

Bernd Sokolowski *Editor*

Auditory and Vestibular Research

Methods and Protocols
Second Edition

EXTRAS ONLINE

Humana Press

METHODS IN MOLECULAR BIOLOGY

Series Editor

John M. Walker

School of Life and Medical Sciences

University of Hertfordshire

Hatfield, Hertfordshire, AL10 9AB, UK

For further volumes:
<http://www.springer.com/series/7651>

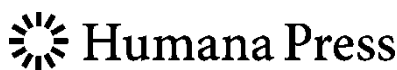
Auditory and Vestibular Research

Methods and Protocols

Edited by

Bernd Sokolowski

*Department of Otolaryngology—Head and Neck Surgery, Morsani College of Medicine,
University of South Florida, Tampa, FL, USA*



Editor

Bernd Sokolowski

Department of Otolaryngology—Head
and Neck Surgery

Morsani College of Medicine
University of South Florida
Tampa, FL, USA

ISSN 1064-3745

Methods in Molecular Biology

ISBN 978-1-4939-3613-7

DOI 10.1007/978-1-4939-3615-1

ISSN 1940-6029 (electronic)

ISBN 978-1-4939-3615-1 (eBook)

Library of Congress Control Number: 2016942277

© Springer Science+Business Media New York 2016

This work is subject to copyright. All rights are reserved by the Publisher, whether the whole or part of the material is concerned, specifically the rights of translation, reprinting, reuse of illustrations, recitation, broadcasting, reproduction on microfilms or in any other physical way, and transmission or information storage and retrieval, electronic adaptation, computer software, or by similar or dissimilar methodology now known or hereafter developed.

The use of general descriptive names, registered names, trademarks, service marks, etc. in this publication does not imply, even in the absence of a specific statement, that such names are exempt from the relevant protective laws and regulations and therefore free for general use.

The publisher, the authors and the editors are safe to assume that the advice and information in this book are believed to be true and accurate at the date of publication. Neither the publisher nor the authors or the editors give a warranty, express or implied, with respect to the material contained herein or for any errors or omissions that may have been made.

Cover illustration: Cover photo shows a confocal image (Leica SP5) of afferents (Neurovue Orange, red) and efferents (Neurovue Maroon, green) to the basal turn of the organ of Corti in a postnatal mouse. Image provided by B. Fritzsch.

Printed on acid-free paper

This Humana Press imprint is published by Springer Nature

The registered company is Springer Science+Business Media LLC New York

Preface

Seven years have passed since the last edition of *Auditory and Vestibular Research, Methods and Protocols*. During this period of time, technological advances and research findings in the field continued at a rapid pace. Thus, no single edition could encompass all the different types of experiments and protocols conducted in the auditory and vestibular fields. With this, the second edition of *Auditory and Vestibular Research, Methods and Protocols*, we expand the previous volume from three to seven major sections. Here, we introduce new protocols that encompass cell culture, tissue engineering, nanotechnology, high-throughput screening, and physiology. The section on physiology alone covers techniques that include optical coherence tomography, patch clamping, and photostimulation of caged neurotransmitters. While the first edition explored the nuances of DNA/RNA and protein protocols, the second edition further expounds on these techniques with new chapters and updates. The imaging section in this edition elucidates traditional areas of fluorescence microscopy, including how to build your own fluorescence microscope, but also contains newer techniques that allow the scanning of live stereocilia at nanoscale resolution and large-scale mapping of the brain using electron microscopy (EM). As in the first edition, the present overview provides a perspective of basic research with both mammalian and non-mammalian animal models. The chapters in Part I focus on RNA delivery and extraction, while those in Part II bring updates to protein protocols such as the yeast two-hybrid system and plasmon resonance, while adding new chapters on protein stoichiometry and colocalization. Part III covers various microscopy techniques, including confocal fluorescence, hopping probe ion conductance, and EM to study connectomics. Part IV describes culture protocols such as those used in organ culture, quantifying neurite behavior, and tissue engineering using umbilical cord cells. Part V focuses on nanotechnology with a general overview of nanoparticle-based delivery in hearing disorders and, more specifically, nanotechnology in membrane electromechanics. Part VI entails a description of inner ear cell sorting techniques and high-throughput chemical screens. Finally, Part VII contains seven chapters describing physiological techniques that measure responses beginning with the basilar membrane, continuing with hair cells, their stereocilia, and spiral ganglion cells, and ending with central auditory circuits. The techniques described herein will be useful to scientists in other fields, especially where tissues are scarce and where a comparative approach is useful in discovering the causes of human disorders.

Tampa, FL, USA

Bernd Sokolowski

Acknowledgements

I would like to give my heartfelt thanks to all of the authors who contributed to the two volumes of *Auditory and Vestibular Research, Methods and Protocols*. A special thanks is extended also to the series editor, John Walker, and to the staff of Springer Verlag for their attention to quality in publishing.

Contents

Preface	v
Acknowledgements	vii
Contributors	xiii

PART I RNA DELIVERY AND EXTRACTION PROTOCOLS

1 Helios® Gene Gun-Mediated Transfection of the Inner Ear Sensory Epithelium: Recent Updates	3
<i>Inna A. Belyantseva</i>	
2 Tol2-Mediated Delivery of miRNAs to the Chicken Ototocyst Using Plasmid Electroporation	27
<i>Michelle L. Stoller and Donna M. Fekete</i>	
3 A Rapid, Cost-Effective Method to Prepare Recombinant Adeno-Associated Virus for Efficient Gene Transfer to the Developing Mouse Inner Ear	43
<i>Michelle M. Gomes, Lingyan Wang, Han Jiang, Christoph A. Kahl, and John V. Brigande</i>	
4 Generation of Noninvasive, Quantifiable, Orthotopic Animal Models for NF2-Associated Schwannoma and Meningioma	59
<i>Sarah S. Burns and Long-Sheng Chang</i>	
5 RNA Extraction from Xenopus Auditory and Vestibular Organs for Molecular Cloning and Expression Profiling with RNA-Seq and Microarrays	73
<i>Casilda Trujillo-Provencio, TuShun R. Powers, David R. Sultemeier, Daniel Ramirez-Gordillo, and Elba E. Serrano</i>	

PART II PROTEIN PROTOCOLS

6 Yeast Two-Hybrid Screening to Test for Protein–Protein Interactions in the Auditory System	95
<i>Iman Moeini-Naghani and Dhasakumar S. Navaratnam</i>	
7 Multiplexed Isobaric Tagging Protocols for Quantitative Mass Spectrometry Approaches to Auditory Research	109
<i>Douglas E. Vetter and Johnvesly Basappa</i>	
8 Protein Quantitation of the Developing Cochlea Using Mass Spectrometry	135
<i>Lancia N.F. Darville and Bernd H.A. Sokolowski</i>	

9	Ultrastructural Identification and Colocalization of Interacting Proteins in the Murine Cochlea by Post-Embedding Immunogold Transmission Electron Microscopy	149
	<i>Margaret C. Harvey and Bernd H.A. Sokolowski</i>	
10	Surface Plasmon Resonance (SPR) Analysis of Binding Interactions of Inner-Ear Proteins	165
	<i>Dennis G. Drescher, Selvakumar Dakshnamurthy, Marian J. Drescher, and Neeliyath A. Ramakrishnan</i>	
11	The Single-Molecule Approach to Membrane Protein Stoichiometry	189
	<i>Michael G. Nichols and Richard Hallworth</i>	

PART III IMAGING PROTOCOLS

12	Visualization of Live Cochlear Stereocilia at a Nanoscale Resolution Using Hopping Probe Ion Conductance Microscopy	203
	<i>A. Catalina Vélez-Ortega and Gregory I. Frolenkov</i>	
13	Design and Construction of a Cost-Effective Spinning Disk System for Live Imaging of Inner Ear Tissue	223
	<i>Federico Ceriani, Catalin D. Ciubotaru, Mario Bortolozzi, and Fabio Mammano</i>	
14	Neuroanatomical Tracing Techniques in the Ear: History, State of the Art, and Future Developments	243
	<i>Bernd Fritzsch, Jeremy S. Duncan, Jennifer Kersigo, Brian Gray, and Karen L. Elliott</i>	
15	Detection of Excitatory and Inhibitory Synapses in the Auditory System Using Fluorescence Immunohistochemistry and High-Resolution Fluorescence Microscopy	263
	<i>Wibke Singer, Hyun-Soon Geisler, Rama Panford-Walsh, and Marlies Knipper</i>	
16	Rapid and Semi-automated Extraction of Neuronal Cell Bodies and Nuclei from Electron Microscopy Image Stacks	277
	<i>Paul S. Holcomb, Michael Morehead, Gianfranco Doretto, Peter Chen, Stuart Berg, Stephen Plaza, and George Spirou</i>	

PART IV CELL CULTURE AND TISSUE ENGINEERING PROTOCOLS

17	Organotypic Culture of the Mouse Cochlea from Embryonic Day 12 to the Neonate	293
	<i>Vidhya Munnamalai and Donna M. Fekete</i>	
18	Quantifying Spiral Ganglion Neurite and Schwann Behavior on Micropatterned Polymer Substrates	305
	<i>Elise L. Cheng, Braden Leigh, C. Allan Guymon, and Marlan R. Hansen</i>	
19	The Use of Human Wharton's Jelly Cells for Cochlear Tissue Engineering	319
	<i>Adam J. Mellott, Michael S. Detamore, and Hinrich Staecker</i>	

PART V NANOTECHNOLOGY

- 20 Nanotechnology in Auditory Research: Membrane Electromechanics in Hearing. 349
Mussie Araya and William E. Brownell
- 21 An Overview of Nanoparticle Based Delivery for Treatment of Inner Ear Disorders 363
Ilmari Pyykkö, Jing Zou, Annelies Schrott-Fischer, Rudolf Glueckert, and Paavo Kinnunen

PART VI SCREENING OF CELLS AND BIOACTIVE COMPOUNDS

- 22 Development of Cell-Based High-Throughput Chemical Screens for Protection Against Cisplatin-Induced Ototoxicity 419
Tal Teitz, Asli N. Goktug, Taosheng Chen, and Jian Zuo
- 23 Profiling Specific Inner Ear Cell Types Using Cell Sorting Techniques 431
Taha A. Jan, Lina Jansson, Patrick J. Atkinson, Tian Wang, and Alan G. Cheng

PART VII PHYSIOLOGICAL PROTOCOLS

- 24 Optical Coherence Tomography to Measure Sound-Induced Motions Within the Mouse Organ of Corti In Vivo 449
Zina Jawadi, Brian E. Applegate, and John S. Oghalai
- 25 Method for Dissecting the Auditory Epithelium (Basilar Papilla) in Developing Chick Embryos. 463
Snezana Levic and Ebenezer N. Yamoah
- 26 Whole-Cell Patch-Clamp Recording of Mouse and Rat Inner Hair Cells in the Intact Organ of Corti 471
Juan D. Goutman and Sonja J. Pyott
- 27 Glass Probe Stimulation of Hair Cell Stereocilia 487
Anthony W. Peng and Anthony J. Ricci
- 28 A Walkthrough of Nonlinear Capacitance Measurement of Outer Hair Cells 501
Lei Song and Joseph Santos-Sacchi
- 29 In Vitro Functional Assessment of Adult Spiral Ganglion Neurons (SGNs) 513
Jeong Han Lee, Choongryoul Sihn, Wangning Wang, Cristina Maria Perez Flores, and Ebenezer N. Yamoah
- 30 Mapping Auditory Synaptic Circuits with Photostimulation of Caged Glutamate 525
Joshua J. Sturm, Tuan Nguyen, and Karl Kandler
- Index.* 539

Contributors

- BRIAN E. APPLEGATE • *Department of Biomedical Engineering, Texas A&M University, College Station, TX, USA*
- MUSSIE ARAYA • *Department of Molecular Physiology and Biophysics, Baylor College of Medicine, Houston, TX, USA*
- PATRICK J. ATKINSON • *Department of Otolaryngology—Head and Neck Surgery, Stanford University School of Medicine, Stanford, CA, USA*
- JOHNVESLY BASAPPA • *Department of Pathology and Laboratory Medicine, Perelman School of Medicine, University of Pennsylvania, Philadelphia, PA, USA*
- INNA A. BELYANTSEVA • *Laboratory of Molecular Genetics, Section on Human Genetics, National Institute on Deafness and Other Communication Disorders, NIH, Bethesda, MD, USA*
- STUART BERG • *Howard Hughes Medical Institute, Ashburn, VA, USA*
- MARIO BORTOLOZZI • *Department of Physics and Astronomy, University of Padua, Padua, Italy*
- JOHN V. BRIGANDE • *Oregon Hearing Research Center, Oregon Health & Science University, Portland, OR, USA*
- WILLIAM E. BROWNELL • *Department of Otolaryngology, Baylor College of Medicine, Houston, TX, USA*
- SARAH S. BURNS • *Center for Childhood Cancer and Blood Diseases, The Research Institute at Nationwide Children's Hospital, Columbus, OH, USA*
- FEDERICO CERIANI • *Department of Physics and Astronomy, University of Padua, Padua, Italy*
- LONG-SHENG CHANG • *Department of Pediatrics, The Ohio State University College of Medicine, Columbus, OH, USA*
- PETER CHEN • *Lane Department of Computer Science and Electrical Engineering, Benjamin M. Statler College of Engineering and Mineral Resources, West Virginia University, Morgantown, WV, USA*
- TAOSHENG CHEN • *Department of Chemical Biology and Therapeutics, St. Jude Children's Research Hospital, Memphis, TN, USA*
- ELISE L. CHENG • *Department of Otolaryngology—Head and Neck Surgery, University of Iowa Hospitals and Clinics, Iowa City, IA, USA*
- ALAN G. CHENG • *Department of Otolaryngology—Head and Neck Surgery, Stanford University School of Medicine, Stanford, CA, USA*
- CATALIN D. CIUBOTARU • *CNR, Institute of Neuroscience, Padua, Italy*
- SELVAKUMAR DAKSHNAMURTHY • *Department of Otolaryngology, Wayne State University School of Medicine, Detroit, MI, USA*
- LANCIA N.F. DARVILLE • *Department of Otolaryngology—Head and Neck Surgery, Morsani College of Medicine, University of South Florida, Tampa, FL, USA*
- MICHAEL S. DETAMORE • *Department of Chemical and Petroleum Engineering, University of Kansas, Lawrence, KS, USA*

- GIANFRANCO DORETTO • *Lane Department of Computer Science and Electrical Engineering, Benjamin M. Statler College of Engineering and Mineral Resources, West Virginia University, Morgantown, WV, USA*
- DENNIS G. DRESCHER • *Department of Otolaryngology, Wayne State University School of Medicine, Detroit, MI, USA*
- MARIAN J. DRESCHER • *Department of Otolaryngology, Wayne State University School of Medicine, Detroit, MI, USA*
- JEREMY S. DUNCAN • *Division of Otolaryngology, University of Utah, Salt Lake City, UT, USA*
- KAREN L. ELLIOTT • *Department of Biology, University of Iowa, Iowa City, IA, USA*
- DONNA M. FEKETE • *Department of Biological Sciences, Purdue University, West Lafayette, IN, USA*
- CRISTINA MARIA PEREZ FLORES • *Department of Physiology and Cell Biology, School of Medicine, University of Nevada Reno, Reno, NV, USA*
- BERND FRITZSCH • *Department of Biology, The University of Iowa, Iowa City, IA, USA*
- GREGORY I. FROLENKOV • *Department of Physiology, College of Medicine, University of Kentucky, Lexington, KY, USA*
- HYUN-SOON GEISLER • *Department of Otolaryngology, Tübingen Hearing Research Centre, University of Tübingen, Tübingen, Germany*
- RUDOLF GLUECKERT • *Department of Otolaryngology, Medical University of Innsbruck, Innsbruck, Austria*
- ASLI N. GOKTUG • *Department of Chemical Biology and Therapeutics, St. Jude Children's Research Hospital, Memphis, TN, USA*
- MICHELLE M. GOMES • *Oregon National Primate Research Center, Oregon Health & Science University, Beaverton, OR, USA*
- JUAN D. GOUTMAN • *Instituto de Investigaciones en Ingeniería Genética y Biología Molecular, Buenos Aires, Argentina*
- BRIAN GRAY • *Molecular Targeting Technologies, Inc., West Chester, PA, USA*
- C. ALLAN GUYMON • *Department of Chemical and Biochemical Engineering, The University of Iowa, Iowa City, IA, USA*
- RICHARD HALLWORTH • *Department of Biomedical Sciences, Creighton University School of Medicine, Omaha, NE, USA*
- MARLAN R. HANSEN • *Department of Otolaryngology—Head and Neck Surgery, University of Iowa Hospitals and Clinics, Iowa City, IA, USA*
- MARGARET C. HARVEY • *Department of Otolaryngology—Head and Neck Surgery, Morsani College of Medicine, University of South Florida, Tampa, FL, USA*
- TAHA A. JAN • *Department of Otolaryngology, Massachusetts Eye and Ear Infirmary, Harvard Medical School, Boston, MA, USA*
- LINA JANSSON • *Department of Otolaryngology—Head and Neck Surgery, Stanford University School of Medicine, Stanford, CA, USA*
- ZINA JAWADI • *Department of Otolaryngology—Head and Neck Surgery, Stanford University, Stanford, CA, USA*
- HAN JIANG • *Oregon Hearing Research Center, Oregon Health & Science University, Portland, OR, USA*
- CHRISTOPH A. KAHL • *Oregon National Primate Research Center, Oregon Health & Science University, Beaverton, OR, USA*
- KARL KANDLER • *Department of Otolaryngology, School of Medicine, University of Pittsburgh, Pittsburgh, PA, USA*

- JENNIFER KERSIGO • *Department of Biology, University of Iowa, Iowa City, IA, USA*
- PAAVO KINNUNEN • *BECS, Department of Biomedical Engineering and Computational Science, Aalto University, Aalto, Finland*
- MARLIES KNIPPER • *Department of Otolaryngology, Tübingen Hearing Research Centre, University of Tübingen, Tübingen, Germany*
- JEONG HAN LEE • *Department of Physiology and Cell Biology, School of Medicine, University of Nevada, Reno, Reno, NV, USA*
- BRADEN LEIGH • *Department of Chemical and Biochemical Engineering, The University of Iowa, Iowa City, IA, USA*
- SNEZANA LEVIC • *School of Pharmacy and Biomolecular Sciences, University of Brighton, Brighton, UK*
- FABIO MAMMANO • *CNR, Institute of Cell Biology and Neurobiology, Monterotondo, RM, Italy*
- ADAM J. MELLOTT • *Department of Plastic Surgery, University of Kansas Medical Center, Kansas City, KS, USA*
- IMAN MOEINI-NAGHANI • *Department of Neurology, Yale School of Medicine, New Haven, CT, USA*
- MICHAEL MOREHEAD • *Lane Department of Computer Science and Electrical Engineering, Benjamin M. Statler College of Engineering and Mineral Resources, West Virginia University, Morgantown, WV, USA*
- VIDHYA MUNNAMALAI • *Department of Biological Sciences, Purdue University, West Lafayette, IN, USA*
- DHASAKUMAR S. NAVARATNAM • *Department of Neurology, Yale University School of Medicine, New Haven, CT, USA*
- TUAN NGUYEN • *Department of Physics, The College of New Jersey, Ewing, NJ, USA*
- MICHAEL G. NICHOLS • *Department of Physics, Creighton University, Omaha, NE, USA*
- JOHN S. OGHALAI • *Department of Otolaryngology—Head and Neck Surgery, Stanford University, Stanford, CA, USA*
- RAMA PANFORD-WALSH • *Department of Otolaryngology, Tübingen Hearing Research Centre Tübingen, University of Tübingen, Tübingen, Germany*
- ANTHONY W. PENG • *Department of Otolaryngology—Head and Neck Surgery, Stanford University School of Medicine, Stanford, CA, USA*
- STEPHEN PLAZA • *Howard Hughes Medical Institute, Ashburn, VA, USA*
- TUSSHUN R. POWERS • *Biology Department, New Mexico State University, Las Cruces, NM, USA*
- SONJA PYOTT • *Department of Otorhinolaryngology, University Medical Center Groningen, Groningen, The Netherlands*
- ILMARI PYYKKÖ • *Department of Otolaryngology, University of Tampere and University Hospital of Tampere, Tampere, Finland*
- NEELIYATH A. RAMAKRISHNAN • *Department of Otolaryngology, Wayne State University School of Medicine, Detroit, MI, USA*
- DANIEL RAMIREZ-GORDILLO • *Biology Department, New Mexico State University, Las Cruces, NM, USA*
- ANTHONY J. RICCI • *Department of Otolaryngology—Head and Neck Surgery, Stanford University School of Medicine, Stanford, CA, USA*
- JOSEPH SANTOS SACCHI • *Department of Surgery, Yale University School of Medicine, New Haven, CT, USA*

- ANNELIES SCHROTT-FISCHER • *Department of Otolaryngology, Medical University of Innsbruck, Innsbruck, Austria*
- ELBA E. SERRANO • *Biology Department, New Mexico State University, Las Cruces, NM, USA*
- CHOONGRYOUL SIHN • *Department of Physiology and Cell Biology, School of Medicine, University of Nevada Reno, Reno, NV, USA*
- WIBKE SINGER • *Department of Otolaryngology, Tübingen Hearing Research Centre, University of Tübingen, Tübingen, Germany*
- BERND H.A. SOKOLOWSKI • *Department of Otolaryngology—Head and Neck Surgery, Morsani College of Medicine, University of South Florida, Tampa, FL, USA*
- LEI SONG • *Department of Surgery, Yale University School of Medicine, New Haven, CT, USA*
- GEORGE SPIROU • *Department of Otolaryngology, West Virginia University School of Medicine, Morgantown, WV, USA*
- HINRICH STAECKER • *Department of Otolaryngology—Head and Neck Surgery, University of Kansas Medical Center, Kansas City, KS, USA*
- MICHELLE L. STOLLER • *Department of Neurobiology and Anatomy, University of Utah, Salt Lake City, UT, USA*
- JOSHUA J. STURM • *Department of Otolaryngology, University of Pittsburgh School of Medicine, Pittsburgh, PA, USA*
- DAVID R. SULTEMEIER • *Biology Department, New Mexico State University, Las Cruces, NM, USA*
- TAL TEITZ • *Department of Developmental Neurobiology, St. Jude Children's Research Hospital, Memphis, TN, USA*
- CASILDA TRUJILLO-PROVENCIO • *Biology Department, New Mexico State University, Las Cruces, NM, USA*
- A. CATALINA VÉLEZ-ORTEGA • *Department of Physiology, College of Medicine, University of Kentucky, Lexington, KY, USA*
- DOUGLAS E. VETTER • *Department of Neurobiology and Anatomical Sciences, University of Mississippi Medical Center, Jackson, MS, USA*
- LINGYAN WANG • *Oregon Hearing Research Center, Oregon Health & Science University, Portland, OR, USA*
- TIAN WANG • *Department of Otolaryngology—Head and Neck Surgery, Stanford University School of Medicine, Stanford, CA, USA*
- WANGING WANG • *Department of Physiology and Cell Biology, School of Medicine, University of Nevada Reno, Reno, NV, USA*
- EBENEZER N. YAMOAH • *Department of Physiology and Cell Biology, School of Medicine, University of Nevada, Reno, Reno, NV, USA*
- JING ZOU • *BECS, Department of Biomedical Engineering and Computational Science, Aalto University, Aalto, Finland*
- JIAN ZUO • *Department of Developmental Neurobiology, St. Jude Children's Research Hospital, Memphis, TN, USA*

Part I

RNA Delivery and Extraction Protocols

Chapter 1

Helios® Gene Gun-Mediated Transfection of the Inner Ear Sensory Epithelium: Recent Updates

Inna A. Belyantseva

Abstract

The transfection of vertebrate inner ear hair cells has proven to be challenging. Therefore, many laboratories attempt to use and improve different transfection methods. Each method has its own advantages and disadvantages. A particular researcher's skills in addition to available equipment and the type of experiment (in vivo or in vitro) likely determine the transfection method of choice. Biostatic delivery of exogenous DNA, mRNA, or siRNA, also known as Helios® Gene Gun-mediated transfection, uses the mechanical energy of compressed helium gas to bombard tissue with micron- or submicron-sized DNA or RNA-coated gold particles, which can penetrate and transfect cells in vitro or in vivo. Helios® Gene Gun-mediated transfection has several advantages: (1) it is simple enough to learn in a short time; (2) it is designed to overcome cell barriers even as tough as plant cell membrane or stratum corneum in the epidermis; (3) it can transfect cells deep inside a tissue such as specific neurons within a brain slice; (4) it can accommodate mRNA, siRNA, or DNA practically of any size to be delivered; and (5) it works well with various cell types including non-dividing, terminally differentiated cells that are difficult to transfect, such as neurons or mammalian inner ear sensory hair cells. The latter advantage is particularly important for inner ear research. The disadvantages of this method are: (1) low efficiency of transfection due to many variables that have to be adjusted and (2) potential mechanical damage of the tissue if the biostatic shot parameters are not optimal. This chapter provides a step-by-step protocol and critical evaluation of the Bio-Rad Helios® Gene Gun transfection method used to deliver green fluorescent protein (GFP)-tagged full-length cDNAs of myosin 15a, whirlin, β-actin, and Clic5 into rodent hair cells of the postnatal inner ear sensory epithelia in culture.

Key words Biostatic transfection, Gene gun, Inner ear, Hair cell, Stereocilia, Myosin, Whirlin, Actin, Clic5, Immunofluorescence, GFP

1 Introduction

During the last few years, there are reports of successful transfections of inner ear hair cells using different methods. One new method, “injectoporation” is just at the beginning of its evaluation by different laboratories [1] and appears to be promising. The technique of intrauterine electroporation is efficient for hair cell transfection, but is not commonly used, likely because of the

special skills required to perform survival surgery on small rodents [2]. Typically, local injections of non-viral and viral vectors into middle or inner ear is a method of choice for transfecting inner ear cells *in vivo*, to attempt restoring hearing function in mutant mice by gene therapy [3–7]. Electroporation *in vitro*, of embryonic and early postnatal organ of Corti explants, is a method of choice in some laboratories [8–14], whereas others have used Helios Gene Gun transfection [15–25]. This chapter is an update on the Gene Gun transfection technique and its place in relation to other methods of transfection of the inner ear sensory epithelia.

Mammalian inner ear hair cells are terminally differentiated, non-dividing cells located within the sensory epithelia of the auditory (organ of Corti) and vestibular periphery (utricle macula, saccular macula, and three cristae ampullares). Hair cells are polarized cells with a cylindrical or pear-like cell body and an apically positioned cuticular plate, which is composed of a dense meshwork of actin. Tight junctions interconnect the apical surfaces of hair cells with surrounding supporting cells. These structural peculiarities of hair cells and their cellular environment may contribute to the ineffectiveness of conventional transfection techniques such as lipofection [26].

An alternative is electroporation-mediated transfection, which is based on the application of an electric field pulse that creates transient aqueous pathways in lipid bilayer membranes, allowing polar molecules to enter a cell [27, 28]. Electroporation causes a brief increase in membrane permeability after which the membrane quickly reseals. This method is effective with a variety of cell types and species and is used in many applications, including transfection *in vivo* of embryonic mouse brain [29] and transfection *in vitro* of immature hair cells from embryonic inner ear explants [13]. One disadvantage of this method is the exposure of the targeted and non-targeted cells to potentially damaging current and electrolysis-generated changes of pH, which may activate stress responses in hair cells. Excessive cell damage and death was a long-standing concern [27] until electroporation devices were improved [28].

A microinjection method of delivering exogenous DNA into a cell, although precise, is labor-intensive. A fully automated robotic system for microinjection was developed and used in zebrafish embryos [30]. Recently, an injectoporation method, combining microinjection of a solution into the sensory epithelium followed quickly by electroporation, was described for the transfection of the mouse organ of Corti [1]. This method of microinjection followed by electroporation was described previously for transfection of planarians, insect larva, and adult insect brain *in vivo* [31–34]. Xiong and co-authors [1] adopted this method to transfet auditory hair cells in postnatal mouse organ of Corti explants from postnatal day 0 to postnatal day 4. This method appeared to be efficient, although effectiveness is decreased with the age of the postnatal mouse organ of Corti explant [1]. The injectoporation procedure requires micro-injection skills under an upright microscope and seems well suited

for electrophysiology laboratories that study functional responses of transfected cells. One drawback of this procedure is the use of antibiotics in the culture media. These drugs are essential to avoid contamination during the prolonged exposure of cultured explants to ambient air, while positioning electrodes and micropipettes within the petri dish filled with culture media and perform microinjection of tissue under the microscope. Another drawback is the potential damage by micropipettes of cell-cell junctions during microinjections, which may affect Ca^{2+} and other signals between hair cells and supporting cells. Avoiding such damage is essential, when studying hair cell innervation or hair cell and Deiters' cell junctions.

The Helios Gene Gun-mediated transfection method of DNA delivery with submicron-sized particles (microcarriers) accelerated to high velocity was developed in the late 1980s by Sanford, Johnston and colleagues [35–38]. This biolistic method was designed to circumvent difficulties in transfecting plant cells with cell walls that prevent simple diffusion and/or internalization of material or vesicles from the cell surface [36]. Subsequently, this method was shown to be applicable to mammalian cells [37]. In the early 1990s, it was used to deliver exogenous DNA to the tissue of a live mouse [38–40]. Since then, biolistic devices were modified for particular applications and used *in vitro* to transfect cultured cells and tissues, from yeast to mouse brain slices [35, 37, 40, 41, 43], and *in vivo* for intradermal vaccination of human and animals using DNA and mRNA vaccines [44, 45]. In the BioRad hand-held Helios® Gene Gun delivery system (BioRad Laboratories, Inc., Hercules, CA), DNA-coated gold particles (bullets) are accelerated to high speed by pressurized helium and are able to overcome physical barriers such as the stratum corneum in the epidermis [46] or the actin-rich cuticular plate of inner ear hair cells [15]. This method is suitable for the delivery of mRNA, siRNA, or cDNA to terminally differentiated cells that are difficult to transfect such as neurons, inner ear sensory cells, or cells from internal cellular layers [44, 47, 48]. It works well with postnatal inner ear sensory epithelial explants [15–18]. This method can be used to co-transfect two or more different plasmids on the same bullets [18]. It is also suitable for delivery of large cDNAs that do not fit in the limited space of a viral vector, for example. Recently, Helios Gene Gun transfection was combined with live cell imaging, to examine whether or not F-actin core treadmills in hair cell stereocilia [49], as proposed previously [15, 17]. Consistent with the results of a study that shows slow protein turnover in hair cell stereocilia using multi-isotope imaging mass spectrometry [50], the study of gene gun-transfected live hair cells of postnatal mouse utricle reveals stable filamentous actin cores with turnover and elongation restricted to stereociliary tips [49].

Over the last 10 years, we successfully transfected hair cells with cDNA expression constructs of GFP-tagged full-length

myosin Ic, myosin VI, myosin VIIa, myosin 15a, whirlin, espin, γ - and β -actin, and Clic5 using the Helios® Gene Gun [15, 16, 18, 19, 51 and unpublished data]. Some of the data from these papers will be used in this chapter to illustrate the versatility of the Gene Gun transfection method. Our data show that Helios® Gene Gun-mediated transfection is a valuable tool to elucidate the function of “deafness” genes and their encoded proteins, when utilized in combination with fluorescence immunostaining as well as genetic and phenotype analyses of mouse models of human deafness.

Various cell types populating inner ear sensory epithelia have apical surfaces with different physical properties. Directly underneath the apical plasma membrane of sensory hair cells of the organ of Corti is a dense actin meshwork referred to as the cuticular plate. The rootlet of each stereocilium extends into the cuticular plate, which provides a support for the stereociliary bundle [52, 53]. Each auditory stereociliary bundle in mammals is composed of two to three rows of stereocilia, which are mechanosensory microvilli-like projections indispensable for normal hearing function.

Stereocilia may be damaged by the pulse of helium pressure as well as by gold particle bombardment. On the other hand, the dense cuticular plate is an obstacle to the introduction of gold particles into sensory hair cells, which requires a substantial pressure pulse. These factors require careful consideration of the many parameters and settings needed for using the Gene Gun to transfect cDNA into sensory hair cells. The variables to be considered include: (1) the distance between the cartridge with bullets and the targeted tissue, (2) the angle at which bullets strike the cells, (3) the helium pressure applied to propel the bullets toward the tissue, (4) the thickness of the residual liquid layer that covers the tissue during bombardment, (5) the density of bombarding gold particles over the surface area of targeted cells, (6) the purity and concentration of DNA, (7) and the general quality of the cartridges and bullets (*see Subheading 3 and Note 1*). The details of the experimental protocol described in this chapter include: (1) preparation of organotypic cultures of the sensory epithelia of the inner ear from postnatal mice and rats, (2) coating microcarriers with plasmid DNA, (3) cartridge preparation, and (4) bombarding tissues with these DNA-coated gold particles accelerated by a pulse pressure of helium gas (*see Note 2*).

2 Materials

2.1 Preparation of the Inner Ear

Sensory Epithelial Explants

1. Experimental animals. Mouse or rat pups of postnatal days 0–4 (*see Note 3*).
2. Dissection tools and microscope (*see Note 4*).
3. Sterile 60 × 15 mm polystyrene tissue culture dishes (Becton Dickinson and Co., Franklin Lakes, NJ).

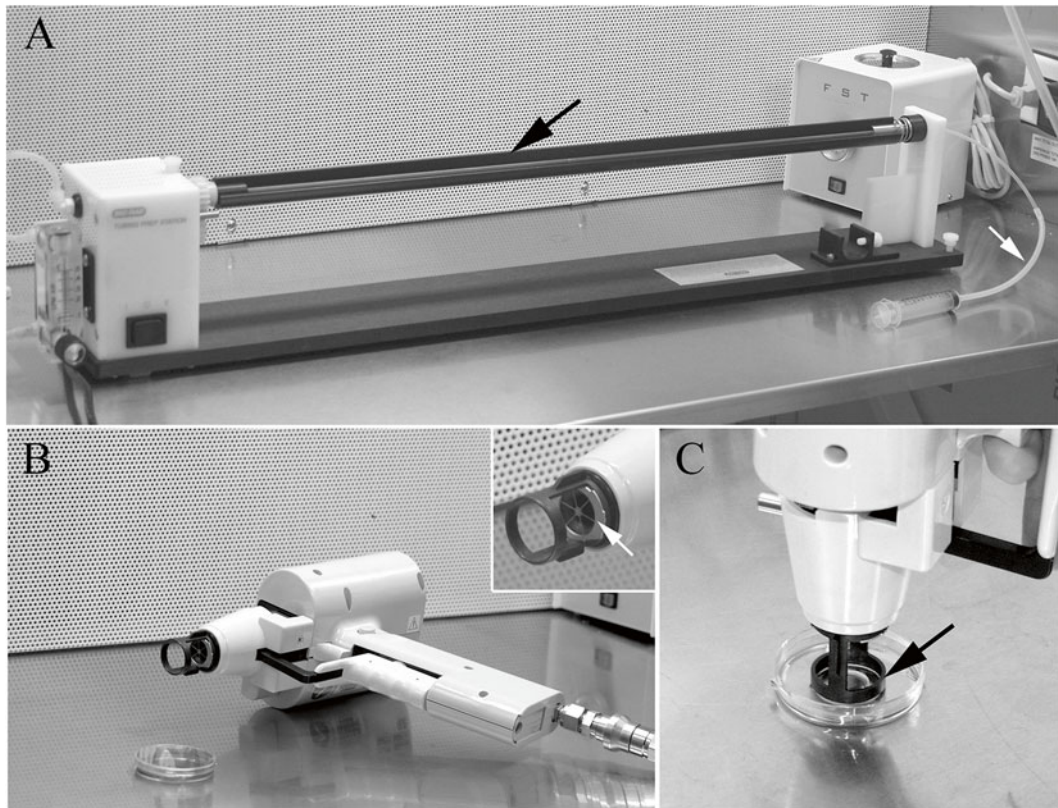


Fig. 1 Bio-Rad Helios® Gene Gun and Tubing Prep Station. **(a)** Tubing Prep Station with Tefzel tubing inserted into the tubing support cylinder (*black arrow*). The right end (~15 cm) of the Tefzel tubing is sticking out and is connected to the 10 cc syringe with adaptor tubing (*white arrow*). **(b)** An assembled Gene Gun with a diffusion screen inserted into the barrel. The insert shows close view of a barrel with a diffusion screen (*white arrow*). Next to the Gene Gun, there is a MatTek glass bottom Petri dish containing the attached sensory epithelium explant in DMEM. **(c)** Correct placement of the Gene Gun while transfecting inner ear sensory epithelium cultured in a MatTek Petri dish. The plastic ring at the end of the barrel (*black arrow*) is positioned so that the explant appears in the center of the ring. DMEM was removed in preparation for firing

4. Leibowitz's L-15 medium without phenol red (Invitrogen, Carlsbad, CA). Store at 4 °C.
5. Sterile MatTek glass bottom Petri dishes (MatTek Corp, Ashland, MA) (*see Note 5* and Fig. 1)
6. 2.18 mg/mL Cell-Tak cell and tissue adhesive (BD Biosciences, San Jose, CA). Store at 4 °C.
7. Tissue culture grade water (Invitrogen).
8. Dulbecco's Modified Eagle's Medium (DMEM) with high glucose content (4.5 g/L) and 25 mM HEPES buffer (Invitrogen) supplemented with 7 % (v/v) fetal bovine serum. Store at 4 °C (*see Note 6*).
9. Sterile microdissecting curette, 12.7 cm, size 3, 2.5 mm (Biomedical Research Instruments, Rockville, MD) (*see Note 7*).
10. Tissue culture incubator set at 37 °C and 5 % CO₂ (*see Note 8*).

2.2 Preparation of Bullets with DNA-Covered Gold Microcarriers

1. 50 µg of plasmid DNA at 1 mg/mL (*see Note 9*). Store at –20 °C.
2. Fresh (unopened) bottle of 100 % ethyl alcohol. Store at room temperature in a cabinet for flammable reagents (*see Note 10*).
3. 1 M CaCl₂: Dilute in the DNase, RNase-free molecular biology grade water from 2 M CaCl₂ molecular biology grade stock solution. Prepared or stock solutions can be purchased from several vendors (e.g., Quality Biological, Inc., Gaithersburg, MD).
4. 1 µm gold microcarriers or tungsten microcarriers (Bio-Rad) (*see Note 11* [38]).
5. 20 mg/mL polyvinylpyrrolidone (PVP, Bio-Rad): weigh out 20 mg of crystallized PVP, add 1 mL of 100 % ethanol and vortex. PVP becomes fully dissolved within 5–10 min at room temperature. Store at 4 °C and use within 1 month (*see Note 12*).
6. 0.05 M spermidine (Sigma-Aldrich Inc., St. Louis, MO) stock solution: dilute the content of one ampule (1 g) of spermidine in 13.6 mL of DNase, RNase-free molecular biology grade water to get a 0.5 M stock solution. Store this solution as single-use aliquots at 20 °C for 1 month. For a working solution to use in bullet preparation, thaw one aliquot of stock solution, take 5 µL and add 45 µL of DNase, RNase-free molecular biology grade water to obtain a final concentration of 0.05 M. Use the same day (*see Note 13*).
7. Two sterile 15 mL conical tubes and sterile 1.5 mL centrifuge tubes.
8. Ultrasonic cleaner (waterbath sonicator) (e.g., Model 50D, VWR International, Chesten, PA) (*see Note 14*).
9. Tubing Prep Station (Fig. 1a) (Bio-Rad). Clean by wiping with 70 % (v/v) ethanol before each use.
10. Nitrogen gas tank, grade 4.8 or higher and nitrogen regulator (Bio-Rad). Also, see the Bio-Rad Helios® Gene Gun System instruction manual for nitrogen gas requirements.
11. Tefzel tubing (Bio-Rad).
12. Tubing cutter and disposable blades (Bio-Rad).
13. 10 cc syringe with ~12–15 cm of syringe adaptor tubing (Fig. 1a, white arrow) (Bio-Rad).
14. 20 mL disposable scintillation vials with caps (Kimble Glass Inc., Vineland, NJ) and desiccating capsules of drycap dehydrators type 11 (Ted Pella, Inc., Redding, CA).

2.3 Helios® Gene Gun Transfection Procedure

1. Helium gas tank grade 4.5 (99.995 %) or higher should be used and a helium pressure regulator (Bio-Rad).
2. Helios Gene Gun System, 100/120 V (Fig. 1b) (Bio-Rad).
3. A diffusion screen (Fig. 1b, white arrow in the insert) (Bio-Rad) can be reused with the same DNA preparation (*see Note 15*).

4. Inner ear sensory epithelial explants attached to the bottom of a glass bottom MatTek Petri dish (prepared as described in Subheading 3).

2.4 Counterstaining, Immunostaining, and Imaging of Transfected Samples

1. 1× Phosphate buffered saline (PBS) without Ca²⁺ and Mg²⁺: 1.06 mM KH₂PO₄, 155.17 mM NaCl, 2.97 mM Na₂HPO₄ (*see Note 16*). Store at 4 °C.
2. 4 % (v/v) Paraformaldehyde fixative: dilute 16 % paraformaldehyde (Electron Microscopy Sciences, Hatfield, PA) 1:4 with 1× PBS (1× PBS is without Ca²⁺ and Mg²⁺, if not specifically mentioned otherwise). Store at 4 °C.
3. 0.5 % (v/v) Triton X-100: dilute 0.25 mL of 100 % Triton X-100 (ACROS Organics, New Jersey, USA) in 50 mL of 1× PBS (*see Note 17*).
4. Blocking solution: dilute 0.2 g of bovine serum albumin fraction V, protease-free (Roche Diagnostics, Indianapolis, IN) and 0.5 mL goat serum (Invitrogen) in 10 mL of 1× PBS. Keep refrigerated and use within 48 h. Every time before use, filter the desired volume of blocking solution using a syringe-driven MF membrane filter unit (25 mm in diameter and 22-μm pore size; Millipore Corporation, Bedford, MA) for sterilization of aqueous solutions.
5. Primary antibody to recognize endogenous native or fluorescently tagged newly synthesized protein. For example, to recognize endogenous whirlin or GFP-tagged whirlin we use polyclonal rabbit anti-whirlin antibody, diluted 1:400 in blocking solution (Fig. 2, [18]). Store at -80 °C.
6. Secondary antibody conjugated to a fluorophore. For example, to bind to polyclonal rabbit anti-whirlin primary antibody (Subheading 2.4, step 5) we use Alexa 643-conjugated goat anti-rabbit secondary antibody (Invitrogen). Store at 4 °C. Dilute 1:500 in blocking solution at the time of use.
7. Rhodamine-phalloidin (Invitrogen). Dilute 1:100 in 1× PBS or blocking solution before use (*see Note 18*).
8. A short (146 mm) glass Pasteur pipette (Ted Pella, Inc., Redding, CA) to transfer inner ear sensory epithelial explant from MatTek Petri dish to a glass slide to mount. To make a tip opening of the Pasteur pipette wider to accommodate the explant, cut the narrow part of the pipette with glasscutter tool.
9. ProLong Gold Antifade Mountant (Invitrogen). Store and use according to the manufacturer's instructions (*see Note 19*).
10. Confocal microscope of any brand suitable for fluorescence imaging. For example, LSM510 or LSM780 confocal microscope (Carl Zeiss Inc., Göttingen, Germany) equipped with a 63× or 100×, 1.4 numerical aperture objective.

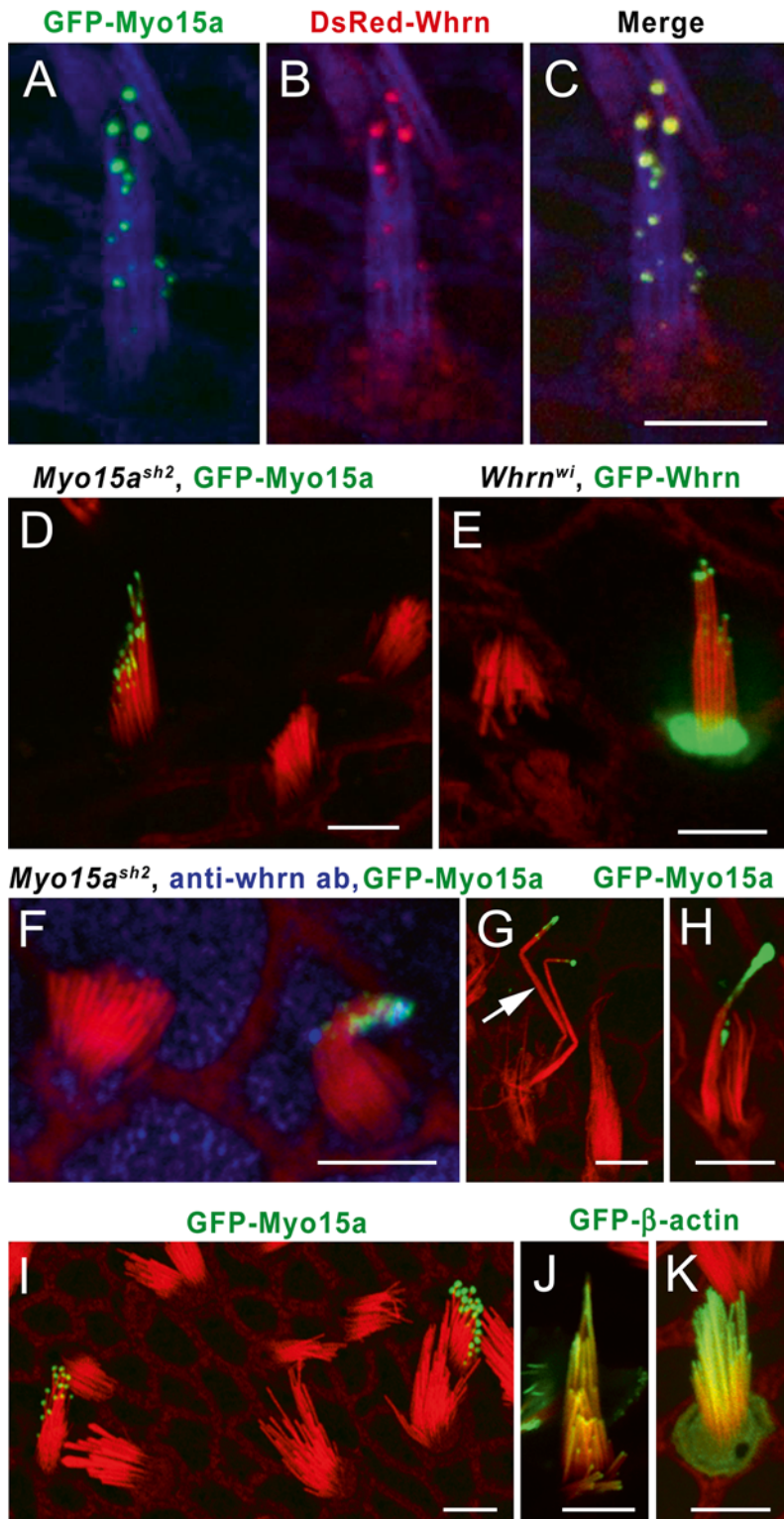


Fig. 2 Gene Gun transfected vestibular hair cells from organotypic cultures of wild-type and mutant mouse inner ear sensory epithelia. (a–c) Simultaneous transfection of GFP-Myo15a and DsRed-Whrn into the vestibular hair cell of a wild-type mouse. GFP-myosin 15a (*left*) and DsRed-whirlin (*middle*) accumulate at the tips of

3 Methods

3.1 Preparation of the Inner Ear Sensory Epithelial Explants

1. Prepare MatTek Petri dishes by coating the entire glass bottom of the dish with Cell-Tak diluted 1:6 (v/v) in tissue culture grade water. Let Cell-Tak dry. Immediately before transferring the tissue into the Cell-Tak covered MatTek Petri dish, wash the dish once briefly with DMEM without FBS (*see Note 20*).
2. Dissect sensory epithelia from postnatal day 0–4 (P0-P4) mouse or rat inner ear in a 60-mm sterile cell culture dish, keeping the tissue submerged in L-15 medium. In the case of the organ of Corti, remove the spiral ligament and the stria vascularis, remove the tectorial membrane, using a 26-gauge needle dissociate the organ of Corti from the modiolus, and then cut the entire organ of Corti into the desired number of pieces. Microdissection of the vestibular sensory epithelia should include gentle removal of utricular and saccular otocystia, calcium-based crystals sitting on top of the sensory epithelia, using a 26-gauge needle.
3. Transfer one or two pieces of the epithelia into the MatTek Petri dish with 2 mL of DMEM supplemented with 7 % (v/v) FBS using a microdissecting curette (*see Note 7*). Submerge all pieces and gently push them against the surface of the dish coated with Cell-Tak to attach them to the substrate (*see Note 21*). Immediately place the dish with attached organotypic culture in an incubator at 37 °C and 5 % CO₂. Let the tissue adhere to the dish while remaining undisturbed overnight.

◀

Fig. 2 (continued) stereocilia in direct proportion to each other and to the length of stereocilia. Merged image (**right**) shows overlapping localizations of GFP-myosin 15a and DsRed-whirlin. Cytoskeletal actin is visualized using phalloidin 633 (*blue*). (**d**) Restoration of the staircase shape of a stereociliary bundle of a homozygous *Myo15ash2* vestibular hair cell 67 h after GFP-Myo15a transfection. Note the short length of stereocilia of non-transfected neighboring *Myo15ash2* hair cells. (**e**) Restoration of the staircase shape of the stereociliary bundle in a homozygous *Whrnwi* vestibular hair cell 48 h after transfection with GFP-Whrn. (**f**) Exogenous GFP-myosin 15a (*green*) recruits endogenous whirlin stained with anti-whirlin HL5136 antibody (*blue*) to stereociliary tips of a *Myo15ash2* transfected vestibular hair cell. Note that there is no anti-whirlin immunoreactivity in the stereocilia of neighboring non-transfected hair cells (*left*). (**g**) Rat vestibular hair cell stereociliary bundle (transfected with GFP-Myo15a) degenerates as a result of excessive helium pressure and particle bombardment. Two giant, over-elongated, and deformed stereocilia (*arrow*) were observed 40 h post-transfection. The stereociliary bundle of a non-transfected neighboring hair cell remains intact. (**h**) Degeneration of a stereociliary bundle transfected with GFP-myosin 15a (GFP-Myo15a), in a mouse vestibular hair cell 26 h post-transfection. There is an enormous accumulation of GFP-myosin 15a at the tips of fused stereocilia. (**i**) Accumulation of variable amount of GFP-myosin 15a at the tips of stereocilia of two transfected mouse vestibular hair cells from the same sensory epithelium explant 45 h post-transfection. (**j, k**) Different patterns of GFP-β-actin distribution in stereocilia of simultaneously transfected mouse vestibular hair cells from the same explant 72 h post-transfection. (**j**) GFP-β-actin is mostly at the tips of stereocilia, whereas, (**k**) GFP-β-actin is distributed along the length of stereocilia. Cytoskeletal actin is visualized by rhodamine-phalloidin (*red*) in panels (**d–k**). Sensory explants were harvested at P2-P5 and transfected the next day. Scale bars: 5 μm

3.2 Preparation of Bullets with DNA-Covered Gold Microcarriers

1. Weigh out 25 mg of gold microcarrier into a 1.5 mL centrifuge tube.
2. Add 100 μ L of 0.05 M spermidine (*see Note 9* and **13**). Vortex for 10–15 s, then sonicate the tube for 30 s by dipping the tube half-way into the water bath of the sonicator.
3. Add 50 μ g of plasmid DNA (50 μ L of 1 mg/mL). Vortex briefly (~5 s) to ensure even distribution of DNA in gold suspension (*see Note 9*).
4. Add 100 μ L of 1 M CaCl_2 one drop at a time to the tube with DNA. Vortex briefly (~3 s) after each drop. If more than 100 μ L of DNA is used, match this volume with the same amount of CaCl_2 . Incubate the tube at room temperature for 10 min.
5. Cut ~76 cm of Tefzel tubing using scissors. Trim both ends using the Bio-Rad Tubing cutter. Position the Tubing Prep Station so that the nitrogen gas meter and the “ON-OFF” switch for rotation are facing toward you (Fig. 1a). Insert the tubing into the Tubing Prep Station, leaving about 10 cm of the tube sticking out on the right-hand side (Fig. 1a).
6. Turn “on” the nitrogen gas to 0.3–0.4 L/min and flush the tubing for 10–15 min.
7. Dilute PVP to 50 μ g/mL using 100 % ethanol (Add 10 μ L of 20 mg/mL of PVP to 4 mL of ethanol in 15 mL conical tube) (*see Note 12*).
8. Microfuge the gold with DNA at $1000 \times g$ for 2 min at room temperature to pellet gold particles. Aspirate excess supernatant using a 1 mL pipette tip, leaving about 20 μ L. Resuspend the gold pellet in this residual volume by gently tapping on the lower part of the tube.
9. Wash three times in 1 mL of 100 % ethanol. Pellet gold by centrifugation at $1000\text{--}2000 \times g$ at room temperature for 10 s, aspirate supernatant as in Subheading **3.2, step 8**, resuspend gold and add 1 mL of 100 % ethanol. After the last wash remove most of the ethanol (*see Note 10*).
10. Add 200 μ L of the 50 μ g/mL PVP in ethanol made in Subheading **3.2, step 7**. Pipette up and down to break up clumps. Transfer the contents of the tube to a 15 mL conical tube. Add another 200 μ L of 50 μ g/mL PVP in ethanol to the centrifuge tube, repeat the pipetting, and transfer to the same 15 mL tube until all the gold particles are transferred. Bring the final volume to 3 mL with fresh 50 μ g/mL PVP in ethanol. Vortex briefly for about 15 s to ensure an even distribution of gold particles in the suspension. Close the tube and keep inverting it by hand to prevent the gold from clumping.

11. Turn off the nitrogen gas on the Tubing Prep Station. Insert the right end of the Tefzel tubing into the adaptor tubing (*see Subheading 2.2, step 13*) attached to an empty 10 cc syringe. Remove the tubing from the apparatus. Remove the cap of the 15 mL tube containing 3 mL of the gold particle suspension (*see Subheading 3.2, step 10*) and immediately place the left end of the Tefzel tubing at the bottom of this tube. Pull the plunger of the syringe and quickly and consistently draw the gold suspension into the tubing. When the entire volume of gold particle suspension is within the Tefzel tubing, continue drawing the suspension into the tubing to empty ~2–3 cm of the left end-segment of the tubing. Make sure that the gold particle suspension is distributed along the Tefzel tubing evenly, without air bubbles, and is not drawn into the adaptor tubing (Fig. 1a, white arrow). Immediately bring the gold-filled tubing to a horizontal position and slide it, with syringe attached, into the tubing support cylinder (Fig. 1a, black arrow) of the Tubing Prep Station until the tubing passes through the O-ring.
12. Let the tubing sit undisturbed for 3 min in the tubing apparatus. The gold will settle to the lower side of horizontally positioned tubing.
13. Use the syringe with adaptor tubing (*see Subheading 3.2, step 11*) attached to the right end of the tube with gold suspension to slowly and consistently pull the supernatant (ethanol) out of the tubing over the course of ~40–45 s. After all of the ethanol is transferred into the syringe and the connecting tubing, disconnect the syringe with adaptor tubing from the Tefzel tube with gold particles.
14. Turn the rotation switch to the “ON” position on the Tubing Prep Station and rotate the tube with gold particles for 20–30 s, allowing the gold to uniformly smear on the inside surface of the tubing.
15. On the Tubing Prep Station, slowly open the valve on the flowmeter regulating the nitrogen gas to 0.35–0.4 L/min, while rotating the tubing with gold particles for 5 min.
16. Stop rotating the tubing. Turn off the nitrogen gas and remove tubing from the apparatus. Trim the ends of the tubing, which usually are not evenly coated with gold. Cut the tubing into ~1.3 cm sections with the Bio-Rad Tubing cutter. These pieces are now the cartridges with bullets.
17. Store these prepared cartridges with bullets in tightly closed scintillation vials (*see Subheading 2.2, step 14*) with one capsule of drycap dehydrators (Ted Pella, Inc., Redding, CA) in each vial (*see Subheading 2.2, step 14*). The coated gold particles stored at 4 °C are usable for about 1 year (*see Note 22*).

3.3 Helios® Gene Gun Transfection Procedure

1. Load bullets with the desired plasmid DNA into the cartridge holder. Leave slot no. 1 empty. Place the cartridge holder into the Gene Gun.
2. Connect the Gene Gun to the helium gas tank via the helium regulator. Open the gas valve and set the pressure to 758.42 kPa (110 psi). Using empty slot no. 1 for firing trial shots, discharge the Helios® Gene Gun two to three times. Be sure that the helium pressure remains stable and does not drop during these trial shots.
3. Switch to slot position no. 2. Insert the diffusion screen into the Helios® Gene Gun barrel as shown in Fig. 1b (see Note 15).
4. Remove a dish with the inner ear sensory explants from the incubator and place it in a sterile laminar flow hood.
5. Aspirate culture medium (as much as possible) from the inner ear organotypic culture attached at the bottom of the MatTek Petri dish (Fig. 1b, c). Immediately position the plastic ring, located at the end of the Helios® Gene Gun barrel (Fig. 1c, black arrow), at the bottom of the Petri dish so that the targeted tissue is located in the center of the ring, and the Gene Gun barrel is perpendicular to the dish bottom. Discharge the Gene Gun (Fig. 1c; see Note 23).
6. Immediately add 2 mL of fresh DMEM medium containing 7 % FBS to the dish. Without delay, place the dish in the incubator for the desired number of hours/days.
7. Repeat steps 1–5 for the other dishes with organotypic culture using fresh bullet cartridges in the consecutive slots of the same cartridge holder.

3.4 Immunostaining and Imaging of Transfected Samples

1. Wash cultures two times in cold 1× PBS (see Note 16).
2. Fix in 4 % paraformaldehyde for 30 min to 1 h at room temperature or overnight at 4 °C.
3. Wash four times with 1× PBS for 5 min.
4. Permeabilize in 0.5 % Triton X-100 for 10–15 min (see Note 17).
5. Wash four times with 1× PBS for 5 min.
6. Incubate in blocking solution (2 % BSA and 5 % goat serum in 1× PBS) for 30 min.
7. Incubate in primary antibody diluted in blocking solution for 1–2 h at room temperature or overnight at 4 °C (see Note 18).
8. Wash four times with 1× PBS for 5 min.
9. Incubate simultaneously for 20 min at room temperature in secondary antibody diluted in blocking solution (see Subheading 2.4, step 6) and phalloidin conjugated to a particular fluorophore (Invitrogen) and diluted 1:100 in blocking solution (see Subheading 2.4, step 7) (see Note 18).

10. Wash four times in 1× PBS.
11. Using a 26-gauge needle, lift the inner ear explant off the glass bottom of the MatTek Petri dish. Transfer the explant to a glass slide by carefully drawing it into a short (146 mm) glass Pasteur pipette (*see Subheading 2.4, step 8*). Position the sensory epithelium on the glass slide with stereocilia facing up; remove the surrounding liquid as much as possible before adding anti-fade mounting medium. Immediately apply a drop of mounting medium. Mount the tissue using the ProLong Gold Antifade Mountant (Invitrogen) according to the manufacturer's instructions (*see Note 24*).
12. Keep slides protected from light in a slide box overnight to let the mounting media solidify (*see Note 25*). Acquire images the next day using a confocal microscope equipped with a 63× or 100×, 1.4 numerical aperture objective.

3.5 Biolistic Transfection of Inner Ear Sensory Epithelium: Interpretation of Results

The advantages and disadvantages of the described method can be illustrated by analyzing the data obtained from Gene Gun-mediated transfections of GFP-myosin 15a and DsRed- or GFP-whirlin into hair cells of inner ear sensory epithelial explants obtained from wild-type and mutant mice [16, 18, 19]. In wild-type hair cells, unconventional motor protein myosin 15a and PDZ domain containing protein whirlin localize together at the tips of stereocilia [18, 19]. We used a Helios® Gene Gun to co-transfect two expression vectors. Gold particles were coated with two different cDNAs at a 1:1 ratio of molecules. GFP-myosin 15a and DsRed-whirlin on the same gold bullet were co-transfected into wild-type hair cells. Both corresponding epitope-tagged proteins were localized to the tips of stereocilia [18]. These data complemented observations of the endogenous myosin 15a and whirlin at the tips of stereocilia as revealed by immunofluorescence [16] and, most importantly, demonstrated that GFP and DsRed epitope tags do not interfere with proper targeting or function of these two proteins (Fig. 2a–c). Moreover, overexpression of GFP-myosin 15a in stereocilia of wild-type hair cells causes distention of stereocilia tips due to an accumulation of an excessive amount of GFP-myosin 15a [18]. No over-elongation of stereocilia of wild-type hair cells due to overexpression of myosin 15a was observed [16, 18].

Myosin 15a mutant (*Myo15ash2*) and whirlin mutant (*Whrnwi*) mice are deaf and have defective hair cell stereocilia that fail to elongate to a normal length due to mutations of these genes [55–57], and thus remain abnormally short [16, 18, 19, 55–58]. Gene Gun-mediated transfections of wild-type GFP-myosin 15a and wild-type GFP-whirlin into the hair cells of sensory epithelial explants from the corresponding mutant mice resulted in the restoration of a normal length of stereociliary bundles (Fig. 2d–e). Moreover, using Gene Gun-mediated transfection of domain-deletion constructs of

myosin 15a and whirlin cDNAs into *Myo15ash2* and *Whrnwi* hair cells, we found that these two proteins interact in vivo through the C-terminal PDZ ligand of myosin 15a and the third PDZ domain of whirlin [18]. This interaction allows myosin 15a to deliver whirlin to the tips of stereocilia. Using an anti-whirlin-specific antibody in combination with Gene Gun transfection, we found that exogenous wild-type GFP-myosin 15a “reawakens” the elongation process in the abnormally short *Myo15ash2* hair cell stereocilia by recruiting endogenous whirlin to stereociliary tips (Fig. 2f and [18]).

3.5.1 Advantages

Using lipofection, viral-mediated transfection, electroporation, or injectoporation, a transfected cell occasionally receives a very small amount of a cDNA expression construct encoding a fluorescently tagged protein. In this case, the amount of synthesized fluorescently tagged protein might be below the threshold of detection by fluorescence microscopy and some transfected cells might be indistinguishable from and mistaken for an untransfected control cells with background fluorescence. Nevertheless, a low level of the epitope-tagged protein may subtly alter the phenotype of the cell. One of the advantages of Helios® Gene Gun transfection is that you can usually find a gold particle inside the body of a transfected cell. This gold particle, marking a transfected cell, allows an investigator to distinguish a likely transfected cell from adjacent non-transfected cells that lack gold particles and can serve as non-transfected controls. Thus, in Helios® Gene Gun transfected epithelia, reliable control non-transfected cells of the same type can be identified in close proximity with transfected cell. Moreover, in our experiments (see Subheading 3.5), stereocilia from *Myo15ash2* and *Whrnwi* inner ear explants undergo elongation only when transfected with wild-type GFP-tagged myosin 15a or whirlin, correspondingly. In contrast, stereocilia bundles of non-transfected hair cells from the same explant remain short, because they are lacking functional myosin 15a (Fig. 2d, f) or whirlin (Fig. 2e). Thus, Gene Gun transfections provide an opportunity to quantitatively measure the induced elongation of stereocilia by comparing the lengths of restored stereocilia of transfected hair cells to the lengths of short hair bundles of non-transfected neighboring control cells. These experiments using Helios® Gene Gun-mediated transfection reveal the functional significance of specific proteins to key developmental events, as demonstrated by the importance of myosin 15a and whirlin interaction to the differential elongation of stereocilia during hair bundle morphogenesis [18].

3.5.2 Disadvantages

There are limitations to using Helios® Gene Gun-mediated transfections of cultured inner ear sensory epithelia. First, stereocilia are sensitive to mechanical disturbances and are easily damaged by an excessive pulse pressure of helium gas, triggering stereocilia degeneration. An early sign of degeneration is an abnormal hair bundle

shape (Fig. 2g–h). Stereocilia may show unrestrained elongation and/or fusion and some proteins in stereocilia become mislocalized, including GFP-tagged proteins introduced via cDNA constructs (Fig. 2g–h). Thus, care should be exercised in interpreting the results if the hair bundle of a transfected cell looks abnormal, especially in explants from mutant mice. For example, an over-elongated, fused, splayed, or otherwise disorganized stereociliary bundle of a transfected *Myo15ash2* hair cell may likely result from degeneration rather than from overexpression of GFP-myosin 15a. Moreover, one can observe a single degenerating over-elongated stereocilium within a short *Myo15ash2* stereociliary bundle, even in non-transfected *Myo15ash2* hair cells that lack functional myosin 15a [16, 18]. Therefore, the presence of abnormal hair bundles with over-elongated stereocilia should not be interpreted as a result of GFP-myosin 15a overexpression in transfected wild-type hair cells (e.g., Fig. 2g–h). Rather, in both transfected and non-transfected *Myo15ash2* hair cells, over-elongation of stereocilia can be interpreted as a consequence of degeneration caused by either mechanical damage due to helium gas pressure, the culture conditions for a prolonged period of time, or the *Myo15ash2* mutation itself. To avoid excessive mechanical damage to stereocilia, the pressure of helium gas should be carefully adjusted for each particular Gene Gun and experimental setup. In our hands, a pressure of 110 psi was used successfully to obtain healthy-looking transfected cells.

Third, different amounts of plasmid DNA on the gold microcarriers may affect the outcome. While only one gold particle may penetrate a hair cell for most transfections, transfected hair cells may show different levels of GFP-tagged protein expression at a specific point in time. Figure 2i shows different amount of GFP-myosin 15a accumulation at the tips of hair cell stereocilia from the same explant 45 h post-transfection. A second example is GFP- β -actin, which first appears at the tips of stereocilia and then supposedly incorporates into actin filaments. Moreover, according to new data obtained from transfected live hair cell time-lapse images, GFP- β -actin may elongate some or all of the stereocilia from the tips, with elongated portions of stereocilia highlighted in green [49]. Hair cells simultaneously transfected with GFP- β -actin in the same explant may show different distribution patterns of newly incorporated GFP- β -actin within stereocilia. Similar variations in GFP- β -actin pattern of distribution in transfected hair cells from the same explant were described for viral infection/delivery to hair cells [54]. Figure 2j–k shows Gene Gun-transfected hair cells from the same explant. Approximately 72 h post-transfection, GFP- β -actin is present primarily at the tips of the stereocilia in one hair cell (Fig. 2j), while GFP- β -actin highlights most of the stereociliary length of another hair cell (Fig. 2k). The time of appearance and the amount of GFP-tagged protein visualized in a transfected cell is probably related to the amount of DNA transfected into a cell.

Therefore, it is important to repeat the above-described experiments (independent determinations each with replicas) to document the range of variations and the kinetics of appearance and localization of the tagged protein. In the absence of such data, one should view any interpretations of time-sensitive expression of GFP-tagged proteins with skepticism. Rigorous evaluation and accurate interpretation of the data from Gene Gun-mediated transfections may require, for example, good antibody to show that endogenous localization of this protein corresponds to the localization of GFP-tagged protein. Time-lapse imaging of transfected cells and the genetic analyses of the phenotype of relevant mutant mice are also useful.

4 Notes

1. Other Gene Gun models, including Accell®, have been developed by Arogen, Inc., a Bio-Rad collaborator (*see* also Helios® Gene Gun System Instruction Manual from Bio-Rad, which is available online at http://www.bio-rad.com/LifeScience/pdf/Bulletin_9541.pdf). Cell penetration, gene expression, and other parameters vary with the model of the Gene Gun. Therefore, users must optimize the operating parameters for their particular model. O'Brien and Lumis [42] developed a modified barrel for the Bio-Rad hand-held Helios® Gene Gun, which improves the penetration of gold particles into cultured brain slices and allows the use of lower gas pressures without the loss of transfection efficiency. This modified Gene Gun barrel is available from Modolistics (*see* <http://www2.mrc-lmb.cam.ac.uk/personal/job/index.html>). Zhao and co-authors [22] reported another protocol improvement for the Gene Gun transfection. Although the efficiency was similar for both original and improved Gene Gun transfections, less damage to stereociliary bundles was claimed with this new procedure. The main differences from the standard procedure were a transbasilar-membrane approach for gold particle bombardment and a shortened version of focusing nozzle originally designed by O'Brien and Lumis [42].

When transfection conditions were optimized for our standard protocol, taking into account all of the above-mentioned variables for our application and using the original Bio-Rad Helios® hand-held Gene Gun, we obtain good efficiency of transfection of both organ of Corti and vestibular sensory epithelia as illustrated in Fig. 3a. Using Clic5-GFP construct, many non-sensory cells as well as 14 hair cells have been transfected in the apical piece of the organ of Corti, but only the most apical portion of this piece is shown on the right panel of

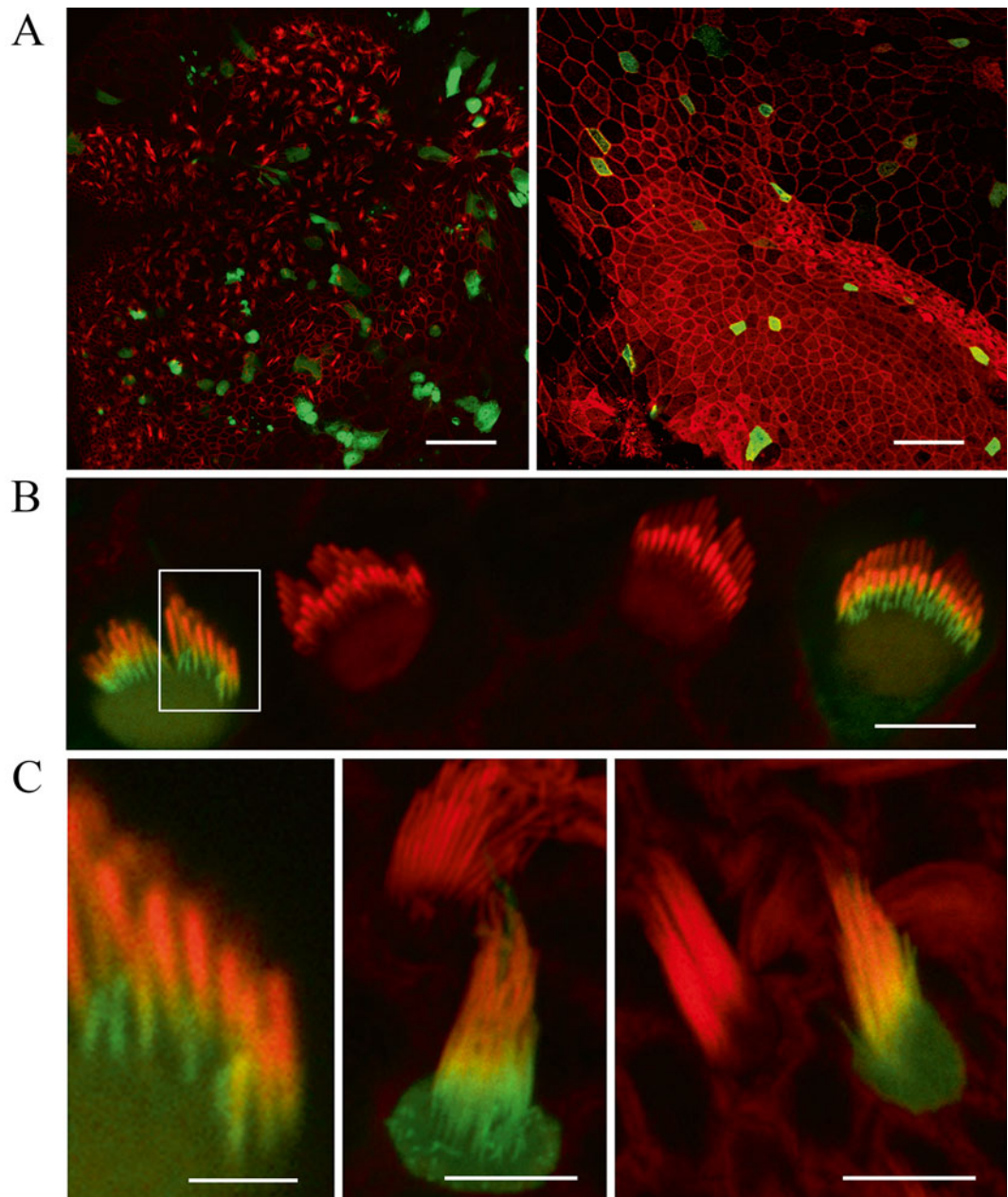


Fig. 3 Gene Gun-mediated Clic5-GFP transfection of the wild-type mouse inner ear sensory epithelia. **(a)** An overview image of the transfected sensory epithelium of the saccule (*left*) and the organ of Corti (*right*) taken with a 40 \times objective. The transfected cells are depicted in green. **(b)** Two non-transfected inner hair cells and two neighboring Clic5-GFP transfected inner hair cells from a P4 C57Bl/6J mouse organ of Corti. Clic5-GFP (green) is concentrated at the base of hair cell stereocilia of all rows. Boxed area in **(b)** is enlarged in **(c)**, *left panel*. **(c)** Middle and right panels show transfected vestibular hair cells next to the non-transfected neighboring hair cells from a P4 C57Bl/6J saccule. Cytoskeletal actin is visualized by rhodamine-phalloidin (red) in all panels. Scale bars: in **(a)** and **(b)** 20 μ m, in **(b)** and **(c)** 5 μ m, except in the *left panel* in **(c)** is 1 μ m

Fig. 3a. Close-up view of transfected hair cells shows that Clic5-GFP targets the tapered region of IHC stereocilia and highlights the entire length of the thinner underdeveloped third row stereocilia (Fig. 3b, c, left panel). In vestibular hair cells of the saccule, Clic5-GFP also targeted near the base of stereocilia (Fig. 3c, middle and right panel), mimicking its reported endogenous localization [51, 59, 60].

2. You can find information about the assembly, operation, maintenance, spare parts, and general optimization of particle delivery in the Helios® Gene Gun System Instruction Manual from Bio-Rad. Also, there is a helpful troubleshooting section.
3. All experimental animals should be handled according to the protocols of the Institutional Animal Care and Use Committee.
4. All microdissections of the inner ear sensory epithelia should be carried out under sterile conditions using autoclaved instruments and preferably, in a laminar flow hood.
5. Glass-bottom Petri dishes of different diameters can also be used and purchased from other companies (e.g., World Precision Instruments, Inc., Sarasota, FL or Electron Microscopy Sciences).
6. DMEM/F12 media supplemented with 7 % (v/v) FBS can be used.
7. This microdissection curette allows transfer of sensory epithelia pieces submerged in a limited volume of L-15 media. Pieces of the sensory epithelia can also be transferred using a glass Pasteur pipette (*see Subheading 2.4, step 8*) attached to a pipette holder (A. Daigger & Co., Vernon Hills, IL), which allows you to control the release of liquid from the pipette tip. To transfer your specimen using this pipette, aspirate the specimen along with some L-15 media, let the specimen settle down toward the opening of the pipette (you can help this along by tapping gently on the glass pipette), and then touch the surface of the liquid (DMEM) with the tip of the glass pipette, when you want to release your specimen into DMEM. This way the specimen will be transferred to the dish containing DMEM with minimum contamination by L-15 media.
8. It is important to frequently check the water level in the incubator tray to maintain an appropriate humidity level.
9. pAcGFP1-Actin vector is available from BD Biosciences. To use a different vector with your cDNA of interest you can purchase a Quantum Prep Plasmid Miniprep Kit (100 preps, Bio-Rad) or Qiagen's QIAfilter plasmid midi kits (Qiagen, Valencia, CA), to prepare plasmid DNA of high purity suitable for Helios® Gene Gun transfection. It is advisable to use endotoxin-free kits to prepare high-purity plasmid DNA. To use more than 100 µL of a less concentrated plasmid DNA preparation, match the volume of spermidine, but try to avoid volumes larger than

150 µL. More concentrated plasmid DNA (>1.0 mg/mL) may cause gold particles to cluster. It is also crucial to use purified plasmid DNA, since impure plasmid DNA may result in a poor transfection outcome as well as gold particle clustering. After purification, DNA should be diluted to 1 mg/mL in molecular biology grade water (*see also [42]*).

10. It is very important that the ethanol is free of water (200 proof). A fresh bottle of 100 % ethanol should be opened on the day of use in bullet preparation procedures.
11. The size of the microcarrier should be optimized for the particular application, cell types, etc. For example, nanoparticles are used in the improved method of neuron transfection in the cultured brain slices [61–63]. However, whether nanoparticles under similar conditions penetrate the cuticular plate of hair cells needs further investigation. Tungsten particles are less expensive, but can oxidize and may be toxic to the cells. It is not recommended to use tungsten particles instead of gold [64].
12. Old PVP may cause uneven gold coating of the Tefzel tubing, inefficient release of gold particles during the shot, lower tissue penetration, and reduced transfection efficiency. Do not keep diluted PVP for more than 1 month. The concentration of PVP should be optimized for each particular instrument and application. The crystallized PVP is hygroscopic. Store it in a tightly closed vial in a desiccator at room temperature.
13. Spermidine solution should be sterile-filtered using a 0.22 µm pore filter, if sterile solution is necessary. Spermidine deamidates with time; solutions should be stored frozen. Old spermidine may cause poor precipitation of DNA onto the gold particles, and subsequently reduce transfection efficiency. Do not keep spermidine for more than 1 month even at -20 °C.
14. O'Brien and Lummis recommend omitting the sonication step [42]. However, sonication seems to be efficient in mixing spermidine with gold particles and keeping gold particles in suspension. In the protocol described in this chapter, as well as in the previous version of this chapter published in 2009 [65], sonication is omitted only in steps when DNA is added to gold particles to avoid the potential destructive effects of sonication on DNA.
15. The use of a BioRad diffusion screen reduces the damage to the inner ear sensory epithelia and especially to hair cell stereociliary bundles, by reducing the density of the gold particles in the center of the shot during bombardment. After repeatedly firing the Gene Gun, gold particles will build up on the center of the diffusion screen, which may become gold colored. Use a dedicated diffusion screen for each plasmid DNA to avoid cross-contamination. A dedicated diffusion screen for a particular plasmid DNA can be reused many times. It does not

require frequent autoclaving. However, it is necessary to clean diffusion screens before using them with a different plasmid DNA. Diffusion screens can be cleaned by soaking in 70 % or 100 % ethanol and by sterilizing them in an autoclave that uses only distilled water to generate steam. Some autoclaves include a detergent in the water and this situation should be avoided.

16. 1× PBS containing Ca^{2+} and Mg^{2+} is used if the presence is required of these ions.
17. Triton X-100 is a viscous solution. It is useful to prepare a 1 % stock solution by adding 500 μL of Triton X-100 to 49.5 mL of 1× PBS. Before introducing Triton X-100 into a 1 mL pipette tip, cut off about 1 cm of the tip to make a wider opening. This help in drawing the viscous solution in and out of the pipette tip.
18. Rhodamine-phalloidin and other phalloidin conjugates can be used to visualize filamentous actin. Phalloidin 633 can be used to highlight the actin cytoskeleton, when cells are co-transfected using two cDNA plasmids tagged with GFP and dsRed.
19. ProLong Gold Antifade Mountant can be stored at room temperature, but have to be tightly closed when not in use.
20. A higher concentration of Cell-Tak may improve the adhesion of the sensory epithelia but it can be toxic to hair cells. While diluting Cell-Tak in a 1.5 mL centrifuge tube, make sure you use it immediately as Cell-Tak quickly adheres to the walls of the tube. Also, you can prepare your dishes using rat-tail collagen, type I (Upstate, Lake Placid, NY). Alternatively, you may choose to attach your sample directly to a glass surface not covered with any substrate. In this case, use DMEM without serum during the attachment period.
21. If you have problems with tissue attachment, try DMEM without serum for several hours or overnight. The next morning change the media to DMEM with 7 % (v/v) FBS. Also, the freshly dissected tissues seem to adhere to Cell-Tak better than tissues kept in L-15 media for more than ~10 min after microdissection. DMEM/F12 medium (Invitrogen) with 7 % (v/v) FBS seems to be better for rat inner ear organotypic cultures.
22. Alternatively, to store cartridges you can use tightly closed 15 mL conical tubes, each with one capsule of dehydrator as described in Subheading [2.2](#), step 14. Some preparations of plasmid DNA coated onto gold particles were used successfully for transfections after more than 2 years of storage with proper desiccation.
23. To prevent culture contamination, wipe the plastic ring of the end of a barrel (Fig. [1c](#), black arrow) with 70 % ethanol after each shot. It is advisable to wear ear protection (earmuffs or earplugs) when firing the Gene Gun.

24. It is important to remove the 1× PBS from the slide as much as possible without over-drying the sample before adding a drop of Antifade solution. Residual liquid around the sample will interfere with anti-fade properties of the mounting media. In general, samples should not be allowed to dry out at any time during the immunostaining and mounting procedures.
25. You can use clear nail polish to seal the perimeter edge of a coverslip onto a slide. This step is not necessary if you intend to keep your slide for less than one week. Let the nail polish dry before using the slide under a confocal microscope. For long-term storage up to a few months, store slides in the slide boxes at 4 °C with several capsules of desiccant (Ted Pella, Inc.).

Acknowledgement

I thank Thomas Friedman for support and encouragement as well as for critical reading of this chapter, Jonathan Gale (University of London, UK) for teaching me the rat organ of Corti explant technique, Erich Boger for preparing myosin 15a and whirlin cDNA expression constructs, Atteeq Rehman for the Clic5-GFP construct; Gregory Frolenkov and Doris Wu for critical reading of the manuscript and helpful discussions. This work was supported by funds from the NIDCD Intramural Program (1ZIADC000039 and 1ZIADC000048) to Thomas B. Friedman.

References

1. Xiong W, Wagner T, Yan L, Grillet N, Müller U (2014) Using injectoporation to deliver genes to mechanosensory hair cells. *Nat Protoc* 9:2438–2449
2. Brigande JV, Gubbels SP, Woessner DW, Jungwirth JJ, Bresee CS (2009) Electroporation-mediated gene transfer to the developing mouse inner ear. *Methods Mol Biol* 493: 125–139
3. Luebke AE, Foster PK, Muller CD, Peel AL (2001) Cochlear function and transgene expression in the guinea pig cochlea, using adenovirus- and adeno-associated virus-directed gene transfer. *Hum Gene Ther* 12:773–781
4. Konishi M, Kawamoto K, Izumikawa M, Kuriyama H, Yamashita T (2008) Gene transfer into guinea pig cochlea using adeno-associated virus vectors. *J Gene Med* 10:610–618
5. Akil O, Seal RP, Burke K, Wang C, Alemi A, During M, Edwards RH, Lustig LR (2012) Restoration of hearing in the VGLUT3 knock-out mouse using virally mediated gene therapy. *Neuron* 75:283–293
6. Chien WW, Isgrig K, Roy S, Belyantseva IA, Drummond MC, May LA, Fitzgerald TS, Friedman TB, Cunningham LL (2016) Gene Therapy Restores Hair Cell Stereocilia Morphology in Inner Ears of Deaf Whirler Mice. *Mol Ther* 24(1):17–25
7. Askew Ch, Rochat C, Pan B, Asai Y, Ahmed H, Child E, Schneider BL, Aebsicher P, Holt JR (2015) Tmc gene therapy restores auditory function in deaf mice. *Sci Translat Med* 7:295ra108
8. Woods C, Montcouquiol M, Kelley MW (2004) Math1 regulates development of the sensory epithelium in the mammalian cochlea. *Nat Neurosci* 7:1310–1318
9. Zheng JL, Gao WQ (2000) Overexpression of Math1 induces robust production of extra hair cells in postnatal rat inner ears. *Nat Neurosci* 3:580–586
10. Driver EC, Kelley MW (2010) Transfection of mouse cochlear explants by electroporation. *Curr Protoc Neurosci Chapter 4:Unit 4.34.1–10*

11. Parker M, Brugaud A, Edge AS (2010) Primary culture and plasmid electroporation of the murine organ of Corti. *J Vis Exp* 36:1685
12. Masuda M, Pak K, Chavez E, Ryan AF (2012) TFE2 and GATA3 enhance induction of POU4F3 and myosin VIIa positive cells in nonsensory cochlear epithelium by ATOH1. *Dev Biol* 372:68–80
13. Haque KD, Pandey AK, Kelley MW, Puligilla C (2015) Culture of embryonic mouse cochlear explants and gene transfer by electroporation. *J Vis Exp* 95:52260
14. Jones JM, Montcouquiol M, Dabdoub A, Woods C, Kelley MW (2006) Inhibitors of differentiation and DNA binding (Ids) regulate Math1 and hair cell formation during the development of the organ of Corti. *J Neurosci* 26:550–558
15. Schneider ME, Belyantseva IA, Azevedo RB, Kachar B (2002) Rapid renewal of auditory hair bundles. *Nature* 418:837–838
16. Belyantseva IA, Boger ET, Friedman TB (2003) Myosin XVa localizes to the tips of inner ear sensory cell stereocilia and is essential for staircase formation of the hair bundle. *Proc Natl Acad Sci U S A* 100:13958–13963
17. Rzadzinska AK, Schneider ME, Davies C, Riordan GP, Kachar B (2004) An actin molecular treadmill and myosins maintain stereocilia functional architecture and self-renewal. *J Cell Biol* 164:887–897
18. Belyantseva IA, Boger ET, Naz S, Frolenkov GI, Sellers JR, Ahmed ZM et al (2005) Myosin-XVa is required for tip localization of whirlin and differential elongation of hair-cell stereocilia. *Nat Cell Biol* 7:148–156
19. Boger ET, Frolenkov GI, Friedman TB, Belyantseva IA (2008) Myosin XVa. In: Coluccio LM (ed) *Myosins: a superfamily of molecular motors*. Springer, The Netherlands, pp 441–467
20. Geng R, Melki S, Chen DH et al (2012) The mechanosensory structure of the hair cell requires clarin-1, a protein encoded by Usher syndrome III causative gene. *J Neurosci* 32:9485–9498
21. Grati M, Kachar B (2011) Myosin VIIa and sans localization at stereocilia upper tip-link density implicates these Usher syndrome proteins in mechanotransduction. *Proc Natl Acad Sci U S A* 108:11476–11481
22. Zhao H, Avenarius MR, Gillespie PG (2012) Improved biolistic transfection of hair cells. *PLoS One* 7:e46765
23. Morín M, Bryan KE, Mayo-Merino F et al (2009) In vivo and in vitro effects of two novel gamma-actin (ACTG1) mutations that cause DFNA20/26 hearing impairment. *Hum Mol Genet* 18:3075–3089
24. Kawashima Y, Gélécoc GS, Kurima K et al (2011) Mechanotransduction in mouse inner ear hair cells requires transmembrane channel-like genes. *J Clin Invest* 121:4796–4809
25. Diaz-Horta O, Subasioglu-Uzak A, Grati M et al (2014) FAM65B is a membrane-associated protein of hair cell stereocilia required for hearing. *Proc Natl Acad Sci U S A* 111: 9864–9868
26. Felgner PL, Gadek TR, Holm M et al (1987) Lipofection: a highly efficient, lipid-mediated DNA-transfection procedure. *Proc Natl Acad Sci U S A* 84:7413–7417
27. Weaver JC (1995) Electroporation theory. Concepts and mechanisms. *Methods Mol Biol* 47:1–26
28. Favard C, Dean DS, Rols MP (2007) Electrotransfer as a non viral method of gene delivery. *Curr Gene Ther* 7:67–77
29. Saito T, Nakatsuji N (2001) Efficient gene transfer into the embryonic mouse brain using in vivo electroporation. *Dev Biol* 240:237–246
30. Wang W, Liu X, Gelinas D, Ciruna B, Sun Y (2007) A fully automated robotic system for microinjection of zebrafish embryos. *PLoS One* 2:e862
31. Gonzalez-Estevez C, Momose T, Gehring WJ, Salo E (2003) Transgenic planarian lines obtained by electroporation using transposon-derived vectors and an eye-specific GFP marker. *Proc Natl Acad Sci U S A* 100: 14046–14051
32. Kunieda T, Kubo T (2004) In vivo gene transfer into the adult honeybee brain by using electroporation. *Biochem Biophys Res Commun* 318:25–31
33. Ando T, Fujiwara H (2013) Electroporation-mediated somatic transgenesis for rapid functional analysis in insects. *Development* 140: 454–458
34. Matsumoto CS, Shidara H, Matsuda K et al (2013) Targeted gene delivery in the cricket brain, using in vivo electroporation. *J Insect Physiol* 59:1235–1241
35. Klein TM, Wolf ED, Wu R, Sanford JC (1987) High-velocity microprojectiles for delivering nucleic acids into living cells. *Nature* 327: 70–73
36. Klein TM, Fromm M, Weissinger A et al (1988) Transfer of foreign genes into intact maize cells with high-velocity microprojectiles. *Proc Natl Acad Sci U S A* 85:4305–4309

37. Zelenin AV, Titomirov AV, Kolesnikov VA (1989) Genetic transformation of mouse cultured cells with the help of high-velocity mechanical DNA injection. *FEBS Lett* 244:65–67
38. Johnston SA (1990) Biolistic transformation: microbes to mice. *Nature* 346:776–777
39. Yang NS, Burkholder J, Roberts B, Martinell B, McCabe D (1990) In vivo and in vitro gene transfer to mammalian somatic cells by particle bombardment. *Proc Natl Acad Sci U S A* 87:9568–9572
40. Williams RS, Johnston SA, Riedy M, DeVit MJ, McElligott SG, Sanford JC (1991) Introduction of foreign genes into tissues of living mice by DNA-coated microparticles. *Proc Natl Acad Sci U S A* 88:2726–2730
41. Sanford JC, Smith FD, Russell JA (1993) Optimizing the biolistic process for different biological applications. *Methods Enzymol* 217:483–509
42. O'Brien JA, Lummis SC (2002) An improved method of preparing microcarriers for biolistic transfection. *Brain Res Protoc* 10:12–15
43. Thomas JL, Bardou J, L'hoste S, Mauchamp B, Chavancy G (2001) A helium burst biolistic device adapted to penetrate fragile insect tissues. *J Insect Sci* 1:9
44. Kim TW, Lee JH, He L et al (2005) Modification of professional antigen-presenting cells with small interfering RNA in vivo to enhance cancer vaccine potency. *Cancer Res* 65:309–316
45. Pascolo S (2006) Vaccination with messenger RNA. *Methods Mol Med* 127:23–40, Review
46. Yang CH, Shen SC, Lee JC et al (2004) Seeing the gene therapy: application of gene gun technique to transfet and decolour pigmented rat skin with human agouti signaling protein cDNA. *Gene Ther* 11:1033–1039
47. Shefi O, Simonnet C, Baker MW, Glass JR, Macagno ER, Groisman A (2006) Microtargeted gene silencing and ectopic expression in live embryos using biolistic delivery with a pneumatic capillary gun. *J Neurosci* 26:6119–6123
48. O'Brien JA, Lummis SC (2006) Biolistic transfection of neuronal cultures using a hand-held gene gun. *Nat Protoc* 1:977–981
49. Drummond MC, Barzik M, Bird JE et al (2015) Live-cell imaging of actin dynamics reveals mechanisms of stereocilia length regulation in the inner ear. *Nat Commun* 6:6873
50. Zhang DS, Piazza V, Perrin BJ et al (2012) Multi-isotope imaging mass spectrometry reveals slow protein turnover in hair-cell stereocilia. *Nature* 481:520–524
51. Belyantseva IA (2013) CLIC5 interacts with taperin at the base of stereocilia. In: Abstracts of the 9th molecular biology of hearing and deafness, Stanford University, Palo Alto, CA, Accessed 22–25 June
52. Furness DN, Mahendrasingam S, Ohashi M, Fettiplace R, Hackney CM (2008) The dimensions and composition of stereociliary rootlets in mammalian cochlear hair cells: comparison between high- and low-frequency cells and evidence for a connection to the lateral membrane. *J Neurosci* 28(25):6342–6353
53. Kitajiri S, Sakamoto T, Belyantseva IA et al (2010) Actin-bundling protein TRIOBP forms resilient rootlets of hair cell stereocilia essential for hearing. *Cell* 141:786–798
54. Di Pasquale G, Rzadzinska A, Schneider ME, Bossis I, Chiorini JA, Kachar B (2005) A novel bovine virus efficiently transduces inner ear neuroepithelial cells. *Mol Ther* 11:849–855
55. Probst FJ, Fridell RA, Raphael Y et al (1998) Correction of deafness in shaker-2 mice by an unconventional myosin in a BAC transgene. *Science* 280:1444–1447
56. Holme RH, Kiernan BW, Brown SD, Steel KP (2002) Elongation of hair cell stereocilia is defective in the mouse mutant whirler. *J Comp Neurol* 450:94–102
57. Mburu P, Mustapha M, Varela A et al (2003) Defects in whirlin, a PDZ domain molecule involved in stereocilia elongation, cause deafness in the whirler mouse and families with DFNB31. *Nature Genet* 34:421–428
58. Delprat B, Michel V, Goodyear R et al (2005) Myosin XVa and whirlin, two deafness gene products required for hair bundle growth, are located at the stereocilia tips and interact directly. *Hum Mol Genet* 14:401–410
59. Gagnon LH, Longo-Guess CM, Berryman M et al (2006) The chloride intracellular channel protein CLIC5 is expressed at high levels in hair cell stereocilia and is essential for normal inner ear function. *J Neurosci* 26:10188–10198
60. Salles FT, Andrade LR, Tanda S et al (2014) CLIC5 stabilizes membrane-actin filament linkages at the base of hair cell stereocilia in a molecular complex with radixin, taperin, and myosin VI. *Cytoskeleton* 71:61–78
61. O'Brien JA, Lummis SC (2011) Nanobiolistics: a method of biolistic transfection of cells and tissues using a gene gun with novel nanometer-sized projectiles. *BMC Biotechnol* 11:66
62. Arsenault J, O'Brien JA (2013) Optimized heterologous transfection of viable adult organotypic brain slices using an enhanced gene gun. *BMC Res Notes* 6:544

63. Arsenault J, Nagy A, Henderson JT, O'Brien JA (2014) Regioselective biolistic targeting in organotypic brain slices using a modified gene gun. *J Vis Exp* 92:e52148
64. Russell JA, Roy MK, Sanford JC (1992) Physical trauma and tungsten toxicity reduce the efficiency of biolistic transformation. *Plant Physiol* 98:1050–1056
65. Belyantseva IA (2009) Helios Gene Gun-mediated transfection of the inner ear sensory epithelium. In: Sokolowski B (ed) Auditory and vestibular research. Methods and protocols. *Methods Mol Biol* 493, Humana Press, Springer, Heidelberg, pp 103–124

Chapter 2

Tol2-Mediated Delivery of miRNAs to the Chicken Ototocyst Using Plasmid Electroporation

Michelle L. Stoller and Donna M. Fekete

Abstract

The avian embryo has a well-documented history as a model system for the study of neurogenesis, morphogenesis, and cell fate specification. This includes studies of the chicken inner ear that employ *in ovo* electroporation, in conjunction with the Tol2 system, to yield robust long-term transgene expression. Capitalizing on the success of this delivery method, we describe a modified version of the Tol2 expression vector that readily accepts the insertion of a microRNA-encoding artificial intron. This offers a strategy to investigate the possible roles of different candidate microRNAs in ear development by overexpression. Here, we describe the general design of this modified vector and the electroporation procedure. This approach is expected to facilitate phenotypic screening of candidate miRNAs to explore their bioactivity *in vivo*.

Key words microRNA, Inner ear, Tol2 transposon, Vestibular, Auditory

1 Introduction

Gene transfer into the chicken embryo is a valuable tool for the study of development. The ease of access to multiple organ systems, low cost, and similarities to the mammalian system are enticing to researchers. These benefits are especially attractive when studying the development of the inner ear. The fluid-filled otic cup/otocyst gives rise to vestibular and auditory organs and the associated statoacoustic neurons, and is readily accessible to experimental manipulation *in ovo* on embryonic days 2–3 [1].

Successful overexpression of protein-coding transgenes has been well-documented within the avian inner ear using retroviral infection [2–4], particularly the RCAS system designed by the laboratory of Steven Hughes [5–7]. High-titer retroviruses can produce robust infection and long-term, high levels of transgene expression. However, these viruses can only infect mitotically active cells, and they are limited to transgenes smaller than 2.4 kb if they are to remain replication-competent [6, 8]. Replication-incompetent

retroviral vectors and plasmid vectors can both accept much larger transgenes (on the order of 10 kb for the former).

A further disadvantage of retrovirus-mediated gene transfer was encountered, when we modified RCAS to produce microRNA (miRNA) or short-hairpin RNA (shRNA). Small non-coding RNAs can be used as tools to limit the protein production of their targets by blocking translation or enhancing degradation of messenger RNA [9–11]. On multiple occasions, we inserted into RCAS, an artificial intron containing sequences designed to form short RNA hairpins following reverse transcription, expecting these to be processed into short single-stranded RNAs by the cell's miRNA processing pathway. However, viral titers were often 10–100-fold lower than standard protein-encoding RCAS vectors. We are unsure whether it is the presence of the hairpins, or the extra splice sites that may be interfering with viral replication in these vectors. Even when moderately high viral titers were achieved, subsequent infection of chicken otocysts with RCAS vectors carrying a pre-miRNA intron consistently failed to produce mature miRNAs detectable by *in situ* hybridization methods. In contrast, inserting identical pre-miRNA-containing introns into plasmid expression vectors, and transducing these into the otocyst via electroporation, were successful [12];unpublished data).

While electroporation of standard expression plasmids [13–15] can bypass certain problems encountered with viral vectors, transgene expression typically lasts only a few days [16, 17]. To circumvent this limitation, the Tol2 transposase system can be employed. This method relies on the integrative properties of transposons. When a plasmid encoding the Tol2 transposase is co-electroporated with a vector containing a transgene flanked by Tol2 sites, the DNA flanked by these sites is excised and inserted into the genomic DNA through the activity of the transposase [18–20]. This process ensures strong, long-term expression of protein-encoding genes within the vestibular and auditory organs [21–23].

An important aspect of gene transfer is to combine the detection of transduced cells with cellular phenotyping methods, such as immunofluorescence. This poses an additional challenge for the delivery and detection of small RNAs, because they require *in situ* hybridization to be detected in tissue sections. To identify which cells have been transfected, a separate reporter plasmid, often encoding a fluorescent protein, can be co-electroporated with the small RNA-expression vector [24]. The reporter fluorescence thus serves as a proxy for localization of the transduced small RNAs. This strategy creates a tenuous link between the observation of reporter protein and the assumption that small RNAs are being co-expressed at the same location. A solution to this problem is to use a bicistronic vector design, as is discussed here, where both the small RNA and the reporter gene are processed from the same primary transcript.

In this chapter, we discuss the combined use of a Tol2 transposase system and electroporation to simultaneously deliver a miRNA and a reporter gene under the control of the same

promoter to the chicken inner ear. To achieve this outcome, we modified the Tol2 vector to include an artificial intron [25–27] that houses the genomic sequences for a miRNA of interest. This design exploits the Pol II pathway to produce both a protein-coding transcript from the exon and a small RNA from the intron (Fig. 1).

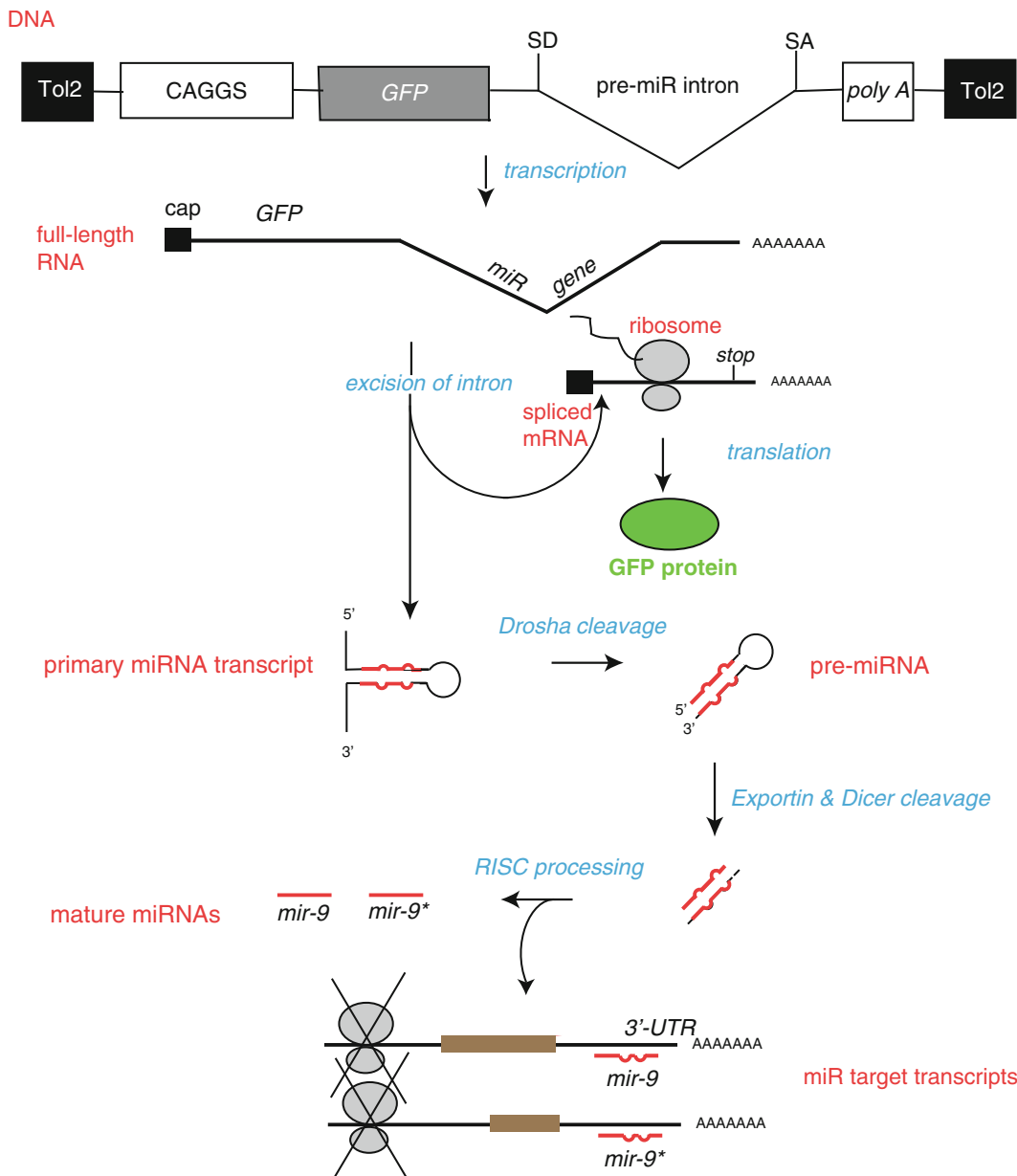


Fig. 1 Modified Tol2-Vector design and processing. When co-expressed with transposase, the DNA region flanked by the Tol2 ends incorporates into the host cell's genomic DNA. The CAAGS promoter drives expression of the exon encoding GFP and the *miR-9* gene from the intron designated by the splice donor (SD) and splice acceptor (SA) sites. Once the DNA is transcribed into RNA, the intron containing the primary miRNA transcript is clipped into a pre-miRNA and exported from the nucleus. It is then processed into mature miRNAs. Separately, the spliced GFP transcript is exported from the nucleus and processed as messenger RNA

Similar designs, using different backbones, have been shown to produce both components and provide a more accurate link between the expression of a reporter and distribution of transduced small RNAs [25–30]. Here, we show how this method generates miRNAs at levels that can be detected by *in situ* hybridization and that corresponds to the localization of green fluorescent protein (GFP) as a reporter on adjacent sections through the inner ear. We describe the overall electroporation method, as well as the construction of an electrode pair specialized for otocyst-stage electroporations. This report complements a previous methods paper describing electroporation at earlier (otic cup) stages, using Tol2 vectors specifically designed for drug-inducible expression of multiple protein-encoding genes [23].

2 Materials

2.1 DNA Plasmid Construction and Preparation

1. pME-MCS-sda (available upon request from the authors).
2. pTol2-GFP-Gateway (available upon request from the authors).
3. Gateway® LR Clonase™ II Plus enzyme mix (Invitrogen; Life Technologies, Grand Island, NY).
4. Genomic DNA from species of interest.
5. Primers and solutions for PCR amplification.
6. Thermal-cycler.
7. Standard reagents and associated buffers for conventional cloning by restriction enzyme digestion and ligation: *Xba*I, *Xho*I, ligase, ethidium bromide-agarose gel reagents and running buffers.
8. Commercial maxi-prep kit for preparation of purified plasmid DNA.
9. Primers for DNA sequencing designed to confirm correct cloning: T3 primer.
10. pCAG-T2TP [20].
11. pTol2-GFP-sd-miR(X)-sa.
12. Fast green FCF (Sigma): Prepare a 0.25 % solution by adding 25 mg of Fast Green FCF crystals to 10 mL of millipure or distilled water. Filter using a 0.45 µm syringe filter, make 1 mL aliquots and store at -20 °C until use.

2.2 Electrode Fabrication Supplies

1. Platinum wire, 0.3 mm diameter (Alfa Aesar, Ward Hill, MA).
2. Tungsten wire, 0.5 mm diameter (Alfa Aesar).
3. Heat shrink tubing, 3/64" × 6" (SPC Technology, Blaine, MN).
4. Bunsen burner.
5. Nail polish.

2.3 Microinjection and Electroporation

1. Micropipette puller: Flaming/Brown Model P-97 (Sutter Instrument Co., Novato, CA).
2. Micropipettes: thin wall borosilicate glass capillary with filament, diameter chosen to match electrode holder. We use 1.5 mm OD × 1.17 mm ID (Harvard Apparatus, Holliston, MA).
3. Manual micromanipulators: $n=2$ (e.g., MM33 roller bearing micromanipulator, Stoelting Co.), each mounted on a magnetic base with articulated arm (Stoelting Co.), and set on an iron base plate (Narishige, Japan).
4. Electroporator (TSS20 Ovodyne) and current amplifier (E21) (Intracel, UK).
5. Pipette holder for tungsten/platinum electrodes (e.g., Tritech Research).
6. Hook cable connector between current amplifier and tungsten/platinum electrodes (Bex Co., Tokyo, Japan).
7. Microinjection apparatus: Pressure injector with nanoliter injection volumes and millisecond resolution, with 60 psi regulator and foot pedal external trigger (e.g., Picospritzer III; Parker Hannifin Corp., Cleveland, OH).
8. Micropipette holder for pressure injection of plasmids: MP Series microinjection electrode holder, straight body with appropriate (male/female) Luer Port, 1.5 mm glass OD (Harvard Apparatus).
9. Manual stereomicroscope with apochromatic correction and magnification to 25 \times or greater.
10. Fiberoptic illuminator, dual gooseneck light guides.
11. Compressed nitrogen tank (>99 % purity).
12. Ice bucket with ice.
13. 1.5 mL Eppendorf tubes
14. Microcapillary pipet tips (Eppendorf MicroloaderTM; Eppendorf, Hauppauge, NY) attached to 10 μ L pipettor to backfill micropipettes.
15. Culture Dishes: two 60 mm dishes and one 35 mm dish.
16. Chick Ringer's Solution: NaCl 123 mM, CaCl₂ 1.53 mM, KCl 5 mM, Na₂HPO₄ 0.8 mM, in 1 L millipure. Bring the pH to 7.4 using NaOH. Once dissolved, filter the solution using a 0.22 μ m Stericup filter unit (Millipore, Billerica, MA). Distribute 100 mL into 125 mL bottles and autoclave and store at room temperature.

2.4 Windowing and Embryo Preparation

1. 3 or 5 mL syringe.
2. 18.5–20-Gauge needle.
3. Scotch tape and clear packing tape.

4. 5 mL plastic disposable transfer pipets.
5. Egg holder: can be fashioned from Styrofoam, plaster-of-paris, or by lining a 60 mm Petri dish with Kimwipes.
6. Dissection tools: one Dumont #55 straight forceps, one Dumont #5 straight forceps with Biology tips, one set of curved dissection scissors (Fine Science Tools, Foster City, CA).
7. Kimwipes.
8. 70 % Ethanol.
9. Humidified egg incubator, benchtop or cabinet (Lyon Technologies, Inc., Chula Vista, CA).

3 Method

3.1 DNA Plasmid Construction and Preparation

1. Figure 2 shows the basic cloning strategy for preparing a bicistronic vector carrying a pre-miRNA of interest. This entails using pME-MCS-sda as a Gateway® donor vector and pTol2-GFP-Gateway as a Gateway® destination vector. As background information, we provide the primer sequences we used to generate the artificial intron cassette found in the pME-MCS-sda Gateway® shuttle vector. The primers, designed based on previous reports [26, 27], are as follows:
 2. Forward: 5'gct gtc gac gta atc tag agg atc cct cga gta cta act ggt acc tct tc 3'.
 3. Reverse: 5' gca agc ttc tgc agg ata tca aaa aaa aaa gaa gag gta cca gtt agt act c 3'.
4. We inserted the amplicon containing the artificial intron into a Gateway® shuttle vector to create pME-MCS-sda as described previously [25]. We placed three restriction enzyme sites (*Xba*I, *Bam*HI, and *Xho*I) in the artificial intron to facilitate entry of any miRNA of interest.
5. Amplify your pre-miRNA of interest from genomic DNA, designing the primers to include *Xba*I and *Xho*I restriction site sequences at the ends (see Note 1). The resulting amplicon should encompass extra base pairs flanking the pre-miRNA sequence for proper processing [31]. We maintained about 60 nucleotides of endogenous sequence on the 5' and 3' ends of pre-miR-9-1. We also had success with constructs containing a larger number of flanking bases [25].
6. Once the amplicon is generated, insert this into pME-MCS-sda using conventional cloning with *Xho*I-*Xba*I double-digestion and ligation. Confirm that this intermediate construct is correct by DNA sequencing using the T3 primer.

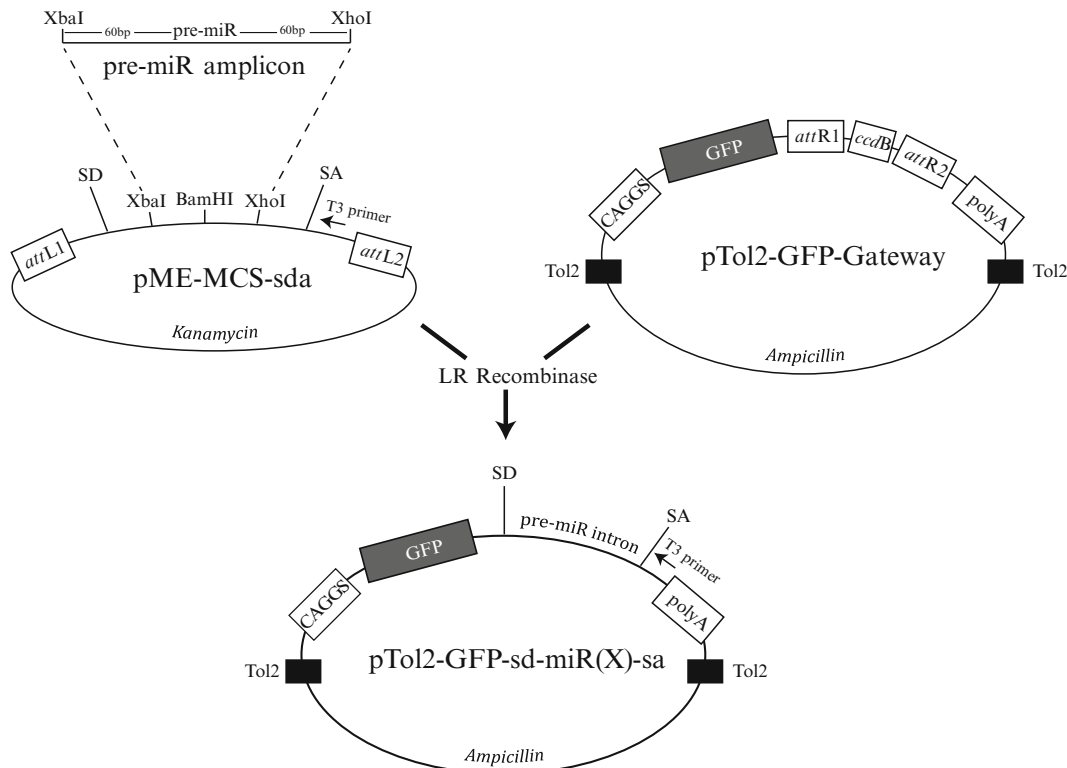


Fig. 2 Cloning strategy for generating a bicistronic Tol2 vector carrying GFP and any pre-miR intron. The pre-miR amplicon is created by amplifying the pre-miRNA of choice from genomic DNA. The amplicon should include genomic sequences predicted to form the pre-miRNA stem-loop (~80 nucleotides) after transcription, along with 60–100 bp of DNA flanking either side of this. Primers should be designed to add *Xba*I and *Xho*I restriction sites to the end of the pre-miR amplicon. These sites facilitate cloning the amplicon into pME-MCS-SDA, which then serves as a Gateway® donor vector (Invitrogen, Life Technologies). The pTol2-GFP-Gateway was created to serve as a Gateway® destination vector. Arrows show the position and direction of T3 primer binding sites that are used to sequence the miRNA intron. SA splice acceptor, SD splice donor

7. Use the LR Clonase™ II enzyme mix (Invitrogen, Life Technologies) according to the manufacturer's protocol to transfer the miRNA-intron into the pTol2-GFP-Gateway vector [12]. This will create the desired miRNA-reporter expression vector, now called pTol2-GFP-sd-miR(X)-sa (substitute miR(X) with the name of your miRNA, e.g., pTol2-GFP-sd-miR9-sa). Confirm the construct is correct by DNA sequencing using the T3 primer and, if desired, a primer located at the 3' end of GFP.
8. Prepare maxiprep plasmid DNA for pTol2-GFP-sd-miR(X)-sa and pCAG-T2TP. Use a standard protocol or commercial kit to yield final DNA concentrations between 3 µg and 5 µg/µL for electroporation (*see Note 2*).

3.2 Electrode Fabrication

1. Cut a piece of tungsten wire to approximately 4–5 cm in length.
2. Cut a piece of platinum wire 1 cm in length.
3. Trim a piece of heat-shrink tubing to encapsulate the tungsten wire piece, leaving a 0.5 cm segment of wire protruding from the tubing at one end.
4. Insert a 0.5 cm segment of platinum wire into the opposite end of the tubing, ensuring it contacts the tungsten wire.
5. Using the Bunsen burner, wave the insulated portion of the wires, back and forth over the flame, to shrink and secure the insulation surrounding the wires. At this point, the platinum wire should be firmly secured by the insulation.
6. Repeat steps 1–5 to create second electrode. Once both electrodes are made, place them side-by-side and secure them together by wrapping the insulated portion of the wire closest to the exposed platinum with Parafilm. Joining the two electrodes is also accomplished by holding the insulated portions over an open flame.
7. Bend the final 2–3 mm of exposed platinum by ~45–60°.
8. Apply nail polish to cover the exposed platinum, except at the tips, where nail polish is applied only to the outer sides of each electrode, to ensure current flows between the two inner surfaces of the tips (*see Note 3*).
9. Place in electrode holder (Fig. 3).
10. Attach to the current amplifier with hook cable connector.

3.3 Micropipette Production

1. Using a micropipette puller, pull borosilicate glass capillary tubes. A short taper (~5 cm) is preferable to minimize clogging.
2. Break the end of the micropipette to create a 10–13 µm opening (*see Note 4*).
3. Pull and break about 10 micropipettes for each batch of embryos, so that clogged micropipettes can be replaced readily.

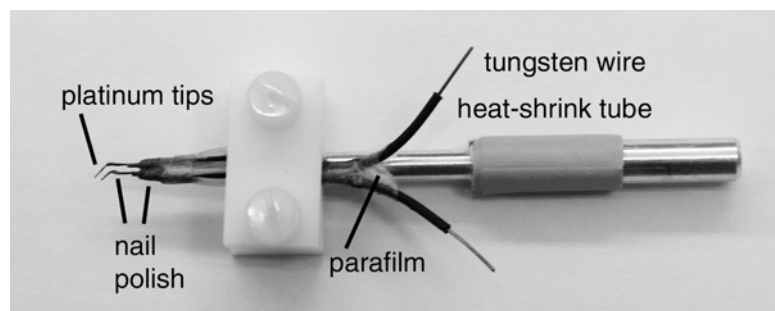


Fig. 3 Platinum-tungsten electrodes secured in electrode holder. See text for details on fabrication

3.4 Embryo Preparation

3.4.1 Egg Windowing

1. Eggs should be placed on their sides in the egg incubator, and the topmost spot indicated with a marker. This is where you can expect to find the embryo on the day of windowing, if the incubator does not rock the eggs.
2. On the second day, place the egg horizontally in an egg holder with the marked position at the top. Create a small hole at the pointed end of the egg using an 18.5–20-gauge needle attached to a 3 or 5 mL syringe.
3. Insert the needle, angled downward as vertically as possible, and remove 1.5–2.5 mL of albumin (*see Note 5*). Cover the hole with Scotch tape.
4. Cover the pre-marked top position of the egg with ~2 cm of Scotch tape. This will minimize dropping broken shell pieces onto the embryo during windowing. Pierce the top portion of the eggshell with the 18.5-gauge needle. Insert the tip of the dissection scissors and remove a circular portion of the eggshell (and Scotch tape) about 1 cm in diameter.
5. Cover the opening with clear packing tape and place back into humidified egg incubator until ready for injection and electroporation.

3.4.2 Injection Day

1. Using the dissection scissors, remove enough of the tape and shell to see the entire chicken embryo.
2. While the egg is in its holder, place it under the stereomicroscope and adjust the fiber optic lighting until it reflects off the chorion.
3. Using #5 forceps, grab a portion of chorion just beyond the dorsal surface of the embryo near the position of the otocyst. Use #55 and #5 forceps to delicately tear the chorion and then the underlying amnion until an area surrounding otocyst is clear. The cleared region must be large enough to accommodate the electrode tips. This is critical for successful electroporation. We have had success using a needle or forceps to pierce the membranes and deliver a small amount of Ringer's solution beneath the amnion to separate it from the embryo before tearing it open, as described previously [23]. The embryonic membranes of each embryo should be pierced immediately before the plasmid injection step as described in Subheading 3.6.

3.5 Preparation of Injection Needle

1. For injection and electroporation of HH16–18 embryos, dilute 9 volumes of plasmid DNA (3–5 µg/µL) with 1 volume of 0.25 % fast green. Use a molar ratio of 2:1 for pTol2-GFP-sd-miR(X)-sa and CAG-T2TP, respectively. Hereafter, we refer to this mix as plasmid DNA. A simplified version of each plasmid is shown schematically in Fig. 4a. Leave the plasmid DNA on ice.

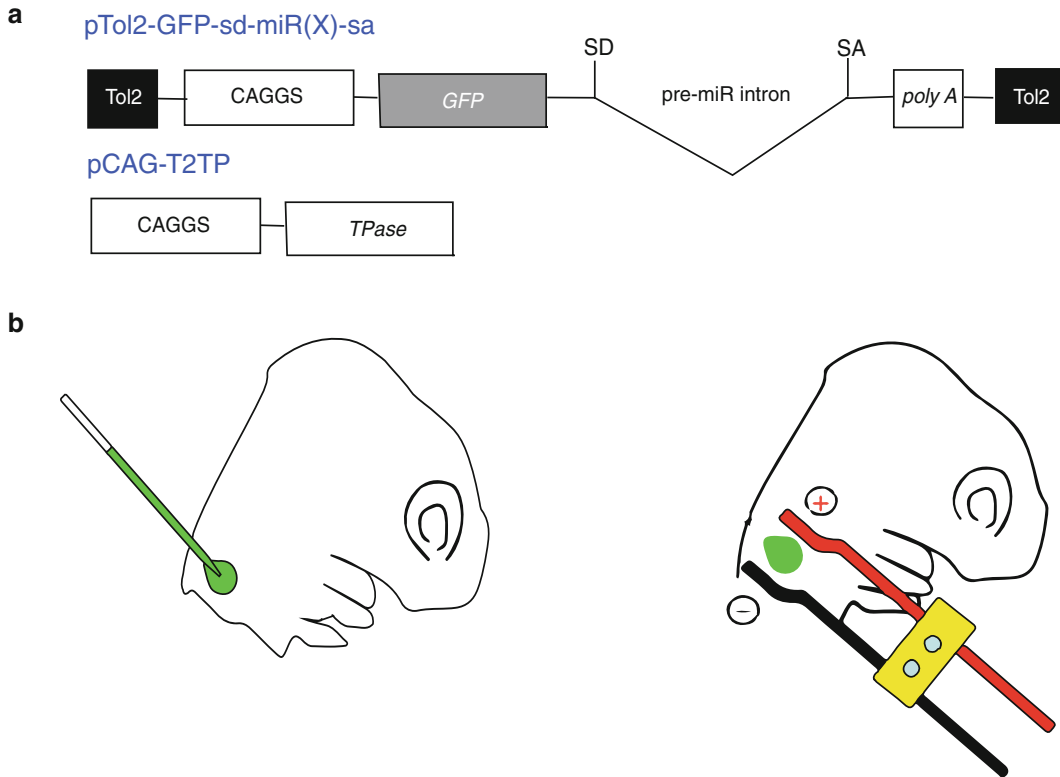


Fig. 4 Electroporation of Tol2-Vectors into the chicken otocyst. (a) Schematic representation of miRNA-containing plasmid and transposase-encoding vector. (b) A mixture of fast-green and plasmid DNA is injected into the otocyst of an E3 (HH16-18) chicken. (c) The platinum tips of the electrode are placed on top of the embryo, with the otocyst in between. The location of positive electrode dictates the direction of DNA migration. This cartoon depicts DNA targeted toward the anterior pole of the otocyst. To target the anterior or posterior poles, the otocyst is approached from either the ventral direction (as shown) or the dorsal direction

2. Backfill the pulled-glass capillary micropipette with 3 μ L of plasmid DNA using microcapillary pipet tips. Place micropipette into the holder connected to the Picospritzer and clamp onto the micromanipulator. Open valve to nitrogen gas cylinder.
3. Ensure that the DNA readily flows out of the tip of the micropipette following a pressure pulse. To accomplish this, place a 35 mm cell culture plate filled with Ringer's solution on top of two 60 mm cell culture plates and view under the stereomicroscope. Lower the micropipette into the solution so its tip barely breaks the surface of the liquid (to avoid excessive backflow of Ringer's solution into the tip). Turn on the Picospritzer and engage airflow until the plasmid DNA is expelled into the surrounding liquid and all air bubbles are removed from the tapered shank of the micropipette.

3.6 Injection and Electroporation of Plasmids into the Otocyst

1. Place embryo prepared in Subheading 3.4.2 under the stereomicroscope. Deposit several drops of Ringer's solution onto embryo using a plastic transfer pipet (*see Note 6*). Adjust lighting obliquely to enhance the visibility of the otocyst. Differences in opacity become more critical as injections are performed on younger embryos because the otic cup or otocyst is more transparent.
2. Use micromanipulator to move the injection micropipette above embryo. The precise injection procedure will differ for otic cup stages (HH11-12) versus otocyst injections (HH13 and beyond). Details for otic cup injections can be found in an excellent methods chapter by Freeman et al. [23]. Here we focus on otocyst stages (*see Note 7*).
3. Slowly lower the micropipette until the tip pierces the epithelium of the otocyst. In some cases, the moment the otocyst is punctured, it can be visualized as a sudden alleviation of resistance applied to the needle tip by the epithelium, causing the embryo to recoil upward.
4. Inject the DNA mixture into the otocyst cavity until it begins to enlarge (Fig. 4b). We typically use pressure settings of 20 psi with 10 ms pulses. Multiple pulses are sometimes required, especially if the micropipette begins to clog after several injections. Take care not to overfill the otocyst to avoid rupturing it. Remove the micropipette. If a delay between injections of more than ~5 min is expected, submerge the tip of the micropipette into the Ringer's solution in the 35 mm plate to avoid it drying out and clogging.
5. Apply two additional drops of Ringer's solution to the embryo. On the opposite side of the embryo, bring into view the electrode holder secured to a second micromanipulator.
6. Place electrodes so the otocyst lies between them, as shown in Fig. 4c. Then, gently lower electrodes until they touch the surface epithelium. Since both electrodes are composed of platinum wire, either side can function as the cathode. Designation of the cathode determines which direction the DNA will travel. In Fig. 4c, the cathode is placed anterior to the otocyst to drive the DNA toward the anterior crista.
7. Deliver two 10-V square wave current pulses, 50 ms long, spaced 10 ms apart using an electroporator and the connected current amplifier. A good indicator of functioning electrodes is a copious amount of bubbles (*see Note 8*).
8. Apply additional Ringer's solution before withdrawing the electrodes. Cover the eggshell window with clear packing tape and place back into the egg incubator until harvest.

9. Clean electrodes after several embryos have been electroporated, by submerging their platinum ends into the liquid contained in the 35 mm plate and delivering several current pluses. Electrodes often become less efficient as tissue debris accumulates on the surfaces. If tissue debris still remains on the electrodes, carefully remove by scraping off using #5 forceps. It may be necessary to reapply nail polish after cleaning electrodes, if they become chipped during the process.
10. When finished with each batch of embryos, clean dissection tools with detergent and a soft bristle brush, then rinse well with water. Clean electrodes as in Subheading 3.6, step 9. Dispose of needles and syringes in a sharps container. If any of the DNA mixture remains, it can be stored at 4 °C or –20 °C, and reused. Turn off nitrogen tank.
11. Embryos should be left in a humidified incubator until the desired embryonic stage. Figure 5 shows evidence of gene transfection in sections through the inner ear 4 days after plasmid electroporation into the E3 otocyst.
12. Visualize GFP by immunofluorescence and miR-9 by in situ hybridization. Our lab has successfully collected transgene-expressing basilar papillae 14 days after electroporation, although survival rates decrease dramatically beyond 3–4 days post-electroporation [12].

4 Notes

1. Most pre-miRNA stem-loop sequences can be found using miRBASE (<http://mirbase.org>; [32]). It is also possible to construct an intron that carries multiple pre-miR sequences in series [12]. See manufacturer for further details of Gateway technology (Invitrogen, Life Technologies). Plasmids pME-MCS-SDA and pTol2-GFP-Gateway are available from the authors upon request.
2. When making high concentration DNA, we often resuspend in a lower volume (~25–50 %) than what is recommended by the manufacturer of a commercial maxiprep kit. The resulting solution can be rather viscous or DNA may precipitate out of solution. Placing the solution in a 55 °C water bath for 30 min on the day of injection may help the DNA redissolve.
3. Nail polish application to the outside of the platinum wire is critical. Without the coating, the electric current will emanate from all of the exposed sides of the electrode. This can cause poor DNA transfection and increased embryo death.
4. Tip diameters less than 10 µm can result in clogging, while diameters greater than 13 µm may create too large of a hole in

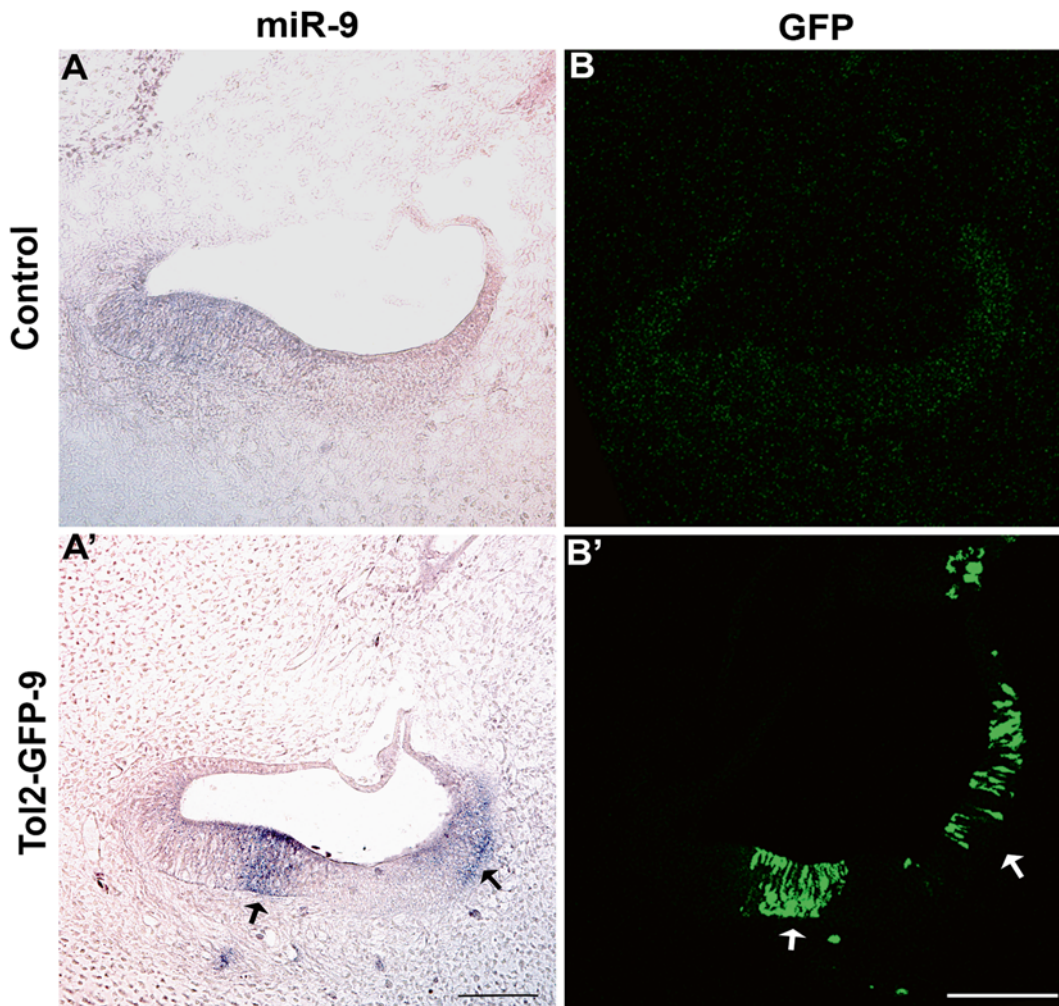


Fig. 5 Tol2-mediated expression of miRNA in the developing chick ear. On E3, pTol2-GFP-sd-miR9-sa and CAG-T2TP plasmids were electroporated into the anterior pole of the otocyst and the embryo was allowed to develop until E7. Alternate sections through the anterior crista were (a') processed by *in situ* hybridization to detect miR-9 or (b') immunostained for GFP. For *in situ* hybridization, we used a 5' and 3' double digoxigenin-labeled LNATM microRNA detection probe (Exiqon) and alkaline phosphatase immunohistochemistry. The miR-9 hybridization signal (a' black arrows) is located in areas that correspond to GFP in the sister section (b' white arrows). (a, b) The control consists of the contralateral (*left*) ear with the image flipped to match the experimental (*right*). Scale bar = 100 μ m

the otocyst, leading to excessive leakage of the plasmid DNA. Although not required, we find it helpful to use a student microscope to break the micropipette and immediately judge the tip diameter using an ocular micrometer at low power (10 \times). To do this, we mount the micropipette on the slide holder using molding clay, and watch as we tap the tip head-on against the edge of a stack of glass slides secured to the stage.

5. The amount of albumin removed is based on the size of the egg. It is better to remove too little than too much. A video is available of the egg windowing protocol [33].
6. During the procedure, note the appearance of the embryo. Make sure the embryo remains moist with regular application of Ringer's solution. The embryo will die if dried out.
7. We describe here a protocol to target the anterior or posterior poles of the otocyst, to transfet the anlagen of the utricular macula/anterior crista or the saccule/posterior cristae, respectively, as described previously [15, 34]. It is not uncommon to find the medial wall of the otocyst, including the endolymphatic duct, also transfected with this method. Delivery of plasmids to other sensory organs or to the otic neuroblasts can be determined empirically, and may require transfection into the otic cup at E1.5-2.5 (Hamburger-Hamilton stages 11–13), as described by others [12, 35–37].
8. If bubbles are absent or substantially decreased compared to previous embryos, transfer electrodes to a plate containing Ringer's solution and remove debris by scraping the electrode tips with dull forceps, and wiping with Kimwipes. In some cases, a few pulses in clean liquid will remove the debris without scraping.

Acknowledgements

We thank Ulrike Sienknecht for providing a protocol for electroporation electrode fabrication and Kaidi D. Zhang for converting pTol2-GFP into a Gateway® destination vector. We thank Vidhya Munnamalai for helping with figure preparation, Andrea Battisti for piloting electroporation techniques in our lab, and M. Katie Scott for reviewing the manuscript. Support from the NIDCD (R01DC002756 to D.M.F. and F31DC0011687 to M.L.S.) is gratefully acknowledged. Plasmid constructions were aided by data obtained from the DNA sequencing facility at Purdue University supported by P30 CA023168.

References

1. Bissonnette JP, Fekete DM (1996) Standard atlas of the gross anatomy of the developing inner ear of the chicken. *J Comp Neurol* 368:620–630
2. Stevens CB, Davies AL, Battista S et al (2003) Forced activation of Wnt signaling alters morphogenesis and sensory organ identity in the chicken inner ear. *Dev Biol* 261:149–164
3. Chang W, Brigande JV, Fekete DM, Wu DK (2004) The development of semicircular canals in the inner ear: role of FGFs in sensory cristae. *Development* 131:4201–4211
4. Sienknecht UJ, Anderson BK, Parodi RM et al (2011) Non-cell-autonomous planar cell polarity propagation in the auditory sensory epithelium of vertebrates. *Dev Biol* 352:27–39

5. Federspiel MJ, Hughes SH (1997) Retroviral gene delivery. *Methods Cell Biol* 52:179–214
6. Hughes SH (2004) The RCAS vector system. *Folia Biol* 50:107–119
7. Hughes SH. The RCAS system. <http://home.ncifcrf.gov/hivdrp/RCAS/index.html>
8. Morgan BA, Fekete DM (1996) Manipulating gene expression with replication-competent retroviruses. *Methods Cell Biol* 51:185–218
9. Winter J, Jung S, Keller S et al (2009) Many roads to maturity: microRNA biogenesis pathways and their regulation. *Nat Cell Biol* 11:228–234
10. Fabian MR, Sonenberg N, Filipowicz W (2010) Regulation of mRNA translation and stability by microRNAs. *Annu Rev Biochem* 79:351–379
11. Krol J, Loedige I, Filipowicz W (2010) The widespread regulation of microRNA biogenesis, function and decay. *Nat Rev Genet* 11: 597–610
12. Zhang KD, Stoller ML, Fekete DM (2015) Expression and misexpression of the miR-183 family in the developing hearing organ of the chicken. *PLoS One* 10(7):e0132796. doi: [10.1371/journal.pone.0030871](https://doi.org/10.1371/journal.pone.0030871)
13. Neves J, Parada C, Chamizo M, Giráldez F (2011) Jagged 1 regulates the restriction of Sox2 expression in the developing chicken inner ear: a mechanism for sensory organ specification. *Development* 138:735–744
14. Neves J, Uchikawa M, Bigas A, Giraldez F (2012) The prosensory function of Sox2 in the chicken inner ear relies on the direct regulation of Atoh1. *PLoS One* 7:e30871. doi: [10.1371/journal.pone.0030871](https://doi.org/10.1371/journal.pone.0030871)
15. Battisti AC, Fantetti KN, Moyers BA, Fekete DM (2014) A subset of chicken statoacoustic ganglion neurites are repelled by Slit1 and Slit2. *Hear Res* 310:1–12
16. Krull CE (2004) A primer on using in ovo electroporation to analyze gene. *Dev Dyn* 229:433–439
17. Muramatsu T, Mizutani Y, Ohmori Y, Okumura J (1997) Comparison of three non-viral transfection methods for foreign gene expression in early chicken embryos in ovo. *Biochem Biophys Res Commun* 230:376–380
18. Kwan KM, Fujimoto E, Grabher C et al (2007) The Tol2kit: a multisite gateway-based construction kit for Tol2 transposon transgenesis constructs. *Dev Dyn* 236:3088–3099
19. Kawakami K (2007) Tol2: a versatile gene transfer vector in vertebrates. *Genome Biol* 8:1–10
20. Sato Y, Kasai T, Nakagawa S et al (2007) Stable integration and conditional expression of electroporated transgenes in chicken embryos. *Dev Biol* 305:616–624
21. Freeman SD, Daudet N (2012) Artificial induction of Sox21 regulates sensory cell formation in the embryonic chicken inner ear. *PLoS One* 7:15–17
22. Costa A, Sanchez-Guardado L, Juniat S et al (2015) Generation of sensory hair cells by genetic programming with a combination of transcription factors. *Development* 142: 1948–1959
23. Freeman S, Chrysostomou E, Kawakami K et al (2012) Tol2-mediated gene transfer and in ovo electroporation of the otic placode: a powerful and versatile approach for investigating embryonic development and regeneration of the chicken inner ear. *Methods Mol Biol* 916:373–385
24. Zelarayan LC, Vendrell V, Zelarayan LC et al (2007) Differential requirements for FGF3, FGF8 and FGF10 during inner ear development. *Dev Biol* 308:379–391
25. Stoller ML, Chang HC, Fekete DM (2013) Bicistronic gene transfer tools for delivery of miRNAs and protein coding sequences. *Int J Mol Sci* 14:18239–18255
26. Lin SL, Chang D, Wu DY, Ying SY (2003) A novel RNA splicing-mediated gene silencing mechanism potential for genome evolution. *Biochem Biophys Res Commun* 310:754–760
27. Lin S-L, Ying S-Y (2004) New drug design for gene therapy—taking advantage of introns. *Lett Drug Des Discov* 1:256–262
28. Du G, Yonekubo J, Zeng Y et al (2006) Design of expression vectors for RNA interference based on miRNAs and RNA splicing. *FEBS J* 273:5421–5427
29. Karwacz K, Bricogne C, MacDonald D et al (2011) PD-L1 co-stimulation contributes to ligand-induced T cell receptor down-modulation on CD8+ T cells. *EMBO Mol Med* 3:581–592
30. Arce F, Breckpot K, Stephenson H et al (2011) Selective ERK activation differentiates mouse and human tolerogenic dendritic cells, expands antigen-specific regulatory T cells, and suppresses experimental inflammatory arthritis. *Arthritis Rheum* 63:84–95
31. Zeng Y, Yi R, Cullen BR (2005) Recognition and cleavage of primary microRNA precursors by the nuclear processing enzyme Drosha. *EMBO J* 24:138–148
32. Griffiths-Jones S, Grocock RS, van Dongen S et al (2006) miRBase: microRNA sequences, targets and gene nomenclature. *Nucleic Acids Res* 34:D140–D144

33. Korn MJ, Cramer KS (2007) Windowing chicken eggs for developmental studies. *J Vis Exp* e306. doi:[10.3791/306](https://doi.org/10.3791/306)
34. Chang W, Lin Z, Kulessa H et al (2008) Bmp4 is essential for the formation of the vestibular apparatus that detects angular head movements. *PLoS Genet* 4:e1000050. doi:[10.1371/journal.pgen.1000050](https://doi.org/10.1371/journal.pgen.1000050)
35. Alsina B, Abello G, Ulloa E et al (2004) FGF signaling is required for determination of otic neuroblasts in the chick embryo. *Dev Biol* 267:119–134
36. Daudet N, Lewis J (2005) Two contrasting roles for Notch activity in chick inner ear development: specification of prosensory patches and lateral inhibition of hair-cell differentiation. *Development* 132:541–551
37. Evsen L, Sugahara S, Uchikawa M et al (2013) Progression of neurogenesis in the inner ear requires inhibition of Sox2 transcription by neurogenin1 and neurod1. *J Neurosci* 33:3879–3890

Chapter 3

A Rapid, Cost-Effective Method to Prepare Recombinant Adeno-Associated Virus for Efficient Gene Transfer to the Developing Mouse Inner Ear

Michelle M. Gomes, Lingyan Wang, Han Jiang, Christoph A. Kahl,
and John V. Brigande

Abstract

There is keen interest to define gene therapies aimed at restoration of auditory and vestibular function in the diseased or damaged mammalian inner ear. A persistent limitation of regenerative medical strategies that seek to correct or modify gene expression in the sensory epithelia of the inner ear involves efficacious delivery of a therapeutic genetic construct. Our approach is to define methodologies that enable fetal gene transfer to the developing mammalian inner ear in an effort to correct defective gene expression during formation of the sensory epithelia or during early postnatal life. Conceptually, the goal is to atraumatically introduce the genetic construct into the otocyst-staged mouse inner ear and transfect otic progenitors that give rise to sensory hair cells and supporting cells. Our long-term goal is to define therapeutic interventions for congenital deafness and balance disorders with the expectation that the approach may also be exploited for therapeutic intervention postnatally.

In the inaugural volume of this series, we introduced electroporation-mediated gene transfer to the developing mouse inner ear that encompassed our mouse survival surgery and transuterine microinjection protocols (Brigande et al., Methods Mol Biol 493:125–139, 2009). In this chapter, we first briefly update our use of sodium pentobarbital anesthesia, our preferred anesthetic for mouse ventral laparotomy, in light of its rapidly escalating cost. Next, we define a rapid, cost-effective method to produce recombinant adeno-associated virus (rAAV) for efficient gene transfer to the developing mouse inner ear. Our immediate goal is to provide a genetic toolkit that will permit the definition and validation of gene therapies in mouse models of human deafness and balance disorders.

Key words Recombinant adeno-associated virus (rAAV) vectors, Virus-mediated gene transfer, Transuterine microinjection, Mouse experimental embryology, Fetal gene transfer

1 Introduction

We previously demonstrated electroporation-mediated gene transfer to the developing mouse inner ear [1] and now establish an adeno-associated virus (AAV)-mediated gene transfer paradigm. AAV is a non-enveloped, 25 nm diameter, single-stranded DNA virus belonging to the *Parvoviridae* family [2]. Recombinant AAV

(rAAV) lacks the ability to self-propagate, and serves as an attractive vector for fetal gene therapy because of its low immunogenicity, its ability to direct long-term gene expression in a variety of tissues, and a lack of disease association in humans [3, 4]. AAV tropism is determined by the viral capsid proteins through interaction with cell surface receptors [5]. Coating the virus with different AAV capsid serotypes alters rAAV host range and can be exploited to optimize the infection efficiency for specific applications such as transducing otic epithelial progenitors in the otocyst-stage mouse inner ear [6].

The goal of this chapter is to provide a modified AAV production protocol to rapidly and cost-effectively produce rAAV vector of sufficient purity and titer to enable efficient gene delivery into the developing mouse inner ear. The key advantages of this protocol are: (1) a streamlined production process that obviates the need for further virus purification by the time-consuming iodixanol gradient ultracentrifugation methodology [7], (2) optimized polyethylenimine transfection conditions that produce high virus yield [8], and (3) a small-scale, “one flask per vector” transfection scheme that routinely yields enough concentrated viral inoculum for at least 100 mouse otocyst injections.

We demonstrate early postnatal transgene expression after transuterine microinjection of rAAV into the otocyst-stage mouse inner ear without toxicity and at comparable efficiencies to rAAV purified through a standard iodixanol gradient ultracentrifugation methodology (Fig. 1). Since rAAV preparations generated by our rapid method are still significantly contaminated with cellular proteins, this approach is primarily useful for studies in which the purity of the viral vector is not a confounding factor. For instance, we have introduced viral inocula produced by this rapid rAAV protocol to evaluate promoter sequences that might guide cell-specific expression and to test the efficacy of epitope-tagging a fluorescent reporter (Fig. 2). The overarching strength of the approach is that it will enable feasibility-level pilot, proof-of-concept, and screening studies that require sustained gene expression in the inner ear from late embryogenesis through early postnatal stages. We predict that this method will be useful for other target tissues and organ systems accessible by fetal gene transfer provided AAV serotype, vector functionality, and potential toxicity are rigorously evaluated.

2 Materials

2.1 General Anesthesia for Mouse Ventral Laparotomy: Update

1. 50 mg/mL Nembutal (pentobarbital sodium solution, United States Pharmacopeia [USP]) stock solution. Pentobarbital sodium anesthesia remains the anesthetic of choice to provide the depth and duration of anesthesia required for ventral laparotomy without adversely affecting the developing embryos subjected to transuterine microinjection [9]. The recent

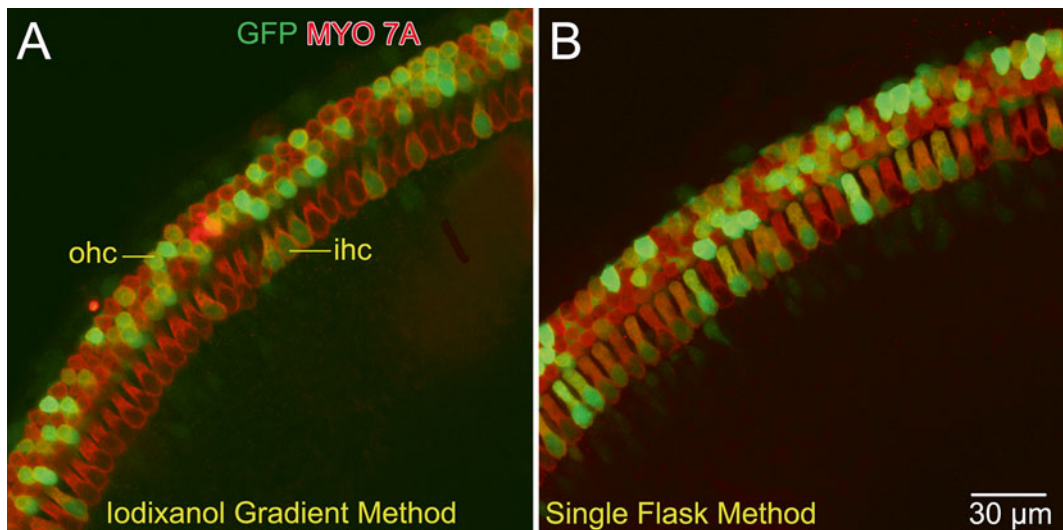


Fig. 1 rAAV produced by the rapid, single flask method demonstrates similar infection dynamics in the mouse inner ear as rAAV purified by iodixanol gradient ultracentrifugation. rAAV1-chick beta actin (CBA)-GFP was produced by the (A) iodixanol and the (B) single flask methods in which the culture supernatant and cellular lysate are pooled and purified by gradient ultracentrifugation or only partially purified by Amicon filtration, respectively. Titers of 7.3×10^{12} and 7.9×10^{12} vg/mL were achieved with the iodixanol and single flask methods, respectively. Viral inocula were introduced into the embryonic day 12.5 (E12.5) mouse otic vesicle by transuterine microinjection until it swelled [9]. The embryos were carried to term, born naturally, and the inner ears of postnatal day 6 (P6) pups were harvested for immunofluorescence localization of myosin 7A (MYO 7A), a hair cell marker [17]. The iodixanol (A) and the single flask (B) purified rAAVs result in GFP expression in inner and outer hair cells as demonstrated in these confocal microscopic projections. In over 200 E12.5 mouse otocyst injections, no embryonic lethality was observed and cochlear maturation to early adult stages is indistinguishable from that of wild-type embryos injected with rAAV purified by iodixanol gradient ultracentrifugation

escalation in Nembutal cost has necessitated an alternative approach to its purchase from commercial sources to preserve its use for mouse survival surgery (*see Note 1*).

2.2 Cell Culture, Transfection, and rAAV Vector Production

- Human Embryonic Kidney (HEK) 293A cells (Life Technologies), or HEK293 cells (American Type Culture Collection; ATCC) (*see Note 2*).
- Dulbecco's Phosphate-Buffered Saline (DPBS) without $\text{Ca}^{2+}/\text{Mg}^{2+}$.
- 1× Trypsin EDTA Solution: 0.05 % trypsin, 0.53 mM EDTA, without, $\text{NaHCO}_3/\text{Ca}^{2+}/\text{Mg}^{2+}$, in 1× Hanks' Balanced Salt Solution (HBSS, Corning Life Sciences).
- Complete media: Prepare Dulbecco's Modification of Eagle's Medium (DMEM) containing 4.5 g/L glucose, L-glutamine, and sodium pyruvate (Corning Cellgro; Media Tech) with 10 % Fetal Bovine Serum (FBS). Add 1× Penicillin/Streptomycin/L-Glutamine (100 international units [I.U.]/mL

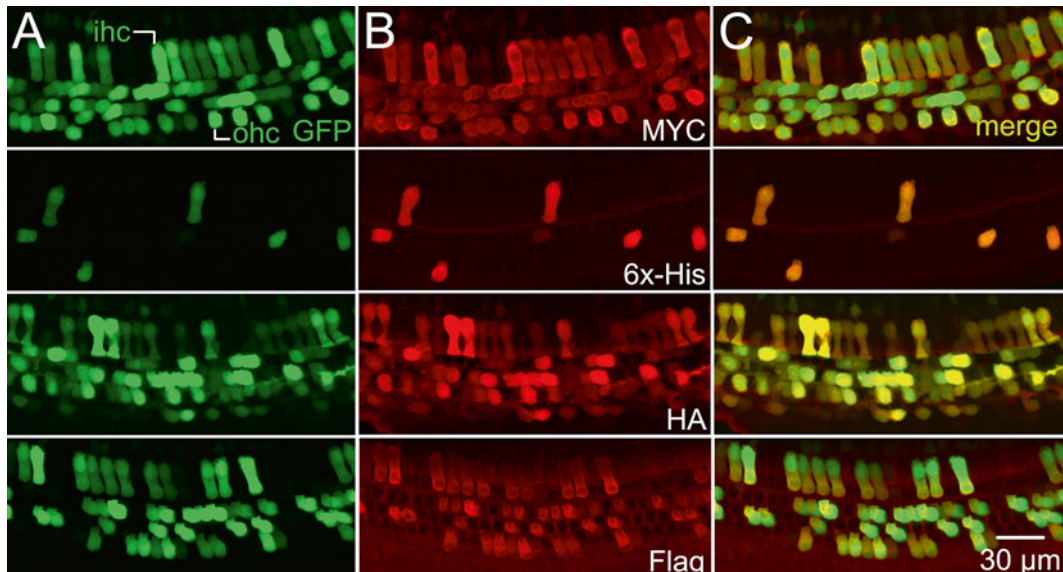


Fig. 2 The single flask method enables rapid evaluation of differentially epitope-tagged GFP constructs for efficacy of expression in the early postnatal mouse inner ear. Four pAAV1-CBA-GFP-[epitope tag] constructs were produced to independently evaluate Myc, 6x Histidine (6x-His), hemagglutinin (HA), and Flag tag detection of GFP. Two copies of the Myc, HA, and Flag tag coding sequences were used against only one 6x-His tag sequence. Four rAAV1-CBA-GFP-[epitope tag] vectors were produced by the single flask method and titers in vg/mL were: Myc— 9.2×10^{11} ; 6x-His— 2.5×10^{12} ; HA— 8.3×10^{11} ; and Flag— 2.4×10^{12} . The viral inocula were independently injected into E12.5 mouse otocysts and inner ears were harvested at P6 for whole mount immunofluorescence with anti-Myc antibody (Abcam #1162); anti-6x-His tag antibody (Abcam #9108); anti-HA tag antibody (Abcam #9110); and anti-DDDDK tag antibody (Abcam #1162) at 1:100 dilution. Representative confocal projections of the apical cochlea for each vector are presented in the images. Column (A), GFP expression in inner (ihc) and outer hair cells (ohc) in P6 apical cochlea. Column (B), Immunofluorescence detection of the four epitope tags in the organs of Corti in Column (A). Column (C), Merged images of (A) and (B). The C-terminal epitope tags were detected by their respective antisera in GFP+-[epitope-tagged] hair cells with extremely high efficiency. Finally, the 6x-Hisx vector was consistently less robustly expressed. These data indicate that the Myc-, HA-, and Flag-tagged GFP are robustly expressed in sensory hair cells by P6 via rAAV-mediated gene transfer to the developing mouse inner ear. Moreover, the single flask method enables a rapid testing scheme to empirically determine which epitope tag to deploy at the N- or C-terminal of the ion channel or transcription factor of interest, for example. Once bioactivity of the tagged protein is confirmed, a fully purified, high-titer iodixanol gradient preparation of only the validated rAAV vector is performed, ultimately saving time and resources

penicillin, 100 $\mu\text{g}/\text{mL}$ streptomycin, and 292 $\mu\text{g}/\text{mL}$ L-glutamine).

5. Post-transfection media: DMEM containing 2 % FBS and 1× Penicillin-Streptomycin-L-Glutamine.
6. Transfection media (serum-free, antibiotic-free): DMEM.
7. AAV rep-cap serotype plasmid (~1 $\mu\text{g}/\mu\text{L}$) expressing the appropriate viral capsid serotype, e.g., pAAV2/1 (*see Notes 3–6*).

8. AAV vector transgene plasmid (~1 µg/µL). This is the plasmid containing the target gene flanked by viral inverted terminal repeats (ITRs), e.g., pAAV-CAG-GFP (Addgene #37825) (*see Notes 4–7*).
9. Adenoviral helper plasmid, e.g., pAd DeltaF6 (Penn Vector Core, Gene Therapy Program, University of Pennsylvania School of Medicine) (~1 µg/µL) (*see Notes 4–6*).
10. High Potency Linear Polyethylenimine (PEI) “MAX” (MW 40,000) stock solution (Polysciences, Inc.): 1 mg/mL in water, pH 7.1. Sterile filter using 0.2 µm filter (*see Notes 8 and 9*).
11. T-150 culture flasks (Corning), 2 mL aspirating pipette, 10 mL pipette, 15 mL conical tubes.
12. Hemocytometer.
13. Class II Biological Safety Cabinet (BSC) (*see Note 10*).
14. Designated cell culture incubator set at 37 °C and 5 % CO₂.
15. Inverted microscope: 4× and 10× objectives.

2.3 Cell Harvest, Lysis, and Pre-clearing

1. 0.5 M EDTA. Sterile filter using an 0.2 µm filter.
2. Benzonase nuclease (≥250 units/µL (*see Note 11*)).
3. 95–100 % ethanol, molecular biology grade.
4. Dry ice (pelleted).
5. 37 °C water bath.
6. Beckman J2-21M/E centrifuge or a centrifuge capable of 3836×*g* (e.g., 5000 rpm in a Beckman Coulter JA-14 rotor).

2.4 AAV Concentration and Buffer Exchange

1. AAV storage buffer: DPBS, 35 mM NaCl, 5 % glycerol (v/v). Sterile filter using an 0.2 µm filter.
2. Amicon Ultra-15 (MWCO 100,000) centrifugal filter (Millipore, Bedford, MA).
3. Pipettors: P-200 µL and P-1000 µL with sterile pipette tips.
4. Allegra 6R centrifuge or equivalent that supports a swinging bucket rotor capable of 2056×*g* (e.g., 3000 rpm in a Beckman Coulter GH-3.8 rotor).

2.5 AAV DNA Preparation and Titration by Quantitative Polymerase Chain Reaction (qPCR)

1. Heating Blocks.
2. DNase I and 10× DNase buffer (Life Technologies).
3. 10 mM Tris, pH 9.0.
4. 50 mM EDTA.
5. Proteinase K (20 mg/mL; Amresco).
6. Chicken beta actin (CBA) promoter, forward primer (100 µM): 5'-CCA CGT TCT GCT TCA CTC TCC-3' (*see Note 12*).
7. Chicken beta actin (CBA) promoter, reverse primer (100 µM): 5'-CCC CAT CGC TGC ACA AAA TA-3' (*see Note 12*).

8. Chicken beta actin (CBA) Probe (10 μ M) (Biosearch Technologies): 5'd FAM-CCC CCT CCC CAC CCC CAA TTT TGT ATT TAT-BHQ-1 3' (*see Note 12*).
9. TaqMan Universal PCR Master Mix (Applied Biosystems, Foster City, CA).
10. Standard plasmid: pAAV-CAG-GFP (Addgene, A gift from Edward Boyden) linearized with EcoRI (5442 base pairs). The CAG promoter is identical to the CBA promoter. Standard dilution series: 10^7 , 10^6 , 10^5 , 10^4 , 10^3 copies/reaction.
11. 7500 Real Time PCR System (Applied Biosystems) or equivalent.

3 Methods

3.1 Seeding HEK293A Cells

1. Plate HEK293A cells in 20 mL of complete media at 7.5×10^6 cells/T-150 flask 24 h prior to transfection in the BSC (*see Notes 2, 10 and 13*).
2. Transfer cells to an incubator at 37 °C and 5 % CO₂. This results in approximately 1.5×10^7 cells/flask on the day of transfection.

3.2 Triple Transfection of HEK293A Cells

On the day of transfection:

1. Check cells under a microscope to ensure they are growing evenly in a monolayer and are 80–90 % confluent (*see Note 14*).
2. Pre-warm 15 mL of post-transfection media in a 37 °C water bath and equilibrate the transfection media to room temperature.
3. Set up two 15 mL tubes, labeled “PEI” and “Plasmids”, in the BSC.
4. To each tube, add 1.5 mL of transfection media.
5. Add 30 μ L of 1 mg/mL PEI “MAX” Stock solution to the “PEI” tube (*see Notes 8 and 9*).
6. Add 3.75 μ g of AAV serotype plasmid, 3.75 μ g of the vector transgene ITR plasmid, and 7.5 μ g of adenoviral helper plasmid, to the “Plasmids” tube. Mix well by vortexing.
7. Add the PEI-transfection media solution to the Plasmid-transfection media solution in the “Plasmids” tube. Mix well by vortexing.
8. To form the transfection complex, incubate the PEI:Plasmid solution at room temperature for 15 min. In the meantime, remove the flask containing the HEK293A cells and aspirate the media. Add 15 mL of pre-warmed post-transfection media to the flask (*see Note 15*).

9. After the transfection complex has formed, vortex the PEI:Plasmid solution again and then add 3 mL of the PEI:Plasmid complex dropwise to the flask containing 15 mL of post-transfection media without disturbing the cells. Gently tilt the flask back and forth so that the transfection complex is evenly distributed over the cells.
10. Return the flask to the incubator at 37 °C and 5 % CO₂ (*see Note 16*).

3.3 Harvesting Cells and Supernatant with Lytic Release of rAAV

1. Harvest cells ~72 h post-transfection. To aid detachment of the cells from the flask surface, add 300 µL of 0.5 M EDTA per T-150 flask for a final concentration of 8–10 mM EDTA. Return the flask to the 37 °C incubator and incubate for at least 15 min. Gently tilt the flask back and forth about 10 times to dislodge the cells. Carefully take up the solution containing cells with a sterile 10 mL serological pipette and release without creating any air bubbles in the media (e.g., maintain a 1 mL residual volume in the pipette until final ejection). Transfer both supernatant containing secreted AAV and the cells containing cell-associated AAV (SN+cells) into a sterile 50 mL conical centrifuge tube (*see Note 17*).
2. Freeze–thaw the SN+cells solution 3 times by cycling between a dry-ice ethanol bath and 37 °C water bath (*see Note 11*). Vortex the cell suspension vigorously after each thaw to encourage the cells to lyse and release any cell-associated AAV into the solution (SN+lysate).
3. Add 6–7 µL Benzonase nuclease (\geq 250 units/µL) to achieve a 100 unit/mL final concentration in the SN+lysate solution. Mix gently and incubate for 1 h in a 37 °C water bath (*see Note 11*). Re-mix the solution every 15 min during the incubation.
4. Centrifuge the SN+lysate at $3836\times g$ (e.g., 5000 rpm in a Beckman Coulter JA-14 rotor) for 15 min at 4 °C. Separate the supernatant containing the rAAV particles from the pellet with a sterile 25 mL serological pipette and transfer to a sterile 50 mL conical centrifuge tube. Discard the pellet containing the cellular debris into a biohazardous waste receptacle.

3.4 Concentration and Buffer Exchange

1. Prepare the Amicon Ultra-15 (MWCO 100,000) centrifugal filter for concentration and buffer exchange by first adding 10 mL of sterile water to the filter membrane and centrifuging at $2056\times g$ (e.g., 3000 rpm in a Beckman Coulter GH-3.8 rotor) for 10 min at room temperature. Discard the flow through. The water wash removes impurities left on the membrane from the manufacturing process.

2. Add 15 mL of AAV storage buffer to the membrane. Centrifuge at $2056 \times g$ for 10 min at room temperature. Discard the flow through. The buffer wash equilibrates the membrane prior to concentration and buffer exchange.
3. Add 15 mL of the rAAV solution to the equilibrated Amicon Ultra-15 (MWCO 100,000) centrifugal filter (*see Note 18*). Centrifuge at $2056 \times g$ for 10 min at room temperature. Discard the flow through.
4. Visually estimate the volume of the retentate, which contains the rAAV particles. If more than 200 μ L of retentate is present, gently pipette the solution up and down three times using a P-1000 pipettor to disturb the concentration gradient of rAAV particles that forms near the membrane. Avoid touching the membrane with the pipette tip, which could mechanically compromise the membrane resulting in loss of rAAV in the flow through. Continue centrifugation with resuspension of retentate in ~10 min intervals until the ~200 μ L target volume is achieved.
5. Mix 15 mL of AAV storage buffer with ~200 μ L of retentate by gently pipetting 3 times with a sterile 5 mL serological pipette.
6. Centrifuge at $2056 \times g$ for 10 min at room temperature, assess retentate volume, and continue Amicon filtration until the 200 μ L target volume is achieved.
7. Repeat the concentration and buffer exchange procedure at least three times using the ~200 μ L volume as the endpoint for each cycle. The final centrifugation step strives to achieve a final volume of 100–120 μ L without evidence of viral precipitation (*see Note 18*).
8. Transfer the concentrated rAAV vector with a P-200 μ L pipettor into a 1.5 mL microfuge tube.
9. Briefly centrifuge to remove any precipitate. Transfer the rAAV supernatant to a new 1.5 mL microfuge tube.
10. Aliquot the rAAV vector in 10 μ L volumes and freeze at –80 °C. Leave at least one 10 μ L aliquot of rAAV vector at 4 °C for quantification of viral genomes present.

3.5 Preparation of rAAV DNA and Titer Determination by Quantitative Polymerase Chain Reaction (qPCR)

rAAV DNA is prepared from the concentrated rAAV vector for quantification by qPCR according to the method described by Rohr and colleagues [10]. Only critical steps are summarized below.

1. DNase treatment: Digest a 1 μ L aliquot of concentrated rAAV with 1 unit DNase I (Life Technologies) in the supplied buffer at 1 \times concentration in a final volume of 50 μ L for 30 min at 37 °C. Inactivate DNase I by addition of 5 μ L 50 mM EDTA and heating for 10 min at 65 °C.

2. Proteinase K digestion: Add 45 μ L of DPBS containing 0.2 μ g/ μ L of Proteinase K to the 55 μ L DNase-treated sample to achieve a final concentration of 9–10 μ g Proteinase K in the 100 μ L reaction volume. Incubate samples at 56 °C for 1 h. Inactivate proteinase K by heating at 95 °C for 20 min.
3. Dilute samples 100-fold in 10 mM Tris, pH 9.0 for qPCR (e.g., add 5 μ L to 495 μ L of 10 mM Tris, pH 9.0).
4. Titer Determination: For titration by qPCR, 10 μ L aliquots of sample dilutions and standards are assayed in duplicate using the CBA promoter primer-probe in a 7500 Real-Time PCR system (Applied Biosystems) (*see Note 12*). Use 10 μ L of PCR-grade water as negative control.
5. The viral genomes (vg)/mL are calculated from the dilution factor and the mean copies of rAAV per reaction determined from the standard curve consisting of 10⁷ -10³ copies of the standard (*see Note 19*).

4 Notes

1. The official transcript (version 4/17/2013) of the Office of Laboratory Animal Welfare (OLAW) Webinar on March 1, 2012 entitled “Use of Non-Pharmaceutical-Grade Chemicals and Other Substances in Research with Animals” included an appendix that addressed a comment submitted in writing after the Webinar, regarding the limited availability and extreme cost of Nembutal [11]. OLAW, the United States Department of Agriculture Animal Care, and the Association for Assessment and Accreditation of Laboratory Animal Care jointly issued the following response: “The Regulatory guidance on this matter specifically allows for use of non-pharmaceutical-grade compounds due to non-availability and with Institutional Animal Care and Use (IACUC) approval. The exorbitant cost of this product has placed it logically into the unavailable category. Pentobarbital from a reagent or analytical-grade powder, properly prepared by your pharmacist or other knowledgeable individual (e.g., chemist, veterinarian, researcher, with assurance of appropriate storage and handling, and approval by the IACUC is acceptable. IACUC approval can be institution-wide for the drug prepared in this fashion for all approved users.” The Brigande Laboratory has secured Oregon Health & Science University (OHSU) IACUC approval to compound a 50 mg/mL solution of pentobarbital sodium solution for mouse survival surgery. Reagent and analytical-grade pentobarbital sodium powder is available from a compounding pharmacist with appropriate DEA licensure and potentially from other commercial sources. Stability testing of the

compounded anesthetic should be conducted to determine safe storage conditions that preserve potency and efficacy. Our formulation is 50 mg/mL pentobarbital sodium in 40 % propylene glycol, (USP), 10 % ethanol, (USP), and the balance water for injection, (USP), and is stable in the dark at room temperature for 12 months. Consult your IACUC for their preferred method of compounding pentobarbital sodium, which typically differs between institutions.

2. HEK293 cells contain integrated adenovirus sequences that provide essential helper functions for AAV production. Transfection efficiency can diminish after prolonged passage in culture or if cells are allowed to become over-confluent. For routine passage, we recommend splitting the cells every 3–4 days before they reach confluence. To maintain cell quality and consistency between virus productions, we recommend creating a low-passage working cell bank from the initial cell stock. A passage limit for efficient transfection should be determined empirically (usually no more than 20–30 passages). After the appropriate cell passage limit is reached, a new cell vial should be thawed from the working cell bank.
3. All stock solutions and buffers are made with endotoxin-free water with a resistivity of 18.2 MΩ cm.
4. The biosafety classification and attendant biosafety procedures required to work with rAAV vectors is dependent on a number of factors that have to be carefully evaluated by the investigator prior to beginning the work. The Institutional Biosafety Committee (IBC) and IACUC at OHSU work in tandem to ensure that appropriate biosafety protocols are in place to protect both investigators and their animal model systems. According to the November 6, 2013 issue of the Guidelines for Research Involving Recombinant or Synthetic Nucleic Acid Molecules, wild-type and recombinant AAVs of all serotypes are generally classified as Risk Group 1 (RG-1) agents (i.e., are not associated with disease in healthy human adults). Therefore, work with RG-1 rAAV requires at a minimum Biosafety Level (BSL)-1 and Animal Biosafety Level (ABSL)-1 containment. Additional modifications may raise the risk profile. For example, BSL-2 and ABSL-2 containment is usually required if the rAAV is produced using a live helper virus and/or encodes a potentially toxic or tumorigenic transgene. In addition, the human-derived HEK293A cell line and the significant cellular material present in unpurified rAAV preparations generally requires BSL-2 as per the blood-borne pathogens standard set by the Occupational Safety & Health Administration (OSHA). All *in vivo* work with rAAV in the Brigande Laboratory is conducted under BSL-2 protocols, though our dams with inoculated embryos are housed at ABSL-1 with permission of the

OHSU IACUC. However, it is essential to consult your institutional biosafety officials and your IACUC for guidance on formulating an appropriate institutional biosafety protocol appropriate for the production and *in vivo* use of rAAV.

5. The basic AAV component plasmids can be obtained from a variety of sources, such as the Penn Vector Core at the University of Pennsylvania, or from one of several commercial vendors. Also, the non-profit Addgene plasmid repository (www.addgene.org) stocks a growing collection of specific AAV vector transgene plasmids deposited by researchers. The AAV triple transfection method outlined here requires three plasmids: a transgene plasmid with flanking inverted-terminal repeats (ITRs); a serotype-specific plasmid expressing AAV rep-cap proteins; and an adenoviral plasmid providing essential virus helper functions [12–14]. The separation of virus functions onto different plasmids makes the system very flexible as plasmids of interest can be swapped into the transfection protocol in order to change virus characteristics without having to alter the virus production methodology. For example, the serotype-specific plasmid determines the tissue tropism of the rAAV vector and influences virus production yields and cellular transduction efficiency. The triple transfection scheme allows screening of several AAV capsid serotypes enabling identification of AAV1 as highly effective for gene delivery to the developing inner ear. Similarly, the transgene plasmid sequence can be modified or exchanged to alter the genetic payload.
6. The serotype-specific plasmid and the adenoviral helper plasmid are grown in common *E. coli* strains (such as TOP10) as high-copy plasmids in Luria Broth containing 50 µg/mL carbenicillin at 37 °C. The inverted-terminal repeat (ITR)-containing plasmids (i.e., the cis or vector transgene plasmids) contain an appropriate transgene sequence flanked by the AAV ITR on each side. The ITRs are critical for proper vector transgene packaging into virus particles, but are prone to deletions and rearrangements. Therefore, ITR-containing plasmids should be grown in recombination-deficient (rec-) *E. coli* strains (such as Sure (Agilent Technologies), Stbl2, or Stbl3 (Life Technologies)) as low-copy plasmids at 30 °C. Using these conditions the plasmid yields are significantly lower, hence we recommend using a rich media like 2XYT and doubling the growth volumes. For example, for a Qiagen Maxi Prep, set up two 100 mL overnight cultures. Use twice the volumes of P1, P2, and P3 buffers for initial resuspension and cell lysis. Then purify over a single Maxi Prep column following the standard Qiagen endotoxin-free Maxi Kit protocol. In addition, to avoid failed rAAV vector productions, the integrity of the ITRs in each new plasmid preparation should be

carefully verified in advance by restriction digests using enzymes that cut within the ITRs (such as *Xma*I, *Msc*I, *Ahd*I, *Pau*I, and *Pvu*II).

7. The wild-type AAV genome size is about 4.7 kb. All viral sequences (except for the two 145 bp inverted terminal repeats (ITRs)) are deleted in rAAV vectors. That provides a transgene capacity of up to ~4.5 kb. Even though slightly larger transgene cassettes can sometimes still be packaged efficiently, there is a risk of non-packaging or incomplete packaging with oversized genomes (i.e., absent or low vector titers, respectively). Therefore, it is recommended not to exceed the AAV packaging capacity.
8. The use of PEI “MAX” as a transfection agent eliminates the need to change media post-transfection since it is non-toxic to cells. In addition, it is chemically stable and functions over a wide pH range.
9. PEI “MAX” is built on the same linear backbone of PEI, but contains more than 11 % additional free nitrogens. The amino groups make it a highly potent cationic polymer allowing it to form ionic interactions with the phosphate backbones of DNA. PEI:DNA complexes are transported into the cell via endocytosis and escape endosomes via a proton sponge effect that promotes osmotic swelling and disruption of the endosomal membrane. In PEI:DNA complexes, the ratio between molar units of PEI nitrogen atoms to units of DNA phosphate atoms, known as the N/P ratio, was found to correlate with transfection efficiency [8, 15]. We optimized our AAV transfection and production protocol using PEI “MAX” by assaying various N/P ratios and DNA amounts. An N/P ratio of 15.3 for PEI “MAX” coupled with 1.0 µg DNA per mL of media (15 µg DNA/T-150 flask) produces the highest AAV yields. The volume (µL) of PEI was calculated based on the following equation [15]: $3 \times D \times R/S$, where D =total amount of plasmid DNA used (15 µg), R =N/P ratio (ratio of nitrogen content in PEI to phosphorous content in DNA= 15.3), S =concentration of the PEI stock (23.2 mM, monomer unit).
10. The BSC is a vertical type of laminar flow hood whose class 100 environment protects the user from exposure to biohazards. The primary route of exposure to rAAV particles is through aerosolization during pipetting. Confining all procedures involved in the production of rAAV to the BSC minimizes the potential for exposure, protecting the investigator and laboratory staff. The Environmental Health and Radiation Safety group at OHSU requires annual recertification of all biological safety cabinets used for production of viral vectors.

Check institutional policy regarding all biosafety requirements to safely work with rAAV vectors.

11. The freeze–thaw cycles initiate cell lysis and the release of cellular DNA and RNA along with unencapsidated viral DNA. Benzonase is an endonuclease that digests all forms of DNA and RNA to 5'-monophosphate terminated oligonucleotides 3–5 bases in length. Cellular debris is cleared from the preparation by a subsequent centrifugation step. Benzonase-treated solutions exhibit reduced viscosity, which facilitates concentration and buffer exchange by Amicon filtration.
12. The PCR primers and probe are specific to the vector transgene sequence (e.g., the CBA promoter), in order to accurately quantify the number of vector genomes in a large background of cellular DNA. If other transgene sequences are used, the primer and probe sequences need to be appropriately designed and the qPCR assay validated.
13. It is also possible to plate HEK293A cells up to 5 days prior to transfection. In this case, plate at 0.9×10^6 cells/T-150 flask in 20 mL of complete growth media. This results in $\sim 1.5 \times 10^7$ cells/flask on the day of transfection. Twenty-four hours prior to transfection, aspirate off the old growth media, feed the cells with 15 mL of fresh complete growth media, and return the flask to the 37 °C incubator.
14. Eighty to ninety percent confluence is equivalent to approximately $12\text{--}15 \times 10^6$ cells per T-150 flask. The number of cells present at the time of transfection is critical given that the expected productivity per cell is about 1×10^4 viral genomes. Vector titers may be reduced if cells are over- or under-confluent.
15. Complete DMEM containing 10 % FBS is used for seeding HEK293A cells, but the amount of FBS in the media is reduced to 2 % post-transfection. The reduced FBS concentration adequately supports cell growth, though at a slower rate; helps boost virus production compared to serum-free growth media; and is comparable to virus production with 10 % FBS. In addition, 2 % FBS compared to 10 % FBS is cost-effective, decreases the viscosity of the media, and prevents clogging of the Amicon ultrafilters due to precipitation of FBS proteins during the concentration and buffer exchange step.
16. rAAV does not produce a clear cytopathic effect (CPE) and this may make it difficult to monitor virus production. Nevertheless, there are general signs that can be observed, e.g., rounded up cells, increased cellular debris, and the presence of floating cells, which suggest that the transfection was successful. When performing this protocol for the first time, we recommend using a marker gene (e.g., GFP) that is

expressed from the viral cassette to assess transfection efficiency by visualizing the number of fluorescent cells present. Transfection is considered efficient when 80–90 % of the cells express the fluorescent marker protein.

17. The prototypical AAV2 virus accumulates to about 90 % inside cells, and so AAV has traditionally been harvested from cells rather than the media. In contrast, many of the more recently discovered AAV serotypes (including AAV1) tend to release a significant and variable amount of virus particles into the media within the first 72 h post-transfection [16]. Furthermore, AAV particles tend to leak into the media during prolonged cell culture; hence harvesting both the cells and supernatant (i.e., the production media) can significantly boost yields and enhance viral titer.
18. The Amicon Ultra-15 (MWCO 100,000) centrifugal filter has three advantages. First, contaminants such as media components and proteins <100,000 kDa pass through the membrane as part of the flow through. For example, Benzonase at 30 kDa is removed from the virus preparation in this step. Second, Amicon filtration concentrates the virus preparation 100-fold by reducing the volume from ~20 mL to ~200 µL or less. Third, the ultrafilter exchanges the rAAV media with a buffer that is compatible for delivery into the embryonic mouse inner ear and suitable for long-term rAAV storage at -80 °C with no significant drop in viral titer or infectivity.
19. Typical titers obtained from a single flask AAV production from supernatant plus cells ranged from 7.3×10^{11} to 7.7×10^{12} vg/mL. The average titer±the standard error of the mean (SEM) obtained from 16 single flask preparations was $3.2 \times 10^{12} \pm 6.0 \times 10^{11}$ vg/mL. The average volume of rAAV concentrate±SEM from these 16 single flask preparations was 107 ± 2.4 µL. In practice, 100 µL of viral inoculum can be managed to enable approximately 100 E12.5 otocyst injections.

Acknowledgements

We thank the members of the Molecular Virology Support Core (MVSC) laboratory for their support, in particular Dr. Don Siess for his technical insights. Research funding for the development of AAV preparation methods was provided by NIH P51 center grant OD011092 to the Oregon National Primate Research Center. The Brigande lab gratefully acknowledges funding from the National Institute on Deafness and other Communication Disorders: R01DC008595, R01DC014160, and R21DC012916 (JVB); P30DC005983 (Oregon Hearing Research Center); and the Hearing Health Foundation through the Hearing Restoration Project.

References

1. Brigande JV, Gubbels SP, Woessner DW, Jungwirth JJ, Bresce CS (2009) Electroporation-mediated gene transfer to the developing mouse inner ear. *Methods Mol Biol* 493:125–139
2. Berns KI (1990) Parvovirus replication. *Microbiol Rev* 54(3):316–329
3. Grimm D, Kleinschmidt JA (1999) Progress in adeno-associated virus type 2 vector production: promises and prospects for clinical use. *Hum Gene Ther* 10(15):2445–2450
4. Jooss K, Yang Y, Fisher KJ, Wilson JM (1998) Transduction of dendritic cells by DNA viral vectors directs the immune response to transgene products in muscle fibers. *J Virol* 72(5):4212–4223
5. Wu Z, Asokan A, Samulski RJ (2006) Adeno-associated virus serotypes: vector toolkit for human gene therapy. *Mol Ther* 14(3):316–327
6. Bedrosian JC, Gratton MA, Brigande JV, Tang W, Landau J, Bennett J (2006) In vivo delivery of recombinant viruses to the fetal murine cochlea: transduction characteristics and long-term effects on auditory function. *Mol Ther* 14(3):328–335
7. Lock M, Alvira M, Vandenbergh LH, Samanta A, Toelen J, Debysier Z, Wilson JM (2010) Rapid, simple, and versatile manufacturing of recombinant adeno-associated viral vectors at scale. *Hum Gene Ther* 21(10):1259–1271
8. Huang X, Hartley AV, Yin Y, Herskowitz JH, Lah JJ, Ressler KJ (2013) AAV2 production with optimized N/P ratio and PEI-mediated transfection results in low toxicity and high titer for *in vitro* and *in vivo* applications. *J Virol Meth* 193(2):270–277
9. Wang L, Jiang H, Brigande JV (2012) Gene transfer to the developing mouse inner ear by *in vivo* electroporation. *J Vis Exp* (64). doi: [10.3791/3653](https://doi.org/10.3791/3653)
10. Rohr UP, Wulf MA, Stahn S, Steidl U, Haas R, Kronenwett R (2002) Fast and reliable titration of recombinant adeno-associated virus type-2 using quantitative real-time PCR. *J Virol Methods* 106(1):81–88
11. Transcript of OLAW On-line Seminar broadcast on March 1, 2012—Use of non-pharmaceutical grade chemicals and other substances in research with animals (v4/17/2013)
12. Grimm D, Kern A, Rittner K, Kleinschmidt JA (1998) Novel tools for production and purification of recombinant adenoassociated virus vectors. *Hum Gene Ther* 9(18):2745–2760
13. Matsushita T, Elliger S, Elliger C, Podsakoff G, Villarreal L, Kurtzman GJ, Iwaki Y, Colosi P (1998) Adeno-associated virus vectors can be efficiently produced without helper virus. *Gene Ther* 5(7):938–945
14. Xiao X, Li J, Samulski RJ (1998) Production of high-titer recombinant adeno-associated virus vectors in the absence of helper adenovirus. *J Virol* 72(3):2224–2232
15. Reed SE, Staley EM, Mayginnis JP, Pintel DJ, Tullis GE (2006) Transfection of mammalian cells using linear polyethylenimine is a simple and effective means of producing recombinant adeno-associated virus vectors. *J Virol Methods* 138(1–2):85–98
16. Vandenbergh LH, Xiao R, Lock M, Lin J, Korn M, Wilson JM (2010) Efficient serotype-dependent release of functional vector into the culture medium during adeno-associated virus manufacturing. *Hum Gene Ther* 21(10):1251–1257
17. Gubbels SP, Woessner DW, Mitchell JC, Ricci AJ, Brigande JV (2008) Functional auditory hair cells produced in the mammalian cochlea by *in utero* gene transfer. *Nature* 455(7212):537–541

Chapter 4

Generation of Noninvasive, Quantifiable, Orthotopic Animal Models for NF2-Associated Schwannoma and Meningioma

Sarah S. Burns and Long-Sheng Chang

Abstract

Schwannomas and meningiomas are nervous system tumors that can occur sporadically or in patients with neurofibromatosis type 2 (NF2). Mutations of the *Neurofibromatosis 2 (NF2)* gene are frequently observed in these tumors. Schwannomas and meningiomas cause significant morbidities, and an FDA-approved medical therapy is currently not available. The development of preclinical animal models that accurately capture the clinical characteristics of these tumors will facilitate the evaluation of novel therapeutic agents for the treatment of these tumors, ultimately leading to more productive clinical trials. Here, we describe the generation of luciferase-expressing *NF2*-deficient schwannoma and meningioma cells and the use of these cells to establish orthotopic tumor models in immunodeficient mice. The growth of these tumors and their response to treatment can be measured effectively by bioluminescence imaging (BLI) and confirmed by small-animal magnetic resonance imaging (MRI). These and other animal models, such as genetically-engineered models, should substantially advance the investigation of promising therapies for schwannomas and meningiomas.

Key words Vestibular schwannoma, Meningioma, Neurofibromatosis type 2 (NF2), *Neurofibromatosis 2 (NF2)* gene, Xenograft, Allograft, Severe combined immunodeficiency (SCID) mice, Intranerve, Stereotactic, Bioluminescence imaging (BLI), Magnetic resonance imaging (MRI)

1 Introduction

Vestibular schwannomas (VS) are tumors originating from Schwann cells covering the vestibular branch of the 8th cranial nerve. These tumors are often slow-growing and can occur sporadically or in association with neurofibromatosis type II (NF2; OMIM #101000), a highly penetrant, autosomal-dominant genetic disorder [1]. Nearly all NF2 patients develop bilateral VS, and up to 60 % of these patients develop meningiomas. Other disease features include ependymomas, spinal schwannomas, astrocytomas, and presenile lens opacities. Patients with VS usually present with tinnitus, hearing loss, and imbalance. These tumors can lead to deafness, facial nerve paralysis, brainstem compression, hydrocephalus, and death, if left untreated.

Meningiomas are derived from cells of the meninges lining the brain. About 80 % of meningiomas are benign (WHO grade I), whereas the remaining are atypical (grade II) and anaplastic (grade III) [2]. These tumors cause significant morbidity, including cranial nerve palsy, seizures, and brainstem compression, which may lead to paralysis, aspiration pneumonia, and death. Approximately 20 % of benign meningiomas recur over ten years, while grade II and grade III tumors possess greater rates of recurrence. Meningiomas in NF2 patients are associated with disease severity and increased risk of mortality [3, 4].

Currently, an FDA (U.S. Food and Drug Administration)-approved drug is not available for the treatment of VS and meningiomas. Treatment options for these tumors are presently limited to observation, surgical removal, and stereotactic radiation [1]. However, surgery may not be possible if the tumor is inaccessible or when there are too many tumors. Radiation treatment may cause malignant transformation and/or growth acceleration of benign tumor cells. In addition, preservation of hearing and balance along with the facial nerve and lower cranial nerves for swallowing and airway protection are often not achieved with current methods. Together, these factors underscore the importance of developing effective medical therapies that stop tumor growth.

Evaluation of potential novel therapeutic agents requires animal models that accurately reflect disease characteristics. Most, if not all, of NF2-associated VS and the more common sporadic unilateral schwannomas harbor mutations in the *Neurofibromatosis 2* (*NF2*) tumor suppressor gene [5, 6]. Additionally, *NF2* mutations are found in most NF2-associated meningiomas and about 50–60 % of sporadic meningiomas [4, 7, 8]. To address the tumor suppressor role of merlin, mice that lack *Nf2* function in Schwann or meningeal cells have been generated and develop schwannomas and meningiomas, respectively [9–11]. These genetically engineered mouse (GEM) models have been used in therapeutic evaluation; however, tumor latency, penetrance, and detection in these GEM models are important considerations. Also, xenograft models in severe combined immunodeficiency (SCID) mice implanted with VS specimens have been established, but the tumors do not exhibit consistent growth [12, 13]. Thus, additional models that closely mimic the clinical presentation of *NF2*-deficient benign schwannomas and meningiomas and that facilitate efficient quantitation of tumor growth will further enhance therapeutic testing.

Accurate measurement of tumor size and longitudinal monitoring of tumor growth are critical in evaluating drug responses. Magnetic resonance imaging (MRI) has been the gold standard for evaluating NF2-associated tumors *in situ* [14]. Likewise, small-animal MRI has been used to noninvasively monitor tumor growth in mouse models. To facilitate longitudinal monitoring of

drug response, bioluminescence imaging (BLI) has significantly advanced the ability to quantitate tumor growth in animal models and is particularly valuable for intracranial tumors whose growth cannot be monitored externally [15]. Here, we describe the use of luciferase-expressing schwannoma and meningioma cells to generate orthotopic animal models. Tumor growth in these models can be quantified over time by BLI and confirmed by MRI.

2 Materials

2.1 Cell Culture

1. Dulbecco's modified Eagle (DME) and DME/F-12 (v/v) media (Life Technologies, Grand Island, NY) are supplemented with 10 % fetal bovine serum (FBS).
2. 100× Penicillin/Streptomycin stock solution: Mix 5000 units/ml penicillin G sodium and 5000 µg/ml streptomycin sulfate in 0.85 % saline (*see Note 1*).
3. Phosphate-buffered saline (PBS) without Ca²⁺/Mg²⁺: 137 mM NaCl, 2.7 mM KCl, 10 mM Na₂HPO₄, and 1.8 mM KH₂PO₄, pH 7.4.
4. Tris-buffered saline (TBS): 50 mM Tris-HCl, pH 7.4 and 150 mM NaCl.
5. Trypsin solution: 0.25 % trypsin-0.53 mM EDTA in Hanks' Balanced Salt Solution (HBSS).
6. Reconstitute recombinant human neuregulin-β1/hereregulin-β1 epidermal growth factor domain (rhuHRG-β1) in PBS, aliquot in small volumes, and store at -80 °C.
7. Forskolin stock solution: Prepare 5 mM forskolin in dimethyl sulfoxide (DMSO), sterilize using a 0.2-µm filter, aliquot, and store at -20 °C. HRG-β1 and forskolin are freshly added to culture medium (*see Subheading 3.1, step 1*).
8. 100× Poly-L-lysine or Poly-D-lysine (molecular weight 75–150 kDa) stock solution: Prepare 5 mg/ml in TBS and store at 4 °C.
9. 250× Laminin stock: Purchased as 1 mg/ml solution from, e.g., Sigma and stored at -80 °C.
10. *Nf2*^{P0} (*P0Cre;Nf2*^{fl/fl}) schwannoma cells.
11. *Nf2*^{P0} schwannoma cell culture medium: DME/F-12 medium supplemented with 10 % FBS, 10 ng/ml HRG-β1, and 2 µM forskolin.
12. *NF2*-deficient benign human meningioma cell line Ben-Men-1.
13. Ben-Men-1 culture medium: Supplement DME medium with 10 % FBS.

2.2 Lentiviral Transduction and Isolation of Luciferase-Expressing Clones

1. Lenti-CMV-Luc lentiviruses containing a cytomegalovirus (CMV) promoter-driven luciferase-expression unit and a puromycin-resistance gene (Qiagen, Germantown, MD).
2. 10,000× Polybrene (hexadimethrine bromide; Sigma-Aldrich) solution: Prepare polybrene by dissolving 80 mg in 1 ml of H₂O, sterilize by filtration, and store at 4 °C (*see Note 5*).
3. Puromycin dihydrochloride stock solution: Prepare a 5 mg/ml solution in DME medium, sterilize by filtration, aliquot, and store at -20 °C (*see Subheading 3.2, step 5*).
4. Cloning cylinders (Bellco Glass, Vineland, NJ) are used to isolate individual puromycin-resistant colonies.
5. The Protein Assay Dye Reagent Concentrate (Bio-Rad, Hercules, CA) is diluted five-fold prior to protein concentration measurements (*see Subheading 3.2, step 7*).
6. The Luciferase Reporter Assay System (Promega, Madison, WI) is used according to the manufacturer's instruction.
7. A SpectraMax microplate reader (Molecular Devices, Sunnyvale, CA) is used to detect luciferase activity in cultured cells (*see Subheading 3.2, step 8*).

2.3 Mice and Tumor Cell Injection

1. SCID C.B17 mice are purchased from a certified vendor, such as The Jackson Laboratory, Charles River Laboratories, and Taconic Biosciences (*see Subheadings 3.3 and 3.4, step 3*).
2. PROTEXIS sterile powder-free surgical gloves, Curity™ gauze sponges, Webcol™ alcohol prep, and Duo-Swab® Povidone-Iodine Cleansing Scrub and Prep Swabsticks.
3. Isoflurane (Forane) and an Inhalation Anesthesia System and Vapor Guard activated charcoal adsorption filters (VET Equip® Instrument, Livermore, CA).
4. Fine surgical instruments, including iris scissors, forceps, scalpels, blades, and a high-speed micro drill with carbon steel burrs (0.5 mm diameter) (Fine Science Tools, Foster City, CA).
5. A Mini ARCO hair clipper (Wahl Clipper Corp, Sterling, IL).
6. A model 940 small-animal stereotaxic instrument with a BENCHMark™ 3-axes digital counter display (Leica Biosystems, Inc., Buffalo Grove, IL) equipped with an inhalation anesthesia system (VET Equip® Instrument) and a KDS310 Nano single syringe infusion/withdraw pump (KD Scientific, Holliston, MA).
7. Hamilton Neuros™ 10 µl syringes with removable 33-gauge or 26-gauge needles are used for intranerve or intracranial injection, respectively.
8. An OPMI Pro Magis surgical microscope (Carl Zeiss Microscopy, LLC, Thornwood, NY).

9. Vetbond™ tissue adhesive (3M, St. Paul, MN).
10. Small-animal thermo-controlled recovery pads, to enhance post-surgical recovery.

2.4 Bioluminescence Imaging

1. D-luciferin potassium stock: D-luciferin potassium salt (Gold Biotechnology, St. Louis, MO) is dissolved as a 15 mg/ml stock in PBS. The stock solution should be sterilized by filtration. Alternatively, a ready-to-inject solution of D-luciferin (Xenolight RediInject; Perkin Elmer, Waltham, MA) is also available (*see Subheading 3.5, step 1*).
2. Insulin syringes with 28-gauge needles are used for luciferin injection into mice.
3. An IVIS Spectrum Preclinical In Vivo Imaging System and Living Image® software (Perkin Elmer) (*see Subheading 3.5, step 4*).
4. Isoflurane (Forane) is used to anesthetize mice throughout the imaging process.

3 Methods

Orthotopic animal models of tumors are essential tools in evaluating the safety and efficacy of potential therapeutics. These models can complement cell culture models by providing the native environment for tumor growth on the organismal level. In addition, they facilitate assessment of drug distribution and the ability of a drug to reach the tumor tissue and to inhibit target molecules. Effective animal models accurately recapitulate the specific features of the human tumors. As benign schwannomas and meningiomas tend to be slow-growing, an ideal animal model for these tumors would incorporate this growth characteristic. We discuss approaches for generating orthotopic, quantifiable schwannoma allograft and meningioma xenograft models, which can be used to evaluate potential therapeutic agents.

3.1 Schwannoma and Meningioma Cell Cultures

1. Dissect and use schwannomas developed in *P0Cre;Nf2^{flax/flax}* (*Nf2^{P0}*) mice with conditional *Nf2* inactivation in Schwann cells [9] to prepare schwannoma cell cultures as described previously [16].
2. Grow *Nf2^{P0}* schwannoma cells in DME/F-12 (*see Subheading 2.1, step 5*) and plate on dishes coated with polylysine and laminin.
3. Confirm *Nf2/Merlin* status of these schwannomas by PCR genotyping and Western blotting [16, 17] (*see Note 2*).
4. Grow *NF2*-deficient benign human meningioma cell line Ben-Me-1 in DME medium supplemented with 10 % FBS on non-coated dishes [18, 19] (*see Note 3*).

3.2 Generation of Luciferase-Expressing Sch10545-Luc Schwannoma and Ben-Men-1-LucB Meningioma Cells

1. Trypsinize and plate Sch10545 schwannoma (derived from an *Nf2^{P0}* mouse) and Ben-Men-1 meningioma cells in fresh growth medium so that they will be about 25–50 % confluent by the next day. An extra dish of cells is plated at the same dilution to determine the number of cells in the dish.
2. The next day, trypsinize and count cells in the extra dish to determine the amount of lentivirus needed for infection (*see Note 4*). We usually infect Sch10545 or Ben-Men-1 cells with Lenti-CMV-Luc lentiviruses at a multiplicity of infection (MOI) of 1 to 10 (*see Note 5*). The MOI is defined as the number of infectious viral particles per cell (*see Note 6*).
3. For lentiviral transduction, remove medium from the dish. Based on the number of cells determined, mix an appropriate amount of lentiviruses with growth media supplemented with 8 µg/ml of polybrene and add to the cells. Incubate dish at 37 °C from 4 h to overnight (*see Note 7*).
4. Change media the next day following transduction and incubate the transduced dish at 37 °C for another day.
5. Two days after transduction, add puromycin to the cells to a final concentration of 2 µg/ml and replenish the growth medium containing puromycin every 3 days until puromycin-resistant colonies are visible (*see Note 8*)
6. Isolate individual puromycin-resistant colonies using cloning cylinders and expand in separate dishes containing growth medium and puromycin (*see Note 9*).
7. Trypsinize cells when dishes containing individual puromycin-resistant clones approach confluence. Expand half of the cells from each clone into a new dish to continue propagating as a stock. Wash the other half of the cells with PBS 2× and lyse in the Luciferase Reporter Lysis Buffer (Subheading 2.2, step 6). To determine the protein concentration, mix 2 µl of each clear lysate with 1 ml of diluted Bio-Rad Protein Assay Dye Reagent (*see Subheading 2.2, step 5*) and measure the absorbance at a wavelength of 595 nm. Generate a standard curve for protein concentration by measuring the absorbance of a series of standards with known amounts of protein at 595 nm and use these data to extrapolate each sample's protein concentration.
8. Measure luciferase activity by using equal amounts of proteins from each lysate (10 µg) using a Promega Luciferase Assay Kit and a microplate reader, according to the manufacturer's instructions. Inject clones expressing robust luciferase activity (e.g., Sch10545-Luc and Ben-Men-1-LucB) into mice to generate luciferase-expressing schwannoma allograft and meningioma xenograft tumors as described in the following sections.

3.3 Intranerve Injection of Luciferase-Expressing Mouse Nf2^{-/-} Schwannoma Cells into the Nerves of SCID Mice

1. Acquire approval from the institutional animal care and use committee (IACUC) prior to initiating any studies involving animals.
2. Trypsinize and count actively-growing, luciferase-expressing Sch10545-Luc schwannoma cells. Wash in PBS 2× and spin down at $2000 \times g$ for 30 s in an Eppendorf microfuge. Resuspend cell pellet in an appropriate volume of PBS and place on ice until injection. To establish schwannoma allografts, inject $\sim 10^5$ Sch10545-Luc cells in 3 μ l of PBS per mouse.
3. To perform intranerve injections, anesthetize an 8-to-10-month-old SCID mouse (*see Note 10*) using 5 % isoflurane in oxygen in an induction chamber until it is under deep anesthesia and does not respond to toe pinches. The induction chamber is connected to an Inhalation Anesthesia System to regulate isoflurane flow rate and to a Vapor Guard activated charcoal adsorption filter to capture the waste gas.
4. Once anesthetized, place the mouse on its stomach with its hind legs outstretched on a clean surgical platform. To maintain anesthesia during surgery, place a nose cone connected to an Inhalation Anesthesia System on the nose to continue administering isoflurane gas. Use a mini-hair clipper to remove hair from the right (or left) thigh and hind leg area, since only one sciatic nerve is injected with cells (*see Note 11*).
5. Disinfect the surgical site with a Povidone-Iodine Cleansing Scrub Swabstick and then with a Povidone-Iodine Antiseptic Prep Swabstick. Make a small incision (~1 cm) in the skin of the flank just below and parallel to the femur. Use scissors to separate the skin from the muscle of the leg. To expose the sciatic nerve, blunt dissect through the biceps femoris muscle using a pair of sharp scissors. The sciatic nerve should appear as a white fascicle of nerve fibers extending parallel to the femur.
6. To access the sciatic nerve for intranerve injection, insert a pair of fine forceps underneath the nerve to gently elevate and stabilize the nerve above the muscle. Load 3 μ l of the Sch10545-Luc cell suspension in a Hamilton Neuros™ 10 μ l syringe with a 33-gauge needle. To inject the cells, the needle of the Neuros™ syringe should be carefully inserted into the nerve by positioning the needle along the nerve. Gradually inject the contents of the syringe into the nerve, while holding the needle steady.
7. Once the syringe is empty, remove the needle slowly and place the nerve back into its original position beneath the muscle. Close and seal the incision using Vettbond™ tissue adhesive. Give the mouse a dose of buprenorphine (0.05 mg/kg) subcutaneously as an analgesic, remove the isoflurane nose cone, and place the animal on a thermo-controlled recovery pad until fully recovered and ambulatory.

**3.4 Stereotactic
Injection
of Luciferase-
Expressing NF2-
Deficient Benign
Meningioma Cells
to the Skull Base
of SCID Mice**

1. As in Subheading 3.3, all animal experiments should be approved by the IACUC before initiating any studies.
2. Harvest actively-growing, luciferase-expressing Ben-Men-1-LucB for injection as described in Subheading 3.3, step 2. We find that injection of approximately 10^6 cells suspended in 5 μ l of PBS per mouse results in reproducible establishment of intracranial tumors.
3. As in Subheading 3.3, step 3, anesthetize 8–12-month-old SCID mice using 5 % isoflurane in oxygen until they are under deep anesthesia and do not respond to toe pinches.
4. Stabilize the anesthetized mouse on a secure platform and position in a small-animal stereotaxic device using a nose cone connected to an Inhalation Anesthesia System. Insert the ear pins carefully into the ear canals. When positioned properly, the head of the mouse is immobilized to minimize movement of the head during stereotactic injection.
5. Remove the hair on the top of the head using a pair of iris scissors and cleanse the surface area of the head from the nose to the back of the skull with Duo-Swab® Povidone-Iodine Cleansing Scrub and Antiseptic Prep Swabsticks. Using a scalpel with a No. 10 surgical blade, make a longitudinal midline incision from the forehead to the back of the skull. Use a sterile cotton-tipped applicator to stabilize the skin to facilitate the incision. Gently push scalp skin to the sides so that an area of the skull is exposed from the bregma, which is located near the middle of the skull, to the eyes. The bregma is a juncture in the cranial plates, where the coronal suture intersects perpendicularly to the sagittal suture.
6. Stabilize a 26-gauge needle attached to a Neuros™ 10 μ l syringe filled with 5 μ l of cell suspension, containing $\sim 1 \times 10^6$ Ben-Men-1-LucB cells, in the stereotactic device and position it above the bregma. An OPMI Pro Magis surgical microscope is helpful in visualizing the bregma.
7. After the needle of the syringe is positioned directly above the bregma, set each of the stereotactic coordinates to zero. Then, using the stereotactic axes, move the syringe 1.5 mm anterior to the bregma and 1.5 mm lateral to the right of the bregma. Make a small burr hole at this location using a high-speed micro drill.
8. Once the drill has completely penetrated the skull so that the brain is exposed, lower the syringe until the tip of the needle is at the surface of the brain. Prior to inserting the needle into the brain, set the coordinate of the Z-axis to zero, and confirm coordinates for the X- and Y-axes (1.5 mm anterior and 1.5 mm lateral to the right of the bregma).

9. Once positioned, lower the needle slowly 4.5 mm into the brain to the skull base (*see Note 12*).
10. Using an automatic injector, inject tumor cells into the skull base at a rate of 1.5 ml/min. After the cells have been completely dispensed, maintain the needle in place for one minute to permit the injected cells to settle, followed by slowly withdrawing the needle from the brain.
11. Using a pair of forceps, close the surgical incision with Vetbond tissue adhesive.
12. As in Subheading 3.3, step 7, inject a dose of buprenorphine (0.05 mg/kg) subcutaneously near the surgical site as an analgesic. Remove the mouse from the stereotactic device and place on a thermo-controlled recovery pad until full recovery.

3.5 Monitoring Growth of Schwannoma Allografts and Meningioma Xenografts by BLI

1. BLI is used to assess successful tumor engraftment and growth. Prior to imaging, inject mice, implanted with Sch10545-Luc or Ben-Men-1-LucB cells, intraperitoneally with 150 mg/kg of d-luciferin (*see Note 11*).
2. As in Subheadings 3.3 and 3.4, steps 3, anesthetize mice using 5 % isoflurane in oxygen. Place the anesthetized mouse in the IVIS Spectrum Preclinical In Vivo Imaging System and position the nose in the nose cone for isoflurane gas administration during imaging.
3. Capture bioluminescent images of tumor-bearing mice at the peak time of luciferase activity following injection of d-luciferin (*see Note 13*).
4. Using BLI, tumor growth is measured noninvasively over time. The intensity of the BL signal correlates with changes in tumor size and is measured in each mouse using region-of-interest analysis in the LivingImage software (*see Note 14*). To determine tumor establishment and growth prior to treatment, at least two bioluminescent images should exhibit robust and increasing signals. We have found that tumor growth in the Sch10545-Luc schwannoma allograft model is effectively detected over one-week time intervals, whereas growth in the Ben-Men-1-LucB meningioma xenograft model is best observed over 1-month intervals.
5. To assess the efficacy of a particular therapeutic agent, compare the intensity of the BL signal (*see Note 15*) and its changes over time among animals treated with a therapeutic agent and untreated controls (*see Note 16*). Treatment responses can be confirmed by small-animal MRI [12, 19].

4 Notes

1. Antibiotics, such as penicillin and streptomycin, are used to reduce contamination, particularly during preparation of primary cultures of VS and meningioma cells. The details regarding preparation of these primary tumor cell cultures have been described previously [16]. However, we try to avoid using antibiotics, whenever it is possible, e.g., culturing established cell lines.
2. To generate an *Nf2*-deficient schwannoma cell line, schwannoma cells from *Nf2^{P0}* mice were cultured for more than 25 passages and subcloned. We isolated a clone, designated Sch10545, which exhibits continuous growth. Loss of the *Nf2* gene in these cells was confirmed by PCR genotyping and Western blotting [16, 17]. Interestingly, these cells are no longer dependent on HRG and can grow in medium supplemented with 10 % FBS.
3. The benign human meningioma cell line Ben-Men-1 was established from a grade I meningioma by telomerase immortalization [18]. By Western blotting and DNA sequencing, we previously showed that Ben-Men-1 cells are Merlin-deficient [19].
4. Lentiviral vectors, such as Lenti-CMV-Luc, are considered Biosafety Level 2 (BSL-2) agents. Although they are replication-deficient, all handling and storage of lentiviral vectors and disposal of contaminated waste must be conducted according to institutional rules and regulations and NIH guidelines. Lentiviral vectors should be aliquoted in small amounts and stored at -80 °C. Repeated freeze-thawing will decrease the viral titer.
5. Other optimized firefly luciferase expression vectors [20–22] can be used, as well as luciferase-expressing vectors from other species [23, 24].
6. The optimal MOI is dependent on the target cell type and should be titrated to enhance viral gene delivery. Infection time may be decreased, or purified viral particles are used if viral toxicity is observed in the cell line of interest, particularly when using viral supernatant.
7. Polybrene is a cation polymer that can enhance retroviral or lentiviral transduction efficiency, by neutralizing the charge repulsion between viral particles and sialic acid moieties on the cell surface [25]. However, polybrene may be toxic to some cell lines, calling for a shorter incubation time. Alternatively, protamine sulfate [26] or other reagent systems, such as ViraDuctin™ or Sigma's ExpressMag bead system, are used to increase the efficiency of viral infection.

8. The optimal concentration of puromycin for the selection of puromycin-resistant clones should be determined in advance. For this purpose, we usually use the minimal concentration of puromycin that is sufficient to kill all non-transduced cells. Puromycin should be added 24 h after infection to allow for sufficient expression of the puromycin-resistant gene.
9. Different sizes of cloning cylinders can be purchased and used to isolate individual puromycin-resistant colonies. Alternatively, dilution cloning can be performed using 96-well plates. Also, it is possible to plate cells at a low density and directly select individual puromycin-resistant colonies in 96-well plates 24 h or more after lentiviral transduction.
10. For engraftment of schwannoma and meningioma cells, we routinely use the *scid* strain of immunodeficient mice, which carry the defective DNA-activated protein kinase *Prkdc*, important for the rearrangement of the immunoglobulin and T-cell receptor genes [27]. Other immunodeficient mouse strains, such as nonobese diabetic (NOD)-*scid* $\beta 2m$ null and NOD-*scid IL2Rynull (also called NSG or NOD *scid* gamma), may be considered as they give rise to more rapid tumor engraftment in some tumor models [28, 29]. Due to the $\beta 2m$ null mutation, NOD-*scid* $\beta 2m$ null mice are deficient in MHC class I expression, and their natural killer (NK) cells are unable to kill susceptible targets upon activation [30]. The NOD-*scid IL2Rynull strain harbors a mutation in *IL2Ry*, which encodes the cytokine-receptor γ -chain shared by IL-2, IL-4, IL-7, IL-9, IL-15, and IL-21 receptors, and exhibits impaired NK cell development [31].**
11. It can be helpful to stabilize mouse legs by taping their toes to the platform during surgery. The sciatic nerve can be accessed from either the dorsal or ventral sides of the mouse. It is preferable to graft only one sciatic nerve in each mouse as grafting both nerves will lead to impaired function of both hind legs due to tumor growth, resulting in early removal of mice from the study.
12. The depth to which the needle needs to be lowered to reach the skull base may vary slightly, depending on the age of the mice. Using 8-to-12-week-old mice, a depth of 4.5 mm is a useful guideline for skull base injection.
13. The sensitivity with which tumors are measured depends on the level of luciferase expression in the clones. Stronger luciferase activity yields a strong BL signal for a smaller number of cells, enabling the detection of fewer cells in a tumor. D-luciferin is commonly used for BLI in mice. Recently, a synthetic luciferin, the cyclic alkylaminoluciferin (CycLuc1), was shown to exhibit improved light output and to enhance BL detection in deep tissues, such as the brain [32].

14. The kinetics of luciferin circulation and uptake by tumor cells may vary in different models. To facilitate accurate quantitation of tumor growth, measurements are performed when luciferase activity is highest. This peak time is determined by measuring in vivo luciferase activity at various time intervals after d-luciferin injection. All subsequent bioluminescence measurements should be performed at this time interval.
15. As a sensitive and efficient way to noninvasively monitor tumor growth, BLI facilitates longitudinal studies, particularly for benign tumors [19]. Studies suggest that BL signals detected in luciferase-expressing tumors correlate with tumor size detected by MRI. BLI and MRI complement each other well by quantifying viable tumor cells and measuring the volume of the tumor mass by clinical standards, respectively.
16. Recently, interest is gaining in orthotopic patient-derived xenografts (PDX) as preclinical models for drug screening and development [33]. Loss of the *NF2* gene product Merlin leads to deregulation of multiple signaling pathways, such as the mitogen-activated protein kinase (MAPK) and PI3K/AKT/mTOR pathways, which may serve as viable therapeutic targets [1]. Study of these pathways has led to the initiation of several clinical trials. These schwannoma and meningioma animal models should enhance evaluation of additional novel therapeutic compounds.

Acknowledgments

The authors would like to thank Dr. D. Bradley Welling for discussion. This work was supported by grants from the Department of Defense, Children's Tumor Foundation, Advocure NF2, Meningioma Mommas, and the Galloway Family.

References

1. Yates C, Welling DB, Chang L-S (2011) Research advances in therapeutics for neurofibromatosis type 2-associated vestibular schwannomas. In: Cunha KS, Geller M (eds) Advances in neurofibromatosis research. Nova Science Publishers, Inc., Hauppauge, NY
2. Wiemels J, Wrensch M, Claus EB (2010) Epidemiology and etiology of meningioma. *J Neurooncol* 99:307–314
3. Baser ME, Friedman JM, Aeschliman D, Joe H, Wallace AJ, Ramsden RT, Evans DG (2002) Predictors of the risk of mortality in neurofibromatosis 2. *Am J Hum Genet* 71:715–723
4. Goutagny S, Kalamarides M (2010) Meningiomas and neurofibromatosis. *J Neurooncol* 99:341–347
5. Rouleau GA, Merel P, Lutchman M et al (1993) Alteration in a new gene encoding a putative membrane-organising protein causes neurofibromatosis type 2. *Nature* 363:515–521
6. Trofatter JA, MacCollin MM, Rutter JL et al (1993) A novel Moesin-, Exrin-, Radixin-like gene is a candidate for the neurofibromatosis 2 tumor-suppressor. *Cell* 72:791–800
7. Bianchi AB, Hara T, Ramesh V et al (1994) Mutations in transcript isoforms of the neurofibromatosis 2 gene in multiple human tumour types. *Nat Genet* 6:185–192
8. Bianchi AB, Mitsunaga SI, Cheng JQ, Klein WM, Jhanwar SC, Seizinger B, Kley N, Klein-Szanto AJ, Testa JR (1995) High frequency of inactivating mutations in the neurofibromatosis

- type 2 gene (*NF2*) in primary malignant mesotheliomas. *Proc Natl Acad Sci U S A* 92:10854–10858
- 9. Giovannini M, Robanus-Maandag E, van der Valk M, Niwa-Kawakita M et al (2000) Conditional biallelic *Nf2* mutation in the mouse promotes manifestations of human neurofibromatosis type 2. *Genes Dev* 14:1617–1630
 - 10. Kalamardes M, Stemmer-Rachamimov AO, Niwa-Kawakita M, Chareyre F, Taranchon E, Han ZY, Martinelli C, Lusis EA, Hegedus B, Gutmann DH, Giovannini M (2011) Identification of a progenitor cell of origin capable of generating diverse meningioma histological subtypes. *Oncogene* 30:2333–2344
 - 11. Gehlhausen JR, Park SJ, Hickox AE et al (2015) A murine model of neurofibromatosis type 2 that accurately phenocopies human schwannoma formation. *Hum Mol Genet* 24:1–8
 - 12. Chang L-S, Jacob A, Lorenz M, Rock J et al (2006) Growth of benign and malignant schwannoma xenografts in severe combined immunodeficiency mice. *Laryngoscope* 116:2018–2026
 - 13. Neff BA, Voss SG, Allen C, Schroeder MA, Driscoll CL, Link MJ, Galanis E, Sarkaria JN (2009) Bioluminescent imaging of intracranial vestibular schwannoma xenografts in NOD/SCID mice. *Otol Neurotol* 30:105–111
 - 14. Lin AL, Gutmann DH (2013) Advances in the treatment of neurofibromatosis-associated tumours. *Nat Rev Clin Oncol* 10:616–624
 - 15. Wang Y, Tseng JC, Sun Y, Beck AH, Kung AL (2015) Noninvasive imaging of tumor burden and molecular pathways in mouse models of cancer. *Cold Spring Harb Protoc* 2015:135–144
 - 16. Chang L-S, Welling DB (2009) Molecular biology of vestibular schwannomas. In: Sokolowski B (ed) Auditory/vestibular research, The Humana Press, Totowa, NJ, *Methods Mol Biol* 493:163–177
 - 17. Spear SA, Burns SS, Oblinger JL, Ren Y, Pan L, Kinghorn AD, Welling DB, Chang L-S (2013) Natural compounds as potential treatments of *NF2*-deficient schwannoma and meningioma: cucurbitacin D and goyazensolide. *Otol Neurotol* 34:1519–1527
 - 18. Püttmann S, Senner V, Braune V, Hillmann B, Exeler R, Rickert C et al (2005) Establishment of a benign meningioma cell line by hTERT-mediated immortalization. *Lab Invest* 85: 1163–1171
 - 19. Burns SS, Akhmetiyeva EA, Oblinger JL, Bush ML, Huang J, Senner V, Chen C-S, Jacob A, Welling DB, Chang L-S (2013) AR-42, a histone deacetylase inhibitor, differentially affects cell-cycle progression of meningeal and meningioma cells and potently inhibits *NF2*-meningioma growth. *Cancer Res* 73:792–803
 - 20. Rabinovich BA, Ye Y, Etto T, Chen JQ, Levitsky HI, Overwijk WW, Cooper LJ, Gelovani J, Hwu P (2008) Visualizing fewer than 10 mouse T cells with an enhanced firefly luciferase in immunocompetent mouse models of cancer. *Proc Natl Acad Sci U S A* 105:14342–14346
 - 21. Kim JB, Urban K, Cochran E, Lee S, Ang A, Rice B, Bata A, Campbell K, Coffee R, Gorodinsky A, Lu Z, Zhou H, Kishimoto TK, Lassota P (2010) Non-invasive detection of a small number of bioluminescent cancer cells *in vivo*. *PLoS One* 5:e9364
 - 22. Harwood KR, Mofford DM, Reddy GR, Miller SC (2011) Identification of mutant firefly luciferases that efficiently utilize aminoluciferins. *Chem Biol* 18:1649–1657
 - 23. Prescher JA, Contag CH (2010) Guided by the light: visualizing biomolecular processes in living animals with bioluminescence. *Curr Opin Chem Biol* 14:80–89
 - 24. Mezzanotte L, Fazzina R, Michelini E, Tonelli R, Pession A, Branchini B, Roda A (2010) *In vivo* bioluminescence imaging of murine xenograft cancer models with a red-shifted thermostable luciferase. *Mol Imaging Biol* 12: 406–414
 - 25. Davis HE, Morgan JR, Yarmush ML (2002) Polybrene increases retrovirus gene transfer efficiency by enhancing receptor-independent virus adsorption on target cell membranes. *Biophys Chem* 97:159–172
 - 26. Cornetta K, Anderson WF (1989) Protamine sulfate as an effective alternative to polybrene in retroviral-mediated gene-transfer: implications for human gene therapy. *J Virol Methods* 23:187–194
 - 27. Shultz LD, Ishikawa F, Greiner DL (2007) Humanized mice in translational biomedical research. *Nat Rev Immunol* 7:118–130
 - 28. Ito M, Hiramatsu H, Kobayashi K et al (2002) NOD/SCID/ γ cnull mouse: an excellent recipient mouse model for engraftment of human cells. *Blood* 100:3175–3182
 - 29. Carreno BM, Garbow JR, Kolar GR, Jackson EN, Engelbach JA, Becker-Hapak M, Carayannopoulos LN, Piwnica-Worms D, Linette GP (2009) Immunodeficient mouse strains display marked variability in growth of human melanoma lung metastases. *Clin Cancer Res* 15:3277–3286
 - 30. Kim S, Poursine-Laurent J, Truscott SM et al (2005) Licensing of natural killer cells by host

- major histocompatibility complex class I molecules. *Nature* 436:709–713
31. Shultz LD, Lyons BL, Burzenski LM, Gott B, Chen X, Chaleff S et al (2005) Human lymphoid and myeloid cell development in NOD/LtSz-scid IL2R gamma null mice engrafted with mobilized human hemopoietic stem cells. *J Immunol* 174:6477–6489
32. Evans MS, Chaurette JP, Adams ST Jr, Reddy GR, Paley MA, Aronin N, Prescher JA, Miller SC (2014) A synthetic luciferin improves bioluminescence imaging in live mice. *Nat Methods* 11:393–395
33. Wilding JL, Bodmer WF (2014) Cancer cell lines for drug discovery and development. *Cancer Res* 74:2377–2384

Chapter 5

RNA Extraction from *Xenopus* Auditory and Vestibular Organs for Molecular Cloning and Expression Profiling with RNA-Seq and Microarrays

Casilda Trujillo-Provencio, TuShun R. Powers, David R. Sultemeier,
Daniel Ramirez-Gordillo, and Elba E. Serrano

Abstract

The amphibian *Xenopus* offers a unique model system for uncovering the genetic basis of auditory and vestibular function in an organism that is well-suited for experimental manipulation during animal development. However, many procedures for analyzing gene expression in the peripheral auditory and vestibular systems mandate the ability to isolate intact RNA from inner ear tissue. Methods presented here facilitate preparation of high-quality inner ear RNA from larval and post-metamorphic *Xenopus* specimens that can be used for a variety of purposes. We demonstrate that RNA isolated with these protocols is suitable for microarray analysis and Illumina-Solexa sequencing (RNA-Seq) of inner ear organs, and for cloning of large transcripts, such as those for ion channels. Genetic sequences cloned with these procedures can be used for transient transfection of *Xenopus* kidney cell lines with fluorescent protein fusion constructs.

Key words RNA, Auditory, Vestibular, *Xenopus laevis*, *Xenopus tropicalis*, Microarray, RNA-Seq, Cloning, Transcriptional profiling, Heterologous gene expression

1 Introduction

Xenopus laevis is a widely used and well-established organism that has contributed to our understanding of embryogenesis and cellular development for well over 50 years [1]. In large part, *X. laevis* is a popular experimental species because the stages of *X. laevis* development have been richly detailed from the fertilized egg to the mature adult, and because the organism is extremely easy to breed and maintain in the laboratory [2]. However, the relatively long generation time (~18 months) and allotetraploid genome have been an impediment to genetic studies with this species. In the last decade, *Xenopus tropicalis* has emerged as another member of the genus *Xenopus* that is a superior alternative for molecular genetic analysis and large-scale sequencing efforts due to its

diploid genome and shorter (~5 months) generation time [3, 4]. Research with *Xenopus* species is furthered by the ability to implement powerful gene editing methods, such as CRISPr/Cas and TALEN/ZFN, to produce transgenic animals for targeted analysis of gene function [5]. The *Xenopus* community also benefits from the existence of sequenced genomes for both species, and the comprehensive resources available on *Xenbase* (<http://www.xenbase.org/entry/>), an open source database [6]. Finally, the *National Xenopus Resource* (NXR; <http://www.mbl.edu/xenopus/>) serves as a center for the maintenance of *X. laevis* and *X. tropicalis* stock. The NXR also provides training for *Xenopus* research applications (e.g., genetics, transgenesis, informatics, husbandry, imaging).

Using *X. laevis* and *X. tropicalis* as our experimental systems, we aim to understand the developmental mechanisms that give rise to the uniquely shaped auditory and vestibular endorgans of the inner ear with their characteristically patterned epithelia comprised of specialized mechanosensory hair cells [7–9]. We are especially interested in the specification of the electrical phenotype of hair cells and in determining the cadre of ion channels that typify endorgans of the inner ear [10–12]. Our target for molecular investigations is the inner ear of both *Xenopus* species. However, the diminutive inner ears that reside in the *Xenopus* otic capsule provide limited amounts of tissue for RNA isolation. This restriction has posed an additional challenge for the identification of genes that are expressed in the inner ear [8, 11].

The protocols that we developed and that are presented here permit isolation of high-quality RNA from larval and postmetamorphic *Xenopus* inner ears of both species. Furthermore, methods that are applicable for RNA isolation from the *Xenopus* inner ear have been validated as suitable for RNA isolation from other *Xenopus* organs such as brain and kidney, as well as *Xenopus* cell lines. Since the inner ear originates from a neurogenic placode [13], many genes expressed in the inner ear are also expressed in nervous tissue. Inner ears also share common sensitivities with kidneys to antibiotics and other drugs [14]. Therefore, these RNA isolation protocols can be used to design experiments that identify genes expressed during development of various *Xenopus* organs, and in the response of organs and cell lines to chemical challenges. The total RNA isolated with our procedures was used in two downstream applications: transcriptional profiling [15] and molecular cloning [11, 16]. Ion channel genes cloned with these methods can be fused to sequences for a fluorescent reporter molecule, such as green fluorescent protein (GFP), and expressed in *Xenopus* kidney cell lines, using lipid-mediated transient transfection and other gene delivery methods [16, 17].

Many methods requiring total RNA as a starting material are significantly affected by the quality of the RNA isolated from the tissue of interest. Furthermore, when tissue is limited, the success

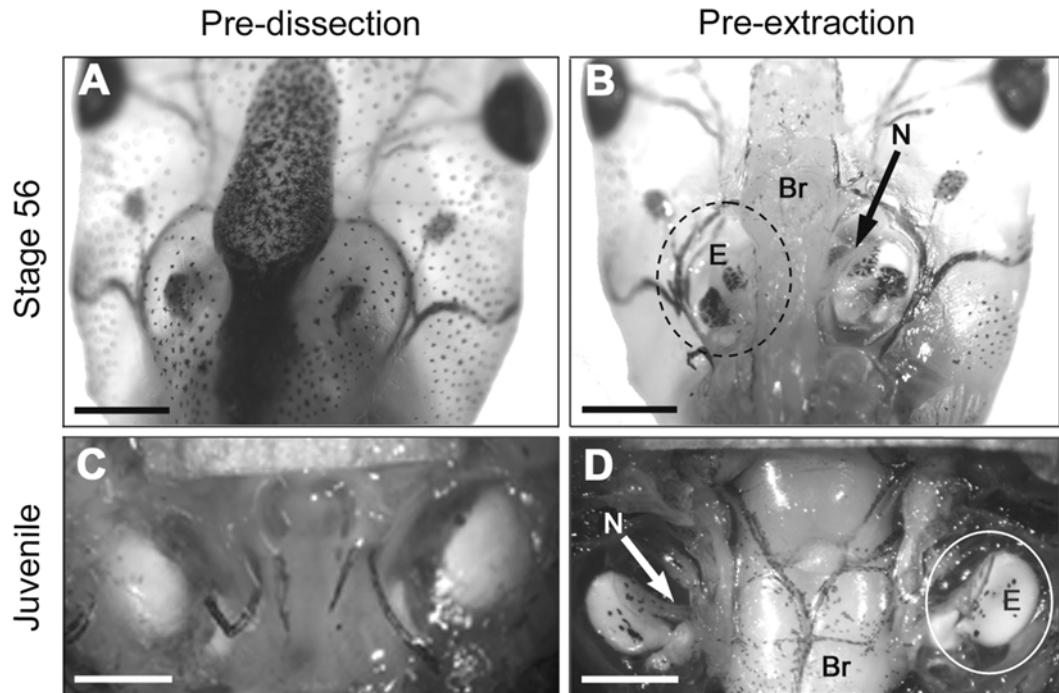


Fig. 1 *Xenopus* inner ear and brain dissections. (a) Dorsal view of *X. laevis* Stage 56 larva prior to dissection. (b) Dorsal view of exposed *X. laevis* Stage 56 inner ear (E) and brain (Br) after the tissue and bone are removed. (c) Ventral view of *X. laevis* juvenile upper jaw prior to dissection. (d) Ventral view of exposed *X. tropicalis* juvenile inner ear (E) and brain (Br) after tissue and bone are removed. Arrows point to the eighth cranial nerve (N). Anterior (top), Posterior (bottom). Scale bar = 1 mm

of methods that dictate a specific amount of starting RNA is hindered, because the amount of retrievable total RNA is diminished. Isolation of total RNA, from the minuscule inner ear of *Xenopus* [8, 10, 11, 15, 16] (see Fig. 1), for molecular pursuits such as transcriptional profiling and molecular cloning, presents such a challenge. In addition, the total RNA must be of very high quality, with a demonstrable lack of degradation and the presence of transcripts greater than 3 kb.

After numerous attempts to isolate a sufficient amount of high-quality total RNA from the inner ear of *Xenopus*, we were able to optimize the method by working quickly through tissue dissections, meticulously cleaning the tools used in the procedure with RNaseZap®, bathing the exposed tissue with RNAlater®, and incorporating the use of the Qiagen RNeasy® Mini Kit. Additionally, the use of the Agilent 2100 Bioanalyzer for RNA characterization greatly enhanced our capacity to detect and analyze isolated total RNA and to standardize protocols (see Fig. 2). Previously, the use of denaturing gel electrophoresis and a spectrophotometer was standard for assessing the quality and quantity of RNA. This procedure resulted in the loss of µg amounts of total RNA.

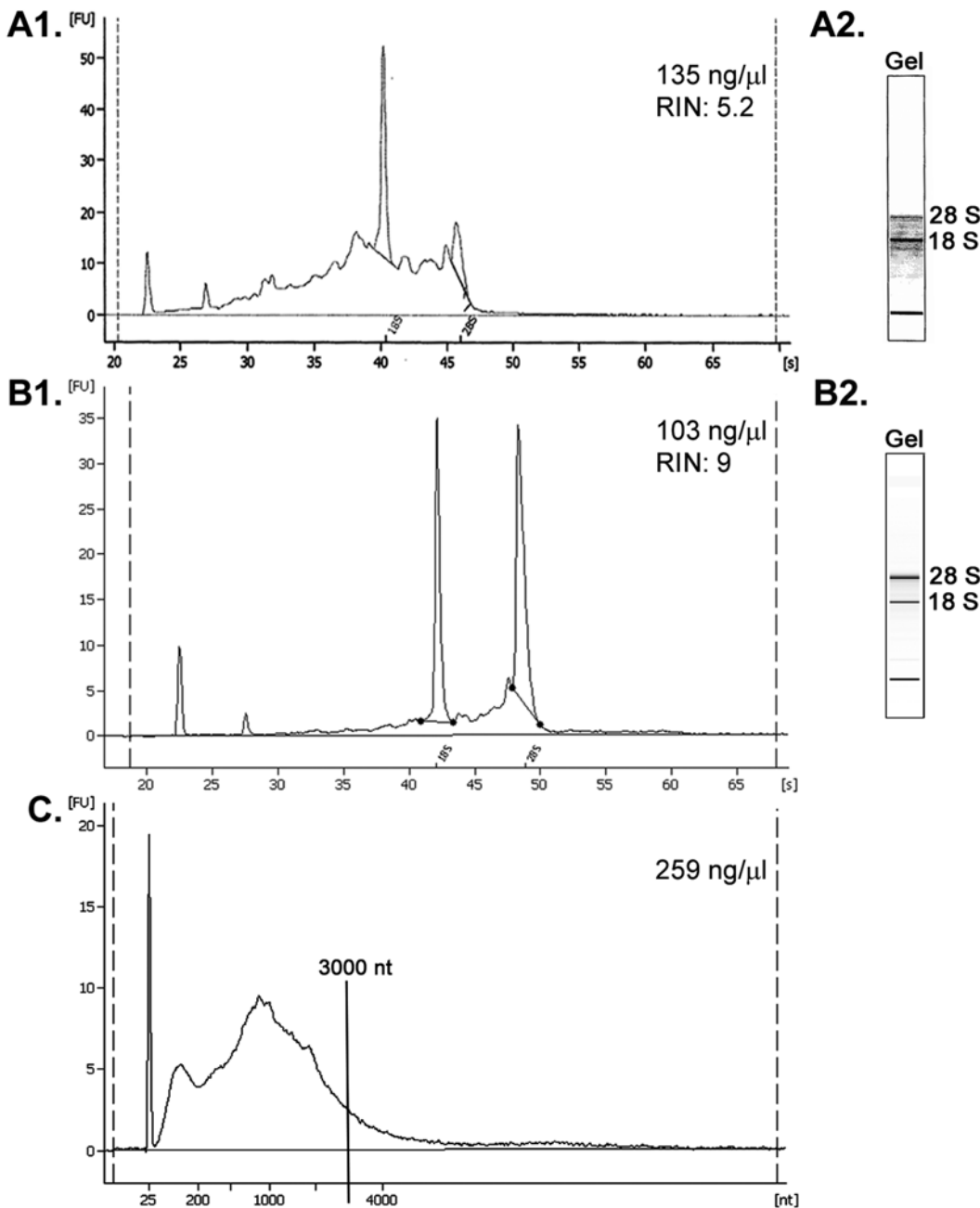


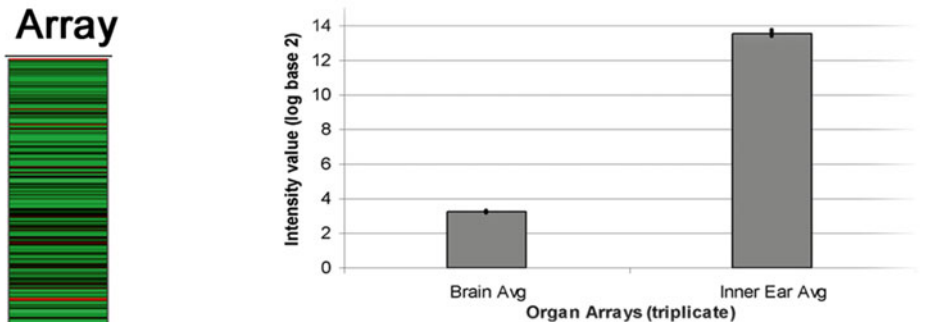
Fig. 2 *X. laevis* inner ear total RNA and cRNA evaluated with an Agilent 2100 Bioanalyzer. **(A1)** Electropherogram of degraded total RNA. This electropherogram is typical of RNA isolated from *X. laevis* juvenile inner ear tissue prior to implementation of the Qiagen RNeasy® Mini Kit. The RNA sample had a low (5.2) RNA Integrity Number (RIN). **(A2)** Gel representation of total RNA shown in **A1**. **(B1)** Electropherogram of high-quality (non-degraded) total RNA. This electropherogram is typical of RNA extracted from *X. laevis* Stage 56 larvae inner ear tissue with the Qiagen RNeasy® Mini Kit using the procedures described in Subheadings 3.2–3.4. The RNA sample had a high (9.0) RNA Integrity Number (RIN). **(B2)** Gel representation of total RNA shown in **B1**. **(C)** Electropherogram of biotin-labeled cRNA synthesized from the total RNA shown in **B1**. The cRNA of inner ear samples typically includes sequences greater than 3000 nt. Axis units: Abscissa **A1** and **B1**, migration time (seconds, s); Abscissa **C**, nucleotides (nt); Ordinate, fluorescence units (FU)

In contrast, the Agilent 2100 Bioanalyzer can detect and assess the *quantity* of as little as 25 ng/ μ L total RNA and the *quality* of as little as 5 ng/ μ L total RNA [18]. The Bioanalyzer characterizes the sample with an RNA integrity number (RIN) that can be used to establish a quantitative standard for RNA quality for each application. We consider this type of equipment and quantitative analysis a major contributor to the success and replicability of our methods, especially for transcriptional profiling.

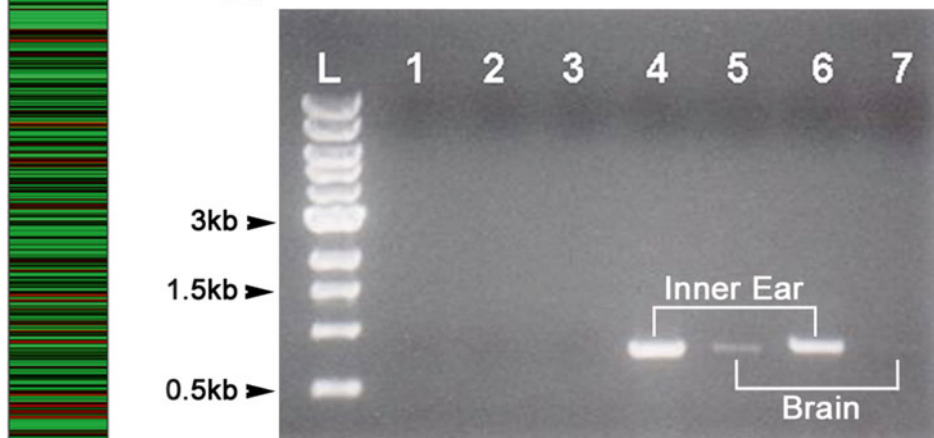
High-quality RNA enhances the success of RT-PCR Rapid Amplification of cDNA Ends (RACE) reactions, especially when long transcripts are sought. With our protocols, we typically visualize one sharp band of a PCR product when gene-specific primers and the PicoMaxx® High Fidelity PCR system are used to amplify a gene of interest (*see Fig. 3c*). The PicoMaxx® High Fidelity PCR system uses a blend of *Taq* and *Pfu* DNA polymerases and an exclusive ArchaeMaxx® polymerase-enhancing factor. The system provides high PCR sensitivity and fidelity which facilitates the detection and amplification of low copy number targets up to 10 kb in size. For example, we routinely obtain target PCR products in the 3–4 kb range [8, 10]. Using the TOPO® XL PCR Cloning Kit in conjunction with the PicoMaxx® High Fidelity PCR system enabled the cloning of transcripts greater than 3 kb [11, 16]. It is crucial to confirm that clones are full length and of the expected identity by sequencing prior to other downstream applications such as heterologous expression in a cell culture system (*see Fig. 3d*).

We enlisted the transcriptional profiling approach, using microarray analysis alone and in conjunction with RNA-Seq technology, in order to better understand global gene expression patterns that underlie *X. laevis* inner ear function (*see Fig. 3a*). By mining *Affymetrix* inner ear microarray transcriptomic data, we identified expression of *Xenopus* orthologs for genes traditionally associated with auditory and vestibular function, as well as “orphan” genes with high expression values and no known function [15]. Our analysis was facilitated by assigning functional significance to microarray probe set identifiers using gene categories such as “deafness,” “transcription factors,” and “ion channels.” Moreover, in comparative organ profiling experiments, we identified hundreds of genes on the GeneChip® *X. laevis* Genome Array that are expressed at different levels in *X. laevis* inner ear as compared with brain microarray data. For example, we noted differential expression of the gap junction protein β 2 (GJB2) [19], a gene that has been implicated in hereditary deafness. The difference in GJB2 expression levels in *X. laevis* inner ear was nearly 4 \times that of the brain (*see Fig. 3b*). The relative GJB2 abundances detected through microarray analysis of inner ear and brain RNA are also apparent when inner ear and brain RNA are used as template in RT-PCR RACE reactions with GJB2 gene-specific primers (*see Fig. 3c*). Thus, RT-PCR RACE reactions replicate the gene’s transcriptional

A. Inner Ear B. GJB2 Expression



C. RT-PCR RACE Reactions



D. GFP-BK Expression in A6 Cells

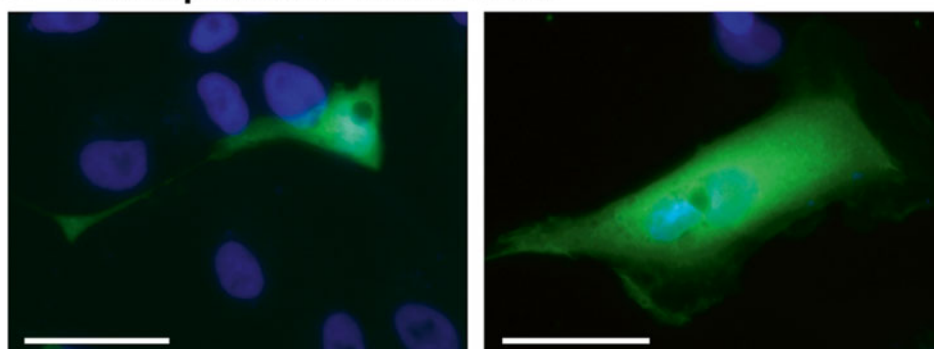


Fig. 3 Applications of RNA for transcriptional profiling (**a, b**), molecular cloning (**c**), and heterologous gene expression in cell culture (**d**). (**a**) Heat map of inner ear microarray data. *X. laevis* juvenile inner ear total RNA (~1 µg) was labeled and hybridized to the GeneChip® *Xenopus laevis* Genome Array. The heat map was constructed using the Spotfire® DecisionSite® 9.0 software. The data are organized numerically by probe set ID with the lowest ID number at the top. In this sample, the normalized intensity values (log base 2) for the 15,491 probe sets ranged from 0.8 (low) to 15.22 (high). The intensity color code for expression: *L* low, *M* intermediate, *H* high. (**b**) Microarray detection of the expression of the gap junction protein beta 2 (GJB2) in inner ear and brain. The average and standard deviation values in the histograms were calculated from three different

profile between organs as detected with microarrays. We interpret these findings as an indication of the indispensable contribution of high-quality RNA to the consistency between replicates and the identification of inner ear-specific genes.

RNA extracted from *Xenopus* inner ears also enabled us to explore the transcriptional profile of the *Xenopus* inner ear that emerges when expression is assessed using both *Affymetrix* GeneChip® *X. laevis* Genome Array and Illumina-Solexa sequencing (RNA-Seq) approaches. By evaluating transcriptomic data captured with the two technologies we were able identify and analyze *Xenopus* inner ear orthologs for Online Mendelian Inheritance in Man® (OMIM®) genes implicated in deafness and vestibular disorders in humans [20]. The results of these transcriptional profiling investigations enhance, and lend credence to, the suitability of *Xenopus* as a relevant model for investigations of hearing and vestibular function.

2 Materials

2.1 Tissue Preparation

1. *Xenopus laevis* and *Xenopus tropicalis* are obtained from Nasco (Fort Atkinson, WI). *X. laevis* larvae are purchased as a unit of Stage 48–55 tadpoles and maintained in aquaria until they reach developmental Stage 55–56. Juvenile animals (*X. laevis* and *X. tropicalis*) are used within a week of arrival. All procedures involving animals are approved by the New Mexico State University Institutional Animal Care and Use Committee.
2. Ethyl 3-aminobenzoate methanesulfonate salt: Prepare a 2 % (w/v) stock solution in water (see Notes 1 and 2). Store the stock solution at 4 °C and discard after 1 month. Working solutions of 0.2 % (larvae) and 0.5 % (juvenile animals) are prepared the day of use by diluting the stock solution with 0.01 M phosphate buffered saline: 1.5 mM KH₂PO₄, 8.1 mM Na₂HPO₄, 138 mM NaCl, 2.7 mM KCl, pH 7.4.
3. Water treated with 0.1 % (v/v) diethyl pyrocarbonate (see Notes 1 and 3).

Fig. 3 (continued) microarray experiments. Low standard deviations characterized the sample replication. (c) RT-PCR RACE detection of GJB2 transcript in *X. laevis* juvenile inner ear and brain. *Lane 1*—inner ear, minus RT control, GJB2 primer pair 1; *Lane 2*—brain, minus RT control, GJB2 primer pair 1; *Lane 3*—PCR reaction control, minus cDNA template, GJB2 primer pair 1; *Lane 4*—inner ear, GJB2 primer pair 1; *Lane 5*—brain, GJB2 primer pair 1; *Lane 6*—inner ear, GJB2 primer pair 2; *Lane 7*—brain, GJB2 primer pair 2. *Lane L*—5 µL of NEB 1 kb DNA ladder. cDNA is detected in lanes 4–7. Expression levels correlate with the microarray data shown in (b). (d) GFP-positive *Xenopus* A6 kidney cells transfected with the GFP-BK clone. Dashed lines encircle transfected A6 cells (GFP) and dotted lines encircle stained nuclei (Hoechst). Scale bar=50 µm

4. RNaseZap® and RNAlater® (Ambion®/Life Technologies, Grand Island, NY).
5. Dissecting tools: Dumont #5 forceps, standard straight fine Iris scissors, scalpel handle #3 (all from Fine Sciences Tools, Foster City, CA); BD Bard-Parker Sterile Stainless Steel Scalpel Blades #11; 60×15 mm glass Petri dish filled with black wax (Nasco, Fort Atkinson, WI).
6. Olympus SZ61 dissecting stereomicroscope.
7. Microcentrifuge tubes sterilized by autoclaving, 1.7 and 2.0 mL; and 22-gauge needles.

2.2 Total RNA Isolation

1. RNeasy® Mini Kit (Qiagen, Valencia, CA).
2. 14.3 M β-mercaptoethanol.
3. Kimwipes®.
4. Brinkmann Polytron PT1200 handheld homogenizer with sawtooth 0.5 mm generator.

2.3 Total RNA Clean-Up and Total RNA Quality and Quantity Determination

1. The DNA-free™ DNA Removal kit, 5 M ammonium acetate, 5 mg/mL linear acrylamide, and THE RNA Storage Solution (Ambion®/Life Technologies).
2. 100 % Ethanol.
3. 70% Ethanol is prepared by diluting 100 % ethanol with DEPC-treated water.
4. Refrigerated centrifuge (e.g., Beckman Coulter AllegraTM 21R Refrigerated Centrifuge).
5. An Agilent 2100 Bioanalyzer and Agilent RNA 6000 Nano Kit (Agilent Technologies, Santa Clara, CA) can be used to determine total RNA quality and quantity.

2.4 Microarray Analysis

1. GeneChip® *Xenopus laevis* Genome Array (Affymetrix, Santa Clara, CA) and Applause 3'-Amp System (NuGEN, San Carlos, CA).
2. gcRMA (Robust multichip averaging) summarization method downloaded from bioconductor.org and executed in the R package (<http://www.r-project.org/>).
3. Spotfire® DecisionSite® 9.0 for Functional Genomics (Spotfire, Inc., Somerville, MA).

2.5 RNA-Seq Analysis

1. Tru-Seq Library Preparation kit (Illumina, San Diego, CA).
2. NanoDrop spectrophotometer.
3. Agilent 2100 Bioanalyzer and Agilent DNA 1000 kit (Agilent Technologies).
4. Illumina Genome Analyzer II Sequencer (Illumina).
5. Illumina software v1.0 (Illumina).

6. Genomic Mapping and Alignment program (GMAP) (University of Minnesota).
7. Alpheus™ Sequence Variant Detection System v3.1 (National Center for Genome Resources, Santa Fe, NM).

2.6 Molecular Cloning of Genes Identified with Transcriptional Profiling

1. SMARTer™ RACE 5'/3' Kit (Clontech Laboratories, Inc., Mountain View, CA).
2. PicoMaxx® High Fidelity PCR System (Agilent Technologies).
3. Thermal cycler (e.g., TC-512, Techne Inc., Burlington, NJ).
4. Lyophilized gene-specific primers, 10 nmol.
5. SeaKem® LE Agarose (Cambrex Bio Science Rockland, Inc., Rockland, ME).
6. Tris-acetate/EDTA electrophoresis buffer (TAE 1×): 0.04 M Tris base, 0.001 M EDTA, 1.0 M glacial acetic acid. A 50× stock solution is prepared in a glass bottle and stored at room temperature (22–26 °C).
7. Agarose gel with ethidium bromide: Prepare by diluting 10 mg/mL ethidium bromide stock solution to a final concentration of 0.25 µg/mL in melted agarose gel. Do not include ethidium bromide in the running buffer.
8. 1 kb DNA ladder.
9. S.N.A.P.™ UV-Free Gel Purification Kit and TOPO® XL PCR Cloning Kit with One Shot® TOP10 Electrocomp™ *E. coli* (Invitrogen™/Life Technologies).
10. Lambda Bio UV/Vis Spectrometer (Perkin Elmer Corp., Norwalk, CT).
11. Electroporator 2510 and electroporation cuvettes (Eppendorf, Westbury, NY).
12. BigDye® Terminator v3.1 Cycle Sequencing Kit (Life Technologies).
13. ABI PRISM® 3100 Genetic Analyzer (Applied Biosystems/Life Technologies).

2.7 Heterologous Inner Ear Gene Expression

1. Living Colors® pAcGFP1-C1 expression vector (Clontech Laboratories, Inc.).
2. *Xba*I and *Spe*I restriction enzymes; Antarctic phosphatase; and Quick Ligation™ Kit.
3. *X. laevis* A6 kidney cell line (American Type Culture Collection, Manassas, VA).
4. Cell culture medium per 100 mL: 75 mL of NCTC-109, 10 mL Newborn Calf Serum, 2 mL of 200 mM L-Glutamine, and 13 mL of Milli-Q water. Combine medium components, then filter-sterilize with a 250 mL Stericup™-GP Filter Unit (EMD Millipore, Billerica, MA). Passage reagent: Filter-sterilized

0.25 % Trypsin-EDTA. Store aliquots consisting of 10 mL of Newborn Calf Serum, 2 mL of L-glutamine, and 10 mL of 0.25 % Trypsin-EDTA at -20 °C.

5. Class II Safety Cabinet and Water-Jacketed CO₂ Incubator Model 2310.
6. Nunc® LabTek™ chamber slide system, two- or four-chamber.
7. Lipofectamine™ 2000 Transfection Reagent (Life Technologies, Grand Island, NY).

2.8 Epifluorescence Imaging

1. 3.7 % Paraformaldehyde: Prepare by diluting 10 % paraformaldehyde in PBS. Paraformaldehyde is prepared fresh for each experiment.
2. Hoechst 33342, 10 mg/mL.
3. SlowFade® Antifade Kit (Life Technologies).
4. VWR® micro cover glasses No.1, 24 × 50 mm.
5. Clear fingernail polish.
6. CoolSNAP™ HQ CCD camera (Photometrics, Tucson, AZ).
7. Nikon TE2000 epifluorescence microscope equipped with a UV-2A filter cube (UV excitation) and a B-2E/C filter cube (Blue excitation).
8. MetaVue™ Imaging System Version 6.0r5 and MetaMorph® Offline Imaging System Version 6.0r5.
9. Adobe® Photoshop® Version 7.0.1 (Adobe Systems Incorporated, San Jose, CA).

3 Methods

3.1 General Recommendations

1. Work quickly and follow established best practices for handling RNA [21].
2. Clean tools with RNaseZap®.
3. Bathe tissue with RNAlater® during surgery.
4. Use Qiagen RNeasy® Mini Kit.
5. High-quality RNA (RIN > 8) is essential; use the Agilent Bioanalyzer or similar equipment to assess RNA quality.
6. At least 1 µg of high-quality RNA (RIN > 8) is optimal.
7. Use total RNA within 72 h for microarray and RNA-Seq experiments.
8. 18–20 µg of biotin-labeled cRNA are required before proceeding to the fragmentation and hybridization steps in microarray experiments.

9. Review electropherograms for size distributions of cRNA/mRNA samples; transcripts greater than 3 kb should be present in the sample, especially if ion channels and other membrane transporters and receptors are target genes.
10. Use the PicoMaxx® High Fidelity PCR System or equivalent.
11. Use the TOPO® XL PCR Cloning Kit or equivalent.

As per standard laboratory procedures, investigators are reminded that they should review chemical MSDS sheets prior to use and ensure that reagents are handled and discarded in compliance with all federal and state regulations. Protocols that use animals in research must be approved by the Institutional Animal Care and Use Committee prior to initiating experiments. Recommended guidelines for the use of *Xenopus* in research are available online [22–24].

3.2 Tissue Preparation

1. Take precautions to eliminate sources of RNase contamination by following rigorous laboratory procedures for working with RNA. Minimal practices include a clean bench, strict adherence to the use of gloves throughout the procedure, a dedicated set of pipettors, and disposable sterile plasticware. Prior to dissections, clean all dissection tools and the Polytron generator with RNaseZap® and rinse thoroughly with DEPC-treated water (*see Note 4*).
2. Partially immerse stage 55–56 larvae and juvenile (2.5–3.5 cm, 1.0–3.0 g) *X. laevis* or juvenile *X. tropicalis* (1.5–2.5 cm, 0.8–2.0 g) in a solution of ethyl 3-aminobenzoate methanesulfonate salt (0.2 % for Stage 55–56 larvae and 0.5 % for juveniles) for 10–30 min at room temperature (22–26 °C). The solution should cover the torso of the animal, but leave the nostrils of the animal exposed to air.
3. Work quickly during the dissections to minimize tissue exposure to RNases. Pierce larval hearts and decapitate juvenile animals prior to aseptic removal of inner ear tissue. Also, extract brain and kidney tissue from juvenile animals.
4. Use a dissecting stereomicroscope (e.g., Olympus SZ61) for the dissection of tissues.
5. Remove larval inner ears by approaching the tissue from the dorsal side of the animal (*see Fig. 1a*). Peel the skin away from the area above the brain and otic capsules and remove the soft bone of the skull and otic capsules, using a surgical scalpel and fine forceps.
6. Once the tissue is exposed (*see Fig. 1b*), bathe it with RNAlater® to prevent degradation of RNA. Extract the inner ear by grasping the eighth cranial nerve and withdrawing the nerve and its target sensory organs from the otic capsule.

7. Remove juvenile inner ears and brains by approaching the tissue ventrally from the roof of the mouth after removing the lower jaw. To facilitate the dissection, pin the top of the head and the exposed spinal cord to the dissecting dish with 22-gauge needles. Despite the animal size difference, *X. tropicalis* inner ears are only slightly smaller than those of *X. laevis*, and overall the inner ears of the two species are of comparable dimensions (see Fig. 1c, d).
8. Remove the skull and otic capsule bone with a surgical scalpel and fine forceps. Bathe the exposed tissue (see Fig. 1d) copiously with RNAlater®. Then, extract the inner ear tissue as described in the larval preparation. After removal of inner ear tissue, sever the brain from all nerve branches and carefully remove with fine forceps.
9. The dissected tissue is placed in a 2.0 mL microcentrifuge tube, containing 200–400 µL of RNAlater® immediately after removal from the animal.
10. Use tissue immediately for RNA isolation or store at –20 °C for several months or at –80 °C indefinitely prior to RNA isolation.

3.3 Total RNA Isolation

1. Use the RNeasy® Mini Kit from Qiagen for total RNA isolation.
2. Remove the dissected tissue from the RNAlater®, blot quickly on a Kimwipe® (from a clean box reserved for RNA work), and immediately place in a pre-weighed 2.0 mL microcentrifuge tube containing 600 µL of Buffer RLT and 6 µL of 14.3 M β-mercaptoethanol.
3. Determine the tissue weight by subtracting the weight of the tube plus Buffer RLT and β-mercaptoethanol from the weight of tube containing the tissue plus Buffer RLT and β-mercaptoethanol.
4. Extract no more than 30 mg of tissue, as recommended by the vendor, for each total RNA isolation (see Note 5).
5. Disrupt the tissue using a homogenizer with a 0.5 mm generator set at the highest setting. Pulse samples 3–5× for ~5–10 s until the tissue is completely homogenized and the solution is uniform in texture and color. Cool the tube on ice between pulses.
6. After the tissue is uniformly homogenized, follow the RNeasy® Mini Kit protocol as described in the manual.
7. Elute total RNA in two steps, first with 50 µL and then with 40 µL of RNase-free water provided with the kit.

3.4 Total RNA Clean-Up

1. Use the DNA-free™ DNA Removal kit from Ambion®/Life Technologies to purify total RNA sample.
2. Treat the total RNA obtained from step 7, Subheading 3.3, with DNaseI to degrade any DNA in the sample. Follow the protocol manual with a DNaseI incubation time of 30 min.
3. Following the DNase inactivation step, transfer the total RNA solution to a clean 1.7 mL microcentrifuge tube and precipitate by adding $0.1\times$ volume of 5 M ammonium acetate, $0.015\times$ volume of 5 mg/mL linear acrylamide, and $2\times$ volume of 100 % ethanol.
4. Incubate the total RNA precipitation reaction overnight at -20°C .
5. Recover the total RNA pellet by centrifugation at $10,000\times g$ for 20 min at 4°C . Discard the supernatant, and wash the pellet with 300 μL of 70 % ethanol. Repeat centrifugation for 10 min.
6. Discard the wash supernatant, and air dry the pellet at room temperature for 15 min.
7. Resuspend total RNA in 8–15 μL of THE RNA Storage Solution and incubate in a 37°C water bath for 5 min.
8. Store the sample at -80°C or place on ice and analyze for quality and recovery.
9. Use RNA within 72 h for downstream methods (see Note 6).

3.5 Determination of Total RNA Quality and Quantity

1. Dilute the total RNA sample 1:3 in THE RNA Storage Solution and use the Agilent RNA 6000 Nano Kit to prepare the RNA for the determination of quality and quantity.
2. Follow the vendor's instructions of the Agilent 2100 Bioanalyzer to generate an electropherogram and an RNA Integrity Number (RIN) for each RNA sample. An electropherogram displaying two well-defined peaks of 1.8 kb (18S rRNA) and 4.0 kb (28S rRNA) and a RIN above 8 are indicative of high-quality RNA (see Fig. 2B1). For typical yields of total RNA isolated from *Xenopus* tissues see Note 7. Figure 2 shows representative electropherograms generated by the 2100 expert software.

3.6 Microarray Analysis

1. Use total RNA, obtained in Subheading 3.4, step 8, from juvenile and larval *X. laevis* in microarray experiments within 72 h of tissue dissection. At least 1 μg (5–10 μL) of high-quality RNA with a RIN above 8 is required for cRNA synthesis (see Note 8).
2. Prepare biotin-labeled cRNA for hybridization to the GeneChip® *Xenopus laevis* Genome Array by using the Applause 3'-Amp System following the vendor's instructions.

3. Determine the amount of biotin-labeled cRNA by analyzing diluted cRNA (1:10 or 1:20) on the Agilent 2100 Bioanalyzer in order to ensure that 18–20 µg of biotin-labeled cRNA are available for the fragmentation and hybridization steps. Review electropherograms, generated by using the 2100 expert software from Agilent, to evaluate the size distributions of the cRNA samples to be used for transcriptional profiling. For inner ear and brain, expect the sample to contain cRNA that is greater than 3 kb (see Fig. 2c for a cRNA sample prepared by the BioMicro Center at the Massachusetts Institute of Technology, Cambridge, MA, using the aforementioned technology).
4. After image acquisition, normalize the raw data using the gcRMA (Robust multichip averaging) summarization method. After normalization, analyze all microarray data using the Spotfire® DecisionSite® 9.0 for Functional Genomics software. A heat map that graphically represents the levels of gene expression from one array of *X. laevis* inner ear tissue is shown in Fig. 3a.

3.7 Illumina-Solexa Sequencing (RNA-Seq)

1. RNA-Sequencing was completed using the Illumina-Solexa platform for sequencing by synthesis.
2. Short-insert paired end (SIPE) libraries were prepared from the total RNA (obtained in Subheading 3.4, step 8) according to the Illumina's mRNA-Seq Sample Prep Protocol v2.0 (Illumina).
3. The resultant double-stranded cDNA concentration was measured on a NanoDrop spectrophotometer, and size and purity were determined on the 2100 Bioanalyzer using a DNA 1000 Nano kit.
4. The cDNA libraries were cluster amplified on Illumina flow-cells, sequenced on the Genome Analyzer II Sequencer as 36-cycle single-end reads, and pipelined using Illumina software v1.0.
5. Illumina reads were aligned to the *X. tropicalis* genome using the algorithm for genomic mapping and alignment program (GMAP) and the Alpheus® Sequence Variant Detection System v3.1 (see Note 9).

3.8 Molecular Cloning of Genes Identified with Transcriptional Profiling

1. The expression of genes detected with microarray analysis can be confirmed with molecular cloning using RT-PCR RACE protocols.
2. Use *X. laevis* and *X. tropicalis* inner ear or brain total RNA, acquired in Subheading 3.4, step 8, as a template for RT synthesis of first-strand cDNA. Prepare 5'-RACE-Ready first-strand cDNA in separate reactions, according to the instruction manual of the SMARTer™ RACE 5'/3' Kit, using 1 µg of

control RNA from the kit and 1 µg of the following experimental samples: *X. laevis* inner ear or brain total RNA, *X. tropicalis* inner ear or brain total RNA.

3. Run control PCR reactions that amplify the first-strand cDNA, prepared from the kit RNA according to the vendor's protocols, to evaluate the success of the 5'-RACE reactions.
4. Analyze control PCR products by agarose gel electrophoresis, as described in the kit manual, before proceeding with the experimental PCR reactions with *Xenopus* samples. If the expected products are observed, use the *Xenopus* first-strand cDNA samples for PCR reactions. If products are not detected, the first-strand synthesis reactions must be repeated following recommendations outlined in the troubleshooting section of the user manual.
5. Use the 5'-RACE-Ready inner ear or brain first-strand cDNA samples (5–10 µL in a 50 µL reaction volume) to amplify second-strand cDNA according to the PicoMaxx® High Fidelity PCR System user manual. The thermal cycler parameters are as follows: initial denaturation, 95 °C for 2 min; 35 cycles of 95 °C for 40 s, Tm minus 3 °C for 30 s, 72 °C for 3 min; final extension 72 °C for 10 min. Design gene-specific primers to the gene of interest and obtain from vendor. The primer Tm's are specified in the Oligonucleotide Data Sheet provided by Eurofins MWG Operon and vary by primer pair.
6. Analyze 7 µL of the PCR reaction on a 1.2 % agarose gel (0.25 µg/mL ethidium bromide) in 1× TAE buffer.
7. Isolate the resultant PCR fragments using the S.N.A.P.™ UV-Free Gel Purification Kit, according to the vendor's instructions, until the quantification step. For quantification, analyze 10 µL of the isolated fragment on a Lambda Bio UV/Vis Spectrometer.
8. Clone the purified PCR product using the TOPO® XL PCR Cloning Kit with One Shot® TOP10 Electrocomp™ *E. coli*, according to the kit manual with a 3:1 molar ratio of insert to vector. After the ligation step, use the Electroporator 2510 to transform the electrocompetent cells with a setting of 1400 V.
9. Analyze between 5 and 10 positive clones by restriction enzyme digestion to confirm the presence of an insert. Sequence clones with inserts following the BigDye® Terminator v3.1 Cycle Sequencing Kit protocol and analyze sequencing reactions using the ABI PRISM® 3100 Genetic Analyzer.
10. Molecular cloning, using the RT-PCR RACE procedures described above, can be used to confirm the differential expression of genes such as the *X. laevis* EST, GenBank Accession no.

BJ076720 (National Institute for Basic Biology Mochii normalized *Xenopus* tailbud library, Clone ID# XL058il6 (3_)). This gene is detected with Affymetrix (Santa Clara, CA) probe set XI.8924.1.A1 at using the GeneChip® *Xenopus laevis* Genome Array. The Affymetrix annotation states that this probe set targets *X. laevis* connexin 26 (gap junction protein β2, GJB2). Microarray analysis suggests that this gene is expressed at higher levels in the inner ear than in the brain (*see Fig. 3b*).

11. Design primers to amplify two regions within the 3292 bp Affymetrix consensus sequence for the XI.8924.1.A1 at probe set. Use the HMMgene v. 1.1 program [25] to determine the putative coding sequence within the consensus sequence for the design of primer pair 1. Use the sequence for the *X. laevis* EST (GenBank Accession #BJ076720) that is arrayed on the chip for the design of primer pair 2.
12. Primer pair 1 amplifies an 804 bp product that includes the entire GJB2 coding sequence. The forward primer (5'-AGTCAGCGCACAGAGACCAA-3') aligns with the 5' UTR sequence (31 bp upstream of the translational start site) and the reverse primer (5'-AGCTGACCTGCCACAGT AAC-3') aligns 7 bp downstream of the stop codon.
13. Primer pair 2 amplifies an 859 bp product within the EST sequence. The forward primer (5'-CGGTCAATCATTAGT-3') aligns 71 bp upstream of the start of the EST sequence and the reverse primer (5'-ACACTCCAGGAAAA CAC-3') is 24 bp downstream from the end of the EST sequence.
14. Prepare the first-strand cDNA from *X. laevis* inner ear and brain total RNA as described previously. The second-strand PCR reactions follow the steps outlined in Subheading 3.8, step 5, with the following annealing temperatures (Tm): 60 °C for primer pair 1 and 53 °C for primer pair 2.
15. Clone and sequence the resultant PCR products (*see Fig. 3c*), following the methods described in Subheading 3.8, steps 6–7. Confirm that cloned inserts correspond to the expected GJB2 and EST targets by sequencing. The relative product intensities on the gel parallel the relative transcript levels detected by microarray analysis.

3.9 Heterologous Inner Ear Gene Expression

1. Subclone a TOPO® XL cloned calcium-activated potassium channel (BK) isoform from *X. laevis* inner ear tissue [11] that share 99 % nucleotide identity with posted *Xenopus* spinal cord GenBank sequences (Accession no. AF274053) into the Living Colors® pAcGFP1-C1 expression vector.
2. Use *Xba*I and *Spe*I restriction enzymes to digest 5 µg of the BK TOPO® XL clone, following the vendor's recommended

reaction conditions. Isolate the insert using the S.N.A.P.TMUV-Free Gel Purification Kit as described in Subheading 3.8, step 7.

3. Prepare the vector, Living Colors[®] pAcGFP1-C1, by digesting 1 µg of plasmid DNA with *Xba*I restriction enzyme and then dephosphorylating with Antarctic phosphatase, following the vendor's protocol.
4. Use the Quick Ligation[™] Kit to clone the BK isoform fragment into the GFP expression vector, following the vendor's protocol. Confirm positive clones by restriction enzyme analysis and subsequent sequencing reactions using the BigDye[®] Terminator v3.1 Cycle Sequencing Kit.
5. Culture the *X. laevis* A6 kidney cell line according to the vendor's recommendations and maintain in antibiotic-free media at 26 °C in 5 % CO₂.
6. Passage A6 cells at a plating density of 4. 5 × 10⁴ cells/cm² on two- or four-chamber culture slides 24 h prior to transient transfections.
7. Transfect cells with a final concentration of 2 µg/mL of Lipofectamine 2000 Transfection Reagent and 1 µg/mL of plasmid diluted in serum-free NCTC-109 medium, following the vendor's protocol. Transfect cultures with Lipofectamine without plasmid in control experiments (see Note 10).

3.10 Epifluorescence Imaging

1. After 24–48 h, wash cells gently in serum-free NCTC-109 medium.
2. Fix cells in 3.7 % paraformaldehyde for 10 min at room temperature and wash with PBS (pH 7.4).
3. Expose cells to 1 µg/mL Hoechst 33342 diluted in PBS (pH 7.4) for 10 min at room temperature followed by a PBS (pH 7.4) wash.
4. Prepare slides for imaging by adding AntiFade Solution C from the SlowFade[®] Antifade Kit to the chambers for 15 min at room temperature. Remove the AntiFade Solution C and detach the side walls of the culture chambers.
5. Add a few drops of AntiFade Solution A from the SlowFade[®] Antifade Kit to the slide prior to applying a cover slip. Seal the cover slip with clear fingernail polish.
6. Capture images using a CCD camera connected to an epifluorescent microscope, as described in Subheading 2.8, and the MetaVue[™] Imaging System software (see Fig. 3d).
7. Process images offline using appropriate software (e.g., MetaMorph[®] Offline Imaging System software and Adobe[®] Photoshop[®] for figure preparation).

4 Notes

1. Prepare all solutions in Milli-Q water ($18 \text{ M}\Omega \text{ cm}$) with a total organic content of less than five parts per billion.
2. Solutions of ethyl 3-aminobenzoate methanesulfonate salt are buffered to pH 7.0 with sodium bicarbonate. Use gloves when preparing and handling solutions of ethyl 3-aminobenzoate methanesulfonate salt. Prepare the stock solution in a chemical fume hood to avoid inhalation of dust.
3. WARNING: DEPC is a combustible explosive and a toxic chemical. It is recommended that users purchase small amounts of DEPC and use all the DEPC as soon as possible. Take appropriate precautions when handling: e.g., always wear personal protective equipment and work in an approved chemical fume hood. Dilute DEPC in water to a final concentration of 0.1 %. After adding the DEPC, close the container tightly and vigorously shake. Allow the solution to sit overnight at room temperature and autoclave for 20 min before use. The DEPC-treated water can be stored at room temperature after autoclaving. Solutions requiring DEPC-treated water are indicated in the text.
4. The Polytron blade can be removed carefully from the outer shaft of the generator, and both the blade and outer shaft must be thoroughly cleaned. RNaseZap® is copiously applied and the surfaces are lightly scrubbed with Kimwipes. Rinse the blade and outer shaft several times with DEPC-treated water, rinse once with 70 % ethanol, and allow to air dry. (Reminder: 70 % ethanol should be made with DEPC-treated water.) This cleaning procedure should be repeated between tissue samples.
5. Typically, the amount of tissue recovered from *Xenopus* juvenile animals is 1 mg per inner ear and 10 mg per brain. The amount of tissue recovered from Stage 56 *X. laevis* is 0.7 mg per inner ear. Total RNA is isolated by combining tissue from at least 3 animals.
6. Resuspended RNA stored at -80°C may have a variable shelf life depending on the tissue source and handling protocols. The RNA should be checked periodically for quality using the Agilent 2100 Bioanalyzer. In our hands, RNA isolated with the Qiagen kit and stored for up to 7 years in the Ambion®/Life Technologies RNA Storage Solution have yielded RIN values of 8 and above.
7. The average yields of total RNA using the Qiagen RNeasy® kit are as follows: *X. laevis* juvenile—1.8 µg per brain and 0.3 µg per inner ear; *X. laevis* Stage 56—0.3 µg per inner ear; *X. tropicalis* juvenile—1.9 µg per brain and 0.2 µg per inner ear. Downstream protocols (i.e., Microarray analysis and RT-PCR) typically require at least 1 µg of total RNA.

8. The Agilent 2100 Bioanalyzer allows precise optimization of total RNA isolation procedures (*see* Fig. 2). The Bioanalyzer can detect ng quantities of nucleic acids in 1 μ L and also quantifies RNA integrity with a number (RIN). Therefore, this instrument is superior to spectrophotometer quantification (260/280 ratios) for evaluating RNA quality.
9. Other software platforms available for the analysis of transcriptomic data include commercial options such as JMP Genomics, and open source workflow tools that use the R programming language (e.g., Bioconductor packages).
10. Transfection can be achieved using chemical, viral, or physical (electroporation) methods. The lipid-mediated transfection protocol presented here can be implemented using routine equipment available in most cell and molecular biology laboratories. However, we have observed higher transfection efficiencies using viral-mediated methods to deliver *Xenopus* inner ear calcium-activated potassium channel $\beta 1$ subunit fluorescent fusion constructs to the *Xenopus* A6 kidney-derived cell line [16].

Acknowledgments

The authors thank Joanna Beeson for technical support with cell culture experiments, and Alicia Arguelles and Erica Koval for their assistance with manuscript preparation. We are grateful to Dr. Charlie Whittaker, of the MIT Center for Cancer Research, and to Manlin Luo and Dr. Rebecca Fry, of the MIT BioMicro Center, for their technical assistance and generous advice. We also acknowledge Dr. Peter Sorger and members of the MIT Cell Decision Processes Center for stimulating intellectual interactions and for facilitating access to essential equipment and computing resources. Funding for this research was provided by awards from the National Institutes of Health (NIDCD R01DC003292; NIGMS P50GM068762).

References

1. Tinsley RC, Kobel HR (eds) (1996) Biology of *Xenopus*. Oxford University Press, Oxford
2. Nieuwkoop PD, Faber J (eds) (1967) Normal table of *Xenopus laevis* (Daudin). A systematical and chronological survey of the development from the fertilized egg till the end of metamorphosis, 2nd edn. North-Holland Publishing, Co., Amsterdam
3. Amaya E (2005) Xenomics. Genome Res 15:1683–1691
4. Showell C, Conlon FL (2007) Decoding development in *Xenopus tropicalis*. Genesis 45:418–426
5. Nakayama T, Blitz IL, Fish MB, Odeleye AO, Manohar S, Cho KW, Grainger RM (2014) Cas9-based genome editing in *Xenopus tropicalis*. Methods Enzymol 546:355–375
6. Karpinka JB, Fortriede JD, Burns KA et al (2014) Xenbase, the *Xenopus* model organism database; new virtualized system, data types and genomes. Nucleic Acids Res 43(Database issue):D756–D763
7. Diaz ME, Varela A, Serrano EE (1995) Quantity, bundle types, and distribution of hair cells in the sacculus of *Xenopus laevis* during development. Hear Res 9:33–42

8. Serrano EE, Trujillo-Provencio C, Sultemeier D, Bullock WM, Quick QA (2001) Identification of genes expressed in the *Xenopus* inner ear. *Cell Mol Biol* 47:1229–1239
9. Quick QA, Serrano EE (2005) Inner ear formation during the early larval development of *Xenopus laevis*. *Dev Dyn* 234:791–801
10. Varela-Ramirez A, Trujillo-Provencio C, Serrano EE (1998) Detection of transcripts for delayed rectifier potassium channels in the *Xenopus laevis* inner ear. *Hear Res* 119: 125–134
11. Sultemeier DR, Trujillo-Provencio C, Serrano EE (2007) Cloning and characterization of *Xenopus* inner ear calcium-activated potassium channel α - and β -subunits. *ARO Abstr* 30:740
12. Gabashvili IS, Sokolowski BH, Morton CC, Giersch AB (2007) Ion channel gene expression in the inner ear. *J Assoc Res Otolaryngol* 8:305–328
13. Schlosser G, Northcutt RG (2000) Development of neurogenic placodes in *Xenopus laevis*. *J Comp Neurol* 418:121–146
14. Humes HD (1999) Insights into ototoxicity: analogies to nephrotoxicity. *Ann NY Acad Sci* 884:15–18
15. Powers TR, Virk SM, Trujillo-Provencio C, Serrano EE (2012) Probing the *Xenopus laevis* inner ear transcriptome for biological function. *BMC Genomics* 13:225
16. Ramirez-Gordillo D, Trujillo-Provencio C, Knight VB, Serrano EE (2011) Optimization of gene delivery methods in *Xenopus laevis* kidney (A6) and Chinese hamster ovary (CHO) cell lines for heterologous expression of *Xenopus* inner ear genes. *Vitro Cell Dev Biol Anim* 47(9):640–652
17. Sultemeier DR, Knight VB, Manuelito SJ, Hopkins M, Serrano EE (2005) Heterologous and homologous expression systems for functional analysis of *Xenopus* inner ear genes. *ARO Abstr* 28:28
18. Agilent Technologies, Inc. (2003) Reagent kit guide: RNA 6000 nano assay. November 2003 Edition, Germany
19. Petersen MB, Willems PJ (2006) Non-syndromic, autosomal-recessive deafness. *Clin Genet* 69:371–392
20. Ramírez-Gordillo D, Powers TR, van Velkinburgh JC, Trujillo-Provencio C, Schilkey F, Serrano EE (2015) RNA-Seq and microarray analysis of the *Xenopus* inner ear transcriptome discloses orthologous OMIM® genes for hereditary disorders of hearing and balance. *BMC Res Notes*. Vol. 8:691
21. Life Technologies (2012) Working with RNA: the basics. Avoiding, detecting and inhibiting RNase. <https://www.lifetechnologies.com/content/dam/LifeTech/migration/files/dna-rna-purification-analysis/pdfs.par.91610.file.dat/co24813%20-%20rna%20basics1-final-high.pdf>
22. Nasco (2008) Animal protocol for *Xenopus laevis*, African Clawed Frog Colony. https://www.enasco.com/page/xen_care
23. Grainger Lab (2001) Grainger Lab X. Tropicalis adult husbandry protocol. <http://faculty.virginia.edu/xtropicalis/husbandry/TropadultcareNew.htm>
24. Reed BT (2005) Guidance on the housing and care of African clawed frog, *Xenopus laevis* Research Animals Department, Royal Society for the Prevention of Cruelty to Animals. <http://science.rspca.org.uk/ImageLocator/LocateAsset?asset=document&assetId=1232712646624&mode=prd>
25. Center for Biological Sequence Analysis (2013) HMMgene v. 1.1 program. <http://www.cbs.dtu.dk/services/HMMgene/>

Part II

Protein Protocols

Chapter 6

Yeast Two-Hybrid Screening to Test for Protein–Protein Interactions in the Auditory System

Iman Moeini-Naghani and Dhasakumar S. Navaratnam

Abstract

We describe a protocol to screen for protein–protein interactions using the Gal-4-based yeast two-hybrid system. In this protocol, we describe serial transformation of bait into an already constructed cDNA library in yeast AH109 cells. We find this method gives the most number of true interactions. Where a premade library in yeast cells is not available, the method outlined can be quickly adapted. AH109 cells can be first transformed with bait containing a vector followed by selection of yeast containing the bait. A second transformation of yeast cells is then accomplished with the cDNA library. The method is quick and can lead to the discovery of significant interactions.

Key words Protein–protein interactions, Yeast two-hybrid, Gal4-based, Cochlea cDNA library, pGBKT7, pGADT7, AH109, Serial transformation

1 Introduction

The yeast two-hybrid system was first developed to detect protein–protein interactions between two known proteins [1]. There are several different yeast two-hybrid systems available and several key papers and reviews have a detailed accounting [2–14]. Yeast two-hybrid systems include the GAL4-based system, the Lex-based system, and the split ubiquitin-based system [11, 14, 15]. In this chapter, we lay out our laboratory protocol on using the Gal4 yeast two-hybrid system. There are presently many exciting and newer uses of the yeast two-hybrid system, including mass screenings to globally define interacting proteins (interactome) [16–19].

A short theoretical description of the GAL4-based system follows, since this method is a recent one. Briefly, the GAL4-based assay described here is based on the fact that eukaryotic transcriptional activators consist of two parts, a DNA binding domain and a transcription activation domain, that need to be in close physical proximity with one another to initiate transcription. The DNA binding domain binds the promoter, whereupon the transcription

activation domain “instructs” RNA polymerase to transcribe a downstream (reporter) gene. The transcripts encoding the protein of interest (“bait”) are tagged to the binding domain and a mixture of different unknown proteins are tagged to the activation domain (cDNA). These are then co-transformed into yeast. Transcription ensues when the activation and binding domains are brought into close proximity, as a result of protein–protein interactions between the bait protein and an unknown second protein. By using a selectable marker downstream of the promoter, the yeast two-hybrid screen allows us to choose colonies, where an interaction has occurred between the bait protein and a second unknown protein. These colonies are then picked and grown, and the transcript encoding the protein that interacts with the bait protein is isolated and sequenced.

Described below is our laboratory protocol using the Matchmaker two-hybrid system from Clontech, a commercially available yeast two-hybrid system. This system uses the Gal4 activation and binding domains with several reporter genes (HIS3 and ADE2 α galactosidase and β galactosidase). The HIS3 and ADE2 gene products allow growth in medium lacking histidine and adenine and, also, permit us to screen with different degrees of stringency (i.e., strength of protein–protein interaction). The HIS3 marker allows for selection with medium stringency while the ADE2 marker allows for selection with high stringency. The galactosidase genes, of which the α form is secreted, allow for easy identification of interacting proteins by blue-white screening. A second feature in using the Matchmaker system is that the inserts and the bait are also epitope-tagged, allowing us to confirm protein–protein interaction *in vitro*.

In the protocol laid out herein, it is assumed that the user has access to a yeast cDNA library from the tissue of interest in AH109 cells. If not, a commercial library can be purchased and used to serially transform yeast. The yeast are then grown in differentially restrictive conditions (Synthetic dropout media (SD)—His—Ade, and Synthetic dropout media—His; *see Note 1*). The plates contain X-alpha-Gal that allows evaluation of galactosidase secretion.

Two methods can be used to introduce the two plasmids into a single yeast cell: chemical transformation and yeast mating. Chemical transformation involves physical incorporation of plasmid DNA into yeast cells, while yeast mating is dependent on haploid yeast cells mating and taking on a diploid configuration. The latter requires the presence of two complementary gene products (MAT and MAT alpha) in the two species of yeast. Yeast strain AH109 contains MAT, whereas Y187 contains MAT alpha. While mating efficiency is high and allows a larger fraction of cells carrying the prey to be interrogated by the bait, the process still involves chemical transformation of yeast strains with the bait plasmid into one strain (usually Y187) and the prey plasmid into another strain (usually AH109), when premade libraries are not available.

2 Materials

2.1 Hardware

1. 150 mm plates.
2. Benchtop centrifuge and microcentrifuge.
3. 15 and 50 mL conicals.
4. 42 and 30 °C water bath.
5. Large platform rocker with speed and temperature controls for growing yeast.
6. Large platform rocker with speed and temperature controls for growing bacteria.
7. 30 °C incubator for yeast plates.
8. 37 °C incubator for yeast plates.
9. Spectrophotometer.
10. Vortexer.
11. Large platform rocker with speed and temperature controls.

2.2 Solutions

All reagents are prepared in Milli-Q water.

1. Yeast Extract Peptone Dextrose (YPD Medium): Prepare 1 L of medium by mixing 10.0 g of yeast extract (Difco, BD Biosciences, CA), 20.0 g of Peptone (Difco), 20.0 g of Glucose, in 950 mL of Milli-Q water. Adjust pH to 6.5 and bring volume to 1 L with water. Autoclave at 120 °C for 15 min.
2. Agar Plates: Mix YPD with 10 g of Bacto-agar (Difco), autoclave at 120 °C for 15 min.
3. 2×YPD Medium: Prepare 1 L of medium by mixing 20.0 g of yeast extract (Difco), 40.0 g of Peptone (Difco), 40.0 g Glucose, and 0.6 g of L-tryptophan in 950 mL of water. Adjust pH to 6.5 with 1 N HCl and bring volume to 1 L with water. Autoclave at 120 °C for 15 min.
4. SD (Synthetic Dropout) Medium: Mix 6.7 g of Yeast Nitrogen Base without amino acids, 20.0 g of Glucose, 100 mL of 10× Dropout Supplement in 950 mL of water. Adjust pH to 5.8 with 1 N HCl and bring volume to 1 L. Autoclave at 120 °C for 15 min.
5. 10× Complete Dropout Solution. Mix the following components in 1000 mL of Milli-Q water: 200 mg of L-adenine hemisulfate, 200 mg of L-arginine HCl, 200 mg of L-histidine HCl monohydrate, 300 mg of L-isoleucine, 1000 mg of L-leucine, 300 mg of L-lysine HCl, 200 mg of L-methionine, 500 mg of L-phenylalanine, 2000 mg of L-threonine, 200 mg of L-tryptophan, 300 mg of L-tyrosine, 200 mg of L-uracil, 1500 mg of L-valine.

6. 10× Dropout Solution (-Ade/-His/-Leu/-Trp). Mix the following components in 1000 mL of Milli-Q water: 200 mg of L-arginine HCl, 300 mg of L-isoleucine, 300 mg of L-lysine HCl, 200 mg of L-methionine, 500 mg of L-phenylalanine, 2000 mg of L-threonine, 300 mg of L-tyrosine, 200 mg of L-uracil, 1500 mg of L-valine.
7. 10× Dropout Solution (-His/-Leu/-Trp). Mix the following components in 1000 mL of Milli-Q water: 200 mg of L-adenine hemisulfate, 200 mg of L-arginine HCl, 300 mg of L-isoleucine, 300 mg of L-lysine HCl, 200 mg of L-methionine, 500 mg of L-phenylalanine, 2000 mg of L-threonine, 300 mg of L-tyrosine, 200 mg of L-uracil, 1500 mg of L-valine.
8. 10× Dropout Solution (-Leu). Mix the following components in 1000 mL of Milli-Q water: 200 mg of L-adenine hemisulfate, 200 mg of L-arginine HCl, 200 mg of L-histidine HCl monohydrate, 300 mg of L-isoleucine, 300 mg of L-lysine HCl, 200 mg of L-methionine, 500 mg of L-phenylalanine, 2000 mg of L-threonine, 200 mg of L-tryptophan, 300 mg of L-tyrosine, 200 mg of L-uracil, 1500 mg of L-valine.
9. 10× Dropout Solution (-Trp). Mix the following components in 1000 mL of Milli-Q water: 200 mg of L-adenine hemisulfate, 200 mg of L-arginine HCl, 200 mg of L-histidine HCl monohydrate, 300 mg of L-isoleucine, 1000 mg of L-leucine, 300 mg of L-lysine HCl, 200 mg of L-methionine, 500 mg of L-phenylalanine, 2000 mg of L-threonine, 300 mg of L-tyrosine, 200 mg of L-uracil, 500 mg of L-valine.
10. 50% Polyethylene Glycol (PEG) Stock Solution: Dissolve 50 g of PEG 3350 in 100 mL of water. The solution may need to be heated to 55 °C to dissolve the polyethylene glycol.
11. 10× Li Acetate: Dissolve 6.6 g of LiAc in 85 mL of water and adjust pH to 7.5 with acetic acid. Autoclave at 120 °C for 15 min.
12. 10× TE buffer: Mix 12.1 g of Tris base, 3.72 g of ethylenediaminetetraacetic acid (EDTA, disodium salt) in 950 mL of water and adjust pH to 7.5 with 1 N HCl. Autoclave at 120 °C for 15 min.
13. PEG/Li Acetate solution: Mix 8 mL of 50 % PEG, 1 mL of 10× Tris-EDTA (TE) and 1 mL of 10× Li Acetate.
14. 3-Amino-1,2,4-triazole (3-AT)should be added to SD/-Trp at varying concentrations before plating cells with AH109 cells that are transformed with bait in pGBK T7 plasmid. Double transformants are then grown in SD/-His/-Leu/-Trp medium using the minimal concentration of 3-ATthat shows no growth of the bait plasmid transformed AH109 cells.
15. cDNA libraries. Chick cochlea cDNA libraries are available upon request. Please contact Dhasakumar.Navaratnam@Yale.Edu.

3 Methods

There are several different yeast two-hybrid systems available. These include the Gal4-based system, the Lex-based system, and the split ubiquitin-based system. In this chapter, we describe our protocol for the Gal4 yeast two-hybrid system.

3.1 Two-Hybrid Screening

3.1.1 Preparing the Bait Vector

1. Three methods are available for yeast two-hybrid screens: co-transformation, yeast mating, and serial transformation. Of these, we find serial transformation and mating to give the greatest number of transformants and potential interactions (see Note 2).
2. Subclone the fragment of cDNA, to be used as bait, into vector pGBK T7. Since the Gal4-based system depends on soluble proteins, it is important that the sequence of interest does not contain potentially membrane-spanning regions. Use PCR amplification to generate the cDNA fragments. Design primers complementary to the nucleic acid sequence in the fragment of cDNA with restriction fragments at their 5' ends. Remember to add an extra 4–5 nucleotides at the 5' end so that the restriction enzyme can “bite.” Also, note that the 5' end should have the protein of interest in frame with the *myc* epitope.

3.1.2 Testing for Leaky His3 Expression

(See Note 3)

1. Streak AH109 (or Y187 if using yeast mating) on YPDA plates and grow until colonies appear (~2–4 days).
2. Pick isolated colony and grow in 5 mL of YPD medium overnight at 30 °C.
3. Transfer cells to 50 mL of YPD medium and continue growing at 30 °C.
4. Periodically assess Optical Density (O.D.) at 600 nm to test that the cells are growing.
5. Once O.D. 600 exceeds 0.15–0.3, centrifuge cells at $700 \times g$ for 10 min at room temperature.
6. Resuspend cell pellet in 50 mL of 2×YPD.
7. Grow cells at 30 °C for 1–3 h with shaking in a 500 mL flask.
8. Once an O.D. 600 reading of 0.4 is attained, centrifuge cells at $700 \times g$ for 10 min at room temperature and discard supernatant.
9. Resuspend cell pellet in 50 mL of water and centrifuge at $700 \times g$ for 10 min at room temperature.
10. Resuspend cell pellet in 1.5 mL of 1.1× TE/LiAc solution centrifuge at $700 \times g$ for 10 min at room temperature, and discard supernatant.
11. Resuspend cell pellet in 0.6 mL of 1.1× TE/LiAc solution.

12. In a 1.5 mL microfuge tube, mix 0.1 µg of bait plasmid in pGBKT7 (>0.5 µg/µL) and 10 µL of denatured sheared herring testes carrier DNA (10 mg/mL). To denature carrier DNA, add desired amount of DNA from Subheading 3.1.1, step 3 to a 0.5 mL PCR tube and set thermal cycler to: 94 °C for 5 min, 4 °C for 5 min, 94 °C for 5 min, and hold at 4 °C.
13. Add 100 µL of AH109 cells from Subheading 3.1.2, step 11. Mix gently by vortexing, then add 0.6 mL of PEG/LiAc solution to each 1.5 mL microfuge tube.
14. Mix gently by vortexing, then incubate at 30 °C for 45 min. Mix cells every 15 min.
15. Add 70 µL of DMSO to each 1.5 mL microfuge tube and mix.
16. Place cells in 42 °C water bath for 15 min and mix cells every 5 min.
17. Centrifuge cells at $700 \times g$ for 2 min at room temperature.
18. Resuspend in 3 mL of 2×YPD medium and incubate cells at 30 °C for 2 h with shaking.
19. Centrifuge cells at $700 \times g$ for 2 min at room temperature.
20. Resuspend each pellet in 0.5 mL of 0.9 % NaCl.
21. Spread 50 µL cells each on two SD/-Trp/plates and two plates each of SD/-Trp/-His, containing 2.5, 5.0, 10, and 15 mM 3-amino-1,2,4-triazole and two plates of SD/-Trp/-His. If there is no growth on SD/-Trp/-His/plates without 3-amino-1,2,4-triazole, the reagent does not need to be added to SD/-Leu/-Trp/-His in Subheading 3.1.3, step 3. If however, there is leaky His3 expression, add 3-amino-1,2,4-triazole to plates at a concentration where no growth is seen (*see Note 3*).

3.1.3 Materials Prepared the Day Before the Y2H Experiment

1. Prepare sufficient subcloned pGBKT7 vector containing cDNA for entire experiment (~10 µg). We use Qiaquick purified plasmid with no further purification.
2. Prepare media and plates the day before the planned experiment and set incubator temperature for 30 °C.
3. Prepare the following number of agar plates with specific dropout medium: 200 SD/-Ade/-Leu/-Trp/-His/X-Gal plates, 200 SD/-Leu/-Trp/-His/X-Gal plates, 4 SD/-Leu plates, 4 SD/-Trp plates, and 4 SD/-Leu/-Trp/plates. Add 3-amino-1,2,4-triazole to a final concentration determined in Subheading 3.1.2 to plates lacking His (-His/), where no growth is seen in previously conducted tests, as described in Subheading 3.1.2, step 21. See also Notes 1 and 4.

3.1.4 Conducting the Y2H Experiment

The following ten steps are performed on the morning of the Y2H experiment. We use chemical transformation that has given us the

most consistent results with good viability (and contrasts favorably with electroporation).

1. Thaw 2 mL of cDNA library ($>5 \times 10^7$ colony forming units per mL) in AH109 cells at room temperature. The library contains the putative protein–protein partners or “prey.”
2. Add entire contents of library into 100 mL of 2×YPD medium.
3. Grow cells at 30 °C for 1–3 h with shaking in a 500 mL flask.
4. Periodically assess O.D. 600 to determine if the cells are growing.
5. Once O.D. 600 exceeds 0.15–0.3, centrifuge cells at $700 \times g$ for 10 min at room temperature.
6. Resuspend pellet in 100 mL of 2×YPD and grow cells at 30 °C for 1–3 h with shaking in a 500 mL flask.
7. Once an O.D. 600 reading of 0.4 is attained, centrifuge cells at $700 \times g$ for 10 min at room temperature.
8. Resuspend cells in 80 mL of water, then centrifuge cells at $700 \times g$ for 10 min at room temperature.
9. Resuspend cells in 3 mL of 1.1×TE/LiAc solution, then centrifuge cells at $700 \times g$ for 10 min at room temperature.
10. Resuspend pellet in 1.2 mL of 1.1×TE/LiAc solution. Divide cells into two 0.6 mL aliquots.
11. Prepare two sterile 15 mL conical tubes by cooling and maintaining them on ice, then add in order: 3 µg of bait plasmid in pGBK T7 ($>0.5 \mu\text{g}/\mu\text{L}$) and 20 µL of denatured sheared herring testes carrier DNA (10 mg/mL). To denature carrier DNA, add desired amount of DNA to 0.5 mL PCR tube and set thermal cycler to: 94 °C for 5 min, 4 °C for 5 min, 94 °C for 5 min, then hold at 4 °C.
12. Add 600 µL of AH109 cells from Subheading [3.1.4, step 10](#).
13. Mix gently by vortexing, then add 2.5 mL of PEG/LiAc solution to each 15 mL conical tube.
14. Mix gently by vortexing then, incubate at 30 °C for 45 min. Mix cells every 15 min.
15. Add 160 µL of DMSO to each 15 mL conical tube and mix.
16. Place cells in 42 °C water bath for 20 min and mix cells every 10 min.
17. Centrifuge cells at $700 \times g$ for 10 min at room temperature.
18. Resuspend each cell pellet in 3 mL of 2×YPD medium and incubate cells at 30 °C for 2 h with shaking.
19. Centrifuge cells at $700 \times g$ for 10 min at room temperature, then resuspend cells in 30 mL of 0.9 % NaCl.
20. Spread 150 µL of cells from conical tube 1 onto each of the 100 150 mm plates containing SD/-Ade/-Leu/-Trp/-His/

X-Gal. Spread 150 µL of cells from conical tube 2 onto each of the 100 150 mm plates containing SD/-Leu/-Trp/-His/X-Gal. Spread 150 µL from each tube on two SD/-Leu/-Trp/plate, two SD/-Leu/plate, and two SD/-Trp/plates. Please also *see Note 4*.

21. Incubate for 4–8 days at 30 °C or until colonies appear. Colonies should appear by 2 days but no longer than 8 days (*see Notes 5–8*).

3.1.5 Yeast Mating Protocol

1. Pick a single colony of Y187 that has been chemically transformed with yeast bait vector (pGBK with bait insert). Inoculate 10 mL SD/-Trp with the single colony. Incubate overnight with shaking (200 RPM on a Brand?) at 30 °C.
2. Centrifuge cells at $700 \times g$ for 10 min at room temperature.
3. Resuspend cells in 10 mL of fresh SD/-Trp and inoculate entire contents into 100 mL of fresh SD/-Trp medium. Incubate overnight with shaking (200 RPM) at 30 °C.
4. Centrifuge cells at $700 \times g$ for 10 min at room temperature. Resuspend pellet in 100 mL of 2×YPD and place in a sterile 2 L flask.
5. Thaw out one 1.5 mL frozen vial of AH109, containing the prey library and inoculate entire vial into 2×YPD medium, containing Y187 GBK bait plasmid.
6. Incubate overnight at 30 °C with shaking at 50 RPM.
7. After 18 h of incubation remove 10 µL and examine under phase contrast to confirm mating. If mating is confirmed centrifuge cells at $700 \times g$ for 10 min at room temperature. If mating is not confirmed incubate cells for another 4 h and centrifuge cells.
8. Resuspend cells in 31 mL TE. Centrifuge cells at $700 \times g$ for 10 min at room temperature. Resuspend pellet in 10 mL of TE.
9. Spread 150 µL of cells onto each of the 100 150 mm plates containing SD/-Ade/-Leu/-Trp/-His/X-Gal. Spread 150 µL of cells onto each of the 100 150 mm plates containing SD/-Leu/-Trp/-His/X-Gal. Spread 150 µL from each tube on two SD/-Leu/-Trp/plate, two SD/-Leu/plate, and two SD/-Trp/plates. Please also *see Note 4*.

3.1.6 Picking Colonies and Controlling for Artifacts

1. Count the number of colonies in the SD/-Leu/-Trp/plate, SD/-Leu/plate, and SD/-Trp/plate to determine the number of double transformants (pGADT7 and pGBKT7), and transformants with pGBK T7 respectively. The number of colonies in SD/-Leu/plate will confirm the number of viable cells in the library (titer) (*see Note 4*).

2. Pick single colonies from each plate and re-streak on similar selective plates. That is, streak colonies from SD/-Ade/-Leu/-Trp/-His/X-Gal onto SD/-Ade/-Leu/-Trp/-His/X-Gal plates, and colonies from SD/-Leu/-Trp/-His/X-Gal onto SD/-Leu/-Trp/-His/X-Gal plates (*see Notes 5–8*).
3. Pick individual colonies from each of the new plates and grow in the corresponding restrictive media by inoculating 0.5 mL of medium with one colony each. That is colonies from SD/-Ade/-Leu/-Trp/-His/X-Gal to be grown in SD/-Ade/-Leu/-Trp/-His/medium, and colonies from SD/-Leu/-Trp/-His/X-Gal on SD/-Leu/-Trp/-His/X-Gal medium.
4. Grow cells at 30 °C for 2 days with shaking at 200 RPM. .
5. Centrifuge cells at $700 \times g$ for 10 min at room temperature.
6. Resuspend cells in 5 mL of sterile SD/-Trp/medium to isolate only yeast containing the pGADT7-cDNA.
7. Grow cells at 30 °C for 2 days with shaking. Remove 0.85 mL and add 0.15 mL of sterile glycerol. Freeze in nalgene cryovials at –80 °C. These stocks serve as a reservoir in the event of unforeseen errors.
8. Centrifuge remaining cells from Subheading 3.1.6, step 7 at $700 \times g$ and proceed to isolate DNA by yeast mini-prep.

3.2 Yeast DNA Isolation and Transformation of Bacteria

3.2.1 Isolation

We have attempted to isolate yeast DNA using a number of methods with variable success (*see Note 9*). We have now settled on using the Zymoprep I/II™ Yeast Plasmid Minipreparation Kit (Zymoresearch, Orange, CA), which gives us the most consistent results. The method is similar to the commonly used alkaline lysis method used with bacteria, but has an antecedent enzyme digestion step for breaking down the cell wall.

1. Centrifuge 1.5 mL of yeast liquid culture in a 2 mL Eppendorf tube.
2. Add 15 µL of Zymolyase™ for each 1 mL of Solution 1 to make a Solution 1-enzyme mixture.
3. Add 200 µL of Solution 1 to each pellet.
4. Add a further 3 µL of Zymolyase™ to each tube. Resuspend the pellet by mild vortexing and incubate at 37 °C for 60 min.
5. Add 200 µL Solution 2 to each tube. Mix well.
6. Add 400 µL Solution 3 to each tube. Mix well.
7. Centrifuge at $18,000 \times g$ for 3 min.
8. Transfer the supernatant to the Zymo-Spin-I column.
9. Centrifuge the Zymo-Spin I column for 30 s at $14,000 \times g$.
10. Discard the flow-through in the collection tube. Make sure the liquid does not touch the bottom part of the column.

11. Add 550 μ L of Wash Buffer (EtOH added) onto the column with the collection tube and centrifuge for 1 min at 18,000 $\times g$.
12. Place column in fresh 1.5 mL microfuge tube and centrifuge at 18,000 $\times g$ for an additional 1 min.
13. Place column in fresh microtube, add 10 μ L of water, and incubate for 5 min at room temperature. Elute plasmid off the column by centrifuging for 1 min at 18,000 $\times g$.

3.2.2 Transforming Bacteria with Isolated Plasmid

The isolated DNA is used to transform bacteria (*see Note 10*). We find electroporation of the DNA (using the manufacturer's instructions) into *E. coli* DH10B (Invitrogen, Carlsbad, CA) gives the best results. Once *E. coli* are transformed, follow these steps.

1. Spread cells onto ampicillin plates using 5 mM glass beads.
2. Pick individual clones using a sterile toothpick to inoculate 3 mL of LB medium, containing 50 μ g of Ampicillin/mL. Isolate DNA using a standard mini-prep kit (e.g., Qiagen plasmid mini-prep kit).
3. Determine the sequence of the inserted cDNA using the T7 primer. We use in-house or commercial sequencing services.

3.3 Confirming Interactions

Interactions demonstrated using the yeast two-hybrid system need to be confirmed by other techniques such as immunoprecipitation or FRET (*see Note 11*). While an in-depth description of these techniques is beyond the scope of this chapter, we will mention briefly the technique of coimmunoprecipitation. We routinely use in vitro synthesized S35 Methionine-labeled protein, as it is the most useful method. The WGA system from Clontech gives us the most consistent results. We are able to use the sequences in the pGKKT7 and pGADT7 vectors without further subcloning. The vectors can be linearized and used to run off RNA using the T7 promoter. Moreover, both vectors are designed to incorporate a *Myc* and Flag tag at the N-terminus of each inserted cDNA sequence. These tags allow for easy immunoprecipitation and visualization by autoradiography of the corresponding two proteins (confirming interactions).

Also, we follow immunoprecipitation experiments *in vitro* with experiments *in vivo*, using antibodies, where available, to the two interacting proteins. When antibodies to the native proteins are not available, we resort to epitope tagging the entire protein. The proteins are then expressed in HEK cells and separately immunoprecipitated. The converse protein is then detected in the immunoprecipitate by western blotting.

3.4 Where cDNA Libraries in Yeast Are Not Available

The method outlined here assumes that you have pGAD T7-cDNA libraries in yeast AH109 cells. This method of serial transformation can be used also to test for interactions using commercial non-yeast libraries. In this case, AH109 cells derived from a fresh single

colony should be made competent as indicated in Subheading 3.1.4, steps 1–10. The cells should be transformed with bait containing pGBKT7 and grown in SD/-Trp medium. A second round of transformation is then performed using the cDNA library in pGADT7 with the same protocol outlined above (*see* Subheading 3.1.4, steps 1–21). Following the second round of transformation, cells are plated on SD/-Ade/-Leu/-Trp/-His/ plates and SD/-Leu/-Trp/-His plates to isolate colonies with interacting proteins.

4 Notes

1. Readers may wonder why we limit ourselves to using relatively stringent conditions for detecting interacting proteins. In our experience, the real difficulty with yeast two-hybrid techniques is not one of sensitivity (number of interactions) but rather one of specificity (number of true interactions). We have therefore not had to use low stringency screens. In these screens yeast after transformation of bait and prey vectors are grown in SD/-Leu/-Trp/. After colonies are identified, they are re-plated on plates with increasing stringency (SD/-Ade/-His/-Leu/-Trp/ and SD/-His/-Leu/-Trp/).
2. We have tried using co-transformation, serial transformation, and yeast mating in trying to detect protein–protein interactions. Of these methods, our data indicate that serial transformation and mating give the most number of interacting proteins. The downside to these methods is that it is possible that the bait protein could be eliminated by recombination in the event that it is toxic to the cell.
3. Leaky His3 expression. At times it is possible that the bait in pGBK T7 can alone activate transcription of the His3 protein. The level of His3 expression is low and can be easily suppressed by the addition of 3-AT. We first test if the bait protein in pGBKT7 activates His3 expression in AH109 cells by transforming these cells with the bait pGBKT7 construct alone. These cells are then plated on SD/-Trp/-His with varying concentrations of 3-AT added to the medium. We then note the concentration of 3-AT at which there is no observed growth. We then add 3-AT to SD/-Trp/-Leu/-His plates used for medium stringency screening of the yeast two-hybrid screen. We do not add 3AT to the high stringency screen (SD/-Trp/-Leu/-His/-Ade).
4. Each of the constructs contains different reporter genes allowing one to select for cells containing that construct. For instance, the pGBKT7 vector contains the tryptophan reporter allowing cells containing this vector to be grown in medium lacking tryptophan. Likewise, the pGAD T7 vector that contains the

cDNA library has the Leucine reporter. Thus, cells containing this plasmid can be grown in medium lacking leucine. Double transformants (that is cells containing both pGBKT7 and pGAD T7) can be grown on media lacking both Leucine and Tryptophan. This must be contrasted with double transformants that show an interaction that will grow in medium lacking leucine, tryptophan, histidine, and adenine. The latter two are reporters that are dependent on an interaction between the GAL4 binding domain and GAL4 activation domain.

5. A feature that must be paid attention to is the shape and the color of yeast in plates incubated in restrictive media. AH109 cells after 2–4 days of growth appear as 2–5 mm sized plaques that resemble a small blob of yoghurt. There are no visible hyphae. Contaminant yeast from ambient air can sometimes grow on these plates, but their morphology makes them easy to identify.
6. The times of incubation in restrictive conditions (SD/-His/-Trp/-Leu/; SD/-Ade/-His -Trp/-Leu/) may vary and depends on the strength of the interacting proteins. For instance, weaker interactions may result in growth that is visible after 5–8 days. The criterion that we use is the size of the yeast colony—they must be 2 mm or larger. Often colonies are seen on day 2 that do not grow to be larger than 2 mm.
7. Colonies that express Ade are white or pale pink in color. Colonies that lack Ade turn brown to red in SD/-Ade/-His/-Trp/-Leu/medium.
8. In our screens, we use both alpha and beta galactosidase assays only at the point of secondary screening. The reason we do not use this assay in the initial screening is owing to cost. Although we do not use it as a method for detecting interactions the amounts of alpha and/or beta galactosidase can also be used as a test of the strength of protein–protein interactions. There are several plate and liquid assays (chromogenic and fluorescent) for both these enzymes.
9. We have attempted to isolate yeast DNA using a number of methods with variable success. We have now settled on using the Zymoprep I/II™ Yeast Plasmid Minipreparation Kit, which has given us the most consistent results. The method is similar to the commonly used alkaline lysis method used with bacteria, but has an antecedent enzyme digestion step for breaking down the cell wall.
10. Isolated DNA from yeast mini-preps should be used to transform bacteria. This will allow adequate amounts of DNA for subsequent experiments (DNA sequencing, making proteins for pull-down assays, subcloning into mammalian expression vectors, etc.). While the commonly used heat shock method can

be used, we find the amount of recovered DNA to be variable and at times too low to effectively transform bacteria. We have instead found electroporation (using the manufacturer's instructions) into *E. coli* DH10B (Gibco BRL Life Technologies, Inc.) to give the best results. Spread cells on ampicillin plates.

11. It is now widely recognized in the field that while yeast two-hybrid technology is a sensitive technique, it is susceptible to nonspecific artifacts. A number of reasons account for this including absent physiological significance, leaky reporters, etc., and are discussed in several of the reviews below. The bait protein too does influence this to some degree. Nevertheless, it is now de-rigueur to confirm interactions detected, using the yeast two-hybrid system, by immunoprecipitation. Additionally, in vivo and subcellular interactions can further be determined using fluorescence resonance energy transfer (FRET).

References

1. Brent R, Finley RL Jr (1997) Understanding gene and allele function with two-hybrid methods. *Annu Rev Genet* 31:663–704
2. Bartel P, Chien CT, Sternglanz R, Fields S (1993) Elimination of false positives that arise in using the two-hybrid system. *Biotechniques* 14(6):920–924
3. Bartel PL, Chien C-T, Sternglanz R, Fields S (1993) Using the two-hybrid system to detect protein-protein interactions. In: Hartley DA (ed) *Cellular interactions in development: a practical approach*. Oxford University Press, Oxford, pp 153–179
4. Chien CT, Bartel PL, Sternglanz R, Fields S (1991) The two-hybrid system: a method to identify and clone genes for proteins that interact with a protein of interest. *Proc Natl Acad Sci U S A* 88:9578–9582
5. Fields S, Sternglanz R (1994) The two-hybrid system: an assay for protein-protein interactions. *Trends Genet* 10:286–292
6. Fritz CC, Green MR (1992) Fishing for partners. *Curr Biol* 2:403–405
7. Golemis EA, Gyuris J, Brent R (1994) Interaction trap/two-hybrid systems to identify interacting proteins. In: *Current protocols in molecular biology*. Wiley, Hoboken, NJ, Ch. 13 and 14
8. Golemis EA, Gyuris J, Brent R (1996) Analysis of protein interactions; and Interaction trap/two-hybrid systems to identify interacting proteins. In: *Current protocols in molecular biology*. Wiley, Hoboken, NJ, Ch. 20.0 and 20.1
9. Guarente L (1993) Strategies for the identification of interacting proteins. *Proc Natl Acad Sci U S A* 90(5):1639–1641
10. Gyuris J, Golemis E, Chertkov H, Brent R (1993) Cdi1, a human G1 and S phase protein phosphatase that associates with Cdk2. *Cell* 75:791–803
11. Johnsson N, Varshavsky A (1994) Split ubiquitin as a sensor of protein interactions in vivo. *Proc Natl Acad Sci U S A* 91:10340–10344
12. Luban J, Goff SP (1995) The yeast two-hybrid system for studying protein-protein interactions. *Curr Opin Biotechnol* 6(1):59–64
13. Mendelsohn AR, Brent R (1994) Applications of interaction traps/two-hybrid systems to biotechnology research. *Curr Opin Biotechnol* 5(5):482–486
14. Stagljar I, Korostensky C, Johnsson N, te Heesen SA (1998) Genetic system based on split-ubiquitin for the analysis of interactions between membrane proteins in vivo. *Proc Natl Acad Sci U S A* 95(9):5187–5192
15. Fields S, Song OA (1989) novel genetic system to detect protein-protein interactions. *Nature* 340:245–246
16. Fields S (2005) High-throughput two-hybrid analysis. The promise and the peril. *FEBS J* 272:5391–5399
17. Goll J, Uetz P (2006) The elusive yeast interactome. *Genome Biol* 7(6):223
18. Stelzl U, Wanker EE (2006) The value of high quality protein-protein interaction networks for systems biology. *Curr Opin Chem Biol* 10(6):551–558
19. Suter B, Auerbach D, Stagljar I (2006) Yeast-based functional genomics and proteomics technologies: the first 15 years and beyond. *Biotechniques* 40(5):625–644

Chapter 7

Multiplexed Isobaric Tagging Protocols for Quantitative Mass Spectrometry Approaches to Auditory Research

Douglas E. Vetter and Johnvesly Basappa

Abstract

Modern biologists have at their disposal a large array of techniques used to assess the existence and relative or absolute quantity of any molecule of interest in a sample. However, implementing most of these procedures can be a daunting task for the first time, even in a lab with experienced researchers. Just choosing a protocol to follow can take weeks while all of the nuances are examined and it is determined whether a protocol will (a) give the desired results, (b) result in interpretable and unbiased data, and (c) be amenable to the sample of interest. We detail here a robust procedure for labeling proteins in a complex lysate for the ultimate differential quantification of protein abundance following experimental manipulations. Following a successful outcome of the labeling procedure, the sample is submitted for mass spectrometric analysis, resulting in peptide quantification and protein identification. While we will concentrate on cells in culture, we will point out procedures that can be used for labeling lysates generated from tissues, along with any minor modifications required for such samples. We will also outline, but not fully document, other strategies used in our lab to label proteins prior to mass spectrometric analysis, and describe under which conditions each procedure may be desirable. What is not covered in this chapter is anything but the most brief introduction to mass spectrometry (instrumentation, theory, etc.), nor do we attempt to cover much in the way of software used for post hoc analysis. These two topics are dependent upon one's resources, and where applicable, one's collaborators. We strongly encourage the reader to seek out expert advice on topics not covered here.

Key words Proteomics, iTRAQ, Quantitative mass spectrometry, Protein expression

1 Introduction

A unique watershed moment in biology occurred with the release of the initial drafts of the entire genome sequence derived from first model organisms. This event led to the completion of whole genomic sequencing of many other organisms, including human. The ability to read genomic sequences and map genes within genomic space is certainly a powerful tool. However, it can also be argued that the vast majority of practicing biologists today actually work on understanding the role of *proteins* in their chosen sub-discipline, whether to seek an understanding of development,

disease states and their progression, or normal cellular processes. Yet the methods used by many biologists to examine the transcriptome only details the state of the transcript and hence the state of gene expression; whereas, it is the protein(s) encoded in each transcript that is more often the actual effector molecule of interest. One assumption tacitly made is that gene expression equals protein expression, but this is clearly not always (some may say rarely!) true [1, 2]. Thus, as we push beyond the genomic age, into a post-genomic epoch of biology, one must increasingly come to terms with techniques that are more suited to assess the effectors of biological processes. The transcriptome is a static entity in terms of sequence (save for the uncommon, or experimentally induced, mutation and methylation), whereas proteins have many more degrees of freedom that make their assessment particularly challenging. These can include post-translational modifications, which can be many (phosphorylation, palmitoylation, sumoylation, etc.), the timing of these changes, alternative splicing from the genome, and RNA editing-induced changes to the protein sequence (and therefore function), which is not even revealed in the genomic sequence. Coupling these issues with the observation that many genes can encode more than one protein (and in some cases hundreds of proteins), one begins to get the sense of the enormous task facing the biologist wishing to examine the state of the proteome in their sample of interest. Indeed, while estimates of the number of genes making up the genome generally are settled between 20,000 and 30,000 genes, estimates of the functional proteome range is in the 100,000s. While biological complexity certainly resides within the genome, a simple comparison of the number and sequence of genes between the worm, *C. elegans*, and humans, illustrates that a major portion of the biological complexity separating these species resides in gene function, and even more importantly, in the interactions between gene products.

The study of proteins in biological processes crossed a watershed point with the coupling of mass spectrometry (MS) with biological samples, even though techniques used for assessing protein expression and quantification were in use for many years before. The “need” that led to this change in approach is traced to the difficulty of assessing large numbers of proteins simultaneously, as well as assessing proteins for which no discriminatory tag is available (either an antibody, or a fusion protein expressed *in vivo*). The chief advance made possible by MS-based proteomics is the freedom to discover otherwise unanticipated changes in protein expression, post-translational modification, etc., that are involved in particular biological processes. The evaluation of these expression states leads to the establishment of protein interaction networks. Many methods exist for establishing and quantifying interaction networks, however, they all result in testable hypotheses of mechanism(s) that regulate phenotypic changes in an organism.

The end result can reveal protein interactions not previously appreciated, as well as altered cellular states observed in disease or experimenter-induced changes in cells/tissues. Thus, an understanding can be attained of how a phenotype occurs when that phenotype is not directly related to an altered gene [3, 4]. Inherent in this kind of approach is the movement away from a purely reductionist view of biology, to a more global, interactive view characterized by the systems biology approach.

Many of the most successful proteomics experiments to date (at least related to higher organisms) have used proteomic approaches to study changes in specific structures such as organelles [5–7], synaptic junctional preparations [8], etc. This illustrates a key principle in proteomics—simplifying the sample results in better discrimination of protein changes.

There are a number of issues that must be considered once a decision is made to tackle a proteomics project. A firm commitment must be made to the type of data collection, since in most cases, strategies adopted may be mutually exclusive for other purposes. Thus, if there is an interest in examining phosphorylation states of proteins, a sample preparation/isolation method is used that is significantly different from more routine protein expression studies. Similarly, if interested in glycosylation states of membrane-associated proteins, isolation may be significantly different than when assessing the nuclear proteome. Other concerns include whether the sample is pre-fractionated prior to further processing, run on a one- or two-dimensional gel or a liquid chromatography column, tagged for future quantification, or whether the protein remains tagless. One rule of thumb is that each time the sample is manipulated there is a likelihood that protein loss *will* occur. The threshold at which these losses might alter the outcome of the experiment is difficult or impossible to know *a priori*.

Finally, although space does not allow a full description of mass spectrometry-based proteomics here, several review articles can help the uninitiated to navigate the decisions that must be made and to allow a better appreciation of the concerns [9–13]. Here, we limit ourselves to detailing the preparation of a protein lysate sample for quantifying expression levels *in vitro* and for giving a quick introduction to the analyses of the resulting data.

1.1 Labeling Methods for Quantitative Differential Mass Spectrometry

1.1.1 Isotope-Coded Affinity Tag (ICAT)

We will outline three of the more common methods of differential labeling in this section and detail one of them further in Section 3. Figure 1 schematically demonstrates the major steps of these methods side by side.

ICAT (Fig. 1a) was one of the first methods by which peptides could be differentially labeled prior to submission for mass spectrometric analysis [14]. Briefly, this technique uses a biotinylated reagent with a specificity toward sulfhydryl groups. The labeling

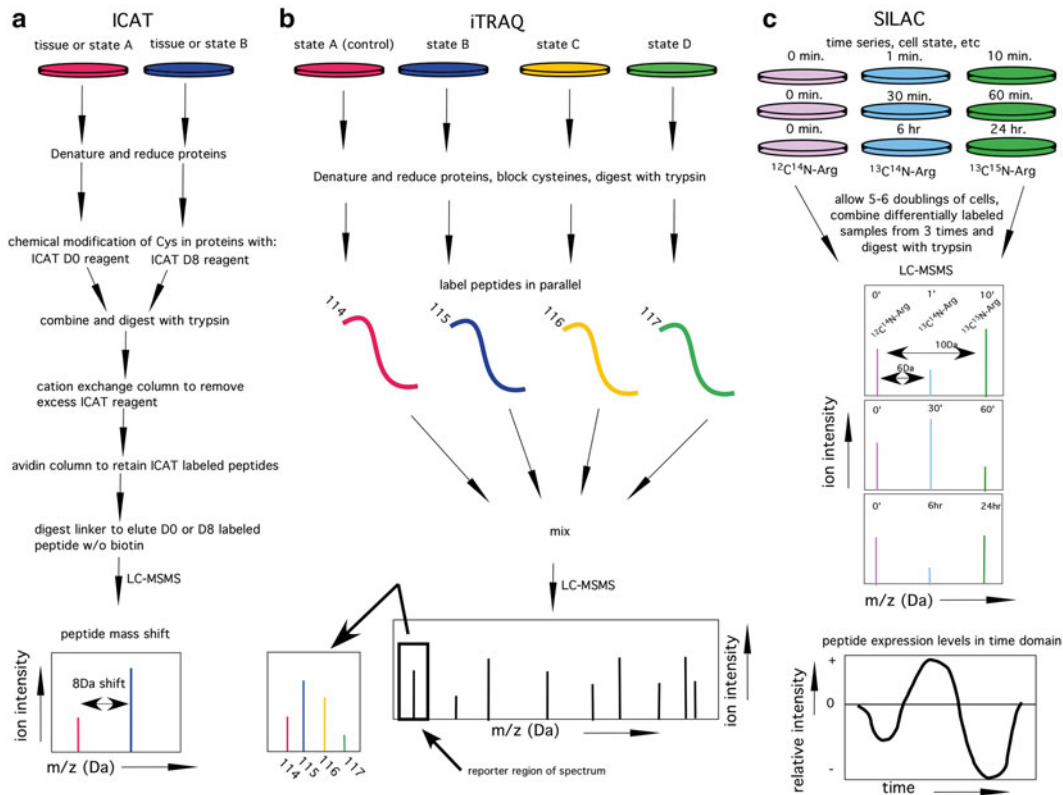


Fig. 1 Comparison of major steps in labeling proteins or peptides for quantitative mass spectrometric analysis. (a) When using ICAT, compare tissues or cells by first denaturing the proteins in the lysate and then labeling all cysteine residues with one of two labels. The light label contains normal hydrogen at specific sites, while the heavy label contains deuterium substituted in place of the hydrogens. In all, the heavy label is 8 Da heavier than the light label. Lysates are mixed at this point and digested with trypsin. Following digestion, the resultant-labeled peptides are selected for and retained over an affinity column, eluted and subjected to liquid chromatography and mass spectrometry. Peptides exactly 8 Da apart are examined and, when matched by sequence, the ion intensity (or the precursor LC peak area) is assessed for quantitation purposes. (b) When using iTRAQ, cells or tissues of different states are lysed, denatured, and digested. Each pool is labeled separately, then mixed, submitted to LC-MSMS, and each label is assessed for ion intensity. Labels are freed during peptide bond cleavage, and are found in a low mass region of the spectrum, separated by 1 Da. (c) In SILAC procedures, one metabolically labels all proteins by allowing the cells to incorporate various heavy-labeled arginine (depicted here) and/or lysine into the generated proteins. Lysates are obtained, mixed, digested, and any post-translational modifications desired are selected and submitted to LC-MSMS. Expression data are plotted in the time domain to gain an understanding of the temporal nature of modifications. For example, if one is looking at phosphorylation events, data can indicate the time course of phosphorylation and dephosphorylation, as depicted in the bottom panel

reagent carries either a “heavy” (d_8) or “light” (d_0) tag (Fig. 2a). This sample is combined with a second, independently labeled sample carrying the other tag, which is then compared to the first. The combined samples are then trypsinized. Labeled peptides are recovered from the mixture via biotin affinity chromatography.

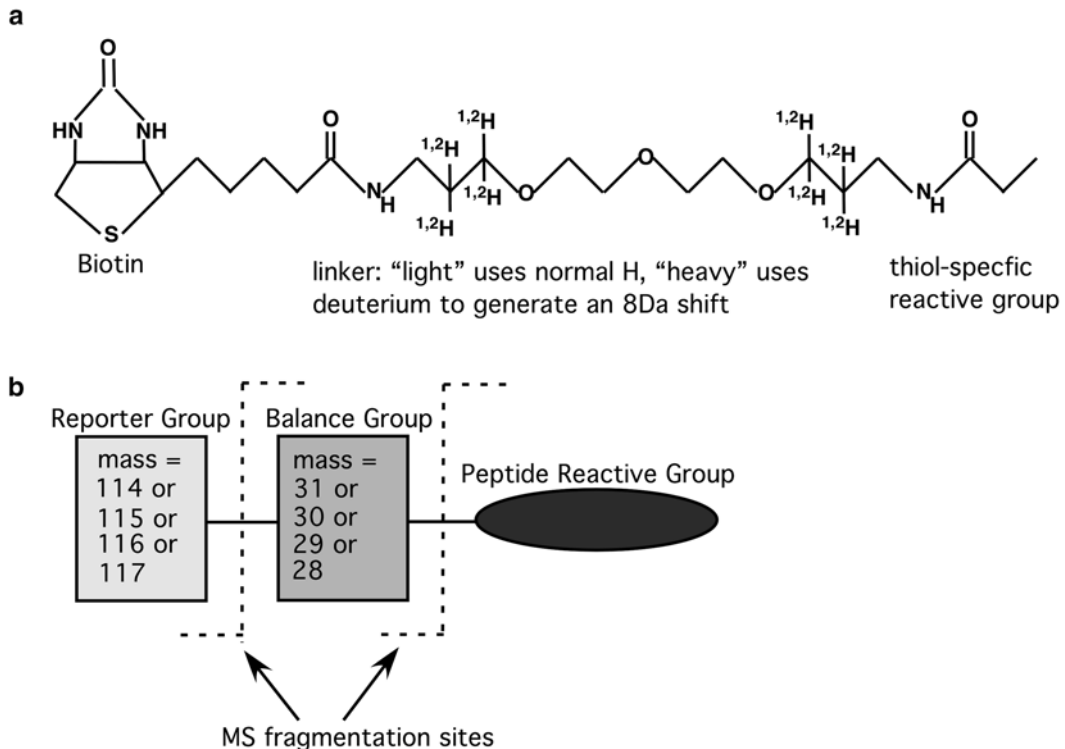


Fig. 2 Labels for ICAT and iTRAQ technologies. **(a)** The ICAT label is composed of a biotin moiety used for affinity selection, a linker, which contains either ¹H or D (²H) substitutions as indicated, and a thiol reactive group that binds to free cysteines of the protein. The biotin group is cleaved after the affinity column selection step and the peptide released. **(b)** The iTRAQ label consists of a reporter group of varying mass and a balance group that is co-varied with the mass of the reporter group, such that each peptide labeled carries an isobaric tag (i.e. a tag of the same mass). The label also contains a peptide reactive group that is reactive toward primary amines and ϵ amines of lysine residues. Upon dissociation in the mass spectrometer, peptide bonds are broken, releasing the peptide and the balance and reporter groups. The peptide undergoes further peptide bond breaks to yield the MSMS peptide sequence, while the balance group is lost in the very low mass region of the spectrum. The reporter group is found in a very quiet region of the spectrum and is assessed for total ion count/intensity to yield the quantitative information needed for analysis

Following cleavage of the sample from the biotin moiety and release from the affinity column, the mixture is analyzed via liquid chromatography coupled mass spectrometry (LCMS). Analysis consists of examining the ratio of ion intensities of the heavy and light sequence-matched peptides in the MS. The final result yields both sequence information of the peptide following tandem MS procedures and quantification of each peptide. Two potential drawbacks of the ICAT approach are its dependence on the occurrence of cysteines in the proteins of interest (a minor difficulty, as most proteins do contain cysteine residues) and the number of cysteine residues. The latter can be more problematic if the proteins of interest contain few cysteine residues. Unambiguous protein

identification from a complex peptide mixture requires good coverage of the parent protein by the recovered peptides. Therefore, if there are few cysteine residues, and thus few labeled peptides, protein identification may be compromised. The advantage of the ICAT system is its relative ease of use, and its applicability to lysates generated from any source (cell culture, tissues, etc.). A number of protocols have been published concerning ICAT [15].

1.1.2 Isobaric Tagging for Relative and Absolute Quantification (iTRAQ)

iTRAQ (Fig. 1b) is similar in concept to ICAT, but differs in that amines are modified to carry a label for quantification (Fig. 2b). With iTRAQ, one also has the ability to multiplex up to four samples for simultaneous differential MS quantification. Unlike the ICAT system, with iTRAQ, samples are trypsinized first prior to labeling. This approach has the advantage of labeling all peptides, since trypsin cuts at lysine/arginine sequences, and the iTRAQ system labels ε amines of each lysine. In addition, other free amines carry a label as well. The manner by which quantification is accomplished in the MS is similar to the way ICAT ratios of ion intensities are used to assess changes in peptide expression between samples. In the mass spectra, the location of the quantified peaks is remote from the peptide sequence peaks, due to the cleavage of the label from the peptide during the collision-induced dissociation phase of the tandem MS run. The advantage here is that all label peaks at mass 114, 115, 116, and 117 are collected in one place in the spectrum that is relatively “quiet” (Fig. 4). Thus, suppression by abundant peptide species is generally very low, and the signal more accurately reflects the true expression level. An added advantage to iTRAQ over ICAT is that peptide coverage of protein sequences is more complete due to the greater number of labeled peptides available for analysis. This coverage leads to a better resolution of protein identification, especially with family members that have a highly conserved sequence. While iTRAQ can be used for samples generated from tissue as well as for cell culture, the majority of work thus far is from in vitro preparations.

1.1.3 Tandem Mass Tags (TMTs)

Labeling techniques for relative quantification of proteins have continued to evolve. The iTRAQ technique has continued to grow in popularity since the original publication of this volume. At the time of writing this update, over 1500 publications can be found on PubMed using iTRAQ as a search term. Perhaps one of the more significant advances in quantitative proteomics has been the continued evolution of instrumentation, but not to be overlooked are the developments occurring in the procedures of peptide labeling. Here we wish to highlight, in abbreviated form, the availability of a new set of mass tags that function very much like the iTRAQ reagents, but which also have some expanded properties that the end user may appreciate and find useful for specific experimental work flows. Thermo Scientific has developed a set of novel reagents

called tandem mass tags (TMTs) for use in peptide labeling [16]. Similar to the standard iTRAQ reagents, the TMT reagents are composed of an amide-reactive NHS-ester group, a spacer arm, and a mass reporter. The mass reporter is cleaved during MSMS, leaving resides in the 126–131 Da region of the MSMS spectrum. The standard kit allows six-plex labeling of complex samples, thus increasing the experimental design toward simultaneous analysis of six different conditions/time points, etc. Using appropriately equipped MS instruments capable of high-energy collision dissociation (HCD), one may take advantage of a 10-plex reagent kit. The 10-plex makes use of differential resolution of ^{13}C and ^{15}N isotopes within the mass reporter, which yield slightly different masses in the MSMS spectrum. For example, the TMT 10 -127N will be visible with a monoisotopic reporter mass of 127.124760, while the same label carrying heavy carbon instead of nitrogen, termed TMT 10 -127C, will have a mass of 127.131079.

Of special interest to investigators wishing to examine peptides potentially involved in disulfide bonds in the parent protein, an iodoacetyl TMT reagent has also become available from Thermo Scientific in either a single label or six-plex version. These kits employ a TMT tag containing a cys-reactive group that allows for quantitative investigations of cysteine containing peptides. The tag produces an irreversible labeling of sulphydryl groups. Because of the presumed lower abundance of such peptides in complex samples, it is suggested that the investigator use an immobilized anti-TMT antibody resin to enrich the final submitted sample for the label. The analysis makes use of standard CID energies for MSMS, although HCD and ETD may also be used.

Finally, another specialty labeling kit produced by Thermo Scientific is the aminoxyTMT kit. This chemistry is useful for quantitative assessments of carbonyl-containing compounds and also comes as a single or six-plex labeling kit. The aminoxy group of the labeling reagent is reactive toward carbonyls. This is predicted to be useful for steroids, oxidized proteins, and especially carbohydrates. The kit is therefore of use for investigating the glycome via analysis of N-linked glycans. Unlike all of the labeling reagents considered to this point, the aminoxyTMT mass tag reagents are used following PNGaseF/G glycosidase treatment of samples (tissue/cells, fluids), which releases N-linked glycans. The N-linked glycans are then separated/enriched from the rest of the material via a simple hydrophobic column, and then labeled with the aminoxyTMT reagent of choice. The labeling occurs at the reducing end of the glycan. Given the complexity of the glycome, and the increasing interest in general glycobiology and variations of the glycome associated with disease states (for example, Huntington's Disease [17], etc.), the aminoxyTMT labeling kit may be very useful in proteome discovery pipelines.

1.2 Absolute Quantification Without Labeling

The techniques described above produce relative assessments of protein expression. They are all based on some basal level of expression from which a change under experimental manipulation is assessed. These analyses are most often pursued using a global discovery approach in which an information-dependent acquisition (IDA) of data is performed and matched across the global proteomic database. In an IDA approach, peptides are picked by the mass spectrometer for analysis based on several user-defined *a priori* rules, but which are generally designed to simply examine the highest peak intensities without a hypothesis driven reason. Additionally, all fragments (transitions) generated from that peptide are passed on for detection. While powerful in discovering the “lay of the land,” it is a well-known problem of such MS approaches that results are too often impossible to fully replicate not only between different labs, but even in the same lab between runs. Potentially interesting peptides are not always observed in all sample replicates due to many factors, including sample complexity and the automated procedure of peak picking for MSMS analysis used in peptide identification. Sample complexity can result in lost identifications due to competition between co-eluting peptides (ion suppression), or simply from the mass spec being busy analyzing one signal while another is present in the chromatography run whose peak is lost (i.e. when the time differential between peaks is too short). To overcome such problems, a *multiple reaction monitoring* (MRM) MS technique can be developed (*see* [18] for review). MRM uses information based on first round discovery-mode (IDA) results to develop a highly specific *targeted-mode* approach to peptide tracking and quantification. MRM-MS tracks single transitions from predefined peptides of interest (i.e. those observed as differentially expressed under IDA mode). Because definitions of transition states are physical constants that are used to follow a peptide, results are highly reproducible between experiments and are obtained with highest sensitivity since only this transition is monitored at any time. Thus, MRM transition definitions also allow for independent follow-up of the peptide across labs. The key to biologically relevant and successful MRM studies lies in knowledge first gained during discovery phase (IDA) work, and depends on a previously complete analysis of proteins expressed in the sample under specific conditions. While *in silico* assumptions may be made concerning proteins and their transition states, this is no substitute for empirically derived data-driven MRM production. The largest challenge to adopting MRM as a standard practice for quantitative proteomics is the issue surrounding the time and cost of assay development. One must first select individual peptides for analysis, and this is required for numerous (dozens to hundreds) proteins. Absolute quantification is attained by producing stable isotope-labeled peptides that are distinguishable from native peptides assayed from the sample. These labeled peptides are

spiked into the mix and used as exemplars against which to compare the target peptide. Previous calibration of MS signal by known concentrations of each labeled peptide is used to determine the concentration of the targeted peptide, when the signal from the targeted peptide is compared to the labeled peptide spiked into the mix. The production of these calibration peptides can be expensive, given the requirement for purity and the use of stable isotopes in their production. Nonetheless, because of the selected monitoring of very specific transitions (fragmentations), MRM is extremely sensitive and highly reproducible. As MRM transition databases continue to grow, thus obviating the need for extensive early phase IDA analysis (and thereby decreasing some expense), MRM-based quantification will become the typical method for quantification of the proteome.

1.3 Stable Isotope Labeling of Amino Acids (SILAC) in Cell Culture

SILAC (Fig. 1c) is significantly different from either ICAT or iTRAQ style approaches. With the SILAC approach, all proteins are labeled *metabolically* via incorporation of labeled arginine, lysine, or both [19, 20]. Additionally, the label can be light, intermediate, or heavy by using the desired amino acid carrying ^{13}C , ^{15}N , or double $^{13}\text{C}^{15}\text{N}$ substitutions. Because of the number of possible labels (four if one also considers the unlabeled control state), multiplexing is possible with SILAC. The key to successful SILAC labeling is allowing the cells to completely incorporate the labeled amino acids into all the proteins. Therefore, cells are passaged a minimum of five to six times in the presence of the labeled amino acids to accomplish full incorporation [20]. SILAC techniques are used to create dynamic temporal maps of protein expression changes in response to various manipulations [21]. The strength of the SILAC approach resides in its tagless approach to differential MS analysis, thus alleviating potential LC problems (co-elution issues, etc.). Additionally, the population of cells analyzed is typically homogeneous, thereby simplifying the proteomic complexity normally inherent in tissue. Thus, signals are cleaner, allowing a deeper probe into the proteome and, thereby allowing access to less abundant and potentially more “biologically significant” proteins. The significant downside to SILAC is its inability to be used in complex organisms, although reports exist of metabolically labeling *Drosophila* and *C. elegans* for quantitative proteomic analysis [22]. Additionally, a potential arginine to proline interconversion can take place if the arginine is not kept at sufficiently low concentrations in the culture media. This inter-conversion can lead to artifactual loss of arginine signal. However, the most likely problem faced when using SILAC techniques is the issue of cost. Stable isotopes of amino acids can be very expensive and specialized cell culture media is required. Also, serum additives generally cannot be used due to the potential for introducing unlabeled amino acids to the cells. Not all cells grow and thrive in serum-free conditions.

Numerous other methods exist [23] for labeling, such as ^{18}O labeling, and peptide acylation, more commonly referred to as a global internal standard technique (GIST). However, ICAT, iTRAQ, and SILAC represent the most commonly used techniques, and it is relatively straightforward to perform the labeling chemistry, as these are available in kit form from vendors.

2 Materials

2.1 Hardware

1. Refrigerated bench-top centrifuge capable of $18\text{--}20,000 \times g$.
2. SpeedVac® or similar vacuum concentrator.
3. 60 °C Heat block.
4. 37 °C Incubator.
5. Vortexer.
6. pH paper.
7. 2.5 mL Hamilton syringe with a blunt 22-gauge needle.
8. Standard lab pipettors.
9. Tissue grinder with ground glass surfaces (Kontes, Vineland, NJ).
10. PepClean C18 columns (Pierce, Milwaukee, WI).
11. Probe sonicator.
12. More sophisticated equipment may be required depending on the level of sample pre-fractionation desired, including Mini-Rotofor® (BioRad, Hercules, CA), FPLC, or HPLC capable of performing reverse phase chromatography. These more specialized pieces of equipment will not be covered further, but may be mentioned where appropriate.

2.2 Specialized Reagents/Solutions

2.2.1 Lysate Generation

1. Hanks' buffered saline solution (HBSS) without CaCl_2 , MgCl_2 , MgSO_4 .
2. RIPA lysis buffer or a similar lysis solution such as Pierce's T-Per: 1 % NP-40 or Triton X-100, 1 % sodium deoxycholate, 0.1 % SDS, 0.15 M NaCl, 0.01 M sodium phosphate, pH 7.2.
3. Protein assay kit.

2.2.2 iTRAQ Labeling

1. iTRAQ labeling system kit (Applied Biosystems, Foster City, CA).
2. Acetonitrile, high purity, stored at room temperature.
3. 0.5 % fresh trifluoroacetic acid in water preferably made from stock TFA packaged in glass ampoules and stored at room temperature.
4. Methanol, high quality, such as HPLC grade and stored at room temperature.

5. Absolute ethanol, high quality, such as HPLC grade, and stored at room temperature.
6. 2 % SDS, molecular biology grade, in ddH₂O.
7. 50 mM Tris-(2-carboxyethyl) phosphine (TCEP) in ddH₂O.
8. 200 mM Methyl methanethiosulfonate (MMTS), or 200 mM iodoacetamide, both in isopropanol.
9. 0.5 M Triethylammonium bicarbonate, pH 8.5 in ddH₂O.
10. 1 M KCl in ddH₂O.
11. Cation exchange loading buffer for chromatographic peptide clean up: 10 mM KH₂PO₄ in 25 % acetonitrile.
12. Cation exchange chromatography cartridge cleaning solution: 10 mM KH₂PO₄, pH 3.0 in 25 % acetonitrile/1 M KCl.
13. Chromatographic elution buffer: 10 mM KH₂PO₄, pH 3.0 using 10 mM K₂HPO₄ in 25 % acetonitrile/350 mM KCl.
14. Trypsin of the highest quality that is treated with 1-tosylamido-2-phenylethyl chloromethyl ketone (TPCK) (*see* Section 3.3). We have successfully used both Applied Biosystems and Sigma-Aldrich. Also, *see* Note 1 on optional use of immobilized trypsin systems. Whatever the source of trypsin, it must be mass spectrometry grade.
15. Acetone of high purity, store at room temperature.
16. Dissolution buffer: 0.5 M triethylammonium bicarbonate, pH 8.5.

3 Methods

Protocols such as those described herein are becoming more commonplace in modern neuroscience research, and many modifications exist when pursuing slightly different goals. Thus, what we describe here should be recognized as simply the beginnings of the dive into proteomic space. However, it deserves reiteration here that without proper handling of samples prior to generation of the spectra and quantification of the results, all downstream applications will be compromised. Thus, it is with this in mind that we attempt here to get the investigator off to a good start by informing them of this technology and the major potential pitfalls along the way.

Conceptually, the labeling of a sample for iTRAQ analysis is straightforward, and uses well characterized chemistries familiar to most protein chemists. As detailed in the stepwise workflow diagramed in Fig. 3 and explained in detail in Section 1.1, the methods describe the following steps:

- Generate protein lysates.
- Reduce disulfide bonds.

- Block the reactive cysteines.
- Digest the proteins to their constituent peptides.
- Differentially label the peptides of each sample with one of the iTRAQ reagents.
- Combine samples.
- Submit for mass spectrometry analysis and analyze results.

Sample preparation, processing, and labeling will be covered stepwise. However, only general points of mass spectrometry data analysis will be covered, due to the variations and complexities introduced by experiment specific issues. We suggest consulting mass spectrometry core personnel. The goal here is to alert and inform the reader to issues directly under the control of the biologist that can impact downstream analysis so that properly informed decisions can be made where necessary.

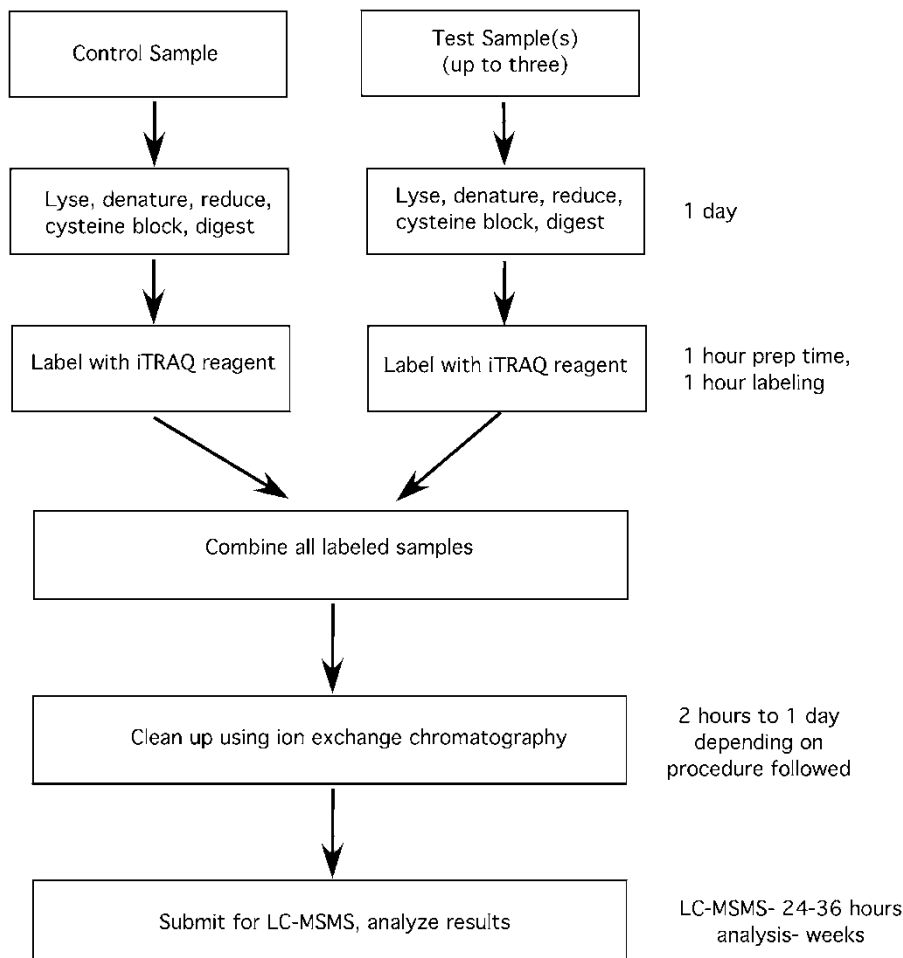


Fig. 3 Flow diagram for iTRAQ labeling procedure. See text for specific information on each step

3.1 Sample Preparation

3.1.1 Cell Culture

1. Generate samples by manipulating flasks/dishes of cells as required for the experiment (i.e. drug application, activation by bioactive molecules, etc.). Keep samples separate through these steps. We use OC-K3 cells, but the steps detailed here are useful for any cell line or primary cell culture. Numerous cell lines are now available for those interested in cell biological processes of auditory system-derived cells [24, 25].
2. Wash cells gently in ice-cold HBSS 2×.
3. Remove HBSS each time by aspiration, but do not allow the cells to dry. It is vitally important to carry out the lysis steps at 4 °C to inhibit proteolysis.
4. Immediately add the minimal volume of lysis buffer needed to cover the cells, and incubate on ice for approximately 10–20 min (*see Note 2*).
5. Scrape and transfer cell/lysis buffer solution to an appropriate sized tube. Usually a 1.5–2 mL snap top eppendorf tube will suffice, but this will depend on the size of the dish being lysed.
6. Optional step: Sonicate, on ice, to further disrupt cells, denature genomic DNA, and decrease viscosity of sample.
7. Centrifuge at 18–20,000 ×*g* in a refrigerated centrifuge at 4 °C for 20 min to pellet cellular debris.
8. Transfer supernatant to fresh tube. Lysate should optimally be used immediately, but can be stored at –80 °C as required.
9. Estimate protein concentration (*see Note 3*). For future use, have on hand approximately 250 µg–1 mg of protein per sample condition. Adjust the concentration of the sample to 10 mg/mL. The final protein lysate can be stored at –80 °C for future use.

3.1.2 Tissues (*See Note 4*)

1. Process tissue to remove blood by transcardial perfusion of ice-cold saline.
2. Dissect quickly and immerse in lysis buffer at 4 °C in a tissue grinder.
3. Grind tissue to fully lyse the sample. When isolating cochlea, care should be taken to extract any cerebellar tissue from the recess holding the flocculus. Entire cochlear samples can be prepared, or cochlea microdissected without the bone capsule prior to lysis.
4. An optional step can be performed utilizing a probe sonicator. Sonication must be performed at 4 °C (*see Note 5*).
5. Follow Section 3.1.1, steps 6–9.

3.1.3 Phosphoprotein Enrichment

At times, the investigator may wish to assess post-translationally modified proteins. Numerous possibilities exist for enriching a sample for proteins/peptides that have undergone post-translational modifications. *See Note 6* for details.

3.2 Sample Processing (See Note 7)

3.2.1 Acetone Precipitation

Standard acetone precipitation techniques can be used to isolate the proteins of a sample from potentially interfering substances, or to concentrate the sample.

1. Transfer sample to a tube that can hold approximately 10× the sample volume.
2. Chill both the sample and the acetone to 4 °C.
3. Add six volumes of the cold acetone to the sample in the larger tube.
4. Cap the tube, and invert the sample 3–5× to thoroughly mix the sample and acetone.
5. Incubate the tube at -20 °C for 4 h. A precipitate should become clearly visible.
6. Briefly centrifuge at 4 °C to pellet the precipitate ($18,000 \times g$ for 2 min).
7. Decant off the acetone from the tube and proceed immediately to the reducing and blocking steps (Subheading 3.2.2). Do not allow the pellet to dry.

3.2.2 Denaturing, Reducing, and Cysteine Blocking the Sample (See Note 8)

1. Add 20 µL of dissolution buffer per tube containing up to 100 µg of protein sample or the acetone precipitated pellet. In order to have ample sample for labeling and processing, one may wish to label 250 µg of protein. Simply scale up the reaction as required (see Note 9). Add 1 µL of the denaturant (2 % SDS).

2. Check the pH of the solution by spotting some of the sample onto pH paper. The pH should be above 8.0.
3. Vortex to mix well, but avoid formation of bubbles/foam. Spin at low speed if necessary to eliminate foam.
4. Add 2 µL of reducing agent (50 mM TCEP) and vortex again to ensure complete mixing.
5. Incubate tubes at 60 °C in a heat block for 1 h.
6. Pulse spin briefly to collect sample at the bottom of the tube.
7. Add 1 µL cysteine blocking reagent (200 mM MMTS or iodoacetamide).
8. Vortex to mix, and incubate at room temperature for 10 min.

3.3 Trypsin Digest (See Note 10)

3.3.1 Digesting Samples with Trypsin

1. Dissolve trypsin at 1 µg/µL in ddH₂O or if using trypsin from the iTRAQ kit, use 25 µL Milli-Q standard H₂O per tube. If preparing more than two samples for analysis, prepare 50–60 µg of trypsin, or two tubes from kit.
2. Vortex to mix thoroughly.

3. To each 100 µg of sample in dissolution buffer from Subheading 3.2.2, step 8, add 10 µL of trypsin solution. Keep the final volume below 50 µL, or SpeedVac® as appropriate prior to the addition of trypsin.
4. Vortex to mix thoroughly.
5. Incubate at 37 °C for 16 h (overnight).

3.4 Labeling Samples with iTRAQ Reagents

The heart of the iTRAQ technology lies in the ability of the investigator to efficiently and completely label each peptide in a sample with a traceable, quantifiable tag. Each sample is processed separately to label the peptides.

1. Equilibrate the iTRAQ reagent to room temperature before use.
2. Add 70 µL of absolute ethanol to each iTRAQ label tube that will be used.
3. Vortex approximately 1 min to ensure complete mixing and dissolving.
4. Transfer the entire volume of one iTRAQ label reagent tube to one sample tube such that each sample tube receives one iTRAQ reagent. Usually, controls are labeled with the 114 reagent, but of course this is up to the investigator. It is critical to keep track of which sample received which label, as downstream quantification depends on the proper ratio of control to manipulated state.
5. Vortex to mix, and then pulse spin to collect all solutions to the bottom of the tube.
6. Incubate at room temperature for 1 h.
7. Combine the label reactions into one tube, such that a single tube receives each label singly, without duplication of labels if doing more than four labels (for the 4-plex kit, 8 if using the soon to be released 8-plex kit).

1. Follow Subheading 3.4, steps 1–6, but only label one digested sample, using the 114 label.
2. Dry sample in a SpeedVac® and resuspend in 20 µL of 0.5 % trifluoroacetic acid (TFA) in 5 % acetonitrile per 30 µg total peptide.
3. Calculate the number of columns required. The number of columns needed depends on the amount of peptide being run. The binding capacity of each column is 30 µg, so calculate the number relative to the binding capacity of the columns and the amount of peptide used.
4. Wet the resin of the spin column with 200 µL of 50 % methanol.

3.4.1 Assessing Completeness of Labeling Reaction (See Note 11)

5. Spin at $1500 \times g$ for 1 min.
6. Repeat **steps 4** and **5**, discarding the flow-through each time.
7. Add 200 μL of 0.5 % TFA in 5 % acetonitrile to each spin column.
8. Spin at $1500 \times g$ for 1 min and discard the flow-through.
9. Repeat **steps 7** and **8**.
10. Apply the labeled sample onto the bed of the spin column.
11. Spin at $1500 \times g$ for 1 min at room temperature.
12. Set flow-through aside in case sample binding needs to be verified.
13. Apply 200 μL of 0.5 % TFA in 5 % acetonitrile to wash the column and spin at $1500 \times g$ for 1 min.
14. Discard flow-through and repeat **step 13**.
15. Elute the sample from the column by adding 20 μL of 70 % acetonitrile to the bed of the column and centrifuging at $1500 \times g$ for 1 min.
16. Repeat **step 15** with fresh 70 % acetonitrile.
17. Dry the sample in a SpeedVac®.
18. Resuspend the sample in 30 μL dissolution buffer.
Repeat the labeling reaction as outlined in Subheading **3.4**, **steps 1–6**, using the 117 iTRAQ labeling reagent (*see Note 12*).

3.5 Preparing the Combined Sample for Mass Spectrometry (See Also Note 13)

The entire volume of all samples is combined in a 1:1:1:1 ratio. The most common method of analyzing the iTRAQ sample is via LC-MS/MS. Thus, the sample must be prepared so that it will be efficiently nebulized during the electrospray introduction into the mass spectrometer. At this stage, it is recommended that personnel who run the samples through the mass spectrometry be consulted, because the type of LC one performs will dictate to some degree the final preparation of the sample. A clean up procedure of the sample is described here as a general guide.

1. Assemble the cation exchange system as per manufacturer's instructions. Most important is the fitting between the syringe and the needle to port adapter. Be sure that the system is snug to keep solutions from backing up and out of the system.
2. Dilute the concentration of undesirable materials such as salts and detergents by adding ten volumes (relative to the sample) of loading buffer.
3. Vortex to mix thoroughly.
4. Spot an aliquot onto pH paper to ensure the pH of the solution. The pH must be between 2.5 and 3.3. Add more loading buffer as needed to attain the proper pH (*see Note 14*). Prepare the

column to accept the sample by injecting 1 mL of conditioning buffer. Allow flow-through to go to waste. All injections should be made with a slow and steady pace.

5. Inject 2 mL of loading buffer into the cartridge and divert flow-through to waste.
6. Inject diluted sample at a rate of approximately 1 drop/s into the column. Collect the flow-through and save until sure that the peptides were maintained on the column.
7. Inject 1 mL of loading buffer to wash the column. Save in the same tube as used in step 7. This step may be repeated as necessary.
8. Elute retained peptides by slowly (~1 drop/s) injecting 500 μ L of elution buffer. Collect the eluate into one tube.

3.6 Mass Spectrometric Analysis of iTRAQ-Labeled Samples

The iTRAQ system makes use of isobaric tagging reagents (Fig. 2b) that carry a highly efficient and accurate peptide reactive group, a balance group, and one of a series of reporter groups of differential mass that is capable of maintaining its charge. The tags co-elute during typical reverse phase liquid chromatography performed prior to injection into the mass spectrometer, and are cleavable under MSMS conditions. Upon cleavage in the collision cell of a mass spectrometer, the tag is released from the peptide, thereby giving rise to two important regions of the spectrum: (1) the sequencing portion of the spectrum, where the data for peptide sequence are maintained; and (2) the reporter region of the spectrum, in which the isobaric tags are found. Figure 4 illustrates these regions as viewed in ProteinPilot (see Note 15). Finally, the reporter region is typically a relatively “quiet” region in the spectrum, and thus one can be confident that the peaks observed are derived from the tag itself. If other peaks are present in the reporter region, this may be an indication of noise resulting from poor sample processing, contaminants, etc.

3.7 What to Do with All of Those Data

Both proteomic and genomic analyses are wonderful in that one receives so much data. However, therein also lies the problem (and the danger)—how to verify the results, and what to do with the results once verified. Lists of proteins expressed are useful, but only at a superficial level. Verification can take the form of western blot analysis, follow-up proteomic analysis, etc. Bioinformatic approaches to proteome analyses are maturing at a steady and ever increasing pace. At this stage, of course, the investigator must decide in which direction to proceed. Listed in Note 15 are URLs that can be used as a jumping off point to investigate various databases and software. Of particular interest are those that detail methods by which protein:protein interactions are modeled [26–29], and tools with which to generate and investigate interaction pathways [30–32].

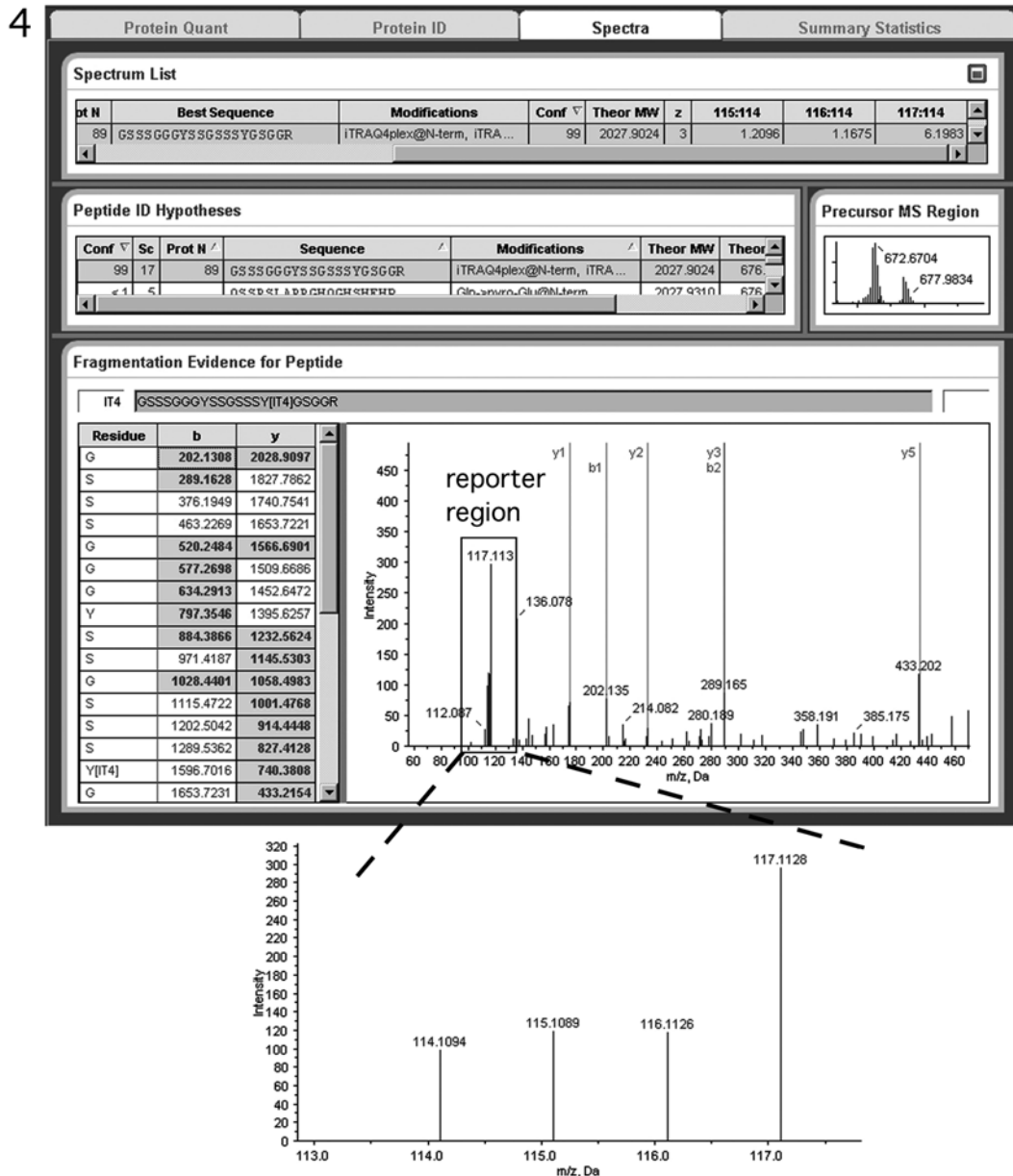


Fig. 4 ProteinPilot screen shot of typical results from an iTRAQ experiment. When examining the spectra of a peptide of interest (spectrum list), ratios of labels are indicated (here, 114 was used as the normal state, and therefore the denominator for the ratio). Additionally, the spectrum is inspected for manual annotation and analysis if desired in the fragmentation window. Regions can be zoomed in as indicated here to visually inspect the reporter region of the spectrum (dashed lines). In this case, this peptide was upregulated only during conditions in state 3 (~6× upregulated), while under conditions 1 and 2 (labeled with 115 and 116 reporters, respectively), no change is detected from baseline (label 114)

4 Notes

1. Immobilized trypsin can be obtained from Pierce or Sigma in which trypsin is cross-linked to agarose beads and is present as a slurry. To use immobilized trypsin, follow these steps:
 - Wash 100–250 µL of the trypsin bead slurry with 500 µL of water or a trypsin digestion buffer without primary amines. Repeat for a total of three times, each time centrifuging the beads down ($\sim 2000 \times g$) and decanting or pipetting off the supernatant. Be sure to thoroughly resuspend the beads with each wash and vortex to ensure complete mixing.
 - Resuspend the slurry in 200 µL of water or a trypsin digestion buffer without primary amines.
 - The sample should be resuspended in water or a trypsin digestion buffer without primary amines at a final concentration of 2 µg/µL.
 - Add the sample to the resuspended trypsin slurry.
 - Vortex to ensure complete mixing.
 - Incubate 16 h (overnight) at 37 °C with end-over-end mixing if possible.
 - Isolate the digest by spinning the slurry down and collecting the supernatant.
 - SpeedVac® the digest and bring back up in dissolution buffer to 30 µL.
 - Any formulation of lysis buffer should suffice (RIPA buffer, T-Per or M-Per from Pierce, etc.), and the exact composition of the lysis buffer will depend on the proteins targeted for analysis. For example, isolation and analysis of membrane proteins will demand a different lysis buffer from the standard lysis buffer for cytoplasmic proteins. Usually, the differences between lysis buffers are in detergent and/or osmolarity used. No protease inhibitors should be present, as this will inhibit the tryptic digest in downstream steps.
2. We have had good success with the Pierce MicroBCA kit.
3. Tissues represent a more difficult sample to deal with, owing primarily to the greater complexity of tissue compared to cells in culture. However, this should not dissuade one from such experiments, but rather alert one to the potential pitfalls associated with working with highly complex material. One major determinant of the success of proteomic analysis of tissue samples is the presence and successful depletion of plasma in the sample. Plasma is in such abundance that it often times masks proteins from detection. Various methods exist for depleting

tissue samples of plasma (or at least lessening the contribution of plasma to the protein mixture). For simplicity, we suggest first perfusing ice-cold saline transcardially through the animal in an attempt to clear the blood while also slowing proteolysis. Here, the investigator may need to adjust the procedure depending on the requirements for the experiment.

4. The advantage to sonication is the resultant decrease in viscosity due to the breakdown of the genomic DNA. Experience with the tissue of interest will reveal whether this is a significant problem to be addressed.
5. Many proteins are regulated by post-translational modifications. One of the most studied modifications is the addition of phosphate groups to distinct residues of proteins. If one is interested in assessing phosphorylation states on proteins in the samples, various enrichment protocols can be followed. The reader is directed to the Pierce Phosphoprotein Enrichment Kit (cat# 90003) as a potential starting point, although others exist from different vendors. These columns are simple to use, and yield a significant enrichment of phosphoproteins, but at the expense of losing non-phosphorylated proteins from the sample.
6. Numerous substances in the sample mixture can potentially interfere with the final labeling reaction. Chief among these are amine-containing compounds such as ammonium sulfate, -bicarbonate, -citrate, etc. These will interfere with the labeling process by competing for the iTRAQ label. Other issues to be concerned with are the presence of thiols that are typically introduced into sample mixtures by the addition of DTT or 2- β -mercaptoethanol (2 β ME), which can interfere with the cysteine blocking steps, and high amounts of detergents or denaturants, which will interfere with the tryptic digest step. Should any of these be present in the sample, one must perform a standard acetone precipitation step to isolate the sample from the interfering substance. If DTT or 2 β ME are present, the acetone precipitation should be performed immediately prior to moving on further in the procedure. If either detergents or primary amines are present, acetone precipitation can be performed either after reducing the sample and blocking the free cysteines (in the case of detergents that might be necessary for maintaining sample solubility), or just prior to tryptic digest (in the case of the presence of primary amines). The best practice is to avoid the need for precipitation at all, as this step represents a major point in the overall procedure where uncontrolled sample loss can occur, thereby, introducing bias in the relative amounts of proteins present in each sample. However, precipitation cannot always be avoided. If the trypsin digest will employ an immobilized trypsin (*see Note 1*),

acetone precipitation will be required, and the sample should be resuspended only in ddH₂O or a buffer without primary amines. In this case, the acetone precipitation should be performed after denaturing, reducing, and cysteine blocking steps detailed in Subheading 3.2.2. Prior to acetone precipitation, one may also wish to enrich for phosphoproteins (*see Note 6*). On occasion, the sample may be insoluble in the dissolution buffer concentration plus SDS as added. Should this be a problem, the dissolution buffer volume can be increased up to 50 µL without adversely affecting the labeling step. If more is required, one should first SpeedVac® the sample to near dryness, and add up to 100 µL of dissolution buffer. Should this still not solve a problem of an insoluble sample, two alternatives exist. One may either use a detergent/denaturant or a different buffer. An addition of 1 µL of 2 % SDS per 20 µL of the dissolution buffer will keep the concentration of SDS low enough so as to not interfere with the future trypsin digest. Use of denaturants or detergents other than SDS are possible, and included octyl β-D glucopyranoside (OG), NP-40, Tween-20, Triton X-100, and CHAPS (all at less than or equal to a 1 % final concentration), or urea at less than 1 M. In all cases, the aqueous partition of the sample must not be higher than 40 % to avoid problems with final labeling. Any other buffers tried should not carry primary amines, and should buffer at pH 8.0–8.5. These include, but are not limited to, BES, BICINE, CHES, HEPES, MOBS, MOPS, and PIPES. Concentration should be kept at approximately 0.3 M such that at the labeling step, the buffer concentration does not fall below 0.06 M.

7. In order to best label the proteins in the sample, one first must denature the sample to allow equal access to all possible modifiable amino acids carrying primary amines. Because denaturing with chemicals such as SDS will unfold proteins, but not destroy secondary structure induced by the presence of disulfide bonds, the denatured proteins must then be chemically reduced, generally using either DTT or some other reducing agent. The iTRAQ kit uses tris-(2-carboxyethyl)phosphine (TCEP) for this purpose. TCEP is used to denature the sample so that thiols are not introduced to the sample (*see* Subheading 3.2). Finally, the reduced cysteines must be blocked. Typically, this is done with iodoacetamide (at a concentration of 200 mM in isopropanol). One may use this, but the iTRAQ kit includes methylmethane-thiosulfonate (MMTS, 200 mM in isopropanol) for cysteine reduction. The advantage of MMTS is that it is a reversible blocker that can be useful should one decide to fractionate the sample by selectively isolating cysteine-containing peptides. We have found the procedure employed by the iTRAQ kit to be easy to follow and to yield excellent labeling.

8. It is critically important, however, to not allow the protein concentration to significantly decrease due to an increase in volume. If the sample is insoluble at a final concentration of 5 mg/mL, *see Note 7* for alternatives.
9. Trypsin is a pancreatic serine endoprotease derived from pancreatic trypsinogen following a removal of its N-terminal leader sequence. Trypsin is highly selective in its cleavage of peptide bonds, and cleaves only those bonds in which the carboxyl group is contributed by arginine or lysine. When trypsin is treated with 1-1-tosylamido-2-phenylethyl chloromethyl ketone (TPCK-treated), any contaminating chymotrypsin activity is irreversibly inhibited. Additionally, when the lysine residues of trypsin are modified by a reductive methylation process, autolytic cleavage of trypsin is also irreversibly inhibited. This results in a loss of tryptic peptide fragments in the mass spectra. Neither treatment alters the trypsin activity toward the proteins present in the lysates. TPCK modification is especially important in iTRAQ-labeled mass spectrometry. Contaminating chymotryptic digests result in cleavage of peptides at the carboxyl side of tyrosine, tryptophan, and phenylalanine (i.e. amino acids containing phenyl rings). With longer digests, chymotrypsin will also hydrolyze other amide bonds, particularly those with leucine-donated carboxyls. These digests do not guarantee that a modifiable residue will be present in each resultant peptide. Following tryptic digestion, one can be sure that each peptide generated possesses at least a single modifiable amino acid that can be labeled by the iTRAQ reagents. Thus, TPCK-modified trypsin should always be used. Immobilized trypsin (*see Note 1*) is also especially useful, since autolysis, and therefore spectral peaks derived from trypsin, is virtually eliminated. However, immobilized trypsin is not provided with the iTRAQ kit. The investigator should determine the need for elimination of trypsin-derived peaks and balance the extra effort/cost with the desired results.
10. The first time one performs the iTRAQ labeling procedure, it may be worth the added effort to first assess one's success in fully labeling a sample. Without complete labeling, some peptides will be unlabeled and not represented in the reporter region of the spectra (see further discussion below) despite the fact that the peptides are actually present in the sample. A simple test can be performed to assess the completeness with which the sample is labeled with the aid of C18 spin columns such as that from Pierce (PepClean C18 columns). These columns are good general tools for purifying and concentrating peptide samples.
11. If the initial labeling reaction was not carried to completeness, the sample should contain both the 114 and the 117 labels in the mass spectrum analysis. As long as no 117 label is detected,

the initial labeling reaction can be considered complete, and there would be little need to further analyze labeling efficiency in the future unless significant changes to sample preparation are encountered.

12. Many compounds potentially present in the sample can interfere with the LC-MS/MS analysis. These include, but are not limited to, the dissolution buffer, ethanol, TCEP, any salts, excess iTRAQ labeling reagent, denaturants, and detergents. Thus, a simple method for cleaning the sample needs to be used. Cation exchange chromatography can be used to isolate the sample from interfering compounds and allows one to replace the sample diluent with a more “mass spec friendly” diluent. A variety of cation exchange systems can be purchased. One system that uses spin column and vacuum plate technology for ion exchange chromatography is the VivaPure system (Sartorius Biotech, Inc., Goettingen, Germany). The system appears straightforward to use, but we have had no first-hand experience with this. Included in the Applied Biosystems Methods Development Kit is a system for performing cation exchange chromatography on the sample prior to submission for mass spectrometry. However, this system is useful only for relatively simple samples such as that obtained from phosphopeptide-enriched samples, samples that have undergone some other type of affinity enrichment, or samples from cell culture. Complex samples such as those obtained from tissue lysates will require more complicated fractionation, perhaps even over a two-dimensional LC system, prior to MS analysis. For complex samples, or if more complex fractionation is desired (thus allowing one to uncover signatures of the less abundant proteins in the sample), the appropriate personnel should be consulted.
13. The cation exchange column will only work properly when the peptides are carrying a cationic charge. The charge allows them to adhere to the column matrix while inorganics, such as salts, and organics such as acetonitrile, can be flushed away.
14. A viewer version of Protein Pilot can be obtained as freeware distributed by Applied Biosystems for use with data generated by their QStar and QTrap mass spectrometers. The exact file type the investigator will receive back from the mass spectrometry facility will depend on the type of instrument used, local preferences for software, etc. Here, we will only present analysis performed with the Protein Pilot software. However, other software will perform in a similar manner. Data represented in ProteinPilot include proteins detected in the sample, the ratio of tags for that protein, individual peptide sequence and tag ratios, and a spectral characterization of tag intensities. From these four simple windows, one can quickly assess relative protein concentrations between the samples analyzed.

However, one should also inspect the protein identification window to make investigator-based decisions concerning identifications. In the best cases, one should expect detection of multiple peptides of the protein being identified and these peptides should span numerous regions of the protein. Thus, peptides from N- and C-term regions, as well as internal regions should be present to allow for the best identification. However, this is not always available, and so further investigation in these cases needs to be done to assess the veracity of the identification in light of incomplete coverage.

15. Useful URLs detailing protein interaction databases, and pathway visualization and structure analysis include:
 - Human–protein interaction database [33], <http://www.hpid.org/>;
 - Human–protein reference database, <http://www.hprd.org>;
 - Mammalian protein–protein interaction database (MIPS);
 - <http://mips.gsf.de/proj/ppi>;
 - Molecular interactions database (MINT) [34], <http://mint.bio.uniroma2.it/mint>;
 - Proteomics Identifications database (PRIDE) [35, 36], <http://www.ebi.ac.uk/pride>;
 - Protein–protein interaction network visualization software Cytoscape [37] GenePro plug-in for Cytoscape, <http://genepro.ccb.sickkids.ca/index.html>;
 - ProViz <http://cbi.labri.fr/eng/proviz.htm>.

Acknowledgements

This work was supported by funding to DEV from NIH R01 DC006258, R21 DC015124, and Univ. Mississippi Medical Center Office of Research.

References

1. Anderson L, Seilhamer J (1997) A comparison of selected mRNA and protein abundances in human liver. *Electrophoresis* 18:533–537
2. Gygi S, Rochon Y, Franza B, Aebersold R (1999) Correlation between protein and mRNA abundance in yeast. *Mol Cell Biol* 19:1720–1730
3. Grant S, Blackstock W (2001) Proteomics in neuroscience: from protein to network. *J Neurosci* 21:8315–8318
4. Gavin A, Aloy P, Grandi P et al (2006) Proteome survey reveals modularity of the yeast cell machinery. *Nature* 440:631–636
5. Coughenour H, Spaulding R, Thompson C (2004) The synaptic vesicle proteome: a comparative study in membrane protein identification. *Proteomics* 4:3141–3155
6. Andersen J, Lam Y, Leung A, Ong S, Lyon C, Lamond A, Mann M (2005) Nucleolar proteome dynamics. *Nature* 433:77–83
7. Yates J, Gilchrist A, Howell K, Bergeron J (2005) Proteomics of organelles and large cellular structures. *Nat Rev Mol Cell Biol* 6:702–714
8. Langnaese K, Seidenbecher C, Wex H, Seidel B, Hartung K, Appeltauer U, Garner A, Voss

- B, Mueller B, Garner CC, Gundelfinger ED (1996) Protein components of a rat brain synaptic junctional protein preparation. *Brain Res Mol Brain Res* 42:118–122
9. Yates J (1998) Mass spectrometry and the age of the proteome. *J Mass Spectrom* 33:1–19
 10. Yates J (2000) Mass spectrometry. From genomics to proteomics. *Trends Genet* 16: 5–8
 11. Fountoulakis M (2004) Application of proteomics technologies in the investigation of the brain. *Mass Spectrom Rev* 23:231–258
 12. Ferguson P, Smith R (2003) Proteome analysis by mass spectrometry. *Ann Rev Biophys Biomol Struct* 32:399–424
 13. Mann M, Hendrickson R, Pandey A (2001) Analysis of proteins and proteomes by mass spectrometry. *Ann Rev Biochem* 70:437–473
 14. Gygi S, Rist B, Gerber S, Turecek F, Gelb M, Aebersold R (1999) Quantitative analysis of complex protein mixtures using isotope-coded affinity tags. *Nat Biotechnol* 17:994–999
 15. Shioi Y, Aebersold R (2006) Quantitative proteome analysis using isotope-coded affinity tags and mass spectrometry. *Nature Prot* 1: 139–145
 16. Quan L, Miao L (2013) CID, ETD, and HCD fragmentation to study protein post-translational modifications. *Mod Chem Appl* 1:e102
 17. Gizaw ST, Koda T, Amano M, Kamimura K, Ohashi T, Hinou H, Nishimura S-I (2015) A comprehensive glycome profiling of Huntington's disease transgenic mice. *Biochem Biophys Acta* 1850:1704–1718
 18. Ebhardt HA, Root A, Sander C, Aebersold R (2015) Applications of targeted proteomics in systems biology and translational medicine. *Proteomics* 15(18):3193–3208
 19. Ong S, Mann M (2006) A practical recipe for stable isotope labeling by amino acids in cell culture (SILAC). *Nat Prot* 1:2650–2660
 20. Amanchy R, Kalume D, Pandey A (2005) Stable isotope labeling with amino acids in cell culture (SILAC) for studying dynamics of protein abundance and posttranslational modifications. *Sci STKE* 2005, pl2
 21. Blagoev B, Ong S, Kratchmarova I, Mann M (2004) Temporal analysis of phosphotyrosine-dependent signaling networks by quantitative proteomics. *Nat Biotechnol* 22:1139–1145
 22. Krijgsveld J, Ketting RF, Mahmoudi T, Johansen J, Artal-Sanz M, Verrijzer CP, Plasterk RH, Heck AJ (2003) Metabolic labeling of *C. elegans* and *D. melanogaster* for quantitative proteomics. *Nat Biotechnol* 21:927–931
 23. Julka S, Regnier F (2004) Quantification in proteomics through stable isotope coding: a review. *J Proteome Res* 3:350–363
 24. Rivolta M, Grix N, Lawlor P, Ashmore J, Jagger D, Holley M (1998) Auditory hair cell precursors immortalized from the mammalian inner ear. *Proc Biol Sci* 265:1595–1603
 25. Rivolta M, Holley M (2002) Cell lines in inner ear research. *J Neurobiol* 53:306–318
 26. Bork P, Jensen LJ, von Mering C, Ramani AK, Lee I, Marcotte EM (2004) Protein interaction networks from yeast to human. *Curr Opin Struct Biol* 14:292–299
 27. Sharan R, Suthram S, Kelley RM, Kuhn T, McCuine S, Uetz P, Sittler T, Karp RM, Ideker T (2005) Conserved patterns of protein interaction in multiple species. *Proc Natl Acad Sci U S A* 102:1974–1979
 28. Sharan R, Ulitsky I, Shamir R (2007) Network-based prediction of protein function. *Mol Systems Biol* 3:88
 29. Fernandez-Ballester G, Serrano L (2006) Prediction of protein-protein interaction based on structure. *Meth Mol Biol* 340:207–234
 30. Iragne F, Nikolski M, Mathieu B, Auber D, Sherman D (2005) Proviz: protein interaction visualization and exploration. *Bioinformatics* 21:272–274
 31. Yan W, Lee H, Yi EC et al (2004) System-based proteomic analysis of the interferon response in human liver cells. *Genome Biol* 5:R54
 32. Suderman M, Hallett M (2007) Tools for visually exploring biological networks. *Bioinformatics* 23:2651–2659
 33. Han K, Park B, Kim H, Hong J, Park J (2004) Hpid: the human protein interaction database. *Bioinformatics* 20:2466–2470
 34. Chatr-aryamontri A, Ceol A, Palazzi LM, Nardelli G, Schneider MV, Castagnoli L, Cesareni G (2007) Mint: the molecular interaction database. *Nucleic Acids Res* 35:D572–D574
 35. Jones P, Cote RG, Cho SY, Klie S, Martens L, Quinn AF, Thorneycroft D, Hermjakob H (2008) Pride: new developments and new datasets. *Nucleic Acids Res* 36(Database Issue): D878–D883
 36. Jones P, Cote RG, Martens L, Quinn AF, Taylor CF, Derache W, Hermjakob H, Apweiler R (2006) Pride: a public repository of protein and peptide identifications for the proteomics community. *Nucleic Acids Res* 34:D659–D663
 37. Shannon P, Markiel A, Ozier O, Baliga NS, Wang JT, Ramage D, Amin N, Schwikowski B, Ideker T (2003) Cytoscape: a software environment for integrated models of biomolecular interaction networks. *Genome Res* 13:2498–2504

Chapter 8

Protein Quantitation of the Developing Cochlea Using Mass Spectrometry

Lancia N.F. Darville and Bernd H.A. Sokolowski

Abstract

Mass spectrometry-based proteomics allows for the measurement of hundreds to thousands of proteins in a biological system. Additionally, mass spectrometry can also be used to quantify proteins and peptides. However, observing quantitative differences between biological systems using mass spectrometry-based proteomics can be challenging because it is critical to have a method that is fast, reproducible, and accurate. Therefore, to study differential protein expression in biological samples labeling or label-free quantitative methods can be used. Labeling methods have been widely used in quantitative proteomics, however label-free methods have become equally as popular and more preferred because they produce faster, cleaner, and simpler results. Here, we describe the methods by which proteins are isolated and identified from cochlear sensory epithelia tissues at different ages and quantitatively differentiated using label-free mass spectrometry.

Key words Cochlea, Label-free quantitation, LC-MS/MS, Mass spectrometry, Proteomics

1 Introduction

Mass spectrometry (MS) is an important tool in proteomics that can provide identification and quantitation of proteins. However, mass spectrometry is not inherently quantitative due to the fact that peptides have a wide range of physiochemical properties, such as size, charge, and hydrophobicity [1]. These differences lead to a significant difference in mass spectrometry response. Therefore, for mass spectrometry-based quantitation there are two approaches, absolute and relative quantitation, which involves labeling or label-free approaches (Fig. 1). MS-based absolute quantitation involving labeling, uses a known amount of isotope-labeled standard that is mixed with the analyte and the absolute amount of the analyte is calculated from the ratio of ion intensity between the analyte and its standard [2] (Fig. 2a). In contrast, absolute quantitation using the label-free approach uses a modified spectral counting method known as absolute protein expression (APEX) [3]. The absolute

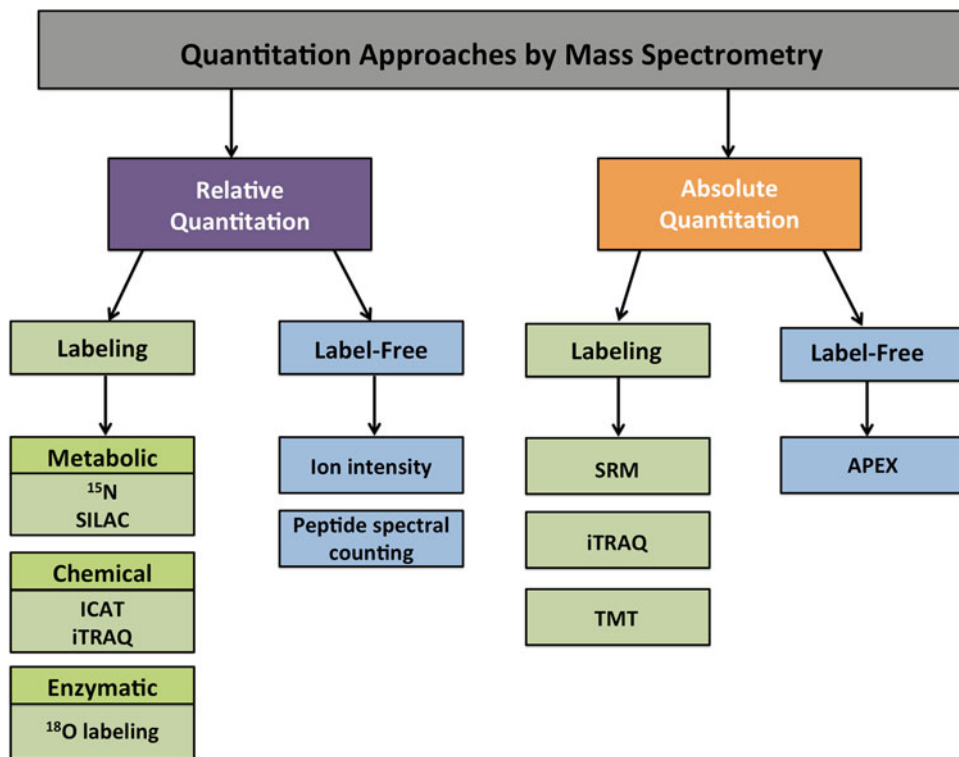


Fig. 1 An overview of the different mass spectrometry-based quantitative approaches in proteomics

protein concentration of each protein in a sample is calculated based on the empirical relationship between the number of spectra or peptides identified for a protein and the protein abundance in the sample [4]. Most commonly used is relative quantitation involving labeled or label-free methods. In the labeled approach, proteins from different samples are labeled differently and the peptides from the different samples are mixed and identified in the same spectra with different masses. Commonly used labeling techniques include metabolic labeling, chemical mass tagging, and enzymatic labeling (Fig. 1). In metabolic labeling, stable isotopes are incorporated into the protein sequence *in vivo*. Stable isotope labeling by amino acids in cell culture (SILAC) [5] is a commonly used metabolic labeling method, however it does not work well for all cell types and limited on the number of samples that can be analyzed per experiment [1]. Chemical mass tagging involves tagging proteins or peptides with stable isotopes *in vitro*. Isobaric tags for relative and absolute quantitation (iTRAQ) [6] and isotope-coded affinity tags (ICAT) [7] are commonly used chemical mass tagging methods. However, these methods are limited by their susceptibility to side reactions that can lead to unwanted products, which can adversely affect the quantitation [1]. Another labeling method is enzymatic addition of stable isotopes, which involves

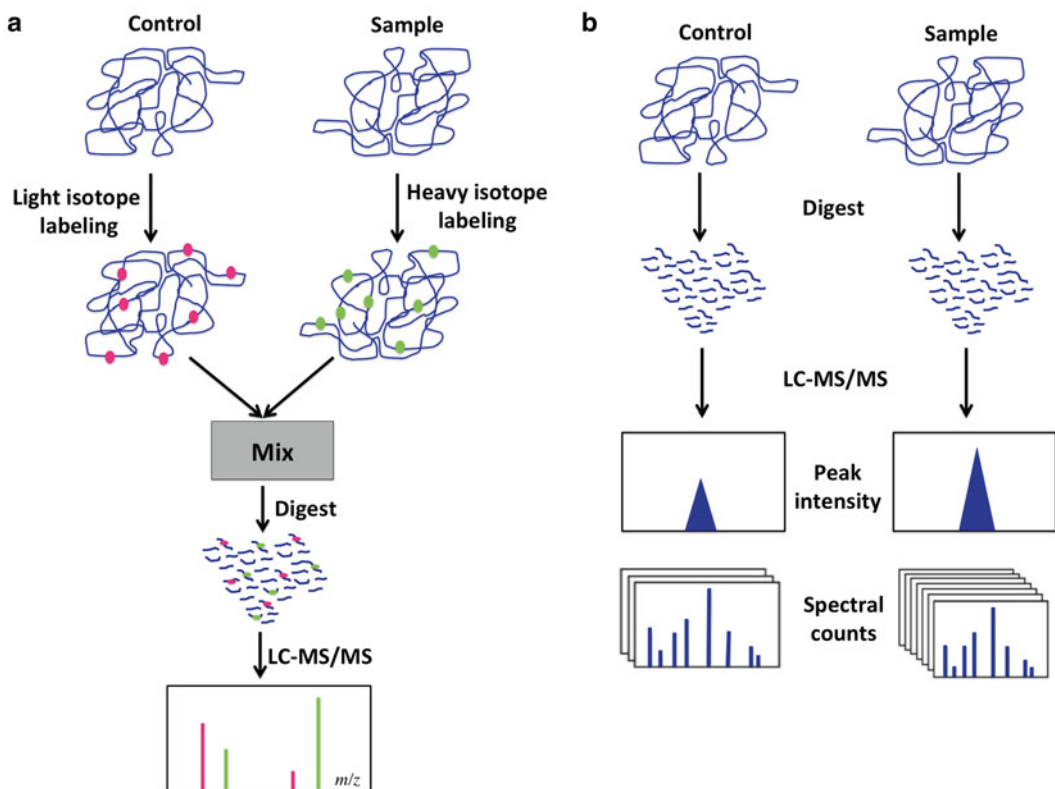


Fig. 2 General quantitative mass spectrometry workflows in differential protein expression analysis. **(a)** Label-based quantitative mass spectrometry and **(b)** label-free quantitative mass spectrometry

peptide digestion and isotope labeling simultaneously, thereby generating peptides that are a few Da heavier. ^{18}O labeling is commonly used and generates peptides 2 or 4 Da heavier due to the exchange of 1 or 2 oxygen atoms with ^{18}O at the carboxyl end of the peptide [3, 8]. However, a limitation with this method is that it has incomplete labeling efficiencies and the rates of labeling for different peptides will vary [1].

Relative quantitation by the label-free approach involves the samples being analyzed separately and the spectra of the peptides are compared for similar masses and retention times (Fig. 2b). In label-free quantitation, two approaches can be used: (1) peak intensities or area under the curve [9] and (2) spectral counting [10]. Measurement of peak area involves calculating and comparing the mean intensity of peak areas for all peptides from each protein in the biological sample [11]. Quantitating proteins based on area under the curve involves measuring ion abundance at a specific retention time for the given peptides [12]. Several factors must be considered when undertaking this approach, such as peak reproducibility and accurate peak detection that may be affected by

biological and technical variations. A limitation associated with this approach is determining a balance between survey scans and fragment scans in order to achieve both protein quantitation and identification [12]. In contrast, spectral counting is based on the number of MS/MS spectra generated from a protein. The more abundant the protein is in the biological sample, the more peptides will be selected for fragmentation [12]. Spectral counting is based on three measures which include observing the number of peptide-to-spectrum match, the number of distinct peptides identified, and the sequence coverage for a select protein in an LC-MS/MS run should correlate with protein quantity [1]. Spectral counting is limited by the differences in peptides' physiochemical properties that can result in variation and bias in MS measurements [12]. However, a comparison of both approaches shows that spectral counting is more reproducible and has a larger dynamic range [13]. As compared to labeling techniques, label-free techniques are less expensive, they can be applied to an array of biological samples, and they have a high analytical depth and dynamic range, which is advantageous when comparing samples with large number of protein changes [4].

Data analysis for label-free quantitation begins with protein identification using database searching via search engines such as MASCOT, SEQUEST, or X!TANDEM [12]. Protein identification is then followed by protein quantitation. Statistical analysis is important in quantitative proteomics experiments to differentiate protein abundance between samples. There are several commercially available software commonly used for label-free quantitation, including Scaffold [14], ProteoIQ, and Elucidator. Here, we describe the methods by which proteins are isolated and identified from cochlear sensory epithelia tissues at different ages and quantitatively differentiated using label-free mass spectrometry with spectral counting.

2 Materials

2.1 Protein Sample Preparation

1. Phosphate Buffered Saline: Prepare 1 L of 1× solution by adding 144 mg of potassium phosphate monobasic, 795 mg of sodium phosphate dibasic heptahydrate, and 9 g of NaCl to 900 mL of water. Bring volume to ~1 L with water (*see Note 1*) then adjust pH to 7.4 with HCl.
2. Protease inhibitor stock solutions: Mix 50 mg/mL of Pefabloc® SC 4-(2-Aminoethyl) benzenesulfonyl fluoride hydrochloride (AEBSF; Fluka St. Louis, MO) in water and store in 100 µL aliquots, 10 mg/mL of leupeptin in water and store in 10 µL aliquots, 10 mg/mL of aprotinin in 10 mM 4-(2-hydroxyethyl)-1-piperazineethanesulfonic acid (HEPES), pH 8.0, and store

in 20 μ L aliquots, 100 μ g/mL of pepstatin A in 95 % ethanol and 1 mM microcystin-LR (Calbiochem/EMD Biosciences, San Diego, CA) in DMSO and store both in 5 μ L aliquots.

3. Lysis buffer stock solutions: 1 M Tris–HCl, pH 8.0 (UltraPureTM, Invitrogen, Carlsbad, CA) and 0.5 M ethylenediaminetetraacetic acid (EDTA) UltraPureTM solution (Invitrogen) pH 8.0.
4. Lysis buffer working solution: Use 100 mM Tris–HCl, pH 8.0, 120 mM NaCl, 50 mM NaF, and 5 mM EDTA. Prepare 100 mL solution by adding 5 mL of 1 M Tris–HCl, pH 8.0, 701 mg of NaCl, 210 mg of NaF, and 1 mL of 0.5 M EDTA. Bring volume to 100 mL with water and store at 4 °C.
5. Complete lysis buffer working solution: Use 100 mM Tris–HCl, pH 8.0, 120 mM NaCl, 50 mM NaF, 5 mM EDTA, 500 μ g/mL AEBSF, 10 μ g/mL leupeptin, 100 μ g/mL pepstatin A, 2 μ g/mL aprotinin, and 1 mg/mL microcystin-LR. Prepare a 1 mL volume immediately before use by mixing the following quantities of stock protease and phosphatase inhibitors: 10 μ L of AEBSF, 1 μ L of leupeptin, 1 μ L of pepstatin A, 2 μ L of aprotinin, and 0.5 μ L of microcystin-LR.
6. Solubilization Buffer: Prepared from complete lysis buffer with 4 % (w/v) sodium dodecyl sulfate (SDS). Other detergents can be used in the solubilization buffer, however careful consideration should be given that the detergent is compatible with the FASP digestion procedure (*see Note 2*).
7. Sonic dismembrator (Model 100; Thermo Fisher).

2.2 Protein Digestion

All solutions are prepared fresh and immediately prior to use.

1. FASP Protein Digestion KitTM (Expedeon, San Diego, CA): 50 mM (NH₄)HCO₃, 100 mM Tris–HCl solution, pH 8.5, 8 M urea, iodoacetamide, 0.5 M NaCl solution, and 30 kDa spin filter.
2. Urea Solution: Prepare 8 M urea solution by dissolving one tube of urea from the FASP kit with 1 mL of 100 mM Tris–HCl.
3. Iodoacetamide Solution: Prepare 10× iodoacetamide solution by dissolving 100 μ L of 8 M urea solution to one tube of iodoacetamide from the FASP kit.
4. Digestion Solution: Prepare 0.1 μ g/ μ L of endoproteinase LysC solution by dissolving 5 μ g LysC in 50 μ L of 50 mM ammonium bicarbonate solution provided with the FASP kit. Prepare 0.4 μ g/ μ L of trypsin solution by dissolving 20 μ g trypsin in 50 μ L of 50 mM (NH₄)HCO₃ solution provided with the FASP kit.
5. Formic acid (*see Note 3*).

6. Benchtop centrifuge (e.g., Microcentrifuge® model 5417R, Eppendorf).
7. NanoDrop spectrophotometer (Model ND 1000; Thermo Fisher Scientific).

2.3 Desalting Peptides Using C₁₈ Spin Columns

1. C₁₈ MacroSpin columns (The Nest Group, Southboro, MA).
2. Acetonitrile, mass spectrometry grade.
3. 0.1 % Formic Acid: 100 µL formic acid in 100 mL of ddH₂O.
4. 90 % Acetonitrile: 90 mL of acetonitrile and 10 mL of ddH₂O.
5. Vacuum concentrator (e.g., SpeedVac® model SPD121P, Thermo Fisher).

2.4 Protein Fractionation Using Ion Exchange Chromatography

1. 200 × 2.1 mm, 5 µm SCX column (Polysulfoethyl A, The Nest Group).
2. Solvent A: 5 mM ammonium formate, pH 3.0 in 25 % acetonitrile and 75 % ddH₂O.
3. Solvent B: 500 mM ammonium formate, pH 6.0 in 25 % acetonitrile and 75 % ddH₂O.
4. 500 µg of Cytochrome C Solution: 100 µL of 1 mg/mL of Cytochrome C in 25 mM NH₄HCO₃. Reduce for 60 min at RT with 5 µL of 200 mM dithiothreitol, followed by alkylation for 60 min with 20 µL of 200 mM iodoacetamide in the dark. Add 20 µL of 20 mM dithiothreitol to consume the remaining alkylating agent. Add 1:100 ratio of trypsin and heat at 37 °C O/N. The following day, add 10 µL formic acid to stop the reaction and dry the cytochrome C digest in a speedvac.
5. High-performance liquid chromatography system (*see Note 4*) and Photodiode array.
6. Fraction collector.

2.5 Nano LC-MS/ MS

1. 100 µm × 25 mm sample trap (New Objective, Woburn, MA).
2. 75 µm × 10 cm C₁₈ column (New Objective, Woburn, MA).
3. Solvent A: 95 % ddH₂O and 5 % acetonitrile containing 0.1 % formic acid.
4. Solvent B: 80 % acetonitrile and 20 % ddH₂O containing 0.1 % formic acid.
5. High-resolution LTQ Orbitrap (Thermo Fisher Scientific, MA, USA) mass spectrometer.

2.6 Bioinformatics Tools for Protein ID and Statistical Analyses

1. MASCOT Search Engine (Matrix Science, London, UK).
2. Scaffold (Version 4.3.2, Proteome Software, Portland, OR).
3. Statistica software (Version 12, StatSoft, Inc.).

3 Methods

3.1 Protein Sample Preparation (See Note 5)

Experiments using animal tissue should be approved by the University's Institutional Animal Care and Use Committee as set forth under the guidelines of the National Institutes of Health.

1. Dissect cochleae from post-natal 3-, 14- and 30-day-old (P3, P14, and P30) CBA/J mice under sterile conditions and place them in aliquots of 16 cochlea per tube and store at -80 °C.
2. On the day of the experiment, wash tissue with 500 µL of 1× phosphate buffered saline (PBS). Centrifuge for 3 min at 1000×g, and remove the supernatant. Repeat 3×.
3. Sonicate tissue for 30 s on ice in 100 µL of complete lysis buffer using a sonic dismembrator. Cool lysate on ice for 1 min between each sonication. Sonicate a total of 3×.
4. Centrifuge the extract at 750×g at 4 °C for 2 min and remove the supernatant to a new microtube. Extract the pellet in 50 µL of complete lysis buffer by sonicating for 30 s on ice. Centrifuge the extract at 750×g at 4 °C for 2 min. Combine both lysates and centrifuge at 28,600×g at 4 °C for 60 min. Remove the supernatant to a new microtube and add 20 µL of solubilization buffer to the pellet. Vortex for 1 min and incubate for 60 min at 4 °C.
5. Incubate the sample on ice for 30 min, then heat at 95 °C for 5 min. Follow with centrifugation at 16,000×g at 4 °C for 15 min. Collect the supernatant and transfer to a new tube.
6. Extract the pellet in complete lysis buffer by sonicating 1× for 30 s on ice.
7. Combine the lysate and previous supernatant and centrifuge at 20,800×g at 4 °C for 60 min and retain the supernatant for digestion (*see Note 6*).

3.2 Protein Digestion

1. Add a 30 µl aliquot (\leq 400 µg) of cochlear protein extract, containing 4 % SDS, 100 mM Tris-HCl, pH 7.6 and 0.1 M dithiothreitol directly to a 30 K spin filter and mix with 200 µL of 8 M urea in Tris-HCl. Centrifuge at 14,000×g for 15 min.
2. Dilute the concentrate with 200 µL of 8 M urea solution and centrifuge at 14,000×g for 15 min.
3. Add 10 µL of 10× iodoacetamide in 8 M urea solution to the concentrate in the filter and vortex for 1 min. Incubate the spin filter for 20 min at RT in the dark followed by centrifugation at 14,000×g for 10 min.
4. Add 100 µL of 8 M urea solution to the concentrate on the filter unit and centrifuge at 14,000×g for 15 min. Repeat this

step 2×. Add 100 µL of 50 mM ammonium bicarbonate solution to the filter unit and centrifuge at 14,000×*g* for 10 min. Repeat this step 2×.

5. Add 0.1 µg/µL of LysC in a 1:50 (w/w) enzyme-to-protein ratio and incubate O/N at 30 °C.
6. Following incubation, add 40 µL of 50 mM ammonium bicarbonate solution to the filter unit and centrifuge at 14,000×*g* for 10 min. Repeat this step 1×.
7. Add 50 µL of 0.5 M NaCl solution to the spin filter and centrifuge at 14,000×*g* for 10 min. Transfer the filtrate containing the LysC peptides to a fresh microtube and acidify with formic acid to 1.0 %.
8. Wash the filter unit with 40 µL of 8 M urea, and then wash 2× with 40 µL 18 MΩ water.
9. Wash the filter unit 3× with 100 µL of 50 mM ammonium bicarbonate solution. After the final wash add 0.4 µg/µL of trypsin in 1:100 (w/w) enzyme-to-protein ratio and incubate O/N at 37 °C.
10. Elute tryptic peptides from the second digest by adding 40 µL of 50 mM ABC solution to the filter unit and centrifuge at 14,000×*g* for 10 min. Repeat this step 1×.
11. Add 50 µL of 0.5 M NaCl solution to the filter unit and centrifuge at 14,000×*g* for 10 min. Transfer the filtrate containing the tryptic peptides to a fresh microtube and acidify with formic acid to 1.0 %.

3.3 Desalting Peptides Using C₁₈ Spin Columns (see Note 7)

1. Activate a C₁₈ spin column by adding 500 µL of acetonitrile and centrifuge at 1100×*g* for 1 min. Discard the flow-through after centrifugation.
2. Equilibrate the column with 500 µL of 0.1 % formic acid and centrifuge at 1100×*g* for 1 min. Discard the flow-through and repeat this step 1×.
3. Add up to 500 µL of the LysC peptide digest to the column and centrifuge at 1100×*g* for 1 min. If the sample volume is greater than 500 µL then repeat this step.
4. Wash the column with 500 µL of 0.1 % formic acid and centrifuge at 1100×*g* for 1 min. Discard the flow-through. Repeat this step 1×.
5. Add 250 µL of a 90:10 acetonitrile-to-water ratio to the column and centrifuge at 1100×*g* for 1 min. Collect the eluent containing the desalted peptides and transfer to a fresh microtube. Repeat this step 1×.
6. Dry the desalted peptide sample in a vacuum centrifuge and avoid letting the sample dry completely.

7. Repeat this procedure to desalt the tryptic peptide digest.
8. The peptide samples were quantified based on absorbance at 280 nm using a NanoDrop spectrophotometer.

3.4 Protein Fractionation Using Ion Exchange Chromatography

1. Inject 100 µg of Cytochrome C digest onto the SCX column to verify column separation.
2. Inject 50–100 µg of LysC peptide digest onto a SCX column to separate peptides.
3. Use a gradient of 2–40 % solvent B over 50 min with a flow rate of 250 µL/min.
4. Monitor the peptide fractions at 280 nm and collect the fractions in 2 min intervals using a fraction collector.
5. Repeat the procedure for the tryptic peptide digest.
6. Dry fractions in a vacuum concentrator and store at –80 °C until ready to use for nano LC-MS/MS analysis (*see Note 8*).

3.5 Nano LC-MS/ MS

1. Reconstitute dried LysC and tryptic peptide digests fractions in 20 µL of 0.1 % formic acid and sonicate for 15 min.
2. Centrifuge samples at 20,000×*g* for 10 min and remove the top 95 % of sample to a new sample vial.
3. Inject 5 µL of each peptide fraction onto a sample trap to remove salts and contaminants and separate peptides on a C₁₈ column.
4. Use a gradient of 2–40 % solvent B over 100 min with a flow rate of 200 nL/min.
5. Collect ten tandem mass spectra for each MS scan on the LTQ Orbitrap.

3.6 Identification of Proteins (See Note 9)

1. Proteins are identified by peptide mass fingerprinting using the MASCOT search engine with the UniProt protein database (*see Note 10*).
2. The following search parameters can be used in MASCOT: *Mus musculus* for taxonomy, set the parent and fragment ion maximum precursors to ±8 ppm and ±1.2 Da, respectively (these parameters are instrument-specific). A fixed modification of carbamidomethyl of cysteine, variable modifications of oxidation of methionine and protein N-terminal acetylation (these are selected based on the reduction and alkylation performed during the digestion procedure), select the enzyme used to digest the proteins, and set a limit of two missed cleavages (*see Note 11*).
3. The peptide and protein identifications can be validated using Scaffold software. Load the MASCOT .dat files for the P3 LysC fractions, then create a new experiment and load the .dat

files for the P3 tryptic fractions. Repeat this for the other P3 biological replicates and give the sample category the name P3 so that all the replicates will be grouped as P3. Perform the same process for P14 and P30. Hence, all three sample categories, P3, P14, and P30 will be contained in one Scaffold file.

4. Scaffold parameters can be set to 95 and 99 % probability for peptide and protein, respectively, and contain a minimum of two identified peptides.
5. Remove decoys and contaminants such as keratin from the list of proteins.
6. Validate peptide identity assigned to spectra for protein identification by observing signal-to-noise ratio, verifying that high intensity peaks are labeled, and the fragment peaks line up with the amino acid assignment (*see Note 12*).

3.7 Normalizing Spectral Counts

Scaffold provides spectral counts for each protein and normalizes the spectral counts between samples, which allows for comparison of protein abundance between samples, whether a protein is up- or down-regulated. If the total amount of protein varies between samples, normalization can be used to create the total amount of all proteins in each sample to be about the same.

1. In Scaffold, select the option Quantitative Value, which allows you to view the normalized spectral counts (*see Note 13*).
2. The normalized spectral count data can then be used to calculate a ratio of the average spectral counts or fold change obtained for each age group, P3/P14, P3/P30, and P14/P30. Proteins with a ratio of average spectral counts that are twofold or greater are considered significant (*see Note 14*).

3.8 Analysis of Differentially Expressed Proteins (See Note 15)

Statistica software can be used for the statistical analysis. Spectral counts correlate with protein abundance. Therefore, the mean normalized spectral counts can be used to determine differential abundance between the age groups.

1. Once the data sets are comparable after normalization, changes can now be determined between the age groups (*see Note 16*).
2. To find differentially abundant proteins, export the mean normalized spectral counts from Scaffold into an excel spreadsheet and import the data into the statistical software, Statistica (*see Note 17*).
3. Analyze the data using a One-way Analysis of Variance (ANOVA) followed by a *post-hoc* test. For example you can use the Bonferroni test. Select “Age Group” as the Category Predictor *aka* Effect and the mean normalized spectral counts as the Dependent Variables (*see Note 18*).

4. Statistica will report *p*-values that are drawn from pairwise comparison between age groups, Sums of Squares (SS), Mean Square (MS), MS between groups divided by MS within groups (*F*-value), tests of all age groups together using ANOVA (P), and Degrees of Freedom (df). Proteins between age groups can be considered significantly different when $p \leq 0.05$.
5. Statistica provides statistical values, including *p*-values comparing all age groups. For example, values are given for P3 vs. P14, P3 vs. P30, and P14 vs. P30. The results can be exported to an excel spreadsheet.
6. Using the ratio of the average spectral counts, as described in Section 3.7, and the *p*-values calculated from Statistica, the differentially expressed proteins can be sorted in an excel spreadsheet to determine which proteins are up- and down-regulated as well as exclusively expressed.

4 Notes

1. All solutions should be prepared using Milli-Q water (minimum of 18 MΩ cm) and chemicals used are at minimum Analytical Reagent Grade quality.
2. SDS is a detergent with relatively small micelles and high critical micelle concentration (CMC), and, therefore, easily passes through the FASPfiltering membrane and is depleted from the protein lysate. In contrast, detergents with large micelles and low CMCs are not easily removed from the FASP filtering membrane which could result in inhibition of the protease(s) used for digestion as well as ion suppression in mass spectrometry. This outcome will result in no data [15].
3. FORMIC ACID can be used in place of the recommended trifluoroacetic acid (CF₃CO₂H) to acidify the digested peptides and stop the digestion.
4. If the SCX column begins to exhibit signs of increased back pressure over extended use, the column should be flushed with 20 column volumes of high salt buffer, followed by 20 column volumes of 40 % methanol, then 20 column volumes of water, followed by column equilibration.
5. Prior to protein quantitation the proteins have to be identified, hence it is important to select a proteomics approach that will reduce the proteome dynamic range. Shotgun proteomics, which involves digesting proteins and separating peptides prior to tandem mass spectrometry is preferred, because we can combine different separation methods prior to mass spectrometry to enrich protein samples, detect different classes of proteins, and identify low abundant proteins.

6. Biological replicates should be performed in order to eliminate random variations. Performing replicates allows random variations to be averaged out and consistent signals to be confirmed.
7. Peptide desalting is important to remove salt and other contaminants that interfere with mass spectrometry analysis.
8. To facilitate the removal of excess salt, 500 µL of 5 % FORMIC ACID in 50:50 ACETONITRILE:H₂O can be added to the partially dried SCX collected fractions. These fractions are then dried again in a vacuum centrifuge. It is important to not dry the samples completely to avoid losing peptide identification during LC-MS/MS.
9. A challenge with using spectral counts is that zero counts can be given for a protein when absent in one sample, but it may be detected in another, which makes it impossible to calculate a fold change. In addition, when comparing samples, there may be peptides that will not be fragmented and detected due to low abundance and low ionization efficiency. Hence, optimizing peptide fractionation and chromatographic separation is critical to peptide identification.
10. It is important to search the data against a decoy database that contains reversed, shuffled, and random protein sequences to reduce the number of false positives.
11. MASCOT search engine uses mass spectrometry data for protein identification. A commonly used approach is peptide mapping, which refers to the identification of proteins using data from intact peptide masses. For peptide mass fingerprinting, MASCOT requires the input of specific parameters. The taxonomy filter allows selection of the species studied, which limits the number of matches in the results. The modification filter allows selection of fixed modifications, which assumes that in every instance a particular residue has been modified and variable modification, which tests each potential site with and without the modification. Variable modification should be used carefully because it can increase the chance of random matches. The parent and fragment ion maximum precursors allow for input of the error window on experimental peptide mass values and the error window for MS/MS fragment ion mass values, respectively. If the parent ion maximum precursor is set too tight this can result in the loss of valid peptide identifications and if set too loose this can result in an increase of false-positive identifications. The missed cleavage filter allows for missed cleavages during protein digestion. If not certain whether the protein digestion was perfect, a selection of 1 or 2 missed cleavage sites may be selected. The selection of a larger number of missed cleavage sites can result in an increased number of random peptide matches.

12. The signal-to-noise (S/N) ratio should be at least 3:1 to be considered significant.
13. To obtain normalized Quantitative Values between samples in Scaffold, the sum of the unweighted spectral counts (the total number of spectra associated with a protein as well as those shared with other proteins) for each sample is scaled by determining a sample specific scaling factor. The scaling factor used for each sample is then applied to all proteins in that sample. The scaling factor is determined by dividing the sum of spectral counts by the average spectral counts across all biological samples.
14. Protein variation between samples can occur for numerous reasons, including differences in protein abundances, variation in sample preparation, sample digestion, protein extraction procedure, change in chromatography, or the MS/MS acquisition. Hence, a normalization process is required to take into account these changes and properly identify significant changes in protein abundance between sample groups.
15. When performing a quantitation study it is important to consider whether the proteins of interest are known or unknown. If the proteins are known they can be targeted. In such a case, we would not use label-free quantitation, but another approach such as Selected Reaction Monitoring (SRM). However, if the proteins of interest are unknown, we can observe differential expression using a label-based or label-free approach.
16. Fold change values should be considered along with *p*-values ≤ 0.05 using ANOVA. The significance of the fold change can vary depending on the average spectral counts being compared. For example, a fold change of 2 is more significant between average spectral counts of 54 and 27 as compared to between 2 and 1.
17. Scaffold has several statistical analysis tools, such as Fold change, *t*-test, and ANOVA that can be used to identify differential protein abundance between samples. However, Scaffold does not have the ability to perform a *post-hoc* test that confirms where differences occur between sample groups. Therefore, additional statistical analyses have to be performed using different statistical software.
18. Data sets can be analyzed using statistical tests such as a Student's *t*-test. However, when there are more than two groups to compare ANOVA should be performed.

Acknowledgements

This work was supported by the NIH/NIDCD Grant R01 DC004295 to BHAS.

References

1. Bantscheff M, Lemeer S, Savitski MM, Kuster B (2012) Quantitative mass spectrometry in proteomics: critical review update from 2007 to the present. *Anal Bioanal Chem* 404:939–965
2. Kito K, Ito T (2008) Mass spectrometry-based approaches toward absolute quantitative proteomics. *Curr Genomics* 9:263–274
3. Mirza SP (2012) Quantitative mass spectrometry-based approaches in cardiovascular research. *Circ Cardiovasc Genet* 5:477
4. Schulze WX, Usadel B (2010) Quantitation in mass-spectrometry-based proteomics. *Annu Rev Plant Biol* 61:491–516
5. Ong SE, Mann M (2007) Stable isotope labeling by amino acids in cell culture for quantitative proteomics. *Methods Mol Biol* 359:37–52
6. Ross PL, Huang YN, Marchese JN, Williamson B, Parker K et al (2004) Multiplexed protein quantitation in *Saccharomyces cerevisiae* using amine-reactive isobaric tagging reagents. *Mol Cell Proteomics* 3:1154–1169
7. Gygi SP, Rist B, Gerber SA, Turecek F, Gelb MH et al (1999) Quantitative analysis of complex protein mixtures using isotope-coded affinity tags. *Nat Biotechnol* 17:994–999
8. Stewart II, Thomson T, Figge D (2001) ¹⁸O labeling: a tool for proteomics. *Rapid Commun Mass Spectrom* 15:2456–2465
9. Chelius D, Bondarenko PV (2002) Quantitative profiling of proteins in complex mixtures using liquid chromatography and mass spectrometry. *J Proteome Res* 1:317–323
10. Liu H, Sadygov RG, Yates JR 3rd (2004) A model for random sampling and estimation of relative protein abundance in shotgun proteomics. *Anal Chem* 76:4193–4201
11. Sun C, Xu G, Yang N (2013) Differential label-free quantitative proteomic analysis of avian eggshell matrix and uterine fluid proteins associated with eggshell mechanical property. *Proteomics* 13:3523–3536
12. Neilson KA, Ali NA, Muralidharan S, Mirzaei M, Mariani M et al (2011) Less label, more free: approaches in label-free quantitative mass spectrometry. *Proteomics* 11:535–553
13. Zyballov B, Coleman MK, Florens L, Washburn MP (2005) Correlation of relative abundance ratios derived from peptide ion chromatograms and spectrum counting for quantitative proteomic analysis using stable isotope labeling. *Anal Chem* 77: 6218–6224
14. Searle BC (2010) Scaffold: a bioinformatic tool for validating MS/MS-based proteomic studies. *Proteomics* 10:1265–1269
15. Wisniewski JR, Zielinska DF, Mann M (2011) Comparison of ultrafiltration units for proteomic and N-glycoproteomic analysis by the filter-aided sample preparation method. *Anal Biochem* 410:307–309

Chapter 9

Ultrastructural Identification and Colocalization of Interacting Proteins in the Murine Cochlea by Post-Embedding Immunogold Transmission Electron Microscopy

Margaret C. Harvey and Bernd H.A. Sokolowski

Abstract

Verification of the presence and location of a protein within tissue can be accomplished by western blotting and immunohistochemistry, using either paraffin or frozen sections. Affinity purification by reciprocal coimmunoprecipitations using the tissue of interest can demonstrate the existence of an interacting pair of proteins. Ultimately, the ability to visualize the interaction at the cellular level is desired. Precise location(s) of interacting proteins *in situ* can be accomplished by ultrastructural localization with high-quality primary antibodies and small-particle-size Au-conjugated secondary antibodies. Visualization can be obtained with a transmission electron microscope fitted with a high-resolution camera permitting magnifications that exceed 2×10^5 , and, to date, resolution capability of 20+ Mpixels, thus enabling localization of the target protein to within nanometers of the actual location. Here, we report the method by which immunolocalization at the level of the electron microscope is accomplished using the post-embedding technique, i.e., performing antibody labeling of proteins on ultrathin sections of tissue embedded in acrylic resin.

Key words Cochlea, Interacting proteins, Immunogold, Transmission electron microscopy, High-resolution imagery, Post-embedding technique

1 Introduction

Novel proteins identified by peptide analyses from mass spectrometry data, by any technique for that matter, require validation within the tissue of interest by, e.g., RT-PCR, western blotting, and immunostaining. Potential interacting proteins can be sourced by a variety of methods, e.g., yeast two-hybrid screenings, affinity purification followed by mass spectrometry, and bioinformatics analyses generating complex interactomes. Validation *in vivo* can then proceed by performing reciprocal coimmunoprecipitations (coIP) and immunohistochemistry followed by techniques *in vitro*, such as affinity-tagging constructs and expressing proteins in heterologous systems, followed by reciprocal coIP, silencing studies,

and immunocytochemistry analyzed by a variety of fluorescence-driven techniques that are able to localize and quantify interactions. The question remains however, what/where are these proteins and interactions within cells of the tissues themselves, i.e., the ultrastructural location(s). A technique, which will hopefully (re)gain favor in the scientific community, is immunolocalization at the level of the electron microscope. There are two general approaches with this technique, pre-embedding and post-embedding, the latter resulting in superior morphology and improved localization [1]. In addition, it is a technique that is quantifiable.

Tissues are rapidly excised and fixed, either in paraformaldehyde or in combination with a small percentage of glutaraldehyde. This decision potentially involves a tradeoff between obtaining optimal morphology at the risk of blocking primary antibody epitopes. After decalcification, tissues are dehydrated and infiltrated/embedded using a water-soluble resin such as LR White. After heat-curing, blocks are first thick–thin sectioned to evaluate both morphology and orientation using a common histochemical stain. Once retrimmed to focus on a particular area of interest, tissue is then thin-sectioned and collected on nickel grids. After a rehydration series, sections are incubated with glycine to quench aldehydes and then blocked to inhibit nonspecific staining. Blocking solutions include normal serum from the animal in which the secondary antibody was made, bovine serum albumin, and small percentages of cold water fish skin gelatin as a blocking agent and Tween® 20 to reduce hydrophobic interactions with gold particles and enable surface wettability. Sections are then briefly rinsed in an acetylated form of BSA (BSA-c) that works as a strong blocking agent. Primary antibody incubation is done at room temperature, overnight, in a diluent containing only BSA-c, at a slightly higher concentration, and Tween 20® in buffer. The primary antibody should first be tested over a range of concentrations while maintaining the gold-conjugated secondary antibody at a constant dilution.

A number of experiments can be accomplished at one time using several grids to collect short ribbons of serially-sectioned tissue. The next day, sections are washed in buffer, this time at an elevated pH, as epitopes are potentially more accessible to antibody binding. The pH is suited to match the pH of the shipped buffer containing the gold conjugates. The next incubation is with colloidal gold particle-conjugated secondary antibodies. For colocalization studies, antibodies must be of different types, i.e., monoclonal and polyclonal, and the gold-conjugated particles must be of different sizes. The protocol described herein suggests use of 5 and 10 nm particles. The trade-off is the operator's ability to distinguish between the two during imaging and the advantage provided by using smaller particles. Thus, the smaller the particle the closer in proximity to the location of the protein(s). At this point, sections are stained for contrast first using osmium, followed by potassium permanganate and uranyl acetate. Sections are evaluated

and photographed at both low magnification (to have context) and higher magnifications.

Technical information supporting the techniques of immunogold staining and use of transmission electron microscopy fill volumes of literature. The aim of this chapter is to outline a protocol that resulted from numerous permutations at each and every step along the way, working with murine cochleae. This method permits the investigator to truly appreciate structure and cellular architecture in the context of the protein(s) of interest in the tissue of interest.

2 Materials

2.1 Dissection Tools, Fixation Equipment

1. Animal sacrifice: Isoflurane, bell jar with grating, gauze padding, plastic transfer pipet, guillotine, crushed ice, and dissection dishes that can be packed in ice and are compatible with a dissection microscope.
2. Forceps: Laminectomy Forceps (Dumont #2, Fine Science Tools (FST) Foster City, CA), #5 and #55 Forceps (Dumostar, FST).
3. Scalpels and blades: #11 and #22 blade holders and scalpel blades.
4. Scissors: Fine straight iris scissors and angled spring scissors.
5. Glass sample: 4 mL bottles with snap caps.
6. Sample rotator (e.g., Pelco Rotator R1 adjustable to 35° (Ted Pella, Redding, CA).
7. A rocking platform that can be placed in a refrigerator.

2.2 Preparation of Tissue Samples

2.2.1 Buffers

The use of ultrapure water (nanopure) is essential. High-quality (molecular biology grade) reagents are advised as is the use of filter-tip pipet tips. A clean environment is necessary. All buffers are to be mixed using a magnetic stirrer unless otherwise noted.

1. Phosphate-Buffered Saline solution (PBS): 150 mM NaCl, 3 mM Na₂HPO₄·7H₂O, 1 mM KH₂PO₄, pH 7.4, in water. Prepare 1 L by adding 9 g NaCl, 0.795 g Na₂HPO₄·7H₂O, and 0.144 g KH₂PO₄ to 950 mL of nanopure water and adjust pH to 7.4. Bring up to a volume of 1 L and mix.
2. Phosphate Buffer (PB): 0.1 M NaH₂PO₄, anhydrous, in water. Prepare 1 L by adding 12.1 g of NaH₂PO₄, anhydrous, to ~950 mL of nanopure water and adjust the pH to 7.4. Bring up to a volume of 1 L and mix.
3. Fixation buffer: 4 % paraformaldehyde (16 % solution, EM grade), 0.1 % glutaraldehyde (8 % solution, EM grade (Ted Pella)) in PB. Prepare 50 mL by adding 12.5 mL of the stock 16 % paraformaldehyde solution and 625 µL of the stock 8 % solution to 45 mL of PB. Mix, adjust pH to 7.4 using pH indicator paper, bring up to a volume of 50 mL and mix. Prepare this buffer freshly.

4. Decalcification buffer: 5 mM ethylenediaminetetraacetic acid (EDTA; 0.5 M UltraPure™ EDTA pH 7.5) in PB. Prepare 50 mL by adding 500 µL of the stock 0.5 M EDTA solution to 45 mL of PB, mix, pH to 7.4, bring to a 50 mL volume and mix. Prepare this buffer freshly.

2.2.2 Resin Embedding

Use goggles and gloves to work with a methacrylate resin. Most common laboratory gloves provide insufficient protection. The manufacturer suggests using Barrier-Brand or gloves with nitrile.

1. Use LR White medium grade resin. Combine the entire contents of catalyst provided to the bottle of resin, add a stir bar and permit both to mix for 30 min using a magnetic stirrer. Place the bottle of resin at 4 °C overnight (O/N).
2. Dehydration/infiltration solutions: Prepare the following dehydration series using a freshly opened bottle of absolute ethanol (EtOH) and combine with nanopure water to achieve a 50, 70, and 85 % EtOH series. Prepare 10 mL each of the 50 and 85 % EtOH, while preparing 50 mL of the 70 % EtOH. Prepare fresh 10 mL of 2:1 resin/70 % EtOH.
3. Acquire the following materials for tissue embedding: Snap-fit® Gelatin Capsules, size 00 (Ted Pella); BEEM® capsule holder size 00 (Ted Pella); oven set to 50 °C.

2.3 Ultramicrotomy

A refurbished ultramicrotome can be purchased from, e.g., International Medical Equipment, Inc. (IMEB, Livonia, MI). It will require a specimen holder compatible with size 00 BEEM® capsules, a collet suitable for use with size 00 BEEM® capsules, and a knife holder.

2.3.1 Semi-thin Sectioning

1. Glass Knives: Fresh glass strips, manual knife breaker, glass knife storage box, silver polyester tape, glass knife boats, clear nail polish. As a more desirable alternative, use a diamond knife.
2. Thick single edge razor blades (WECPREP™ Blades, Ted Pella) for coarse trimming of blocks; a wooden block for holding a collet.
3. 1 mL syringe fitted with a Nalgene 0.2 µm syringe filter (25 mm SFCA).
4. Wooden applicator stick with whittled beveled edge; a modified wooden applicator stick to which is fastened a cat/dog whisker.
5. Small, dark glass bottle with a phenolic screw-on cap, containing a small cotton applicator swab immersed in a few mL of chloroform.
6. Standard glass microscope slides, coverslips, mounting medium, e.g., Cytoseal™, slide storage box; extra-fine point waterproof marking pen; hot plate adjustable to ~45 °C.

7. Histochemical Staining Solution: 1 % Toluidine Blue O in 2 % $\text{Na}_2\text{B}_4\text{O}_7 \cdot 10\text{H}_2\text{O}$. Add 1 g of Toluidine Blue O and 2 g of $\text{Na}_2\text{B}_4\text{O}_7 \cdot 10\text{H}_2\text{O}$ to 100 mL of nanopure water. Mix by stirring on a magnetic stirrer and filter into a dark glass bottle using Whatman #1 qualitative filter paper. At the time of use, dispense using a 1 mL syringe fitted with a 0.2 μm filter.
8. pH meter and probe compatible with Tris-based buffers.

2.3.2 Ultrathin Sectioning

1. Diamond Knives: These knives are available from, e.g., DiATOME. A standard 45° knife angle with a 4 mm edge length is preferable as the former has a hydrophilic edge for ultrathin sectioning, while the latter provides room for cutting larger sections.
2. 5 mL syringe fitted with an angled needle.
3. Angled tweezers (5/90, Dumont antimagnetic 90°-angled positive action tweezers, EMS); Inox N4 negative action tweezers (EMS).
4. Lens paper and lens tissue, two 100 mm plastic petri dishes lined with filter paper.
5. Grids (EMS): Factors to consider include section support, retention, and viewing area. Consider acquiring a selection of grid types, e.g., standard 100 hexagonal nickel grids (EMS), 200 mesh Nickel Gilder Grids, 200 mesh Gilder Thin Bar Grids, which provide 40 % greater viewing area or preferably, to increase retention of sections; 100 hexagonal mesh nickel Formvar-coated grids (standard thickness, i.e., 10 nm). Formvar is always placed on the shiny side of the grid, therefore sections must be collected on that side.
6. Grid cleaning reagents (*not to be used on Formvar-coated grids!*): 0.1 M HCl, acetone and absolute EtOH.
7. Grid storage and transport: BEEM® Dial-A-Grid storage boxes (EMS) provide easy access and permit retrieval of one grid at a time, thus eliminating the risk of losing grids.
8. Centrifuge tubes: Sterile, polypropylene 15 and 50 mL sizes.
9. Microcentrifuge tubes: Sterile, polypropylene 1.5 mL size.

2.4 Immunochemistry

2.4.1 Materials

1. pH meter and probe compatible with Tris-based buffers
2. Polypropylene, sterile centrifuge and microcentrifuge tubes, 15 and 50 mL sizes, and 1.5 mL tubes.
3. A series of 23 covered, stackable watch glasses or petri dishes, with lids, of at least 60 mm diameter. Line each with filter paper to enable a humid environment. Cut extra hard dental wax (Ted Pella) into 23 pieces and place in each dish so that several grids can be safely manipulated in one experiment.

2.4.2 Antibodies

1. Primary Antibodies: Perform a thorough search of the literature to determine if your protein(s) of interest have been identified by antibodies proven to work for this application. Barring that unlikely probability, purchase antigen/immuno-gen affinity-purified antibodies (e.g., Novus Biologicals, Proteintech™ Group). Colocalization will require pairing of antibodies by type.
2. Secondary gold-conjugated antibodies of appropriate type and different particle sizes for colocalization: EM Goat anti-Mouse IgG Heavy and Light Chains (H + L) 5 nm gold; EM Goat anti-Mouse IgG (H + L) 10 nm gold; EM Goat anti-Rabbit IgG (H + L) 5 nm gold; EM Goat anti-Rabbit IgG (H + L) 10 nm gold; BBI International, all available from Ted Pella, Inc. (Cautionary note—there is the possibility of back-order status from time-to-time).

2.4.3 Contrast Staining Buffers and Solutions

1. Tris-Buffered Saline Solution (TBS, pH 7.4): 50 mM Tris-HCl, 150 mM NaCl in nanopure water. Prepare 100 mL by adding 5 mL of stock 1 M Tris-HCl pH 7.5 (1 M UltraPure™ Tris-HCl pH 7.5, 15567-027, Invitrogen, Grand Island, NY) and 0.88 g of NaCl to 95 mL nanopure water. Adjust pH to 7.4 and bring volume up to 100 mL. Mix by using a magnetic stirrer. Store at 4 °C.
2. Aldehyde Quenching Solution: 50 mM glycine in TBS, pH 7.4. Prepare 50 mL by adding 0.188 g of glycine to 50 mL of nanopure water and mix by vortexing. Store at 4 °C.
3. Blocking Solution for use with a mouse monoclonal primary antibody on mouse tissue, to be prepared freshly: 5 % goat anti-mouse IgG (AffiniPure Fab Fragment Goat Anti-Mouse IgG (Jackson ImmunoResearch)), 1 % bovine serum albumin (BSA, Fraction V), 0.1 % Cold Water Fish Skin Gelatin (40 % CWFG, AURION, EMS), and 0.05 % Tween® 20 in TBS pH 7.4. Prepare a volume sufficient for the number of grids to be stained. For example, using 30 µL for each of six grids would require 180 µL. Prepare 200 µL by adding 10 µL of goat anti-mouse IgG, 2 mg of BSA, 0.5 µL of CWFG and 0.1 µL of Tween® 20–189.4 µL of TBS pH 7.4. Mix well by vortexing. From this point onward, examples will assume the staining of six grids. Maintain on ice until use.
4. Blocking Solution, to be prepared freshly: 5 % normal goat serum, 1 % BSA, 0.1 % CWFG, 0.05 % Tween® 20 in TBS pH 7.4. Prepare 200 µL by adding 10 µL of normal goat serum, 2 mg of BSA, 0.5 µL of CWFG and 0.1 µL of Tween® 20–189.4 µL of TBS pH 7.4. Mix well by vortexing, then maintain on ice until use.
5. Blocking Buffer Rinse Solution, to be prepared freshly: 0.1 % BSA-c in TBS pH 7.4. Prepare 200 µL by adding 2 µL of stock

BSA-cTM (10 %, AURION BSA-CTM (acetylated BSA), EMS) to 189.4 µL of TBS pH 7.4. Mix well by vortexing and maintain on ice until use.

6. Primary Antibody Diluent, to be prepared freshly: 0.2 % BSA-c, 0.05 % Tween[®] 20 in TBS pH 7.4. Prepare 200 µL by adding 4 µL of BSA-c, 0.1 µL of Tween[®] 20–196 µL of TBS pH 7.4. Mix well by vortexing, then maintain on ice until use.
7. Tris-Buffered Saline Solution (TBS, pH 8.2): 50 mM Tris-HCl, 150 mM NaCl in nanopure water. Prepare 100 mL by adding 5 mL of stock 1 M Tris-HCl pH 8.0 (1 M UltraPure[™] Tris-HCl pH 8.0, Invitrogen) and 0.88 g of NaCl to 90 mL of nanopure water. Adjust pH to 8.2 using 1 M NaOH and bring volume to 100 mL with nanopure water. Mix using a magnetic stirrer and store at 4 °C.
8. Secondary Antibody Diluent, to be prepared freshly: 0.1 % BSA-c, 0.05 % Tween[®] 20 in TBS pH 8.2. Prepare 200 µL by adding 2 µL of BSA-c and 0.1 µL of Tween[®] 20–198 µL of TBS pH 8.2. Mix by vortexing briefly.
9. Osmium Tetroxide (OsO₄) Solution, to be prepared freshly: This chemical is *only* to be used in a fume hood!! 1 % OsO₄ in nanopure water. Prepare 200 µL by adding 50 µL of stock 4 % OsO₄ solution (aqueous; 10×2 mL ampoules, EMS), to 150 µL of nanopure water. Maintain at room temperature (RT). Discard in a dedicated hazardous waste container upon completion of the experiment.
10. Potassium Permanganate (KMnO₄) Solution (*see Note 17*) to be prepared freshly: 1 % KMnO₄ in nanopure water. Prepare 100 mL by adding 1 g of KMnO₄ (EMS) to 100 mL of nanopure water. Mix well using magnetic stirrer. Maintain at RT.
11. KMnO₄ Stop Solution, to be prepared freshly: 0.025 % citric acid in nanopure water. Prepare 50 mL by adding 0.0125 g of Na₃C₆H₅O₇·2H₂O, to 50 mL of nanopure water and mix by vortexing. Discard any remainder as hazardous waste.
12. Uranyl Acetate (UAcO₄) Solution, to be prepared freshly: 2 % UAcO₄ (aqueous) in nanopure water. Prepare 50 mL by adding 1 g of UAcO₄·2H₂O (Ted Pella) to 50 mL of nanopure water. Mix by vortexing. Store the solution in a dark glass bottle at 4 °C.

3 Methods

3.1 Preparation of Tissue Samples

Experiments using animal tissue should be approved by the University's Institutional Animal Care and Use Committee as set forth under the guidelines of the National Institutes of Health.

1. Euthanasia: Do the following under a hood. Add Isoflurane to several gauze pads and place on a metal grating in a glass bell jar. For an adult mouse, 2–3 min of exposure to an Isoflurane overdose should be sufficient to euthanize the animal. Check for cessation of respiration and lack of response to a tail pinch (neonatal mice are born hypoxic, therefore permit longer exposure to Isoflurane). While working very quickly, decapitate using appropriate instrument (*see Note 1*).
2. Removing the brain: Using a dorsal approach, bisect the head with a #22 scalpel along the midline to separate the hemispheres (*see Note 2*). If the animal is very young and the cranial vault is not completely ossified, use a #11 blade. Remove the pinnae and surrounding surface tissue/fur and immediately place the half-heads on crushed ice. Move to the dissecting microscope. Use a dissecting dish embedded in ice, containing ice-cold PBS in an amount sufficient to completely immerse the entire $\frac{1}{2}$ head to perform gross dissection. Lift the brain gently and carefully transect the cranial nerves including the nerves of the inner ear by using #2 mouse laminectomy forceps to hold the half-head in place (*see Note 3*) and spring scissors (*see Note 4*). Proceed to remove the brain in the direction of rostral to caudal.
3. Dissection of the inner ear: Using fine iris scissors, remove the otic capsule from the temporal bone, trim excess muscle and bone and transfer the otic capsule to a smaller hexagonal weighing dish containing ice-cold PBS embedded in ice. Using a #2 forceps to hold the inner ear upright and a #11 feather blade, isolate the tympanic bulla from the otic capsule so as to expose the cochlea surrounded in translucent bone. After trimming away excess bone with iris scissors, while holding the otic capsule with the nondominant hand at an $\sim 45^\circ$ angle, carefully pierce the round and oval windows using a #11 blade. (If the dissection microscope is situated in a laminar flow hood, add a few mL of Fixation Buffer to the dish.) Remove the overlying vestibular portion of the inner ear by inserting a #11 blade in the small space separating the bones. Scratch a portion of bone surrounding the cochlea with a scalpel at the apex to remove a small portion of the tympanic bulla and partially expose the sensory epithelium.
4. Fixation: Immersion-fix the tympanic bulla for 2 h in Fixation Buffer, while rotating under slow speed in a tissue rotator set at an $\sim 35^\circ$ angle at RT. Transfer tissues to a fresh bottle containing PBS with rotation for 2×30 min, each time transferring to a fresh bottle. Return the samples to the dissecting apparatus and dissect away the bony portion of the cochlea by carefully entering the space between the bone and the spiral ligament with a fresh #11 blade and slowly and with great care, flick small pieces of bone away from the sensory epithelium

along with the spiral ligament and stria vascularis, unless these tissues are of interest as well (*see Note 5*).

5. Decalcification: Transfer tissues to bottles containing the Decalcification Buffer and place them in a refrigerator or cold room under gentle rocking. Change to fresh Decalcification Buffer on a daily basis. Test for pliability of the cochlea gently using forceps (*see Note 6*). Upon determination that decalcification has been achieved, rinse every 15 min with nanopure water over the course of 2 h with gentle rocking.
6. Dehydration/Resin Infiltration: Immerse tissues in 50 % EtOH for 15 min, 70 % EtOH for 2×30 min (*see Note 7*), then 1×30 min in 85 % EtOH. Then place in a ratio of 2:1 70 % EtOH/resin for 1 h, 2×100 % resin for 1 h each followed by 100 % resin O/N with gentle rotation (*see Note 8*). The next day, continue infiltration by placing tissue in 100 % resin for 1 h while maintaining rotation. During this period, ensure that the oven temperature is maintained at 50 °C.
7. Embedding and Curing: Place 00 gelatin capsules in the BEEM® Capsule Holder and move to an upright microscope. Remove the cap of the gelatin capsule, over-fill with 100 % resin and quickly place tissue into the capsule so that when the cochlea sinks to the center of the bottom of the capsule, it resides on its side. Rapid embedding is important, as the resin is readily oxidized if exposed to air (*see Note 9*). Quickly place the cap on the capsule firmly, ensuring tight closure and maintaining the capsule upright. Since there will be resin overflow, place paper towels beneath the embedding stand. Place the capsule holder in the 50 °C oven for 48 h for polymerization/curing.

3.2 Ultramicrotomy: Semi-thin Sectioning

1. Coarse trimming of the tissue blocks: After testing the blocks of embedded tissues for hardness (this can be determined by the inability to penetrate the resin with a fingernail), remove the gelatin capsule by first removing the cap and then the capsule containing the tissue from the holder. Score the block with a (thick) razor blade, peel away the gelatin capsule, and secure firmly in the collet/block trimming base. Under a standard upright binocular microscope, locate the embedded tissue. Using one-half of a double-edged Personna razor blade with a piece of tape running along one side to prevent injury, create a quadrangle-shaped block face encompassing the area of tissue. To achieve this shape, trim the block so as to have a narrow apical edge and a wider basal edge. Connect the apical and basal edges by cutting at ~45° angles. Remove the coarsely trimmed block and insert it into the specimen holder such that the narrower edge engages the knife edge first; it is more effective to have this side cut first as you are likely working with decalcified tissue. For soft tissue, the basal portion of the block should encounter the knife edge first.

2. Adjusting the settings on the microtome: Refer to the manual and/or a trained professional familiar with your microtome. As an example, these instructions apply to an MT2B Porter-Blum Sorvall ultramicrotome. Apply settings for the acquisition of semi-thin sections to collect and evaluate for disposition; 0.5 μm sections are best, for which the interference color appears green in the collection trough. (Acquire a continuous interference color and thickness scale reference for estimation purposes.)
3. Preparation of glass knives using a manual knife breaker: Refer to the manual and/or a trained professional familiar with the knife breaker. As an example, these instructions apply to an LKB 7800B KnifeMaker. Remove a fresh strip of glass and wash it carefully with a laboratory detergent (e.g., Alconox); rinse copiously with nanopure water and permit to dry. Place the glass strip onto the breaker so as to break it in half. Using one piece, score the glass and permit to break so as to produce a diamond shape; store the remaining piece in a clean environment. Rotate the diamond 45° to the right, gently and firmly secure the blade, score again, and apply pressure slowly and stop such that the diamond breaks on its own. There are now two knives; the one on the right can be used for trimming the block face to approach the tissue while the left knife will be used for fine cutting. The quality of the knives must be assessed by examining them under a dissecting microscope; the edges should be straight and the left knife should have a lengthy edge, as determined by the location of a feathery landmark located near the right edge of the knife, from which point the left portion of the knife edge is used to cut sections.

3.3 Ultramicrotomy: Ultra-thin Sectioning

3.3.1 Cleaning Non-Formvar-Coated Grids

3.3.2 Set Up and Acquiring Semi-thin Sections

Using straight tweezers, immerse each grid in 0.1 N HCl for ~15 s. This etches the grids and assists in section retention, especially for LR White. Gently blot the grid on tissue paper and briefly immerse the grid in water, blot, acetone, blot, absolute EtOH, blot and place grids on filter paper in petri dish to dry.

1. Ensure the knife holder is clean, then insert the freshly prepared glass knife. Adjust the height using the guide and tighten the knife in the holder. Inexperienced users should practice with a blank block. Angle the stage such that the knife is exactly parallel to the apical portion of the quadrangle. Do not over-tighten any setting.
2. Slowly move the block such that it approaches the knife-edge. Face the block by sectioning away resin until tissue is detected by close observation of sections in the well. Move the glass knife periodically as needed by first backing away from the block a short distance and then re-approaching, thus maintaining a sharp edge.

3. As sections float into the boat spread the sections by briefly passing a chloroform-containing cotton applicator stick over the well, to smooth out any wrinkles. Do not permit the applicator to touch either the sections or water.
4. Capture each section by using the whisker brush to manipulate the section onto the beveled wooden applicator stick and transferring it to a drop of nanopure water warmed to 45 °C on a fresh slide placed partially on a hotplate. The sections float onto the droplet by placing the applicator at an ~90° angle to the water droplet and turning the stick until the sections float off.
5. Allow the sections to warm for a minute or so, then carefully decant or wick away the remaining water while tilting the slide carefully until the section adheres.
6. Quickly encircle the area in which the section was placed on the opposite side using an indelible marking pen (e.g., Sharpie) while the section can still be seen, before it is completely dry.
7. While the slide is on the hotplate, apply a small drop of Toluidine Blue Staining Solution contained within the syringe fitted with a 0.2 µm filter and permit that to stain for some 15–30 s while observing. Wick/decant the remaining stain and gently wash the section using a wash bottle containing nanopure water. Blot around and then dry the section briefly using the hotplate and examine with a standard upright microscope.
8. Continue semi-thin sectioning until the area of interest has been reached. This should be done frequently so as not to pass the area of interest in its optimal plane of section. To ensure the likelihood of this, mount the slide with a coverslip and examine under 100x oil objective. This step is of great import, as much time/funds can be lost performing an experiment with the area of interest missing, the tissue in an undesirable plane of section and/or poor morphology.

3.3.3 Fine Trimming the Block and Ultrathin Sectioning

1. After backing the knife a sufficiently safe distance from the tissue block, remove the knife/knife holder. Remove the block from the specimen holder and return to the collet in the block-trimming base under the upright microscope.
2. Using a thin Personna razor blade, transform the shape of the block face such that a narrow, long rectangular shape is achieved directly over the area of interest, while retaining a border of resin. Great care must be taken during this step.
3. Return the block to the specimen holder and align it and the knife so that the narrow portion of the block face is parallel to the knife.

4. Fill the knife boat with fluid using a 5 mL syringe, so that the surface has a slightly concave shape and the entire edge of the knife is wetted.
5. Tweezers, chloroform, grids, lens paper, and lens tissue should all be close at hand.
6. Slowly approach the knife edge; once engaged, change the setting of the microtome to thin sectioning and adjust to a slower cutting speed. Again, this can be monitored by observing the interference color of the sections. Aim to acquire sections of silver (200–500 Å), gold (500–800 Å), or purple (800–1300 Å) (*see Note 10*).
7. Sections should come off the knife-edge as a straight contiguous ribbon. Make subtle changes to either the knife-edge, the block itself, or the fluid level in the knife boat so as to ensure this result.
8. Collect sections on the dull side of the grid (3 mm in diameter) unless using Formvar-coated grids, in which case sections are to be collected on the shiny side, as this is the side upon which the Formvar was placed; check with the manufacturer.
9. Ideally, sections should reside only on the grids and preferably in the center, not the edges, as this risks section loss during processing and impairs data collection on the area of interest. The use of angle-tip tweezers to hold the grid permits the collection of sections with greater ease. In addition, the grid can be slightly bent at the very edge to help maintain its position during collection. The 45° angle tweezers suffice to maintain control.
10. Coordinate holding the section manipulator in one hand and the tweezers in the other. Collect the section by grasping the grid by the edge and entering the fluid in the knife boat at a steep angle. Once the sections are floating above the grid, lift the grid slowly to capture the sections.
11. Carefully wick water from between the tines of the tweezers by using lens paper. Very gently touch only the grid edge to lens tissue to further remove any remaining fluid.
12. Store the grid sample side up in a filter paper-lined petri dish with the lid slightly open so as to permit air-drying. One can perform IEM after drying the grids for one hour, however, keeping them O/N is a safer bet.
13. As experiments are more likely to be successful with freshly cut sections, do not collect more grids than can be used in a timely manner (*see Note 11*).

3.3.4 Immunogold Labeling

1. Using a pipeter, place 30–50 µL droplets on the dental wax corresponding to the number of grids used in the experiment (*see Notes 12 and 13*).

2. Rehydrate the tissue sections by gently placing grids section-side down on drops of TBS pH 7.4 for 3×5 min.
3. Transfer grids to the next dish (humid) containing droplets of Aldehyde Quenching Solution for a period of 30 min.
4. Block tissue sections by placing grids on droplets of Blocking Solution for 30 min (humid) (*see Note 14*).
5. Wash grids on droplets of Blocking Buffer Rinse Solution for 5 min.
6. This step is to be used only if a mouse monoclonal antibody is used on mouse tissue, otherwise skip to **step 7**. Place grids in dish containing droplets of Blocking Solution for use with a mouse monoclonal primary antibody on mouse tissue for a period of 30 min (humid).
7. Transfer grids to dish containing Blocking Buffer Rinse Solution for 1 min.
8. Transfer grids to primary antibody diluted in Primary Antibody Diluent and incubate O/N at RT (humid) (*see Note 15*).
9. The next day, set up three dishes containing droplets of TBS pH 8.2 and wash grids 3×5 min.
10. Set up two dishes so each contains a drop of corresponding gold-conjugated secondary antibody/antibodies diluted in Secondary Antibody Diluent. Place the grids on the first drop for 5 min. Transfer the grids to the second drop for a period of 90 min (*see Note 16*).
11. Set up three dishes containing droplets of TBS pH 7.4 and wash grids 3×5 min.
12. Set up two dishes with droplets of nanopure water and wash grids 2×5 min.

3.3.5 Contrast Staining

1. The following is to be performed in a chemical fume hood. Osmicate tissue sections by placing grids in a dish with droplets of OsO₄ solution for 15 min.
2. Rinse grids in very slowly running droplets of nanopure water using a wash bottle and a small plastic beaker for collection. Each droplet of water should cling to the grid momentarily.
3. Dispense drops of KMnO₄ solution (*see Note 17*) in another dish and permit staining for 15 s followed by a gentle rinse in slowly running droplets of water.
4. Set up a dish with KMnO₄ Stop Solution droplets and place grids on droplets for 45 s. Rinse once again in running droplets of water.
5. Set up a dish with UAcO₄ solution droplets. Provide conventional contrast by staining grids in UAcO₄ solution for 30 min followed by 3×5 min washes (three separate dishes) in nanopure water.

6. Store grids in a grid box that permits easy access but does not expose a number of grids at the same time, thus reducing the risk of losing grids.
7. Transport grids in a filter paper-lined petri dish on which to place each grid prior to mounting on the TEM stage.

3.4 Imaging

Always obtain a relatively low magnification image, for context. Scan for general area of interest using low beam intensity and magnification. Once identified, increase magnification and then beam intensity. Use the wobbler to assist in focusing; ensure that it is not engaged when imaging. Opt for use of the highest resolution camera, should there be a choice. Back up images on an external hard drive.

4 Notes

1. Tissues must be extracted rapidly and always submerged in ice-cold PBS so as to avoid hair cell exposure to hypoxic conditions.
2. It is essential to precisely bisect the head along the midline, which separates the two hemispheres of the brain; any deviation will endanger the integrity of the cochlea.
3. The laminectomy scissors are ideal for dissections of small animals as they have a ridged area near the tips permitting a firm yet gentle grasp of the tympanic bulla at the particular angle necessary to remove the bony portions of the cochlea.
4. The spring scissors enable the careful transection of cranial nerves, thereby minimizing the potential damage from pulling and ripping the nerves.
5. Decalcification Buffer can be made up with 2 % paraformaldehyde in the interests of preserving morphology should a significant time period be required for decalcification. This of course, depends partly on the age of the animal, reflecting the degree of bone mineralization. Should the stria vascularis not be included in the tissue sample, note that it is more difficult to separate it from the spiral ligament in the presence of fixative.
6. It is imperative that all bony tissue be decalcified as tissue cannot otherwise be sectioned for ultramicrotomy without damaging both the tissue and the knife-edge.
7. The first step in the infiltration series, i.e., 2:1 resin:70 % EtOH, is an appropriate stopping point, should time be an issue. Keep the tissues at 4 °C without rocking.
8. Cautionary guidelines should be followed in the technical notes accompanying the LR White resin.

9. Provided the following can be accomplished swiftly, should the tissue reside in an undesirable position, an extremely fine wire is used to reposition it.
10. Very thin sections, e.g., light silver to grey sections are not compatible for LR White work vs. increased resolution of, e.g., mitochondrial features. Thicker sections diminish section loss, folding, and tears/wrinkles.
11. At the outset, use unstained thin sections to evaluate fixation (e.g., examine mitochondrial membranes, they should be well resolved), quality of sectioning (chatter, compression, folding of sections), resolution of area of interest, and proper plane of sectioning.
12. Thirty microliters is generally considered the minimum volume to enable the sections on the grid to be exposed sufficiently well to each reagent in the series.
13. Sinking grids—a problem with routine EM let alone Immunolectron Microscopy (IEM), so be sure to adjust water level of droplet. Importance of collecting serial sections—adjust water level in boat. Sections tearing, falling off—Formvar is worth it, when you consider the time involved and the possibility of losing perfect cross-sections! Go for light gold sections—thinner (light grey interference) sections are not necessarily to one's advantage; the sections must not wrinkle and be capable of withstanding the entire IEM protocol and imaging.
14. BSA-c is described as a partly linearized, chemically modified BSA possessing an increased negative charge due to the acetylation of amino groups on basic amino acids. Its use improves signal-to-noise ratios; however, avoid incorporating it in the blocking buffer, as it may reduce signal intensity. The wash duration can be adjusted up or down, not to exceed 5 min; consult with the company for technical expertise. CWFG is a potent inhibitor of background staining; BSA up to 5 % can be added along with normal serum, and blocking duration can be decreased. Together with Tween® 20, nonspecific staining in the nucleus due to charge interactions can be diminished. Wash steps of 3×5 min can be used prior to primary antibody incubation (using diluent). Antibodies do NOT penetrate the resin sections. Substitution of BSA as the main blocking agent is an option, as normal serum might have impurities and introduce cross-reactivity. Formvar coating on grids can produce nonspecific staining but the advantage of increased section retention far outweighs this possibility.
15. Quality of the antibody is everything. Avoid purchasing an antibody unless it has been *antigen* affinity-purified. Confirm this with technical support from the seller should purification be described as “affinity-purified,” as this most likely refers

solely to the use of a protein A/G to purify the antibodies from the antiserum/ascites. Only purchase antibodies for which the downstream applications require recognition of the epitope under native conditions, i.e., immunocytochemistry, immunohistochemistry. Antibody concentration should be determined by titration. Provided a range is given, estimate by using a lower dilution or if none is given, try 1:10 to 1:100, on sections that are of lesser quality. Primary antibody incubation can be changed in terms of concentration (1–5 µg/mL) and duration (30–60 min at 37 °C). Have a positive control (tissue in which the protein is known to be expressed) and negative controls as well, e.g., the use of secondary antibody/antibodies in the absence of primary antibody/antibodies and a known negative tissue. For additional validation, use antibodies targeting different epitopes of same protein(s) of interest.

16. The use of two successive droplets of secondary antibody is recommended, as the first drop will remove excess buffer and the second is used for the gold labeling. A permutation of this protocol, to be found in BBI Life Sciences technical support literature, is to fix the grids after secondary antibody labeling in 1 % glutaraldehyde in water pH 7.4 for 10 min, the rationale being potential increased retention of gold particles. However, post-fixation washes are needed prior to contrast staining. It is important to bear in mind, with respect to precise localization, that an antibody is ~8 nm in length to which is attached a gold particle of either 5 nm or 10 nm diameter. Therefore, the protein(s) of interest is/are ~13–18 nm from the gold labeled colloid. This harkens back to the fact that antibodies do not penetrate the resin. This information is also found within the above-cited technical literature.
17. The addition of a short period of contrast staining with KMNO₄ is useful for increased resolution of membranes; however, incubation time is critical.

Acknowledgements

This work was supported by NIH/NIDCD grant R01 DC004295 to BS.

Reference

1. Hayat MA (2000) Principles and techniques of electron microscopy: biological applications, 4th edn. Cambridge University Press, Cambridge

Chapter 10

Surface Plasmon Resonance (SPR) Analysis of Binding Interactions of Inner-Ear Proteins

Dennis G. Drescher, Selvakumar Dakshnamurthy, Marian J. Drescher, and Neeliyath A. Ramakrishnan

Abstract

Surface plasmon resonance is an optical technique that is utilized for detecting molecular interactions. Binding of a mobile molecule (analyte) to a molecule immobilized on a thin metal film (ligand) changes the refractive index of the film. The angle of extinction of light that is completely reflected after polarized light impinges upon the film, is altered, and monitored as a change in detector position for a dip in reflected intensity (the surface plasmon resonance phenomenon). Because the method strictly detects mass, there is no need to label the interacting components, thus eliminating possible changes of their molecular properties. We have utilized surface plasmon resonance to study interaction of proteins of inner-ear sensory epithelia.

Key words Surface plasmon resonance (SPR), Hair cell, Molecular cloning, Protein–protein interaction, Fusion protein, Interaction kinetics, Sensor chip CM5, Biacore 3000

1 Introduction

Surface plasmon resonance (SPR) binding methodology is used to study molecular interactions [1–3]. It is an optical technique for detecting the interaction of two different molecules in which one is mobile and one is fixed on a thin gold film [2]. Over the last several years, technical advances and new applications have further increased the usefulness of SPR [4]. This technique has been used for characterization of antibodies [5], receptor–ligand screening [6], hormone detection [7], and assay of cancer markers, cardiac proteins, immune-disorder markers, nucleic acid point mutations, microRNA, bacterial nucleic acids, and viruses [7]. A recent technique, label-enhanced SPR, increases the signal-to-noise ratio of bimolecular interactions (up to 100-fold) and can be used in conjunction with conventional SPR [8].

Inner-ear samples generally comprise small amounts of tissue and are thus well suited for molecular analysis by SPR. SPR provides

sufficient sensitivity for quantitatively determining interactions of key molecules involved in sensory neurotransmission, mechano-transduction, and receptor–ligand binding. For example, the interaction of exocytotic synaptic proteins [9] has been investigated with determination of binding constants. Calcium-dependent interaction of the calcium-sensor otoferlin with SNAREs (soluble NSF attachment protein receptor proteins) has been described in several studies [10, 11]. The interactions of proteins implicated in hair-cell mechano-transduction and ion transport have been investigated [12–16]. Also, receptor–ligand interactions of aminoglycosides with endocytotic receptors in the neonatal inner ear, determined by SPR, have been examined [17].

In the work described here, affinity-purified fusion proteins/polypeptides are immobilized by an amine-coupling reaction on a sensor chip (Biacore, Piscataway, NJ, USA) inserted into the flow chamber of a Biacore 3000 instrument (Biacore, Uppsala, Sweden). Addition of a second protein to the chamber, the flow-through *analyte*, results in binding to the immobilized protein *ligand*, producing a small change in refractive index at the gold surface and conversion of light waves to electron density waves or plasmons [18], resulting in an intensity dip whose angle can be quantitated with precision [19]. Binding affinities can be obtained from the ratio of rate constants, yielding a straightforward characterization of protein–protein interaction. SPR directly detects mass (concentration) with no need for special radioactive or fluorescent labeling of proteins/polypeptides [20] before measurement, presenting a great advantage in minimizing time and complexity of the studies.

2 Materials

2.1 Selection of Sensor Chip

1. A CM5 chip, research grade (Biacore-GE Healthcare Life Sciences, Piscataway, NJ, USA), is commonly used (see Note 1).

2.2 Production of Ligands and Analytes

1. All reagents are prepared with Milli-Q water. The protein, used as immobilized ligand or mobile analyte, is purified either directly from a tissue source or by recombinant technology with overexpression in bacterial cells (see Subheading 3.2.4). Ligand or analyte can be a fusion protein tagged with hexahistidine or glutathione-S-transferase (GST) (as an aid to purification), or can be a synthetic oligopeptide, 20–30 amino acids in length.
2. Mouse brain QUICK-clone cDNA (BD Biosciences-Clontech, Palo Alto, CA, USA) or custom cDNA.
3. Expression vectors pRSET (Life Technologies, Carlsbad, CA, USA) or pGEX (GE Healthcare-Amersham, Piscataway, NJ,

USA), for producing fusion proteins/polypeptides by in-frame cloning.

4. Restriction enzymes *BamH*1, *EcoR*1, *Hind*3, *Bgl*2, *Not*1.
5. QIAEX-II gel extraction kit (Qiagen, Valencia, CA, USA).
6. *E. coli* Subcloning EfficiencyTM DH5αTM cells (Life Technologies).
7. One Shot Top 10 cells (Life Technologies) for cloning and plasmid isolation.
8. *E. coli* BL 21 StarTM (DE3) pLysS cells (Life Technologies) for protein expression.
9. LB liquid medium: 1 % bacto-tryptone, 0.5 % yeast extract, 1 % NaCl, adjusted to pH 7.0 with 5 N NaOH.
10. LB agar.
11. S.O.C. medium: 2 % tryptone, 0.5 % yeast extract, 10 mM NaCl, 2.5 mM KCl, 10 mM MgCl₂, 10 mM MgSO₄, 20 mM glucose.
12. Wizard plus SV Miniprep Kit (Promega, Madison, WI).
13. IPTG (isopropylthio-β-d-galactoside) stock solution: 100 mM in water. Sterilize by filtration and store at -20 °C.
14. Ampicillin stock solution: 100 mg/mL in water. Sterilize by filtration and store at -20 °C.
15. Protease Inhibitor Cocktail for use in polyhistidine tagged protein.
16. Protease Inhibitor Cocktail for general use.
17. Pre-cast SDS-PAGE (sodium dodecyl sulfate-polyacrylamide gel electrophoresis) gels (4–12 % gradient, NuPAGE (Life Technologies)).
18. Electrophoresis running buffer (20× NuPAGE SDS Running Buffer). Dilute buffer appropriately.
19. Coomassie Blue electrophoresis stain.
20. BenchMarkTM pre-stained protein ladder.
21. Cell lysis buffer: 500 mM KCl, 20 mM Tris pH 7.9, 0.2 % NP-40, 10 % glycerol, 10 mM imidazole, 5 mM mercaptoethanol and freshly added protease inhibitor.
22. Nickel-nitrilotriacetic acid (Ni-NTA) spin columns for purification of hexahistidine-tagged proteins (Qiagen).
23. Sonication lysis buffer for protein purification: 1× PBS, 100 mM EDTA, 0.5 mM DTT, 1× Protease Inhibitor Cocktail for general use, pH 7.4.
24. Glutathione-Sepharose 4B beads for GST fusion tags (GE-Healthcare Life Sciences).
25. L-Glutathione, reduced.

26. Amicon Ultra Centrifugal Filter Unit with Ultracel membrane (EMD Millipore, Billerica, MA, USA).
27. Anti-X-Press HRP antibody (Life Technologies).
28. Anti-GST antibody.
29. Coomassie Plus-200 Protein Assay Reagent.
30. Quant-iTTM Protein Assay Kit for use with Qubit fluorometer (Life Technologies).
31. Phosphate-buffered saline (PBS): 0.01 M NaH₂PO₄, 0.138 M NaCl, 0.0027 M KCl, pH 7.4.

2.3 Ligand Immobilization

1. HEPES buffered saline-NaCl (HBS-N buffer): 0.15 M NaCl, 0.01 M HEPES, pH 7.4.
2. HBS-P buffer: HBS-N with 0.005 % v/v surfactant P20 (Biacore).
3. HBS-EP buffer: HBS-N with 3 mM EDTA, 0.005 % v/v P20 (Biacore).
4. EDC amine coupling reagent: 0.4 M 1-ethyl-3-(3-dimethylaminopropyl)carbodiimide hydrochloride in water (Biacore).
5. Ethanolamine solution: 1.0 M ethanolamine-HCl, pH 8.5.
6. NHS amine coupling reagent: 0.1 M N-hydroxysuccinimide in water (Biacore).
7. Sodium acetate buffers for immobilization in the acidic range: 10 mM, pH 4.0, 4.5, 5.0, 5.5.
8. 10 mM disodium tetraborate buffer for immobilization in the basic range: 10 mM, pH 8.5 (Biacore).
9. 1.0 M NaCl solution.
10. Glycine-HCl solutions: 10 mM, pH 1.5, 2.0, 2.5, 3.0. Use for regeneration.
11. 50 mM NaOH solution. Use for regeneration.
12. BIAdesorb Solution 1: 0.5 % SDS.
13. BIAdesorb Solution 2: 50 mM glycine, adjusted to pH 9.5 with 5 N NaOH.

2.4 Experimental Binding Measurements

1. HBS-N buffer (buffer compositions in Subheading 2.3).
2. HBS-P buffer.
3. HBS-EP buffer.
4. Phosphate-buffered saline with Tween (PBST): 10 mM NaH₂PO₄, pH 7.5, 2.4 mM KCl, 138 mM NaCl, 0.05 % Tween-20.

5. Non-specific binding reducer (NSB): 10 mg/mL carboxymethyl dextran sodium salt in 0.15 M NaCl, containing 0.02 % sodium azide (Biacore).
6. Bovine serum albumin (BSA): 2 mg/mL.

3 Methods

We perform surface plasmon resonance experiments with a Biacore 3000 instrument [21]. The immobilization involves activation of carboxymethyl groups on a dextran-coated chip by reaction with N-hydroxysuccinimide, followed by covalent bonding of the ligands to the chip surface via amide linkages and blockage of excess activated carboxyls with ethanolamine [22]. Reference surfaces are prepared in the same manner, except that all carboxyls are blocked and no ligand is added. During analysis, each cell with an immobilized fusion protein is paired with an adjacent cell on the chip, the latter serving as a reference. The final concentration of bound ligand, expressed in response units (RU), is calculated by subtracting the reference RU from the ligand RU. HBS-N, HBS-P, HBS-EP, or PBST buffer may be used as both running and analyte-binding buffer. Purified fusion protein (analyte), typically at 100 nM, is allowed to flow over the immobilized ligand surface and the binding response of analyte to ligand is recorded. The chip surface is regenerated by removal of analyte with a regeneration buffer. The maximum RU with each analyte indicates the level of interaction, and reflects comparative binding affinity.

3.1 Equilibration of the Sensor Chip

1. Store the CM5 sensor chip at 4 °C. Bring the chip to room temperature just before the experiment.
2. At the analysis step, dock chip in the instrument. Prime with immobilization running buffer (HBS-N or HBS-EP). The priming process flushes the pumps, the integrated fluidic cartridge, autosampler, and flow cells of the sensor chip with the chosen running buffer. In the *Biacore 3000 Control* program, click the TOOLS tab and then select WORKING TOOLS. Place the running buffer in the buffer shelf, select PRIME, and click START.

3.2 Production of Ligands and Analytes

3.2.1 Design of PCR Primers for Production of Insert

1. Design primers so that the target insert will remain in frame when ligated (by adding additional nucleotides to the primer sequence, if necessary).
2. Use a different restriction site for each member of the primer pair to support directional cloning.
3. Amplify desired cDNA message, e.g., from mouse brain cDNA, with the primer pair.

4. Purify the PCR product containing the desired restriction sites by electrophoresis in agarose gels, followed by band excision and sequencing (*see Note 2*).

3.2.2 Ligation of Insert into Plasmid Expression Vector

1. Digest the PCR product at 37 °C overnight with appropriate restriction enzymes corresponding to the restriction sites of the PCR product. If the buffer supplied for both restriction enzymes is the same, the two enzymes can be incubated simultaneously with the PCR product. Otherwise, perform the two incubations, as well as Subheading 3.2.2, step 2, for each enzyme consecutively.
2. Extract the digested product (insert) with phenol-chloroform and precipitate it in ethanol (*see Note 2*).
3. Digest, extract, and precipitate the expression vector (e.g., pRSET) in a manner similar to that used for the PCR product (*see Note 3*).
4. Measure the concentration of the vector and insert by gel analysis using a molecular mass standard of known quantity, by spectrophotometry at 260 nm, or by fluorescence with a Qubit fluorometer (*see Note 4*).
5. Perform a standard ligation reaction using T4 DNA ligase. Use a 3:1 insert:vector ratio (*see Note 5*).

3.2.3 Transformation of Bacteria by Plasmid Expression Vector

1. Mix 1–2 µL of the vector ligation product with *E. coli* DH5α competent bacterial cells and incubate on ice for 30 min [3].
2. Heat-shock the cell mixture at 42 °C for 45 s.
3. Add 1 mL of S.O.C. medium and mix vigorously in an orbital shaker at 37 °C for 90 min.
4. Spread a 50- to 200-µL aliquot onto an LB agar plate (1.2 % agar in LB liquid medium), containing 75 µg/mL final concentration of ampicillin, and incubate at 37 °C overnight.
5. Select 10 or more colonies from the plate and culture them in 3–10 mL of liquid LB medium containing 75 µg /mL ampicillin overnight.
6. Pellet the cells by centrifugation at 4,000×*g* for 5 min.
7. Isolate plasmids with the Wizard plus SV Miniprep Kit.
8. Verify presence of insert by digestion with the two restriction enzymes that were used for cloning (*see Note 6*).

3.2.4 Protein Expression from Plasmid Expression Vector

1. Transform *E. coli* BL 21 Star™ (DE3) pLysS cells (Invitrogen) with the expression vector construct as in Subheading 3.2.3, steps 1–3.
2. Spread cells onto LB agar plates containing 75 µg/mL ampicillin, and allow them to grow overnight.

3. Culture resulting colonies in LB liquid medium containing 75 µg/mL ampicillin for 8 h or until the absorbance at 600 nm reaches an optical density (OD) reading of 0.3.
4. Add IPTG stock solution to yield a final concentration of 1 mM to induce protein expression.
5. Culture cells for another 3–4 h at 37 °C.
6. Pellet cells at 4,000× g , add lysis buffer, vortex, and incubate at room temperature for 30 min. Sonicate if necessary to increase protein yield.
7. Centrifuge at 18,000× g for 25 min and collect the clear supernatant.
8. Electrophoretically analyze 5 µL of the supernatant with a molecular mass standard in a pre-cast SDS-PAGE gel. Stain with Coomassie Blue.
9. Repeat Subheading 3.2.4, steps 1–8, using the expression vector not containing an insert, as a negative control.
10. As a further control, repeat Subheading 3.2.4, steps 1–8, with the omission of the inducer IPTG (*see Note 7*).

3.2.5 Purification of Protein (Ligand or Analyte) using Ni-NTA Affinity Purification (See Note 8)

If required, this purification step is preceded by scaling up of the culture, following Subheading 3.2.4, steps 1–7. All procedures are performed at room temperature.

1. Equilibrate a Ni-NTA spin column with 600 µL of cell lysis buffer and centrifuge for 2 min at 700× g at room temperature.
2. Load up to 600 µL of the cleared lysate supernatant from Subheading 3.2.4, step 7 onto the Ni-NTA spin column. Centrifuge at 700× g for 2 min and collect the flow-through. Add another 600 µL, if required, and centrifuge again.
3. Wash the column with 600 µL of wash buffer, centrifuge for 2 min at 700× g . Repeat the wash steps three to five times.
4. Elute the bound fusion protein by adding 200 µL of elution buffer to the spin column and centrifuge at 700× g for 2 min. Repeat the elution two more times.
5. Analyze the protein sample for purity as in Subheading 3.2.4, step 8, on an SDS-PAGE gel, and stain with Coomassie Blue (*see Note 9*).

3.2.6 Purification of Protein (Ligand or Analyte) Using Glutathione-Agarose Beads

This purification step is preceded by verification of overexpression and scaling up of the culture (to 50 mL or more), following Subheading 3.2.4, steps 1–5 (*see Note 10*).

1. Pellet the cells at 4,000× g , wash the pellet by resuspending in sonication lysis buffer, and pellet again. Repeat this wash procedure three times.

2. For subsequent steps, keep the cells on ice.
3. Sonicate cells on ice for 1 min three times, with 30 s pauses between exposures. Add Triton X-100 or Tween-20 to yield a final concentration of 1 %, and mix well.
4. Centrifuge at $18,000 \times g$ for 25 min at 4 °C and collect the supernatant.
5. Prepare the GST-sepharose 4B beads by washing four times in PBST buffer and preparing a 50 % slurry in PBST (*see also the GE-Amersham manual*).
6. Add 100 µL of GST-sepharose slurry for each 1 mL of the supernatant.
7. Incubate at 4 °C overnight with gentle mixing on a rotator. Spin the mix at $600 \times g$, remove the supernatant, and wash the beads three to five times with 1× PBST.
8. Elute the bound fusion protein by mixing the beads with 10 mM reduced glutathione, centrifuge at $600 \times g$, and collect the supernatant. Repeat three times and pool the eluted protein.
9. Check purity of the protein with SDS-PAGE gels, for the aliquots of lysate, sample flow-through fluid, and buffer washes.

3.2.7 Assay of Purity of Protein Samples (Ligands and Analytes) Used for Binding Studies

1. Dialyze the purified protein extensively (at least 16 h, with 6–7 changes of buffer) at 4 °C against the running buffer to be used in the SPR binding experiment (*see Notes 11 and 12*).
2. To check purity, run protein on SDS-PAGE and visualize with Coomassie Blue or silver stain.
3. Measure spectrophotometric absorbance of the sample at 595 nm (for Coomassie Blue stain) and calculate the concentration from a standard Coomassie Blue absorbance curve constructed from protein at known concentrations.
4. One may also determine protein concentration by fluorescence methods, such as with the Qubit fluorometer, which is sensitive enough to detect sub-nanogram concentrations of protein (*see Note 4*).
5. Store purified protein solutions at –20 °C in separate aliquots to avoid repeated freeze–thaw cycles that may inactivate proteins.
6. Prior to SPR studies (Subheading 3.4), thaw the protein on ice and centrifuge at 4 °C for 30 min at $18,000 \times g$ to pellet any precipitated protein.
7. Carefully collect the supernatant.
8. De-gas the sample solution before use (*see Note 13*).

3.2.8 Preparation of Cell Lysate Containing Analyte for Binding Studies

- Pellet bacterial cells that express the analyte protein by centrifuging at $4,000 \times g$.
- Instead of placing cells in lysis buffer (as in Subheading 3.2.4, step 6), sonicate the cells as described in Subheading 3.2.6, step 3. Centrifuge sample at $18,000 \times g$ for 25 min at 4°C .
- Collect the clear supernatant. As prepared here, non-purified analyte can sometimes be used if the ligand partner is pure, as determined by detection of the ligand as a single band by polyacrylamide gel electrophoresis (*see Note 11*).
- Estimate total protein in the filtered sample by the Coomassie Blue spectrophotometric method or the fluorescent method, as described previously.
- Dilute sample in SPR running buffer (HBS-N or HBS-EP) to the desired concentration, starting with $10 \mu\text{g}/\text{mL}$ total protein. Typical analyte concentrations are $10\text{--}250 \mu\text{g}/\text{mL}$, depending on the analyte affinity.

3.3 Ligand Immobilization

3.3.1 Preparation for Pre-concentration: Determining the Ligand Concentration for Optimal Immobilization

- Utilize 10 mM buffer solutions at three to four pH values, e.g., pH 4.0, 5.5, and 6.0, for “pH scouting” (Fig. 1). The pH range is chosen to be below the estimated pI of the fusion protein (*see Note 14*).
- Dilute protein sample in buffer solutions of different pH values (Subheading 3.3.1, step 1). The concentration of ligand should be in the range of $2\text{--}200 \mu\text{g}/\text{mL}$ (*see Note 15*)
- Using a sample volume of $100 \mu\text{L}$, determine the pH value that gives maximum surface retention for immobilization (Fig. 2). The Biacore 3000 instrument is automated, so once the program is loaded and samples are placed, the entire reaction sequence proceeds.
- Open *Biacore 3000 Control* software, click on RUN tab, and then click on APPLICATION WIZARD, then select SURFACE PREPARATION and click on START. In the next panel select pH SCOUTING and click NEXT.
- In the opening panel select BUFFERS or add a NEW BUFFER and then click on NEXT, type the LIGAND NAME, specify the INJECTION TIME, FLOW RATE, and FLOW CELL to use.
- In the next panel select WASH METHOD, WASH FLOW RATE, SOLUTION TO INJECT (*see Note 16*), and INJECTION TIME.
- In the next panel, assign RACK POSITIONS to samples and solutions, click on NEXT and click START. The result of a pH scouting run is shown in Fig. 1.

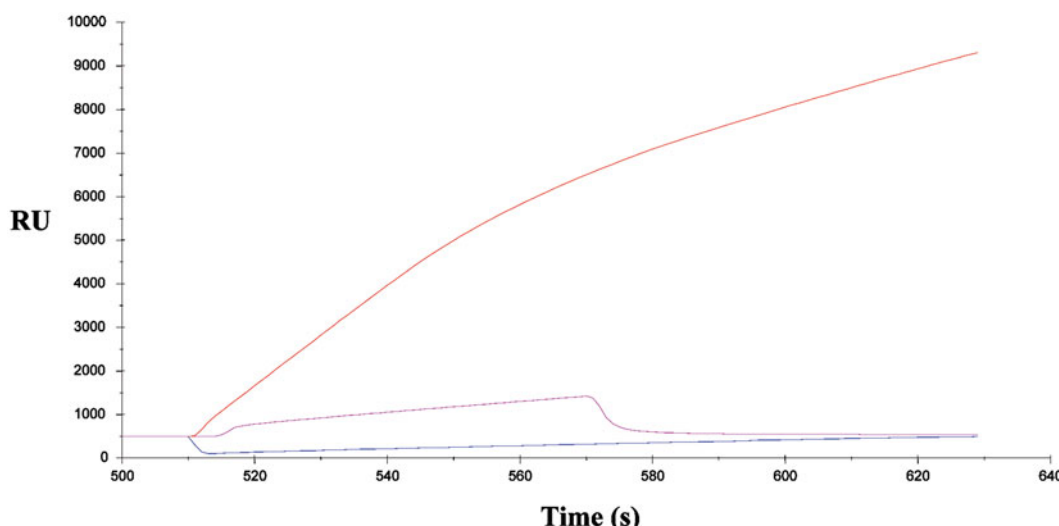


Fig. 1 The “pH scouting” of mouse syntaxin 1A hexahistidine fusion protein (model protein of 36 kDa molecular mass and pI 5.67) as ligand. The protein was diluted in 10 mM sodium acetate to a final concentration of 50 µg/mL, at three different pH values (4.0, 5.5, and 6.0), prior to the “pre-concentration” testing (see Fig. 2). For pH 4.0 (red curve), the surface concentration of ligand on the chip was much higher than that obtained for pH 5.5 and 6.0 (magenta and blue curves, respectively). Thus, for immobilization of the syntaxin 1A fusion protein via the amine coupling reaction (Fig. 2), pH 4.0 was chosen (a value less than the pI).

3.3.2 Preparation for Immobilization via the Amine Coupling Reaction (See Note 17)

1. Run a DESORB step with a maintenance chip docked (see Note 18).
2. Prepare two vials each containing 115 µL of EDC.
3. Prepare two vials each containing 115 µL of NHS.
4. Prepare two empty vials for mixing the reagents in Subheading 3.3.2, steps 2 and 3. (The vials are inserted in the instrument racks for automated mixing of reagents.)
5. Prepare sample (typically 200 µL) by mixing the required amount of ligand with sodium acetate solution at a pH determined by the pH scouting step.
6. Prepare two vials each containing 80 µL of ethanolamine solution, for blocking the unreacted active sites on the chip.
7. Prepare a vial containing 100 µL of 50 mM NaOH, for surface regeneration after pre-concentration.
8. Dock the CM5 sensor chip using the *Biacore 3000 Control* software, and prime the chip with the running buffer (see Note 19).

3.3.3 Setting Up the Pre-concentration and Immobilization Steps

1. Open the *Biacore 3000 Control* software (Fig. 2).
2. Click on the RUN tab, then click on to RUN APPLICATION WIZARD, select SURFACE PREPARATION, and START.
3. When the SURFACE PREPARATION STEPS window opens, select IMMOBILIZATION pH SCOUTING, and then select

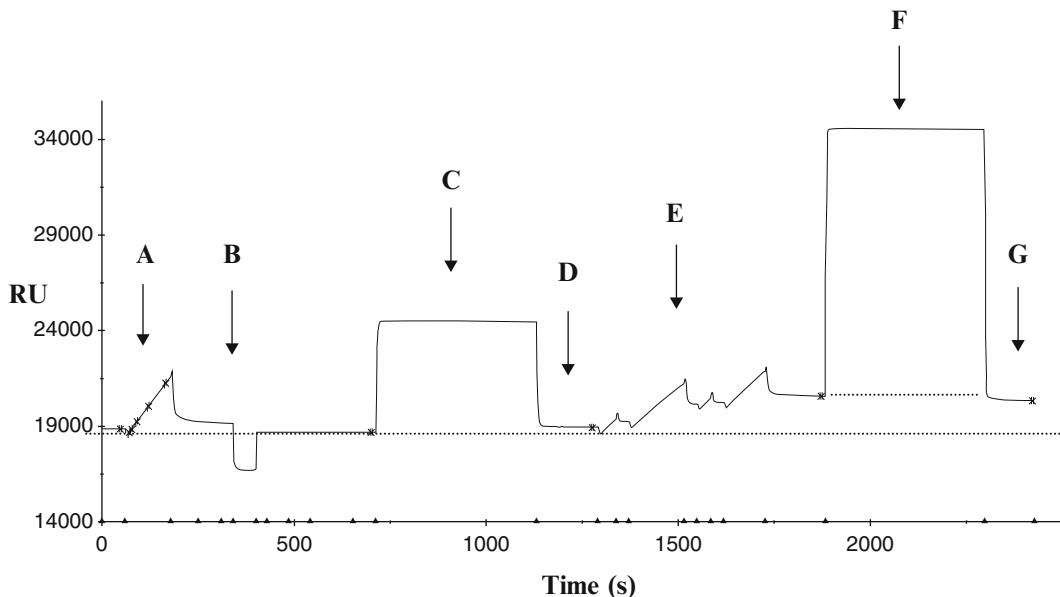


Fig. 2 Steps in the immobilization of purified syntaxin 1A fusion protein ligand on a CM5 research-grade sensor chip via the amine coupling reaction. **(a)** “Pre-concentration” test to determine how much of the ligand to inject to reach a targeted (aimed) level of response (RU, response units), here, 1500 RU. The injection period ends after attainment and overshoot of this criterion value above the baseline of approximately 19,000. The pre-concentration test reflects the proclivity of the ligand for the carboxymethylated dextran surface in its *non-activated* state, maximizing compatibility during the actual covalent binding step **(e)**, providing an estimate of the mass necessary for optimizing the association. **(b)** Washing of the non-covalently bound ligand with 50 mM NaOH to remove the ligand completely and obtain baseline. **(c)** Injection of the reaction mix (*see Subheading 3.3.2*) onto the surface, activating the carboxymethyl group by forming a highly reactive succinimide ester [24], followed by termination of the injection. **(d)** Slight elevation in the RU reflecting the activation, compared to the baseline between **(b)** and **(c)**. **(e)** After surface activation, injection of ligand sample diluted in buffer of the appropriate, pre-determined pH, with continuation of injection resulting in covalent binding of ligand to the reactive surface to yield the targeted RU value of 1500 (difference between the achieved constant level just before **(f)** and the baseline at **(d)**). **(f)** Blockage of remaining non-reacted, activated carboxymethyl groups by injection of ethanolamine, followed by cessation of injection. **(g)** Point of attained immobilization of ligand. Small triangles on time line below designate the events of injection, end of injection, and re-filling.

BUFFER (a list of buffers will appear). Click NEXT after selecting the buffer or buffers.

4. Type the NAME of the ligand to be tested, select INJECTION TIME, FLOW RATE, and FLOW CELL (FC; any of the four flow cells, FC 1, 2, 3, or 4 can be used for testing). An injection of 2-min duration, which is the default time, is usually sufficient to test the surface retention of the ligand for the selected pH. The flow rate is set to 5 $\mu\text{L}/\text{min}$ (*see Note 20*). Click NEXT to continue.
5. For the immobilization reaction, click RUN APPLICATION WIZARD, select IMMOBILIZATION, and click NEXT to select the type of SENSOR CHIP (CM5).

6. Select the IMMOBILIZATION METHOD, then in the next box select AIM FOR IMMOBILIZED LEVEL and click NEXT (*see Note 21*).
7. Select the WASH SOLUTION. Use the same wash solution(s) that were used for the pH scouting wash.
8. Select the SAMPLE POSITIONS for the vials to be placed in the instrument rack. Pipette out the required amount of each reagent, including the ligand solution. Manually insert the vials in the rack (*see Note 22*).
9. Click NEXT to start the run. At the completion of the run, a table is displayed showing the immobilization achieved (*see Note 23*).

3.3.4 Surface Preparation: Regeneration Scouting and Surface Performance Test

1. Open the control software. Perform DESORB, dock the CM5 chip containing the ligand, and prime with running buffer.
2. Click RUN tab, select RUN APPLICATION WIZARD, select SURFACE PREPARATION, and click START when the panel opens.
3. Select REGENERATION SCOUTING and click NEXT. In the panel, enter the ANALYTE NAME, INJECTION TIME, FLOW RATE, and FLOW CELL that contains the ligand. Click NEXT and select the rack positions. Click START and save the file to begin the run.
4. Select SURFACE PERFORMANCE TEST and click NEXT to enter the analyte name. Specify INJECTION TIME, FLOW RATE, AND NUMBER OF CYCLES (2–5 cycles). Select the FLOW CELL (1, 2, 3, 4, 2-1, or 4-3) and click NEXT to set the regeneration conditions.
5. In the panel, select a REGENERATION METHOD (dissociation in buffer, single injection, or two injections), FLOW RATE, SOLUTION/INJECTION (e.g., 10 mM glycine HCl, pH 3.0), and INJECTION TIME. Click on the box for STABILIZATION TIME, set the time (2 min or more), and click NEXT.
6. Select the RACK POSITIONS and click START to save and run the experiment (*see Note 24*).

3.4 Experimental Binding Measurements

3.4.1 Experimental Binding Run

1. Run DESORB with the maintenance chip docked. Remove the maintenance chip, dock the CM5 ligand chip, and prime.
2. Click RUN, then select APPLICATION WIZARD. Select BINDING ANALYSIS and click START.
3. Choose DIRECT BINDING, click NEXT to select the FLOW CELL, FLOW RATE, and the NUMBER OF SAMPLE INJECTIONS. Set the SAMPLE INJECTION TIME and WAIT AFTER INJECTION time.

4. Click NEXT to enter the ANALYTE NAME, NUMBER OF REPLICATIONS, and the ORDER in which the sample is to be analyzed (as entered or random).
5. Select the regeneration (wash) method. Choose SINGLE INJECTION or TWO INJECTIONS.
6. Select FLOW RATE for the regeneration run.
7. Select the TYPE OF SOLUTION (*see Note 24*).
8. Click NEXT to reach the next panel to assign the sample positions in the rack. Drag and drop each sample to whichever position is wanted, but make sure the programmed placement corresponds exactly to the subsequent actual placement. This panel also tells one how much of each solution is required.
9. Pipette out the required amount of the solutions and keep in the assigned racks.
10. Press NEXT, and then once again verify if all the samples are in the correct position and in the correct rack.
11. Click START to run the experiment. Begin with a low analyte concentration with a flow rate of 30 $\mu\text{L}/\text{min}$, and choose a reference cell and the ligand cell.

3.4.2 Experimental Kinetic Run (Fig. 3)

1. Run DESORB and then dock the CM5 chip with ligand and prime in running buffer.
2. On the *Biacore 3000 Control Software*, click RUN, and select RUN APPLICATION WIZARD.
3. Select KINETIC ANALYSIS and click START.
4. Tick the box for CONCENTRATION SERIES and select as a control experiment MASS TRANSFER.
5. Next, select DIRECT BINDING and click NEXT.
6. In the panel, select the flow cell (2-1, 4-3, 1, 2, 3, or 4), set the FLOW RATE, STABILIZATION TIME, INJECTION TIME, and DISSOCIATION TIME. Select the RUN ORDER (random or as entered). Enter ANALYTE NAME, MOLECULAR MASS in Daltons, NUMBER OF REPLICATIONS, and required CONCENTRATIONS. Click NEXT. Select at least five different concentrations and include a buffer blank.
7. In the MASS TRANSFER control panel, select a CONCENTRATION to be analyzed. If using a range of 0–200 nM, use a concentration that is in the range of 100 nM. Click NEXT.
8. Select the REGENERATION METHOD, FLOW RATE, REGENERATION SOLUTION, and the INJECTION TIME. Set the STABILIZATION TIME after regeneration.
9. Select RACK POSITIONS, click NEXT, and click START to begin the run and save the file (*see Note 25*).

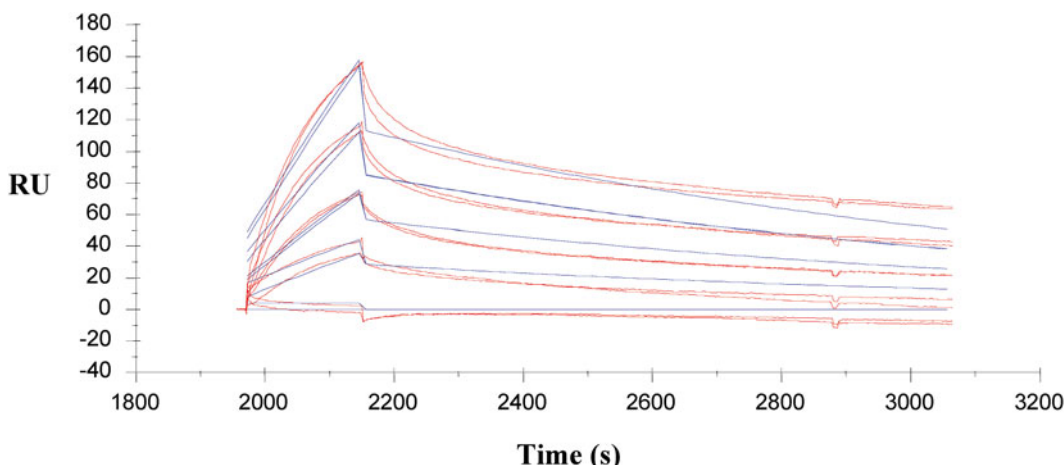


Fig. 3 Plots illustrating experimental curve-fitting methodology for a simple binding model (1:1 Langmuir). Association and dissociation phases can be seen in each plot. Pairs of red traces at each concentration indicate duplicate experimental determinations and blue traces show the corresponding binding model curves. In these studies, a syntaxin 1A fusion protein ligand was immobilized on a CM5 sensor chip by the amine coupling method to a final targeted RU of 707 (immobilization targeting is illustrated in Fig. 2). A range of concentrations (0, 10, 20, 40, and 80 nM) of the analyte, a model hexahistidine fusion protein of the calcium channel $\text{Ca}_v1.3$ II-III loop with molecular mass 18 kDa, was used for the kinetic evaluation

3.4.3 Data Analysis and Determination of Kinetic Constants

1. Using *BIAevaluation* software (*see Note 26*), select the data to be analyzed and create an overlay file by selecting the relevant curves. Align all the curves to the start of the injection. Remove the portions of the plots that lie outside the relevant regions of the association and dissociation curves, since the measurements require only the relevant portions.
2. Choose FIT: KINETICS SIMULTANEOUS k_a/k_d to start the kinetic evaluation wizard and perform the curve-fitting process. Set the baseline to zero at a point at the start of the injection in the most stable region. Performing a Y-TRANSFORM command in the wizard panel enables alignment of all the desired curves.
3. Select START TIME and STOP TIME for the injection and select the DATA RANGE, for association and dissociation, to be used in the fitting process. Make necessary adjustments by zooming out and inspecting the selected region visually (*see Notes 27 and 28*).
4. In the next panel, select the BINDING MODEL. Depending on the binding data, choose the model which best fits the ligand-analyte interaction. (a) 1:1 Langmuir binding, (b) 1:1 binding with shifting baseline, (c) 1:1 binding with mass transfer, (d) bivalent analyte, (e) heterogeneous analyte, (f) heterogeneous ligand, (g) two-state reactions [25].

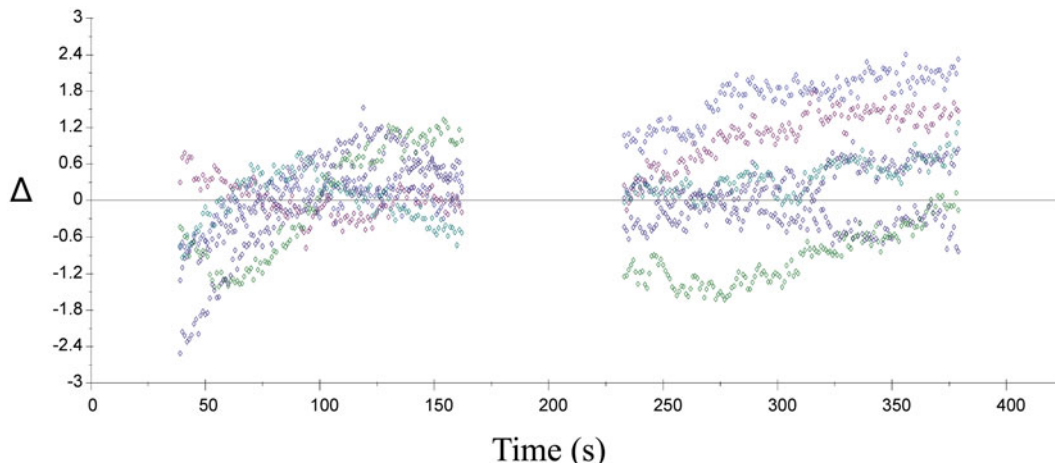


Fig. 4 “Residual” plots [23] reflecting minimal deviation between experimental and fitted data for a kinetic study (not shown) in which the data match the model. Left and right data sets correspond to chosen association and dissociation portions, respectively, of the kinetic curves. Colors represent different concentrations of analyte (top to bottom, see dissociation portion): *light blue*, 2 nM; *magenta*, 0 nM; *black*, 4 nM; *blue-green*, 8 nM; *dark blue*, 32 nM; *green*, 16 nM. Note that the scatter in the residual plots is within or around the criterion ± 2 RU, indicating that the experimental and model kinetic curves, in this case for a 1:1 Langmuir interaction (see Subheading 3.4.3, step 4), show a good fit. Larger deviations from the zero line would indicate that the data should be refitted using another kinetic model

5. Fit the data and observe the progress. For simple 1:1 reactions, the computation process is almost instantaneous, but a delay of several seconds to minutes may indicate complex binding or heterogeneity in the data set.
6. After the fit, the curves will appear as an overlay of the experimental and fitted data (Fig. 3). Close overlap, observed visually, is a good first indication of the validity of the fit.
7. The result is displayed as a report, with all the constants in numerical form. Examine the “residual plot,” which is the calculated difference between the experimental and fitted data (Fig. 4), by clicking on the RESIDUALS tab. If there are systematic deviations between the experimental and fitted curves, the plot will indicate them by displacement from the zero line. A stable baseline is critical to optimal kinetic analysis (Fig. 5). Ideally, the noise level in the plot should be on the order of ± 2 RU (also *see Note 29*).

4 Notes

1. The Biacore CM5 chip is widely employed for SPR interaction studies. Carboxymethylated dextran molecules are attached to a gold-coated surface. The CM5 chip can detect nucleic acids,

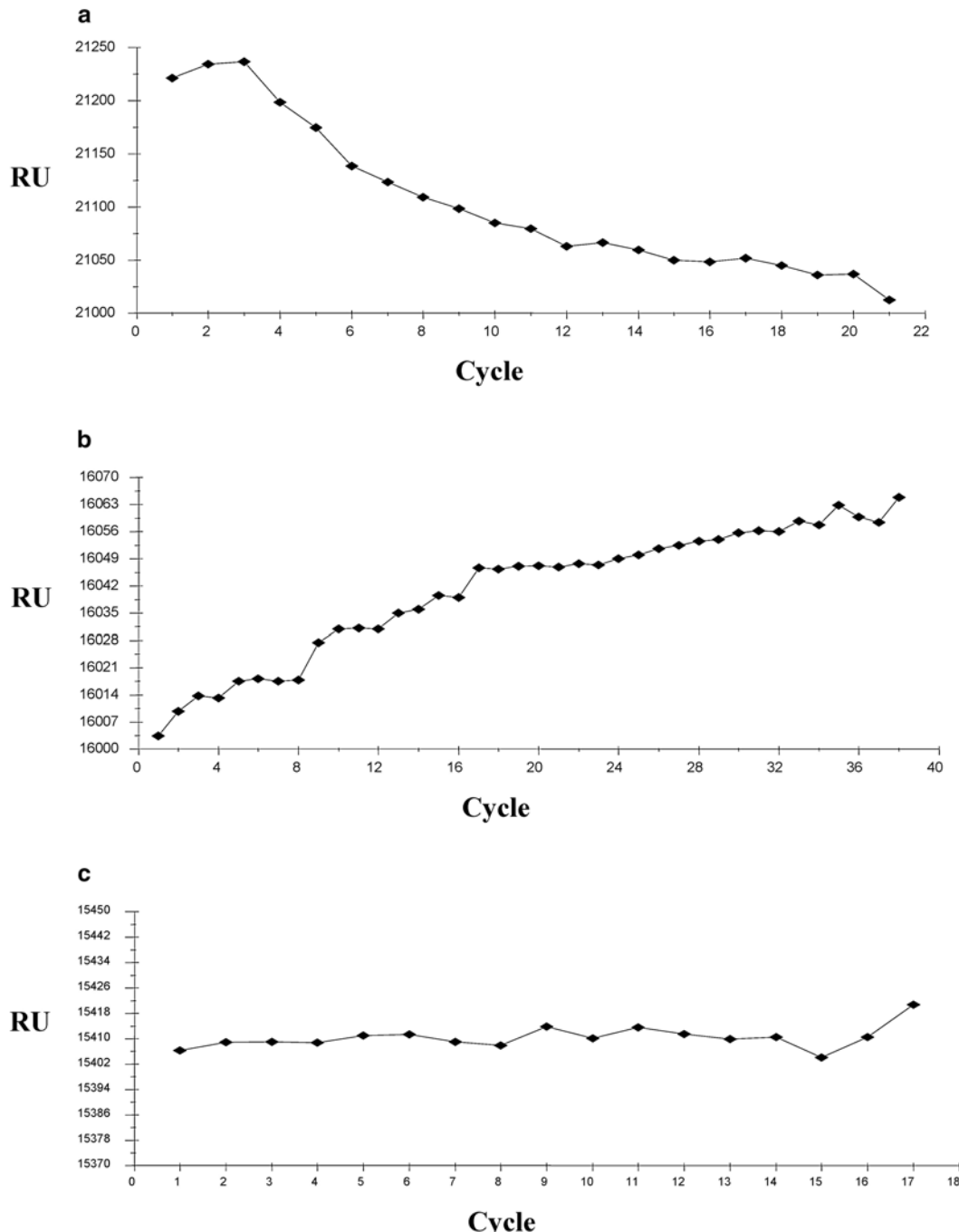


Fig. 5 Illustration of unstable vs. stable SPR baselines. Baseline stability is critical to obtaining accurate kinetic data. Plot (a) shows a decreasing baseline after each cycle, commonly due to loss of the bound ligand. Plot (b) indicates an increase in the baseline after each cycle, reflecting partial dissociation of analyte and poor regeneration. Plot (c) shows a stable baseline, indicating minimum loss of bound ligand as well as maximum regeneration. The latter reaction is most likely to yield accurate kinetic data. (Fig. 3 illustrates a data set where the baseline was stable and duplicate determinations were similar.)

carbohydrates, and small molecules, in addition to proteins. The chip surface is prepared for binding studies by coupling ligand molecules to the carboxymethyl group via NH₂, -SH, -CHO, -OH, or -COOH linkages. As alternatives to the CM5 chip, CM4, CM3 and C1 chips can be used, which have a lower matrix density of functional groups. Another chip, SA, can be used for immobilization of biotinylated peptides, proteins, nucleic acids, and carbohydrates. HPA and L1 chips are employed for lipid or liposome immobilization. NTA chips are utilized for capturing histidine-tagged molecules [24].

2. If no non-specific PCR bands are present, the product can be purified by phenol-chloroform extraction and alcohol precipitation. Adjust the sample volume to 200 µL by adding deionized water. Add an equal volume of phenol-chloroform (50 % phenol saturated with 0.1 M Tris-HCl, pH 7.6, 48 % chloroform, 2 % isoamyl alcohol) to the sample and vortex to mix. Centrifuge at 14,000 × g for 5 min. Carefully pipette out the upper phase into a fresh tube and add an equal volume of chloroform, vortex, and centrifuge as before. To the supernatant, add 1/10 volume of 3 M sodium acetate, pH 4.5, and 2.5 volumes of ethanol. Incubate at -20 °C for 1 h. Centrifuge at 14,000 × g for 10 min at room temperature. Remove the supernatant. Wash pellet in excess 70 % ethanol, centrifuge as before, decant supernatant, and dry pellet in air.
3. The pRSET vector contains sequences for six contiguous histidine residues upstream of the multiple cloning site, and thus the his-tagged fusion protein expressed in bacteria can be purified using a nickel affinity column (Qiagen). Immediately adjacent and upstream to the multiple cloning site is an eight-amino-acid epitope (Xpress™) against which antibodies are commercially available (Invitrogen), facilitating antibody-based detection. The pGEX expression vector can also be used (*see Note 10*).
4. The Qubit fluorescence spectrometer (Life Technologies) is a convenient instrument for measurement of nucleic acid and protein concentration by fluorescence. In a 0.5-mL tube, pipette 190 µL of the Quant-iT working solution (1/200 dye in buffer; buffer is double-stranded DNA Broad-Range reagent). Add DNA sample (1–10 µL) and bring to a total of 200 µL with water. Vortex 2–3 s, incubate for 2 min, and read the fluorescence.
5. Add, to an autoclaved 0.5-mL microcentrifuge tube, 4 µL of 5× ligase reaction buffer, 15–60 fmol vector DNA, 45–180 fmol insert DNA (0.1–1.0 µg total DNA), and 1 unit of T4 DNA ligase in 1 µL (Invitrogen). Bring the total volume to 20 µL, mix gently, and centrifuge briefly to collect the contents at the bottom of the tube. Incubate at 4 °C overnight.

6. Further confirmation of correct insert sequence should be accomplished by nucleotide sequencing of the insert before carrying out the protein expression.
7. In verifying the expression of protein, there should be a heavily stained protein band at the estimated molecular size of the fusion product for the IPTG-induced sample. There may be a low-to-moderately stained band in the non-induced samples. There should be no comparable band in the empty vector sample. Once expression is verified, proceed to the purification step.
8. After protein overexpression for the clonal sequence is established, the bacterial cells are grown in cultures for scaled-up protein purification. For purification of the fusion protein, generally 50–250 mL of culture is sufficient for small-to-medium-scale protein yield. From a 50 mL culture, one can purify up to 250 µg of protein.
9. For Ni-NTA spin-column (Qiagen) purification [11], as much as 100 µg of pure protein can be obtained from 1.2 mL of the lysate solution, depending on the level of expression. In some cases, minor bands are visible in the purified sample, and a re-purification step with a fresh spin column is required.
10. For purification using glutathione-agarose beads [10], PCR primers for domains of interest containing desired restriction sites are used in PCR reactions to clone the domains into the pGEX-6P-1 vector. This vector contains a 5' glutathione S-transferase (GST) coding region followed by a multiple cloning site. The fusion protein product will contain an N-terminal, 26-kDa GST tag, which allows affinity purification through the binding of GST to glutathione covalently bound to the resin. The pGEX-6P-1 vectors are utilized to transform *E. coli* BL21 (DE3) as described in Subheading 3.2.3, and the protein is purified by the glutathione-agarose beads.
11. In general, both ligand and analyte should be as pure as possible, particularly for kinetic analysis of interactions. However, if a well-purified ligand is used, it is possible to determine the concentration of the analyte even if the latter is present in a mixture [23].
12. It is critical that there be no glycerol in the protein samples and buffers, since glycerol may alter data due to its elevated refractive index.
13. De-gas solutions by fitting a rubber stopper, with inlet tube attached to an aspirator and trap, to the top of a vessel containing the solution and reduce the pressure until air bubbles are expelled.
14. The pH should be adjusted so that the protein has a net positive charge. The pI and molecular mass of the protein can be

estimated using the COMPUTE pI/MW tool found at http://au.expasy.org/tools/pi_tool.html.

15. The ligand should be at least 95 % pure. Generally, a ligand protein of smaller molecular mass should be paired with a protein of higher molecular mass as analyte, because the SPR response will be higher, due to the more advantageous (higher) density that can be achieved for the smaller molecular-mass molecule bound to the surface.
16. A single injection of 50 mM NaOH at a flow rate of 20 $\mu\text{L}/\text{min}$ will usually remove all the ligand from the surface (inspect the baseline to see if it returns to the same level as before the run). If the baseline remains elevated, a second wash with the same or another buffer should be performed to remove the ligand completely.
17. The amine coupling reaction is the reaction most generally used for proteins because of readily available amine groups in proteins. (A sensorgram of a typical immobilization experiment using amine coupling reaction is shown in Fig. 2.) However, amine coupling is not suitable if the ligand is too acidic ($\text{pH} < 3.5$), if the amine groups are present in the active site, or if there are too many amine groups. In such situations, if thiol groups are present in the ligand, thiol coupling is preferred as an alternative [24]. If neither is suitable, capture techniques such as streptavidin-biotin or His-tag nickel affinity methods can be selected. If a well-characterized antibody is available against the ligand, the antibody can be immobilized and the ligand captured for binding studies. Non-amine-coupling protocols are not covered in detail here.
18. It is important to perform DESORB before each run in order to clean the microfluidic tubes, chamber, and injection port. Such recommended instrument maintenance should be carried out on a regular basis. In the *Biacore 3000 Control* program, click the TOOLS tab and then WORKING TOOLS. Place one vial each of BIAdesorb Solution 1 and BIAdesorb Solution 2 in the rack designated by the program. Click DESORB and then START. Use a maintenance chip (chip lacking gold or other surface coatings) during the DESORB; do not use the CM5 chip.
19. As noted in Subheading 3.1, step 2, the sensor chip should be primed before each run. The total duration for the priming is 6.3 min.
20. A slow flow rate (5 $\mu\text{L}/\text{min}$) is best, since the chance for the ligand to adsorb to the surface increases as the flow rate decreases.
21. All the buffers, solutions, and sensor chips should be brought to room temperature before the run. De-gas all solutions. The

buffers and regeneration solutions must also be filtered through standard 0.2- μm or 0.4- μm filters.

22. When analyzing the samples, make sure that there are no air bubbles trapped in the sample solution. Even with prior degassing, bubbles can form during the sample dilution, and sometimes the bubbles may not be clearly visible. The way to eliminate bubbles is to spin the tube at top speed ($18,000 \times g$) in a benchtop centrifuge for 10–15 s.
23. To minimize the mass transport effect (Fig. 6), a low level of ligand immobilization is preferred [25].
24. Regeneration is achieved with the optimal pH and ionic concentration that keep the ligand active. A series of regeneration tests should be performed with regeneration buffers, from mild to more stringent conditions of pH and ionic strength. In most cases where the binding affinity is low or moderate, begin with a pH close to neutral (pH 4.5–8.5) and an ionic strength in the range of 0.5–1.0 M. 1.0 M NaCl should be sufficient to dissociate most of the bound protein.
25. When undocking the chip from the instrument, it is often advantageous to select *not* to remove the buffer from the flow cells by un-checking EMPTY FLOW CELL. The chip can then be wrapped in soft tissue paper or a piece of paper towel and stored in a tight container at 4 °C. The sensor chips with immobilized ligands can be stored for few days to more than a month.
26. SPR binding measurements are generally performed in duplicate or triplicate. Such experimentally obtained data can be evaluated with the SPR kinetic evaluation software, *BIAevaluation*. In general, analysis of kinetic data involves the following steps: (a) make overlay plots of several interaction curves, (b) select analysis region, (c) select interaction model and curve fitting, (d) store results of the fitting procedure into an analysis results file.
27. In selecting the data range for analysis of kinetic plots with *BIAevaluation* software, a short period before the injection start and before the stop (the beginning and end of association phase of the kinetic plot) should be excluded in the selection to avoid the dispersion effect (the complex response in refractive index at the beginning and end of injection, not clearly defined mechanistically).
28. Perform separate fits for different regions of the association and dissociation phases to ascertain if the calculated constants are consistent.
29. Although not detailed here, association and dissociation constants can also be obtained directly by determining the concentrations of analyte and ligand under steady-state conditions [23].

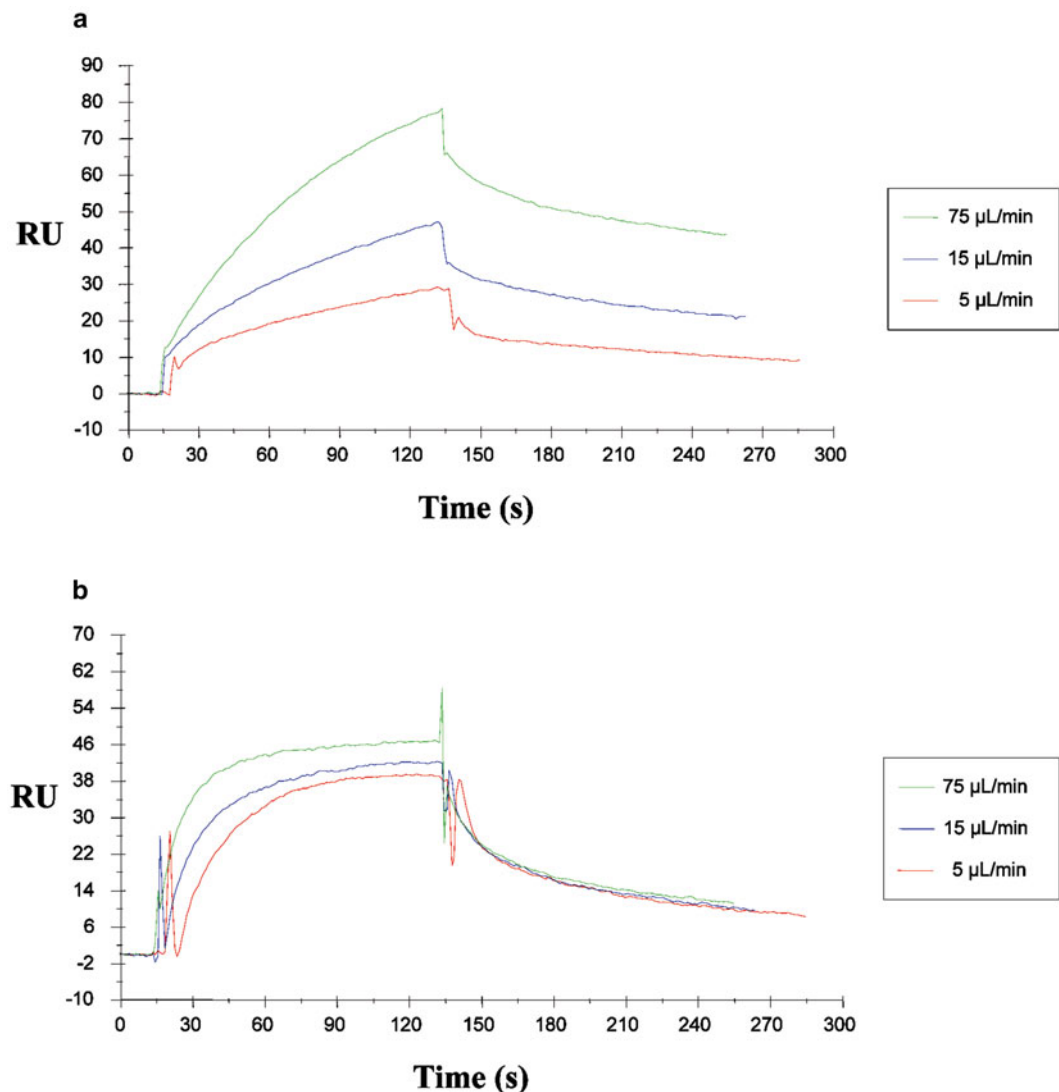


Fig. 6 Effect of flow rate on mass transfer. If the association rate constant of an interaction of interest is high, the measured binding rate may reflect the rate of *transfer* of analyte into the matrix (as the limiting rate) rather than the rate of the binding itself [25]. This limitation can be regarded as the failure to maintain the bulk concentration of the free mobile reactant at the sensor surface in the vicinity of the binding sites, and such mass transfer limitation may yield erroneous rate constants. Mass transfer problems, if present, are commonly detected by injecting a certain concentration of analyte sample at different flow rates, as shown. In diagram (a), the same analyte concentration gives considerably different RUs with different flow rates, indicating the presence of a mass transfer limitation. In diagram (b), the RUs at different flow rates are more similar, with almost identical dissociation phases, suggesting a minimal mass transfer limitation. If mass transfer limitation is present, as in (a), choosing a relatively high flow rate, low ligand density, and experimentally optimal analyte concentration can considerably reduce the limitation [26]

Acknowledgments

This work was supported by NIH R01 DC000156 and NIH R01 DC004076.

References

1. Panagiotis L, Kastritis PL, Bonvin AM (2012) On the binding affinity of macromolecular interactions: daring to ask why proteins interact. *J R Soc Interface* 10:1–27
2. Schuck P (1997) Use of surface plasmon resonance to probe the equilibrium and dynamic aspects of interactions between biological macromolecules. *Annu Rev Biophys Struct* 26: 541–566
3. Ramakrishnan NA, Drescher MJ, Sheikali SA, Khan KM, Hatfield JS, Dickson MJ, Drescher DG (2006) Molecular identification of an N-type Ca^{2+} channel in saccular hair cells. *Neuroscience* 139:1417–1434
4. Nguyen HH, Park J, Kang S, Kim M (2015) Surface plasmon resonance: a versatile technique for biosensor applications. *Sensors* 15: 10481–10510
5. Kowalczyk C, Dunkel N, Willen L, Casal ML, Mauldin EA, Gaide O, Tardivel A, Badic G, Etter AL, Favre M, Jefferson DM, Headon DJ, Demotz S, Schneider P (2011) Molecular and therapeutic characterization of anti-ectodysplasin A receptor (EDAR) agonist monoclonal antibodies. *J Biol Chem* 286:30769–30779
6. Aristotelous T, Ahn S, Shukla AK, Gawron S, Sassano MF, Kahsai AW, Wingler LM, Zhu X, Tripathi-Shukla P, Huang XP, Riley J, Besnard J, Read KD, Roth BL, Gilbert IH, Hopkins AL, Lefkowitz RJ, Navratilova I (2013) Discovery of $\beta 2$ adrenergic receptor ligands using biosensor fragment screening of tagged wild-type receptor. *ACS Med Chem Lett* 4:1005–1010
7. Mariani S, Minunni M (2014) Surface plasmon resonance applications in clinical analysis. *Anal Bioanal Chem* 406:2303–2323
8. Episente Application Note # 020 Label-Enhanced SPR (2015) Label-enhanced SPR: a primer on technology & applications. EAN 020–02-15-03-01
9. Leveque C, Ferracci G, Seagar M, Miquelis R (2003) Biacore's SPR technology applied to the study of the molecular machinery of exocytosis. *Biacore J* 1:8–11
10. Ramakrishnan NA, Drescher MJ, Morley BJ, Kelley PM, Drescher DG (2014) Calcium regulates molecular interactions of otoferlin with soluble NSF attachment protein receptor (SNARE) proteins required for hair cell exocytosis. *J Biol Chem* 289:8750–8766
11. Ramakrishnan NA, Drescher MJ, Drescher DG (2009) Direct interaction of otoferlin with syntaxin 1A, SNAP-25, and the L-type voltage-gated calcium channel $\text{Ca}_{v}1.3$. *J Biol Chem* 284:1364–1372
12. Selvakumar D, Drescher MJ, Drescher DG (2013) Cyclic nucleotide-gated channel α -3 (CNGA3) interacts with stereocilia tip-link cadherin 23 + exon 68 or alternatively with myosin VIIa, two proteins required for hair cell mechanotransduction. *J Biol Chem* 288:7215–7229
13. Selvakumar D, Drescher MJ, Dowdall J, Khan KM, Hatfield JS, Ramakrishnan NA, Drescher DG (2012) CNGA3 is expressed in inner ear hair cells and binds to an intracellular C-terminus domain of EMILIN1. *Biochem J* 443:463–476
14. Ramakrishnan NA, Drescher MJ, Khan KM, Hatfield JS, Drescher DG (2012) HCN1 and HCN2 are expressed in cochlear hair cells. HCN1 can form a ternary complex with protocadherin 15 CD3 and F-actin-binding filamin A or can interact with HCN2. *J Biol Chem* 287:37628–37646
15. Bahloul A, Michel V, Hardelin JP, Nouaille S, Hoos S, Houdusse A, England P, Petit C (2010) Cadherin-23, myosin VIIa and harmonin, encoded by Usher syndrome type I genes, form a ternary complex and interact with membrane phospholipids. *Hum Mol Genet* 19:3557–3565
16. Ramakrishnan NA, Drescher MJ, Barreto RL, Beisel KW, Hatfield JS, Drescher DG (2009) Calcium-dependent binding of HCN1 channel protein to hair cell stereociliary tip-link protein protocadherin 15 CD3. *J Biol Chem* 284:3227–3238
17. Tauris J, Christensen EI, Nykjaer A, Jacobsen C, Petersen CM, Ovesen T (2009) Cubilin and megalin co-localize in the neonatal inner ear. *Audiol Neurotol* 14:267–278
18. Kretschmann E, Raether H (1968) Radiative decay of non-radiative surface plasmons excited by light. *Z Naturforsch Teil A* 23:2135–2136
19. Karlsson R, Roos H, Fägerstam L, Persson B (1994) Kinetic and concentration analysis

- using BIA technology. *Methods Companion Methods Enzymol* 6:99–110
- 20. Stenberg E, Persson B, Roos H, Urbaniczky C (1991) Quantitative determination of surface concentration of protein with surface plasmon resonance using radiolabeled proteins. *J Colloid Interface Sci* 143:513–526
 - 21. Gopinath SCB (2010) Biosensing applications of surface plasmon resonance-based Biacore technology. *Sensor Actuator B* 150: 722–733
 - 22. Johnsson B, Lofas S, Lindquist G (1991) Immobilization of proteins to a carboxymethyl dextran-modified gold surface for biospecific interaction analysis in surface plasmon resonance sensors. *Anal Biochem* 198:268–277
 - 23. BIACORE (1998) BIAsimulation version 3 software handbook. Chapter 4: evaluating kinetic data, 4.1–4.31. Chapter 5: evaluating concentration data, 5.1–5.10
 - 24. Steffner P, Markey F (1997) When the chips are down. *BIA J* 1:11–15
 - 25. Myszka DG, He X, Dembo M, Morton TA, Goldstein B (1998) Extending the range of rate constants available from BIACORE: interpreting mass transport-influenced binding data. *Biophys J* 75:583–594
 - 26. Schuck P, Zhao H (2010) The role of mass transport limitation and surface heterogeneity in the biophysical characterization of macromolecular binding processes by SPR biosensing. *Methods Mol Biol* 627:15–54

Chapter 11

The Single-Molecule Approach to Membrane Protein Stoichiometry

Michael G. Nichols and Richard Hallworth

Abstract

The advent of techniques for imaging solitary fluorescent molecules has made possible many new kinds of biological experiments. Here, we describe the application of single-molecule imaging to the problem of subunit stoichiometry in membrane proteins. A membrane protein of unknown stoichiometry, prestin, is coupled to the fluorescent enhanced green fluorescent protein (eGFP) and synthesized in the human embryonic kidney (HEK) cell line. We prepare adherent membrane fragments containing prestin-eGFP by osmotic lysis. The molecules are then exposed to continuous low-level excitation until their fluorescence reaches background levels. Their fluorescence decreases in discrete equal-amplitude steps, consistent with the photobleaching of single fluorophores. We count the number of steps required to photobleach each molecule. The molecular stoichiometry is then deduced using a binomial model.

Key words Prestin, Single-molecule, Green fluorescent protein, Stoichiometry

1 Introduction

Observation of the fluorescence emitted by single fluorescent molecules, once difficult, is now readily performed in many laboratories. This has been made possible by improvements in detectors, primarily highly sensitive digital cameras (EM-CCD or sCMOS). One technical advance made possible by single-molecule technology is the determination of subunit stoichiometry in membrane proteins. Traditional methods of determining the stoichiometry of oligomerization, such as Western blots, often yield ambiguous results, perhaps because the protein is no longer in its native environment, the plasma membrane. An ingenious approach to this problem was described by Ulbrich & Isacoff in 2007 [1]. They expressed membrane proteins, coupled to the enhanced green fluorescence protein (eGFP), in frog oocytes. They used a high quantum efficiency electron-multiplying charge-coupled device (EM-CCD) camera and total internal reflection (TIRF) imaging to isolate single fluorescent molecules of membrane

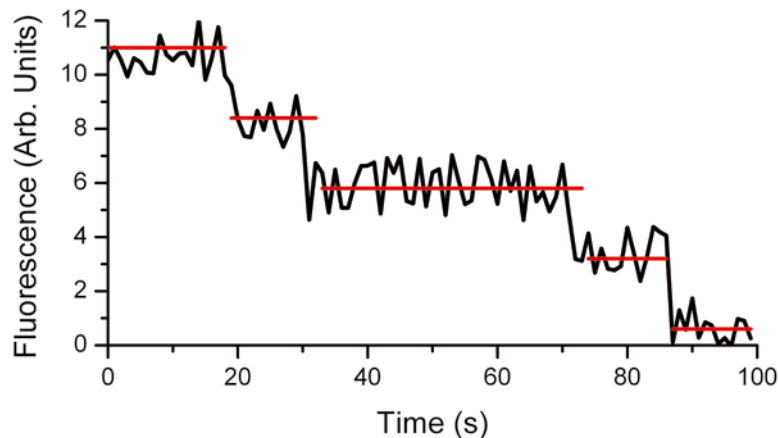


Fig. 1 Illustration of the single-molecule subunit counting method. The figure is a hypothetical plot of the fluorescence intensity of a single tetrameric molecule, as a function of time, with each subunit covalently linked to a fluorophore, under continuous excitation sufficient to cause fluorophore photobleaching of the fluorophores. The fluorescence decreases in approximately equal amplitude steps until background levels are reached. The molecular diagrams indicate the number of active fluorophores (depicted in green) at each stage. The number of steps (in this case four) in theory yields the stoichiometry of the molecule. From [16]

proteins. Under continuous excitation, the fluorescence of regions of interest (ROIs) enclosing putative single molecules were observed to decrease in approximately equal-amplitude steps, consistent with the photobleaching of single fluorophore molecules. By counting the number of steps to photobleach the fluorophores to background, they were able to estimate the stoichiometry of the molecule (Fig. 1). The method has since been applied by many others [2–7].

We have recently applied the method to the stoichiometry of a membrane protein important in mammalian hearing, prestin [8]. The stoichiometry of prestin has been in dispute, with both dimer and tetramer configurations being advanced by Western blot analyses [9, 10], biophysical analysis [11], and an electron-density mapping of purified prestin protein [12]. We studied prestin coupled at its carboxy terminal to eGFP, incorporated in the plasma membrane of a cultured cell line. To immobilize the molecules, we prepared membrane fragments adherent to the culture dish, by osmotic shock and lysis. In this paper, we discuss our implementation of the technique and give practical suggestions for applying the method to other systems (*see Notes 1 and 2*).

2 Materials

2.1 Cell Culture, Transient Transfection, and Cell Imaging Preparation

1. Culture medium: Dulbecco's Modified Eagle Medium (DMEM) with added glucose, glutamine, and pyruvate with 10 % Fetal Bovine Serum (FBS).
2. 0.25 % Trypsin-EDTA.
3. Cell culture flasks: 25 mm² surface area, with a 0.2 µm vent cap (Corning, Inc., Corning, NY).
4. Glass-bottomed dishes. We use 35 mm glass-bottom dishes (MatTek Corp., Ashland, MA). Number 1.5 coverslips are essential for use with high numerical aperture (NA) objectives (*see Subheading 2.4, step 2*).
5. Cells: Human Embryonic Kidney (HEK) cells from ATCC (Manassas, VA).
6. Prestin c-terminal eGFP plasmid was obtained from the Dallos laboratory. Contact Jing Zheng (jzh215@northwestern.edu) for further information.
7. Transient transfection reagents: Lipofectamine 2000 transfection reagent (Invitrogen), DMEM.
8. 15 mL sterile centrifuge tubes.
9. Lysis and imaging hypoosmotic buffer: 4 mM PIPES, 30 mM KCl, pH 6.2, 80 mOsm.
10. Cell lysis requires a 29 G hypodermic needle, blunted, on a 1 mL syringe.

2.2 Imaging and Analysis

1. Microscope: The microscope should be an inverted model with a camera port, preferably 100 % switchable. We use an Olympus IX-70.
2. Objective: A 100× 1.4 numerical aperture UPlanSApo objective from Olympus, and low-fluorescence non-drying immersion oil (Type HF, Cargille Laboratories, Cedar Grove, NJ).
3. Excitation: A 100 W mercury lamp for wide-field UV and blue excitation, its intensity attenuated by neutral density filters (*see Notes 3 and 4*).
4. Total internal reflection (TIRF) imaging may be considered as an alternative (*see Note 5*).
5. Filters: High quality steep cut-off filters from Chroma (Bellows Falls, VT) or Semrock (Rochester, NY) are preferred. Our emission filter for eGFP is an ET535/30 m from Chroma.
6. Detector: An Andor DU-897E back-thinned EMCCD camera with >90 % quantum efficiency in the visible range (Andor Technology, Belfast, Northern Ireland).

7. Image Acquisition: Andor Solis software for image acquisition, which is provided with the camera. To determine the single molecule image size in pixels, *see Note 6*.
8. Analysis: Singlmol, written in Matlab version R20008b with the Image Processing Toolbox (MathWorks, Natick, MA), which is freely available from the authors.

3 Method

3.1 Cell Preparation

1. Grow HEK cells in 5 mL of DMEM plus 10 % FBS in a 25 mm² flask in a CO₂ incubator at 37 °C.
2. For passage at confluence (70–90 %), liberate the cells using 2 mL per flask of 0.25 % trypsin-EDTA for 10 min in the incubator. Quench the enzyme with 3 mL of culture medium, and then spin down the cells at 40 × g for 4 min at 4 °C in a 15 mL tube. Resuspend the cells in 1 mL culture medium. Cell passage should be performed in a laminar flow hood. Start new cells from stocks once the passage number reaches 30.
3. To plate passaged cells for experimentation, incubate glass-bottom dishes containing culture medium for 20 min in the incubator. Add the resuspended cells to the dishes. Adjust the volume of cells so that the dishes reach 70 % confluence after 3 days. Cell plating should be performed in a laminar flow hood.
4. Transfection: Transfect cells with 15 µg of plasmid per dish using Lipofectamine 2000 the day after plating. Follow the manufacturer's instructions for preparation of transfection medium. Transfection should be performed in a laminar flow hood.
5. Cell Lysis (Fig. 2): Remove a dish of cells from the incubator, then remove the culture medium by aspiration and replace it with cold lysis medium. Incubate on ice for 30 min. Remove

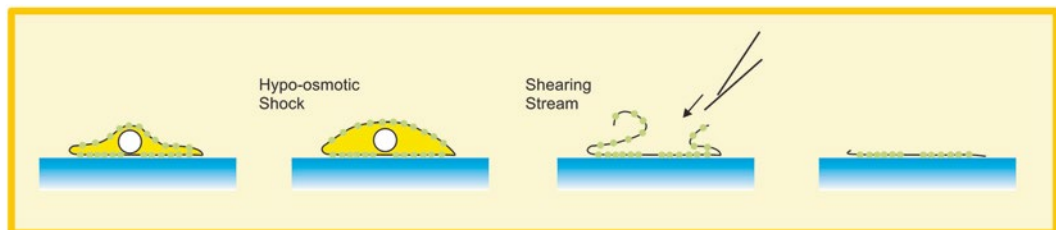


Fig. 2 The osmotic shock and lysis method of preparing membrane fragments. Starting at *left*, the cell containing fluorophore-conjugated molecules in its membrane is exposed to a hypoosmotic solution causing it to swell and its membrane to weaken. The cell is exposed to a stream of buffer, which lyses the cell and removes its contents, leaving behind basolateral membrane fragments containing immobilized fluorescent molecules (*right*)

adherent cells using a stream of cold lysis buffer forced through a 29 G needle. Replace the lysis medium with fresh lysis medium to remove cell fragments. Allow the dish to come to room temperature before imaging in lysis medium, or any medium without pH-sensitive dyes such as Phenol Red.

3.2 Imaging Procedure

1. Experiment in a darkened room to minimize collection of stray light. Cover the microscope with photographic darkroom cloth.
2. Establish the focal plane using the camera image, then translate the specimen in the x - or y -direction a small amount, but greater than one image field, and only then start data acquisition. Similarly, stop down the excitation field so that it is no more than the camera's field of view. The focal plane must be established exactly for maximum fluorophore brightness, but it is equally important to minimize photobleaching during establishment of the focal plane, since exposure to even the attenuated UV excitation that we use results in some photobleaching, which subtracts potentially detectable steps.
3. Acquire images stacks under UV excitation at 5 frames/s until all single molecules are photobleached (usually 500–1000 frames). Use electron-multiplying gains of 100–200 and cool the electronics to -70°C to reduce noise. Save files as 12-bit TIFs.

3.3 Analysis Procedure

1. Import image stacks into MatLab for analysis using the Singlmol script. The user interface of the code is shown in Fig. 3. The program subjects the images to two passes of a 3×3 Gaussian spatial filter to reduce noise before display and analysis. The interface enables background subtraction, thresholding and gain adjustment of the images and permits them to be viewed in sequence. Sequential viewing assists in separating transient high-value points from the persistent fluorescence of single molecules.
2. Perform background subtraction by first selecting an ROI close to but not encompassing the single molecule of interest (click on *BacSelect*). Some background fluorescence is always observed, although inconsistent across the field of view, and it decays approximately exponentially over the imaging period. The program determines and plots the average background fluorescence in the ROI as a function time. Accept the function by clicking on the *Accept* button on the plot. To use background subtraction, click on *BacSubOn*.
3. Click on the *ROI* button to select an ROI containing a putative single molecule for analysis, via a cursor. The program shows an enlarged image of the 5×5 displayed ROI in a separate window for inspection. Adjust the cursor position if the single molecule image is not centered over time (individual images may not appear centered). The average fluorescence in

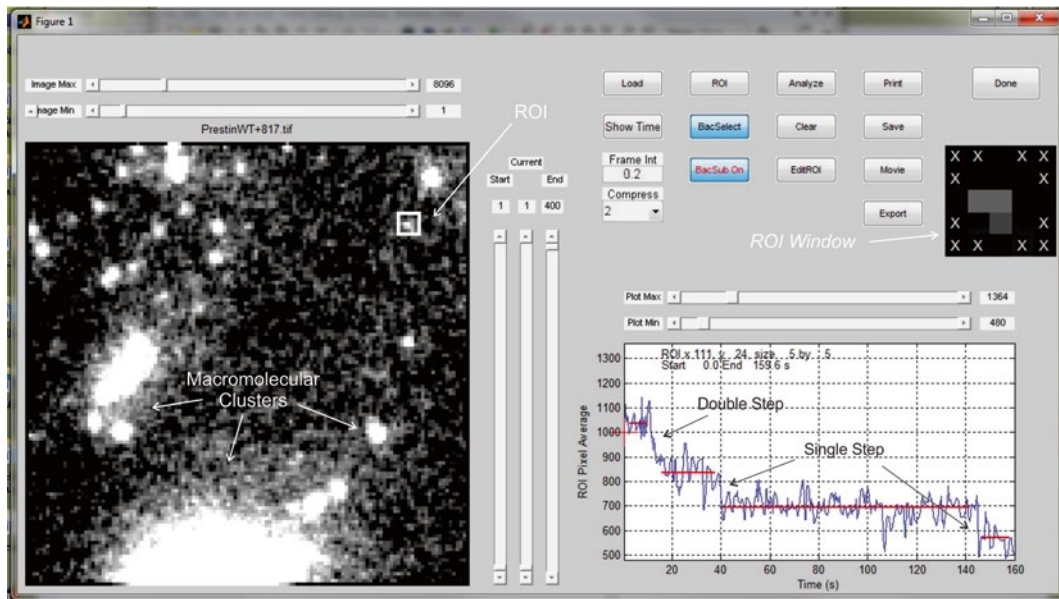


Fig. 3 The user interface of program SinglMol. The *left* window shows a single frame, with sliders controlling display maximum and minimum on *top* and the sequence counter at *right*. The images show typical large clumps of fluorescent molecules (labeled “Macromolecular Clusters”) and some putative single molecules, one of which is indicated by the rectangular region of interest (labeled “ROI”). An enlarged view of the ROI is shown in the window at *right* (labeled “ROI Window”). The time plot below *right* shows the average fluorescence in the ROI over the acquisition period, with the background subtracted. Cursors were used to establish the steps. Labels on the plot indicated apparent single steps and a double step

the ROI as a function of time is then calculated and the background values subtracted. The program then subjects the background-subtracted fluorescence values to a three-point median filter and plots the result in a separate window, with upper and lower plot bounds that can be manipulated for ease of viewing.

4. The corner points of the square ROI are farther from the centroid of the image than the Airy disk radius, and thus contribute little information. In calculating the average ROI fluorescence, the program employs a mask that zeros the corner points of the ROI thereby reducing the noise without sacrificing the fluorescence in the Airy disk image. The mask is:

$$\begin{bmatrix} 0 & 0 & 1 & 0 & 0 \\ 0 & 1 & 1 & 1 & 0 \\ 1 & 1 & 1 & 1 & 1 \\ 0 & 1 & 1 & 1 & 0 \\ 0 & 0 & 1 & 0 & 0 \end{bmatrix}$$

5. Click on the *Analyze* button to measure the step sizes. Use cursors to delineate time ranges corresponding to the beginning and end of fluorescence levels corresponding to two discrete states. The program calculates the average fluorescence in those two states and the difference between them, which is the step size. Repeat the operation until all steps have been measured for that molecule. Store the step sizes in a file by clicking on the *Save* button. To start over, click on the *Clear* button.
6. Import the saved data for that image sequence into Excel. Calculate the average step size for the entire image sequence. Inspect the step sizes for each molecule and manually enter the step count in a separate column. Use the average step size to arbitrate any steps not clearly unitary (see Notes 7 and 8). Sort the step counts into a histogram using the *Histogram* function of Excel. Usually, at least 100 molecules must be studied to obtain a histogram that can be analyzed. An example of the results is shown in Fig. 4

3.4 Fitting the Binomial Distribution

1. Rationale for the Binomial Fit. If a molecule is a tetramer, then the step count ought in theory to be four for every molecule. We observe instead that some molecules exhibit four steps, but more exhibit three, some two, and a few even exhibit a single step. Our model, discussed in greater detail in Note 9, is that some eGFP fluorophores do not fluoresce. Thus, a single molecule composed of randomly selected prestin-eGFP molecules with fluorescing and non-fluorescing eGFPs will have an unknown number of fluorescing eGFPs. The distribution of step counts, representing the number of fluorescing eGFPs, will be described by a binomial distribution, where n repre-

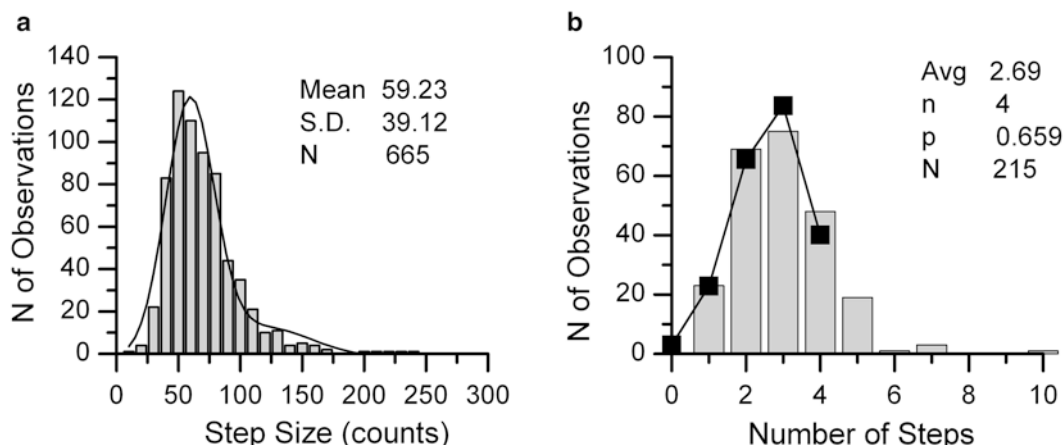


Fig. 4 Representative example of the analysis of single molecules of prestin-eGFP. Histograms of step amplitudes (a) and step counts (b) in a single experiment, for 2315 molecules. The binomial fit parameters are given in the figure. From [16]

sents the molecular stoichiometry and p represents the average fraction of functioning fluorophores in a given experiment (*see also Note 10*).

2. Distinguishing Between Possible Stoichiometries. It is not possible to use a goodness-of-fit comparison between different putative stoichiometries because the number of points fitted, and therefore the number of degrees of freedom, is different in each case. We have therefore used two methods to establish stoichiometry.
 - One is to use a molecule of known stoichiometry for comparison [8]. If the same fluorophore is used, and if the p values are similar, then the stoichiometries are likely to be the same.
 - Another approach is to establish a baseline value of p , p_0 , for the fluorophore using a molecule of known stoichiometry [13]. For molecules of unknown stoichiometry, first calculate the mean of the distribution μ . Then n is calculated as μ/p_0 , rounding to the nearest integer.

4 Notes

1. In principle, this method will work with other fluorescent proteins or organic fluorophores. However, antibody-conjugated fluorophores are inappropriate because multiple fluorophores are attached to each secondary antibody, and an unknown number of secondary antibodies will have bound to the primary antibody. With any fluorophore, the experimenter must balance the need to minimize bleaching with the need for sufficient brightness for single molecules to be detectable.
2. The method can be readily applied to determining hetero-oligomeric stoichiometries in membrane oligomers, by combining labeled and unlabeled component monomers. It can also be applied to cytoplasmic proteins if the proteins can be isolated and immobilized.
3. The excitation should be properly centered at 100 \times and should be as even as possible. This may be assisted by a slight defocus after normal adjustment. Note that mercury bulbs rapidly lose brightness and stability toward the end of their lives. It is wise to start a new series of experiments with a new bulb. Allow 24 h or so of operation to stabilize a new bulb.
4. The excitation intensity at the specimen is severely attenuated by neutral density filters. This is to prolong the time required to bleach the molecules. We use a stack of 25 mm neutral density filters from ThorLabs Inc. (Newton, NJ) mounted in a custom-built holder.

5. Observation of fluorescent proteins in membranes may seem like a natural application of TIRF imaging. Indeed, the reduced excitation levels afforded by TIRF may help to reduce the rate of bleaching. However, the background-rejection advantages of TIRF imaging are less apparent in our isolated membrane fragment preparation, since most of the background-contributing cellular contents have been removed. In addition, TIRF systems suffer from fringing due to internal reflections of polarized light, and the image field is usually unevenly illuminated. In our hands, this contributed to a greater scatter in the estimates of single step size, which led us to return to wide-field illumination.
6. A point source of light, such as a fluorophore, when processed by an imaging device such as a microscope, is observed in the form of a spatial function referred to as an Airy function (Fig. 5). The radius at the first minimum, r_0 , (the Airy disk radius, which encompasses approximately 84 % of the light in the image), is given by

$$r_0 = 0.61\lambda / na$$

where λ is the wavelength of the light and na is the numerical aperture of the microscope objective. For our experiments, using eGFP, the objective na was 1.4 and we assumed $\lambda=520$ nm. This led to a calculated Airy disk diameter of 450 nm. We used a stage micrometer to determine the pixel size of our camera image, and thereby determined that a single molecule would comfortably fit in a 5×5 pixel ROI.

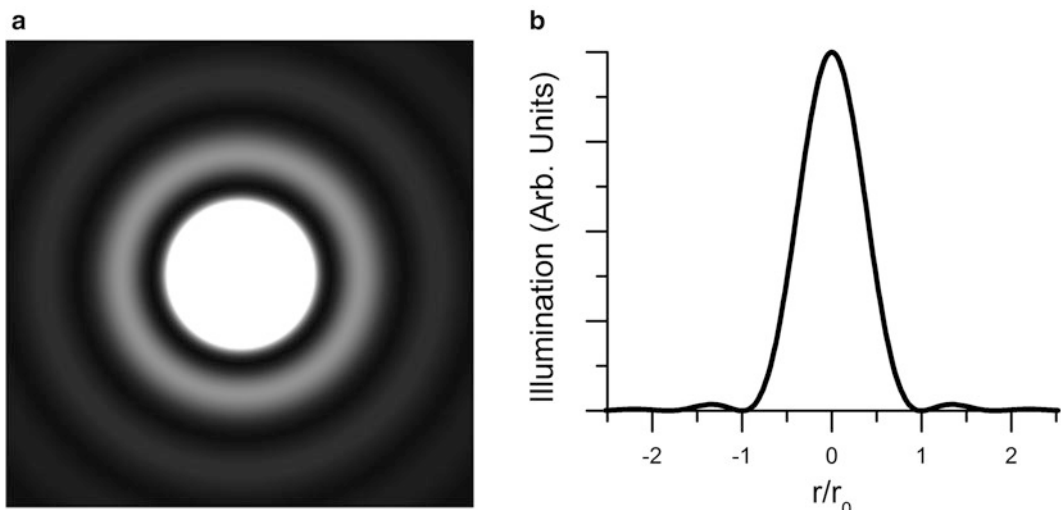


Fig. 5 The image of a point fluorescence source in a microscope. (a) Simulation of the image of a single source, in the form of an Airy disk. (b) Plot of illumination of the Airy disk as a function of normalized radial distance from the centroid, normalized to r_0 . From [16]

7. There is an upper limit to the stoichiometries that this method can assess because the shot noise (noise associated with the random arrival of photons) increases as the square root of the number of subunits, while the step size remains constant. In our hands this limit is seven.
8. We have experimented with several methods of automating the determination of step counts, including Hidden Markov Modeling [14] and the Chung–Kennedy algorithm [15]. However, each method requires some empirical determination of parameters. In-side-by-side comparisons, we found no difference in the results.
9. As we and others have reported [1, 8], the number of steps is variable from molecule to molecule, and the mean step count is non-integer. One explanation is that a fraction of fluorescent proteins fold correctly but do not fluoresce. Thus the experiment resembles a binomial sampling procedure, in which a small sample of n items is removed without replacement from a larger population, some of which are defective. If the probability that the individual item is defective is q , the probability that it is not defective is p , which is $1 - q$. Our observations can then be understood if q is the probability that the fluorophore is defective. The distribution of step counts for N observations of single molecules is then given by:

$$A(x) = N \frac{n!}{x!(n-x)!} p^x (1-p)^{n-x}, \quad x = 0, 1, 2, \dots, n$$

where $A(x)$ is the number of single molecules that bleached in x steps (and x is an integer), N is the number of single molecules observed, n is the presumed stoichiometry (also integer), and p is the fraction of fluorophores that are functional ($0 < p < 1$). The mean of the binomial sampling distribution μ is equal to np .

10. As is clear from Fig. 4, with prestin we occasionally observed step counts greater than four. We assume that these ROIs contained two or more prestin molecules.

Acknowledgments

This work was supported by the State of Nebraska LB 692 administered by Creighton University and N.S.F.-Nebraska E.P.S.Co.R. EPS-0701892 to RH, and National Institutes of Health GM085776 to MGN and RH. Research was conducted in a facility constructed with support from Research Facilities Improvement Program C06 RRI17417-01 from the late, lamented N.C.R.R. of N.I.H. We thank Max Ulrich and Ehud Isacoff for

initial encouragement and advice, Peter Dallos for the prestin-eGFP plasmid constructs, and David Z.Z. He, Heather Jensen-Smith and John Billheimer for comments on the manuscript. We also thank Fang Xiang & Chris Wichman for statistical advice.

References

- Ulbrich MH, Isacoff EY (2007) Subunit counting in membrane-bound proteins. *Nat Methods* 4:319–321
- Bartoi T, Augustinowski K, Polleichtner G et al (2014) Acid-sensing ion channel (ASIC) 1a/2a heteromers have a flexible 2:1/1:2 stoichiometry. *Proc Natl Acad Sci U S A* 111:8281–8286
- Das SK, Darshi M, Cheley S et al (2007) Membrane protein stoichiometry determined from the step-wise photobleaching of dye-labelled subunits. *ChemBioChem* 8:994–999
- Durisic N, Godin AG, Wever CM et al (2012) Stoichiometry of the human glycine receptor revealed by direct subunit counting. *J Neurosci* 32:12915–12920
- Hastie P, Ulbrich MH, Wang HL et al (2013) AMPA receptor/TARP stoichiometry visualized by single-molecule subunit counting. *Proc Natl Acad Sci U S A* 110:5163–5168
- Ji W, Xu P, Li Z et al (2008) Functional stoichiometry of the unitary calcium-release-activated calcium channel. *Proc Natl Acad Sci U S A* 105:13668–13673
- Lioudyno MI, Kozak JA, Penna A et al (2008) Orai1 and STIM1 move to the immunological synapse and are up-regulated during T cell activation. *Proc Natl Acad Sci U S A* 105:2011–2016
- Hallworth R, Nichols MG (2012) Prestin in HEK cells is an obligate tetramer. *J Neurophysiol* 107:5–11
- Detro-Dassen S, Schanzler M, Lauks H et al (2008) Conserved dimeric subunit stoichiometry of SLC26 multifunctional anion exchangers. *J Biol Chem* 283:4177–4188
- Zheng J, Du GG, Anderson CT et al (2006) Analysis of the oligomeric structure of the motor protein prestin. *J Biol Chem* 281:19916–19924
- Wang X, Yang S, Jia S et al (2010) Prestin forms oligomer with four mechanically independent subunits. *Brain Res* 1333:28–35
- Mio K, Kubo Y, Ogura T et al (2008) The motor protein prestin is a bullet-shaped molecule with inner cavities. *J Biol Chem* 283:1137–1145
- Hallworth R, Stark K, Zholudeva L et al (2013) The conserved tetrameric subunit stoichiometry of Slc26 proteins. *Microsc Microanal* 19:799–807
- McKinney SA, Joo C, Ha T (2006) Analysis of single-molecule FRET trajectories using hidden Markov modeling. *Biophys J* 91: 1941–1951
- Chung SH, Kennedy RA (1991) Forward-backward non-linear filtering technique for extracting small biological signals from noise. *J Neurosci Methods* 40:71–86
- Hallworth R, Nichols MG (2012) The single molecule imaging approach to membrane protein stoichiometry. *Microsc Microanal* 18:771–780

Part III

Imaging Protocols

Chapter 12

Visualization of Live Cochlear Stereocilia at a Nanoscale Resolution Using Hopping Probe Ion Conductance Microscopy

A. Catalina Vélez-Ortega and Gregory I. Frolenkov

Abstract

The mechanosensory apparatus that detects sound-induced vibrations in the cochlea is located on the apex of the auditory sensory hair cells and it is made up of actin-filled projections, called stereocilia. In young rodents, stereocilia bundles of auditory hair cells consist of 3–4 rows of stereocilia of decreasing height and varying thickness. Morphological studies of the auditory stereocilia bundles in live hair cells have been challenging because the diameter of each stereocilium is near or below the resolution limit of optical microscopy. In theory, scanning probe microscopy techniques, such as atomic force microscopy, could visualize the surface of a living cell at a nanoscale resolution. However, their implementations for hair cell imaging have been largely unsuccessful because the probe usually damages the bundle and disrupts the bundle cohesiveness during imaging. We overcome these limitations by using hopping probe ion conductance microscopy (HPICM), a non-contact scanning probe technique that is ideally suited for the imaging of live cells with a complex topography. Organ of Corti explants are placed in a physiological solution and then a glass nanopipette—which is connected to a 3D-positioning piezoelectric system and to a patch clamp amplifier—is used to scan the surface of the live hair cells at nanometer resolution without ever touching the cell surface.

Here, we provide a detailed protocol for the imaging of mouse or rat stereocilia bundles in live auditory hair cells using HPICM. We provide information about the fabrication of the nanopipettes, the calibration of the HPICM setup, the parameters we have optimized for the imaging of live stereocilia bundles and, lastly, a few basic image post-processing manipulations.

Key words Scanning ion conductance microscopy, Organ of Corti, Hair cell, Stereocilia, Live cell imaging, Nanopipette

1 Introduction

The sensory hair cells of the inner ear have mechanosensitive actin-filled projections, termed stereocilia, on their apical surface [1, 2]. In the mammalian auditory inner and outer hair cells, stereocilia are arranged in bundles composed of three rows of decreasing height. In the inner hair cells, stereocilia also vary in diameter between the rows [1]. The tallest (first) and second row stereocilia

are \sim 300–500 nm in diameter in live, unfixed, and non-dehydrated mouse or rat inner hair cells. Therefore, individual stereocilia in these rows are visualized easily with optical microscopy. However, the shorter rows of inner hair cell stereocilia and all rows of outer hair cell stereocilia have diameters of \sim 100–200 nm, which is below the resolution of optical microscopy. In bright field imaging, the resolution is proportional to $\sim\lambda/NA$, where λ is the wavelength of the light source and NA is the numerical aperture of the objective lens. In the best possible scenario, the resolution cannot be better than \sim 200 nm for bright field imaging. It can be somewhat improved in fluorescent microscopy, using confocal [3] or super-resolution [4] techniques. However, most of these techniques face substantial challenges and significant resolution degradation when imaging live cells, especially in thick tissue [4, 5]. As of today, the best-known example of optical imaging of live functional auditory stereocilia is the imaging of Ca^{2+} entry into individual stereocilia through mechanotransduction channels [6, 7]. Obviously, the optical techniques do resolve some individual stereocilia in the auditory hair cells, but they are still far from imaging any fine details of the stereocilia bundle structure, such as the links between stereocilia.

Images of the complex architecture of stereocilia bundles at the resolution of single nanometers can be obtained using scanning or transmission electron microscopy (SEM or TEM, correspondingly) [8–10]. However, the samples for electron microscopy are “dead,” since they typically undergo chemical fixation and dehydration processes. Even freeze-substitution and cryo-electron microscopy techniques [11, 12], which can bypass chemical fixation, still result in static preparations that cannot be used to study any dynamic changes in the ultrastructure of the hair cell bundle. Therefore, our knowledge of such potential dynamic changes in the morphology of hair cell stereocilia bundles is largely limited.

In theory, high-resolution imaging of live cells in physiological conditions can be obtained with scanning probe microscopy techniques such as atomic force microscopy (AFM) [13, 14]. However, the AFM probe, a cantilever with a sharp tip, often makes physical contact with the scanned sample. Since hair cell stereocilia are tall structures that protrude from a relatively flat surface, the AFM cantilever tends to crash against them [15, 16] and typically disrupts the bundle cohesiveness, causing irreparable damage to the hair cell. In contrast to AFM, scanning ion conductance microscopy (SICM) is a non-contact scanning probe technique that uses a glass pipette with a nanometer-scale tip [17–19]. An ionic current (I_p) flows through this nano-pipette into the bath solution that contains live cells or tissue in a near-physiological environment (Fig. 1a, left). When the tip of the nano-pipette approaches the surface of the sample, I_p decreases. A feedback system monitors the changes of the I_p and moves the pipette up or down to keep I_p at a

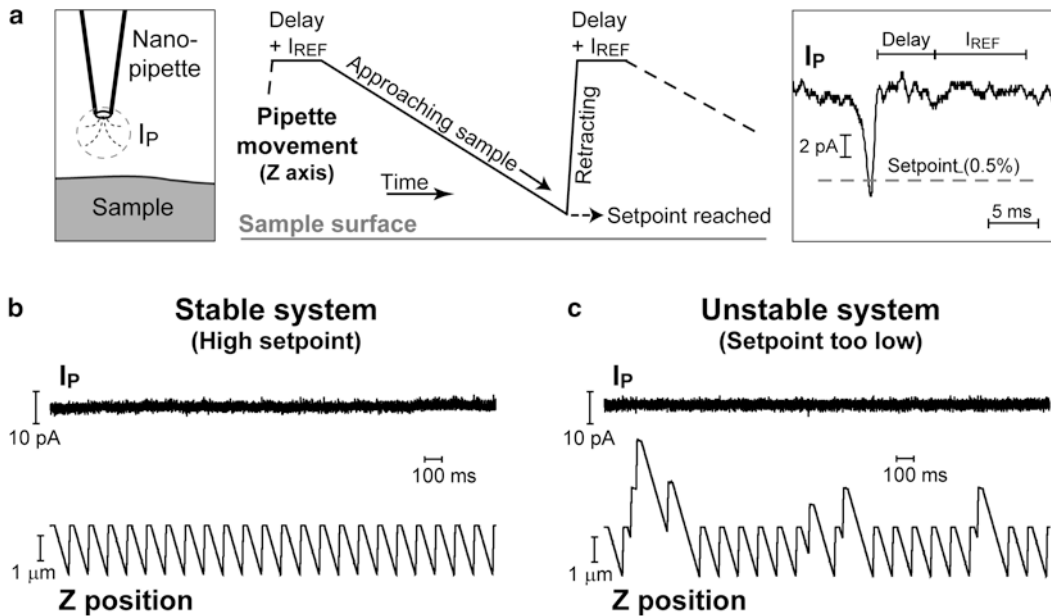


Fig. 1 HIPCM approach curve and setpoint stability. **(a)** *Left*, in hopping probe ion conductance microscopy (HIPCM), the ionic current flowing through a nanopipette (I_P) is monitored while the pipette “hops” above the sample surface. *Middle*, hopping probe approach curve steps over time. *Right*, representative decrease in I_P , when the nanopipette is in close proximity to the sample. *Middle* and *right*, while the pipette is in a resting position away from the sample surface, a reference baseline recording is established of the ionic current (I_{REF}). Next, the pipette is moved down toward the sample surface at a constant speed (Fall Rate). The approach is stopped when I_P decreases below a predefined threshold or “setpoint” (typically 0.3–0.6 %), indicating that the pipette tip has reached the vicinity of the sample surface. The Z position of the pipette at this point is recorded as an imaging pixel. Then, the pipette is quickly retracted away from the sample (at a speed set by the “hop rise rate”) and a new I_{REF} is recorded (after a short delay, to avoid artifacts in I_P induced by the fast movement of the pipette). Finally, a new downward approach is initiated, after the pipette is moved to a new X–Y position (not shown). **(b, c)** Representative recordings of I_P (*top*) and the pipette Z position (*bottom*), when the pipette is in the bath solution away from the sample surface. **(b)** Recordings obtained with a setpoint value of 1.0 %, showing a stable approach curve. The user should find the lowest setpoint value that maintains the stability of the approach. **(c)** Recordings obtained with a setpoint value of 0.45 %, showing an unstable approach curve. If the setpoint value is too low, minor fluctuations in I_P will lead to false-positive “detections” by the HIPCM system and result in noisy images

certain “setpoint” level, thereby maintaining a constant probe-to-sample distance, while the surface is scanned in X–Y directions. To prevent the pipette from hitting the hair cell stereocilia bundles, we developed a modified SICM technique, which is known as hopping probe ion conductance microscopy (HIPCM) [20]. In each step of HIPCM, the “reference” current through the pipette (I_{REF}) is measured while the pipette is far from the sample. Then, the scanning pipette approaches the sample until I_P decreases from I_{REF} to a predefined threshold or “setpoint” (Fig. 1a). This position is recorded as the sample height at this point. Then, the pipette is retracted from the sample before moving to a new X–Y position

and repeating the approach. Using this technique, it was possible to obtain topographic images of mouse inner and outer hair cell stereocilia bundles, and to even resolve the small links (~5 nm in diameter) that connect stereocilia [20].

Here, we describe the steps to perform the successful imaging of live inner hair cell stereocilia bundles in early-postnatal mouse or rat cochlea explants. We describe in detail (1) the fabrication of the nanopipettes, (2) the calibration of the HPICM set up, (3) the preparation of the cochlear explant cultures, (4) the parameters of HPICM imaging that allow resolving stereocilia bundles, and (5) the most common imaging post-processing manipulations.

2 Materials

2.1 SICM Imaging Setup

We have successfully imaged stereocilia bundles in live auditory hair cells using a custom-built SICM setup with the controller and the software from Ionscope Ltd. (United Kingdom). The other SICM systems commercially available are the Park NX-Bio and Park XE-Bio setups (Park Systems, Korea) (*see Note 1*). Users can decide to try any of these commercially available SICM setups but, to date, the successful HPICM imaging of auditory stereocilia bundles has been performed only using Ionscope software and custom-built setups [20]. In addition, keep in mind that some hardware components mentioned below may or may not be integrated in the commercial SICM systems. Finally, it might be needed also to modify the software code that controls the movements of the SICM probe.

1. SICM setup, e.g., ICnano-S2 (Ionscope Ltd.).
2. Inverted research optical microscope, e.g., Eclipse Ti-U (Nikon, Japan) or IX73 (Olympus, Japan).
3. Vibration isolation system, e.g., 63–500 series lab table (Technical Manufacturing Corporation, Peabody, MA) or BM-1 bench top platform (Minus K Technology, Inc., Inglewood, CA).
4. Low-noise patch clamp amplifier, e.g., Axopatch 200B (Molecular Devices, Sunnyvale, CA) or EPC 800 USB (HEKA Elektronik, Germany).
5. Multi-channel low-noise high-resolution digitizer, e.g., Digidata 1322A (Molecular Devices) or BNC-2090A (National Instruments Corporation, Austin, TX).
6. AFM calibration standards, e.g., HS-20MG and HS-100MG (Ted Pella, Inc., Redding, CA).
7. Non-conductive transparent and thin double-sided tape, e.g., Scotch 666 (Electron Microscopy Sciences, Hatfield, PA).

2.2 SICM Software

We optimized the hopping probe parameters for the imaging of stereocilia bundles in live auditory hair cells using the HPICM Control software (Imperial College London, United Kingdom). If different software is used, users may need to adjust the approach curve parameters described in Fig. 1.

1. SICM software with hopping probe capability, e.g., ICnano2000 Software (Ionscope Ltd.) or HPICM Control (Imperial College London) (*see Note 1*).
2. Software for signal monitoring and recording, e.g., ICnano2000 Controller (Ionscope, Ltd.), WinWCP software (University of Strathclyde, United Kingdom), or pClamp (Molecular Devices, LLC.).
3. Software for image post-processing, e.g., ScanIC Image or ICnano2000 (Ionscope Ltd.), or HPICM Control (Imperial College London) (*see Note 2*).

2.3 Glass Nanopipettes

1. Borosilicate glass capillaries with an inner filament (World Precision Instruments, Inc., Sarasota, FL) (*see Notes 3 and 4*). We typically use fire-polished capillaries that are 100 mm in length with outer/inner diameters of 1/0.58 mm.
2. Micropipette puller model P-1000 or P-2000 (Sutter Instrument, Novato, CA).
3. Disposable 1 mL syringes.
4. Patch pipette microloaders (World Precision Instruments, Inc.).
5. Ca²⁺-containing Hank's balanced salt solution (HBSS).
6. Small observation microscope equipped with a 10× objective lens, e.g., LCD Digital Microscope Model 44340 (Celestron, LLC., Torrance, CA) (*see Note 5*).

2.4 Dissecting and Culturing Organ of Corti Explants

1. Early postnatal mouse or rat pups. To establish organotypic cultures, we typically dissect the organs of Corti from animals not older than postnatal day 4 (P4).
2. Stereo microscope for tissue dissection equipped with a light source and fiber optic light guides.
3. Dissecting tools: Dumont tweezers #5.
4. Standard 60 × 15 mm polystyrene tissue culture dishes.
5. Leibovitz's L-15 medium without phenol red.
6. Disposable borosilicate glass 14.6 cm Pasteur pipettes (Fisher Scientific).
7. Uncoated 35 mm glass-bottom dishes.
8. Dulbecco's Modified Eagle Medium (DMEM) with high glucose (4500 mg/L), 25 mM 4-(2-hydroxyethyl)-1-piperazineethanesulfonic acid (HEPES) buffer, 4 mM l-glutamine and phenol red.

9. Ampicillin.
10. Heat-inactivated fetal bovine serum (FBS).
11. Parafilm.
12. Temperature- and CO₂-controlled incubator for cell culture.

3 Methods

The following protocol assumes the user's general experience with patch clamp techniques and the relevant equipment. Users who have no experience in patch clamping are advised to learn the principles of operation of a patch clamp amplifier [21] and the basic techniques of pipette manufacturing (e.g., download the Pipette Cookbook from Sutter Instrument at http://www.sutter.com/PDFs/pipette_cookbook.pdf).

3.1 Pulling and Filling Glass Nanopipettes

1. Place a capillary glass in the micropipette puller (*see Note 6*) and run a "Ramp test" following the puller's *operation manual* to find a safe heat value for the glass. This step is only required the first time the micropipette puller is used for a specific capillary glass.
2. Create a program in the micropipette puller using the parameters given in Table 1. These programs have been designed to create pipettes with a resistance of 200–400 MΩ and estimated inner tip diameters of 50–70 nm (*see Notes 7 and 8*).
3. Place a new capillary glass in the micropipette puller bar grooves and center its position to obtain two nanopipettes of ~50 mm length. To fabricate shorter nanopipettes *see Note 9*.
4. Run the program previously created in the micropipette puller.

Table 1
Pipette puller settings to obtain ~200–400 MΩ borosilicate nanopipettes

Sutter P-1000 puller					
	Heat	Pull	Velocity	Time	Pressure
Line 1	Ramp + 7	0	33	200	500
Line 2	Ramp + 7	250	50	200	
Sutter P-2000 puller					
	Heat	Filament	Velocity	Delay	Pull
Line 1	Ramp	4	40	170	10
Line 2	Ramp + 20	2	16	155	250

5. Use a disposable syringe connected to a flexible filament needle to backfill the freshly pulled nanopipette using Ca^{2+} -containing HBSS (*see Note 10*). Make sure not to overfill the pipette (*see Note 11*).
6. Use a small LCD digital microscope to ensure no bubbles are present in the HBSS-filled nanopipette.

3.2 Checking Pipette Resistance and Signal Noise

The successful imaging of live auditory stereocilia bundles using HPICM relies on the use of pipettes with small tip diameters (~50 nm) and, importantly, low noise ($\leq 5 \text{ pA}$). Therefore, each time a new nanopipette is used, it is necessary to check whether it meets the acceptable diameter and noise criteria.

1. Mount a freshly pulled HBSS-filled nanopipette into the SICM head (*see Note 12*).
2. Place the ground electrode in the bath solution where the sample is located (i.e. into the dish where either a calibration sample or organ of Corti explant is present, as described below in Subheadings [3.3](#) and [3.5](#)).
3. Zero the voltage applied to the pipette by the patch clamp amplifier.
4. Immerse the pipette tip into the bath solution.
5. Adjust the pipette offset to minimize the ion current flowing through the pipette to zero.
6. Apply +100 mV to the pipette and measure the ion current. The value of the current allows calculating the pipette resistance and estimating the tip diameter (*see Notes 13 and 14*).
7. Increase the voltage applied to the pipette until the current reaches a value of 1–2 nA (*see Note 15*).
8. Start with a high setpoint value (e.g., 1–5 %) to obtain a stable hopping-probe approach behavior (Fig. [1b](#)).
9. Slowly decrease the setpoint to the lowest value that maintains the stability of the hopping-probe approach (the “optimal setpoint”). The system is unstable if the pipette position sensor demonstrates a “jumping” behavior (Fig. [1c](#)). In this case, the setpoint is too low and it needs to be increased slightly. From our experience, smaller setpoints produce hair bundle images of better quality. Typically, we use setpoint values lower than 0.6 % to successfully image live hair cell bundles.
10. If the optimal setpoint value is slightly higher than desired, the user can modify one or more of the following parameters from the HPICM approach curve (*see Fig. 1a* for details) to obtain a more stable system. For these parameters, we provide a range of values in Table [2](#) that we typically use during the HPICM imaging of live hair cell bundles and calibration samples.

Table 2

Reference HPICM parameters for the imaging of calibration samples and live hair cell stereocilia bundles^a

~20 or 100 nm calibration samples					
Resolution	Scan size (μm)^b	Lateral resolution (nm)	Hop amplitude (μm)	Fall rate (nm/ms)	Min. Scan hop (nm)^c
Low	≥20×20	~300–400	~0.5–1	~90–110	100–200
High		~100–200	~0.1–0.5		50–100
Live organ of Corti explant					
Resolution	Scan size (μm)^b	Lateral resolution (nm)	Hop amplitude (μm)	Fall rate (nm/ms)	Min. Scan hop (nm)^c
Low	≥20×20	~300–400	~6–8	~60–100	500–1000
Live rat inner hair cell stereocilia bundle^d					
Resolution	Scan size (μm)	Lateral resolution (nm)	Hop amplitude (μm)	Fall rate (nm/ms)	Min. Scan hop (nm)^c
Low	~8×8	~150–200	~4–5	~60–100	500–1000
High		~50–100	~3–4		300–800

^aFor all of these samples, the following parameters can be used: Delay of 1–5 ms; I_{REF} measurement for 3–10 ms; I_p filters ≥5 kHz; and Hop Rise Rate of 700–1000 nm/ms

^bThe full X and Y range of the SICM setup can be used

^cThese values are needed when using the “adaptive” HPICM compression algorithm [20]

^dHPICM imaging parameters for mouse and rat inner hair cell stereocilia bundles are very similar. After locating a mouse inner hair cell stereocilia bundle, the scan size area to be used can be smaller (~6×6 μm) and the hop amplitude can be reduced by ~1–2 μm, while the other parameters remain the same

- Decrease the speed of approach (i.e. fall rate).
 - Decrease the retraction speed (i.e. hop rise rate).
 - Decrease the cutoff value of the current filters (*see Note 16*).
 - Increase the length of the reference ion current measurement (i.e. I_{REF}).
 - Increase the delay before the reference ion current is measured.
11. If the lowest setpoint value remains high, replace the nanopipette for a new one and repeat all previous steps.
 12. When a stable low setpoint value is achieved (i.e. <0.6 %), approach the sample with the nanopipette as described in Subheadings 3.3 and 3.5.

3.3 HPICM Calibration

Before attempting to image live hair cells, it is recommended to use pre-fabricated calibration standards with features of known shapes and sizes to test the X – Y – Z resolution of the HPICM

setup. We recommend starting with the HS-100MG calibration standard for AFM, which represents a silicon chip with pillars and holes of different shapes (i.e. circles, squares, and lines). Each of these features has a height of 100 nm. Once this 100 nm calibration standard is successfully imaged, we suggest moving to the HS-20MG calibration chip to guarantee the *Z* resolution of the system is below 20 nm. These 5 × 5 mm calibration chips come glued to a 12 mm metal disk that needs to be fixed to the bottom of a dish before imaging.

1. Cut a ~13 × 13 mm piece of double-sided tape and place it to the bottom of a glass-bottom dish.
2. Place the calibration standard disk on the tape and make sure it is firmly secured to the bottom of the dish (*see Note 17*).
3. Add Ca²⁺-containing HBSS to the dish (~2 mL) and make sure the calibration chip is covered with the solution.
4. Place the dish in the SICM chamber (*see Note 18*).
5. Set the HPICM approach curve parameters as described in Table 2.
6. Follow the steps described in Subheading 3.2 to check the pipette resistance, set the ion current, test the signal noise and, if necessary, adjust the HPICM parameters.
7. Set the scan size to the full *X*–*Y* range of the system.
8. Use the coarse *X*–*Y* movement to center the pipette position over the calibration chip.
9. Approach the sample with the nanopipette at a slow speed (e.g., 5–25 μm/s).
10. Once the nanopipette is “in control” (i.e. in the vicinity of the sample), start HPICM imaging at low resolution (*see Table 2*).
11. If it is necessary to move to a new *X*–*Y* location (i.e. a different field of view), it is recommended to temporarily retract the pipette by at least 50 μm before the coarse *X*–*Y* movement. Once in the new position, it will be necessary to repeat steps 9 and 10 (i.e. approach to the sample and low-resolution scan).
12. When the calibration chip is successfully visualized at low resolution, choose a region of interest within the field of view and start a high-resolution scan (*see Table 2, Note 19* and Fig. 2).

3.4 Culturing Organ of Corti Explants

1. Dissect cochlear epithelia from early postnatal mouse or rat pups (<P5), removing the organ of Corti from the modiolus and the stria vascularis, but leaving the tectorial membrane attached (*see Note 20*).
2. Using a disposable glass Pasteur pipette, transfer the dissected organ of Corti to a clean glass-bottom dish.

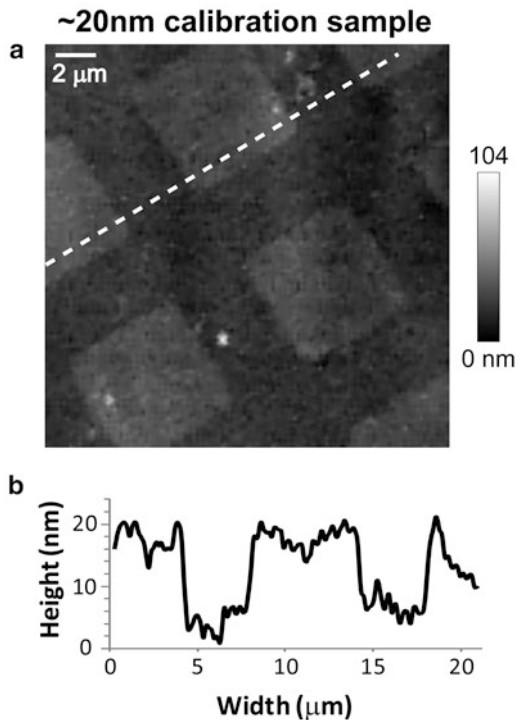


Fig. 2 Determining the resolution of the HPICM system. (a) Representative HPICM image (with a lateral step size of 221 nm) of the HS-20MG calibration chip, from an area filled with squared pillars. (b) Z-axis topography of the sample along the *dashed line* in A. Note that the heights of the pillars are approximately 20 nm

3. Add ~400 μ L of culture medium (i.e. DMEM supplemented with 7 % FBS and 10 μ g/mL ampicillin) to the glass-bottom dish.
4. Using a pipette tip, spread the culture medium around the glass bottom making sure it makes contact with the plastic edges surrounding the glass.
5. Remove ~200 μ L of the culture medium to guarantee that the surface tension of the liquid keeps the tissue explants pressed against the glass bottom (*see Note 21*).
6. Carefully seal the dishes with a small piece ~1 \times 2.5 cm of Parafilm.
7. Place the dishes in a cell culture incubator set at 37 °C and 5 % CO₂.
8. After ~10–14 h incubation, the organ of Corti explants should attach directly to the glass bottom. Carefully remove the Parafilm and add ~1–2 mL of culture medium to each dish and place the dishes back in the incubator (*see Notes 22 and 23*).

3.5 HPICM Imaging of Live Hair Cells

1. Take a dish from the incubator and remove the culture medium.
2. Carefully rinse the organ of Corti explant with L-15 medium at room temperature.
3. Add ~2–3 mL of fresh L-15 medium to the dish.
4. Remove the tectorial membrane with fine tweezers.
5. Repeat steps 2 and 3.
6. Place the dish in the SICM chamber (*see Note 18*).
7. Set the HPICM approach curve parameters as described in Table 2.
8. Follow the steps described in Subheading 3.2 to check the pipette resistance, adjust the current parameters and test the signal noise.
9. Set the scan size to the full $X - Y$ range of the system.
10. Use the coarse $X - Y$ movement to position the pipette over the hair cell rows on the organ of Corti explant.
11. Approach the sample with the nanopipette at a slow speed (e.g., 5–10 $\mu\text{m}/\text{s}$).
12. Once the nanopipette is “in control” (i.e. in the vicinity of the explant), start the HPICM imaging at low resolution (*see Table 2*).
13. If it is necessary to move to a new $X - Y$ location, retract the pipette by at least 200 μm before using the coarse $X - Y$ movement to avoid hitting the tissue with the pipette. In the new position, repeat steps 9 and 10.
14. When the hair cell rows are successfully visualized, choose a region of interest (i.e. a hair cell bundle) within the field of view, and repeat the scan (*see Table 2, Note 19 and Fig. 3a*).
15. If the stereocilia within the hair cell bundle appear abnormally thin (Fig. 3b), it is necessary to decrease the setpoint value. Keep in mind that a few noise pixels on the HPICM image are corrected easily as described in Subheading 3.6.
16. If the thicknesses of the hair cell stereocilia appear normal, start a high-resolution HPICM imaging scan (*see Table 2*).

3.6 HPICM Image Processing

3.6.1 Noise Filtering

Small fluctuations in I_p can sometimes stop the nanopipette approach far from the sample surface and lead to isolated bright pixels in the image (Fig. 4a). These imaging artifacts are particularly common when working with low setpoint values.

- Open an image in the HPICM Control software.
- Select the *Image Processing* tab.
- Check the *Noise Reduction* box.
- Set the threshold filter (in μm) for the pixels that need to be removed.

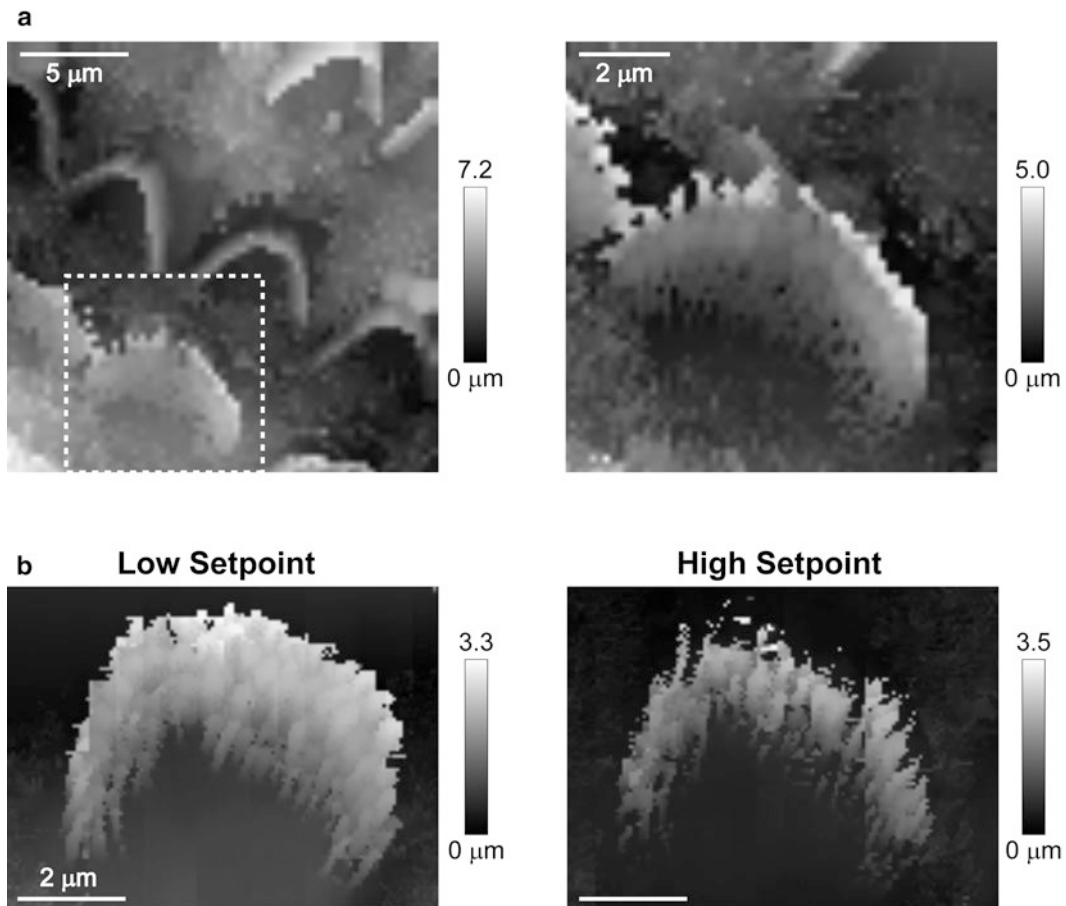


Fig. 3 Selecting an area of interest and adjusting the setpoint. (a) Low-resolution HPICM images of a live rat organ of Corti (*left*) and a stereocilia bundle of an inner hair cell (*right*) within the region highlighted on the left panel. The lateral resolutions of the images are 313 nm (*left*) and 148 nm (*right*). (b) HPICM images of the same inner hair cell bundle obtained with a low setpoint (*left*) or with a setpoint that was too high (*right*). The lateral resolution of the images is 62.3 nm

3.6.2 Line Alignment

Depending on the complexity of the sample to be imaged (i.e. the “hop” amplitude and the speed of approach) and the desired image resolution (i.e. the total imaging points), HPICM images of live hair cell bundles can take a considerable amount of time (e.g., ~16 min for an $8 \times 8 \mu\text{m}$ image with a lateral resolution of 62.5 nm). Therefore, any drifts in the tissue or the HPICM setup could cause visible image artifacts. Any sources of drift in the X and Y axes need to be corrected or minimized, since they typically lead to imaging artifacts that cannot be corrected (*see Note 24*). However, small thermal drifts in the Z -axis of the system result in misaligned lines of the image that are fixed easily (Fig. 4b):

1. Open an image in the ScanIC Image software (*see Note 25*).
2. Select the *Correct Slope* tab.

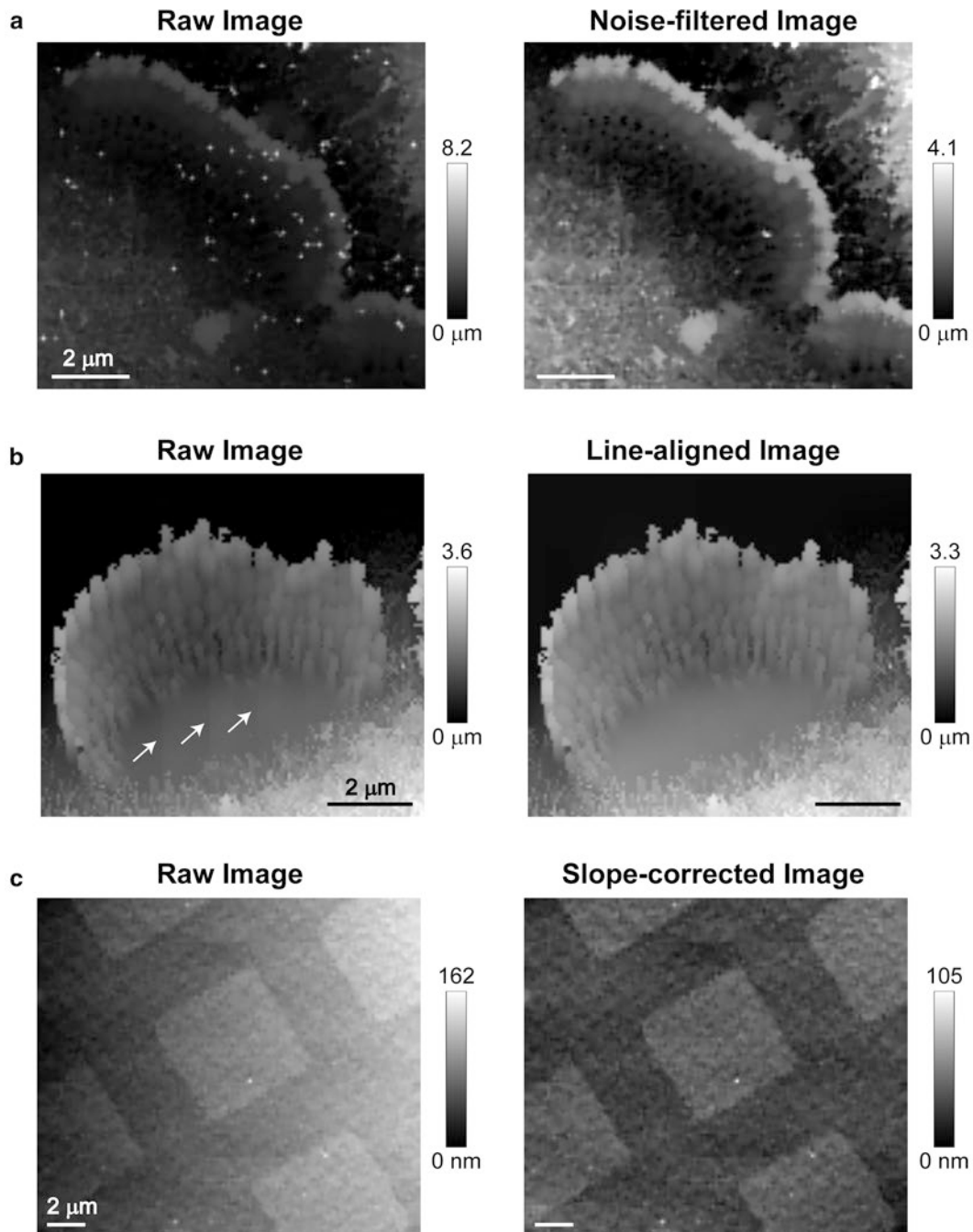


Fig. 4 Imaging post-processing. (a) Raw (left) and noise-filtered (right) HPICM images (lateral resolution of 110 nm) of a stereocilia bundle in a live rat inner hair cell. The noise was filtered using the *Noise Reduction* feature of the HPICM Control software to exclude pixel values higher than 6 μm . (b) Raw (left) and line-aligned (right) HPICM images (lateral resolution of 70 nm) of another stereocilia bundle of a live rat inner hair cell. The lines were aligned using the *ButtonDestripeLineFit* feature of the ScanIC Image software. The arrows highlight some of the lines that are not perfectly aligned due to potential thermal drifts along the Z-axis. (c) Raw (left) and slope-corrected (right) HPICM images of the HS-20MG calibration chip. The *Correct Slope* feature of the ScanIC Image software was used. The images have a lateral resolution of 221 nm and were both line-aligned as described in (b)

3. Choose the width of the lines that need to be aligned and press the *ButtonDestripeLineFit* button for an automated alignment.

3.6.3 Slope Correction

When HPICM images are shown in 2D representations, they exhibit a better contrast if the overall slope of the sample is minimized. Given that the HPICM images are composed of a matrix of points with information in all three dimensions, the slope correction simply changes the “angle of view” (Fig. 4c).

1. Open an image in the ScanIC Image software (*see Note 26*).
2. Select the *Correct Slope* tab.
3. Press the *Correct Slope* button for an automated correction.

4 Notes

1. Although we have only used SICM controller and software from Ionscope, we are aware that other commercially available SICM setups possess the capabilities required to perform high-resolution imaging of live cell samples. We are also aware of developments of an open source code for SICM control. Unfortunately, as of today, an open source solution is not yet available. The most critical feature of the SICM setup for imaging auditory hair cell stereocilia bundles, is a control algorithm with the hopping-probe capability. In addition, the fine pipette movement should be controlled by piezoelectric systems with a nanometer precision and with a range of at least 10 μm in the Z-axis and at least $20 \times 20 \mu\text{m}$ in the X-Y axes. Lastly, the entire SICM setup should exhibit minimal drifts.
2. SICM images represent matrix data with information from a 3D surface. Users are welcome to use any post-processing software that is able to handle these types of data. For example, the MATLAB® software (MathWorks, Natick, MA) can be used to visualize the SICM images. In addition, custom-made scripts can be created to perform image corrections and analyses.
3. Other types of glass can be used for the fabrication of nanopipettes. We obtained similar tip sizes (~50–70 nm inner diameters, ~200–400 $M\Omega$ pipette resistances) and similar HPICM imaging qualities using borosilicate and aluminosilicate glass capillaries. In addition, we have obtained smaller nanopipette tips (~30 nm inner diameter, ~1 $G\Omega$ pipette resistance) with quartz capillaries. To fabricate nanopipettes with aluminosilicate glass capillaries, users would need to set up and optimize a new program in either the P-1000 or P-2000 Sutter pipette pullers. When using the P-1000 puller, use the *Sutter Cookbook* manual (available for download at http://www.sutter.com/PDFs/pipette_cookbook.pdf) for instructions. If quartz nanopipettes are desired, users need to use the laser-based Sutter

P-2000 pipette puller, which has also an *Operation Manual* (http://www.sutter.com/manuals/P-2000_OpMan.pdf) for general guidelines in selecting program values.

4. Users should always make sure that the capillaries contain an inner filament. Otherwise, due to the very small diameter of the tip, the pulled nanopipettes are nearly impossible to backfill with HBSS (or L-15 medium), without leaving small air bubbles at the pipette tip or tapered region.
5. A critical step, before starting any HPICM imaging, is to ensure a lack of air bubbles in the nanopipette after backfilling with HBSS or L-15 medium. Therefore, we recommend inspecting the pipette taper region using a low magnification LCD microscope equipped with a 10× objective lens.
6. Always make sure the puller bars are moved all the way to the center of the stage, when the knobs are tightened, and avoid over-tightening the knobs.
7. Users may need to perform small adjustments to the pipette puller programs provided in Table 1 to get nanopipettes with the correct size and resistance. To do so, please refer to the puller's *Operation Manual* for detailed information about program parameters.
8. The lateral resolution of SICM ultimately relies on the inner tip diameter of the pipette. The first high-resolution HPICM images of mouse hair cell stereocilia bundles were obtained using borosilicate pipettes with an ~30 nm inner tip diameter (i.e. ~1 GΩ resistance) [20]. However, we can successfully visualize individual stereocilia from rat and mouse inner hair cell bundles using borosilicate pipettes with an ~50–70 nm inner tip diameter. We recommend that users start imaging stereocilia bundles using the latter pipettes, since they are easier to manufacture and typically provide lower electrical noise.
9. We recommend using the shortest pipettes the SICM pipette holder can utilize, to minimize the mechanical resonance in the lateral direction at the pipette tip. When 100 mm glass capillaries are centered in the middle of the pipette puller, two nanopipettes are produced of ~50 mm in length. Therefore, to obtain shorter pipettes (~30 mm), either shorter glass capillaries are used (e.g., 70 mm) or a 100 mm glass capillary is placed in the pipette puller with an alignment offset (i.e. not centered).
10. Pulled nanopipettes can be backfilled with L-15 cell culture medium. However, we seem to obtain longer recordings when we use HBSS as the pipette solution instead of L-15 medium.
11. Depending on the length of the electrode and the nanopipette length, we recommend backfilling pipettes with HBSS (or L-15 medium) to the point where only ~1–2 mm of the electrode tip are immersed in the solution.

12. We recommended pulling nanopipettes on the same day of use, since pipette tips become more hydrophobic with time and backfilling with HBSS (or L-15 medium) becomes more difficult.
13. Based on Ohm's law, pipette resistance is easily calculated as follows:

$$R = \frac{V}{I}$$

where R is the resistance of the nanopipette in megaohms, V the potential applied to the pipette in millivolts, and I the ion current flowing through the pipette in nanoamperes.

14. The resistance value of the nanopipette, which is measured in the bath solution, is inversely correlated with the area of the tip opening. Therefore, if the inner diameter of the pipette is halved, the area at the tip opening is reduced to a quarter and the pipette resistance quadruples. Given that a $1\text{ M}\Omega$ pipette has a tip inner diameter of $\sim 1\text{ }\mu\text{m}$ and assuming that the inner/outer diameter ratio of the glass is maintained throughout the entire length of the pulled nanopipette, one can quickly estimate the tip inner diameter using the following equation:

$$\text{ID}_{\text{Tip}} = \frac{1000}{\sqrt{R}}$$

where R is the resistance of the nanopipette in megaohms and ID_{Tip} is the inner diameter at the tip in nanometers.

15. For nanopipettes with resistance values between 200 and $400\text{ M}\Omega$, we obtain the best results applying an ion current of $1\text{--}2\text{ nA}$. However, for smaller nanopipettes with resistance values near $1\text{ G}\Omega$, we recommend an ion current of $\sim 0.5\text{ nA}$.
16. Both analog and digital ion current (I_p) filters can be modified. They are found in the patch clamp amplifier and the HPICM Control software, correspondingly. When the cutoff values of the filters are lowered, the I_p floor noise is reduced, but the reaction speed of the HPICM system also decreases. That is, a fast decrease of I_p might be filtered, when the pipette tip approaches the sample. As a result, the setpoint is reached later, when the pipette is closer to the surface of the sample. To help compensate for this error, the user can decrease the speed of approach.
17. Once glued to a glass-bottom dish using double-sided tape, calibration chips are not removed. Instead, after each use (i.e. HPICM imaging), they are rinsed with distilled water, air-dried, and stored in a dust-free chamber.

18. To minimize drifts during HPICM imaging, small pieces of double-sided tape are used to firmly secure the dishes onto the SICM stage.
19. The HPICM Control software offers an “adaptive” compression profile to set up different lateral resolution values, depending on the complexity of the sample [20]. Values provided in Table 2 should be used for regions with high complexity.
20. Remove the tectorial membrane immediately before HPICM imaging and not during the dissection. The tectorial membrane is still growing in young, postnatal organ of Corti explants. Its premature mechanical disruption results in secretion and accumulation of a large amount of unorganized extracellular matrix that eventually covers the stereocilia bundles and easily sticks to the nanopipette. Therefore, HPICM imaging of the hair cell bundles becomes extremely difficult.
21. If an excess of culture medium is left in the dish, organ of Corti explants do not attach to the glass properly. However, if too much culture medium is removed, explants may dry out during the overnight incubation, causing stereocilia bundle disruptions or even death of the hair cells.
22. Be careful when adding fresh culture medium or rinsing organ of Corti explants, since they can easily detach from the glass-bottom dishes. Similarly, avoid shaking the dishes while explants are transported from the incubator to the SICM setup.
23. After adding fresh cell culture medium and returning the dishes with the organ of Corti explants to the incubator, we recommend waiting for at least 2–4 h before starting the HPICM imaging. This time allows the explants to firmly attach to the glass. Alternatively, the explants can be left in the incubator for up to 1 week before HPICM imaging.
24. The most common sources of drift during HPICM imaging are: tensioned or improperly fixed cables, loose mechanical connections (e.g., loose pipette holder), and even small temperature changes. Anecdotally, an SICM setup without proper thermal insulation exhibited dramatic drifts in the Z-axis when a person entered or left the room.
25. Users can use the ScanIC Control Software as well. Select the *Image Processing* tab, check the *De-striping* box, type the line width (“Reference stripe”) and the sensitivity of vertical alignment.
26. Alternatively, HPICM Control Software can be used to manually correct the slope of the image. Select the *Image Processing* tab, check the *Slope correction* box, and input the slope values for the X and Y axes.

Acknowledgments

We thank Yuri E. Korchev, Pavel Novak and Andrew I. Shevchuk for providing advice on all stages of this project and for the guidance on the use of the HPICM Control and ScanIC Image software, Oleg A. Belov and Samir A. Rawashdeh, for their help with software manipulations, and Julián Vergara-Rojas, for his assistance during the HPICM imaging of rat inner hair cell stereocilia bundles. This work was supported by the National Institute of Deafness and Other Communication Disorders grants R01 DC008861 and R01 DC014658.

References

- Engstrom H, Engstrom B (1978) Structure of the hairs on cochlear sensory cells. *Hear Res* 1(1):49–66
- Tilney LG, Derosier DJ, Mulroy MJ (1980) The organization of actin filaments in the stereocilia of cochlear hair cells. *J Cell Biol* 86(1):244–259
- Conchello JA, Lichtman JW (2005) Optical sectioning microscopy. *Nat Methods* 2(12):920–931
- Maglione M, Sigrist SJ (2013) Seeing the forest tree by tree: super-resolution light microscopy meets the neurosciences. *Nat Neurosci* 16(7):790–797
- Godin AG, Lounis B, Cognet L (2014) Super-resolution microscopy approaches for live cell imaging. *Biophys J* 107(8):1777–1784
- Castellano-Munoz M, Peng AW, Salles FT, Ricci AJ (2012) Swept field laser confocal microscopy for enhanced spatial and temporal resolution in live-cell imaging. *Microsc Microanal* 18(4):753–760
- Beurg M, Fettiplace R, Nam JH, Ricci AJ (2009) Localization of inner hair cell mechanotransducer channels using high-speed calcium imaging. *Nat Neurosci* 12(5):553–558
- Bullen A, Taylor RR, Kachar B, Moores C, Fleck RA, Forge A (2014) Inner ear tissue preservation by rapid freezing: improving fixation by high-pressure freezing and hybrid methods. *Hear Res* 315:49–60
- Pickles JO, Comis SD, Osborne MP (1984) Cross-links between stereocilia in the guinea pig organ of Corti, and their possible relation to sensory transduction. *Hear Res* 15(2):103–112
- Furness DN, Katori Y, Nirmal Kumar B, Hackney CM (2008) The dimensions and structural attachments of tip links in mammalian cochlear hair cells and the effects of exposure to different levels of extracellular calcium. *Neuroscience* 154(1):10–21
- Studer D, Gruber W, Al-Amoudi A, Egli P (2001) A new approach for cryofixation by high-pressure freezing. *J Microsc* 203(Pt 3):285–294
- Lucic V, Rigort A, Baumeister W (2013) Cryo-electron tomography: the challenge of doing structural biology *in situ*. *J Cell Biol* 202(3):407–419
- Dufrene YF (2008) Towards nanomicrobiology using atomic force microscopy. *Nat Rev Microbiol* 6(9):674–680
- Muller DJ (2008) AFM: a nanotool in membrane biology. *Biochemistry* 47(31):7986–7998
- Langer MG, Koitschev A, Haase H, Rexhausen U, Horber JK, Ruppertsberg JP (2000) Mechanical stimulation of individual stereocilia of living cochlear hair cells by atomic force microscopy. *Ultramicroscopy* 82(1–4):269–278
- Langer MG, Fink S, Koitschev A, Rexhausen U, Horber JK, Ruppertsberg JP (2001) Lateral mechanical coupling of stereocilia in cochlear hair bundles. *Biophys J* 80(6):2608–2621
- Hansma PK, Drake B, Marti O, Gould SA, Prater CB (1989) The scanning ion-conductance microscope. *Science* 243(4891):641–643
- Lab MJ, Bhargava A, Wright PT, Gorelik J (2013) The scanning ion conductance micro-

- scope for cellular physiology. *Am J Physiol Heart Circ Physiol* 304(1):H1–H11
19. Korchev YE, Bashford CL, Milovanovic M, Vodyanoy I, Lab MJ (1997) Scanning ion conductance microscopy of living cells. *Biophys J* 73(2):653–658
20. Novak P, Li C, Shevchuk AI, Stepanyan R et al (2009) Nanoscale live-cell imaging using hopping probe ion conductance microscopy. *Nat Methods* 6(4):279–281
21. Molecular Devices L (2012) The Axon guide: electrophysiology and biophysics laboratory techniques. 3rd edn. [http://info.moleculardevices.com/acton/fs\(blocks/showLandingPage/a/2560/p/p-023c/t/page/fm/0](http://info.moleculardevices.com/acton/fs(blocks/showLandingPage/a/2560/p/p-023c/t/page/fm/0)

Chapter 13

Design and Construction of a Cost-Effective Spinning Disk System for Live Imaging of Inner Ear Tissue

Federico Ceriani, Catalin D. Ciubotaru, Mario Bortolozzi, and Fabio Mammano

Abstract

Confocal imaging of fluorescent probes offers a powerful, non-invasive tool which enables data collection from vast population of cells at high spatial and temporal resolution. Spinning disk confocal microscopy parallelizes the imaging process permitting the study of dynamic events in populations of living cells on the millisecond time scale. Several spinning disk microscopy solutions are commercially available, however these are often poorly configurable and relatively expensive. This chapter describes a procedure to assemble a cost-effective homemade spinning disk system for fluorescence microscopy, which is highly flexible and easily configurable. We finally illustrate a reliable protocol to obtain high-quality Ca^{2+} and voltage imaging data from cochlear preparations.

Key words Confocal spinning disk microscopy, Calcium imaging, Voltage imaging, Spontaneous activity, Calcium action potentials, Calcium signaling, Inner hair cells, Non-sensory cells, Connexins

1 Introduction

Virtually all living cells use Ca^{2+} ions as a signal for a variety of physiological processes. Due to its importance as a second messenger, signaling mechanisms which involve Ca^{2+} are probably the best characterized in cell biology. Ca^{2+} in the inner ear is fundamental for hearing and balance functions, due to its critical involvement in hair cell mechanotransduction and synaptic activity. Ca^{2+} signaling is also important in the developing cochlea, where cochlear non-sensory cells display spontaneous and ATP-dependent Ca^{2+} transients that spread from cell to cell in a wave-like fashion [1], while sensory inner hair cells fire spontaneous Ca^{2+} -dependent action potentials [2].

Electronic supplementary material: The online version of this chapter ([doi:10.1007/978-1-4939-3615-1_13](https://doi.org/10.1007/978-1-4939-3615-1_13)) contains supplementary material, which is available to authorized users.

Optical imaging offers an ideal tool to study Ca^{2+} dynamics as it allows simultaneous recording of signals from several cells in an intact tissue, such as the organ of Corti, using fluorescent probes that are well characterized and commercially available. Confocal microscopy is the best choice to visualize thin optical sections of the fluorescence signal arising from a given cell. In conventional laser-scanning confocal microscopy, the sample is illuminated point-by-point by a finely focused laser beam while spatial filtering through a pinhole located close to the detection system (typically, a photomultiplier) enables rejection of out-of-focus fluorescence background resulting in a dramatically improved contrast compared to wide field microscopy [3]. This is particularly important for imaging through thick samples, such as organs or organ slices.

A spinning disk confocal microscope parallelizes the point-by-point illumination and detection processes, as light from the excitation source is distributed over multiple foci and the image is formed over a 2D sensor instead of a single photomultiplier. Therefore, this technique is intrinsically faster and less prone to photo bleaching than point-wise laser scanning. A spinning disk confocal microscope typically uses a rotating element (disk) located in a plane that is optically conjugated with that of the specimen (object plane). Disk transmittance is non-uniform, resulting in the projection of an intensity-modulated light pattern onto the specimen. In the Nipkow disk configuration, thousands of pinholes are arranged in an Archimedes spiral so that light traversing pinholes traces concentric arcs across the sample as the disk revolves [4]. Transmittance patterns other than pinhole arrays have also been used, such as striped disks, in which pinholes are replaced by two orthogonal Ronchi ruling patterns [5].

When the sample contains fluorescent molecules, the emitted fluorescence light returns along the same path of excitation, passing through the objective lens and the disk, and is projected through a relay lens onto a CCD or a sCMOS camera sensor, which also sits in a plane conjugated with the object plane. Fast rotation of the disk permits one to uniformly scan the whole field of view in 10 ms or less to form a (confocal) image onto the detector. Thus, the overall speed of acquisition is normally limited by camera sensitivity and maximal frame rate.

Here, we provide a detailed description of a cost-effective, highly configurable spinning disk confocal microscope (Figs. 1, 2, 3, 4, and 5), which is suitable to perform simultaneous (two-color) imaging and electrophysiological recordings. We show how to test microscope performance (Fig. 6) and provide some illustrative examples (Figs. 7, 8, and 9) of intracellular and intercellular signalling mechanisms in mice cochlear epithelia [6–10].

We hope that the skilled reader will benefit from the information we provide here, which should be sufficient to duplicate the architecture we developed.

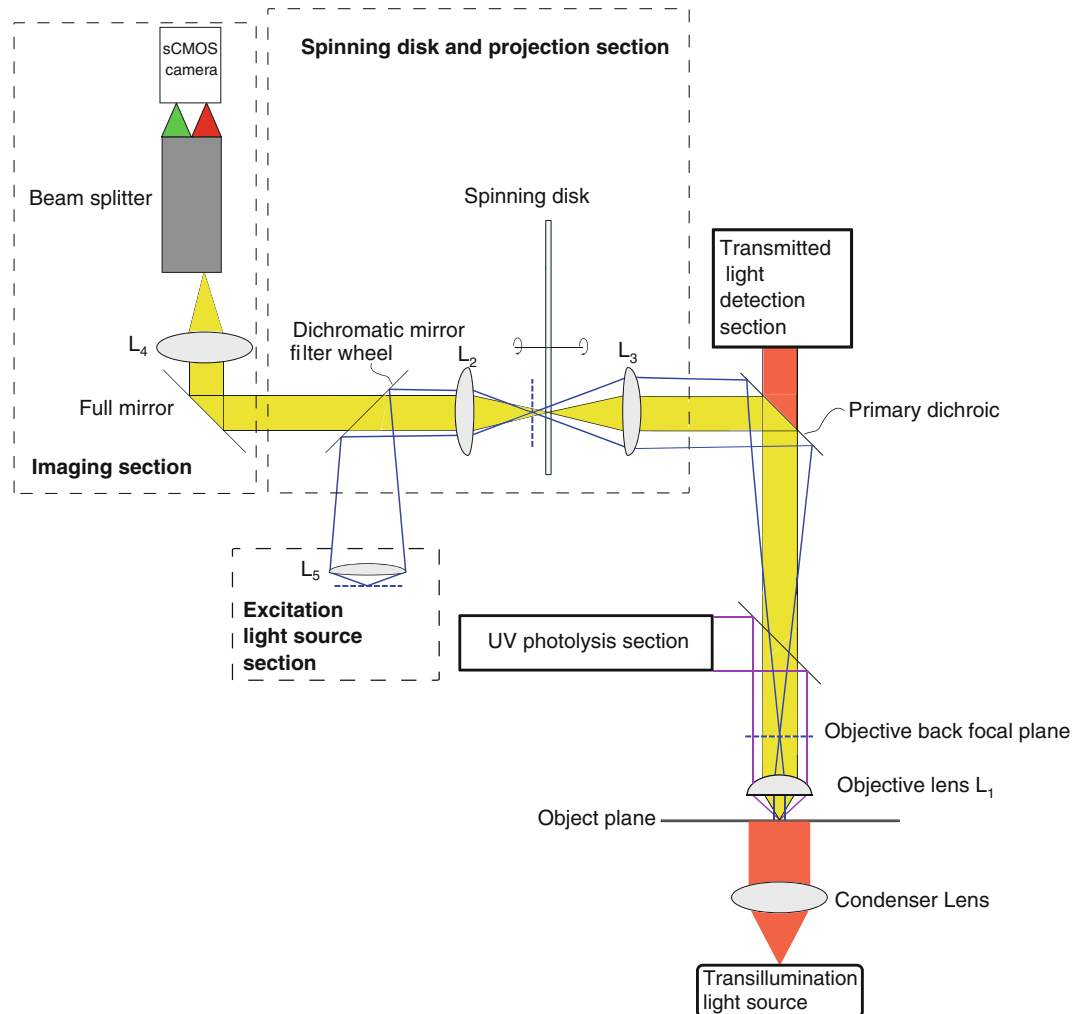


Fig. 1 Scheme of the confocal microscope system developed in our laboratory (see Subheading 2.1 for parts list). L4 sets the overall magnification of the system (as both telescope and the image duplicator have unit magnification), therefore its focal length must be carefully chosen depending on the objective and the final magnification of the image projected by an apochromatic lens onto the camera sensor

2 Materials

2.1 Optical Components

2.1.1 Microscope and Fluorescence Imaging Components (Fig. 1)

1. Fixed stage microscope (e.g. Olympus BX51WI, Olympus) mounted on an anti-vibration table (e.g. 63–560, TMC).
2. Epifluorescence illuminator (e.g. BX-URA2, Olympus).
3. Full mirror (e.g. CM1-G01, Thorlabs, Newton, NJ).
4. Infinity-corrected imaging lens (L4, e.g. ITL200, Thorlabs).
5. Digital scientific camera, preferably with a sCMOS sensor (e.g. PCO.EDGE 5.5, PCO).

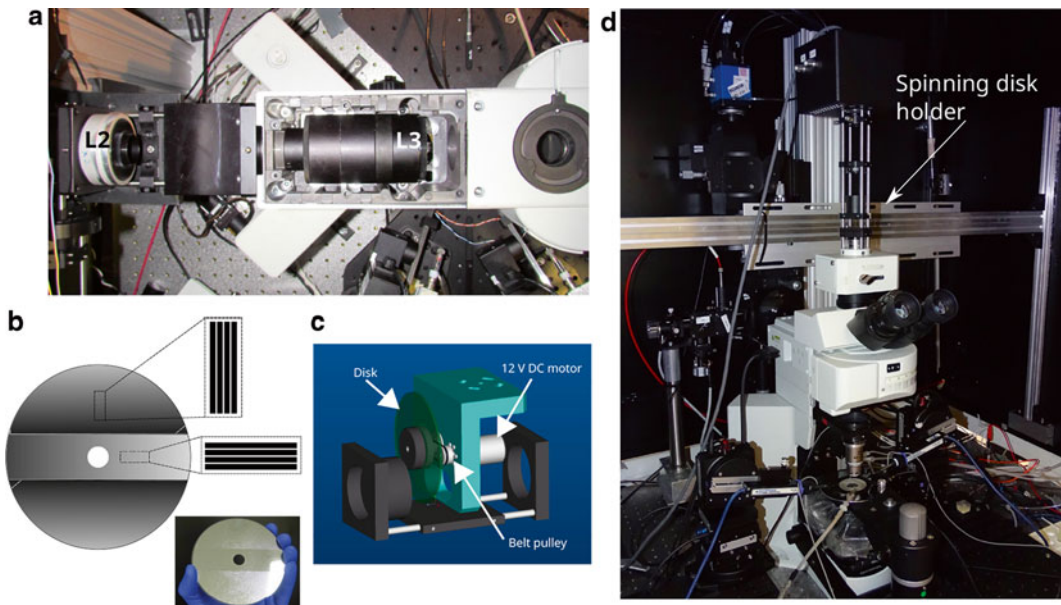


Fig. 2 Spinning disk section. (a) The epifluorescence illuminator was customized to allow the insertion of additional optics in the optical path. The two achromatic doublets forming the confocal telescope (L2 and L3) share the same focal plane (*dashed line*) where the spinning disk is positioned. (b) Confocal disk obtained by laser ablation of chromium deposition on a round glass window; the pattern consists of two orthogonal sets of stripes (38 μm width, 400 μm pitch) that permit to scan the field of view once the disk rotates. (c) Home-made rotary disk mount that connects the DC motor to the disk. (d) To avoid direct transmission of mechanical vibrations to the microscope due to disk rotation, the rotary disk mount is connected to a transversal bar anchored to the Faraday cage, which is mechanically isolated from the optical table

2.1.2 Spinning Disk and Projection Section (Fig. 1)

1. L2, L3: identical achromatic doublets, 50 mm diameter (\varnothing), 100 mm effective focal length (efl), Ultraviolet-Visible coating (e.g. 85–878, Edmund Optics, Barrington, NJ).
2. Spinning disk (Fig. 2b): Use a round glass window (e.g. WFS-1001, UQG Ltd., UK), to form the spinning disk by drilling a precision hole in its center. One face of the window carries a light-modulating pattern (holes or stripes) which can be obtained by laser ablation of a chromium deposition (e.g. Altechna, Vilnius, Lithuania).
3. Rotary disk mount (Fig. 2c): This custom-built component can be requested from Tecnomotive snc (<http://www.tecnomotive.it>, Padova, Italy).
4. DC motor (e.g. A-max 121394, Maxon Motor, Fall River, MA).
5. $x-y-z$ Micromanipulator (e.g. PT3, Thorlabs): This part is used to connect the rotary disk mount (Fig. 2c) to the transversal support bar (Fig. 2d) and to precisely position the disk in the light path between L2 and L3 (Figs. 1 and 2a).

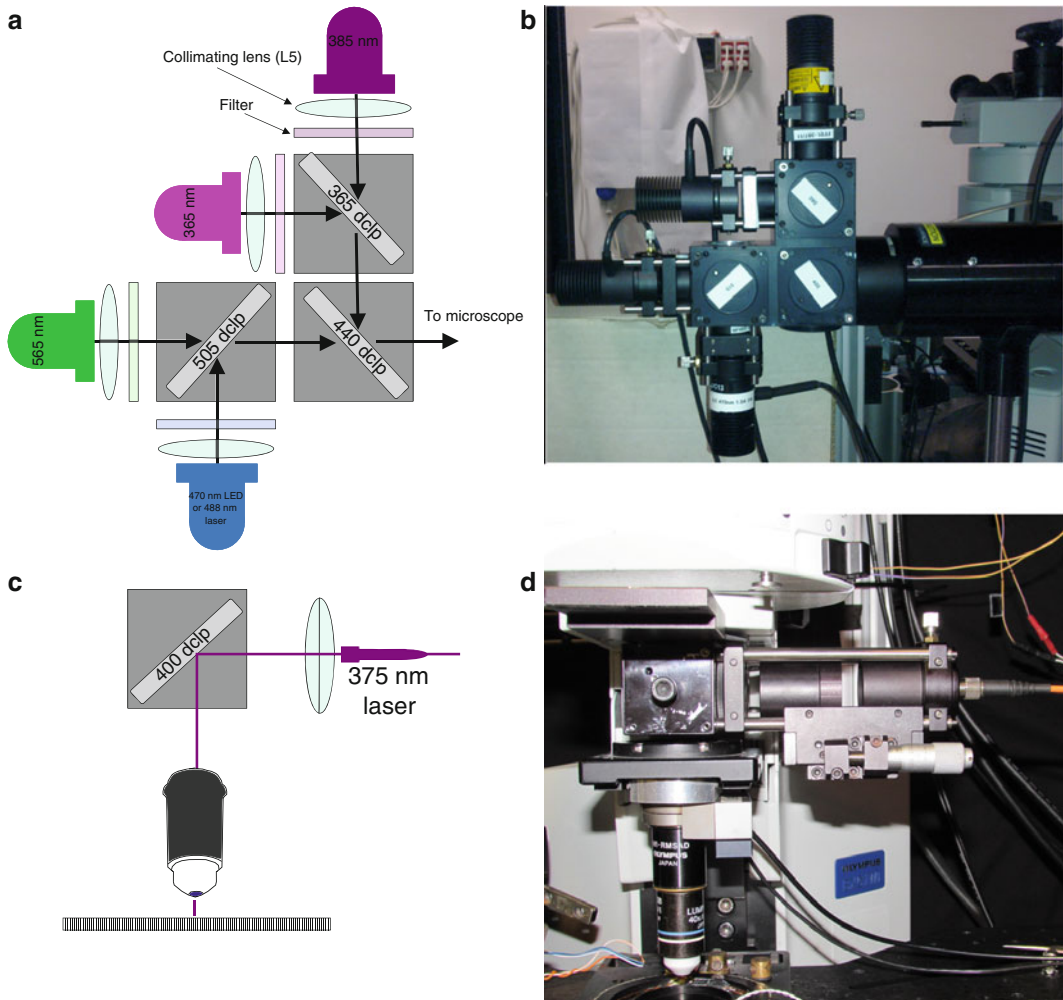


Fig. 3 Fluorescence excitation and photoactivation of caged compounds. **(a, b)** Fluorescence illumination uses up to four high-powered LEDs at pre-selected wavelengths. This arrangement, which consists of dichroic mirrors and filters, enables the selection of one or more wavelengths simultaneously (under TTL control) without altering the optical path. **(c, d)** UV photolysis of caged compounds (e.g. NP-EGTA): delivery of light from a UV laser (379 nm) is TTL-controlled by the same microcontroller board that triggers the excitation LEDs and the acquisition camera. The UV collimated beam is focused onto a small spot by the imaging objective. The optical fiber is mounted on an x - y - z micromanipulator, which permits precise positioning and focusing of the uncaging spot in the field of view

2.1.3 Fluorescence Excitation (Fig. 3a, b)

1. 365 nm LED (e.g. M365L2, Thorlabs).
2. 365 nm LED filter (e.g. Hg01-365-25, Semrock Inc., Rochester, NY).
3. 385 LED (e.g. M385L2, Thorlabs).
4. 385 nm LED filter (e.g. D390/70X, Chroma Technology, Bellows Falls, VT).

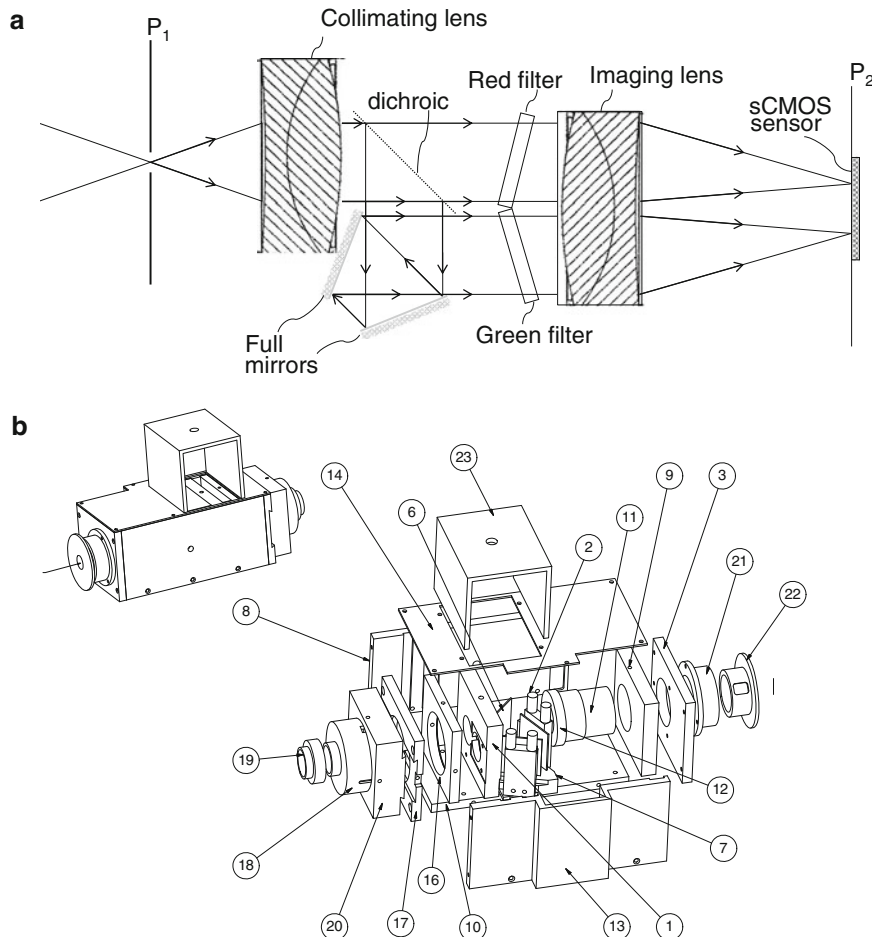


Fig. 4 Custom-made optical image duplicator. (a) This optical device is intercalated between the microscope output port and the 2D solid state sensor of the camera, and is used to acquire two simultaneous and spectrally distinct images of the same field of view; P1 the plane of variable slit aperture and P2 the image plane. (b) Exploded-view diagram: (1) Filter holder, (2) adjustable mirror holder, (3) enclosure, (6) dichromatic mirror, (7) mirror holder, (8) left wall, (9) internal threaded separation, (10) rail, (11) external threaded lens holder, (12) diaphragm, (13) right wall, (14) top enclosure, (16) projection lens holder, (17) back enclosure, (18) telescopic mount, (19) camera mount, (20) rail, (21) slit holder, (22) slit, (23) enclosure

5. 470 nm LED (e.g. M470L3, Thorlabs).
6. 470 nm LED filter (e.g. BP460-480, Olympus).
7. 565 nm LED (e.g. M565L3, Thorlabs).
8. 565 nm LED filter (e.g. 67-019, Edmund Optics).
9. Set of dichroic mirrors to combine light from different sources (e.g. 380DCLP, 440DCLP and 505DCLP, Chroma).
10. LED Collimating Lenses (L5, e.g. AC2520, Thorlabs; one lens per LED).

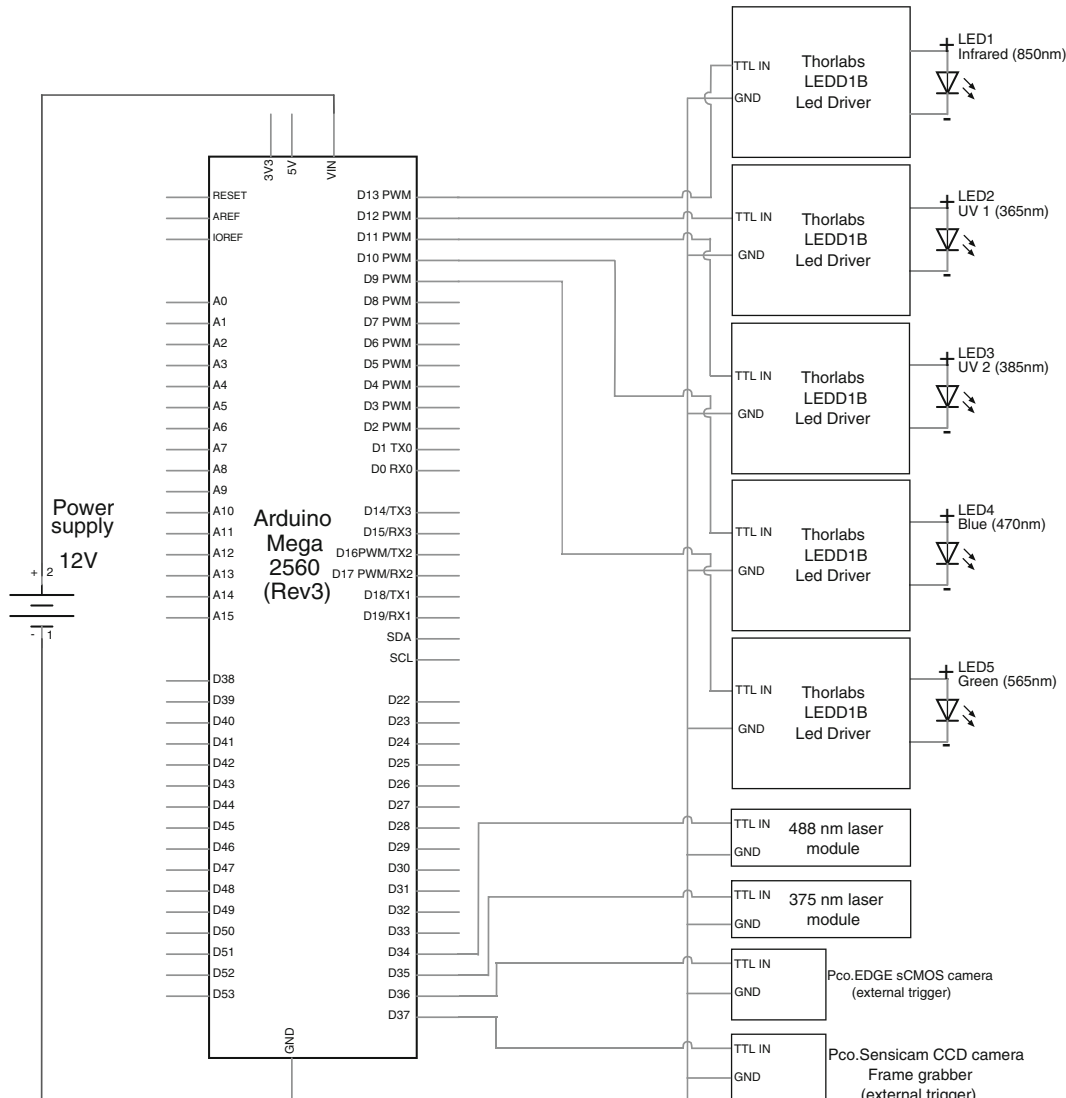


Fig. 5 Control electronics. All light sources are rapidly switched between the ON and OFF states by a home-made control board with a microcontroller (Arduino Mega 2560 Rev3) as main component. The same control board also triggers frame acquisition in both cameras. LEDs are driven by adjustable TTL-controlled LED drivers (LEDD1B, Thorlabs)

11. $x-y$ translators: Used to center LED image in the back focal plane of the objective lens (e.g. CXY1, Thorlabs; one translator per LED).
12. Mechanical assembly: This custom-built part can be requested from Step Engineering Snc (Treviso, Italy; <http://www.stepconsulting.eu/>) (Fig. 3b).
13. Dichroic filter wheel (e.g. CDFW5/M, Thorlabs).

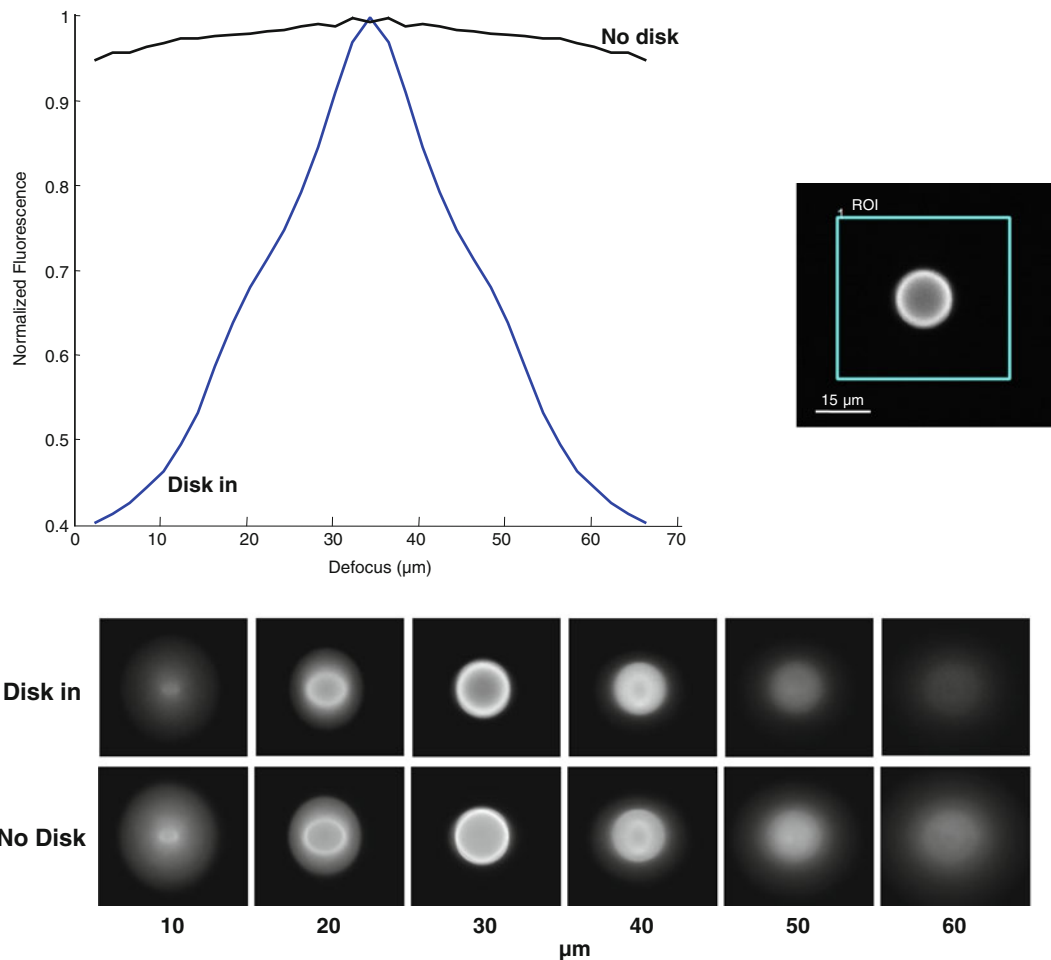


Fig. 6 Testing the optical sectioning capabilities of the confocal apparatus. (a) A 15 μm diameter fluorescent bead was imaged by a z-stack with and without insertion of the spinning disk in the optical path. (b) A square region of interest (ROI) around the bead was used to quantify the emitted fluorescence as shown in the graph (c, normalized for comparison)

14. Dichroic mirror (e.g. 515DCXR, Chroma) to separate excitation and emission light.
- 2.1.4 Transmitted Light Equipment (Fig. 1)**
1. Infrared LED: Used to visualize the preparation with infrared (IR) differential interference contrast (DIC) (e.g., M850 Thorlabs).
 2. Widefield/transmitted light camera (e.g. Sensicam, PCO, Kelheim, Germany).
 3. Infinity-corrected water/oil immersion objective (L1), magnification 20–60 \times , with the highest practicable numerical aperture (NA) (e.g. LUMPLANFL 60 \times , 0.9NA, Olympus).

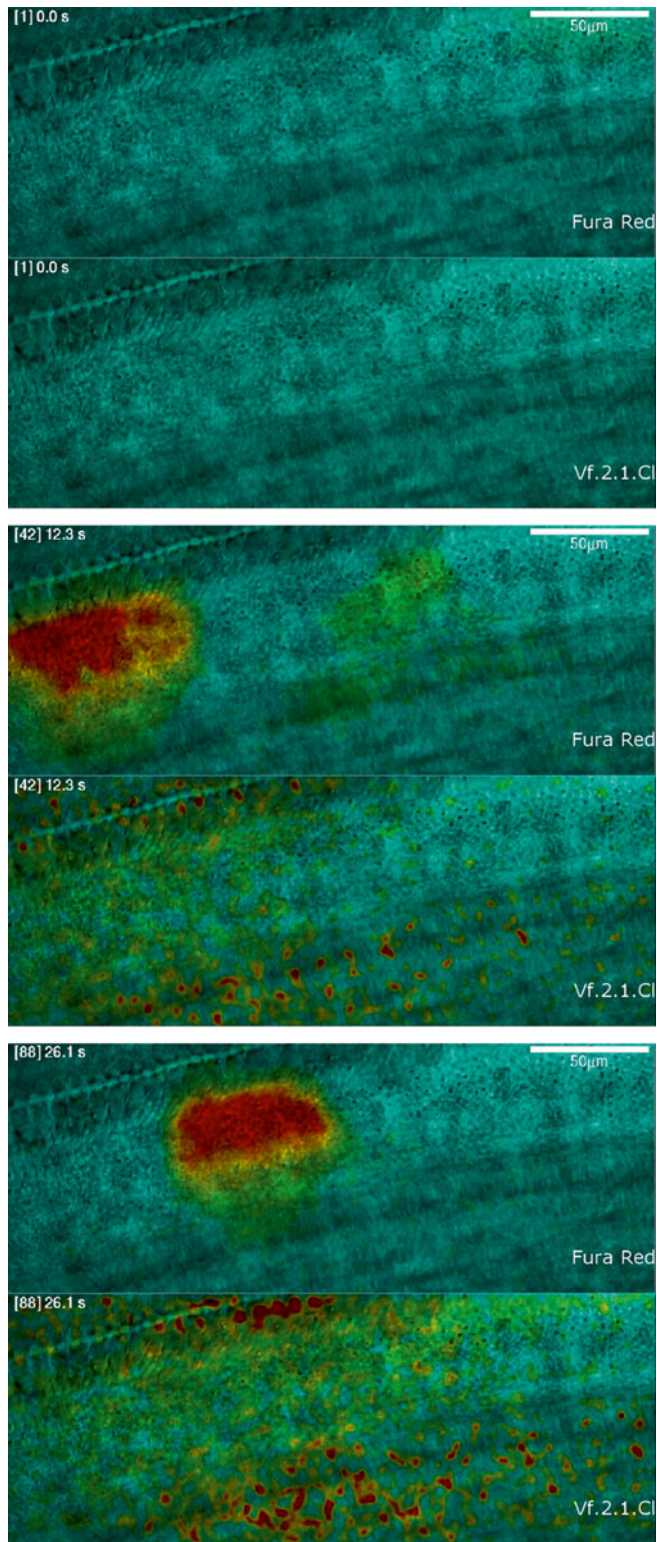


Fig. 7 Simultaneous Ca²⁺ and voltage imaging. Spontaneous Ca²⁺ activity and membrane depolarizations were recorded simultaneously using Fura-Red and Vf2.1.Cl, respectively, to show Ca²⁺ and voltage waves propagating through non-sensory cells coupled by gap-junctions in the greater epithelial ridge of the mouse postnatal cochlea (P5). See also Supplementary Video 1

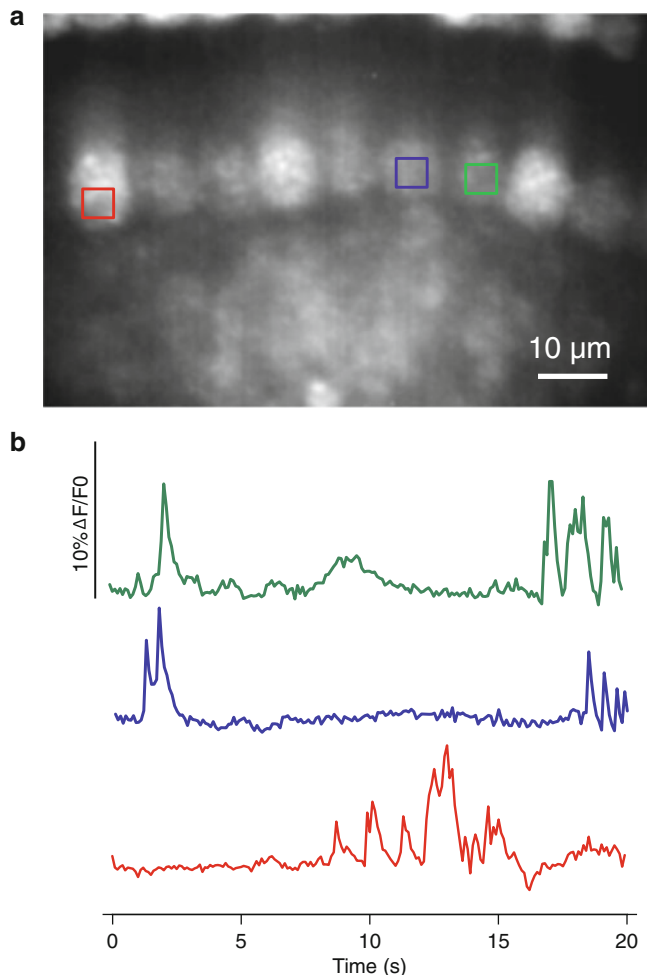


Fig. 8 Recording of spontaneous Ca^{2+} action potentials in immature cochlear inner hair cells. (a) Ca^{2+} dynamics during synaptic activity recorded in inner hair cells of the postnatal cochlea loaded with Fluo-4AM. (b) Local Ca^{2+} transients (“hotspots”) due to spontaneous action potentials (see Supplementary Video 2) were clearly detectable by the confocal apparatus. Signals were post-processed by subtracting the Fluo-4 bleaching component and the slow fluorescence modulation due to out-of-focus non-sensory cells encasing hair cells

4. Piezoelectric objective lens positioning system (e.g. MIPOS 100 SG, Piezojena and related driver, NV 40/1 CLE) (Fig. 3d).
 5. Primary dichroic mirror (e.g., 790DCXXR Chroma).
- 2.1.5 UV Photolysis (Fig. 3c, d)**
1. TTL-controlled continuous-wave diode laser (370–380 nm center wavelength) coupled to 50–100 μm \varnothing UV-permissive optical fiber, with fiber output power ≥ 100 mW (e.g. FC-375-050-MM1-PC-1-0, RGBLase LLC, Fremont, CA).
 2. Collimating achromatic doublet (e.g. AC254-075-A, Thorlabs).
 3. Dichroic mirror (e.g. 400DCLP, Chroma).

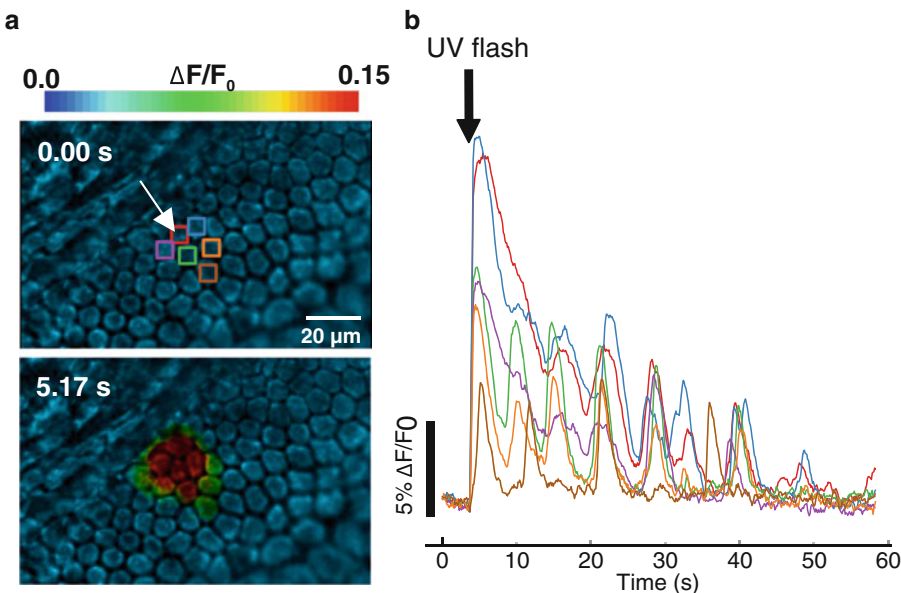


Fig. 9 Focal photoactivation of caged IP_3 in non-sensory cell of the lesser epithelial ridge of the cochlea. (a) Single-cell UV photoactivation of caged IP_3 (170 ms) stimulates propagation of an intercellular Ca^{2+} wave followed by spontaneous Ca^{2+} oscillations. (b) Traces correspond to ROIs in (a). Ca^{2+} concentration was measured by Fluo-4AM, co-loaded with caged IP_3 AM (see Subheading 3 and Supplementary Video 3). Note: the size of UV laser spots in the focal plane ($\sim 10 \mu\text{m}$ using Nikon 60 \times /1.0 NA Water Objective) can be estimated by measuring the dimension of the spot carved in a thin film of black ink deposited on a microscope coverslip

2.1.6 Image Duplicator Components (Fig. 4)

4. Dichroic cage cube (e.g. CM1-DCH, Thorlabs).
5. Cage translation stage: Used to position optical fiber output in the focal plane of the achromatic doublet (e.g. CT1, Thorlabs).
6. $x-y$ translator: Used to position the focal spot in the field of view (e.g. CXY1, Thorlabs).
1. Green/yellow emission filter (e.g. ET535/30M, Chroma).
2. Red emission filter (e.g. D650/50M, Chroma).
3. Dichroic mirror (e.g. 585DCXR, Chroma).
4. Pair of identical achromatic doublets (e.g. AC508-100-A, Thorlabs). These lenses should have high (>90 %) transmittance in the visible region (400–700 nm) and suitable anti-reflection coating.
5. Adjustable mirror mount (e.g. 56–344, Edmund Optics).
6. Adjustable mechanical slit (e.g. VA100C/M, Thorlabs).
7. Mechanical assembly (Fig. 4b).

2.1.7 Optics Alignment Tools

1. Optical test target (e.g. R3L3S1N, Thorlabs).
2. Fluorescent microspheres (e.g. F-7238, ThermoFisher).
3. Fluorescent test target: Used for light source optimization (e.g. VRC2, Thorlabs).

2.1.8 Image Acquisition**Hardware and Software**

1. Computer workstation.
2. Programmable microcontroller (e.g. Arduino/Genuino MEGA 2560 Rev. 3, Arduino) or computer I/O board (e.g. Model 826, Sensoray) to control image exposure trigger and light switching (Fig. 5).
3. High-power TTL-controlled LED drivers (e.g. LEDD1B, Thorlabs).
4. Image acquisition software: We use software developed in our laboratory. Alternatives are Metamorph (Molecular Devices) or MicroManager (University of California, San Francisco).

2.2 Cochlear Dissection Materials

1. Sterile dissection tools.
2. Cell-Tak solution (Becton Dickinson).
3. 0.1 M sodium bicarbonate solution (pH 8.0).
4. Sterile water.
5. Ice-cold Hank's Balanced Salt Solution (HBSS) supplemented with 10 mM Hepes Buffer (~4 mL for each cochlea).
6. Culture medium (~2 mL for each culture): DMEM/F12 supplemented with 5 % Fetal Bovine Serum (FBS, Thermo Fisher), ampicillin (0.1 mg/mL), and fungizone (0.1 mg/mL).

2.3 Fluorescent Dyes and Photoactivatable Compounds

1. VoltageFluor (Vf) 2.1.Cl voltage-sensitive dye [11], kindly provided by Professor Roger Y. Tsien (University of California, San Diego).
2. Pluronic F-127 (Thermo Fisher), 20 % w/v solution in DMSO.
3. Sulfinpyrazone (Sigma-Aldrich): Prepare a 20 mM stock solution in water. Bring pH to ~11 using NaOH and stir, then bring back to ~8.5 using HCl once dissolved.
4. Ca²⁺ dyes Fluo-4AM and Fura-Red AM (Thermo Fisher): Solubilize dyes in DMSO to make 2 mM stock solutions. Mix using a vortexer until solution is homogeneous.
5. Caged IP₃ (ENZO Life Sciences): Prepare 1 mM stock solutions in DMSO.

2.4 Solutions

1. Perfusion medium (EXM) (mM): 135 NaCl, 5.8 KCl, 1.3 CaCl₂, 0.7 NaH₂PO₄, 0.9 MgCl, 10 HEPES-NaOH, 6 D-glucose, 2 pyruvate, amino acids and vitamins (from kit), and pH to 7.48 using NaOH. Amino acids (without L-Glutamine) and vitamins are added from concentrates (50× and 100×, respectively, Sigma-Aldrich). The final osmolarity of the solution is ~307 mOsm/L.

3 Methods

An ethics committee of the University of Padua approved all protocols, according to Italian law on animal Welfare and Experimentation and the 3R criteria.

3.1 Optical Alignment

Using Fig. 1 as a reference, the microscope is conveniently subdivided into the following categories.

1. Spinning disk and projection section, which consists of a unit gain keplerian telescope (lenses L2 and L3) and the disk itself (*see Note 1* and Fig. 2).
2. Fluorescence excitation section, which consists of the light sources and the collimation lenses L5 (*see Note 2* and Fig. 3a, b).
3. Imaging section, which consists of a projection lens (L4), the image duplicator (Fig. 4) and the camera (*see Note 3*).
4. UV photolysis section (*see Note 4* and Fig. 3c, d).
5. Transmitted light detection section, which consists of trinocular/camera (*see Note 5*, Fig. 2d).
6. Control electronics (*see Note 6* and Fig. 5).

3.1.1 Alignment Guidelines

1. Using the eyepiece of the microscope and the transmitted light source, focus a test target as a sample.
2. Remove the lenses L2, L3, the image duplicator (if present) and the spinning disk from the optical path.
3. Move the sCMOS camera along the optical axis until a sharp image of the target lines is formed.
4. Insert L3 as close as possible to the objective inside the modified epifluorescence illuminator (Fig. 2a). The exact position of this lens is not important, provided that (1) it is sufficiently close to the objective to minimize light dispersion and (2) its back focal plane lies sufficiently outside the epifluorescence illuminator to allow the insertion of the spinning disk.
5. Insert L2 in the optical path. Regulate the position of the lens until a sharp image of the test target is formed on the camera. The relative position of L2 and L4 along the optical axis is irrelevant. Relative misalignment and tip/tilt of L2 and L3 lenses should be carefully avoided.
6. Remove the test target and insert the spinning disk in the optical path at L2 and L3 focus. Finely regulate its position along the optical axis until a sharp image of the disk stripes/holes is acquired on the camera.
7. Remove the disk and L4 and insert the image duplicator in the optical path.

8. Remove the image duplicator collimating lens and open the aperture P1 completely (*see* Fig. 4).
9. Using the eyepiece of the microscope and the transmitted light source, focus the test target as a sample.
10. Adjust the position of the camera until a sharp image of the target appears.
11. Insert the collimating lens of the image duplicator. Adjust the position of the lens relative to the aperture P1 until a sharp image of the aperture borders appears on the camera sensor.
12. Insert L4 again. Maintaining the relative distance between the image duplicator and the camera, move the entire image duplicator/camera until a sharp image of the target appears.
13. Close the aperture until the image in the red channel occupies half of the camera sensor.
14. Adjust the full mirrors inside the image duplicator until the image in the green channel occupies the other half of the camera sensor.
15. The UV photolysis laser should form a focused spot on the image plane. Using a marker pen, deposit a film of ink on the surface of a glass coverslip. Focus the UV laser on the surface to carve a spot in the ink. Adjust the optical fiber by the *x*-*y*-*z* micromanipulator in order to obtain the smallest spot as possible.

3.2 Assessing Optical Sectioning

1. To test the optical sectioning capabilities of the microscope, image fluorescent beads (15 μm diameter, Fig. 6) while stepping the objective in small ($<1 \mu\text{m}$) increments along its optical axis (*z* direction) by a piezoelectric actuator.
2. Measure the average fluorescence intensity collected by the sCMOS camera sensor within a ROI containing the bead image. Graphs in Fig. 6 show normalized intensity as a function of objective position (defocus) when the disk was excluded from the optical path and when it was inserted in the path. The system's capability to reject out-of-focus fluorescence appears evident.

3.3 Preparation of Cochlear Organotypic Cultures

1. Dilute Cell-Tak 1:10 using the sodium bicarbonate solution.
2. Immediately dispense a drop of the solution on a glass coverslip ($\sim 10 \mu\text{L}$).
3. Let the coverslip dry completely at room temperature for at least 30 min.
4. Wash the coverslip with sterile water to remove residual bicarbonate. Coated coverslips can be stored at 2–8 °C for 1 week if not used immediately.

5. Quickly dissect the cochlea in ice-cold Hepes buffered (pH 7.2) HBSS. Removal of the stria vascularis during cochlear culture preparation helps to correctly position the cochlea on the coverslip, thereby, greatly improving visualization for action potential recording.

6. Place the cochlea onto the glass coverslip coated with Cell-Tak.

7. Incubate overnight at 37 °C in DMEM/F12 supplemented with 5 % FBS.

3.4 Loading of Dyes and Caged Compounds

3.4.1 Dye Loading for Simultaneous Ca^{2+} and Voltage Imaging

1. Incubate cochlear cultures for 40 min at 37 °C in DMEM/F12 supplemented with 10 μM Fura-Red AM. The incubation medium contains pluronic F-127 (0.1 %, w/v) and sulfinpyrazone (250 μM) to maximize dye sequestration and to prevent its loss, respectively.
2. Incubate cultures for 15 min in DMEM/F12 supplemented with 200 nM VF2.1.Cl and pluronic F-127 (0.1 % w/v).
3. Transfer the culture onto the microscope stage and perfuse it with extracellular solution for 20 min at 2 mL/min in the dark before starting the experiment in order to complete dye de-esterification.
4. Example: Fig. 7 and Supplementary Video 1 show a representative simultaneous recording of spontaneous Ca^{2+} and depolarizing transients and membrane depolarizations in cochlear non-sensory cells, due to spontaneous ATP release from connexin hemichannels [10]. The cochlear culture was co-loaded with Fura-Red AM and VF2.1.Cl and the image duplicator beam splitter was inserted in the optical path for simultaneous two-color imaging.

3.4.2 Dye Loading for Detection of Calcium Action Potentials in Inner Hair Cells

1. For detection of Ca^{2+} action potentials in inner hair cells, incubate cochlear cultures for 40 min at 37 °C in DMEM/F12, supplemented with Fluo-4AM (16 μM), pluronic F-127 (0.1 % w/v), and 250 μM sulfinpyrazone.
2. Transfer the culture onto the microscope stage and perfuse with extracellular solution for 20 min at 2 mL/min in the dark before starting the experiment in order to complete dye de-esterification.
3. Example: Fig. 8 and Supplementary Video 2 display a representative recording of spontaneous action potential activity in cochlear inner hair cells. Single action potential detection was prevented during high frequency bursts due to the relatively long fluorescence decay time constant of Fluo-4 (300 ± 11 ms, Mean \pm S.E.) [12].

3.5 Focal Photostimulation with Caged IP_3

1. Incubate cochlear cultures for 60 min at 37 °C in DMEM/F12 supplemented with Fluo-4AM (16 μM), caged IP_3 AM (5 μM), pluronic F-127 (0.1 %, w/v), and sulfinpyrazone (250 μM).

2. Transfer the culture on the microscope stage and perfuse in extracellular solution for 20 min at 2 mL/min in the dark to allow for de-esterification.
3. In a typical experiment, baseline (pre-stimulus) fluorescence emission (F_0) is recorded for a few seconds, thereafter a UV laser pulse of 100–200 ms is applied to release IP₃ and fluorescence emission is monitored for 1 min or more.
4. Example: Fig. 9 and Supplementary Video 3 show a representative recording of Ca²⁺ transients evoked by focal UV photo-stimulation by caged IP₃.

3.6 Fluorescence Excitation and Acquisition

1. Appropriate dichroic, excitation, and emission filters should be selected for the particular application (see Note 7). Fluo-4, Vf2.1.Cl, and Fura-Red are efficiently excited with blue light (470 nm LED). Emission spectra of Vf2.1.Cl (green) and Fura-Red (red) are suitable for simultaneous recording without the need of spectral cross-talk correction.
2. Image exposure and frame rate should be selected depending on the phenomena under study (see Note 8).
3. To minimize photobleaching and phototoxic effects, it is important that excitation light and image acquisition are carefully synchronized (see Note 9) in order to illuminate the sample only during frame exposure.

3.7 Image Analysis

1. Calcium or voltage signals are quantified pixel-by-pixel as relative changes of fluorescence emission intensity ($\Delta F/F_0$), where F_0 is fluorescence at the beginning of the recording, F is fluorescence at time t during the experiment, and $\Delta F=F-F_0$ (see Note 10).
2. Signal extraction and data analysis can be performed using software for numerical analysis (e.g. ImageJ and ImageJ-based software or Matlab).

4 Notes

1. Spinning disk—After reflection off a dichromatic mirror, excitation light is fed to a unit-gain keplerian telescope formed by two identical UV permissible achromatic doublets (L2 and L3; to position this critical pair of lenses, we removed all intermediate optics from our epifluorescence microscope and replaced them with L3). An x - y - z precision manipulator is used to place the striped disk in the focal plane shared by these two doublets, which is also a primary image plane for the entire microscope. The two achromatic doublets replace the standard lens in the BX-URA2 Olympus epifluorescence illuminator (Fig. 2a) and

are mounted using a combination of 30 and 50 mm lens tubes and holders available from Thorlabs GmbH (Dachau, Germany). The custom-made disk has a pattern on its face of chromium stripes obtained by laser ablation (Fig. 2b) and is spun by a DC motor up to a speed of 7200 rpm (Fig. 2c). To avoid transmission of mechanical vibrations to the microscope and the optical table due to the disk rotation, the disk *x-y-z* manipulator is coupled to a suspended horizontal beam attached to the frame of the Faraday cage that encases the entire system (Fig. 2d).

2. Fluorescence excitation—The rotating disk acts as a spatial filter, blocking a substantial amount (~90 %) of the excitation light. Thus, spinning disk confocal microscopy requires a light source with substantial (>200 mW) power at the relevant excitation wavelengths. High-power LEDs are the preferred option, and their combination permits fast switching between different wavelengths. Each LED is used in combination with a bandpass filter (Fig. 3a, b). Light from each LED is collimated by an aspheric lens (AC2520, Thorlabs, L5 in Figs. 1 and 3a). Note: the 470 nm LED can be replaced with a 488 nm diode laser (e.g. COMPACT-150G-488-SM, World Star Tech) that is more efficient, although considerably more expensive to excite fluorophores such as Fluo-4.
3. Fluorescence imaging—Emitted fluorescence light collected by the objective is spatially filtered through the striped spinning disk, traverses the illumination dichroic and emission filter and is finally focused onto a sCMOS detector (PCO. edge, PCO, Germany) by a projection lens (L4 in Fig. 1, ITL200, Thorlabs). The detector must be located in a plane optically conjugated with the disk as well as the object plane. For two-color acquisition, light emitted by different fluorophores is separated by the optical image duplicator (Fig. 4) and imaged onto separated halves of the sCMOS sensor (Fig. 1).
4. UV photolysis section—The output of a TTL-controlled semiconductor laser module (150 mW, 379 nm, RGBLase LLC, CA, USA) is injected into a UV permissive optical fiber (multimode step index 0.22 NA, 105 μm core, part number AFS105/125YCUSTOM, Thorlabs). Fiber output is projected onto the specimen plane by an achromatic doublet (75 mm effective focal length, part number AC-254-75-A, Thorlabs) and the re-collimated beam is directed onto a dichromatic mirror (400 DCLP, Chroma) placed at 45° just above the objective lens of the microscope (Fig. 3c, d). The image of the fiber core is projected as a circular spot in the focal plane by the (infinity corrected) objective. To obtain a sharp spot profile, an *x-y-z* manipulator is used to adjust the fiber

position with respect to the aspheric lens for light re-collimation. Under these conditions, the optical fiber diameter accurately sets the laser-irradiated area, which encompasses from one to a few cells (depending on the objective).

5. Transmitted light detection section—Light from a substage infrared LED passes through the primary dichroic mirror (Fig. 1) and forms differential interference contrast (DIC) images on a scientific grade CCD camera.
6. Control electronics—LEDs (or lasers) are activated by TTL-controlled drivers in sync with the acquisition camera using a programmable microcontroller (Arduino Mega 2560 Rev3, Arduino, Italy) connected to a computer (Fig. 5). Reprogramming the microcontroller on the fly enables a local scheduler to run commands with extreme precision and flexibility. In fact, the microcontroller device eliminates the latency and jitter intrinsic in a system under direct computer (CPU) control. Combined with an electronically simulated digital ON/OFF switch, this approach achieves a temporal precision on the order of a few microseconds.
7. In our experience, Fluo-4, Vf2.1.Cl, and Fura-Red fluorescence are all efficiently excited by 470 nm LED light (M470L2, Thorlabs) passing through a BP460–480 bandpass filter (Olympus) and directed onto the sample through a 515 DCXR dichromatic mirror (Chroma). For standard calcium imaging, Fluo-4 emission is filtered through a 535/43M bandpass filter (Edmund). For simultaneous voltage and calcium imaging, Vf2.1.Cl and Fura-Red emission are separated by a dichromatic mirror (585DCXR, Chroma) located within the optical image duplicator (Fig. 4), followed by an ET535/30M filter (Chroma) for Vf2.1.Cl and a D650/50M filter (Chroma) for Fura-Red. With or without an image duplicator, fluorescence images are collected by a water immersion objective (typically 60 \times , 1.0 NA, Fluor, Nikon) and projected onto a scientific-grade camera (PCO.Edge 5.5; PCO AG) controlled by software developed in our laboratory.
8. Some guidelines for deciding the correct frame rate and exposure are:
 - Deliver excitation light to the sample only during frame exposure, in order to minimize photobleaching, by switching on the excitation LED source a few milliseconds before exposure starts and switching off a few milliseconds after.
 - The duration of frame exposure should be long enough to obtain a fluorescence signal-to-noise ratio (SNR) higher than 1. The goal is to achieve the minimal SNR that permits discrimination between noise and fluorescence variations related to the biological phenomenon under study.

- The duration of frame exposure should be short enough to avoid camera pixel saturation during the experiment, which results in loss of biological information.
 - The frame rate should be fast enough to track the biological phenomenon under study. For periodic phenomena, a lower bound to the acquisition frequency is set by the Nyquist criterion.
9. Miller et al. [11] reported that Vf2.1.Cl and other PeT-based voltage indicators have a slower rate of photobleaching and are less toxic than FRET-based dyes. We did not perform direct comparisons between these two classes of indicators. However, in our hands, patch clamp recordings from cochlear non-sensory cells in Vf2.1.Cl-loaded cultures were stable for tens of minutes during continuous illumination by the excitation LED. In addition, we did not notice any visible sign of cellular degeneration.
10. When excited at 470 nm, Fura-Red fluorescence emission decreases upon binding Ca^{2+} .

Acknowledgments

This work was supported by Telethon Italy grants GGP13114 and GGP12269 to FM and MB, respectively.

References

1. Mammano F (2013) ATP-dependent intercellular Ca^{2+} signaling in the developing cochlea: facts, fantasies and perspectives. *Semin Cell Dev Biol* 24:31–39
2. Marcotti W (2012) Functional assembly of mammalian cochlear hair cells. *Exp Physiol* 97:438–451
3. Pawley J (2006) Handbook of biological confocal microscopy, vol 236. Springer, New York, NY
4. Gräf R, Rietdorf J, Zimmermann T (2005) Live cell spinning disk microscopy. *Adv Biochem Eng Biotechnol* 95:57–75
5. Confocal Microscopy System (2005) <http://www.biosciencetechnology.com/articles/2005/01/confocal-microscopy-system>
6. Beltramello M, Piazza V, Bukauskas FE, Pozzan T, Mammano F (2005) Impaired permeability to $\text{Ins}(1,4,5)\text{P}_3$ in a mutant connexin underlies recessive hereditary deafness. *Nat Cell Biol* 7:63–69
7. Piazza V, Ciubotaru CD, Gale JE, Mammano F (2007) Purinergic signalling and intercellular Ca^{2+} wave propagation in the organ of Corti. *Cell Calcium* 41:77–86
8. Ortolano S, Di Pasquale G, Crispino G, Anselmi F, Mammano F, Chiorini JA (2008) Coordinated control of connexin 26 and connexin 30 at the regulatory and functional level in the inner ear. *Proc Natl Acad Sci U S A* 105:18776–18781
9. Anselmi F, Hernandez VH, Crispino G et al (2008) ATP release through connexin hemichannels and gap junction transfer of second messengers propagate Ca^{2+} signals across the inner ear. *Proc Natl Acad Sci U S A* 105: 18770–18775
10. Rodriguez L, Simeonato E, Scimemi P et al (2012) Reduced phosphatidylinositol 4,5-bisphosphate synthesis impairs inner ear Ca^{2+} signaling and high-frequency hearing acquisition. *Proc Natl Acad Sci U S A* 109: 14013–14018
11. Miller EW, Lin JY, Frady EP, Steinbach PA, Kristan WB, Tsien RY (2012) Optically monitoring voltage in neurons by photo-induced electron transfer through molecular wires. *Proc Natl Acad Sci U S A* 109:2114–2119
12. Mammano F, Canepari M, Capello G, Ijaduola RB, Cunei A, Ying L, Fratnik F, Colavita A (1999) An optical recording system based on a fast CCD sensor for biological imaging. *Cell Calcium* 25:115–123

Chapter 14

Neuroanatomical Tracing Techniques in the Ear: History, State of the Art, and Future Developments

Bernd Fritzsch, Jeremy S. Duncan, Jennifer Kersigo, Brian Gray, and Karen L. Elliott

Abstract

The inner ear has long been at the cutting edge of tract tracing techniques that have shaped and reshaped our understanding of the ear's innervation patterns. This review provides a historical framework to understand the importance of these techniques for ear innervation and for development of tracing techniques in general; it is hoped that lessons learned will help to quickly adopt transformative novel techniques and their information and correct past beliefs based on technical limitations. The technical part of the review presents details of our protocol as developed over the last 30 years. We also include arguments as to why these recommendations work best to generate the desired outcome of distinct fiber and cell labeling, and generate reliable data for any investigation. We specifically focus on two tracing techniques, in part developed and/or championed for ear innervation analysis: the low molecular multicolor dextran amine tract tracing technique and the multicolor tract tracing technique with lipophilic dyes.

Key words Neuronal tracing, Lipophilic dyes, Dextran amines, Ear, Innervation, Efferents, Afferents

1 Introduction

The inner ear, and more broadly the dorsolateral placode-derived system of mechano- and electrosensory organs, has been at the cutting edge of novel tracing techniques ever since Retzius adopted the Golgi technique to show that hair cells are contacted by nerve fibers derived from ganglia positioned between the ear and the brain [1]. The emerging neuron theory of Cajal was supported by showing hair cells are discontinuous from each other and neurons using the Golgi technique [2]. This finding conflicted sharply with the reticular hypothesis of Golgi himself [3]. Retzius also championed another technique that allowed him to show the entire pattern of innervation of vertebrate ears in unprecedented detail using osmium tetroxide for myelinated nerve fiber staining [4]. This technique continues to be used to show the distribution of myelinated nerve fibers in the ear today [5]. Not only was the myelinated

nerve fiber staining an excellent technique to show the innervation in whole-mounted ears, but this approach facilitated the identification of distinct sensory epithelia. Comparative analysis of innervation patterning led to identifying the basilar papilla as a precursor for the organ of Corti as well as the amphibian papilla being a unique and unifying feature across for amphibians [4, 6].

Despite all the information provided by these early techniques, the “early masters” also made some profound mistakes in their interpretation as a consequence of technical limitations. For example, Retzius did not know that myelin will lose lipids through alcohol preservation and thus cannot be stained by osmium. Using such alcohol-treated specimens, he failed to identify nerve fibers to a ninth inner ear sensory epithelium only found in gymnophionans [7]. This lack of understanding the technique’s limitations led to a heated debate at its time [8, 9]. It took modern approaches to rectify this mistake [6] and demonstrate that the neglected and amphibian papilla are innervated by the same nerve twig, but are two parts of a single epithelium that end up in two different parts of the ear during development: the saccular recess (amphibian papilla aka saccular papilla) and the utricular recess (the neglected papilla aka utricular papilla). Even more profound were misinterpretations by Cajal (the master of Golgi staining) and his student, Lorente de No. Cajal stained fibers of what is now known as the olivo-cochlear bundle crossing in the hindbrain but believed this to be primary afferents forming an acoustic commissure similar to retinal fibers that cross to the contralateral side [10]. Lorente de No identified a rich variety of “afferent fibers” going to inner and outer hair cells, which he categorized into a multitude of fiber types [11, 12] not knowing that some of his more peculiar fiber types were in fact olivo-cochlear efferents, later identified using novel staining techniques for degenerating nerve fibers [13, 14]. While we now know that only two types of afferents and two types of efferents enter the organ of Corti [15], reaching that conclusion required applications of several new tracer techniques, each providing both lasting as well as sometimes transient insights.

Degeneration techniques in frogs implicated Purkinje cells as the source of efferent fibers to the ear. The first modern tract tracing technique, horseradish peroxidase (HRP) revealed this not to be true. The original reports implicating Purkinje fibers projecting to the inner ear were incorrect due to a technical error using evidence of degeneration of terminals as an indicator of connections [16]. Many first-generation retrograde fluorescent tracers to reach laboratories were injected into the ear and led to the identification of variably sized populations of extremely diverse cell types that were claimed to be efferents [17]. Only the detailed fiber tracings possible with HRP showed that efferents were distributed bilaterally in the brainstem of many vertebrates, and that efferents to the vestibular and cochlear/auditory endorgans exhibit various degrees

of segregation [18]. Additionally, HRP was used to show that efferents are derived facial motoneurons that segregate through selective migration away from facial branchial motoneurons [19, 20]. However, it took the invention of multicolor tract tracing with dextran amines [21, 22] and lipophilic dyes [21, 23] to demonstrate beyond a doubt the distribution of efferents in the hindbrain and their segregation through differential migration from the facial branchial motoneurons [24].

Most problematic was the early use of Golgi staining to sort out development of inner and outer hair cell innervation. These “insights” were derived in part by the technical inability to recognize the four different afferent and efferent fiber types in early embryos. For example, despite the visual clarity and stunning details of Poljak and Lorente de Nò’s drawings [12, 25], they were unable to categorize what they considered a multitude of afferent types with unknown quantitative ratios to the two types of hair cells. Obviously, growth of the fibers running along outer hair cells was the easiest to follow and both got the progressive expansion of this fiber type right. Other researchers utilized these insights in order to interpret their TEM data, which would have been impossible to interpret otherwise given the limited overview provided by this technique. In large part, based on the inability to distinguish between different fiber types, ideas were proposed that aimed to interpret the data in a hypothetical context of transient efferent and afferent connections [26, 27]. These transient fibers were reported by some to persist in the adult system [28], thereby generating lasting debates. Only modern tracing techniques, which allow complete filling of fibers from a specific source, could distinguish between afferents and efferents and clarified that afferents and efferents arrive at hair cells nearly simultaneously and that growth of afferents and efferents to outer hair cells is also tightly correlated in time [29]. Indeed, without filling fibers from their respective sources such a distinction would be impossible to make, as later markers making afferents and efferents distinct from one another are not present during the early sorting phase. More recent techniques using molecular approaches to label fibers have largely confirmed the earlier tract tracing data [30]. Moreover, the bilateral distribution of efferents was finally solved, when nerve fibers were found in mammals to project across the floor plate [31] and neurons were found to migrate across the floor plate in chicken [32].

The peripheral fiber-sorting problem of afferents and efferents found its match by the significant challenge to sort the projection pattern of afferents into the hindbrain. Using simple silver techniques or even Golgi staining did not allow detailing both the peripheral source of a given fiber (or fibers) and its central presentation. Different sources of afferents from vestibular and auditory endorgans, including the lateral line, were all believed to mingle in a large area called the acoustico-lateral (or octavo-lateral) area of

the hindbrain [33]. In contrast to these claims, Golgi staining already showed that the afferents of the cochlea ended in a topological fashion in the cochlear nuclei, projecting information from different parts of the cochlea (different sound frequencies) to different parts of the cochlear nuclei [12]. However, it took modern HRP tracing to demonstrate that afferents from different parts of the lateral-line and inner ear each ended in distinct and non-overlapping areas and that the lateral line system of many aquatic vertebrates consists of both mechanosensory and electrosensory modalities, each projecting into their own target area of the hindbrain [34, 35]. Another finding related to modern tracing techniques was the discovery that hair cells with opposite polarity are in general each connected to unique afferents that project to distinct areas of the hindbrain [36–38].

The gain of insights using modern tracing techniques should not be mistaken as an indication that our current techniques are not also prone to artifacts such as false positives and false negatives. Given the past history of misinterpretations based on technical limitations, one can only guess what might happen with our current “insights” once new techniques come on line. As with past techniques, the limits of current techniques and thus the interpretations of data based on the “truth” revealed by them need to be understood to avoid entering data into the literature that require corrections that could have been avoided with proper precautions. As we present the detailed protocols below for dextran amine and lipophilic dye tracings in the ear, we also present our rationale for doing things the way we propose, minimizing known problems with these techniques exemplified in current and past publications.

2 Materials

2.1 Laboratory Equipment

1. Stereomicroscope with light source (*see Note 1*).
2. Peristaltic pump with 24–30G needles for perfusion of mice starting at embryonic day (E) 12.5 (*see Note 2*).
3. Sylgard (Dow-Corning, Midland, MI) coated petri dishes (variable sizes depending on application) for dissections (*see Note 3*).
4. Fine forceps and Vannas scissors for the dissection (Geuder G-19775, Heidelberg, Germany) (*see Note 4*).
5. Sealable glass containers for tissue storage (variable sizes depending on size of tissue).
6. Compressstome (Precisionary Instruments, Greenville, NC) (*see Note 5*).

2.2 Chemicals for Dextran and Lipophilic Dye Tracing

1. NeuroVue dye (Molecular Targeting Technologies, West Chester, PA) (*see Note 6*).
2. 3000 Molecular weight Dextran amine dye (Life Technologies, Grand Island, NY).
3. Fixation solution consisting of 4 % PFA made in 1× PBS and 0.3 M sucrose to preserve extracellular space (*see Note 7*).
4. Glycerol for mounting media (*see Note 8*).
5. Glass slide and coverslips.
6. 0.5 M EDTA in water.
7. 70 % Ethanol in water.

3 Methods

3.1 Dye Labeling

3.1.1 Dextran Amine Dye Application in Live Animals

Two major techniques for neuronal tracing *in vivo* and in fixed tissue are dextran amine tract tracing [21, 35, 39, 40] and lipophilic dye tracing [41–43]. We will first describe the procedure for *in vivo* or *ex vivo* tract tracing (dextran amines) followed by the procedure for lipophilic dye tracing in aldehyde fixed tissue (NeuroVue).

All experiments with animals should be approved by the institute's IACUC according to the guidelines set forth by the NIH. Dextran amines were introduced in 1986 [39, 40] and are now available in colors tuned to all wavelengths compatible with confocal imaging and conjugated to various sized dextrans (*see Notes 9–11*).

1. Dissolve dextran amine crystals in a drop of water until you have a saturated solution. Allow the edges of the water drop to recrystallize.
2. Pre-load a tungsten needle with a small amount of dye by dragging it across the recrystallized edge. The amounts of dye on the tip can be varied by multiple sweeps through the partially crystallized fluid. We prefer to load the needle with a bolus of dye about two to four times the diameter of a tungsten needle.
3. Anesthetize animals with appropriate anesthesia. For mice isoflurane works well, and for amphibians we recommend 0.02 % Benzocaine.
4. Determine the area for dye application under a dissecting scope. Gently open up the tissue with vannas scissors to expose the neuronal population (brain applications) or nerve you want to label.
5. Make a cut/incision and use the tungsten needle to apply immediately the dye to the cut axons. Hold needle in place to let the dye dissolve for approximately 3–4 s and rinse the area with PBS multiple times to wash away all excess dye. Rapid application after nerve cutting and thorough washing are crucial steps that retain only dye diffused into severed fibers to

anterogradely, retrogradely, or transganglionically filled neurons.

6. Maintain the animals under a low dose of anesthesia while the dye diffuses or maintain ex vivo preparations in tissue culture medium [44, 45]. 3000 molecular weight dextran amine dyes diffuse at a rate of 2 mm/h at room temperature but the quality of labeling falls off steeply over distance. We do not exceed 3 h (or approximately 6 mm) to reliably label nearly all cut nerve fibers [32] (*see Note 12*).
7. Fully anesthetize, then perfuse the animal transcardially with fixation solution. Use immersion for small animals, such as *Xenopus* larvae or ex vivo preparations (*see Note 13*).
8. Prepare tissue as whole mounts [46] or sections using various embedding techniques, including methacrylate embedding [47].

3.1.2 NeuroVue Application in Fixed Tissue

NeuroVue dyes come in various colors suitable for all confocal laser wavelengths and allow, if combined with two photon microscopy, the segregation of up to six different colors for distinct labeling (Figs. 1, 2, 3, 4, 5, and 6) [41].

1. Animals/tissue should be transcardially perfused with fixation solution and allowed to incubate in fixation solution at 4 °C for a minimum of 24 h (*see Note 13*).
2. Determine a dye application site to selectively label the neuronal population under consideration using a dissecting scope (*see Note 14*).
3. Apply dye as far from the area of interest as possible (1–2 mm). Choose a site where other neuronal populations will not project to as the neuronal population under consideration. A good understanding of neuroanatomy helps in this process (*see Note 14*).
4. Cut the pre-loaded NeuroVue dye filter strips into appropriately sized triangular pieces with vannas scissors. The optimal size will be as small of a piece as possible, to avoid labeling other structures, while remaining large enough to label the population of interest and not become dislodged. The scissors used to cut the dye need to be rinsed in alcohol to remove dye residue and need to be clean of alcohol when cutting (70 % EtOH in water). This eliminates unintended contamination of tissue/cells with dye (*see Note 15*).
5. When inserting into soft tissue, such as the brain, we recommend to directly insert the filter using a point of the filter cut in a triangle to pierce the tissue (Fig. 1). This ensures the dye contacts all intended structures. For more rigid tissues, we suggest making an incision with scissors. Do not use a dissecting needle or other apparatus to push filter into tissues as this inad-

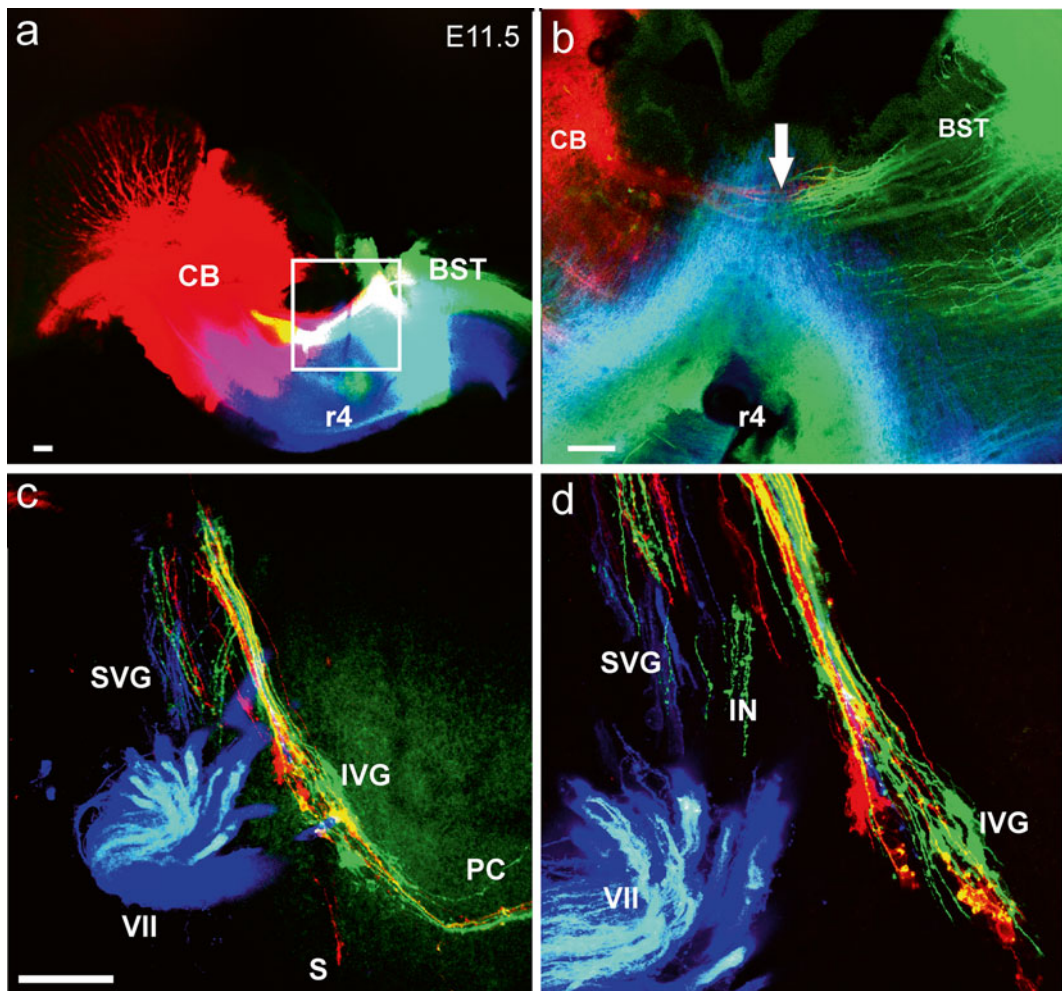


Fig. 1 Early growth of afferents and efferents to the ear. Top images (**a, b**) show the injection sites of three different lipophilic dyes into the hemisected brainstem of an 11.5-day-old mouse embryo. *Green* is NeuroVue Jade, *red* is NeuroVue Orange, *blue* is NeuroVue Maroon. Square in (**a**) indicates position of (**b**). Note how brainstem (BST) and cerebellar (CB) afferents enter the VIII nerve (arrow in **b**). The whole-mounted ear (**c, d**) shows afferents filled from the cerebellum and brainstem (*red* and *green*) as well as efferents (*blue* to extend toward the targets). The higher power image shows the segregation of different vestibular ganglion neurons. *IVG* inferior vestibular ganglion, *PC* posterior canal crista, *S* saccule, *SVG* superior vestibular ganglion, *VII* facial nerve, *r4* rhombomere 4. Bar indicates 100 μ m. Modified after [38]

vertently leads to unintended labeling. For very small applications, we recommend compressing the filter wedge with forceps, to make the tip even sharper and the application site smaller.

6. Place the specimens in a securely closed vial with 4 % PFA and incubate at $\sim 36\text{--}65$ °C in the dark for 2–7 days, depending on

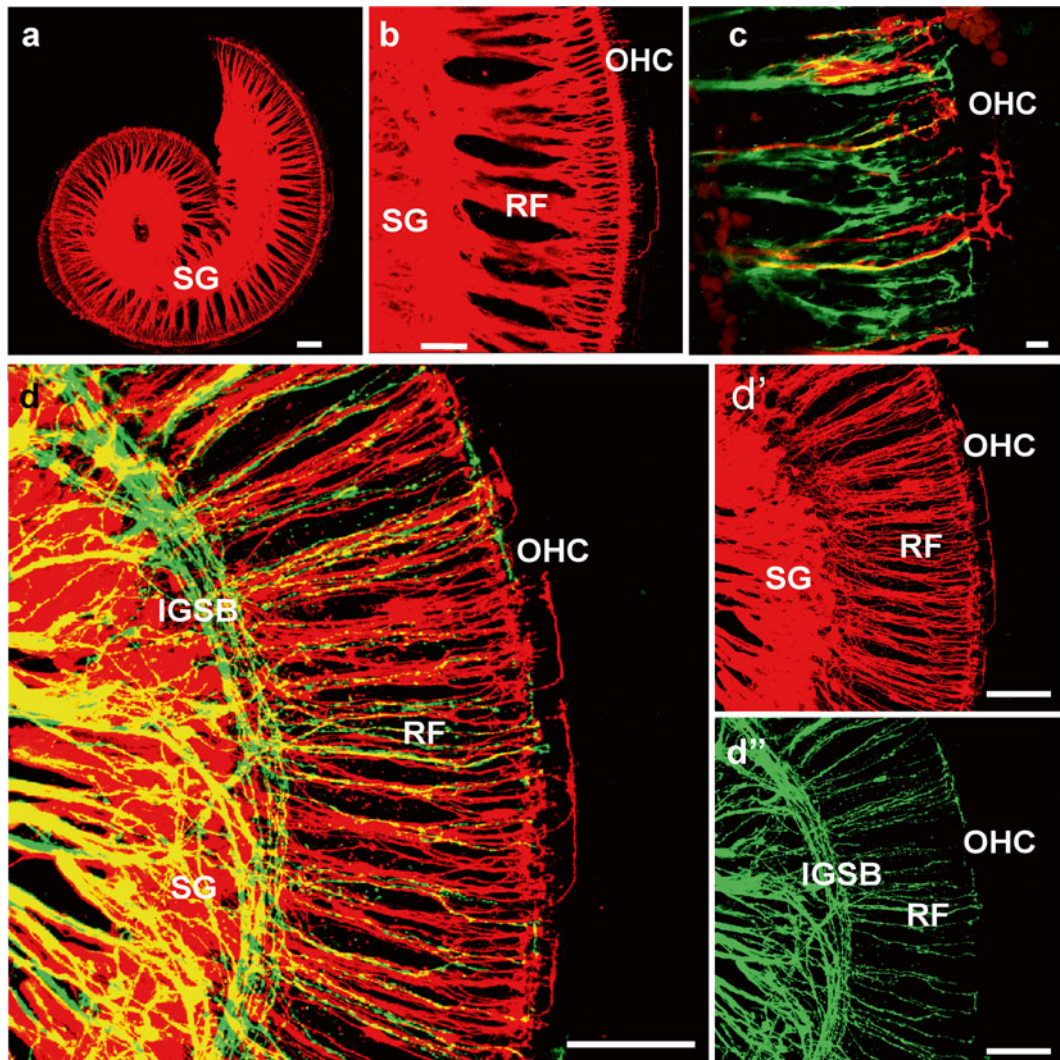


Fig. 2 Dye labeling of afferent and efferent fiber to the organ of Corti after central applications to cochlear nuclei (NeuroVue Orange, red) and crossing efferent fibers (NeuroVue Maroon, green). Whole mounted in glycerol and viewed within 1 h after mounting. (a, b) Single and (c, d) double labeling of afferents (red) and efferents (green) to the organ of Corti of a newborn mouse. Labeled spiral ganglion neurons (SG) send radial fibers (RF) to reach the IHC region with few fibers expanding to OHC. Efferents form intraganglionic spiral bundle (IGSB), join radial fibers and reach to IHC but only rarely to OHC. Bar = 100 μm in (a, b, d) 10 μm in (c). Modified after [23, 29]

age and diffusion distance to be covered (~2 mm per day at 65 °C). Elevated temperatures accelerate diffusion but also risk unusual labeling as membranes become unstable. We recommend parafilm to seal the container.

7. Verify that the dye has diffused to the desired location, and dissect out tissue of interest, using a dissecting scope with epifluorescence (*see Note 16*).

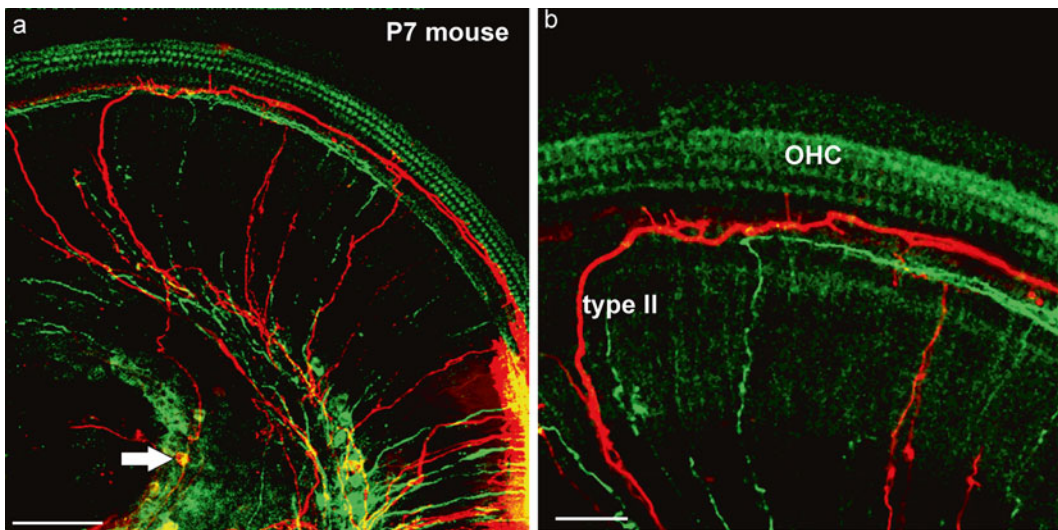


Fig. 3 Dye labeling of afferents and efferents using peripheral applications. Two different lipophilic dyes (green, red) (a) were inserted next to each other in the dissected apex of a 7-day-old mouse. Note that both green and red (arrow) spiral ganglion cells are labeled next to the injection site (lower right in a). Two type II afferents are filled toward the apex before the turn into radial fibers and reach the spiral ganglion neurons (arrow in a). (b) The higher power image shows the fine branches emanating from type II fibers to reach the area of inner hair cells. Bar equals 100 µm in (a), 50 µm in (b). Modified after [65]

8. Whole mount the specimen on a slide with glycerol and cover-slip for imaging with a confocal microscope (see Note 17). If tissue is too large to be mounted on a slide, either remove extraneous tissue or section tissue.
9. We found that sectioning with the compresstome leads to better results compared to vibratomes. However, both are suitable techniques to obtain thick (100–200 µm) sections.
10. Mount sections with spacers to avoid compression in 100 % glycerol. Our experience with other mounting media has been negative, except for Moviol.
11. Stay alert about future developments in tract tracing techniques using modern molecular approaches (see Note 18).

3.2 3-Dimensional Reconstruction

Tissues labeled with either dextran amine or lipophilic dyes or by immunohistochemistry can be subjected to 3-dimensional (3D) reconstruction of the confocal images obtained as described in [46, 48].

1. Perform dye tracing following protocols outlined above.
2. Decalcify tissue in ethylenediaminetetraacetic acid (EDTA) if bone is present.
3. Mount tissue in a clearing solution or glycerol. Use spacers or vacuum grease so that the tissue is not compressed and obtain confocal images.

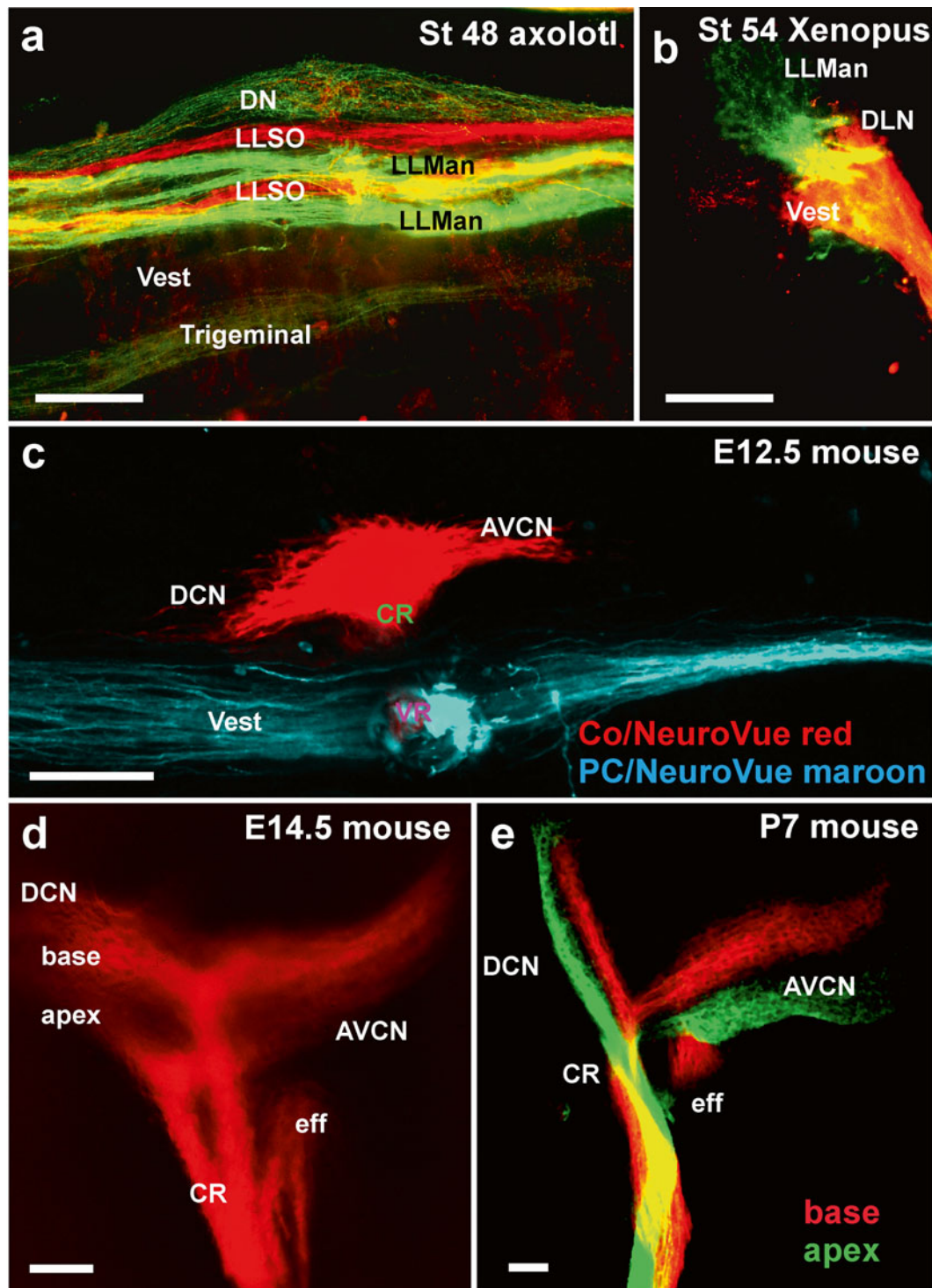


Fig. 4 Afferent projections revealed by dextran amine and lipophilic dye tracing. **(a, b)** Dextran amine can be used effectively to trace different sensory organ innervation to their CNS target. The axolotl brainstem shows the termination of mandibular (LLMan) and supraorbital (LLSO) afferents in two distinct fascicles that may represent the different hair cell polarity. In contrast, afferents from the electroreceptive ampullary organs

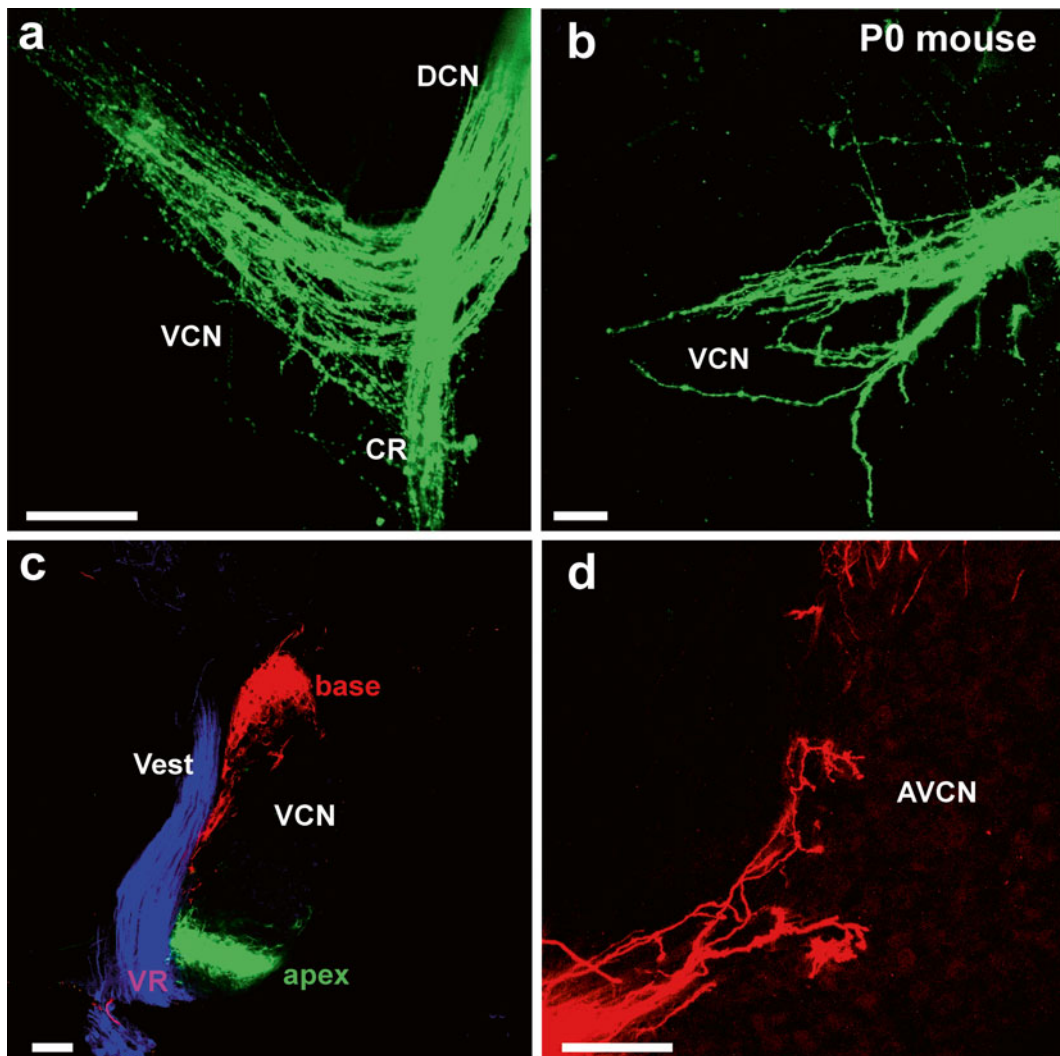


Fig. 5 Details of afferents to cochlear nuclei revealed in (a, b) whole mounts and (c, d) sections. Lipophilic dyes can reveal the pattern of innervation of cochlear afferents and deviations from normal projections in mutant mice (a, b) or can be used in vibratome sections (c) to show the segregation of basal, apical, and vestibular projections to the cochlear nucleus and the nearby vestibular nucleus. (d) Higher magnifications show the Golgi-like filling of afferents beginning to form endbulbs of Held. *AVCN* anteroventral cochlear nucleus, *CR* cochlear root, *VCN* ventral cochlear nucleus, *Vest* vestibular nucleus, *VR* vestibular root. Bar equals 100 μm . Modified after [67]

←
Fig. 4 (Continued) terminate overlappingly in the dorsal nucleus (DN). Frogs do not have electroreception and their lateral line projections are segregated from vestibular (Ves) and auditory projections to the dorsolateral auditory nucleus (DLN). (c) Inner ear fibers are segregated for the vestibular and cochlear afferents as early as E12.5. (d, e) Already at E14.5 the basal and apical area of the cochlea project into distinct fascicles, which can also be labeled with different colored dyes. *AVCN* anteroventral cochlear nucleus, *CR* cochlear root, *eff* efferent fibers; *DCN* dorsal cochlear nucleus, *DLN* dorsolateral nucleus. Bar equals 100 μm , modified after [35, 66]

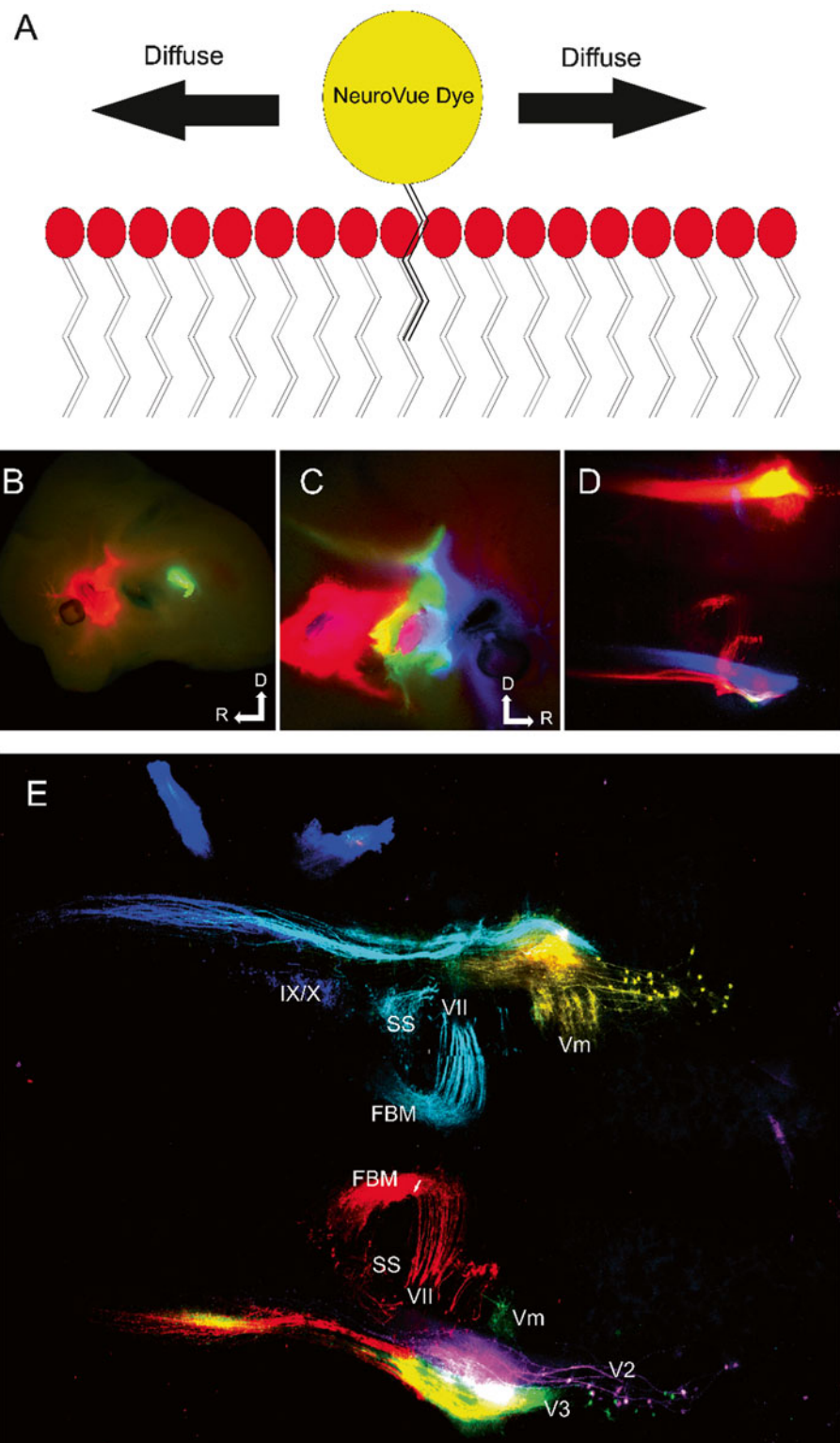


Fig. 6 Dye diffusion and six-color labeling of NV-labeled cranial nerve distribution in hindbrain. **(a)** Drawing of how NeuroVue labels neurons. When the dye is added to the neuronal membrane, lipophilic chains on the

4. Load the confocal file into Amira, Imaris, or similar 3D reconstruction software programs and manually segment the area(s) of interest to create a 3D rendering of the dye or immunohistochemistry stain.

4 Notes

1. We strongly recommend a stereoscope with epifluorescent capacity to take images of application sites for documentation purposes. It is also advantageous to use an epifluorescent dissection scope for checking the diffusion of the dyes. After diffusion we recommend using confocal microscopy for image acquisition.
2. In our experience the tissue preparation using transcardial perfusion is so far superior to immersion fixation that we strongly recommend the former approach.
3. There are multiple ways to work with tissue, but we find sylgard-covered Petri dishes the easiest way to manipulate embryos or to cut dye wavers without dulling sharp and/or pointed tools.
4. There are many suppliers on the market, but we found that the Geuder forceps and scissors are most useful for our techniques.
5. We obtained better sections of fresh tissue with the compresstome compared to traditional vibratome sections. We do not recommend embedding tissue in any organic solvent to allow infiltration with wax, as this will invariably lead to a reduction in clarity of labeling and individual fibers will only be visible in a halo of washed out lipophilic dye. However, fixable dextran amines can be processed by these means or even methacrylate embedding without much negative effects.

Fig. 6 (continued) fluorophore become lodged within the lipid bilayer. Through Brownian motion and diffusion gradients the dye is able to diffuse through the bilayer along the entire neuron. The entire cell can be visualized, because the dyes do not rely on actin or subcellular structures. (b) E12.5 mouse showing dye injection sites of NVO (red), NVB (non-fluorescent), and PTIR334 (green) labeling trigeminal (V), facial (VII) and glossopharyngeal/vagal (IX/X), respectively. Dorsal is up and rostral is to the left. (c) Opposite side of same mouse in (b) showing dye injections NVM (blue), NVJ (green), NVR (red) labeling the maxillary branch of trigeminal (V2), mandibular branch of trigeminal (V3) and facial nerves (VII), respectively. Dorsal is up and rostral is to the right. (d) Hindbrain of same mouse in (b) and (c) imaged, using conventional epifluorescence to visualize the central projections of labeled nerves. With conventional Texas red (566 nm), fluorescein (488 nm), and Cy5 (625 nm) filter cubes, NVO and NVR cannot be distinguished, PTIR334 and NVJ cannot be distinguished, and NVB cannot be imaged. (e) Confocal of same hindbrain shown in (d); NVO, (yellow), NVB (cyan), PTIR334 (blue), NVM (magenta), NVJ (green) and NVR (red). Modified after [41]

6. Since the dyes are photosensitive, store them in a cool dark area in their original package to minimize exposure to light and air.
7. It is paramount to keep in mind that there is no easy way to avoid shrinking of the extracellular space with concomitant expansion of neurons [49], leading to rupture of the surrounding lipid bilayers of neurons. We highly recommend adding sucrose (0.3 M) to the perfusion to avoid excessively shrinking the extracellular space at the expense of neuron expansion [50, 51]. Increasing the concentration of PFA up to 10 % works also to fully preserve membranes and avoid any diffusion of lipophilic dyes out of ruptured membranes, as typically obtained with simple perfusion and most notably with immersion. If immersion is necessary, a 1 min pretreatment with 0.3 M sucrose followed by fixation in 4 % PFA is paramount to reduce membrane disruptions due to neuronal swelling [51].
8. We have used glycerol extensively in the past and have non-recommendable experiences with some of the more recent clearing agents. It is important to realize that lipophilic dyes will diffuse out of membranes as membrane lipids are dissolved in organic clearing agents leading to a blurred appearance of nerve fibers [52] instead of the detailed fiber imaging possible when avoiding organic solvents [53, 54]. A good overview of modern clearing agents was recently published [55] that appears to work better than most other recently proposed clearing agents, including preservation of membranes for electron microscopy. In our hands, it leads to rapid loss of lipophilic dyes.
9. Injection of dextran amines has the risk of dye expansion away from the injection site and this needs to be checked to guess the effective uptake area of dextran amines [56]. If at all possible, we suggest using a topical application rather than injections, to increase non-vesicular Golgi-like filling of fibers and neurons predominantly through passive dye diffusion along the concentration gradient inside the cell both retrograde and anterograde. It has been suggested that this procedure resembles chromatography, likely because sugar residues abound on the outside of cells slowing down diffusion relative to the inside of neurons [21].
10. Dextran amines diffuse only in live tissue [21] with a speed that depends on their molecular weight, but are also actively transported in vesicles in live tissue [56]. Labeling with dextran amines, therefore, needs to be conducted prior to any fixation either in vivo or as ex vivo explants such as the ear. The latter is possible simply because decay of tissue can be slower than filling with dextran amines under favorable circumstances, but care must be taken to avoid artifacts. The diffusion time of different dextran amines are directly related to their molecular

weight [21] and should be taken into consideration when labeling neuronal populations as nerves are only viable after severance for a few hours in ex vivo preparations. Dextran amines can be effectively used for ex vivo tracing [39, 45] or in live embryos [35, 57], but care needs to be taken to avoid technical artifacts such as partial or incomplete filling of neurons and processes. If properly controlled, such an artifact of differential filling can be used to highlight specific fiber types over others in the developing cochlea [44]. However, we strongly recommend to carefully compare such data with other tracing data using different techniques such as lipophilic dyes in fixed tissue [23], to verify data generated by ex vivo dextran amine tracing.

11. Instead of fluorescent dyes, the use of biocytin as a tracer is also possible. However, while biocytin is certainly small enough to fill even the tiniest branch of a neuron, it has one disadvantage compared to fluorescent dextran amines: it requires visualization using the high affinity of streptavidin to biotin. Streptavidin, when conjugated to HRP, is a very large molecule that cannot easily be used for whole mount staining. Larger molecular weight dextran amines are not recommended as they tend to label only larger caliber fibers and cells, much like HRP [21]. Smaller molecules such as rhodamine can also be used but are difficult to fix and can pass through disrupted neuronal membranes, in particular in ex vivo preparations, leading to false positive labeling.
12. Viability of the tissue for proper diffusion with or without transport is crucial. Do not attempt to label long distances in ex vivo fibers. Even labeling of a subpopulation is suspect of being incomplete in analogy with the Golgi technique that labeled only 1 % of neurons. As with Golgi staining, those fibers labeled tend to be completely labeled thus generating no indication of a labeling problem. Since ex vivo preparations can have a differential effect on viability and filling of different fiber types, compare the data to those derived from other techniques to verify the conclusions.
13. For transcardial perfusion, a syringe can be used; however, utilizing a small peristaltic pump with appropriately sized needles is preferred, to maintain a constant pressure as recommended [51]. For best results in all portions of this protocol, the perfusion fixation step should be performed. For example, we perfuse mice starting with E12.5 and older. The tissue can be stored in 4 % PFA at 4 °C for 1 day to 6 months as long as exposure to bright light is avoided. Dextran amines remain stable after fixation, but can be bleached and are difficult to use in thick brain tissue or whole mount (due to lower fluorescence intensity), in particular when using 488 nm excitable

dyes that are within the range of tissue autofluorescence. We do not recommend combining them with gluteraldehyde fixation, as this increases the fluorescence of the tissue dramatically, essentially wiping out the contrast.

14. Like other lipid tracers such as DiI and related substances, Neurovue fills entire neurons from an application site through its membranes (Fig. 6) by passive diffusion within the lipid bilayer surrounding each intact neuron. It is therefore paramount that the neuronal anatomy is fully understood in terms of background of connections, in order to place the dye on the most appropriate nerve for a given analysis [41]. Placing a dye too close to the desired imaging location results in both lateral diffusion of the dye, causing labeling of unwanted cell types and uneven fluorescence along the neuronal tract. Extract all extraneous tissue for good visualization of the chosen site for dye placement. However, some surrounding tissue may need to be kept to stabilize the inserted dye, and to make sure the dye does not become physically dislodged. If labeling two separate neuronal populations with different dyes, the placement of the dyes can be sequentially staggered if diffusion differences vary. It is important to realize that axonal and dendritic filopodia can extend for 100 µm or more with limited content of small actin bundles that are difficult to image in whole-mounted tissue [58]. Using lipophilic dyes easily allows imaging of structures such as filopodia, even in whole-mounted cochlea (Figs. 1, 2, and 3), or studying the transformation of growth cones into synapses in whole-mounted or sectioned cochlear nuclei (Figs. 4 and 5).
15. It may be beneficial to use forceps to compress the dye filter strips, if they are too thick for the application, as this enhances the rigidity of the filter for easy piercing of the tissue. We do not recommend the use of crystals for these applications, as even the smallest amount of crystal can easily lead to unintended labeling of fiber, thus ruining the preparation. In particular, when using mutant mouse tissue, we do not recommend using crystals because of possible artifacts that could lead to misinterpretation, such as alleged mis-wiring that may be related to inadvertent labeling with small crystals. It is absolutely essential, in our hands, to take images of the application site at the time of application as well as after completion of the diffusion, to make sure that the intended application is indeed what was labeled (Fig. 1). Excellent data for controlling application problems are provided in several publications [54, 59]. Failing to provide images of application sites should result in rejection of papers by reviewers, in particular if aberrant wiring in the ear is claimed without being demonstrated, as we did in several of our papers [53, 59].

16. Visualizing dye diffusion with epifluorescence will underestimate the diffusion of the dye seen with a confocal microscope, which is much more sensitive. Usually visualization of 50–75 % of the desired diffusion length will indicate the dye diffused to the area of interest to be imaged by confocal microscopy. If dye is allowed to diffuse until it can be visualized with epifluorescence at the area of interest, there will be quenching when using confocal imaging.
17. Confocal settings can be gleaned from the information supplied with the dye or as described previously [41].
18. Future directions—Tract tracing will always be used as a simple way to analyze mutant phenotypes or normal development without the need to do additional breeding, as is required with other techniques such as BRAINBOW [60] or CONFETI [61]. However, several new techniques are in the making that can potentially help to detail some of the open issues related to the development of fiber connections with hair cells. Cre-induced expression of various protein markers is a technique [30] that has recently been replaced by a next generation of fluorescent proteins that allow multicolor labeling [62], as demonstrated here with dextran amines and lipophilic dyes (Figs. 1 and 6). These approaches can be combined with high-resolution EM imaging, to obtain complete information about connections at the synaptic level [63], using correlated light and electron microscopy [64].

Acknowledgements

Confocal images were obtained at the University of Iowa Carver Center for Imaging. We thank the Office of the Vice President for Research (OVPR), University of Iowa College of Liberal Arts and Sciences (CLAS), and the P30 core grant for support (DC 010362). This work was in part supported by a NASA base grant (Bernd Fritzsch) and 1R43GM108470-01 (Gray, Fritzsch).

References

1. Retzius G (1881) Über die peripherische Endigungsweise des Gehörnerven. Biologische Untersuchungen 3:1–51
2. Ramón y Cajal S (1906) In: Nobel lectures, physiology or medicine 1901–1921
3. Golgi C (1906) The neuron doctrine: theory and facts. Nobel Lecture 1921:190–217
4. Retzius G (1881) Das Gehörorgan der Fische und Amphibien. Samson & Wallin, Stockholm
5. Kersigo J, Fritzsch B (2015) Inner ear hair cells deteriorate in mice engineered to have no or diminished innervation. *Front Aging Neurosci* 7:33
6. Fritzsch B, Wake M (1988) The inner ear of gymnophione amphibians and its nerve supply: a comparative study of regressive events in a complex sensory system (Amphibia, Gymnophiona). *Zoomorphol* 108(4):201–217

7. Sarasin P, Sarasin F (1888) Zur Entwicklungsgeschichte und Anatomie der ceylonesischen Blindwühle *Ichthyophis glutinosus*. Das Gehörorgan. Ergebnisse Naturwiss Forsch auf Ceylon, Bd 2. Kreidels Verlag, Wiesbaden
8. Sarasin P, Sarasin F (1892) Über das Gehörorgan der Caeciliiden. Anat Anz 7: 812–815
9. Retzius G (1891) Das Gehörorgan von caecilia annulata. Anat Anz 6:82–86
10. Ramón y Cajal S (1995) Histology of the nervous system of man and vertebrates, vol 1. Oxford University Press, New York, USA
11. Lorent De No R (1981) The primary acoustic nuclei. Raven Press, New York
12. Lorente de No R (1937) The sensory endings in the cochlea. Laryngoscope 47:373–377
13. Rasmussen GL (1946) The olfactory peduncle and other fiber projections of the superior olfactory complex. J Comp Neurol 84(2): 141–219
14. Rasmussen GL (1953) Further observations of the efferent cochlear bundle. J Comp Neurol 99(1):61–74
15. Brown M, Pierce S, Berglund A (1991) Cochlear-nucleus branches of thick (medial) olivocochlear fibers in the mouse: a cochaleotopic projection. J Comp Neurol 303(2): 300–315
16. Hillman DE (1969) Light and electron microscopical study of the relationships between the cerebellum and the vestibular organ of the frog. Exp Brain Res 9(1):1–15
17. Strutz J, Schmidt CL, Stürmer C (1980) Origin of efferent fibers of the vestibular apparatus in goldfish. A horseradish peroxidase study. Neurosci Letts 18(1):5–9
18. Roberts BL, Meredith GE (1992) The efferent innervation of the ear: variations on an enigma. In: DB Webster, RR Fay, AN Popper. The evolutionary biology of hearing. Springer, New York, pp 185–121
19. Fritzsch B, Wahnschaffe U (1987) Electron microscopical evidence for common inner ear and lateral line efferents in urodeles. Neurosci Letts 81(1):48–52
20. Sienknecht UJ, Köppl C, Fritzsch B (2014) Evolution and development of hair cell polarity and efferent function in the inner ear. Brain Beh Evol 83(2):150–161
21. Fritzsch B (1993) Fast axonal diffusion of 3000 molecular weight dextran amines. J Neurosci Meth 50(1):95–103
22. Hellmann B, Fritzsch B (1996) Neuroanatomical and histochemical evidence for the presence of common lateral line and inner ear efferents and of efferents to the basilar papilla in a frog, *Xenopus laevis*. Brain Beh Evol 47(4):185–194
23. Simmons D, Duncan J, de Caprona DC, Fritzsch B (2011) Development of the inner ear efferent system. In: DK Ryugo, RR Fay, AN Popper. Auditory and vestibular efferents. Springer, New York, pp 187–216
24. Yang T, Bassuk AG, Stricker S, Fritzsch B (2014) Prickle1 is necessary for the caudal migration of murine facial branchiomotor neurons. Cell Tissue Res 357(3):549–561
25. Poljak S (1927) Über den allgemeinen Bauplan des Gehörsystems und über seine Bedeutung für die Physiologie, für die Klinik und für die Psychologie. Zeitschrift für die gesamte Neurologie und Psychiatrie 110(1):1–49
26. Echteler SM (1992) Developmental segregation in the afferent projections to mammalian auditory hair cells. Proc Natl Acad Sci U S A 89(14):6324–6327
27. Bulankina A, Moser T (2012) Neural circuit development in the mammalian cochlea. Physiology 27(2):100–112
28. Sobkowicz HM, August BK, Slapnick SM (2004) Synaptic arrangements between inner hair cells and tunnel fibers in the mouse cochlea. Synapse 52(4):299–315
29. Fritzsch B, Dillard M, Lavado A, Harvey NL, Jahan I (2010) Canal cristae growth and fiber extension to the outer hair cells of the mouse ear require Prox1 activity. PLoS One 5:e9377
30. Koundakjian EJ, Appler JL, Goodrich LV (2007) Auditory neurons make stereotyped wiring decisions before maturation of their targets. J Neurosci 27(51):14078–14088
31. Cowan CA, Yokoyama N, Bianchi LM, Henkemeyer M, Fritzsch B (2000) EphB2 guides axons at the midline and is necessary for normal vestibular function. Neuron 26(2): 417–430
32. Fritzsch B, Christensen M, Nichols D (1993) Fiber pathways and positional changes in efferent perikarya of 2.5-to 7-day chick embryos as revealed with dil and dextran amine. J Neurobiol 24(11):1481–1499
33. Ayers H, Worthington J (1908) The finer anatomy of the brain of *Bdellostoma dombeyi*. I. The acoustico-lateral system. Am J Anat 8(1):1–16
34. Fritzsch B (1981) The pattern of lateral-line afferents in urodeles. Cell Tissue Res 218(3): 581–594
35. Fritzsch B, Gregory D, Rosa-Molinar E (2005) The development of the hindbrain afferent

- projections in the axolotl: evidence for timing as a specific mechanism of afferent fiber sorting. *Zoology* 108(4):297–306
36. Fritzsch B (1981) Electoreceptors and direction specific arrangement in the lateral line system of salamanders? *Zeitschrift für Naturforschung C* 36(5–6):493–496
 37. Maklad A, Kamel S, Wong E, Fritzsch B (2010) Development and organization of polarity-specific segregation of primary vestibular afferent fibers in mice. *Cell Tissue Res* 340(2):303–321
 38. Fritzsch B, López-Schier H (2014) Evolution of polarized hair cells in aquatic vertebrates and their connection to directionally sensitive neurons. In: H Bleckmann, J Mogdans, SL Coombs. *Flow sensing in air and water*. Springer, New York, pp 271–294
 39. Glover J (1995) Retrograde and anterograde axonal tracing with fluorescent dextran-amines in the embryonic nervous system. *Neurosci Prot* 30:1–13
 40. Fritzsch B, Wilm C (1990) Dextran amines in neuronal tracing. *Trends Neurosci* 13(1):14
 41. Tonniges J, Hansen M, Duncan J, Bassett MJ, Fritzsch B, Gray BD, Easwaran A, Nichols MG (2010) Photo- and bio-physical characterization of novel violet and near-infrared lipophilic fluorophores for neuronal tracing. *J Microsc* 239(2):117–134
 42. Godement P, Vanselow J, Thanos S, Bonhoeffer F (1987) A study in developing visual systems with a new method of staining neurones and their processes in fixed tissue. *Development* 101(4):697–713
 43. Wilm C, Fritzsch B (1992) Ipsilateral retinal projections into the tectum during regeneration of the optic nerve in the cichlid fish *Haplochromis burtoni*: a dil study in fixed tissue. *J Neurobiol* 23(6):692–707
 44. Huang L-C, Thorne PR, Housley GD, Montgomery JM (2007) Spatiotemporal definition of neurite outgrowth, refinement and retraction in the developing mouse cochlea. *Development* 134(16):2925–2933
 45. Bleckmann H, Niemann U, Fritzsch B (1991) Peripheral and central aspects of the acoustic and lateral line system of a bottom dwelling catfish, *Ancistrus* sp. *J Comp Neurol* 314(3):452–466
 46. Elliott KL, Houston DW, DeCook R, Fritzsch B (2015) Ear manipulations reveal a critical period for survival and dendritic development at the single-cell level in Mauthner neurons. *Dev Neurobiol*. doi:[10.1002/dneu.22287](https://doi.org/10.1002/dneu.22287)
 47. Fritzsch B, Northcutt R (1992) A plastic embedding technique for analyzing fluores-
 - cent dextran-amine labelled neuronal profiles. *Biotech Histochem* 67(3):153–157
 48. Kopecky BJ, Duncan JS, Elliott KL, Fritzsch B (2012) Three-dimensional reconstructions from optical sections of thick mouse inner ears using confocal microscopy. *J Microsc* 248(3):292–298
 49. Thorne RG, Nicholson C (2006) In vivo diffusion analysis with quantum dots and dextrans predicts the width of brain extracellular space. *Proc Natl Acad Sci U S A* 103(14): 5567–5572
 50. Fritzsch B (1979) Observations on degenerative changes of Purkinje cells during early development in mice and in normal and otocyst-deprived chickens. *Anat Embryol* 158(1):95–102
 51. Cragg B (1980) Preservation of extracellular space during fixation of the brain for electron microscopy. *Tissue Cell* 12(1):63–72
 52. Lu CC, Cao X-J, Wright S, Ma L, Oertel D, Goodrich LV (2014) Mutation of Npr2 leads to blurred tonotopic organization of central auditory circuits in mice. *PLoS Genetics* 10(12), e1004823
 53. Jahan I, Kersigo J, Pan N, Fritzsch B (2010) Neurod1 regulates survival and formation of connections in mouse ear and brain. *Cell Tissue Res* 341(1):95–110
 54. Maklad A, Fritzsch B (2003) Partial segregation of posterior crista and saccular fibers to the nodulus and uvula of the cerebellum in mice, and its development. *Dev Brain Res* 140(2):223–236
 55. Costantini I, Ghobril J-P, Di Giovanna AP et al (2015) A versatile clearing agent for multi-modal brain imaging. *Sci Rep* 5:9808
 56. Tsuriel S, Gudes S, Draft RW, Binshtok AM, Lichtman JW (2015) Multispectral labeling technique to map many neighboring axonal projections in the same tissue. *Nat Methods* 12(6):547–552
 57. Manns M, Fritzsch B (1991) The eye in the brain: retinoic acid effects morphogenesis of the eye and pathway selection of axons but not the differentiation of the retina in *Xenopus laevis*. *Neurosci Letts* 127(2):150–154
 58. Gehler S, Gallo G, Veien E, Letourneau PC (2004) p75 neurotrophin receptor signaling regulates growth cone filopodial dynamics through modulating RhoA activity. *J Neurosci* 24(18):4363–4372
 59. Pauley S, Lai E, Fritzsch B (2006) Foxg1 is required for morphogenesis and histogenesis of the mammalian inner ear. *Dev Dyn* 235(9):2470–2482
 60. Cai D, Cohen KB, Luo T, Lichtman JW, Sanes JR (2013) Improved tools for the Brainbow toolbox. *Nat Methods* 10(6):540–547

61. Abe T, Fujimori T (2013) Reporter mouse lines for fluorescence imaging. *Dev Growth Differ* 55(4):390–405
62. Viswanathan S, Williams ME, Bloss EB et al (2015) High-performance probes for light and electron microscopy. *Nat Methods* 12: 568–576
63. Mikula S, Denk W (2015) High-resolution whole-brain staining for electron microscopic circuit reconstruction. *Nat Methods* 12: 541–546
64. de Boer P, Hoogenboom JP, Giepmans BN (2015) Correlated light and electron microscopy: ultrastructure lights up! *Nat Methods* 12(6):503–513
65. Fritzsch B (2003) Development of inner ear afferent connections: forming primary neurons and connecting them to the developing sensory epithelia. *Brain Res Bull* 60(5): 423–433
66. Fritzsch B, Pan N, Jahan I, Elliott KL (2015) Inner ear development: building a spiral ganglion and an organ of Corti out of unspecified ectoderm. *Cell Tissue Res* 361:7–24
67. Maricich SM, Xia A, Mathes EL, Wang VY, Oghalai JS, Fritzsch B, Zoghbi HY (2009) Atoh1-lineal neurons are required for hearing and for the survival of neurons in the spiral ganglion and brainstem accessory auditory nuclei. *J Neurosci* 29(36):11123–11133

Chapter 15

Detection of Excitatory and Inhibitory Synapses in the Auditory System Using Fluorescence Immunohistochemistry and High-Resolution Fluorescence Microscopy

**Wibke Singer, Hyun-Soon Geisler, Rama Panford-Walsh,
and Marlies Knipper**

Abstract

In sensory systems, a balanced excitatory and inhibitory circuit along the ascending pathway is not only important for the establishment of topographically ordered connections from the periphery to the cortex but also for temporal precision of signal processing. The accomplishment of spatial and temporal cortical resolution in the central nervous system is a process that is likely initiated by the first sensory experiences that drive a period of increased intracortical inhibition. In the auditory system, the time of first sensory experience is also the period in which a reorganization of cochlear efferent and afferent fibers occurs leading to the mature innervation of inner and outer hair cells. This mature hair cell innervation is the basis of accurate sound processing along the ascending pathway up to the auditory cortex. We describe here, a protocol for detecting excitatory and inhibitory marker proteins along the ascending auditory pathway, which could be a useful tool for detecting changes in auditory signal processing during various forms of hearing disorders. Our protocol uses fluorescence immunohistochemistry in combination with high-resolution fluorescence microscopy in cochlear and brain tissue.

Key words Protein, Antibody, Immunohistochemistry, Fluorescence, Microscopy

1 Introduction

In the visual, somatosensory, olfactory, and auditory system, detection and identification of environmental stimuli depends on the developmental induction of intracortical inhibition (for review see [1]). Intracortical inhibition is partly induced by brain-derived neurotrophic factor (BDNF), which is released from pyramidal neurons and initiates the formation of inhibitory contacts of parvalbumin-expressing interneurons (basket cells), onto the somata of excitatory neurons (for review see [2–5]). This sharpening of spatial and temporal cortical resolution is likely initiated by the first

sensory experience, a commonality among sensory organs. In the auditory system, sensory input starts with hearing onset, which is around postnatal day 12 in rodents [6]. At this age, functionally relevant maturation steps occur in the cochlea, including the maturation of cholinergic and dopaminergic feedback from the olivary complex to inner and outer hair cells (IHCs, OHCs). In the immature state, spontaneous Ca^{2+} action potentials (APs) of IHCs are modified by olivocochlear efferent fibers, projecting from the medial portion of the superior olivary complex to the cochlea (for review *see* [7]). They remain in axosomatic contact with IHCs, until they are eliminated and IHCs are innervated mainly by afferent fibers, having few, if any, remaining efferent contacts [8]. One major modulator of these developmental changes in the organ of Corti is thyroid hormone (TH). TH drives the termination of Ca^{2+} APs, including the elimination of cholinergic axosomatic efferent contacts [9]. The mature cochlear afferent fibers are innervated by efferent axodendritic input, which can suppress or facilitate sound-evoked and spontaneous afferent activity through the release of inhibitory (GABA, glycine, dopamine) or excitatory (acetylcholine) transmitters [10–16]. Another TH dependent step is the upregulation of otoferlin, a C2-domain protein essential for IHC exocytosis by acting as a Ca^{2+} sensor in vesicle fusion [17–20]. The presynaptic vesicles of the IHC are tethered to so-called ribbons [21–24]. The presynaptic ribbon's role is proposed to support the continuous release of a high number of vesicles [25–27], enabling an extremely high rate of exocytosis through maintenance of a large readily releasable pool. This ensures the coding of sound intensity in postsynaptic neurons over a wide dynamic range [28, 29] and enables precise sound processing along the ascending auditory pathway [30]. For this reason, peripheral cochlear changes in signal transmission can lead to central compensation mechanisms, which might be related to an imbalance of excitation and inhibition, resulting in changes of central auditory plasticity (for review *see* [31–34]). These changes can be analyzed at the molecular level by studying the expression of marker proteins for excitatory or inhibitory neurons (e.g. glutamate transporters, parvalbumin) and markers for plasticity changes (e.g. activity-regulated cytoskeletal protein Arg3.1/arc).

We describe here our methodology of fluorescence immunohistochemistry including preparation of cochlear and brain tissue to visualize different marker proteins in the auditory system that can give insight into excitatory and inhibitory processes along the ascending auditory pathway [1, 32, 35]. At the level of the IHC, as shown in Fig. 1, the analyses of presynaptic ribbon structures (Fig. 1b, c) in combination with the postsynaptic marker parvalbumin (PV) (Fig. 1b), which labels postsynaptic swellings [36, 37], might give insight into a possible loss of synaptic contacts that are associated with hearing disorders [36]. Analyzing IHC ribbon

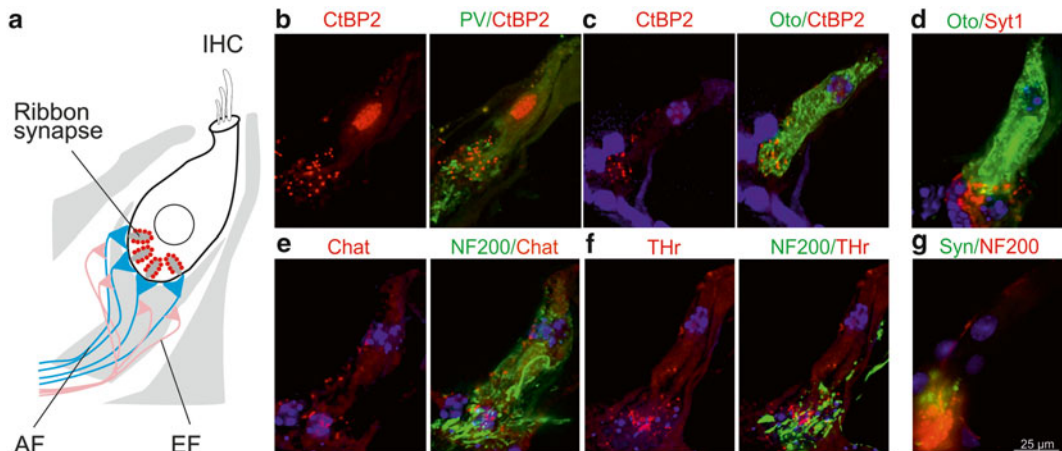


Fig. 1 Immunohistochemistry of the mouse inner ear. All images show inner hair cells (IHCs). **(a)** Cartoon of the IHC, including ribbon synapses (red dots) and afferent (AF, blue) and efferent (EF, pink) innervation. The supporting cells are delineated in grey. **(b)** CtBP2/RIBEYE immunostaining (red) labels presynaptic structures in the IHC, while parvalbumin staining (PV, green) labels postsynaptic regions. **(c)** CtBP2/RIBEYE immunostaining (red) labels presynaptic structures in the IHC, whereas staining for otoferlin (Oto, green) labels the IHC. **(d)** Immunostaining for otoferlin (Oto, green) labels the IHC and staining for synaptotagmin 1 (red) labels a presynaptic marker protein. **(e)** Immunostaining for NF200 (green) labels afferent fibers, while staining for cholinacetyltransferase (Chat, red) labels mature cholinergic efferent contacts. **(f)** Immunostaining for NF200 (green) labels afferent fibers and staining for tyrosinhydroxylase (THr, red) labels mature dopaminergic contacts. **(g)** Immunostaining for synaptophysin (Syn, green) labels efferent fibers, whereas staining NF200 (red) labels afferent fibers. Cell nuclei are counterstained with DAPI, scale bar = 25 μ m

structures in combination with otoferlin (Fig. 1c), which serves as a Ca^{2+} sensor for synaptic vesicle release at hair cell ribbon synapses [17, 18, 38], might give insight into the functionality of presynaptic structures [39]. Changes in postsynaptic structures (e.g., a reduced number of afferent fibers) can indicate alterations in hearing function. Therefore, neurofilament NF200 (Fig. 1e, f), a marker for afferent fibers [36], can be studied in combination with cholinacetyltransferase (Chat) (Fig. 1e), a marker for mature cholinergic input [7], tyrosinhydroxylase (THr) (Fig. 1f), a marker for dopaminergic nerve terminals [10], or synaptophysin (Fig. 1g), a marker for efferent fibers [40]. Alterations in these markers might point to changed cholinergic and dopaminergic feedback from the olivary complex or to developmental deficits which could lead to changed signal transmission [41].

In higher order auditory centers, such as the inferior colliculus (IC) (Fig. 2) or the auditory cortex (AC) (Fig. 3), neuronal markers for excitation and inhibition can be used to analyze probable imbalances of excitation and inhibition occurring, for example, during hearing disorders. In the IC, we show in Fig. 2a the combination of glutamate-decarboxylase (GAD67), a marker for

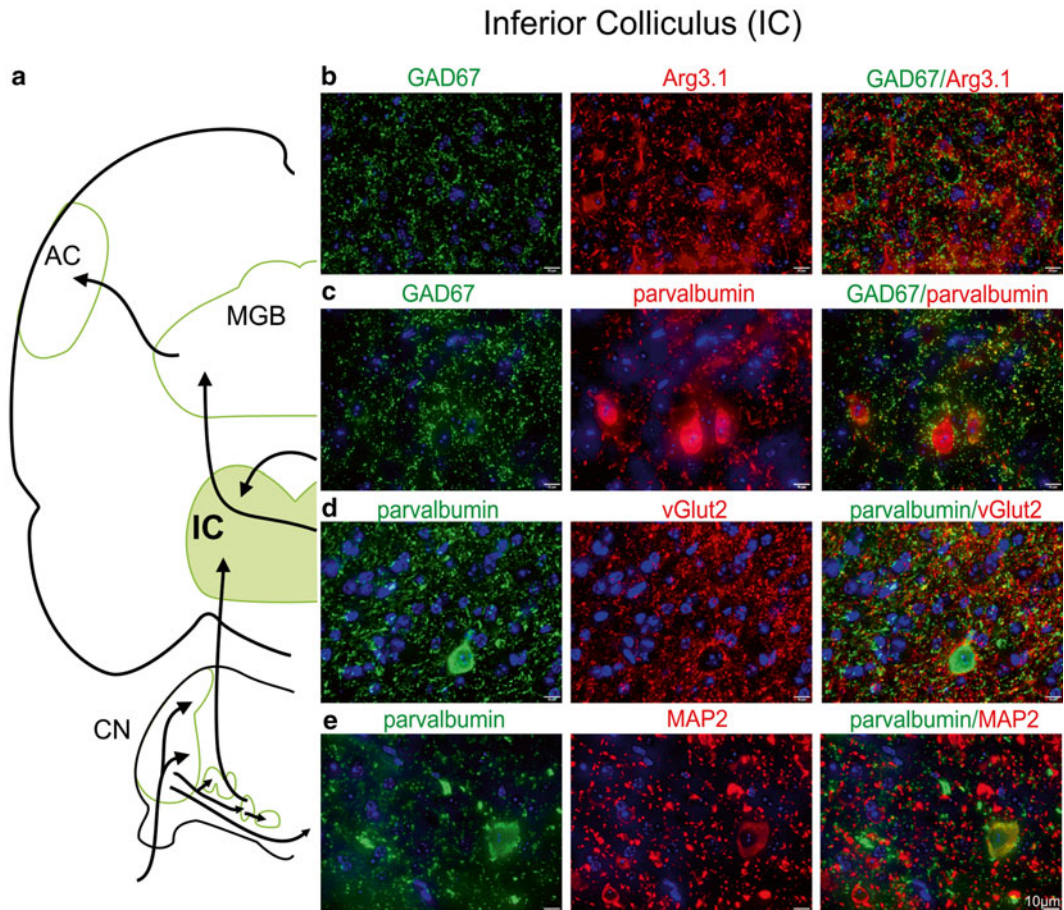


Fig. 2 Immunohistochemistry of the mouse inferior colliculus. **(a)** Cartoon of the ascending auditory pathway (black arrows) showing the cochlear nucleus (CN), the inferior colliculus (IC), the medial geniculate body (MGB), and the auditory cortex (AC). The IC is highlighted in green. **(b)** Immunostaining for GAD67 (green) labels GABAergic inhibitory neurons, whereas staining Arg3.1/arc (red) labels excitatory glutamatergic neurons. **(c)** Immunostaining for GAD67 (green) labels GABAergic inhibitory neurons, while staining parvalbumin (red) labels inhibitory interneurons. **(d)** Immunostaining for parvalbumin (green) labels inhibitory interneurons and vGlut2 (red) staining localizes to excitatory axon terminals. **(e)** Immunostaining for parvalbumin (green) labels inhibitory interneurons, whereas MAP2 (red) staining labels a neuronal marker protein. Cell nuclei are counter-stained with DAPI. Scale bar = 10 μm

inhibitory neurons [42], in combination with the activity regulated gene Arg3.1/arc, a marker for excitatory neurons [43] that was correlated with changes in central auditory activity [44–47]. GAD67 can also be co-stained with other inhibitory marker proteins, such as PV, shown in the IC (Fig. 2b) and AC (Fig. 3a), which is a marker for inhibitory interneurons [48] and is associated with perisomatic inhibition [49] and plasticity [50]. Another possibility is the costaining of GAD67 (Fig. 3c) with vGAT (Fig. 3c), a marker for GABAergic nerve endings [51].

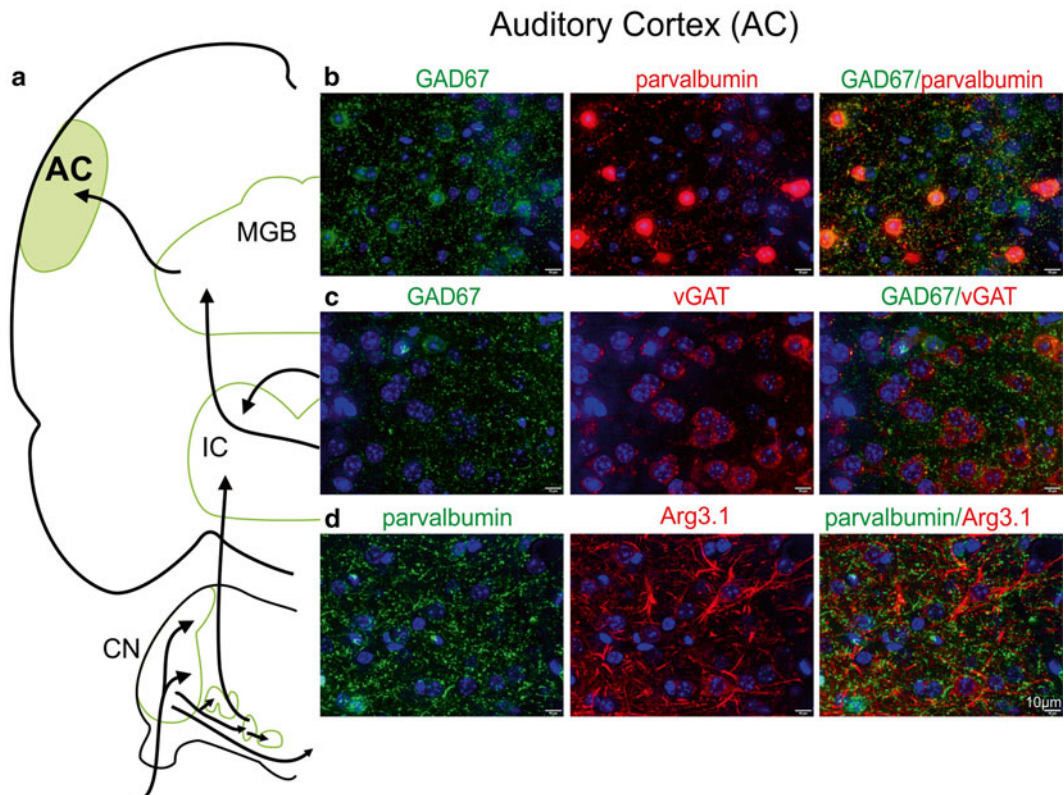


Fig. 3 Immunohistochemistry of the mouse auditory cortex. (a) Cartoon of the ascending auditory pathway (black arrows), showing the cochlear nucleus (CN), the inferior colliculus (IC), the medial geniculate body (MGB), and the auditory cortex (AC). The AC is highlighted in green. (b) Immunostaining for GAD67 (green) labels GABAergic inhibitory neurons, while parvalbumin (red) staining labels inhibitory interneurons. (c) Immunostaining for GAD67 (green) labels GABAergic inhibitory neurons, while vGAT (red) staining labels GABAergic nerve endings. (d) Immunostaining for GAD67 (green) labels GABAergic inhibitory neurons and Arg3.1/arc (red) staining labels excitatory glutamatergic neurons. Cell nuclei were counterstained with DAPI, scale bar = 10 μ m

PV (Fig. 2d) can be combined with markers for glutamatergic excitatory neurons such as vGlut2 (Fig. 2d), which is localized in excitatory axon terminals [52], and either Arg3.1/arc (Fig. 3c) or the neuronal marker protein MAP2 (Fig. 2d) [53]. All of these antibody combinations can illustrate alterations in excitation or inhibition on different cellular levels that in turn are likely associated with changes in signal transmission along the ascending auditory pathway. The pictures shown in Figs. 1, 2, and 3 show examples of antibody combinations in different tissues along the ascending auditory pathway. Readers may of course feel free to use other antibodies, to study other proteins and tissues of interest.

2 Materials

Prepare all solutions using ultrapure water, which is prepared by purifying deionized water to attain a sensitivity of $18\text{ M}\Omega\text{ cm}$ at $25\text{ }^{\circ}\text{C}$. Prepare and store all reagents at room temperature (RT) (unless otherwise indicated). Diligently follow all waste disposal regulations when disposing waste materials. All solutions should be autoclaved unless otherwise indicated. In addition, make sure that all experiments involving animals are in accordance with relevant guidelines and regulations.

2.1 Tissue Preparation (See Note 1)

All protocols using animals should be approved by the institutional animal care and use committee.

1. Tools for tissue preparation: Sharp scissors for decapitation, stable forceps to remove the skull, bended forceps to remove the whole brain, actuated tweezers to open the bulla and remove the cochlea.
2. Binocular microscope to visualize removing the cochlea from the bulla.

2.2 Tissue Fixation

1. $10\times$ Phosphate-Buffered Saline (PBS): Mix $0.5\text{ M Na}_2\text{HPO}_4$ ($2\text{H}_2\text{O}$), 1.5 M NaCl in 900 mL ultrapure water and adjust to pH 7.0 with HCl, then top-off to 1 L . For $1\times$ PBS dilute $10\times$ PBS in water.
2. $2\text{ \%}/4\text{ \%}$ Paraformaldehyde (PFA): Mix $20\text{ g}/40\text{ g}$ PFA in 900 mL $1\times$ PBS. Leave at $54\text{ }^{\circ}\text{C}$ in a water bath until the powder is completely dissolved (see Note 2). Adjust the volume to 1 L with $1\times$ PBS, prepare 50 mL aliquots and store at $-20\text{ }^{\circ}\text{C}$. Do not autoclave.
3. Rotating mixer.

2.3 Embedding Solution for the Cochleae

1. RDO: Rapid decalcifier (e.g., Apex Engineering Product Corporation, Aurora, IL).
2. 25 % Sucrose-Hanks solution: Dilute $10\times$ Hanks' balanced salt solution (HBSS), which is stored at $4\text{ }^{\circ}\text{C}$, with dd H_2O , to a 1:10 solution. Add 250 g sucrose to 1 L of $1\times$ HBSS, and store in aliquots of 15 or 50 mL at $-20\text{ }^{\circ}\text{C}$. Do not autoclave.
3. Optimal Cutting Temperature (O.C.T.) compound.

2.4 Embedding Solutions for Brain Tissue

1. $1\times$ PBS.
2. 4 % Agarose: Mix 4 g agarose in 100 mL $1\times$ PBS + 0.4 % PFA (see Note 3). Heat agarose in microwave until it melts ($\sim 55\text{ }^{\circ}\text{C}$). Prepare fresh every time and do not autoclave.
3. Cryoprotectant: Mix 150 g of sucrose in 200 mL $1\times$ PBS and 150 mL Ethylene glycol. Adjust the volume to 500 mL with $1\times$ PBS. Store at $-20\text{ }^{\circ}\text{C}$.

4. Vibratome to section tissue (e.g., Leica VT 1000S (Leica Biosystems, Wetzlar, Germany)).

2.5 Immunohistochemistry

2.5.1 Reagents for Both Cochlea and Brain Immunohistochemistry

1. Washing buffer for all specimens: 1× PBS.
2. Primary antibodies (*see Note 4*).
3. Secondary antibodies: Use a fluorescence-conjugated antibody against the species that generated the primary antibody. Dilute the secondary antibody in the same buffer as the primary antibody.
4. Size four art paintbrush.
5. Glass cuvettes for washing or transferring brain sections to microscope slides (*see Subheading 3.3, step 10*).
6. In the present description, we used a Cy3-conjugated anti-rabbit antibody (Jackson Immuno Research, West Grove, PA) diluted 1:1500 and an Alexa488-conjugated anti-mouse antibody (Life Technologies, Darmstadt, Germany) diluted 1:500. Store according to the manufacturer's instructions.

2.5.2 Reagents Only for Immunohistochemistry on Cochlear Tissue

1. Permeabilization buffer for cochlear sections: 10 mL 1× PBS, 50 µL Triton-X 100. Prepare 1× PBS + 0.5 % Triton. Store at 4 °C.
2. Blocking solution for cochlear sections: 0.4 g Normal Goat Serum (NGS), 10 mL 1× PBS. Prepare 4 % NGS (*see Note 5*).
3. Reaction buffer for antibody dilution on cochlear sections: Prepare by mixing 2 g (2 %) NaCl, 100 µL Triton X-100, 1 mL NGS in 100 mL 1× PBS (*see Note 6*).

2.5.3 Reagents Only for Immunohistochemistry on Brain Sections

1. Blocking and permeabilization solution: Prepare by mixing 0.3 g bovine serum albumin (BSA) and 20 µL Triton-X 100 in 10 mL of 1× PBS (*see Note 7*). Store at 4 °C.
2. Buffer for antibody dilution: Prepare BSA in a range of 0.5–1.5 % in 10 mL of 1× PBS and 10 µL Triton-X 100 (*see Note 8*).
3. Mounting and nuclear staining (can be used on all different types of tissue sections): Vectashield mounting medium with or without DAPI (Vector Laboratories, Burlingame, CA, USA) (*see Note 9*).

3 Methods

Carry out all steps at room temperature (RT) unless otherwise indicated.

3.1 Tissue Preparation (*See Note 1*)

1. After decapitation open the skull along the lateral ridges (*see Note 10*), remove the complete brain in one piece after cutting the cranial nerves and transfer immediately to 50 mL of 2 % or 4 % PFA for mice and rats, respectively. If you only use brain tissue, *see Subheading 3.1, step 8*.

2. Take the residual skull and cut it in half. Use a dissecting microscope to remove the cochlea. Use actuated tweezers, to open the bulla and remove the cochlea by breaking out the attached part of the cochlea to the temporal bone (*see Note 11*).
3. Transfer the cochleae to 2 % PFA (*see Note 12*) and fix for 2 h at 4 °C on a rotating wheel.
4. Before decalcification remove the PFA and rinse the tissue in ddH₂O. Transfer the tissue to filtered R.D.O. (*see Note 13*) until the tissue is soft (*see Note 14*).
5. Transfer the decalcified cochlea to Sucrose-Hank's solution and keep rotating the tissue at 4 °C overnight.
6. Embed the cochleae in Tissue-Tek, freeze and store at -80 °C (*see Note 15*).
7. Cochleae are cut in 10 µm sections using a Cryostat (Leica Cryostat 1720 Digital Leica, Wetzlar, Germany) and transferred to microscope slides (Superfrost Plus). Store slides at -20 °C until use.
8. Fix brain tissue for 48 h at 4 °C on a shaker. After 24 h exchange the PFA.
9. Take the tissue out of the PFA and rinse with ddH₂O.
10. Embed the tissue in 4 % agarose (*see Note 16*) and store in 0.4 % PFA in 1× PBS at 4 °C.
11. Brains are sectioned at 40–60 µm on a vibratome (e.g., VT1000S; Leica, Wetzlar, Germany).
12. Slices are stored in a 24-well plate in Cryoprotectant at -20 °C.

3.2 Immunohistochemistry for Cochlear Tissue (See Note 17)

1. Take the microscope slides with the cochlear sections out of the -20 °C freezer and allow them to thaw at RT for ~30 min.
2. Add 1 mL of permeabilization buffer to each slide and incubate for 10 min.
3. Rinse the slides with 1× PBS.
4. Pipette 100 µL of blocking solution on each slide and incubate for 30 min in a humidified chamber (*see Note 18*).
5. Dilute the primary antibodies in reaction buffer to the desired concentration (*see Note 4*).
6. After removing the reaction buffer apply 100 µL of antibody solution to each slide. Incubate at 4 °C overnight in a humidified chamber.
7. Rinse slides with 1× PBS.
8. Wash 3× for 30 min in 1× PBS using a glass cuvette.
9. Dilute secondary antibody in reaction buffer.

10. Take the slides out of the glass cuvette, apply 100 µL of secondary antibody to each slide, and incubate in a humidified chamber for 1 h at RT.
11. Rinse the slides with 1× PBS.
12. Wash 3× for 30 min in 1× PBS using a glass cuvette.
13. Mount the tissue slices using Vectashield mounting medium with or without DAPI (*see Note 9*).

3.3 Immunohistochemistry for Free-Floating Brain Slices (See Notes 19 and 20)

1. Take the slices out of the cryosolution using a paintbrush and transfer to a fresh 24-well plate containing 1× PBS.
2. Wash 2× for 15 min in 1× PBS (*see Note 21*).
3. Permeabilization and blocking step: After removing PBS, incubate slices for 30 min in 3 % BSA containing 0.2 % Triton-X 100.
4. Dilute primary antibodies in 0.5–1.5 % BSA, containing 0.1 % Triton-X 100, to the desired concentration (*see Notes 4 and 8*).
5. After removing the permeabilization/blocking buffer, cover the sections with antibody solution and incubate at 4 °C overnight in a humidified chamber (*see Note 22*).
6. After removing the antibody solution, wash the slices 3× for 15 min in 1× PBS.
7. Dilute secondary antibodies in 0.5–1.5 % BSA, containing 0.1 % Triton-X 100, to the desired concentration (*see Note 8*).
8. After removing PBS, cover sections with antibody solution and incubate for 1 h at RT in a humidified chamber (*see Note 22*).
9. After removing the antibody solution, wash 3× for 15 min in 1× PBS.
10. To transfer the brain sections onto microscope slides, place them one at a time in the glass cuvette filled with water and use a paintbrush to transfer them to microscope slides.
11. Mount the slices with Vectashield mounting medium with or without DAPI (*see Note 9*)

3.4 Microscopy

1. Sections shown here were viewed using an Olympus BX61 microscope (Olympus, Center Valley, PA, USA) equipped with an X-Cite Lamp (Olympus). Images were acquired using an Olympus XM10 CCD monochrome camera and analyzed with cellSens Dimension software (OSIS).
2. To increase spatial resolution, slices were imaged over a distance of 10–60 µm (*see Note 23*) in steps of 0.49 µm within an image-stack along the z-axis (z-stack) followed by 3-dimen-

sional deconvolution, using a cellSens Dimension built-in algorithm. Typically z-stacks consisted of 5–30 layers (*see Note 23*), for each layer one image was acquired per fluorochrome (*see Note 24*).

4 Notes

1. Animal care procedures and treatments were performed in accordance with institutional and national guidelines, following approval by the University of Tübingen, Veterinary Care Unit, and the Animal Care and Ethics Committee of the regional board of the Federal State Government of Baden-Württemberg, Germany.
2. Shake the bottles in between to help the powder to dissolve. Work under a hood as the PFA powder is toxic.
3. The amount of agarose depends on the number of samples to be embedded.
4. The primary antibody depends on the gene of interest. Follow the manufacturer's instructions for storage and dilution. The following antibodies were used as seen in Figs. 1, 2, and 3: anti-CtBP2/RIBEYE antibody (Cell Applications, San Diego, CA, USA) diluted 1:100; mouse anti-parvalbumin antibody (Sigma-Aldrich, Munich, Germany) diluted 1:100 for cochlear tissue or 1:500 for brain tissue; mouse anti-otoferlin antibody (Life Spam, Echingen, Germany) diluted 1:100; rabbit anti-synaptotagmin 1 antibody (Synaptic Systems, Göttingen, Germany) diluted 1:50; mouse anti-NF200 antibody (Sigma) diluted 1:8000 and a rabbit NF200 antibody (Sigma) diluted 1:6000; rabbit anti-cholinacetyltransferase antibody (Merck Millipore, Darmstadt, Germany) diluted 1:150; rabbit anti-tyrosinhydroxylase antibody (Merck Millipore) diluted 1:100; goat anti-synaptophysin antibody (Santa Cruz, Heidelberg, Germany) diluted 1:50; mouse anti-GAD67 antibody (Merck Millipore) diluted 1:300; rabbit anti-Arg3.1/arc antibody (Synaptic Systems) diluted 1:500; rabbit anti-parvalbumin (Merck Millipore) diluted 1:3000; rabbit anti-vGlut2 antibody (Synaptic Systems) diluted 1:100; rabbit anti-MAP-2 antibody (Synaptic Systems) diluted 1:500; rabbit anti-vGAT antibody (Merck Millipore) diluted 1:100.
5. Blocking solution is prepared freshly for each immunostaining procedure.
6. Store the remaining reaction buffer at 4 °C, to dilute the secondary antibody the next day. Do not store longer.
7. Use a magnetic stir bar.

8. The amount of BSA depends on the antibody. The investigator evaluates final concentrations.
9. Nuclear staining is not obligatory. If you do not want a nuclear stain use mounting medium without DAPI. Here, we used Vectashield.
10. To open the skull, cut along the lateral ridges on the upper sides of the skull. Do not destroy the bulla containing the cochlea.
11. Cochlea dissections require practice, so start with young adult animals around P20, as the bone is not too hard yet.
12. Use approximately 10 mL of PFA for two cochleae.
13. RDO is a black liquid and that is filtered before use. Use a 0.22 μm sterile filter attached to a syringe. A yellow clear solution is obtained after pressing the RDO through the filter.
14. The time for decalcification depends on the age of the animal. Decalcification is unnecessary for mice and rats up to P7. Generally do not decalcify with RDO longer than 90 min. For animals older than P7, perform the decalcification in a small Petri dish and check every few minutes with tweezers, to determine if the tissue is soft. The investigator determines the final time for different ages and species.
15. Make small pots of aluminum foil to embed the cochleae in Tissue Tek.
16. For embedding use a 12-well plate. Apply 4 % agarose at ~55 °C to the well and place the whole brain into the agarose, leaving a little space between the bottom of the well and the tissue. When the agarose is hard, remove the brain with the agarose from the well, using a spatula, and place in a 50 mL tube containing 0.4 % PFA in 1× PBS. Store at 4 °C.
17. Do not allow tissue slices to dry out during the immunohistochemistry procedure as drying will stop the reaction. Take care that slices are always covered with enough solution. For longer incubation steps use a humidified chamber.
18. Place paper tissue soaked with ddH₂O on the bottom of the humidified chamber. Place little wood sticks or part of plastic pipettes (2 mL) on the moistened tissue. The chamber for cochlear slides should offer the possibility of setting the microscope slides horizontally next to each other on the wood sticks/plastic pipettes. Close the lid without touching the slides.
19. Remove and apply solutions by pipetting. Be careful not to aspirate brain slices into the tip of the pipette.
20. Gently shake the 24-well plate for all steps.

21. Choose volumes so that tissue slices are covered and the liquid does not evaporate. We suggest 300 µL per well.
22. For the humidified chamber, use a box that will accommodate a 24-well plate. Cover the bottom with tissue paper soaked in ddH₂O and close with a lid.
23. The distance of imaging for a *z*-stack, and thereby, the number of layers, depends on the thickness of the tissue and the staining and has to be determined by the investigator.
24. The theoretical resolution (Abbe's law of diffraction of monochromatic light) of this system along the *x*- and *y*-axes was estimated at 203 nm for Cy3 (emission maximum $E_{\text{max}} = 570$ nm) and 185 nm for Alexa488 ($E_{\text{max}} = 517$ nm), respectively. The deconvolution process in the *z*-axis is likely to improve the resolution further, since it reduces the object size in the *x*- and *y*-axes for a projected *z*-stack, due to a reduction of blur in both axes.

References

1. Singer W, Panford-Walsh R, Knipper M (2014) The function of BDNF in the adult auditory system. *Neuropharmacology* 76(Pt C):719–728
2. Heimel JA, van Versendaal D, Levelt CN (2011) The role of GABAergic inhibition in ocular dominance plasticity. *Neural Plast* 2011:391763
3. Huang ZJ, Kirkwood A, Pizzorusso T, Porciatti V, Morales B, Bear MF, Maffei L, Tonegawa S (1999) BDNF regulates the maturation of inhibition and the critical period of plasticity in mouse visual cortex. *Cell* 98(6):739–755
4. Lein ES, Finney EM, McQuillen PS, Shatz CJ (1999) Subplate neuron ablation alters neurotrophin expression and ocular dominance column formation. *Proc Natl Acad Sci U S A* 96(23):13491–13495
5. Jiao Y, Zhang Z, Zhang C, Wang X, Sakata K, Lu B, Sun QQ (2011) A key mechanism underlying sensory experience-dependent maturation of neocortical GABAergic circuits in vivo. *Proc Natl Acad Sci U S A* 108(29):12131–12136
6. Kraus HJ, Aulbach-Kraus K (1981) Morphological changes in the cochlea of the mouse after the onset of hearing. *Hear Res* 4(1):89–102
7. Simmons DD (2002) Development of the inner ear efferent system across vertebrate species. *J Neurobiol* 53(2):228–250
8. Liberman MC (1990) Effects of chronic cochlear de-efferentation on auditory-nerve response. *Hear Res* 49(1–3):209–223
9. Sendin G, Bulankina AV, Riedel D, Moser T (2007) Maturation of ribbon synapses in hair cells is driven by thyroid hormone. *J Neurosci* 27(12):3163–3173
10. Darrow KN, Maison SF, Liberman MC (2006) Cochlear efferent feedback balances interaural sensitivity. *Nat Neurosci* 9(12):1474–1476
11. Dlugaczyk J, Singer W, Schick B et al (2008) Expression of glycine receptors and gephyrin in the rat cochlea. *Histochem Cell Biol* 129(4):513–523
12. Eybalin M (1993) Neurotransmitters and neuromodulators of the mammalian cochlea. *Physiol Rev* 73(2):309–373
13. Guinan JJ Jr, Gifford ML (1988) Effects of electrical stimulation of efferent olivocochlear neurons on cat auditory-nerve fibers. I. Rate-level functions. *Hear Res* 33(2):97–113
14. Rajan R (1988) Effect of electrical stimulation of the crossed olivocochlear bundle on temporary threshold shifts in auditory sensitivity. I. Dependence on electrical stimulation parameters. *J Neurophys* 60(2):549–568
15. Reisinger E, Bresee C, Neef J et al (2011) Probing the functional equivalence of otoferlin and synaptotagmin 1 in exocytosis. *J Neurosci* 31(13):4886–4895
16. Ruel J, Wang J, Rebillard G, Eybalin M, Lloyd R, Pujol R, Puel JL (2007) Physiology, phar-

- macology and plasticity at the inner hair cell synaptic complex. *Hear Res* 227(1–2):19–27
17. Ramakrishnan NA, Drescher MJ, Drescher DG (2009) Direct interaction of otoferlin with syntaxin 1A, SNAP-25, and the L-type voltage-gated calcium channel CaV1.3. *J Biol Chem* 284(3):1364–1372
 18. Roux I, Safieddine S, Nouvian R et al (2006) Otoferlin, defective in a human deafness form, is essential for exocytosis at the auditory ribbon synapse. *Cell* 127(2):277–289
 19. Beurg M, Michalski N, Safieddine S, Bouleau Y, Schneggenburger R, Chapman ER, Petit C, Dulon D (2010) Control of exocytosis by syntaptotagmins and otoferlin in auditory hair cells. *J Neurosci* 30(40):13281–13290
 20. Johnson CP, Chapman ER (2010) Otoferlin is a calcium sensor that directly regulates SNARE-mediated membrane fusion. *J Cell Biol* 191(1):187–197
 21. Fuchs PA (2005) Time and intensity coding at the hair cell's ribbon synapse. *J Physiol* 566(Pt 1):7–12
 22. Lysakowski A, Goldberg JM (2008) Ultrastructural analysis of the cristae ampullares in the squirrel monkey (*Saimiri sciureus*). *J Comp Neurol* 511(1):47–64
 23. Moser T, Brandt A, Lysakowski A (2006) Hair cell ribbon synapses. *Cell Tissue Res* 326(2):347–359
 24. Schmitz F (2009) The making of synaptic ribbons: how they are built and what they do. *Neuroscientist* 15(6):611–624
 25. LoGiudice L, Matthews G (2009) The role of ribbons at sensory synapses. *Neuroscientist* 15(4):380–391
 26. Parsons TD, Sterling P (2003) Synaptic ribbon. Conveyor belt or safety belt? *Neuron* 37(3):379–382
 27. Zenisek D (2008) Vesicle association and exocytosis at ribbon and extraribbon sites in retinal bipolar cell presynaptic terminals. *Proc Natl Acad Sci U S A* 105(12):4922–4927
 28. Johnson SL, Marcotti W, Kros CJ (2005) Increase in efficiency and reduction in Ca²⁺ dependence of exocytosis during development of mouse inner hair cells. *J Physiol* 563(Pt 1):177–191
 29. Khimich D, Nouvian R, Pujol R, Tom Dieck S, Egner A, Gundelfinger ED, Moser T (2005) Hair cell synaptic ribbons are essential for synchronous auditory signalling. *Nature* 434(7035):889–894
 30. Klinke R (1987) Processing of acoustic stimuli in the inner ear—a review of recent research results. *HNO* 35(4):139–148
 31. Kraus KS, Canlon B (2012) Neuronal connectivity and interactions between the auditory and limbic systems. Effects of noise and tinnitus. *Hear Res* 288(1–2):34–46
 32. Knipper M, Zimmermann U, Müller M (2010) Molecular aspects of tinnitus. *Hear Res* 266(1–2):60–69
 33. Knipper M, Van Dijk P, Nunes I, Ruttiger L, Zimmermann U (2013) Advances in the neurobiology of hearing disorders: recent developments regarding the basis of tinnitus and hyperacusis. *Prog Neurobiol* 111:17–33
 34. Eggermont JJ, Roberts LE (2004) The neuroscience of tinnitus. *Trends Neurosci* 27(11):676–682
 35. Knipper M, Müller M, Zimmermann U (2012) Molecular mechanism of tinnitus. In: Fay RR, Popper AN, Eggermont JJ (eds) Springer handbook of auditory research: neural correlates of tinnitus. Springer, New York, pp 59–82
 36. Kujawa SG, Liberman MC (2009) Adding insult to injury: cochlear nerve degeneration after "temporary" noise-induced hearing loss. *J Neurosci* 29(45):14077–14085
 37. Eybalin M, Ripoll C (1990) Immunolocalization of parvalbumin in two glutamatergic cell types of the guinea pig cochlea: inner hair cells and spiral ganglion neurons. *CR Acad Sci III* 310(13):639–644
 38. Yasunaga S, Grati M, Chardenoux S, Smith TN, Friedman TB, Lalwani AK, Wilcox ER, Petit C (2000) OTOF encodes multiple long and short isoforms: genetic evidence that the long ones underlie recessive deafness DFNB9. *Am J Hum Genet* 67(3):591–600
 39. Duncker SV, Franz C, Kuhn S et al (2013) Otoferlin couples to clathrin-mediated endocytosis in mature cochlear inner hair cells. *J Neurosci* 33(22):9508–9519
 40. Knipper M, Zimmermann U, Rohbock K, Kopschall I, Zenner HP (1995) Synaptophysin and GAP-43 proteins in efferent fibers of the inner ear during postnatal development. *Brain Res Dev Brain Res* 89(1):73–86
 41. Knipper M, Panford-Walsh R, Singer W, Ruttiger L, Zimmermann U (2015) Specific synaptopathies diversify brain responses and hearing disorders: you lose the gain from early life. *Cell Tissue Res* 361(1):77–93
 42. Pinal CS, Tobin AJ (1998) Uniqueness and redundancy in GABA production. *Perspect Dev Neurobiol* 5(2–3):109–118
 43. Bramham CR, Worley PF, Moore MJ, Guzowski JF (2008) The immediate early gene arc/arg3.1: regulation, mechanisms, and function. *J Neurosci* 28(46):11760–11767

44. Mahlke C, Wallhauser-Franke E (2004) Evidence for tinnitus-related plasticity in the auditory and limbic system, demonstrated by arg3.1 and c-fos immunocytochemistry. *Hear Res* 195(1–2):17–34
45. Tan J, Rüttiger L, Panford-Walsh R et al (2007) Tinnitus behavior and hearing function correlate with the reciprocal expression patterns of BDNF and Arg3.1/arc in auditory neurons following acoustic trauma. *Neuroscience* 145(2):715–726
46. Singer W, Zuccotti A, Jaumann M et al (2013) Noise-induced inner hair cell ribbon loss disturbs central arc mobilization: a novel molecular paradigm for understanding tinnitus. *Mol Neurobiol* 47(1):261–279
47. Rüttiger L, Singer W, Panford-Walsh R et al (2013) The reduced cochlear output and the failure to adapt the central auditory response causes tinnitus in noise exposed rats. *PLoS One* 8(3):e57247
48. Kawaguchi Y, Kondo S (2002) Parvalbumin, somatostatin and cholecystokinin as chemical markers for specific GABAergic interneuron types in the rat frontal cortex. *J Neurocytol* 31(3–5):277–287
49. Ferando I, Mody I (2014) In vitro gamma oscillations following partial and complete ablation of d subunit-containing GABA receptors from parvalbumin interneurons. *Neuropharmacology* 88:91–98
50. Jonas P, Buzsaki G (2007) Neural inhibition. *Scholarpedia* 2(9):3286
51. Chaudhry FA, Reimer RJ, Bellocchio EE, Danbolt NC, Osen KK, Edwards RH, Storm-Mathisen J (1998) The vesicular GABA transporter, VGAT, localizes to synaptic vesicles in sets of glycinergic as well as GABAergic neurons. *J Neurosci* 18(23):9733–9750
52. Landry M, Bouali-Benazzouz R, El Mestikawy S, Ravassard P, Nagy F (2004) Expression of vesicular glutamate transporters in rat lumbar spinal cord, with a note on dorsal root ganglia. *J Comp Neurol* 468(3):380–394
53. Johnson EW, Eller PM, Jafek BW, Norman AW (1992) Calbindin-like immunoreactivity in two peripheral chemosensory tissues of the rat: taste buds and the vomeronasal organ. *Brain Res* 572(1–2):319–324

Chapter 16

Rapid and Semi-automated Extraction of Neuronal Cell Bodies and Nuclei from Electron Microscopy Image Stacks

Paul S. Holcomb, Michael Morehead, Gianfranco Doretto, Peter Chen, Stuart Berg, Stephen Plaza, and George Spirou

Abstract

Connectomics—the study of how neurons wire together in the brain—is at the forefront of modern neuroscience research. However, many connectomics studies are limited by the time and precision needed to correctly segment large volumes of electron microscopy (EM) image data. We present here a semi-automated segmentation pipeline using freely available software that can significantly decrease segmentation time for extracting both nuclei and cell bodies from EM image volumes.

Key words Connectomics, Segmentation, 3D reconstruction, Electron microscopy, ilastik

1 Introduction

Connectomics is at the forefront of modern neuroscience research. With the advent of programs such as the BRAIN Initiative and the Human Brain Project, increasing numbers of research groups are attempting large-scale mapping of the mammalian nervous system. However, these research endeavors present significant challenges in data acquisition, storage, segmentation, and interpretation [1]. In particular, the segmentation of electron microscopy (EM) images for accurate nanoscale reconstruction of neurons and related structures requires significant time and effort on the part of researchers. Automated software for segmentation is being developed [2–5], but still requires training data in the form of precise—and usually manual—segmentation of subsets of the data to be analyzed, known as ground truth. There exists a host of software tools for performing semi-automated segmentation, each with a unique set of tools, which can make difficult the selection of software best suited for solving a particular segmentation problem. Indeed, it is quite common that several different software solutions must be applied in order to converge on a solution. Additionally,

most semi-automated software techniques perform segmentation on an entire image volume, whereas the specific research questions being asked may only require local segmentation near features of interest. Here, we detail one method for rapid and semi-automated segmentation of nuclei and cell bodies consisting of four steps: image conversion (if necessary), pixel classification, cell identification, and cell segmentation. Using this segmentation pipeline, a cell body and nucleus segmentation that manually may take up to 30 h can be accomplished in as little as 1 h.

2 Materials

2.1 Hardware

Hardware requirements will vary widely depending upon the size and resolution of the data set. Overall, a large amount of fast access memory (32GB+, DDR3/4) and solid state disk (SSD) storage for fast read/write times will significantly decrease the major bottlenecks of dealing with large data volumes. Processor speed, number of cores, and multithreading capability are also important, but secondary to RAM and SSD in boosting performance. This section will provide details on the baseline system that our lab uses, which can be tailored to suit experimental requirements.

1. SuperMicro ATX Server Motherboard Socket G34 AMD (Model: MBD-H8SGL-O; Super Micro Computer, Inc., San Jose, CA).
2. AMD Opteron 6320 Abu Dhabi 2.8GHz 8 core Server Processor (Model: OS6320WKT8GHKWOF; AMD, Sunnyvale, CA).
3. 128GB Kingston 240-pin DDR3 SDRAM ($8 \times 16\text{GB}$, Model: KVR16R11D4K4/64; Kingston Technology, Fountain Valley, CA).
4. XFX HD 5000 Radeon HD 5450 1GB Video Card (Model: HD-545X-ZQH2; AMD).
5. Hec 585W ATX12V Power Supply (Model: HP585DB; Intel, Santa Clara, CA).
6. Corsair Force LS 480GB SATA Solid State Drive (Model: CSSD-F480GBLSB; Corsair Components, Inc., Fremont, CA).
7. Seagate Barracuda 7200.14 3TB SATA Hard Drive (Model: ST3000DM001; Seagate Technology, LLC, Longmont, CO).

2.2 Software

This chapter assumes that you have the following software installed:

1. Python 2.7. Python is the second most commonly used programming language [6], and is the major backbone of all of the software used in this chapter.

2. ImageMagick (<http://www.imagemagick.org>). ImageMagick is a lightweight and versatile tool for converting images between different file formats.
3. ilastik 1.1.6 or later (<http://lastik.org>). The ilastik software [7], developed by the Heidelberg Collaboratory for Image Processing at the University of Heidelberg, provides a graphical user interface (GUI)-driven method for segmentation of image data using multiple classification methods.
4. CellSeeker (<http://www.github.com/SpiroULab/CellSeeker>). CellSeeker, developed by the authors, utilizes EM images and nucleus segmentation from ilastik to provide rapid proofreading of nuclei and extraction of EM subvolumes for further processing in ilastik.

3 Methods

The method described below assumes a high-resolution (<10 nm) fully registered EM image stack. Lower resolutions or misaligned images may significantly affect results.

3.1 Image Conversion, If Necessary

Convert EM image stack to tiff format.

1. ImageMagick should be installed and added to the system PATH (see installation instructions at <http://www.imagemagick.org/script/binary-releases.php>).
2. Open a console window.
 - For Windows, press  Windows Key + r, then type “cmd” (no quotation marks).
 - For Linux, most distributions will use the Ctrl + Alt + t shortcut to open a terminal window.
 - For Mac, in OS X and later, navigate to Applications -> Utilities and double-click on Terminal.
3. Change the directory to where your EM images are stored.
4. Type “convert [input directory/file] [output file]” (no quotation marks) and press Enter. The input directory/file can be either a single file (in the case of a single non-tiff image stack) or a directory containing sequential image files (i.e., image01.tiff, image02.tiff, etc.). If a directory is specified, an asterisk (*) denoting “any file”) and the file type of the images must also be supplied. For example, a set of TIFF files would be specified as “*directory*/*.tiff.” The output should be a single multi-page tiff file specified with the TIFF file extension (i.e., “*directory*/output.tiff”). EM images may also be reduced in size and resolution by adding the “-scale #” command before the input file, where “#” is the scale factor desired (i.e., to scale images by a

factor of 2, a scale factor of 0.5 would be used). This may be desirable to speed up subsequent processing (*see Note 1*).

3.2 Pixel Classification

3.2.1 Training *ilastik* to Recognize Cell Nuclei in EM Images (Fig. 1)

1. Import EM images into *ilastik*'s “Pixel Classification” workflow. Pixel classification utilizes pixel information gained by applying multiple image filters (Gaussian blur, gradient magnitude, etc.) to build a feature vector representing each pixel in an image. Based on training data provided by a user, pixel classification attempts to group pixels with similar feature vectors into subsets that, when taken together, completely segment the image.
2. Run *ilastik* and select the “Pixel Classification” workflow.
3. Provide a project name and location to save the project.
4. On the Input Data screen, under the Raw Data tab, click “Add New” and select the “Add Separate Images” option.
5. Navigate to the location of the EM image data and select the file (or folder, for a directory of sequential images), then click Open.
6. In the “Raw Data” tab, double click on the axis labels under the “Axes” column header.
7. In the axes field, define axes as either “zyxc” for isotropic data or “txyc” for anisotropic data (*see Note 2*) and click OK.
1. After the data have been successfully imported, click the “Feature Selection” tab in the menu options on the left side of the screen.
2. Under “Feature Selection,” click “Select Features....”
3. In the “Features” dialog box, select the filters to use for training the classifier (*see Note 3*). A good rule of thumb is to start with as many classifiers as your data set will allow (a dialog box will provide a warning if a classifier is out of range) and reduce the features if necessary as training progresses to get a better segmentation. In our hands, the number of classifiers used is usually 18-22. Click OK to compute the selected features (*see Note 4*).
4. Click the “Training” tab in the menu options on the left side of the screen. Click “Add Label” twice to create a training label for nuclei and background segmentation. The color of the label is customizable by clicking the colored square next to each label. Change label names, if necessary, by double-clicking the label name.
5. Using Shift + left-click on the mouse to pan, Shift + the mouse wheel to scroll through images, and the “+” and “-” keys to zoom in and out, respectively, locate a nucleus within the EM image.

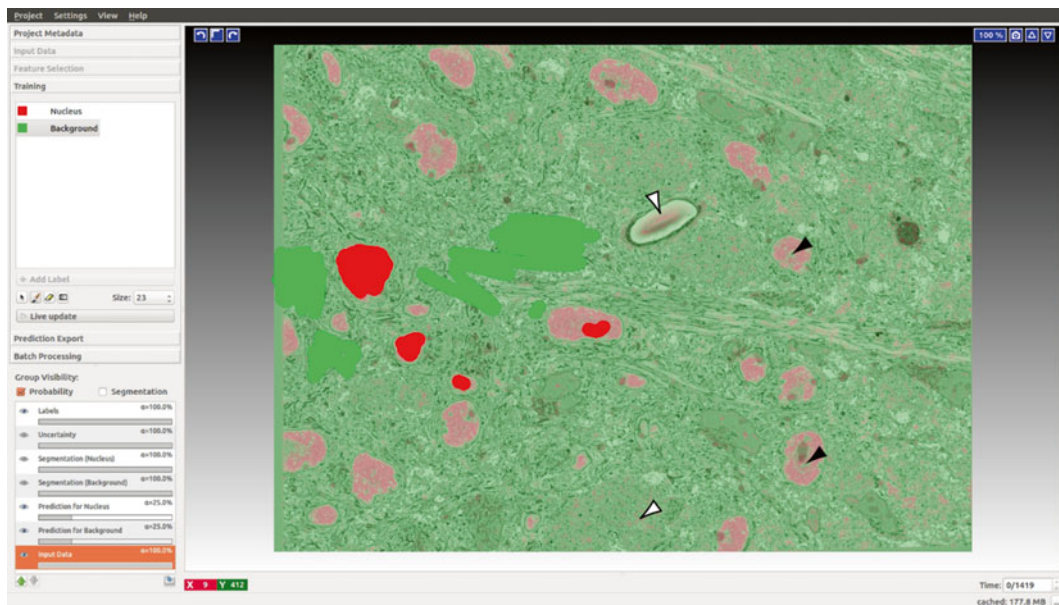


Fig. 1 ilastik pixel classification. Classification for nucleus segmentation performed on serial block-face scanning EM image stack. Nucleus (*solid red*) and background (*solid green*) training data are used to define pixel properties of each region. Pixel classification then sorts each pixel into either nucleus (*translucent red*) or background (*translucent green*) for segmentation. Additional training data can be added to misclassified pixels (i.e., nucleus as background (*black arrowheads*) or background as nucleus (*white arrowheads*)) to refine the segmentation. The output of this step is used as the input to CellSeeker for cell identification

6. Left-click on the label for the nucleus, and select the Paintbrush button (underneath the “Add Label” button on the left side of the screen). Adjust your brush size using the “Size” drop-down menu to a size that will allow for quick painting of the interior of the nucleus without going outside of the nuclear envelope.
7. Left-click and hold inside the nucleus and paint the interior (Fig. 1).
8. Left-click on the label for the background, and repeat the two previous steps for the background outside of the nucleus.
9. Zoom in to a small section of the EM image using the “+” key. Click “Live update” to see the training results. ilastik computes the training results only for the area of the image visible on the screen, so to reduce the time it takes to see a result, keep the visible area relatively small (single nuclei, for example). Ideally, if only a small area is visible, this process should take one minute or less (*see Note 5*). Visibility and opacity of the results can be controlled under the “Group Visibility” section in the lower left of the screen.

10. Modify the nucleus and background labels by painting in areas trained incorrectly (nucleus in background area, and vice versa, white and black arrowheads, respectively, in Fig. 1) until obtaining an acceptable segmentation of the nucleus.
11. Zoom out to view an entire image slice (use the upward-pointing triangle key in the upper-right corner of the image).
12. Ensure that other nuclei in the image are also being accurately segmented. If not, zoom in (“+” key) to trouble areas and paint using the nucleus and background labels until an acceptable segmentation is obtained.
13. Switch to an image in another section of the data set (use Shift + mouse wheel or manually input the slice number in the Z location box in the top left of the image screen) to ensure that training is uniform throughout the volume.

3.2.2 Exporting ilastik Nucleus Segmentation

1. Under “Group Visibility” in the lower left area of the screen, locate the nucleus segmentation entry (e.g., Segmentation (Nucleus)).
2. Right-click on the nucleus segmentation entry, and select “Export....”
3. Under “Output File Info,” click the “Select...” button next to the “File:” entry.
4. In the navigation window, specify a folder and filename for the nucleus segmentation. Click OK.
5. Click OK in the “Image Export Options” window. ilastik should now automatically export the segmentation, which may take several minutes for larger data sets (*see Note 6*)

3.3 Cell Identification

Process nucleus segmentation using CellSeeker to identify cells and create EM subvolumes.

1. Download CellSeeker (<http://www.github.com/SpirouLab/CellSeeker>).
2. Open a terminal window (see above) and navigate to the CellSeeker folder.
3. Run CellSeeker by typing “python cellseeker.py” and press Enter.
4. Within the “CellSeeker:Initialization” window that appears, provide the following:
 - The location of the nucleus segmentation, either by typing the path in the text box beside “Nucleus Segmentation:” or clicking the “Search...” button to the right of the text box, navigating to and selecting the file and clicking “OK.”
 - The location of the EM images in the “EM Images:” field by following the instructions detailed for the nucleus segmentation.

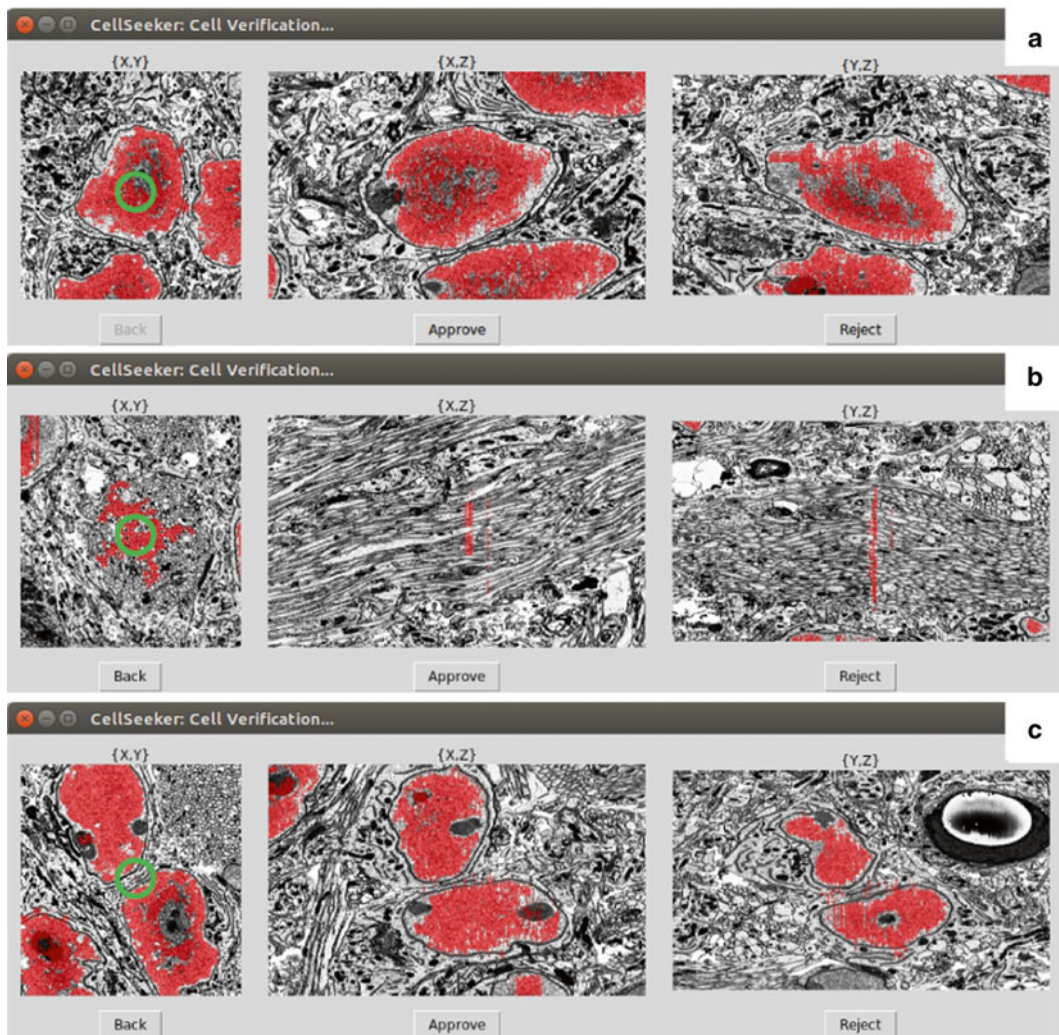


Fig. 2 Cell verification in CellSeeker. EM images are presented in all three image planes with associated nuclear segmentations (red). The cell being identified should have its nucleus centered in the viewing windows (*centers marked with green circles*). (a) This panel demonstrates a successfully identified cell, which would be kept using the “Approve” button. False positives usually appear as either (b) non-nuclei incorrectly identified as nuclei or (c) two nuclei incorrectly fused together. In either case, the “cell” would be rejected using the “Reject” button. Users can navigate backwards to change decisions using the “Back” button. EM of cells verified in this manner will be processed and output for carving in ilastik

- The linear pixel dimension in nanometers (nm) for the EM images (i.e., for a $5 \text{ nm} \times 5 \text{ nm}$ pixel size, this value would be 5) in the text box next to “Pixel dimension (nm):”. CellSeeker assumes isotropic pixel dimensions in x and y.
- The distance between images in z in nm in the text box next to “Z-slice thickness (nm).”

- The estimated cell diameter in micrometers (μm) of cells being extracted from the data volume. This value will be used to calculate the extents in x, y, and z for cropping the EM volume and for filtering (see Note 7).
5. Click “OK.” CellSeeker will perform a size filtering in 2D and 3D based on the largest object found in each image, followed by a connected component analysis to enumerate the presumptive nuclei.
 6. When the filtering step completes, CellSeeker will present an image of a possible extracted nucleus in 2D in all three planes ($\{X, Y\}$, $\{X, Z\}$, $\{Y, Z\}$) overlaid on the associated EM image.
 - If the segmentation has correctly identified the nucleus, click the “Approve” button or press the up arrow key (Fig. 2a).
 - If the segmentation has incorrectly identified a structure as a nucleus, click the “Reject” button or press the down arrow key (Fig. 2b, c).
 - If a classification was incorrectly performed, click the “Back” button or press the left arrow key to return to the previous set of images and reclassify it.
 7. Repeat the verification process for each possible nucleus identified.
 8. After proofreading is complete, click the “Extract Cell Volumes” button.
 9. Specify a location where EM subvolumes representing individual cells should be extracted. If desired, a higher resolution version of the EM volume can be substituted at this point by checking the “Use different EM volume for subvolumes” box and supplying the path to the new EM volume. The new volume *must* be a multiple of the original volume in the $\{x, y\}$ axis (i.e., a $400 \times 400 \times 200$ volume could be substituted for a $100 \times 100 \times 200$ volume), or an error will occur.
 10. Click the OK button. CellSeeker will automatically create sub-folders within the directory for each identified cell (“Cell_1,” “Cell_2,” etc.), as well as folders within each cell folder to hold later segmentation (“Nucleus,” “CellBody,” “Axon,” “Dendrites,” “Inputs,” and “AdditionalStructures”). Within the “CellBody” folder for each cell, CellSeeker produces a multipage TIFF file, containing the EM images for that cell, a text file (“coordinates.txt”), defining where the subvolume was extracted from in the context of the full EM volume, and an ilastik project file, containing the preprocessed images for use in the ilastik “Carving” workflow. This may take some time depending on the data volume size and relative size of each cell.
 11. At this point, for each verified cell, a subvolume of EM data and an associated ilastik project file for carving has been produced.

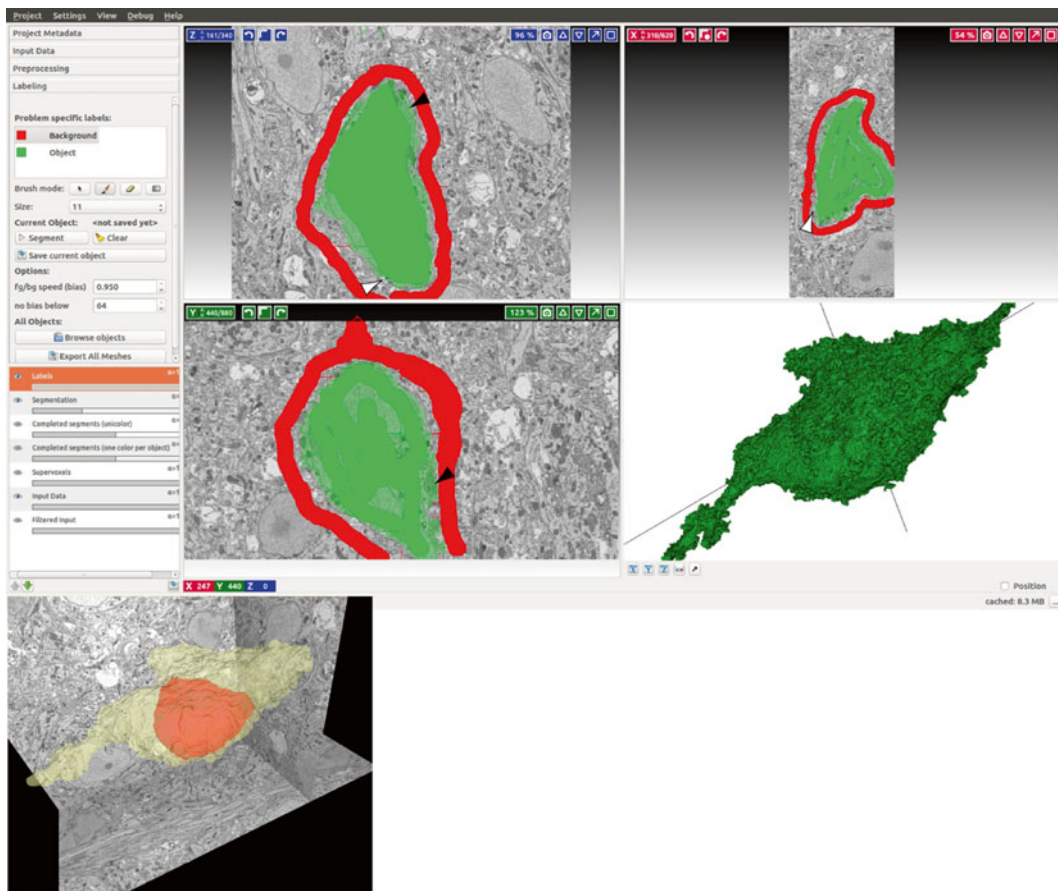


Fig. 3 Carving cells in ilastik (*top*). Training data for cell interior (*solid green*) and background (*solid red*) in all three dimensions is used by ilastik to define the cell segmentation. The result of the segmentation is overlaid on the EM images (*translucent green*). Additional training data can be added to missed pieces of the cell (*white arrowheads*) and background that was incorrectly identified as cell (*black arrowheads*) in an iterative fashion to refine the segmentation. A 3D representation of the current segmentation is displayed in the lower right panel to assist in refinement. This process can produce both a mask of the cell segmentation for further refinement, or a 3D mesh in OBJ format (*bottom*, shown with nucleus (*red*), cell body (*tan*) and EM in the Seg3D software (*see Note 11*) for measurement and display

3.4 Cell Segmentation

Carve nucleus and cell body for each cell in ilastik. The carving workflow in ilastik provides a fast and straightforward method for segmentation of single objects such as cell bodies [8]. Using an oversegmentation of the data into supervoxels (automated groupings of pixels based on intensity and intensity gradient characteristics) and training data supplied by the user, ilastik combines the supervoxels into “object” and “background” segmentations.

1. Run ilastik.
2. Click the “Project” menu option at the top of the screen and select “Open Project...” or use the Ctrl + o (Command + o for Mac) shortcut key.

3. In the “Open ilastik Project” window, navigate to the folders created by CellSeeker containing the preprocessed cells.
4. Select the project file for the cell to be segmented and click “Open.”
5. When the project has finished loading, click the “Labeling” tab in the menu options on the left side of the screen.

**3.4.1 Segmenting
the Nucleus and Cell Body
(Fig. 3)**

1. Left-click on the “Object” label under the “Problem specific labels” heading in the “Labeling” tab.
2. Left-click and hold to paint the interior of the cell nucleus in the X, Y, and Z slices displayed in the image windows. Cover the interior of the nucleus as thoroughly as possible while staying within the nuclear envelope.
3. Left-click on the “Background” label under the “Problem specific labels” heading in the “Labeling” tab.
4. Left-click and hold in the EM image slices displayed in the image windows to paint the area surrounding the nucleus as background in the X, Y, and Z. Make sure the background label covers a subset of pixels that represent the majority of the background (i.e., non-nuclear) image (*see Note 8*).
5. Left-click on the “Segment” button under the “Current Object” heading in the “Labeling” tab. ilastik will produce an initial segmentation of the nucleus based on the training data provided, as well as a three-dimensional representation of the object.
6. Using the slice number controls in the top-left of each image window, navigate to trouble spots in the segmentation (nucleus incorrectly labeled as background and vice-versa) and add additional labels to refine the segmentation. Once changes are made, the “Segment” button must be clicked again to update the segmentation.
7. Once an acceptable nucleus segmentation is obtained (*see Note 9*), click the “Save current object” button under the “Current Object” heading in the “Labeling” tab. Name the object “nucleus” and click the “OK” button.
8. In the list of layers at the bottom-left corner of the window, right-click on the “Segmentation” layer and click “Export....”
9. In the “Image Export Options” window, under the “Output File Info” header, click the “Select...” button next to the “File” option. Select a directory and filename for the nucleus segmentation and click “Save.” Click “OK” on the “Image Export Options” window to output the nucleus segmentation to an HDF5 file (*see Note 10*). Click “Finished!” when the export is complete.

10. Click the “Clear” button under the “Current Object” heading in the “Labeling” tab, then click “Clear” to clear the nucleus segmentation.
11. Repeat steps 1–10, Subheading 3.4.1 to segment and save the cell body.
12. To create three-dimensional mesh objects for the nucleus and cell body (for use in programs such as MeshLab, Blender, or any software that supports the OBJ file format) click the “Export All Meshes” button under the “All Objects:” header. Select a folder for output and click “OK” (*see Note 11*).
13. When finished, click “Project” in the menu options at the top of the window, and select “Save Project.”
14. Repeat the carving process for each verified cell.
15. At this point, two additional HDF5 files (or other format specified by the user) containing either nucleus or cell body segmentation masks for each cell have been produced. Additionally, if “Export All Meshes” was used, two OBJ files containing mesh representations of the nucleus and cell body have been produced.

4 Notes

1. As nuclei are large compared to other organelles, have a clear border (the nuclear envelope) and have a generally uniform internal texture in images, a high-resolution image is not needed to identify them. In order to increase the speed of cell identification, we recommend binning EM images to a low resolution before beginning this process. For example, our original data set for testing was a 250GB image stack with dimensions of $11,000 \times 8000 \times 1420$ at an {x, y} pixel dimension of 11.4 nm and a slice thickness of 60 nm. Before training in ilastik, we binned our images (using either the “*-scale*” command in ImageMagick or the “*newstack -bin*” command in the IMOD software (University of Colorado, Boulder; <http://bio3d.colorado.edu/imod/>). When binned by a factor of 9, the resulting image stack was a more manageable 3.1GB in size and sufficient for identifying nuclei in ilastik. If higher resolution subvolumes are desired, use the “Use different EM volume for subvolumes” option during the subvolume extraction step in CellSeeker.
2. For anisotropic data, you may want to force ilastik to see your data as individual 2D images rather than a 3D image stack to get better segmentation during nucleus training. You can do this during the data import step (*see* above, “Import EM

images into ilastik’s ‘Pixel Classification’ workflow”). In the “Raw Images” tab, next to the data set you will be working with, double-click in the “Axes” column. This will open a “Dataset Properties” window, with one of the options being “Axes.” Change the axes from “zyx” to “tyx” and click OK. If successful, you will see a “Time” indicator at the bottom-right corner of the ilastik window, with a maximum equal to the number of images in your data set. This tricks ilastik into treating your data as a set of 2D images taken at different time points, rather than a 3D volume. All other steps in the process are completed as written.

3. The feature sets provided by ilastik for training the pixel classifier are “Color/Intensity,” “Edge,” and “Texture.” For nuclei in electron microscopy images, usually all three of these categories apply; nuclei in neurons tend to be lighter in color, have clearly defined edges, and a unique speckled texture. Each feature also has an associated range of pixel sizes to choose from, the choice of which will vary depending on the resolution of the EM used. When in doubt, select as many combinations of features and pixel sizes as ilastik will allow, and refine these settings after some pixel classifier training has been completed.
4. Feature selection during the ilastik pixel classification step has a significant impact on the resulting nucleus segmentation. Typically, an iterative approach works best: select features, add training labels, check the segmentation, change the feature selection, and see if the segmentation improves. More details on feature selection can be found in the ilastik documentation at <http://ilastik.org/documentation/pixelclassification/pixelclassification.html#selecting-good-features>.
5. As often as possible, stay zoomed into a small area in ilastik when “Live Update” is on. To save computational time, ilastik only computes the segmentation for the area currently viewed, so the larger the area, the longer the computation time. When verifying that all nuclei are being segmented appropriately, it may take several minutes for the segmentation to appear in ilastik.
6. Exporting the nucleus segmentation from ilastik may take approximately 1 h per gigabyte of original image data. This will produce a nucleus segmentation file in Hierarchical Data Format (HDF5), which will be used in subsequent steps in the segmentation pipeline. This format, designed by the National Center for Supercomputing Applications, is designed for efficient storage and access of large three-dimensional data sets. The HDF5 file format has both benefits and drawbacks. For saving masked or binary information, the amount of compression obtained by using this format is significant (>30×). For more

complex images, such as EM images, the compression is more modest ($\approx 2\times$). In our hands, the HDF5 format is also slower to load into a Numpy array in Python, increasing the wait time in CellSeeker. A mixture of HDF5 and TIFF formats is allowed in CellSeeker, so it is possible to load EM images from a TIFF stack and nucleus segmentation from a HDF5 file.

7. If the size of the cell or cells is unknown, we recommend performing a rough measurement in a program such as ImageJ to get an estimate of the cell size. In this case, it is best to err the cell diameter on the smaller side; although this may produce more false positives, it is also more likely to result in complete identification of all cells in the volume.
8. For the initial training step, when carving a cell in ilastik, we have found that training on three images—one containing a cell body near the “top” of the image stack, one through the center of the cell, and one near the “bottom” of the image stack—in each image plane ($\{x, y\}, \{x, z\}, \{y, z\}$) is sufficient to obtain a reasonable segmentation quickly (usually <5 min). The amount of time for refinement of the segmentation will depend on the image resolution and level of required accuracy.
9. The number of iterations of training, proofing, and retraining will depend on the resolution of the image data and accuracy of training. For the nucleus and cell depicted in the lower panel of Fig. 3, three and five retraining iterations were necessary, respectively.
10. Although HDF5 is our recommended format for export of masks, it is advisable to make sure that the software you plan to use for post-processing can read HDF5 format. If it cannot, make sure to change the export setting in ilastik from HDF5 to your preferred format (i.e., multipage TIFF, JPEG, etc.).
11. Although 3D models can be generated directly from ilastik, we recommend importing the nucleus and cell body masks along with the corresponding EM subvolume into a proofreading tool such as Seg3D (Scientific Computing and Imaging Institute, University of Utah, <http://www.sci.utah.edu/cibc-software/seg3d.html>). This software provides powerful tools for editing the masks created by ilastik to ensure the accuracy of the segmentation, as well as allowing for 3D mesh export.

Acknowledgements

This work was supported by grants NIH F31 DC014393 to PSH, NIH R01 DC007695 to GAS, and NIH/NIGMS CoBRE P20 GM103503 to the WVU Center for Neuroscience.

References

1. Lichtman JW, Pfister H, Shavit N (2014) The big data challenges of connectomics. *Nat Neurosci* 17:1448–1454
2. Kaynig V, Vazquez-Reina A (2013) Large-scale automatic reconstruction of neuronal processes from electron microscopy images. *IEEE Trans Med Imaging* 1:1–14
3. Seyedhosseini M, Sajjadi M, Tasdizen T (2013) Image segmentation with cascaded hierarchical models and logistic disjunctive normal networks. *IEEE Int Conf Comput Vis* 2013: 2168–2175
4. Jain V, Turaga SC, Briggman KL et al (2011) Learning to agglomerate superpixel hierarchies. *Adv Neural Inform Process Syst* 24:648–656
5. Funke J, Andres B, Hamprecht FA et al (2012) Efficient automatic 3D-reconstruction of branching neurons from em data. *Computer Vision and Pattern Recognition (CVPR), IEEE Conference* 2012:1004–1011
6. Kim BYL (2015) 10 Most popular programming languages today. Inc. <http://www.inc.com/larry-kim/10-most-popular-programming-languages-today.html>. Accessed 16 Feb 2016
7. Sommer C, Straehle C, Ullrich K, Hamprecht FA (2011) Interactive learning and segmentation toolkit. *Biomedical Imaging: From Nano to Macro, IEEE International Symposium* 2011: 230–233
8. Straehle C, Köthe U, Knott G, Hamprecht FA (2011) Carving: scalable interactive segmentation of neural volume electron microscopy images. *Med Image Comput Comput Assist Interv* 14:653–660

Part IV

Cell Culture and Tissue Engineering Protocols

Chapter 17

Organotypic Culture of the Mouse Cochlea from Embryonic Day 12 to the Neonate

Vidhya Munnamalai and Donna M. Fekete

Abstract

The development of the mammalian cochlea is a complex process involving several intersecting signaling pathways to ultimately generate its highly organized cellular architecture. In humans, and in the mouse, there is one row of inner hair cells aligned next to three rows of outer hair cells. The support cells intercalate between the hair cells to create a cellular mosaic across the organ of Corti (OC). Organotypic culture of the cochlea is a valuable technique for investigating the early stages of OC development. Cultures can be established at proliferative stages and maintained *in vitro* until cellular differentiation commences. It is straightforward to monitor differentiation in response to perturbations of key signaling pathways using pharmacological agents. While postnatal cochlea organ cultures have already been adapted for *in vitro* studies, it is more challenging to establish cultures at early embryonic stages due to the small size of the organ primordium. The protocol described in this chapter is permissive for all stages of development from E12 cochleas to day 5 neonatal murine cochleas, allowing culture survival up to 2 weeks *in vitro*.

Key words Organotypic, *In vitro*, Mouse, Cochlea, Embryonic, Neonate

1 Introduction

Modern developmental biologists utilize transgenic mouse knock-out and knock-in strategies such as Cre-lox technology to reveal the function of various signaling components that underlie cell, tissue, and organ formation [1]. While transgenic mouse technology is invaluable to study mouse cochlear development, it can be a costly and time-consuming approach that sometimes provides limited flexibility for additional manipulations. In comparison, organotypic culture of the mouse cochlea permits one to observe, sometimes directly, changes during development, and they can offer more temporal control for drug treatments. They can also be cost-effective, or used in combination with transgenic mouse lines to fine-tune the cell types that can be manipulated. Overexpression of genes in the cochlear anlage by electroporation (from E13.5), or viral infection (from E12.5) can be readily performed *in vitro*, thus

bypassing the requirement of in utero surgery [2–4]. Organotypic culture also allows manipulation of several signaling pathways simultaneously, which is less feasible *in vivo*. Similarly, the addition of signaling factors, such as morphogens, can strengthen transgenic mouse studies, or can be applied in conjunction with pharmacological agents [5]. Thus, the applications for this technique are wide and varied. Moreover, they offer an advantage as a preliminary approach that can be explored before applying transgenic or surgical methods.

At the developmental stages considered in this chapter, the texture of the tissue surrounding the inner ear capsule is soft, forcing the experimenter to rely on visual cues, rather than tactile feedback. The dissection procedure described here can be divided into two parts: extraction of the inner ear capsule and a finer dissection of the inner ear capsule. In this chapter, we will describe how to identify and remove the inner ear using developmental landmarks at E12.5, the finer dissection of the cochlea using enzymatic and mechanical separation, and the culture preparation. These methods have been modified from previously published protocols [5, 6].

2 Materials

2.1 Media and Solutions

1. Hank's Balanced Salt Solution Ca/Mg plus (HBSS): In a pre-autoclaved beaker with a stir bar, add the contents of one bottle of HBSS powder (Sigma, St. Louis, MO) to 850 mL of sterile water. Add 1.2 g HEPES and mix well on a stir plate. Adjust the pH to 7.6 with 10 mM NaOH, then add H₂O to fill up to 1 L. Filter through a 0.2 µm Steritop filter unit (Millipore, Billerica, MA) into an autoclaved sterile bottle.
2. Dispase/Collagenase enzyme mix: Add 100 mg Dispase and 100 mg Collagenase, Type 1 (Life Technologies, Grand Island, NY) to 10 mL of sterile HBSS. Mix well and filter with a 0.2 µm syringe filter. Make 400 µL aliquots and store at -20 °C (*see Note 1*).
3. DNase Solution: Add the contents of one vial of deoxyribonuclease (DNase) (15 K units, Sigma, St. Louis, MO) to 10 mL of HBSS and filter with a 0.2 µm syringe filter. Make 600 µL aliquots and store at -20 °C. A 600 µL aliquot will serve 3 procedures (200 µL each) (*see Note 2*).
4. Matrigel Mix: Thaw a 5 mL vial of "reduced growth factor Matrigel" (BD Biosciences, San Jose, CA) in a beaker of ice at 4 °C overnight. Make 0.5 mL aliquots with pre-chilled pipette tips and Eppendorf tubes. Store at -20 °C (*see Note 3*).
5. Collagen Mix: On the same day that the Matrigel is set to thaw overnight, prepare the collagen by adding 5 mL of ice-cold,

0.02 M acetic acid to a vial of 25 mg of lyophilized type IV rat-tail collagen (Sigma, St. Louis, MO). The collagen is mixed on a nutator overnight at 4 °C. The next day, add 2 mL of cold, 5× DMEM: F12 (Reh's modified medium) and 3 mL of sterile H₂O into the vial and pipette up and down. Keep this solution on ice to avoid coagulation. Make 0.5 mL aliquots and store at -20 °C. Add 120 µL of 7.5 % NaHCO₃ to an aliquot of collagen. Check that the pH is 7.4, using pH indicator strips (*see Note 4*). Keep this neutralized collagen solution on ice.

6. Collagen-Matrigel Mix: Add 0.5 mL of the aliquoted and thawed Matrigel and 0.4 mL of sterile H₂O to the neutralized collagen. Mix well by pipetting and store in 50 µL aliquots at -20 °C. This Collagen-Matrigel mix will be used to coat Millicell culture inserts.
7. DMEM-F12 Reh's modified medium 5×: Aliquots 3.9 g of a powdered DMEM-F12 Reh's modified media (US Biologicals, Salem, MA) to a 50 mL conical tube (*see Note 5*). Store the powdered aliquots at 4 °C, until ready for use. Add H₂O up to 50 mL, mix well and filter with a 50 mL 0.2 µm Steriflip filter unit (Millipore, Billerica, MA).
8. DMEM-F12 organ culture media (50 mL): Add 10 mL of 5× DMEM-F12 media, 25 mL of sterile water, 500 µL 30 % d-glucose, 200 µL L-Glutamine, and 100 µL penicillin to a 50 mL conical tube. Add 850 µL of 7.5 % NaHCO₃ and mix well. Check to see that the pH is 7.6 by adding a drop onto a pH indicator strip and, if required, add 1 mM NaOH to adjust the pH. Filter the medium through a 0.2 µm filter into a new conical tube. Add 10 mL of fetal calf serum (FCS), 500 µL of N2, 1 mL of B27 without retinoic acid and 200 µL of Hybrimax DMSO. Add H₂O up to 50 mL, mix well and filter media with a 50 mL Steriflip filter unit.
9. Additional solutions and materials: Sterile tissue culture H₂O, 30 % d-Glucose solution sterile-filtered with an 0.2 µm filter, 200 mM L-Glutamine, 50,000 units/mL Penicillin-G, 7.5 % NaHCO₃ sterile-filtered with a 0.2 µm filter, 1 mM NaOH, sterile-filtered with an 0.2 µm filter, heat-inactivated FCS (*see Note 6*), N2 supplement (Life Technologies, Grand Island, NY), B27 supplement without retinoic acid (Life Technologies, Grand Island, NY), Hybrimax DMSO (Sigma, St. Louis, MO) and pH indicator strips (pH 6.5–10).

2.2 Materials for Dissection

1. Sterile HBSS.
2. Dissection Tools: Two #5 fine forceps, two #55 fine forceps, one pair of dissection scissors, Moria perforated spoon (8 mm tip diameter, 1 mm depth), scalpel blade holder and scalpel blades.

3. Kimwipes.
4. Two Sylgard dissection dishes dedicated for cell culture (one—6 cm and one—35 mm diameter). These can be made in-house using the Sylgard 184 kit from Dow Corning. Measure 10:1 of Part A liquid to Part B liquid. Mix well in a beaker with a spatula. Avoid mixing vigorously to prevent bubbles forming. Add activated charcoal powder to the solution and mix until it is well incorporated. Fill glass dissection dishes until one-third full. Remove excess bubbles by placing in a degassing chamber under vacuum. Leave to cure in the chamber for a few hours, then, very carefully, release pressure from the chamber. Additional bubbles may be released when releasing pressure. Use a kitchen lighter and lightly torch the surface to release any remaining bubbles. Allow the dishes to cure overnight on a flat surface.
5. Culture plates: Five 35 mm plastic cell culture dishes and one 6-well tissue culture plate
6. 12 mm 0.4 µm PTFE membrane Millicell culture inserts (Millipore, Billerica, MA).
7. Two 10 cm autoclaved glass Petri dishes, wrapped in foil to keep sterile.
8. Three individually wrapped, sterile transfer pipettes.
9. Ice bucket filled with ice.
10. Dissection microscope and light source with flexible light guides.
11. Alcohol lamp filled with 100 % ethanol.

3 Methods

3.1 Tissue Culture Preparation

3.1.1 Matrigel-Coated Inserts

1. Thaw a 50 µL aliquot of Collagen-Matrigel on ice and keep on ice to avoid polymerization.
2. Add 10 µL Collagen/Matrigel to the center of each insert and spread it out using the pipet tip to apply a thin layer of Collagen-Matrigel. Incubate at 37 °C for 1 h in a 24-well plate.
3. Add 300–500 µL of DMEM-F12 to each insert. The inserts can be stored at 4 °C for up to 2 weeks.

3.1.2 Preparing a 6-Well Culture Plate

1. In a biosafety hood, turn on the UV light for 20 min. Spray the surface with 70 % ethanol. Any items entering the hood should be sprayed off with ethanol to ensure sterility.
2. Spray ethanol onto a Kimwipe, neatly fold it into the lid of a plastic 6-well cell culture plate, and allow to dry on the lid. This will keep the Kimwipe sterile.

3. When Kimwipe is dry, add 1 mL of sterile tissue culture H₂O to the Kimwipe. This humidifies the 6-well chamber and prevents the cultures from drying out.
4. Add inserts coated with Collagen/Matrigel to each well and add 1 mL of DMEM-F12 to each well.

3.2 Embryo Collection

Experiments using animal tissue should be approved by the University's Institutional Animal Care and Use Committee as set forth under the guidelines of the National Institutes of Health.

1. Euthanize pregnant dam by CO₂ inhalation, followed by a secondary method of euthanasia such as decapitation, or cervical dislocation.
2. In a biohazard bag, lay the pregnant dam on her back and spray her abdomen with 70 % ethanol. With forceps, lift the skin over the abdominal cavity and make a deep vertical incision into the skin and the abdominal wall along the midline using scissors. Take care not to cut into the uterus or internal organs. Open the abdominal cavity and with forceps, carefully pick up one uterine horn containing embryos. Cut out the entire uterus (both uterine horns) containing embryos. Spray the uterus with 70 % ethanol and transfer to a clean sterile Petri dish. Add HBSS to the dish containing the uterus and keep on ice. Dispose of the carcass according to proper institutional procedures.
3. Clean the dissection surface with a 1 % bleach solution, wipe down with a paper towel and allow to air dry. Wipe once again with 70 % ethanol solution. Dip the forceps and Moria spoon into 100 % ethanol and flame-sterilize with the alcohol lamp. Line up tools on a paper towel drenched with 70 % ethanol. Spray the Sylgard dishes with 70 % ethanol and turn upside down to drip dry.

3.3 Dissection:

Part 1

1. Unless otherwise noted, #5 dissection forceps are used when referring to forceps. Under a dissection microscope, use forceps to carefully tease apart the uterine wall to reveal the amniotic sack containing an embryo. Early-stage embryos (e.g. E12.5) are very delicate, so avoid exerting too much force. Remove the embryos from each sack by pulling on the umbilical cord. Using the Moria spoon, transfer all embryos to a new sterile dish containing HBSS on ice.
2. Transfer one embryo into a 6 cm Sylgard dissection dish containing HBSS. Cut the embryo below the front limbs by pinching with forceps and severing the posterior half from the anterior half of the embryo (Fig. 1a, Cut 1). Make the second cut at the midbrain of the embryo (Fig. 1a, Cut 2) and peel back the ectoderm along the dorsal side (Fig. 1a, Cut 3) to

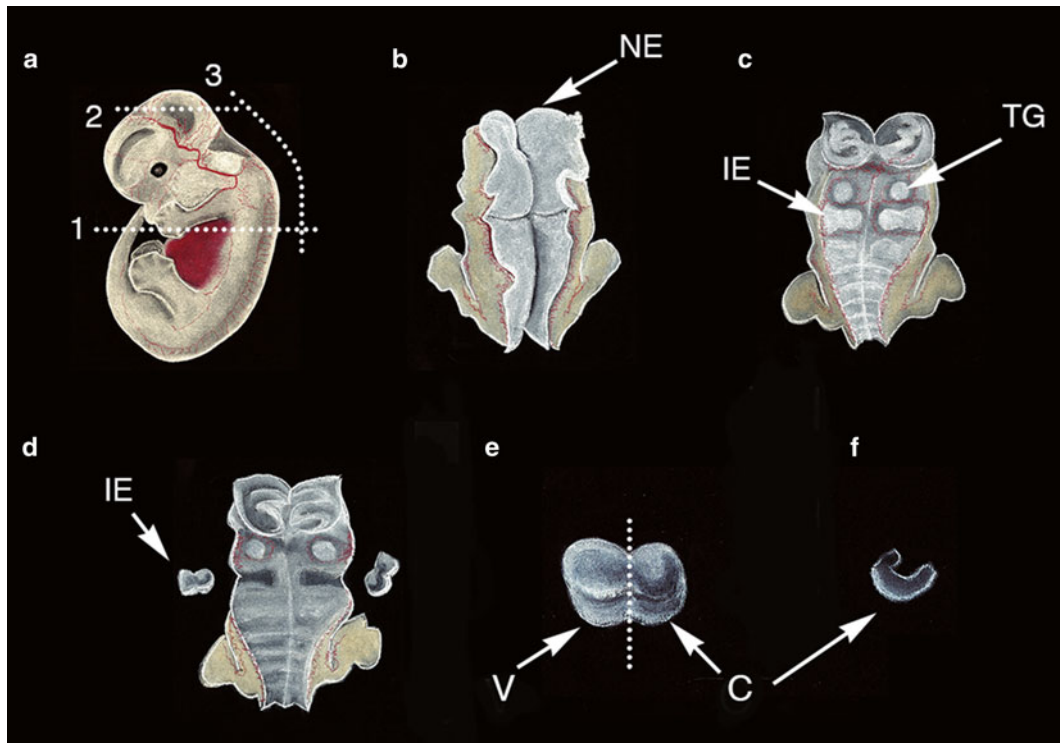


Fig. 1 Schematic of embryonic cochlear dissection at E12.5. (a) A cut is made across the dorsoventral axis below the forelimbs (1), followed by a cut along the midbrain to expose the brain cavity (2). (b) The ectoderm is peeled along the dorsal midline of the embryo (3) to reveal the neuroepithelium, NE. The neuroepithelium layer is removed to access the inner ear capsule. (c) The inner ear (IE) capsule is positioned posterior to the trigeminal ganglion (TG). (d) The inner ear capsules are dissected out and transferred to a dish with cold HBSS. (e) Following enzymatic digestion, the vestibular half (V) of the inner ear is separated from the cochlear half (C), allowing access to the cochlea. (f) The surrounding capsule tissue is then carefully scored and peeled away with fine forceps, to reveal the cochlear duct

reveal the neuroepithelium, NE (Fig. 1b). Remove the neuroepithelium by sliding forceps under the epithelium, and separating it from the main body. Once the neuroepithelium has been removed, the inner ears are not visible from a dorsal view. The inner ears are located posterior to the trigeminal ganglion, with the cochlear half oriented toward the midline (Fig. 1c). The tissues surrounding the otic capsule and the trigeminal ganglion are relatively more transparent, so reposition the light guides, if necessary, to study the differences in opacity.

3. Use #55 fine forceps for all subsequent dissections. Once the inner ear capsules have been visually identified, remove each (IE in Fig. 1d) and transfer to a 35 mm dish containing cold HBSS with a sterile plastic transfer pipette. As the embryo develops, the inner ear capsules become easier to identify. Keep

on ice until all inner ear capsules have been collected. At E12.5, the inner ear capsules are very delicate; therefore, remove the inner ears by making clean cuts around the capsule. From E13.5 onwards, the cartilage in the capsule has sufficiently differentiated from the surrounding tissue that they can be “scored” using the tips of fine forceps. At E15.5, the capsules can be easily extracted by sliding forceps beneath the capsule.

3.4 Dissection:

Part 2

1. Add 4 mL of HBSS to four 35 mm dishes. To the first, add 400 μ L of the Dispase/Collagenase solution. The remaining three dishes are for wash steps after enzymatic digestion. Add 2–4 otic capsules to the Dispase/Collagenase dish and incubate at room temperature for 3–5 min (*see Note 1*). Transfer the capsules from the protease solution to the first HBSS wash dish and pipette up and down a few times, then transfer to the second, repeat and finally transfer to the third dish to wash off the Dispase/Collagenase. Transfer the ear capsules to a new Sylgard dish with 6 mL of HBSS. Add 200 μ L of the DNase solution to the dissection dish.
2. Transfer the digested inner ears into a 35 mm Sylgard dissection dish with a new transfer pipette (*see Note 7*). Cut the inner ear in half to separate the ventral cochlear half from the dorsal vestibular half (Fig. 1e), using #55 fine forceps. Carefully, peel away the pre-cartilage capsule tissue layer, while trying to keep as much loose mesenchyme around the cochlea as possible (Fig. 1f). At E12.5, the capsule tissue is very soft and offers no tactile feedback. From E13.5 to E15, the capsule tissue is relatively easy to peel away without pulling off the mesenchyme. From E15.5 onwards, the capsule tissue becomes cartilaginous. Dispase/Collagenase digestion is not required for E16.5 cochlea dissections. The cartilage from the capsule can be separated from the cochlea by merely pinching and cutting with forceps. If the cochleas are to be cultured in the presence of purified signaling factors, which unlike pharmacological agents cannot pass through the non-sensory anlagen of the cochlea, then the duct should be sliced open. Slide the forceps through the duct and pinch along the non-sensory side to open the cochlear duct (*see Note 8*). The non-sensory side is identified by inspecting the mesenchyme and the spiral ganglion. The sensory side has a slightly thicker layer of mesenchyme than the non-sensory side of the duct. Also, the neurites of the spiral ganglion can be traced to the sensory side. Removing the spiral ganglion is optional and is not required for differentiation of the OC. After E16.5, it is highly recommended to cut away the non-sensory side of the duct if the explants are to be used for fluorescence imaging.

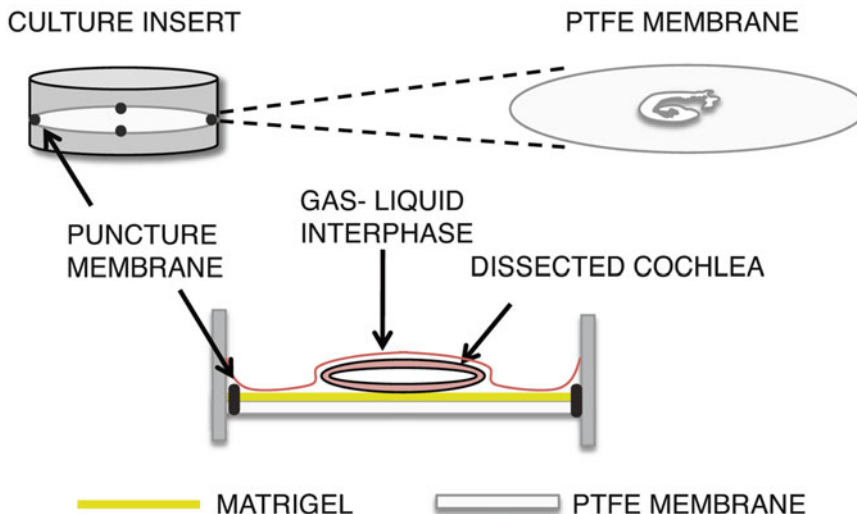


Fig. 2 Schematic of cochlear duct cultures in cell culture inserts. The dissected cochlear duct is placed on the PTFE membrane with the sensory side of the duct touching the Matrigel coated surface of the insert and the non-sensory side upward. The hair cells are oriented upwards within the lumen of the duct. Using forceps, carefully puncture the PTFE membrane close to the walls of the insert, as shown, to allow the outflow of excess media. With a sterile pipette, remove enough media leaving a thin film of media to coat the cochleas. Four to six explants from E12.5 embryos can be cultured on a single insert. (Image not drawn to scale)

3. Transfer cochleas onto the Collagen/Matrigel-coated inserts containing organ-culture media. Orient the cochleas so that the sensory side contacts the insert membrane surface. Puncture the PTFE membrane against the walls of the insert, using forceps to allow excess media to flow out. Alternatively, draw up the excess media from outside the insert with a transfer pipette. With either method, the goal is to leave a thin film of media covering the explant. This keeps the cochlea at the gas-liquid interphase and will also help it to adhere to the insert (Fig. 2).
4. Incubate the cultures at 37 °C, 5 % CO₂ for 5–6 days in vitro or for the desired incubation period. The longest we have successfully cultured the tissue is 15 days. Replace all the medium every 2–3 days. Always check to make sure that a thin film of media is covering the explants. Rehydrate the Kimwipe lining the lid with sterile water, if necessary, to maintain humidity.
5. Fix cochleas or process tissue as desired. Whole membranes containing the cochleas can be cut out with a scalpel blade and used for whole-mount immunostaining or in situ hybridization. The inserts can also be cut out and directly transferred into Trizol for RT-qPCR analysis. Figure 3 shows examples of cochleas fixed and immunolabeled for Sox2 at E12.5 (Fig. 3a),

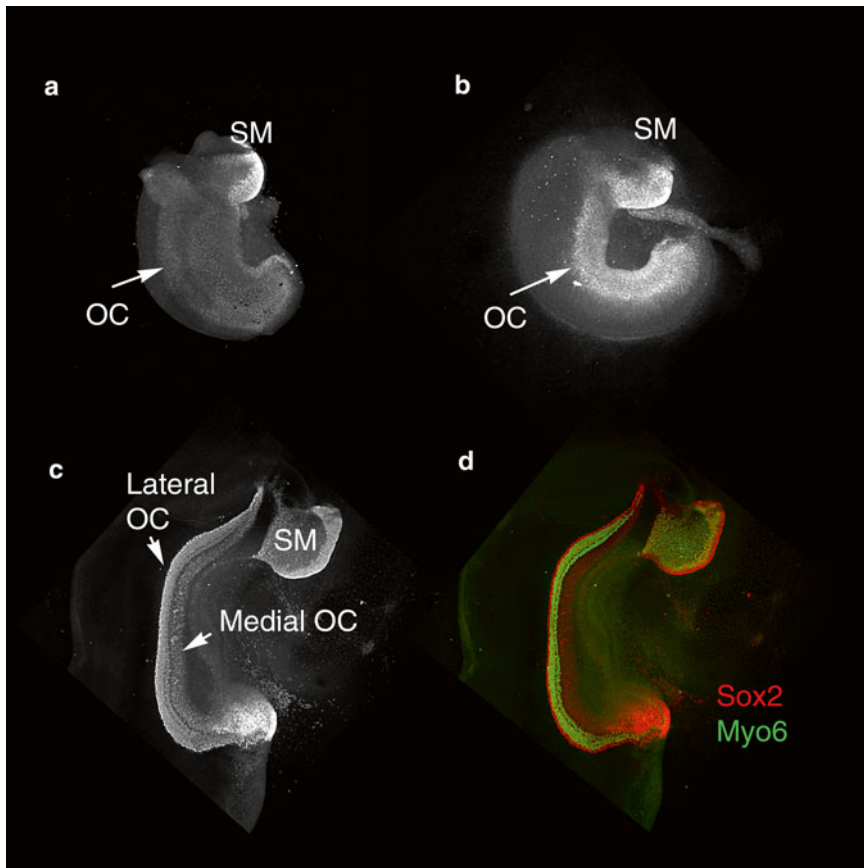


Fig. 3 Progression of an E12.5 cochlea through development. It is useful to ensure that the organ cultures are developing properly in vitro. Sox2 is a useful marker to follow the development of the organ of Corti (OC). Including the Saccular Macula (SM) is optional but allows for easy identification of the base versus the apex, especially if the duct is sliced open. (a) At E12.5, the cochlea consists of a homogeneous population of progenitor cells. Sox2 is homogeneously expressed across the cochlear duct. (b) After 24 h, Sox2 expression shows the sensory domain becomes refined across the radial axis. (c) After 6 days in vitro, Sox2 immunolabeling demonstrates the complexity of differentiated support cells across the radial axis. Both, the medial and lateral compartments of the OC can be readily identified because the Sox2-positive nuclei in both compartments show distinct morphology, with larger nuclei in the lateral compartment. (d) The same cochlea in (c) is immunolabeled for Sox2 for the sensory domain (red) and Myo6 for hair cells (green)

E12.5 + 24 h (Fig. 3b), and E12.5 + 6 days in vitro (Fig. 3c). When practicing dissections, it is helpful for the experimenter to immunolabel cochleas with Sox2 and make sure development progresses as expected. A well-developed cochlea from E12.5 will show the formation of both supporting cells and hair cells (Fig. 3d).

6. Clean tools using ethanol and a nailbrush with soft bristles. Soak Sylgard dishes with 1 % bleach for 10 min and rinse thoroughly (*see Note 9*).

4 Notes

1. Dispase and Collagenase are proteases that help separate layers of tissue surrounding the cochlea for easier separation by forceps. Dispase is a mild protease that maintains cell membrane integrity and is suitable for primary organ culture, while Collagenase helps separate the connective tissue between the cochlea and the collagen in the capsule [7]). Extended exposure to Dispase/Collagenase will sometimes cause the mesenchyme to peel off. This culture protocol, particularly at E12.5, requires that the mesenchyme is present. The mesenchyme tissue adheres quickly to the extracellular matrix proteins in the Matrigel coating of the insert. The mesenchyme is also required for optimal development of the OC with minimal cell death.
2. The inclusion of DNase helps counteract the sticky genomic DNA released from damaged cells during the dissection. This can be especially problematic in cochleas of younger stages (E12.5–E14) [8].
3. Matrigel polymerizes at 10 °C, thus, care must be taken to avoid excessive handling. Aliquots are thawed on ice. Multiple freeze–thaws are acceptable; however, it is advisable making small aliquots of the Collagen/Matrigel mix.
4. When using pH strips, always add the solution to the strips. Avoid dipping the strips into the solution as this may introduce contaminants.
5. The DMEM-F12-powdered media is very hydrophilic, so aliquot in a space with low humidity. Store powdered media at 4 °C with dessicant, such as Drierite, to keep dry.
6. FCS or FBS is heat-inactivated by a 56 °C water bath for 30 min.
7. To avoid excess exposure to Dispase/Collagenase, use dedicated transfer pipettes for each step: one for the protease incubation, a second for the washes, and the third for transferring in and out of the Sylgard dissection dish.
8. Avoid pulling on the tissue as this exerts stress and can sometimes be inhibitive to growth and development. Neat clean cuts will produce better results. One technique that is guaranteed to produce clean cuts is exemplified in Fig. 1a. Pinch the embryo across the dorsoventral axis (Cut 1) with one forceps, and run the tip of the other fine forceps along the long-axis of the pinched pair of forceps toward the tip. This guided “shearing” of the tissue along the edges of the forceps will produce very clean cuts.
9. Do not clean tools or Sylgard dishes with soap. Soak in 1 % bleach solution and rinse thoroughly with distilled H₂O. Keep

dedicated Sylgard dishes for live tissue dissections separated from those used for fixed tissue: formaldehyde can seep out from the Sylgard and into the fresh cochlear tissue.

Acknowledgments

The authors thank the members of the Fekete lab for helpful suggestions included in the protocol. Work in the Fekete lab using this culture technique is funded by NIH/NIDCD grant R01 DC002756.

References

1. Oumard A, Qiao J, Jostock T, Li J, Bode J (2006) Recommended method for chromosome exploitation: RMCE-based cassette-exchange systems in animal cell biotechnology. *Cytotechnology* 50(1–3):93–108. doi:[10.1007/s10616-006-6550-0](https://doi.org/10.1007/s10616-006-6550-0)
2. Brigande JV, Gubbel SP, Woessner DW, Jungwirth JJ, Bresce CS (2009) Electroporation-mediated gene transfer to the developing mouse inner ear. *Methods Mol Biol* 493:25–139. doi:[10.1007/978-1-59745-523-7_8](https://doi.org/10.1007/978-1-59745-523-7_8)
3. Gubbel SP, Woessner DW, Mitchell JC, Ricci AJ, Brigande JV (2008) Functional auditory hair cells produced in the mammalian cochlea by *in utero* gene transfer. *Nature* 455(7212):537–541. doi:[10.1038/nature07265](https://doi.org/10.1038/nature07265)
4. Wang L, Jiang H, Brigande JV (2012) Gene transfer to the developing mouse inner ear by *in vivo* electroporation. *J Vis Exp* (64). doi: 3791/3653
5. Munnamalai V, Hayashi T, Birmingham-McDonogh O (2012) Notch prosensory effects in the mammalian cochlea are partially mediated by Fgf20. *J Neurosci* 32(37):12876–12884. doi:[10.1523/JNEUROSCI.2250-12.2012](https://doi.org/10.1523/JNEUROSCI.2250-12.2012)
6. Hayashi T, Kokubo H, Hartman BH, Ray CA, Reh TA, Birmingham-McDonogh O (2008) Hesr1 and Hesr2 may act as early effectors of Notch signaling in the developing cochlea. *Dev Biol* 316(1):87–99. doi:[10.1016/j.ydbio.2008.01.006](https://doi.org/10.1016/j.ydbio.2008.01.006)
7. Chen SY, Hayashida Y, Chen MY, Xie HT, Tseng SC (2011) A new isolation method of human limbal progenitor cells by maintaining close association with their niche cells. *Tissue Eng Part C Methods* 17(5):537–548. doi:[10.1089/ten.TEC.2010.0609](https://doi.org/10.1089/ten.TEC.2010.0609)
8. Gong Q (2012) Culture of mouse olfactory sensory neurons. *Curr Protoc Neurosci Chapter 3:Unit3 24*. doi: [10.1002/0471142301.ns0324s58](https://doi.org/10.1002/0471142301.ns0324s58)

Chapter 18

Quantifying Spiral Ganglion Neurite and Schwann Behavior on Micropatterned Polymer Substrates

Elise L. Cheng, Braden Leigh, C. Allan Guymon, and Marlan R. Hansen

Abstract

The first successful in vitro experiments on the cochlea were conducted in 1928 by Honor Fell (Fell, Arch Exp Zellforsch 7(1):69–81, 1928). Since then, techniques for culture of this tissue have been refined, and dissociated primary culture of the spiral ganglion has become a widely accepted in vitro model for studying nerve damage and regeneration in the cochlea. Additionally, patterned substrates have been developed that facilitate and direct neural outgrowth. A number of automated and semi-automated methods for quantifying this neurite outgrowth have been utilized in recent years (Zhang et al., J Neurosci Methods 160(1):149–162, 2007; Tapias et al., Neurobiol Dis 54:158–168, 2013). Here, we describe a method to study the effect of topographical cues on spiral ganglion neurite and Schwann cell alignment. We discuss our micro-fabrication process, characterization of pattern features, cell culture techniques for both spiral ganglion neurons and spiral ganglion Schwann cells. In addition, we describe protocols for reducing fibroblast count, immunocytochemistry, and methods for quantifying neurite and Schwann cell alignment.

Key words Photopolymerization, Topographical micropattern, Spiral ganglion, Primary culture, Dissociated culture, Explant

1 Introduction

Spiral ganglion neurite and Schwann cell guidance is an important therapeutic aim in the treatment of hearing loss and design of cochlear implants. Microfabrication of patterned substrates to direct cell growth has had a significant impact on understanding Schwann cell and neurite guidance [1–4]. Imposed topography on engineered substrates can promote cell adhesion, spreading, alignment, and changes in morphology and gene expression [5]. The conventional microfabrication technique, to form topographical micro- and nanopatterns, is photolithography, which most often involves a clean room and numerous coating and washing steps to generate substrates [6]. This approach is often time-consuming and expensive, and results in sharp patterns with zero-one transitions and a virtually infinite slope.

In contrast to photolithography, photopolymerization is a simple one-step method to quickly and inexpensively form substrates with smooth topographies and gradually sloping transitions between ridges and grooves. The amplitude of these linear patterns is easily controlled; channel depths may range from 250 nm to 10 μm . These micropatterns guide spiral ganglion neurite pathfinding *in vitro* [7]. Here, we describe the one-step fabrication method to generate parallel groove-ridge topographies. Spiral ganglion cultures can then be plated on the photopatterned substrates and observed for alignment to the pattern.

Both explant and dissociated spiral ganglia may be plated on these micropatterned materials. While neurite behavior can be observed in explant cultures, it is sometimes difficult to quantify, because of high cell densities. However, explants may be advantageous, if large numbers of cells are needed within a small area or when preserving native tissue structure. In contrast, dissociated culture is best for observing single cell morphology. It should be noted that dissociated spiral ganglion cultures have a mixed population of cells with distinct shapes. Spiral ganglion neurons typically have round cell bodies with eccentric nuclei and a variable number of thin hair-like neurites extending out from the soma. These neurons require trophic support for survival, since they will typically die within 48 h without neurotrophins or other sources of support [8]. Schwann cells typically are spindle-shaped, though in some cases the cell edges have a ruffled appearance. Fibroblasts have a variable morphology, but tend to be multipolar and flattened. Immunocytochemical staining for cell type specific markers is always used to confirm cell identity.

We also describe the system we developed to quantify the effect of patterned substrates on neurite alignment. A number of automated and semi-automated methods for quantifying neurite outgrowth have been developed in recent years [2, 3], but most methods focus on measuring neurite length rather than directionality. To determine the alignment of neurites to linear patterns, we calculate an alignment ratio of each neurite relative to the pattern, using the measurement tool in ImageJ (NIH). This measurement is defined as the overall traced neurite length divided by the length of a line parallel to the pattern (end-to-end distance) (Fig. 1). Using this method, we are able to measure neurite alignment to a linear feature, as well as neurite segment angle distribution relative to the linear feature [7, 9]. For more complex patterns, we developed a simple custom MATLAB (MathWorks)-based algorithm for parsing neurite segments and binning angle measurements [7].

Finally, we describe a simple method for quantifying the alignment of Schwann cells on patterned substrates. An ellipse is fit to the outline of the Schwann cell, and the major axis of this ellipse is used as a measurement of the directionality of the cell relative to the pattern [10].

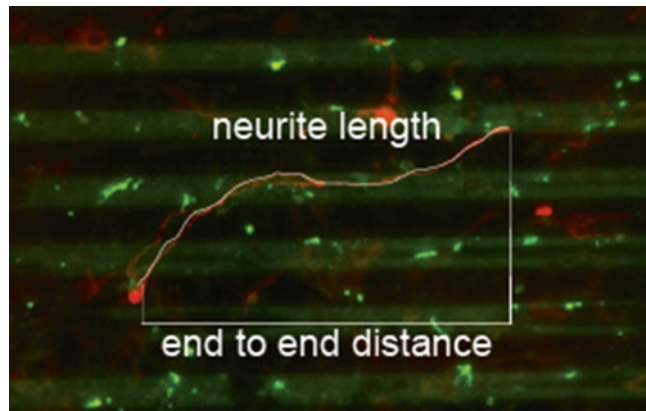


Fig. 1 Method for quantifying neurite alignment to linear patterns. Alignment ratio is defined as the ratio of neurite length to end-to-end distance. As the length of the neurite increases over the end-to-end distance, the alignment ratio increases. A perfectly aligned neurite would have an alignment ratio of 1

2 Materials

2.1 Monomer and Silane Coupling Agent Solutions

1. General Monomer Solutions: Weigh 1 wt% of 2,2-Dimethoxy-1,2-diphenylethan-1-one (Irgacure 651(I-651)), a photoinitiator used for photopolymerization, in a glass vial.
2. Place the vial onto a balance, pipette the appropriate amounts of monomers into the vial (*see Note 1*) and vortex until completely dissolved [10, 11].
3. Store the resulting pre-polymer solution in the dark at room temperature until needed. This storage will avoid any unwanted premature polymerization (*see Note 2*).
4. Silane Coupling Agent Solution: Pipette 1 mL of 3-(trimethoxysilyl) propyl methacrylate (silane coupling agent) into a glass bottle containing 100 mL of hexanes. Swirl the solution gently to ensure mixing.

2.2 Micropattern Substrate Fabrication and Characterization

1. Mercury vapor arc lamp equipped with a collimator lens to ensure uniform intensity throughout illuminated region.
2. Unfrosted glass microscope slides (2.54 cm × 7.62 cm).
3. Quartz or glass photomasks (10–100 μm periodicity).
4. Glass cutter.
5. Glass dish with a sealable lid large enough to store several glass slides without stacking.
6. Non-sterile Petri dish.
7. 95 % v/v ethanol solution.

8. Hexanes.
9. White light interferometer.
10. Scanning electron microscope.

2.3 Surgical Instruments

1. Heavy scissors.
2. Tissue scissors (small Iris scissors work well).
3. Fine forceps x2 (size 55 forceps work particularly well).
4. Bucket of ice.
5. Sterile normal saline.
6. Two sterile Petri dishes.
7. Sterile scalpel blades (11 or 15 blades will work well).

2.4 Cell Culture Reagents

1. Tissue culture hood with UV germicidal lamp.
2. N2 media with 10 % fetal bovine serum (FBS): To make 10 mL of media use 8.7 mL 1× Dulbecco's Modified Eagle Medium, 1 mL FBS, 100 µL of 1 mg/mL insulin stock for a final concentration of 10 µg/mL, 200 µL of 100× N-2 Supplement (Gibco, Life Technologies, Grand Island, NY).
3. Hank's Buffered Saline Solution with Ca²⁺/Mg²⁺ (HBSS^{+/+}).
4. Hank's Buffered Saline Solution without Ca²⁺/Mg²⁺(HBSS^{-/-}).
5. Poly-L-Ornithine 0.01 % aqueous solution.
6. Laminin at 20 µg/mL in HBSS^{-/-}.
7. Neurotrophin 3 (NT-3): Mix NT-3 in N2 medium for a 50 ng/mL final concentration.
8. Brain-derived neurotrophic factor (BDNF): Mix BDNF in N2 medium for a 50 ng/mL final concentration.

2.5 Immunocytochemistry, Protease, and Anti-fibroblastic Reagents

1. 50 mL Blocking buffer: Dissolve 1 g of powdered bovine serum albumin (BSA) in 25 mL of PBS and vortex. Add 2.5 mL of Normal Goat Serum (NGS), top off to 50 mL with additional PBS, then add 50 µL of Triton-X.
2. 10× PBS stock solution: 1.37 M NaCl, 27 mM KCl, 80 mM Na₂HPO₄, 20 mM KH₂PO₄ in 1 L of ddH₂O. Heat to dissolve and adjust to pH 7.4 using 10 N NaOH and/or 2 N HCl.
3. 0.8 % Triton-X in PBS: Add 0.4 mL of Triton-X to 49.6 mL of PBS.
4. 4 % Paraformaldehyde (PFA) in PBS: Dissolve 2 g of PFA in ~48 mL of PBS.
5. 0.25 % Trypsin solution in HBSS^{-/-} (Gibco by Life Technologies, Grand Island, NY).
6. 0.2 % Collagenase solution in HBSS^{-/-}: For 15 mL of solution, weigh 30 mg of collagenase powder (Sigma-Aldrich, St. Louis,

MO) and dissolve in 15 mL of HBSS^{-/-}. Sterile filter and store in 0.5–1 mL aliquots at -20 °C until needed.

7. Minimum Essential Medium Eagle with D-valine modification (Sigma-Aldrich) (*see Note 3*).
8. Cytosine β-D-arabinofuranoside (AraC, Sigma-Aldrich).

2.6 Microscopy and Software

1. Epifluorescent microscope with digital camera.
2. MetaMorph® Microscopy Automation and Image Analysis Software.
3. Computer with a large, high-quality monitor.
4. ImageJ (Rasband, W.S., ImageJ, U. S. National Institutes of Health, Bethesda, Maryland, USA, <http://imagej.nih.gov/ij/>, 1997–2014).
5. MATLAB (R2013b, Natick, Massachusetts: The MathWorks Inc., 2013).

3 Methods

3.1 Glass Slide Activation

1. Arrange standard 2.54 cm × 7.62 cm glass microscope slides in an O₂ plasma cleaner with the slides placed side by side. Expose the slides with plasma at 30 W RF for at least 3 min to ensure sufficient surface polarization.
2. Remove the glass slides from the plasma chamber and quickly transfer them to a sealed glass dish for further functionalization.
3. To this container, pour 100 mL of silane coupling agent solution over the glass slides with the plasma exposed side of the slide face up. Verify that all slides are completely submerged in the coupling agent solution. Cover the glass dish with aluminum foil or parafilm to prevent solvent evaporation overnight (*see Note 4*).
4. After letting the slides react overnight gently remove each slide, using tweezers, and wash in hexanes, then let the slides air-dry (*see Note 5*). Cut activated slides in half, using a glass cutter, forming two 2.54 cm × 3.81 cm slides, then transfer the activated glass slides into a sealed container.

3.2 Polymer Microfabrication and Characterization

1. Place an activated 2.54 cm × 3.81 cm slide on a small movable platform (an inverted Petri dish works well) and pipette 20 µL of monomer solution on the middle of the glass slide.
2. Lower a clean, lint-free, photomask slowly until it contacts the monomer droplet and the solution evenly disperses between the glass slide and the photomask.
3. Move the inverted Petri dish with the slide under a mercury vapor lamp and illuminate the sample, without disrupting the

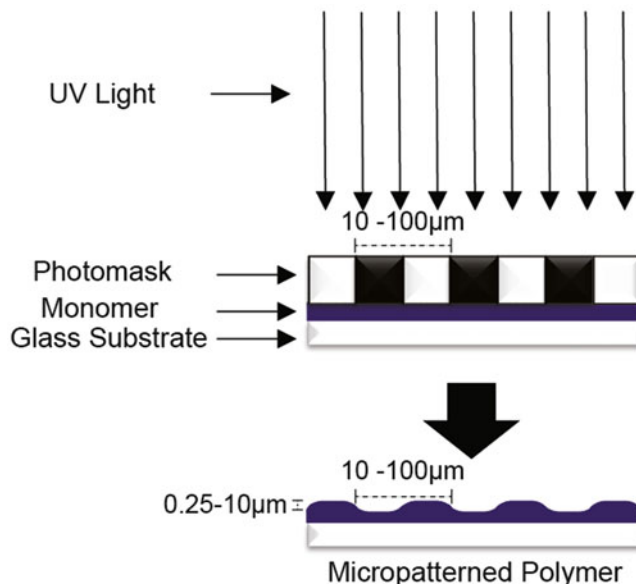


Fig. 2 Schematic of photopatterning process. Monomer is selectively exposed to UV light through transparent bands of the photomask, resulting in raised micro-features across the polymer surface

position of the photomask on the glass slide (*see Notes 6 and 7*). After polymerization, remove the photomask from the polymer by wedging a razorblade between one of the corners of the photomask and the polymer. Once the blade is secured, gently lift and the photomask should release without difficulty (*see Note 8*).

4. Wash the polymer copiously with 95 % v/v ethanol. Let the polymer air-dry and store in a covered container to avoid dust collection. The resulting polymers have microstructure as represented in Fig. 2.
5. Clean the photomask by rinsing with 95 % v/v solution.
6. Micropattern periodicity, channel amplitude, and general surface morphology of polymer samples are characterized by standard white light interferometry methods or scanning electron microscopy. Channel amplitudes will vary from 0.25 to 10 μm depending on the polymerization conditions (Fig. 3, *see Note 7*).

3.3 Preparing Polymers for Culture

1. Sterilize micropatterned polymers in a tissue culture hood by irradiating with a UV germicidal lamp in the hood for at least 5 min. Be sure that no laminin or poly-L-ornithine solutions are in the hood during this process, as the UV germicidal lamp may inactivate proteins.
2. Pour poly-L-ornithine to coat the micropatterned polymers for tissue culture and allow to coat at room temperature for 30 min, then remove.

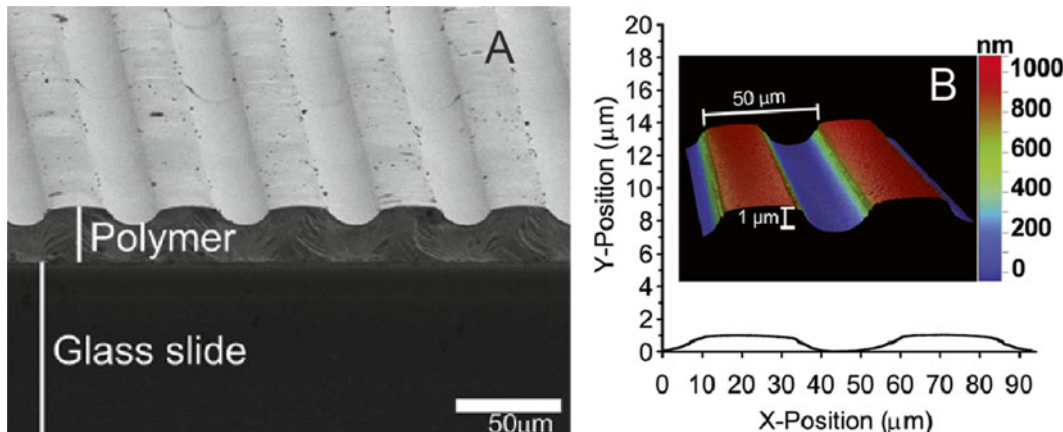


Fig. 3 Characterization of micropatterned surfaces. **(a)** Representative SEM images showing gradually sloping transitions of a parallel line patterned polymer of 8 μm amplitude and 50 μm periodicity. **(b)** 2-D profile of micropatterned polymer using white light interferometry, showing 1 μm amplitude and 50 μm periodicity. Inset: 3-D representation of 100 μm^2 area of the same polymer (Figures adapted from ref. [3]; permission for reproduction granted by Elsevier)

3. Pour 20 $\mu\text{g}/\text{mL}$ laminin solution on the poly-L-ornithine-coated micropatterned polymer and allow to coat at room temperature for 30 min or overnight at 4 °C, then remove.

3.4 Dissection

We recommend perinatal (p3–p6) rats or mice for cell cultures. All protocols should be approved by the Institutional Animal Care and Use Committee under the guidelines set forth by the National Institutes of Health.

1. Decapitate the animal using heavy scissors and bisect the head in the midline with tissue scissors (*see Note 9*). Using a blunt instrument (such as the side of the scissors), gently remove the brain tissue from the cranial cavity, clipping attached cranial nerve roots with scissors as needed.
2. Once the brain is removed, the tentorium cerebelli should be visible as a thin shelf of tissue just posterior to the temporal bone/otic capsule. Cut the area containing the otic capsule away from the rest of the skull and place in a Petri dish of PBS on ice under a dissecting microscope (*see Note 10*).
3. Remove excess tissue and bone around the otic capsule (*see Notes 11 and 12*). Stabilize the bone by grasping the lateral semicircular canal with forceps held in the non-dominant hand.
4. Remove the bony capsule of the cochlea by flicking the bone off the exterior of the cochlea using forceps held in the dominant hand.
5. Scrape off the spiral ligament and Organ of Corti, transecting the radial fibers extending outwards from the modiolus. The modiolus, containing the spiral ganglion neurons, should now

look approximately like a pine tree, tapering toward the apex and widening toward the base.

6. Using fine forceps, remove as much of the modiolar connective tissue as possible without damaging the ganglion. Incomplete removal of connective tissue is acceptable in the interest of achieving a higher neuron yield, though it may increase fibroblast count.
7. Once cleaning is complete, place the ganglion in a 1.5–2 cc tube of HBSS^{+/−} on ice and continue to harvest as many spiral ganglia as indicated by experimental needs.
8. When you have harvested as many spiral ganglia as needed, process the tissue for explants or dissociated culture.

3.5 Preparation of Explants

1. Place a single ganglion in a Petri dish of PBS on ice under the dissecting microscope. Grasp the base of the ganglion or the stump of the cochlear nerve with fine forceps to stabilize.
2. Gently uncurl the ganglion so that it lies as flat as possible using the blunt side of a scalpel blade or a second set of forceps.,
3. Cut the ganglion into four pieces (or as many as desired), using a fresh scalpel blade. Keep track of which pieces are closest to the apex vs. the base if these data are important.
4. Carefully place these explants in the desired position on your prepared substrate, using fine forceps,. It is best to have a very thin film of N2 medium on the surface of the substrate before putting the explants down, as surface tension and gravity will help keep the explant from floating away.
5. Allow the explants to settle down for 1–2 h and attach to the substrate, then add more N2 medium. Be sure to supplement the N2 medium with NT-3 and BDNF if neuronal survival is desired.

3.6 Preparation of Dissociated Cultures

1. Gently spin the tissue to the bottom of the tube of HBSS^{+/−} or simply allow the tissue to settle to the bottom of the Eppendorf vial. Remove the HBSS^{+/−} and in its place add 500 mL of warmed 0.25 % trypsin and 0.2 % warmed collagenase. Close the vial and incubate at 37 °C for 20 min with intermittent agitation.
2. Add 100 µL of FBS to the Eppendorf vial to inactivate the trypsin. Allow the tissue to settle or spin briefly in a microfuge. Remove the supernatant and add a small amount of N2 medium. Shake lightly to rinse, allow to settle again, then repeat N2 rinse a second time.
3. After the final rinse, add 0.5 mL of N2 medium to the tissue.
4. Triturate by pipetting the digested tissue up and down five to eight times using the cut-off 1000 µL pipette tip. The solution should now be turbid.

5. Triturate again 5–8× using an uncut 1000 µL pipette tip.
6. Triturate again 5–8× using an uncut 200 µL pipette tip. It is acceptable that some small, un-dissociated pieces of tissue remain at this point.
7. Add the cell suspension onto your prepared substrate (*see Note 13*). Add N2 medium, which is now supplemented with NT-3 at 50 ng/mL and BDNF at 50 ng/mL, to the desired final volume and incubate at 37 °C in 6 % CO₂.

3.7 Enriching for Spiral Ganglion Schwann Cells

1. To treat with D-valine, make serum-free N2 medium using MEM with D-valine modification (*see Note 3*). Change the cell culture medium using this formulation (*see Note 14*). This type of medium may be used constantly and indefinitely.
2. To treat with cytosine arabinoside (AraC) (*see Note 15*), supplement N2 medium with serum with AraC (20 µM, we keep our stock AraC at 200 mM so that it can be diluted 1:1000). Change the cell culture medium using the AraC supplemented medium, and incubate for 24 h. After 24 h, change to serum-free N2 medium for 48 h.

3.8 Fixation and Immunocytochemistry

1. Remove your culture from the incubator. Remove medium, then add 4 % PFA solution. Incubate at room temperature on shaker for 10–15 min.
2. Rinse 3× in PBS.
3. Permeabilize in 0.8 % Triton in PBS for 30 min at room temperature on shaker.
4. Incubate in blocking buffer for 1 h at room temperature on shaker.
5. Dilute primary antibodies in blocking buffer as desired (*see Notes 16–18*). Replace blocking buffer with primary antibody and incubate overnight at 4 °C or at room temperature for 2 h.
6. Rinse 3× in PBS.
7. Dilute secondary antibodies in blocking buffer as desired (*see Note 19*). Incubate overnight at 4 °C on shaker or at room temperature for 1 h.
8. Rinse 3× in PBS.
9. Coverslip and proceed to imaging; microscopy instructions vary by manufacturer; we use the scan slide tool in Metamorph to generate an image of the entire substrate surface using a 20× objective. This provides sufficient resolution to score neurite and Schwann cell alignment.

3.9 Quantifying Neurite Alignment

1. Open a scan-slide image in ImageJ (*see Note 20*).
2. In the toolbar, right-click the Line tool and select “Freehand line” option.

3. Click Measure under the Analyze menu to open a window with measurements. Ensure that angle and distance are being measured (*see Notes 21 and 22*).
4. Select the neurite(s) to be measured in the scan slide image and trace the neurite using the Freehand line tool (*see Note 23*). Record the length and angle for each segment by pressing Control-M, on a PC, or Command-M, on a Macintosh. Next, trace and measure the end-to-end distance of the pattern from the neuronal soma to the end of the neurite and corresponding distance along the pattern to calculate alignment ratio (Fig. 1). Repeat these measurements as many times as needed within the image. Data can be imported and saved for analysis in Microsoft Excel, SigmaPlot, or other data analysis software.

3.10 Quantifying Schwann Cell Alignment

1. Within ImageJ, open the images of the Schwann cell cultures (*see Note 20*).
2. Select the “Freehand selections” tool and outline the periphery of the cell. Ensure that Major axis, Minor axis, and Angle are being measured (*see Notes 21 and 22*).
3. Once the cell has been outlined, click Edit>Selection>Fit Ellipse in order to fit an ellipse to the outline of the cell (*see Notes 24–26*).
4. Press control-M on a PC or command-M on a Macintosh to measure the angle of the major axis to the horizontal plane. A window with measurements (Major axis, Minor axis, Angle) should appear.
5. Once you have measured the desired number of cells in each image, you can copy the measurement data into the data analysis software.
6. After importing the data into a spreadsheet, correct all angles that are greater than 90° by subtracting from 180° (*see Notes 27 and 28*).

4 Notes

1. Although a number of monomer formulations are compatible with this method [11], a 40 wt% hexyl methacrylate/60 wt% hexanediol dimethacrylate system is the typical formulation of choice. For an approximately 1 g solution of this formulation specifically, weigh 0.01 g of I-651 in a glass vial and pipette 0.40 g of hexyl methacrylate and 0.60 g of hexanediol diacrylate monomer into the vial.
2. New monomer solutions should be made every 30 days. The solutions will gradually form oligomers, which will affect kinetics of polymerization and polymer micropatterns.

3. Unmodified MEM usually has L-valine at 46 µg/mL whereas MEM with D-valine modification substitutes L-valine with D-valine at 92 µg/mL.
4. The seal between the container and the aluminum should be as air tight as possible to prevent solvent release. Do not use a plastic lid to cover the dish, as solvent will swell and potentially dissolve the plastic.
5. When handling glass slides the surface must not be scratched, as it will remove the activation layer. Handle the slides from the edges when possible.
6. An intensity of 16 mW/cm² at 365 nm is recommended, when using a mercury vapor arc lamp.
7. For a given photomask bandspacing, the amplitude of the surface features is highly dependent on illumination time, illumination intensity, and photoinitiator concentration. Varying polymerization time is the most practical method to reach target amplitudes. More information regarding channel amplitude as a function of the aforementioned variables is found in [7].
8. The photomask should release easily for HMA/HDDMA polymer systems, but may strongly adhere for other polymers. A small coating of Rain-X® water repellent or a release film will allow the photomask to be removed from most polymers. If the polymer strongly adheres to the photomask, soak in acetone overnight to soften the polymer and remove the photomask.
9. Spray the rat or mouse pups with 70 % EtOH and wipe prior to decapitation. This reduces the bacterial load on the skin and the chance for culture contamination.
10. Dissecting the otic capsule against a black background makes the tissue more visible. In order to perform dissections on ice, we will typically place a black rubber mat over a frozen cold pack. We mount a microscope in the laminar flow hood in order to maintain sterility of the tissue during dissection.
11. Rat middle ear anatomy features a tympanic bulla, a thin capsule of bone located on the inferior-lateral side of the skull, posterior to mandibular head. The tympanic bulla contains all the middle ear structures and the cochlea is located in the medial wall of the tympanic cavity. When inserting forceps into the external auditory canal, to remove the lateral wall of the tympanic bulla, avoid damaging the medial wall of the tympanic cavity with the forceps. A clean dissection of the spiral ganglion is difficult, after damaging the bony capsule of the cochlea.
12. Because the otic capsule is harder than the surrounding bone, the surrounding bone can usually be flicked away from the otic capsule with relative ease. To separate the otic capsule from the remainder of the temporal bone, a quick and easy method is to

grip one of the semicircular canals seen from the inside of the skull, then apply ventrally directed pressure. The otic capsule, including the cochlea, should separate cleanly from the rest of the temporal bone.

13. To plate on only a small area of your surface, add a thin layer of N2 to the area of interest, then carefully add the cell suspension. After adding the cells, wait at least 30 min, but preferably 1 h, to allow cells to adhere. Then add the remainder of the medium.
14. Fibroblast count can be reduced by using medium containing only D-valine, an enantiomer of L-valine that Schwann cells metabolize, due to the expression of an enzyme that fibroblasts lack, D-amino acid oxidase [12].
15. AraC is used to preferentially inhibit fibroblast growth. However, keep in mind that treating cells with this antimitotic agent also limits Schwann cell growth. Treatment with AraC is a 3-day process. Make N2 media with 10 % FBS and 20 μ M AraC and incubate cells for 24 h with this solution. After 24 h of incubation, change media to serum-free N2 media and incubate for 48 h.
16. S100 β is an excellent marker for Schwann cells, for which multiple antibodies are available from vendors. Our lab has the best results with Abcam's rabbit anti-S100 β antibody. We typically store this reagent at a dilution of 1:2 in glycerol for better preservation, whereas we use the antibody at a dilution of 1:400 or 1:800 final.
17. Neurofilament 200 (NF200) is an excellent marker for neurons, for which multiple antibodies are also available. We have the best results with Invitrogen's mouse anti-NF200, which we typically use at a 1:800 dilution.
18. Vimentin is a marker for mesenchymal cells including fibroblasts, but it should be noted that not all fibroblasts stain for vimentin.
19. We typically use secondary antibodies conjugated to Alexa Fluor[®] dyes (Life Technologies, Grand Island, NY). Alexa Fluor[®] dyes are available in a variety of excitation and emission spectra. Be sure to co-stain with secondary antibodies conjugated to dyes with sufficiently different excitation and emission spectra to avoid bleed-through across stains. It is recommended to use dyes with emission spectra that are at least 100 nm wavelength apart.
20. A scan-slide of the sample is taken and stitched together using MetaMorph software, when quantifying neurite alignment. This approach is taken to avoid a bias toward neurites shorter than the size of the capture window, when only capturing single-frame images. For Schwann cell alignment, randomly taken

pictures are sufficient, as they are almost always smaller than a capture window. However, only quantify alignment on Schwann cells that are entirely captured within your image.

21. Go to the “Select Measurements” tab under Measure and ensure that the Angle and Distance boxes are checked, if after selecting Measure or pressing control/command-M, you find that angle and distance are not recorded., Re-open the Measure tool to record measurements.
22. It is important to have the degree of magnification saved into the image so pixel-to-micron conversions are calculated automatically, when opening in another program (such as ImageJ). This save is crucial for the MATLAB program. If this is not the case, then be sure that a pixels-to-actual measurement conversion factor is known for the magnification of the images taken, so you can convert your measurements to microns.
23. At high cell densities, neurites may overlap and make tracing difficult. Furthermore, cells at high densities may tend to direct each other’s neurite growth, clouding the substrate’s influence on neurite alignment. Therefore, it is generally easier to use a low-density cell culture.
24. Zoom in to the image in order to improve the outline of your Schwann cells. This approach allows you to more closely follow the outline of the cell, though a perfect outline is usually not critical to fitting the best ellipse.
25. Because overlapping or adjacent cells can make this method difficult, and also because at higher cell densities Schwann cell alignment is increasingly affected by adjacent cells, it is best to use a lower-density culture.
26. When Schwann cells grow to confluence, it can be helpful to split them into containers with larger surface areas. When performing this procedure, you should expect a moderate amount of cell loss, and increased fibroblast growth given the additional room for cell proliferation. To split the cells, first prepare as many containers as desired by plating with poly-L-ornithine then laminin as described above. Then, replace the cell culture medium with 0.25 % trypsin-EDTA solution and incubate at 37 °C for 5 min or until the cells appear to be free-floating and round in shape when viewed with a light microscope. Using a pipette tip, suck up the trypsin-cell solution and transfer to a 15 mL conical centrifuge tube. Rinse the cell culture container with several mL of N2 medium and transfer this solution to the previous 15 mL conical tube containing the solution of cells. Spin down at $1250 \times g$ for 5 min at 23 °C. Remove the supernatant, resuspend the cells in culture medium, and plate onto prepared surfaces as described previously.

27. Because we investigate linear patterns where 0 and 180° alignment is equivalent, we correct all Schwann cell alignment measurements to a range of 0–90°. For example, a measurement of 150° is actually equivalent to a measurement of 30°, except that it is left-leaning rather than right-leaning.
28. If the pattern is not horizontally aligned in the image you have taken, you may correct for the difference by measuring the angle of the pattern relative to horizontal in this image, then subtract this measurement from the major-axis angle measurements. Be sure to do this prior to correcting your measurements to the 90° range.

References

1. Fell HB (1928) The development in vitro of the isolated otocyst of the embryonic fowl. *Arch Exp Zellforsch* 7(1):69–81
2. Zhang Y, Zhou X, Degterev A, Lipinski M, Adjeroh D, Yuan J, Wong ST (2007) A novel tracing algorithm for high throughput imaging screening of neuron-based assays. *J Neurosci Methods* 160(1):149–162
3. Tapias V, Greenamyre JT, Watkins SC (2013) Automated imaging system for fast quantitation of neurons, cell morphology and neurite morphometry in vivo and in vitro. *Neurobiol Dis* 54:158–168
4. Hoffman-Kim D, Mitchel JA, Bellamkonda RV (2010) Topography, cell response, and nerve regeneration. *Annu Rev Biomed Eng* 12:203–231
5. Li S, Tuft BW, Xu L, Polacco MA, Clarke JC, Guymon CA, Hansen MR (2015) Microtopographical features generated by photopolymerization recruit RhoA/ROCK through TRPV1 to direct cell and neurite growth. *Biomaterials* 53:95–106
6. Qin D, Xia Y, Whitesides GM (2010) Soft lithography for micro- and nanoscale patterning. *Nat Protoc* 5(3):491–502
7. Tuft BW, Li S, Xu L, Clarke JC, White SP, Guymon BA, Perez KX, Hansen MR, Guymon CA (2013) Photopolymerized microfeatures for directed spiral ganglion neurite and Schwann cell growth. *Biomaterials* 34(1):42–54
8. Hegarty JL, Kay AR, Green SH (1997) Trophic support of cultured spiral ganglion neurons by depolarization exceeds and is additive with that by neurotrophins or cAMP and requires elevation of [Ca²⁺]_i within a set range. *J Neurosci* 17(6):1959–1970
9. Tuft BW, Xu L, White SP, Seline AE, Erwood AM, Hansen MR, Guymon CA (2014) Neural pathfinding on uni- and multidirectional photopolymerized micropatterns. *ACS Appl Mater Interfaces* 6(14):11265–11276
10. Clarke JC, Tuft BW, Clinger JD, Levine R, Figueroa LS, Guymon CA, Hansen MR (2011) Micropatterned methacrylate polymers direct spiral ganglion neurite and Schwann cell growth. *Hear Res* 278(1–2):96–105
11. Tuft BW, Zhang L, Xu L, Hangartner A, Leigh B, Hansen MR, Guymon CA (2014) Material stiffness effects on neurite alignment to photopolymerized micropatterns. *Biomacromolecules* 15(10):3717–3727
12. Kaewkhaw R, Scutt AM, Haycock JW (2012) Integrated culture and purification of rat Schwann cells from freshly isolated adult tissue. *Nat Protoc* 7(11):1996–2004

Chapter 19

The Use of Human Wharton's Jelly Cells for Cochlear Tissue Engineering

Adam J. Mellott, Michael S. Detamore, and Hinrich Staecker

Abstract

Tissue engineering focuses on three primary components: stem cells, biomaterials, and growth factors. Together, the combination of these components is used to regrow and repair damaged tissues that normally do not regenerate easily on their own. Much attention has been focused on the use of embryonic stem cells (ESCs) and induced pluripotent stem cells (iPSCs), due to their broad differentiation potential. However, ESCs and iPSCs require very detailed protocols to differentiate into target tissues, which are not always successful. Furthermore, procurement of ESCs is considered ethically controversial in some regions and procurement of iPSCs requires laborious transformation of adult tissues and characterization. However, mesenchymal stem cells are an adult stem cell population that are not ethically controversial and are readily available for procurement. Furthermore, mesenchymal stem cells exhibit the ability to differentiate into a variety of cell types arising from the mesoderm. In particular, human Wharton's jelly cells (hWJCs) are mesenchymal-type stem cells found in umbilical cords that possess remarkable differentiation potential. hWJCs are a highly desirable stem cell population due to their abundance in supply, high proliferation rates, and ability to differentiate into multiple cell types arising from all three germ layers. hWJCs are used to generate several neurological phenotypes arising from the ectoderm and are considered for engineering mechanosensory hair cells found in the auditory complex. Here, we report the methods for isolating hWJCs from human umbilical cords and non-virally transfected for use in cochlear tissue engineering studies.

Key words Mesenchymal stem cells, Human Wharton's jelly cells, ATOH1, Non-viral gene delivery, Nucleofection, Characterization

1 Introduction

In tissue engineering, both neuronal and sensory tissues, genetic manipulation, and tailored growth factor induction methods are popular for guiding pluripotent stem cells such as embryonic stem cells (ESCs) or induced pluripotent stem cells (iPSCs) toward a target phenotype [1–6]. In cochlear tissue engineering, methods developed by Hashino et al. [7–9] and Ito et al. [10, 11] have both seen success in using induction methods to form the pre-placodal epithelium and otic prosensory vesicles to induce the development

of mechanosensory hair cells. However, while much focus has remained on ESCs and iPSCs for differentiating neuronal phenotypes, there is another stem cell type that has shown potential in engineering neuronal phenotypes.

Mesenchymal stem cells (MSCs) isolated from the bone marrow have long been a standard in tissue engineering for regenerating cartilage, bone, and adipose tissues [12–15]. In addition to bone marrow-derived MSCs, a mesenchymal-type stem cell isolated from the gelatinous connective tissue, Wharton's jelly, of the human umbilical cord, has shown great promise for tissue engineering applications. Human Wharton's jelly cells (hWJCs) are a highly desirable stem cell population due the fact that hWJCs are abundant in supply, ethically non-controversial, exhibit no risk to the donor, are highly proliferative, and have demonstrated differentiation potential similar to human bone marrow stem cells [16, 17]. In addition, hWJCs have shown a remarkable ability to differentiate toward additional phenotypes such as those arising from neuronal lineages with exposure to growth factors or manipulation of gene expression [18, 19]. hWJCs are amenable to non-viral gene delivery methods such as Nucleofection™ [20, 21], and have shown the capability to differentiate toward a mechanosensory phenotype, when genes are manipulated in the NOTCH pathway [22]. Thus, hWJCs are a reliable stem cell type worth investigating and exploring for applications focused on engineering sensory epithelium in the cochlear and vestibular systems.

The aim of this chapter is to provide insights into the protocols used for isolation, sub-culture, preservation, transfection, and associated analyses and characterization of hWJCs. The use of hWJCs in cochlear tissue engineering may prove advantageous for regenerating mechanosensory hair cells and studying mechanisms of development and damage to sensory epithelia.

2 Materials

Chemicals are at minimum Biological Grade quality, unless otherwise noted.

2.1 Isolation of hWJCs from the Umbilical Cord, Culture, and Sub-culture

1. **1× Phosphate buffered saline (PBS):** Dissolve 1 PBS packet (Sigma-Aldrich, St. Louis, MO) in 1 L deionized water. Autoclave and sterifilter through a 1000-mL EMD Millipore Stericup™ Sterile Vacuum Filter Unit (Fisher Scientific, Pittsburgh, PA).
2. **Wash Solution:** Mix 2 % 100× Antibiotic-Antimycotic solution (Life Technologies, Grand Island, NY) in sterile 1× PBS from step 1, Subheading 2.1.

3. Digestion Medium: Dissolve 100 mg Type II Collagenase (Worthington-Biochem, Lakewood, NJ) in 49 mL of Dulbecco's Modified Eagle Medium (DMEM) with low glucose and pyruvate (Life Technologies). Sterifilter solution through 50-mL Steriflip-GV unit (EMD Millipore, Billerica, MA). Add enough (~0.5 mL) of penicillin-streptomycin (10,000 U/mL) (Life Technologies) to digestion medium to obtain a final concentration of 1 % antibiotic in 50 mL of medium.
4. hWJC Culture Medium: Mix 445 mL DMEM containing low glucose and pyruvate with 50 mL of Fetal Bovine Serum (FBS) that is mesenchymal stem cell-qualified (MSC; Life Technologies). Store in aliquots of 25 mL at -20 °C. When ready to use, thaw aliquots O/N in 4 °C refrigerator, then heat-deactivate aliquots at 72 °C for 30 min the next day. Cool to 37 °C before use and add 5 mL penicillin-streptomycin (10,000 U/mL). Gently mix all components together by pipetting.
5. 0.05 % Trypsin-EDTA phenol red. Store aliquots of 25 mL at -20 °C, then thaw aliquots in 37 °C bead bath before use.

2.2 Freezing and Thawing hWJCs

1. hWJC Culture Medium (*see Subheading 2.1, step 4*).
2. Recovery™ Cell Culture Freezing Medium (Life Technologies).
3. 10 mM stock Y27632 Rho-associated coiled-coil kinase (ROCK) inhibitor (Reagents Direct, Encinitas, CA): Reconstitute 2 mg of inhibitor in 624 µL of Dimethyl Sulfoxide (DMSO) (Sigma-Aldrich). Store in 104 µL aliquots in dark at -20 °C, until use.
4. hWJC Thawing Medium: Mix 500 µL of reconstituted Y27632 ROCK Inhibitor with 395 mL of DMEM by gently pipetting. Protect solution from light. Sterifilter DMEM and Y27632 ROCK inhibitor solution through a 500-mL EMD Millipore Stericup™ Sterile Vacuum Filter Unit. Add 100 mL of FBS-MSC-qualified (*see Subheading 2.1, step 4*) to DMEM to obtain a 20 % solution. Then add 5 mL of penicillin-streptomycin (10,000 U/mL) to DMEM to obtain a 1 % solution.
5. 0.05 % Trypsin-EDTA, phenol red (Life Technologies).
6. PBS (*see Subheading 2.1, step 1*).

2.3 Stem Cell Characterization

1. Primary Blocking Solution: Mix 0.6 g of 10 % BSA in 1 mL of Normal Donkey Serum (NDS). Use serum from secondary host. For example, if the secondary antibody label comes from a donkey host, then use normal donkey serum. Donkey, Rabbit, and Goat are common secondary hosts. Adjust volume to 10 mL with 1× PBS (*see Subheading 2.1, step 1*).

2. Secondary Blocking Solution: Mix 0.6 g of BSA in 10 mL of 1× PBS (*see Subheading 2.1, step 1*)
3. SYTOX® Red Dead Cell Stain (Life Technologies).
4. Isotype controls: Fluorescein isothiocyanate (FITC) IgG₁, Allophycocyanin (APC) IgG₁, R-Phycoerythrin (PE) IgG₁, Brilliant Violet (BV) IgG₁ (BD Biosciences, San Jose, CA).
5. Fluorescent secondary antibodies: Donkey Anti-Mouse Alexa Fluor 568 IgG, Donkey anti-mouse Qdot® 525 IgG (Life Technologies).
6. Primary antibodies: FITC mouse anti-human CD73, APC mouse anti-human CD90, PE mouse anti-human CD45, and BV421 mouse anti-human CD34 from BD Biosciences. Human STRO-1 antibody and human endoglin/CD105 antibody from R&D Systems (Minneapolis, MN).
7. hWJC Culture Medium (*see Subheading 2.1, step 4*).
8. 0.05 % Trypsin-EDTA, phenol red (Life Technologies).
9. PBS (*see Subheading 2.1, step 1*).

2.4 Transfection

1. P1 Primary Cell 4D-Nucleofector® X Kit (24 RCT) (Lonza Group Ltd, Basel, Switzerland).
2. Transfection Medium: Mix 500 µL of thawed 10 mM Y27632 ROCK Inhibitor (*see Subheading 2.3*) with 440 mL of Basal Medium from MSCGM™ Mesenchymal Stem Cell Growth Medium BulletKit via gentle pipetting. Sterifilter Basal Medium and Y27632 ROCK inhibitor through a 500-mL EMD Millipore Stericup™ Sterile Vacuum Filter Unit. Add remaining components of MSCGM™ Mesenchymal Stem Cell Growth Medium BulletKit to Basal Medium according to the manufacturer's instructions. Protect from light.
3. HATH1-CMV-plasmid (1 µg/µL): The HATH1 sequence (NCBI Reference Sequence: NC_000072.6) was sub-cloned into a PrecisionShuttle mammalian vector with N-terminal mGFP (Origene, Rockville, MD).
4. 0.05 % Trypsin-EDTA, phenol red (Life Technologies).
5. PBS (*see Subheading 2.1, step 1*).

2.5 Cell Staining

1. Dyes: Hoechst 33342 and FM® 1-43FX (Life Technologies).
2. 4 % Paraformaldehyde fixation solution: In a glass beaker on a stir plate in a well ventilated fume hood, Heat 800 mL of Hank's Balanced Salt Solution (HBSS) without Ca²⁺ and Mg²⁺ to 60 °C. Add 40 g of paraformaldehyde (96 % extra pure) and then slowly add 1 mol/L NaOH drop-wise until the solution clears. Allow solution to cool to RT and adjust volume to 1 L with HBSS. Adjust pH to 6.9 by adding 1 mol/L HCl.

3. Mounting medium with DAPI.
4. Hank's Buffered Saline Solution (HBSS).
5. PBS (*see* Subheading 2.1, step 1).

2.6 Gene Expression Analysis

1. RNA purification kit (e.g., RNeasy; Qiagen, Valencia, CA).
2. Tissue homogenizer (e.g., QIAshredder; Qiagen).
3. 18 MΩ Milli-Q Water.
4. 100 % EtOH.
5. RNA ScreenTape system, including sample buffer and ladder (Agilent Technologies, Santa Clara, CA).
6. D1000 ScreenTape system, including reagents and ladder.
7. 10, 200, and 1000 μL aerosol barrier filter pipette tips.
8. cDNA reverse transcription kit.
9. DEPC-treated H₂O.
10. Primer-probe RNA detection kit (e.g., TaqMan® Fast Universal PCR Master Mix).
11. RNase decontamination reagent (e.g., RNase AWAY™).
12. 0.2-mL PCR tubes and caps, RNase-free.
13. 0.1-mL 96-well reaction plate with barcode (e.g., MicroAmp® Fast Optical; Life Technologies).
14. MicroAmp® optical adhesive film kit (Life Technologies).
15. TaqMan® Assays: *ATOH1*, *BARHL1*, *GAPDH*, *GFI1*, *HES1*, *HES5*, *JAG1*, *JAG2*, *MYO6*, *MYO7A*, *NOTCH1*, *POU4F3*, *SOX2* (Life Technologies).

2.7 Immunohistochemistry

1. 4 % Paraformaldehyde fixation solution in PBS: Heat 800 mL of PBS to 60 °C in a glass beaker on a stir plate in a well-ventilated fume hood. Continue as in Subheading 2.5, step 2, except use PBS.
2. PBS (*see* Subheading 2.1, step 1).
3. Detergents: Triton X-100, Tween 20.
4. Primary and Secondary Blocking Solutions (*see* Subheading 2.3, steps 1 and 2).
5. Histological mounting solution.
6. Secondary antibodies: Donkey anti-rabbit IgG (H+L), donkey anti-mouse IgG (H+L), donkey anti-goat IgG (H+L), Qdot® 525, 605 and 655 (Life Technologies).
7. Qnuclear™ Deep Red Stain (Life Technologies).
8. Primary antibodies: Rabbit anti-human Myosin VIIA (Novus Biologicals, Littleton, CO), mouse anti-human Neurogl (Antibodies-Online, Atlanta, GA), goat anti-human Sox2 (R&D Systems).

2.8 Specialized Equipment and General Supplies

2.8.1 Equipment

1. Spinning disk confocal inverted microscope (e.g., Olympus IX81).
2. Inverted epifluorescence microscope (e.g., Olympus IX81).
3. Cell sorter.
4. Nucleofector (e.g., Lonza Group Ltd. 4D).
5. Thermo Scientific NanoDrop 2000.
6. Tape Station (e.g., Agilent Technologies 2200).
7. Thermocycler (e.g., Eppendorf Mastercycler®).
8. Instrument sterilizer (e.g., Lab Armor Bead Bath).
9. Biosafety cabinet.
10. Water-jacketed CO₂ incubator.
11. Centrifuge (e.g., Sorvall™ ST 40R) and microcentrifuge.
12. Smart tissue processor (e.g., Leica ASP300).
13. Paraffin embedding station (e.g., Leica EG1150C).
14. Microtome (e.g., Leica RM2255).
15. Vacuum pump.
16. Sterilizer (e.g., Primus PSS500).
17. Cryogenic storage unit (e.g., Thermo Scientific Locator™ 6 Plus Rack and Box System).

2.8.2 Supplies

1. NIH Style Neuro Punches (Fine Science Tools).
2. Scalpel handle #3 with scalpel blades #10, 11, and 12.
3. Fine Scissors and extra fine Graefe forceps.
4. Bright-Line™ hemacytometer.
5. Tubes and Bottles: 15 and 50-mL conical tubes, sterile 5-mL polypropylene tubes, 2-mL microcentrifuge tubes, 2-mL round-bottom cryogenic vials, and autoclavable Pyrex glass bottles (250-mL, 500-mL, 1000-mL).
6. Tissue culture filter flasks: TPP—T75, T150, T300 (MidSci).
7. 6-Well tissue culture-treated plate.
8. 100-mm mono plate (Fisher Scientific).
9. 35-mm sterile petri dish.
10. Pipettes: 2-mL aspirating pipettes, 25-mL serological pipettes.
11. Sterile 70-µm cell strainer (Biosciences).
12. Single Channel Auto-Pipettors (2-µL, 20-µL, 200-µL, 1000-µL) and pipette tips (10-µL, 200-µL, 1000-µL).
13. Mr. Frosty™ Freezing Container (Thermo Scientific).
14. Small and large Kimwipes.

3 Methods

3.1 Isolation of hWJCs from Umbilical Cord

1. Sterilize tissue culture hood for 30 min with UV light.
2. Turn on tissue culture hood blower and lift sash ~24 cm. Allow circulation in tissue culture hood to flow for 10 min before use.
3. Spray down all interior surfaces of tissue culture hood with 70 % EtOH (*see Note 1*).
4. Prepare tissue culture hood with drop cloth, 100-mm mono plates, tools (scalpels, forceps, scissors, etc.), and 50-mL conical tubes.
5. Prepare and sterifilter both Wash Solution and Digestion Medium (*see Subheading 2.1, steps 1–3*). Warm the Wash solution and Digestion medium in 37 °C bead bath (*see Note 2*).
6. After wiping down with EtOH, transfer specimen cup/container containing umbilical cord in sterile saline into the tissue culture hood.
7. Carefully, transfer umbilical cord from specimen cup/container to 100-mm mono plate. Remove ends of umbilical cords in 100-mm mono plate with scalpel. Section cord into ~3 cm increments. Squeeze out any residual or remaining blood from tissue sections with forceps.
8. Wash umbilical cord segments 2x with Washing Solution. Move cord segments around and aspirate off waste between. (It is imperative that as much blood is removed as possible.)
9. Transfer umbilical cord segments to new 100-mm mono plate.
10. Wash umbilical cord segments 2x with Washing Solution. Moving cord segments around and aspirate off waste between. (Remove all blood if possible.)
11. Transfer umbilical cord segments to a fresh 100-mm mono plate. Discard previous mono plates. Add just enough Wash Solution to keep umbilical cord segments moist.
12. Remove blood vessels from each umbilical cord segment (Fig. 1). Discard vessels (*see Notes 3 and 4*).
13. Wash umbilical cord segments twice with Wash Solution. Move umbilical cord segments around and aspirate waste between.
14. Transfer tissue segments to new 100-mm mono plate. Use scalpel to physically degrade tissue (*see Note 5*).
15. Once umbilical cord tissue is degraded to the consistency of “pulp,” add Digestion Medium to the 100-mm mono plate via a pipette. Cut any floating large tissue pieces to smaller sizes (*see Note 6*).

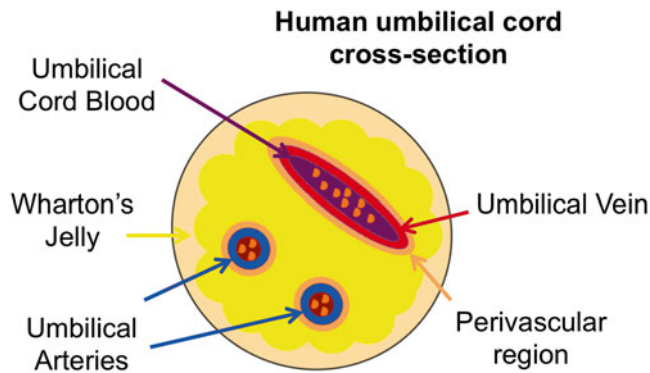


Fig. 1 Cross-section of human umbilical cord. The human umbilical cord contains three blood vessels that must be removed when harvesting human Wharton's jelly cells. Wharton's jelly is the gelatinous connective tissue found between the blood vessels in the human umbilical cord

16. Place the lid over the mono plate and place in a 37 °C incubator with 5 % CO₂ on an orbital shaker for a minimum of 4 h at 50 rpm (*see Note 7*).
17. Remove 100-mm mono plate from incubator. (If any large tissue pieces are still floating, place the mono plate back on the shaker in the incubator for 1 h.) Dilute digested tissue at a ratio of 1:4 with Washing Solution in 50-mL conical tubes.
18. Centrifuge conical tubes for 10 min at ~500 × g. Check for pellet. If no pellet is visible, dilute with additional Washing Solution to a ratio of 1:8 and centrifuge. A dilution of 1:16 is sometimes necessary for a pellet to form.
19. Aspirate supernatant from tubes. Resuspend pellet in hWJC Medium.
20. Count cells using a hemocytometer.
21. Plate 7000 cells/cm² in a T-flask.
22. Gently wash cells with sterile PBS and replace medium every 6–8 h in the first 24 h following plating, to remove residual blood cells.
23. Replace medium every 48 h and sub-culture cells when culture vessel reaches 80 % confluence.

3.2 Culturing and Sub-culturing hWJCs

3.2.1 Culturing hWJCs

1. Place hWJC Culture Medium in 37 °C bead bath for 30–40 min (*see Note 8*).
2. Prepare tissue culture hood as in Subheading 3.1, steps 1–3.
3. Turn on vacuum pump, and spray inside and outside of tubing.
4. Spray and wipe down all reagents and tools with 70 % EtOH before placing in tissue culture hood (e.g., pipettors, culture medium, conical tubes, etc.) (*see Note 9*).

Table 1
Medium recommendations for well plates

Well-plate format	Medium volume to add per well (mL)
96-Well plate	0.2
48-Well plate	0.5
24-Well plate	1
12-Well plate	1.5
6-Well plate	3

Table 2
Medium recommendations for T-flasks

T-flask size	Medium volume to add (mL)
T-25 cm ²	5
T-75 cm ²	15
T-150 cm ²	25
T-300 cm ²	30

5. Gently clean stage of inverted light microscope with 70 % EtOH.
6. Remove cell culture vessel from 37 °C CO₂ incubator.
7. Check cell confluence and health using an inverted light microscope (*see Note 10*).
8. Gently wipe outside of cell culture vessel with 70 % EtOH and place in tissue culture hood.
9. Open wide end of aspirating pipette and hook up to aspirating tubing.
10. Remove pipette wrapper, and carefully remove well plate cover or T-flask cap.
11. Aspirate out all medium, but *do not* touch cell surface with aspirating pipette (*see Notes 11 and 12*).
12. After removing medium, *carefully and slowly* add fresh warm medium to cell culture vessel (Tables 1 and 2) (*see Notes 13 and 14*).
13. Replace lid or cap on culture vessel and return to 37 °C CO₂ incubator (*see Note 15*).

3.2.2 Sub-culturing hWJCs (Passaging)

1. Aspirate all medium off of cells.
2. Wash cells by adding sterile PBS to cells in an amount equivalent to the cell culture medium.
3. Rock T-flask or well plate back and forth gently to spread PBS over entire cell-covered surface, then aspirate all PBS off of cells.
4. Repeat steps 2 and 3, Subheading 3.2.2 one more time.
5. Add 0.05 % Trypsin-EDTA to cells in an amount equivalent to the cell culture medium.
6. Rock T-flask or well plate back and forth briefly to spread 0.05 % Trypsin-EDTA over the entire cell-covered surface.
7. Place T-flask or well plate in 37 °C incubator for 3–5 min.
8. While T-flask or well plate is in incubator, label and prepare 50-mL conical tube(s) under the tissue culture hood with an amount of growth medium that is equivalent to the 0.05 % Trypsin-EDTA used to detach cells. For example, if 2 mL of 0.05 % Trypsin-EDTA was added to each well of a 6-well plate, then add 2 mL of growth medium to an empty 50-mL conical tube under the tissue culture hood.
9. Prepare a separate conical tube for each well or flask in which cells are being detached. Label all conical tubes accordingly to keep track of source for lifted cells.
10. Remove T-flask or well plate from incubator and verify that cells have detached from the surface using a light-inverted microscope. If 90 % \leq cells have detached, gently tap side of flask or well plate, to enhance cell detachment, and verify detachment using microscope.
11. Place T-flask or well plate underneath the tissue culture hood and transfer 0.05 % Trypsin-EDTA into designated conical tube containing equivalent amount of growth medium. The ratio of growth medium to 0.05 % Trypsin-EDTA should be 1:1, to deactivate the enzyme.
12. Pellet the cell suspension down by spinning the conical tube in the centrifuge at $\sim 500 \times g$ for 5 min.
13. Aspirate off all 0.05 % Trypsin-EDTA/hWJC Medium solution (see Note 16) and resuspend cells in 1 mL of hWJC Medium.
14. Count cells using a hemocytometer or automated cell counter.
15. Once total cell number is determined, dilute cells accordingly and split into new T-flasks or wells. hWJCs grow most efficiently at a density of 7000 cells/cm³.

3.3 Freezing and Thawing hWJCs

3.3.1 Freezing Cells

1. Pre-label 2-mL cryogenic vials with threaded caps denoting: date, cell type, name, and passage number. Reference notation to umbilical cord (internal numbering of deidentified sample).
2. Follow sub-culture protocol (*see Subheading 3.2.1, steps 1–14*).
3. Make note of how many cells are in 1 mL of medium. Repellet cell suspension, by centrifuging at $\sim 500 \times g$ for 5 min.
4. Aspirate supernatant and resuspend cells in RecoveryTM Cell Culture Freezing Medium (*see Subheading 2.2, step 2*) at a concentration of 1×10^6 cells/mL. Work quickly as this medium contains Dimethyl sulfoxide (DMSO).
5. Aliquot 1 mL of cell suspension into each pre-labeled cryogenic vial and cap vials.
6. Transfer vials into a Mr. FrostyTM Freezing container filled with isopropanol and place container into a -80°C freezer for up to 12 h.
7. Remove container from -80°C freezer and quickly transfer cryogenic vials into a liquid nitrogen-filled cryopreservation storage unit.
8. Store samples until ready for use.

3.3.2 Thawing Cells

1. Warm hWJC Thawing Medium (*see Subheading 2.3, step 4*) and 50 mL of sterile PBS to 37°C .
2. Place a 35-mm petri dish and appropriate number of T-75 flasks under the tissue culture hood, and label accordingly. Use two T-75 flasks per vial.
3. After hWJC Thawing Medium and PBS are warm, place under tissue culture hood.
4. Fill a 50-mL conical tube with 49 mL of pre-warmed thawing medium.
5. Fill 35-mm petri dish with warm PBS.
6. Quickly retrieve frozen vials of cells from cryopreservation storage unit and spray vials with 70 % EtOH, then place under tissue culture hood.
7. Place bottom of cryogenic vials in warm PBS (*see Note 17*).
8. Draw up ~ 0.5 mL of hWJC Thawing Medium from the 50 mL conical tube, using the 2-mL aspirating pipette.
9. Carefully pipette hWJC Thawing Medium into cryogenic vial containing frozen cells. *Do not take vial out of PBS*. Slowly transfer cell solution and hWJC Thawing Medium between cryogenic vial and 50 mL conical tube until vial is empty of cell solution.
10. Gently mix cells in hWJC Thawing Medium by gently pipetting up and down, or gently rocking closed 50-mL conical tube back and forth.

11. Aliquot 25 mL of cell suspension into each pre-labeled T-75 flask (2/cryogenic vial).
12. Lay T-75 flask on side and swirl medium and cells around to evenly distribute them across the bottom, then place flasks in 37 °C incubator.
13. Repeat steps 10–12, Subheading 3.3.2 for each additional vial of cells.
14. After 24 h, replace hWJC Thawing Medium with hWJC Culture Medium and culture hWJCs according to hWJC culture protocol described in steps 1–13, Subheading 3.2.1.

3.4 Stem Cell Characterization

It is highly recommended that 1.6×10^7 or more cells are used for this protocol to ensure enough cells are available for flow cytometry analysis.

1. Pre-label 16 2-mL microcentrifuge tubes and 16 5-mL polypropylene tubes for cell characterization as follows:
 - One tube for cells that will not be stained and are used for baseline measurements.
 - One tube for each CD marker (6 tubes total).
 - One tube for each isotype control (6 controls total).
 - Three tubes with cells stained for all CD markers.
2. Follow sub-culture protocol (*see* Subheading 3.2.2, steps 1–15).
3. Make note of how many cells are in 1 mL of medium. Repellet cell suspension by centrifuging at $\sim 500 \times g$ for 5 min.
4. Aspirate off supernatant and resuspend cells in Primary Blocking Solution (*see* Subheading 2.3, step 1) at a concentration of 1×10^6 cells/mL. Aliquot 1×10^6 cells/mL cells into pre-labeled 2-mL microcentrifuge tubes. Place cells on ice and keep in the dark for 20 min.
5. Microcentrifuge samples at $\sim 1556 \times g$ for 5 min at 4 °C, then decant supernatant.
6. Add appropriate amount of cell marker or isotype (Table 3) and corresponding amount of Secondary Blocking Solution (*see* Subheading 2.3, step 2), so that cells in each microcentrifuge tube are suspended in a total volume of 200 µL. Mix each suspension well with gentle pipetting (*see* Note 18).
7. Incubate cells on ice, and keep in dark for 20 min.
8. Add 800 µL of Secondary Blocking Solution to each centrifuge tube to bring the total volume to 1000 µL.
9. Centrifuge samples at $\sim 1556 \times g$ for 5 min at 4 °C.
10. Decant supernatant.

Table 3
Cell marker volumes

CD marker/isotype	Recommended marker volume (μ L)	Cell number	2° Blocking solution (μ L)
Unstained	0	1,000,000	200
Mouse anti-human STRO-1 (1°)	2.5	1,000,000	197.5
Donkey anti-mouse Alexa Fluor 568 (2°)	2	1,000,000	198
Mouse anti-human human CD105 (1°)	2.5	1,000,000	197.5
Donkey anti-mouse Qdot 525 (2°)	2	1,000,000	198
CD45 PE	5	1,000,000	198
PE isotype control	5	1,000,000	198
Mouse anti-human FITC CD73	5	1,000,000	195
FITC isotype control	5	1,000,000	195
Mouse anti-human brilliant violet CD34	5	1,000,000	195
Brilliant violet isotype	5	1,000,000	195
Mouse anti-human APC CD90	5	1,000,000	195
APC isotype control	5	1,000,000	195

11. Add appropriate amount of secondary antibody-fluorophore and Secondary Blocking Solution to samples that require secondary labeling as prescribed in Table 3 (see Note 19). Cells that do not require secondary labeling should be suspended in 1000 μ L of Secondary Blocking Solution.
12. Incubate cells on ice and keep in dark for 20 min.
13. Add 800 μ L of Secondary Blocking Solution to secondary labeled cells.
14. Centrifuge secondary labeled samples at $\sim 1556 \times g$ for 5 min at 4 °C.
15. Decant supernatant.
16. Suspend cells that do not require further labeling in 1000 μ L of Secondary Blocking Solution and place on ice. Continue sequential labeling of cell markers for samples to be stained with all cell markers by repeating steps 7–17, Subheading 3.4, until designated samples are labeled for all markers.
17. After all samples are labeled, centrifuge cells at $\sim 1556 \times g$ for 5 min at 4 °C.
18. Decant supernatant.
19. Resuspend all samples in 400 μ L of PBS.

20. Carefully strain each cell suspension through a 70- μm nylon cell strainer into its respective polypropylene tube to break up cell aggregates.
21. Add optional dyes to cell suspensions if desired (e.g., Hoechst, SYTOX® Red Dead Stain).
22. Analyze cell samples with Beckman Coulter MoFlo XDP cell sorter (*see Notes 20 and 21*).

3.5 Transfection

1. Culture hWJCs, used for transfection experiments, with medium components provided in the Lonza BulletKit. Medium provided in BulletKit is mixed and handled according to the manufacturer's instructions. hWJCs are cultured to 80 % confluence before beginning transfection protocol.
2. Warm PBS, Transfection Medium, and Trypsin to 37 °C 2 h prior to transfection.
3. Remove medium from hWJCs, and gently wash cells 2x with PBS, 1 h prior to transfection. After removing PBS, replenish cell cultures with Transfection Medium (*see Subheading 2.4, step 2*) and place in a 37 °C CO₂ incubator for 1 h.
4. While hWJCs are incubating, place HATH1 plasmid DNA on ice. If necessary, reconstitute fresh 4D Nucleofector P1 Primary cell solution, according to the manufacturer's instructions, and refrigerated at 4 °C. Label 100- μL 4D-Nucleofector cuvettes accordingly. Label 6-well plates, fill with 2.4 mL of Transfection Medium and place in a 37 °C cell culture grade incubator.
5. After 1 h, detach hWJCs according to Sub-culture procedure (*see Subheading 3.2.2, steps 1–14*).
6. After counting cells, repellent cell suspension by centrifuging at $\sim 500 \times g$ for 5 min.
7. Resuspend cells in 4D-Nucleofector P1 Primary cell solution at a concentration of 5×10^6 cells/1 mL. Separate cells corresponding to experimental parameters (e.g., untreated controls, HATH1-transfected cells, any other designated treatment groups). Plate non-transfected cells immediately into designated wells containing transfection medium. Pipette 100 μL of cell suspension into each well designated as an untreated control.
8. Add appropriate amount of HATH1 plasmid DNA (1 $\mu\text{g}/\mu\text{L}$) to cells designated for transfection.
 - Up to 5 μg of HATH1 plasmid DNA per 5×10^5 cells can be added for efficient transfection. Depending on experiment parameters between 2 and 3 μg of HATH1 plasmid DNA per 5×10^5 works well for most applications.
 - The volume of plasmid DNA should not exceed 10 % of total volume of cell suspension.

9. Gently mix DNA with cell suspension by tapping tube containing cells.
10. Aliquot 100 μL of DNA/cell suspension into 100- μL 4D Nucleofector cuvettes. After transferring cell suspension into cuvettes, gently tap cuvettes twice to evenly distribute cell suspension between electrodes.
11. Transfer cuvettes to 4D Nucleofector X-unit. Select Human MSC cell type and program FF-104 on the touch screen interface of the 4D Nucleofector Core-unit. Follow software prompts, and Nucleofect cells.
12. After Nucleofection, allow cuvettes to incubate at RT for 10 min.
13. Using the transfer pipette provided with the 4D Nucleofector MSC kit, transfer 100 μL of cells from each cuvette to the designated well in a 6-well plate. Gently swirl plate to evenly distribute cells.
14. Place 6-well plates in 37 °C CO₂ incubator.
15. After 24 h, replace transfection medium with Lonza MSC BulletKit Medium.
16. Culture cells and analyze according to experimental parameters.

3.6 Cell Staining

All cells designated for staining are sub-cultured and plated on a fibronectin-coated glass cover slip. Culture cover slips in 6-well plates until ready to stain.

3.6.1 Hoechst Staining

1. Remove medium, and wash 2× with HBSS, then add 1 mL of HBSS to each well.
2. Add 0.5 μL of Hoechst 33342 to each well and incubate cells at 37 °C in an incubator for 10 min.
3. Image cells using an inverted epifluorescent microscope (e.g., Olympus IX81) or a spinning disk confocal inverted microscope (e.g., Olympus IX81) and use the guide parameters in Table 4 to view and image labels.

3.6.2 FM 1-43 FX

1. Prepare a working staining solution of 5 $\mu\text{g}/\text{mL}$ of FM 1-43 FX in ice-cold HBSS. Keep solution on ice.
2. Remove medium from cover slip, and immerse cover slip in FM 1-43 working staining solution on ice for 1 min.
3. Remove cover slip from FM 1-43 FX working staining solution and immerse with ice-cold 4 % paraformaldehyde in HBSS for 10 min to fix cells. Keep cover slip and 4% paraformaldehyde on ice.
4. Rinse the cover slip at least three times with HBSS.

Table 4
Excitation and emission parameters

Marker	Microscope	Light source	Excitation (nm)	Emission (nm)
Hoechst 33342	IX81 Inverted Epi	Mercury Arc Lamp	387±11	446±60
GFP	IX81 Inverted Epi	Mercury Arc Lamp	494±20	531±22
Alexa Fluor 555	IX81 Inverted Epi	Mercury Arc Lamp	575±25	624±40
Alexa Fluor 647	IX81 Inverted Epi	Mercury Arc Lamp	650±25	684±25
FM 1-43 FX	IX81 Inverted Confocal	405 nm solid-state laser	405	625±11
Qdot 525	IX81 Inverted Confocal	405 nm solid-state laser	405	531±22
Qdot 565	IX81 Inverted Confocal	405 nm solid-state laser	405	560±25
Qdot 605	IX81 Inverted Confocal	405 nm solid-state laser	405	613±20
Qdot 655	IX81 Inverted Confocal	405 nm solid-state laser	405	655±15
Qdot 800	IX81 Inverted Confocal	405 nm solid-state laser	405	788±20
Qnuclear™ Deep Red Stain	IX81 Inverted Confocal	642 nm solid-state laser	642	655±15

GFP green fluorescent protein

3.7 Gene Expression Analysis

3.7.1 RNA Isolation

- Follow manufacturer's instructions, and mount and seal cover slip with ProLong® Gold Antifade Reagent with DAPI.
- Image cells (Fig. 2) as in Subheading 3.6.1, step 3.

3.7.2 NanoDrop 2000 RNA Analysis

- Remove medium from cells, and wash 2× with PBS.
 - Harvest RNA using RNeasy Plus Mini isolation kit following manufacturer's instructions (see Subheading 2.6, step 1).
 - RNA may be stored and preserved at -80 °C for later use, if not immediately converted to cDNA. Avoid multiple freeze-thaw cycles.
- Perform steps 1–5, Subheading 3.7.2, before starting NanoDrop 2000 RNA analysis.
- Set bead bath to 72 °C.
 - If necessary, thaw RNA on ice.
 - Remove Agilent Technologies RNA ScreenTape and RNA ScreenTape buffer from refrigerator, and bring to RT in ~30 min.
 - Pipette 5 µL of DEPC-treated water (see Subheading 2.6, step 9) on the NanoDrop 2000 quartz crystal pedestal and lower the arm. Allow DEPC-treated water to incubate for 5 min to clean quartz crystal and then remove water with a Kimwipe.

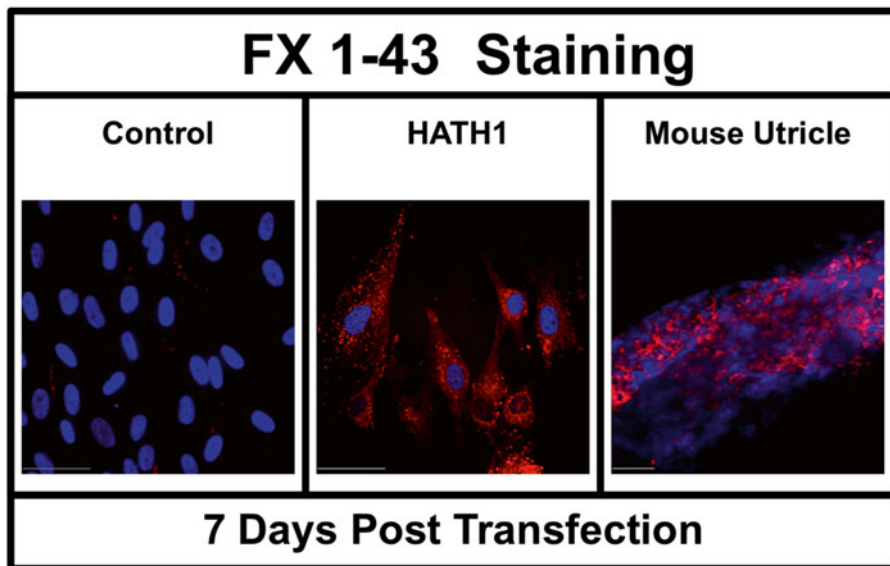


Fig. 2 FM 1-43 staining of lipid membranes. FM 1-43 is a lipophilic dye that is used to identify transfection channels found in mechanosensory hair cells. Sensory epithelium containing hair cells found in the mouse utricle and HATH1-transfected hWJCs revealed positive infiltration of FM 1-43 (*Red*) into cells. Cell nuclei were stained with DAPI (*Blue*). Scale Bars = 50 μ m

5. Turn on Agilent TapeStation.
6. Once steps 1–5, Subheading 3.7.2 are completed, open NanoDrop 2000/2000c software and close NanoDrop 2000 arm, if not already closed.
7. Select “Nucleic Acids” Button in software.
8. Select RNA in the drop-down menu in the upper right corner.
9. Raise NanoDrop 2000 arm, pipette 1 μ L of RNase-Free water on the quartz crystal, and close NanoDrop 2000 arm carefully.
10. Hit “Blank” button to measure background of RNase-Free water. Be sure to use the same solution that is suspending your RNA sample as the Blank, to get an accurate background reading.
11. When the “Measure” button becomes selectable, raise the NanoDrop 2000 arm and wipe off the quartz crystal carefully with a Kimwipe. Pipette 1 μ L of RNA sample onto the quartz crystal, and carefully close the NanoDrop 2000 arm. In the upper right corner of the screen, name the sample being tested. Then select “Measure” (*see Notes 22 and 23*).
12. After measuring is complete, carefully raise the NanoDrop 2000 arm, and wipe off the quartz crystal with a Kimwipe. Load 1 μ L of RNA from the next sample and lower the NanoDrop 2000 arm. Label the sample accordingly in the software and measure.

13. Repeat **step 7**, Subheading 3.7.2 for each new sample. Wipe off quartz crystal every time after measuring a sample.
14. After measuring all samples, create a report to export all the information. Wipe off the quartz crystal, load 5 μL of DEPC-treated water on the quartz crystal and lower the NanoDrop 2000 arm to clean. Allow the DEPC-treated water to spread over the crystal for 5 min, then wipe off the quartz crystal with a Kimwipe.

3.7.3 Agilent Technologies 2200 TapeStation RNA Analysis

1. Start up Agilent TapeStation software, but *not* the Agilent Analyzer Software.
2. Briefly vortex RNA ScreenTape Reagents.
3. Briefly centrifuge RNA ScreenTape Reagents.
4. Load RNA ScreenTape into TapeStation.
5. Label up to 16 optical tubes (2 8-tube strips) on the side accordingly.
6. Add 4 μL of R6K reagent buffer to each tube.
7. Add 1 μL of RNA sample to each tube.
8. Denature RNA samples by heating samples in a 72 °C water bath for 3 min. Immediately place RNA samples on ice and incubate for 2 min.
9. Briefly centrifuge RNA samples to collect contents.
10. Load tubes into TapeStation and remove tube-strip caps. *It is imperative to remove tube-strip caps, otherwise the internal TapeStation automated pipettor will break.*
11. Load appropriate number of pipette tips into TapeStation.
12. In software, label tubes to be analyzed.
13. Close TapeStation Lid and save RNA file, then click “START” program.
14. After running the program, there should be clear bands in the gel image. The peaks should also be sharp and well-defined in the electropherogram. The RNA Integrity Number (RIN) should be between 7 and 10. Do not use any RNA with a RIN below 7. Any RNA with a RIN below 7 is too far degraded to be reliable in downstream applications.

3.7.4 RNA to cDNA Conversion

1. Before starting, thaw High Capacity cDNA reverse transcription kit components (*see* Subheading 2.6, **step 8**), then mix Master Mix according to the manufacturer’s instructions.
2. Pipette 10 μL of 2 \times RT Master Mix into each well of a 96-well reaction plate or individual tube.
3. Pipette 10 μL of RNA sample into each well, pipetting up and down 2 \times to mix.

4. Seal the plates or tubes.
5. Briefly centrifuge the plate or tubes to spin down the contents and to eliminate any air bubbles.
6. Place the plate or tubes on ice until ready to load the thermal cycler.
7. Program thermal cycler using the following parameters: 25 °C for 10 min, 37 °C for 120 min, 85 °C for 5 min, hold at 4 °C until ready to remove.

3.7.5 NanoDrop 2000

cDNA Analysis

1. Thaw DNA on ice.
2. Pipette 5 µL of DEPC-treated water onto the NanoDrop 2000 quartz crystal pedestal and lower NanoDrop 2000 arm. Allow DEPC-treated water to incubate for 5 min to clean quartz crystal, then remove water with a Kimwipe.
3. Open NanoDrop 2000/2000c software and close NanoDrop Arm, if not already closed.
4. Select “Nucleic Acids” button.
5. Select DNA in the drop-down menu in the upper right corner.
6. Raise NanoDrop 2000 arm, and pipette 1 µL of DEPC-treated water onto the quartz crystal and close NanoDrop 2000 arm carefully.
7. Hit “Blank” button to measure background of RNase-Free water. Be sure to use the same solution that is suspending your cDNA sample in the Blank, to get an accurate background reading.
8. When the “Measure” button becomes selectable, raise the NanoDrop 2000 arm and wipe off the quartz crystal carefully with a Kimwipe. Pipette 1 µL of cDNA sample onto the quartz crystal and carefully close the NanoDrop 2000 arm. In the upper right corner of the screen, name the sample being tested. Then select “Measure” (*see Note 24*).
9. Carefully, raise the NanoDrop 2000 arm and wipe off the quartz crystal with a Kimwipe. Load 1 µL of cDNA from the next sample and lower the NanoDrop 2000 arm. Label the sample accordingly in the software and measure.
10. Repeat step 7 for each new sample. Wipe off quartz crystal every time after measuring a sample.

3.7.6 cDNA Gene Expression Analysis via RT-qPCR

1. Turn On Eppendorf Realplex and computer, open Realplex software and login with appropriate user account.
2. Fill a cooler with ice. Remove Universal Fast Master Mix (*see Subheading 2.6, step 10*) from refrigerator and place contents on ice.

Table 5
TaqMan primers used for RT-qPCR

Gene name	Gene symbol	Species	Dye	Entrez gene ID	Life technologies ID
Atonal homolog 1	ATOH1	Human	Fam	474	Hs00944192_s1
BarH-like homeobox 1	BARHL1	Human	Fam	56751	Hs01063929_m1
Glyceraldehyde-3-phosphate dehydrogenase	GAPDH	Human	Fam	2597	Hs02758991_g1
Growth factor independent 1 transcription repressor	GFI1	Human	Fam	2672	Hs00382207_m1
HES family bHLH transcription factor 1	HES1	Human	Fam	3280	Hs00172878_m1
HES family bHLH transcription factor 5	HES5	Human	Fam	388585	Hs01387463_g1
jagged 1	JAG1	Human	Fam	182	Hs01070032_m1
jagged 2	JAG2	Human	Fam	3714	Hs00171432_m1
Myosin VI	MYO6	Human	Fam	4646	Hs01568216_m1
Myosin VIIA	MYO7A	Human	Fam	4647	Hs00934542_m1
Notch 1	NOTCH1	Human	Fam	4851	Hs01062014_m1
POU class 4 homeobox 3	POU4F3	Human	Fam	5459	Hs00231275_m1
SRY (sex determining region Y)-box 2	SOX2	Human	Fam	6657	Hs01053049_s1

3. Remove cDNA samples and TaqMan Assays (*see Subheading 2.6, step 15*) from -20 °C freezer and thaw on ice (Table 5).
4. Spray off gloves and countertop with RNase Away (*see Subheading 2.6, step 12*).
5. Program “Plate Layout” within Realplex software.
6. Program the RT-qPCR Cycle, following the manufacturer’s instructions.
7. Add 10 µL of Master Mix (2×) to each well.
8. Add 1 µL of TaqMan Assay to each well. Remember to change tips after pipetting TaqMan Assay into each well.
9. Add 9 µL of sample to each well. Remember to change tips after pipetting sample into each well. Mix reagents and samples directly in 96-well plate by pipetting up and down 2×.
10. Seal plate with optical film. Use applicator to seal film tightly, but be careful not to bump the plate and cause liquid to splatter onto optical film.

11. Run the plate within 2 h, otherwise place the plate in a 4 °C refrigerator for short-term storage or in the –20 °C for long-term storage.
12. Run the RT-qPCR program and save file.
13. Use the $\Delta\Delta Ct$ method to calculate changes in gene expression.
14. Run gel electrophoresis on samples and control DNA to verify fragment size for further verification of DNA amplification. May be executed with 2200 TapeStation and D1000 Screen Tape and Reagents, according to the manufacturer's instructions.

3.8 Immunohistochemistry

3.8.1 Processing Cells

Cells should be grown on tissue-coated glass cover slips for this process.

1. Remove medium, and wash cover slips with PBS 2×.
2. Immerse cover slips in 4 % Paraformaldehyde fixation solution (*see Subheading 2.7, step 1*) for 15 min.
3. Wash cover slips with PBS 3× for 5 min each.
4. Immerse cover slips in 0.25 % Triton X-100 in PBS for 15 min to permeabilize cells at RT.
5. Wash cover slips with PBS 3× for 5 min each.
6. Proceed with immunostaining immediately.

3.8.2 Processing Tissue Constructs

1. Remove medium, and wash tissue construct with PBS 2× for 15 min each.
2. Immerse tissue construct in 4 % Paraformaldehyde fixation solution (*see Subheading 2.7, step 1*) in a volume 10×>the volume of the sample for 12–16 h (e.g., if your sample has a volume of 1 cm³, immerse the sample in 10 mL of 4 % Paraformaldehyde fixation solution).
3. Using a Leica ASP300 smart tissue processor, use the following protocol to process tissues: Rinse tissue construct in tap water for 1 h, then wash in a graded increase of EtOH for 2 h each (30 %, 50 %, 70 %, 80 %, 90 %, 95 %), followed by three 1 h washes in 100 % EtOH and two 1 h washes in 100 % xylene. Then, immerse tissue construct 3× in fresh paraffin for 1 h each and embed tissue construct in paraffin.
4. Section paraffin-embedded tissue construct in 10 µm sections on a microtome and float onto a 40 °C water bath containing distilled water.
5. Carefully transfer the sections onto glass slides suitable for immunohistochemistry.
6. Place slides in a metal slide rack at a 45° angle inside an oven and incubate for 20–40 min at 65 °C to allow tissues to release moisture and bond to slide.

Table 6
Antibodies and labels

Primary antibody	Primary dilution	Secondary antibody	Secondary dilution
Rabbit anti-human MYOSIN VIIA	1:100	Donkey anti-rabbit Qdot 525	2:100
Mouse anti-human NEUROG1	1:100	Donkey anti-mouse Qdot 605	2:100
Goat anti-human SOX2	1:100	Donkey anti-mouse Qdot 655	2:100

7. Remove from oven and allow tissues to dry O/N at RT (*see Note 25*).
8. Deparaffinize and rehydrate tissues by submerging tissue for 3 min each in the following solutions: 100 % Xylene, 50 % xylene/ethanol (v/v), a graded decrease in ethanol (100 %, 95 %, 70 %, 50 %), followed by rinsing 2× in PBS for 5 min each. Once rehydrated, rinse tissue sections in 0.2 % Tween 20 in PBS 2× for 10 min each.
9. Wash tissue sections in PBS 2× for 5 min each.

3.8.3 Immunostaining

1. Block samples with Primary Blocking Solution (*see Subheading 2.3, step 1*) for 1 h.
2. Incubate samples with primary antibody in appropriate dilution of Secondary Blocking Solution (*see Subheading 2.3, step 2*) O/N at 4 °C (Table 6).
3. Wash samples with PBS 3× for 5 min each.
4. Incubate samples with secondary antibody label in appropriate dilution of Secondary Blocking Solution O/N at 4 °C (*see Table 6*) (*see Note 26*).
5. Wash samples with PBS 3× times 5 min each.
6. Counterstain samples with Qnuclear™ Deep Red Stain (*see Subheading 2.8*), according to the manufacturer's instructions.
7. Wash samples with PBS 3× 5 min each.
8. Dehydrate samples according to the following protocol (EtOH is diluted in ddH₂O): Submerge samples in increasing concentrations of EtOH for 5 s each: 30 %, 50 %, 70 %, 90 %, followed by submersion 2× in 100 % for 5 s each, and finally 2× 100 % xylene for 5 s each.
9. Immediately mount with mounting medium.
10. Image samples as in Subheading 3.6.1, step 3 (Table 4).

4 Notes

1. Spray gloved hands with 70 % ethanol each time before placing in tissue culture hood.
2. Measure the umbilical cord length to the nearest centimeter. Prepare 50 mL of Digestion medium (*see Subheading 2.1, step 3*) for every 10 cm of umbilical cord. For example, for a 20 cm umbilical cord, prepare 100 mL of Digestion Medium. Do not allow umbilical cord tissues to dry out during isolation process. Always keep tissues moist with Washing Solution.
3. There are two arteries and one vein. The two arteries are typically 2–3 mm in diameter and look like “rubbery” white fibers. The vein looks like a large flattened “tube” with a thin tissue wall. The diameter of the vein may be twice the size of the arteries.
4. There are two ways to remove the blood vessels:
 - Method 1: Use two pairs of forceps. Use one pair of forceps to grab the end of a blood vessel and pull. Use the other pair of forceps to gently “peel” away the surrounding tissue. The arteries tend to pull out of the umbilical cord segment smoothly. The vein does not detach easily.
 - Method 2: Carefully, use the scalpel to make a length-wise incision through the amniotic epithelium to allow the umbilical cord segment to “unroll” from a tube to a flat piece of tissue. Use the forceps to gently pull the blood vessels away the umbilical cord segment. CAUTION: *When using this method, be careful not cut through a blood vessel, or the blood vessel will be difficult to identify and remove. Locate blood vessels before cutting into umbilical cord segment, and make incision away from blood vessels.*
5. Mince up the tissue until it has a “pulp-like” consistency.
6. For every 10 cm of umbilical cord, divide minced tissue into separate 100-mm mono plates for digestion. Add 50 mL of Digestion medium to each 100-mm mono plate. For example, if an umbilical cord is initially 30 cm in length, divide minced up tissue equally between 3 100-mm mono plates, and add 50 mL of Digestion medium to each 100-mm mono plate.
7. The length of the umbilical cord and physical degradation affect the amount of time needed to digest the umbilical cord tissue. The digestion process is more efficient when umbilical cord tissue is physically degraded into fine pieces than medium to large pieces. Digestion can take between 4 and 8 h, depending on the quantity of umbilical cord tissue processed and how well umbilical cord tissue was physically degraded.

8. If there is potential for a tube cap or bottle neck to come in contact with water, seal tube cap or bottle neck with parafilm.
9. When removing reagents from bead bath, they should feel warm to the touch, but not hot. If reagents feel cold, continue warming in the bead bath.
10. Cells should appear either spindle-shaped (“Crescent Moon”) at low confluence, and fibroblastic (“Webbed”) when over 50 % confluence. In addition, cells should have well defined edges and nuclei. Cells *should not* display signs of “blebbing.”
11. For well plates, tilt plate at a 30°–45° so that medium is up against the well wall. Then aspirate medium from the wall without touching cell surface (floor of the well).
12. For T-flasks, gently turn flask over so that medium moves from the floor of the T-flask (cell culture surface) to the ceiling of the T-flask. Carefully insert the aspirating pipette into the T-flask without touching the edge or inside of the neck of T-flask and aspirate medium from the ceiling of the T-flask.
13. When adding medium to a well plate, use a pipette and aim for the wall of the well. *Do not* add medium directly to the cell surface (floor of the well), as cells may detach. Add medium slowly, so as not to disrupt the cell monolayer. Sometimes, it is helpful to aliquot medium from the main stock solution into a smaller container, when feeding cells in well plates, to avoid potentially contaminating the main stock solution of medium. For example, if the main stock solution of medium is in a 500-mL bottle and medium needs to be changed in three different 6-well plates, then pipette 54 mL of medium from the main stock into two 50-mL conical tubes. This way, medium is pipetted directly out of the conical tube, instead of the main stock.
14. When adding medium to a T-flask, position the T-flask so that it is nearly vertical and gently add medium to the ceiling of T-flask. Then, gently turn the T-flask over and lay down so that the medium covers the cell surface (floor of T-flask). *Do not* add medium directly to the cell surface.
15. Special Notes regarding cell culture:
 - Check cells and feed on a regular schedule, such as every 48 h.
 - Check cells before feeding. If cells have reached a confluency of 80–90 %, then cells need to be sub-cultured, that is, passaged (*see* Subheading 3.2.2).
 - Confluency—Coverage of cell surface area. For example, 50 % confluency means that cells cover 50 % of the surface area of the cell culture vessel.

- If black dots are observed that move against the motion of the liquid or if “segmented arms” are observed branching out across the surface area of the cell culture vessel, then cells are most likely contaminated with bacteria or fungi, respectively. Contaminated cell cultures will need to be disposed of according to state and local regulations of the institution.
16. Keep aspirating tip near mouth of tube and tilt tube to direct liquid toward aspirating tip. *Do not* place aspirating tip near cell pellet inside of tube.
 17. Make sure the tip of the vial is submerged in PBS so that the vial does not explode.
 18. Samples being labeled for all CD markers (CD34, CD45, CD73, CD90, CD105, STRO-1) will need to be sequentially labeled, to avoid cross-reactivity. One antibody or label can be applied at every incubation-wash step. An incubation-wash step consists of incubating a cell sample with an antibody or label for 20 min on ice in the dark. Afterward, the cell sample is washed with Secondary Blocking Solution and centrifuged to pellet the sample. The supernatant is decanted and the next incubation-wash step started. It is recommended that the STRO-1 primary antibody be added first, followed by the secondary donkey anti-mouse Alexa Fluor 568 label. Afterward, the CD105 primary antibody is added, followed by the secondary donkey anti-mouse Qdot 525 label. Afterward, all remaining markers (CD34, CD45, CD73, CD90) are added, as the remaining markers are pre-conjugated to fluorophores.
 19. Samples, receiving STRO-1 and CD105, require secondary labeling with Alexa Fluor 568 and Qdot 525, respectively.
 20. Positive identification of cell markers are defined by a fluorescent emission that exceeds the fluorescent threshold of cells stained with corresponding isotype (negative) controls.
 21. It is highly recommended that no less than 20,000 events be analyzed for each sample. In addition, it is recommended that samples be analyzed at least 3x.
 22. Pure RNA has a 260/280 absorbance ratio ~2.0 (1.9–2.1). Any sample that has a 260/280 ratio under 1.9 has contaminants and may not provide reliable data in downstream applications [23].
 23. The 260/230 ratio is a secondary measurement of nucleic acid purity. Pure nucleic acids should have a 260/230 ratio between 2.0 and 2.2.
 - If the 260/280 absorbance ratio is below 1.8, check the 260/230 ratio. If the 260/230 ratio is below 2.0, then there may be protein contaminates (*see* [24]).

- If both the 260/280 ratio and the 260/230 ratio are below ~2.0 and 2.0, respectively, then the pH of the blanking solution may have shifted. If the pH of the blanking is slightly below 7.5, it can shift the 260/280 and 260/230 ratios. To determine if pH is affecting the 260/280 ratio, resuspend 1 μ L of the RNA sample in 2 μ L of TE Buffer (Tris and EDTA). Run TE Buffer as the “Blank” on the NanoDrop 2000, then test the RNA sample suspended in TE Buffer (*see* [24]).
 - If the 260/280 and 260/230 ratio are still outside of recommended limits, then there are most likely contaminants in RNA sample. The RNA sample can be re-cleaned with the components of a Qiagen RNeasy Kit (*see* Subheading 2.6, step 1). To do this, bring the total volume of RNase-Free water that the RNA sample is suspended in up to 100 μ L. If using a Qiagen RNeasy Kit, add 350 μ L of RLT buffer and 200 μ L of 100 % EtOH. Mix well, transfer to a brand new RNeasy column, and repeat according to Subheading 2.6, step 1. Re-test the RNA sample on the NanoDrop 2000 (*see* [24]).
24. *Pure cDNA has a 260/280 absorbance ratio between 1.8 and 2.0.* Any sample that has a 260/280 ratio under 1.8 or over 2.0 has contaminants and may not provide reliable data in downstream applications.
 25. Tissues are preserved once embedded in paraffin and bonded to a slide. When ready to proceed with immunohistochemistry, deparaffinize tissues and keep moist. *Do not* allow tissues to dry out.
 26. Reserve a set of samples to incubate only with secondary antibody label to reveal non-specific binding.

Acknowledgments

This work was supported by NIH R01-AR056347 and the State of Kansas.

References

1. Chen J, Steit A (2013) Introduction of the inner ear: stepwise specification of otic fate from multipotent progenitors. *Hear Res* 297: 3–12
2. Collado MS, Holt JR (2009) Can neurosphere production help restore inner ear transduction? *Proc Natl Acad Sci U S A* 106:8
3. Dhara SK, Gerwe BA, Majumder A, Dodla MC, Boyd NL, Machacek DW, Hasneen K, Stice SL (2009) Genetic manipulation of neural progenitors derived from human embryonic stem cells. *Tissue Eng Part A* 15:3621–3634
4. Dhara SK, Majumder A, Dodla MC, Stice SL (2011) Nonviral gene delivery in neural progenitors derived from human pluripotent stem cells. *Methods Mol Biol* 767:343–354
5. Wang L, Ott L, Seshareddy K, Weiss ML, Detamore MS (2011) Musculoskeletal tissue engineering with human umbilical cord mesenchymal stromal cells. *Regen Med* 6:95–109

6. Wataya T, Muguruma K, Sasai Y (2008) Human pluripotent stem cell and neural differentiation. *Brain Nerve* 60:1165–1172
7. Koehler KR, Hashino E (2014) 3D mouse embryonic stem cell culture for generating inner ear organoids. *Nat Protoc* 9:1229–1244
8. Koehler KR, Mikosz AM, Molosh AI, Patel D, Hashino E (2013) Generation of inner ear sensory epithelia from pluripotent stem cells in 3D culture. *Nature* 500:217–221
9. Longworth-Mills E, Koehler KR, Hashino E (2015) Generating inner ear organoids from mouse embryonic stem cells. *Methods Mol Biol* 1341:391–406
10. Ohnishi H, Skerleva D, Kitajiri S, Sakamoto T, Yamamoto N, Ito J, Nakagawa T (2015) Limited hair cell induction from human induced pluripotent stem cells using a simple stepwise method. *Neurosci Lett* 599:49–54
11. Yamahara K, Yamamoto N, Nakagawa T, Ito J (2015) Insulin-like growth factor 1: a novel treatment for the protection or regeneration of cochlear hair cells. *Hear Res* 330:2–9
12. Bancroft GN, Sikavitsas VI, van den Dolder J, Sheffield TL, Ambrose CG, Jansen JA, Mikos AG (2002) Fluid flow increases mineralized matrix deposition in 3D perfusion culture of marrow stromal osteoblasts in a dose-dependent manner. *Proc Natl Acad Sci U S A* 99:12600–12605
13. Barry F, Boynton RE, Liu B, Murphy JM (2001) Chondrogenic differentiation of mesenchymal stem cells from bone marrow: differentiation-dependent gene expression of matrix components. *Exp Cell Res* 268:189–200
14. Romanov YA, Darevskaya AN, Merzlikina NV, Buravkova LB (2005) Mesenchymal stem cells from human bone marrow and adipose tissue: isolation, characterization, and differentiation potentialities. *Bull Exp Biol Med* 140:138–143
15. Rose RA, Jiang H, Wang X et al (2008) Bone marrow-derived mesenchymal stromal cells express cardiac-specific markers, retain the stromal phenotype, and do not become functional cardiomyocytes in vitro. *Stem Cells* 26:2884–2892
16. Bailey M, Wang L, Bode C, Mitchell K, Detamore MS (2007) Comparison of human umbilical cord matrix stem cells and temporomandibular joint condylar chondrocytes for tissue engineering temporomandibular joint condylar cartilage. *Tissue Eng* 13:2003–2010
17. Detamore MS (2013) Human umbilical cord mesenchymal stromal cells in regenerative medicine. *Stem Cell Res Ther* 4:142
18. Devarajan K, Forrest ML, Detamore MS, Staerker H (2013) Adenovector-mediated gene delivery to human umbilical cord mesenchymal stromal cells induces inner ear cell phenotype. *Cell Reprogram* 15:43–54
19. Mitchell KE, Weiss ML, Mitchell BM, Martin P, Davis D, Morales L, Helwig B, Beerenstrauch M, Abou-Easa K, Hildreth T, Troyer D, Medicetty S (2003) Matrix cells from Wharton's jelly form neurons and glia. *Stem Cells* 21:50–60
20. Baksh D, Yao R, Tuan RS (2007) Comparison of proliferative and multilineage differentiation potential of human mesenchymal stem cells derived from umbilical cord and bone marrow. *Stem Cells* 25:1384–1392
21. Mellott AJ, Godsey ME, Shinogle HE, Moore DS, Forrest ML, Detamore MS (2014) Improving viability and transfection efficiency with human umbilical cord Wharton's jelly cells through use of a ROCK inhibitor. *Cell Reprogram* 2:91–97
22. Mellott AJ, Devarajan K, Shinogle HE et al (2015) Nonviral reprogramming of human Wharton's jelly cells reveals differences between ATOH1 homologues. *Tissue Eng Part A* 21:1795–1809
23. Bustin SA, Mueller R (2005) Real-time reverse transcription PCR (qRT-PCR) and its potential use in clinical diagnosis. *Clin Sci (Lond)* 109:365–379
24. Qiagen (2010) Critical factors for successful real-time PCR [E-Reader Version]. Accessed from <https://www.qiagen.com/us/resources/resourcedetail?id=f7efb4f4-fbcf-4b25-9315-c4702414e8d6&lang=en>

Part V

Nanotechnology

Chapter 20

Nanotechnology in Auditory Research: Membrane Electromechanics in Hearing

Mussie Araya and William E. Brownell

Abstract

The soft, thin membranes that envelop all living cells are 2D, nanoscale, fluid assemblies of phospholipids, sterols, proteins, and other molecules. Mechanical interactions between these components facilitate membrane function, a key example of which is ion flow mediated by the mechanical opening and closing of channels. Hearing and balance are initiated by the modulation of ion flow through mechanoreceptor channels in stereocilia membranes. Cochlear amplification by the outer hair cell involves modulation of ion movement by the membrane protein prestin. Voltage-gated ion channels shape the receptor potential in hair cells and are responsible for the initiation of action potentials that are at the heart of sensory processing in the brain. All three processes require a membrane and their kinetics are modulated by the mechanical (i.e., material) properties of the membrane. This chapter reviews the methodology for measuring the mechanics of cellular membranes and introduces a method for examining membrane electromechanics. The approach allows examination of electromechanically mediated interactions between the different molecular species in the membrane that contribute to the biology of hearing and balance.

Key words Membrane electromechanics, Optical tweezers, Patch clamp, Neurons, Ion channels, Outer hair cells, Prestin, Membrane/protein interactions, Phospholipids, Sterols

1 Introduction

Membrane molecules are amphipathic, having both hydrophilic and hydrophobic domains. The hydrophilic domains are located on the membrane surface, while the hydrophobic regions are located inside. The membrane is stabilized by the surface tension arising at both the inner and outer membrane/water interfaces. Living cells expend energy to maintain an asymmetry in the number of phospholipid-associated fixed charges on the inner and outer membrane surfaces. The electrical polarization resulting from the charge asymmetry sets the stage for force generation. Electromechanical force by the membranes of living cells is driven by a diffusion potential of ~100 mV. This potential is generated by the active pumping of ions to maintain electrochemical gradients.

The resulting transmembrane electric field is huge (>10 MV/m—compare to the ~ 3 MV/m fields associated with atmospheric lightning) because the membrane is very thin (>5 nm). Electromechanical coupling occurs naturally in simple lipid bilayers, where it is called the flexoelectric effect. Flexoelectricity is analogous to the electromechanical behavior of piezoelectric crystals and appears to be a universal property of all cell membranes.

Membrane mechanical properties, such as tension, bending stiffness, viscosity, and the active modulation of these properties by membrane electric potential, are important for many physiological functions. Mechanical connections with the cytoskeleton also alter membrane properties and important membrane proteins, such as ion channels and transporters that are anchored to the cytoskeleton. Changes in membrane tension in response to changes in membrane potential and subsequent dissipation of the tension by viscoelastic relaxation are relevant to synchronized gating and inactivation/closing of stretch-activated and voltage-gated ion channels and transporters. Synchronized gating or cooperative gating of ion channels at the axon initial segment permits rapid charge transfer and fast action potential initiation [1]. The rapid onset of the action potential allows for phase locking at high frequencies and rapid temporal processing in the auditory system. Similarly, the cooperative gating of prestin may permit high frequency charge transfer in outer hair cells.

Several methods have been developed to probe the mechanical properties of cellular membranes, including atomic force microscopy, aspiration pipettes, optical and magnetic tweezers, cell stretching, and microelectromechanical systems (MEMs). Each method will be reviewed and its advantages and limitations with respect to the others identified. A new method will then be presented that combines optical tweezers and whole cell voltage clamp to characterize the physical mechanism underlying electromechanical force production by membranes. This new method allows investigation of outer hair cell electromotility, ion channel gating, and rapid temporal processing of auditory information.

The simplest way to investigate cell membrane mechanics is by attaching them to a flexible substrate and pulling or compressing the substrate. Cells are cultured directly on a thin polymer sheet. Whose surface is coated with extracellular matrix molecules to encourage adhesion of the cells to substrate. Systematic altering of the mechanical properties of the substrate material can be made by changing the degree of crosslink in the polymeric substrate and/or mechanical deformation of the substrate. The effects of mechanical forces, loading on the individual and collective interactions of the membrane with the substrate can be investigated. Several varieties of actuators, such as microelectromechanical systems (MEMs), have been used to improve the sensitivity and resolution of force measurement [2]. When using MEMs, the substrate topography

can be micro-manipulated and moved to apply and measure force. Further improvement can be achieved by fractionalization and micro-designing of the substrate with specific cellular matrix targets. Because the membrane of living cells is directly moved, the cells cannot be voltage clamped and the modulation of membrane mechanics by electric potential cannot be measured directly. Measurement of mechanical properties of voltage-clamped cells can be made using atomic force microscopy (AFM) [3]. AFM uses a sharp tip at the end of flexible cantilever to generate a local deformation to the cell surface. Changes in membrane tension will move the cantilever and the membrane tension can be quantified using a calibrated cantilever tip. The measured force includes contributions from the cytoskeleton and does not allow direct quantification of membrane mechanical properties. AFM sensitivity is however great and the technique allows determination of the force required to pull a protein from a membrane or the force that will break bonds and allow a protein to unfold.

The separation of the membrane from the cytoskeleton and direct measurement of mechanical properties of cell membranes can be accomplished using aspiration micropipettes [4–6] or optical tweezers [7, 8]. Aspiration pipettes suck a portion of a cell into the micropipette. By measuring the force required to pull a “tongue,” the force required to separate the membrane from the cytoskeleton and estimates of stiffness and tension can be obtained. This method permits the measurements of forces as small as 1 pN, but does not allow simultaneous voltage clamping. Measures of membrane force in response to electrical stimulation can be achieved using optical tweezers combined with whole-cell patch-clamp, which is the topic of this chapter.

Optical tweezers (Fig. 1) consist of an optically trapped bead that functions as “tweezers,” attaching to and deforming components of the cell. A powerful, highly focused laser beam produces an attractive force on dielectric beads, having a high index of refraction (Fig. 2a). The force required for the deformation pulls or pushes the bead from the center of the trap. The force is proportional to the displacement of the bead from the center of the trap resulting in a sensitive force biosensor. An isolated cell that is adherent to the glass surface of a Petri dish is brought into contact with a trapped bead by moving the microscope stage. The beads are fluorescent and coated with sulfate surface groups to facilitate their adhesion with cell membranes. When the cell is pulled away after attachment, the force pulling on the bead increases until a maximum is reached and the membrane separates from the cytoskeleton. A membrane nanotube (tether) is then extracted from the cell. The force required to hold the tether is less than that required to break the cytoskeletal adhesion. Measurement of the tether force can be used to compute mechanical properties of the membranes such as bending rigidity, surface tension, and viscosity.

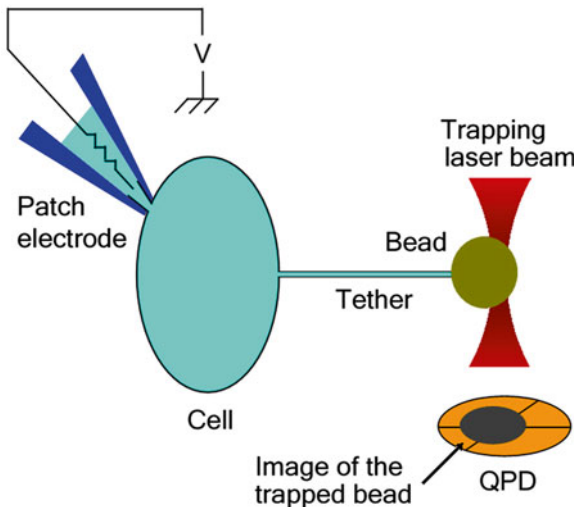


Fig. 1 Cartoon showing membrane tether formation with optical tweezer from voltage-clamped cell. Both constant and sinusoidal electrical stimuli are delivered to the cell through the whole-cell tight-seal patch electrode. Electromechanical force is quantified by measuring the bead displacements along the tether axis using the quadrant photodetector [11]

An analysis of the force measurement allows the understanding of the membrane–cytoskeleton adhesion and modulation of membrane mechanics by electric potential or pharmacological agents. Fundamental energy considerations allow membrane mechanical properties to be calculated from measurements of the tether force and the tether diameter [8, 9].

Electrical stimulation of the cell membrane while membrane tether force is measured is accomplished by maintaining the cell in whole-cell, tight-seal, voltage-clamp (Fig. 1). The materials and methods for patch-clamp experiments are presented in chapters of the present volume (*see* Goutman & Pyott in this edition for details). The only variation on standard techniques arises from the fact that the cell is moved during tether formation and the patch pipette must remain attached to the cell. This is achieved by mounting a low mass micro-manipulator on the microscope stage. Tethers are pulled from plasma membranes, while the membrane is held at different holding potentials, and the tether force is measured, while changing the membrane potential. Measuring biologically relevant mechanical properties typically involves applying mechanical, chemical, and electrical stimuli and recording the evoked mechanical response. Lipid protein interactions convey the mechanical force resulting from changes in the transmembrane electric field and contribute to ion channel cooperative gating and transport. Electromechanical force production by the membrane is altered on

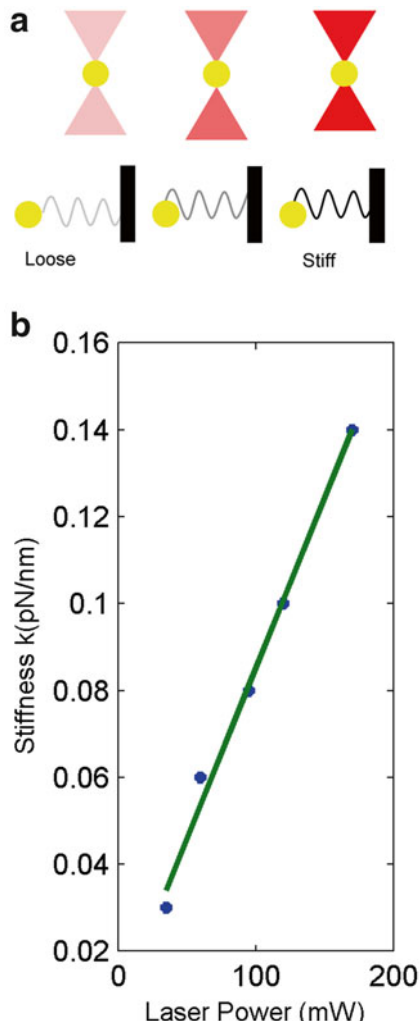


Fig. 2 Cartoon of optical trap and plot of trap stiffness as a function of laser power. **(a)** Dielectric objects are attracted to the center of focused beam. The trapping force applied on the bead depends linearly on its displacement from the trap center just as with a simple spring system. **(b)** Trapping stiffness as a function of laser power. Regression line shown in green was obtained by fitting the stiffness of optical trap as a function of laser power, indicating that the stiffness of the optical trap varies linearly with laser power ($R^2=0.99$). The force that results from a bead displacement X is equal to the stiffness (k) times X .

application of a variety of pharmacological agents or changing cytoplasmic pressures. These treatments also alter ion channel kinetics. Testing for concomitant variation between electromechanical force and channel function can provide experimental support on the membrane's role in ion channel gating.

2 Materials

2.1 Hair Cell and Neuron Culture Preparations

1. Neurobasal medium containing B27 supplement.
2. Glass bottom 35 mm Petri dish, 14 mm Micro-well, No. 1.5 cover glass (0.16–0.19 mm) poly-d-lysine coated.
3. Incubators, biological safety hoods, freezers, and other equipment.
4. Trypsin, dissection, and maintenance media.
5. Dissection tools.

2.2 Optical Trapping Using Optical Tweezers and Tether Pulling

1. Sound-insulated room to house the device as well AVAC for temperature stability.
2. An optical table with a STACIS active damping system.
3. Continuous wave, tunable (650–1100 nm) titanium–sapphire laser (Spectra-Physics, 3900S), with a frequency-doubled Nd: YVO₄ laser (spectra-physics, Millennia V).
4. Inverted microscope (Nikon Eclipse Ti-U).
5. 60× Oil immersion objective, high numerical aperture: NA 1.4.
6. A piezoelectric translation stage (Physik Instrument, P-527.3CL).
7. Other optical instruments: Beam expanders and attenuators (lambda quarter plate with polarized beam splitter should be used as an attenuator to avoid photo-damage to cells), focusing lenses (2-f 250, 2-f 150, 1-f 75 mm lenses in this specific case), 10 mirrors (in kinematic mount with vertical drive, mounting base, and 1 dichroic mirror).
8. Polyethylene fluorescent dielectric beads with a sulfate surface group and a diameter of 4.5 mm (Poly-Sciences, Niles, IL).
9. 300 W light emitting diode (TLED) lamp (Sutter Instrument, Novato, CA).
10. Position-sensing device, a quadrant photodetector (QPD) placed at the Right port, 1 focusing lens.
11. Personal computers, Field programmable gated Array (FPGA, National Instruments PCIe-7852R, Austin, TX), Data Acquisition card (DAQ, National Instruments PCIe-6363), DAQ device drivers (NI-DAQmx).
12. LabVIEW (Ver. 6.0; National Instruments, Austin, TX), Matlab.
13. Calibration equipment: Optical power meter and Acousto-optic deflectors.
14. Imaging optics for bright field microscopy: 100 W Halogen Lamp for bright field microscopy and visualization of cells and charge-coupled device (CCD) camera.

3 Methods

3.1 Alignment and Calibration of Optical Tweezers

This procedure is to be performed for each bead used. Begin by aligning the laser.

1. Turn on the solid-state laser and wait for ~30 min until the pump laser reaches 5 W.
2. Prepare ~0.2 % stock bead solution in PBS.
3. Turn on the AODs to allow the first-order beam to pass (*see Note 1*) and the run application program (*see Note 2*).
4. Open the shutter and measure the laser power (~1.5 W) and spectrum of the bead.
5. Align the laser by adjusting the mirrors (*see Note 3*).
6. Measure the power of the laser at the objective by placing the power meter directly at the objective lens of the microscope. Adjust AODs to produce at least 130–140 mW power at the objective. This is required to trap 4 μm beads with sufficient restoring force to maintain beads in stable equilibrium without thermal damage to the cell.
7. Turn on the piezoelectric controller and set the (x , y , and z) coordinates for the piezoelectric stage at (100, 100, and 70 μm). The coordinates are specific to our microscope and may vary from configuration to configuration.
8. Focus the laser center at about 5 μm above the bottom of the dish. This will place the high convergence angle required for trapping at 5 μm above the coverslip when oil immersion objective is used.
9. Place a bead at the bottom of the dish. Turn on the LED light to excite the bead and turn off other source of light including the room light.
10. Align the fluorescence of the bead at the center QPD after the trapping laser is aligned at the center of the objective.

3.2 Calibrate QPD Output and Stiffness of Optical Tweezers

1. Calibrate the position sensor by moving the microscope stage a known distance (± 2500 nm, ± 2000 nm, ± 1500 nm, ± 1000 nm, and ± 500 nm) and recording the output (in mV). The QPD signal varies linearly with bead displacement up to 2000 nm from the center of the QPD. The slope of this relation is used to convert the QPD signal to displacement of the bead in nanometers.
2. Apply radio frequency signal 50 MHz to the Acousto-optical deflectors (AODs). The AODs have two voltage inputs for the amplitude and frequency of the RF wave (0.5 and 6.2 V, respectively) (*see Note 2*).

3. The tweezers are stepped for ± 500 nm for 40 ms every 80 ms for 1 min. To move the beam 1 nm, change voltage of the frequency input by 0.178 mV in X or 0.189 mV in Y .
4. Take periodic average of the time course and the magnitude of the bead position to enhance the signal-to-noise ratio of the QPD output. (QPD output contains high frequency noise and displacement of the bead cannot be readily quantified from a single trace.)
5. Fit the measured movement of the bead to a stepwise deflection of the trap with an analytic expression for an over-damped harmonic oscillator.
6. Estimate the decay time constant (τ , which is proportional to the ratio of viscosity over the stiffness ($\tau = b/k$)) using fitting algorithm. Use a fitting routine such as polyfit in Matlab.
7. Compute the trapping stiffness. The drag coefficient is known ($b = 6\pi R\eta$, where R is stokes radius=bead radius and η is the viscosity of the solution). Trap stiffness can be solved for from the time constant and drag coefficient. We find that it varies with the power of the laser as a linear function of laser intensity (Fig. 2).

3.3 Hair Cell and Neuron Cultures

All procedures using animals should be approved by the Institutional Animal Care and Use Committee according to the guidelines set forth by the NIH.

1. Guinea pig outer hair cells (OHCs) are easy to isolate, their hearing is similar to that of humans, and the methods are well characterized [5, 10, 11].
2. Dissect the ventral cochlear nucleus from the fetal animal brain (usually at gestation day 16–18) following decapitation. Neurons are then trypsinized, dissociated, and plated onto the glass bottom of poly-d-lysine-coated microwell Petri dishes (MatTek, Ashland, MA) and maintained in Neurobasal medium containing the B27 supplement. Embryonic neurons can be maintained well in culture for up to about 4 weeks and will undergo distinct stages of differentiation and eventually form synaptic connections (see Note 4).
3. Bushy cells are the principal cells of the VCN. If other cell types are found in the culture system, differentiate them based on their morphology and ion channel profile.

3.4 Pull Membrane Tether and Measure Force

1. A tether is formed and elongated by placing the cell in contact with an optically trapped bead and moving the cell away from the trapped bead at a preset velocity. Open the application software to generate the voltage protocol to automate the movement of the piezoelectric stage and tether formation (see Note 2).
2. Enter inputs of the application software that include: (1) the distance of the cell from the trapped bead (usually 25–30 μm);

- (2) the move in speed of the cell toward the trapped bead ($0.1\text{--}1 \mu\text{m/s}$), (3) the hold time between the cells (1–5 s), (4) the move away speed of the cell from the bead ($0.1\text{--}1 \mu\text{m/s}$), and (5) the final distance of the cell from the bead (25–30 μm).
3. Place dish containing cultured cell in the piezoelectric stage and focus the trapping beam at $\sim 5 \mu\text{m}$ over the Petri dish cover slide.
 4. Add fluorescent beads to cell culture solution. Add $\sim 2 \mu\text{L}$ of 0.2 % bead solution into one corner of the square plate of the Petri dish. This addition will help prevent the entrance of multiple beads into the field of view of the QPD when a bead is trapped.
 5. Search for floating beads using manual or coarse control of the piezoelectric stage, and move the floating bead toward the center of the beam very fast by moving the piezoelectric stage very fast. If the bead is trapped, it will not move.
 6. Search for healthy looking cells and bring the cell or (voltage-clamped cell if electromechanical force measurement is being made) near the trapped bead by moving the piezoelectric stage manually. Bring the cell close, $\sim 20\text{--}30 \mu\text{m}$, to the bead and note the precise distance.
 7. Run the application program (*see Note 2*).

3.5 Measurement of Passive Membrane Mechanics

1. The measurement of bending stiffness requires a measurement of tether radius. Achieve this measurement by taking a microscopic image of the tether and analyzing the tether morphology from the saved image.
2. To measure membrane viscosity, pull membrane tethers at several speeds (typically, 1, 2, 3, and 4 $\mu\text{m/s}$). Move the cell away from the trapped bead at 1 $\mu\text{m/s}$ for 30s as described above, then increase the pulling rate every 3 s by 1 $\mu\text{m/s}$ until it reaches 5 $\mu\text{m/s}$.

3.6 Measurement of Membrane Electromechanics

1. Pull, coat, and fill pipette electrode prior to starting the experiment (*see Goutman & Pyott in this edition for details*).
2. Voltage-clamp the cells prior to forming and pulling tethers at different holding potentials (-120, -60, 0, 60, and 120 mV) during electromechanical force measurements.
3. Stage movement is stopped when tether length reaches a preset value and allows the tether to relax for 60 s.
4. Apply a sinusoidal electrical stimulus after the tether force reaches steady state. The sinusoidal voltage ($\pm 20 \text{ mV}$, [10 Hz–5 kHz]) is superimposed on the holding potentials for 10 s and the mechanical response of the tether measured.
5. When measuring tether electromechanical force, whole-cell currents may be simultaneously recorded to monitor the tight seal during the entire force measurements.

3.7 Data Processing and Analysis

1. Take a running average of the QPD signal to remove high-frequency noise.
2. Convert QPD signal in (mV) to displacement of the bead from the center of the QPD (in nm) (*see* Subheading 3.2, step 1).
3. Multiply bead displacement by trap stiffness to compute tether force. The tether formation force is at the peak of the tether force profile, when the membrane has detached from the cytoskeleton and a tether is formed (Fig. 3). The electromechanical tether force at each holding potential should be normalized to tether force at 0 mV. High-frequency electromechanical force measurement requires normalization (*see* Note 5).
4. Calculate the membrane–cytoskeleton adhesion energy using measurements of tether force on a region of a cell where the membrane is supported by the cytoskeleton and on blebs lacking cytoskeleton support (i.e., where the adhesion term equals 0).
5. Calculate bending stiffness (B) with the equilibrium force required to hold the elongated tether (F_{eq}) and the tether diameter (d) using the relation $B=2\pi^*F_{eq}^*d$.

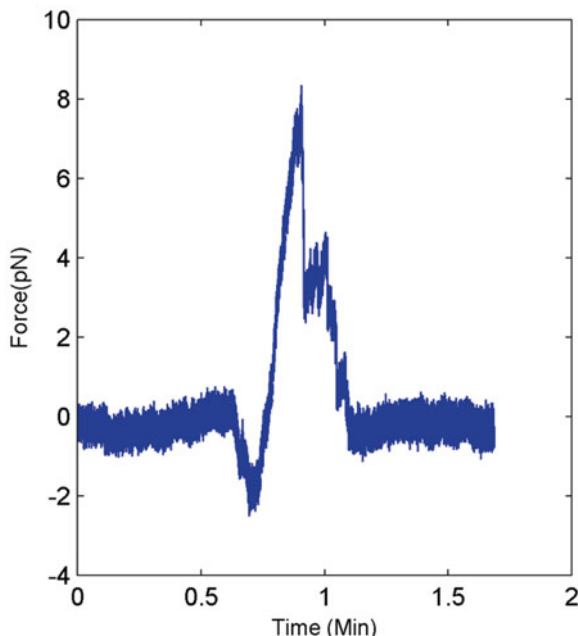


Fig. 3 Representative force profile showing tether formation. The soma of an isolated neuron is brought into contact with the bead and pushes it in the negative direction (downward deflection). The neuron is then moved away from the bead at a constant velocity (0.1 $\mu\text{m}/\text{s}$) for the remainder of the trace. The membrane is attached to the cytoskeleton until a peak force is reached at which point the membrane separates and the force on the bead drops as membrane flows into the resulting tether. The peak value is the tether formation force and is proportional to the cytoskeleton–plasma membrane adhesion energy [8, 15]

6. Calculate membrane viscosity. Fit the data for different pulling rates, V_{pull} , to an exponential function to obtain the asymptotic value of the steady-state force for the different pulling segments (*see Note 6*). Fit a set of steady-state force and the pulling rate to the linear function $F_{\text{ss}}(V_{\text{pull}}) = F_{\text{ss}}(0) + 2\pi\eta V_{\text{pull}}$, to get an estimation of the steady-state force at zero pulling rate $F_{\text{ss}}(0)$ and the viscosity (η).
7. Assess the role of the membrane force generation in channel gating and transport. Add (1, 5, 10, 50, and 100 mM) salicylate to the bath solution and measure the changes in electro-mechanical gain and channel function. Whole-cell membrane currents are used to assess channel function.

4 Notes

1. We developed a calibration scheme utilizing Acousto-optical deflectors (AODs) to control the position of the trapping beam. A radio frequency signal is applied to solid crystal through a piezoelectric transducer of AODs to control the diffraction of light. Several properties of diffracted light are independently controlled with AODs, including the angle, amplitude, and frequency. The diffraction angle is proportional to the sound frequency and the intensity of the diffracted beam is proportional to the sound amplitude. The ability to control the refraction angle allows the beam to be moved rapidly (<10 μ s). Two orthogonally oriented AODs, AODX and AODY are used to scan the laser beam in the XY plane. The AODs are driven by RF signals 40–60 mHz generated by the FPGA (*see Notes 4*) and the frequency and amplitude of the RF pulse is determined by two voltage inputs generated by the FPGA. The position of the bead at the objective is determined by the center frequency of the AOD (50 mHz). The AOD is designed such that the zeroth-order beam has the highest efficiency at about 80 % of the incident light and the first-order beam has about 12.5 % of the incident center frequency. Drive the AODs using voltage signals (0.5 V, 6.2 V to control the amplitude and frequency of the RF wave at the center frequency of the AOD) to provide at least 530–570 mW in the first-order beam of the AOD crystal (yielding 130 mW at the objective). But as the acoustic wave frequency deviates from its center value, diffraction efficiency decreases, causing a decrease in laser power. Spatial filters are used to block zeroth-order beam and the first-order beam is deflected by slightly changing the frequency of the RF pulse from the center frequency of the AOD.
2. Integration of computer with instruments—automation of measurements. The extensive data collection protocol and

limited time for maintaining cellular integrity requires automation of the movement of the piezoelectric stage (to elongate tether) while recording the displacement of the bead for further analysis. Patch-clamp amplifiers, piezoelectric stages, and QPDs have features that allow extensive interaction with the laboratory computer. Some are inputs and some are outputs. The interfacing of these devices with a computer can be achieved with data acquisition (DAQ) or field programmable-gated array (FPGA) systems. Using a terminal block, cables, and a DAQ device, the measured signal can be transferred, digitized, and stored in the computer for later analysis. From the DAQ device, the signal can be transferred to the computer through a variety of different bus structures that plug into the PCI bus of a computer. Most DAQ devices have four standard elements—analog input, analog output, digital I/O, and counters. Analog input is used to measure the voltage (mV) signal from the QPD device and the current delivered to the cell by the patch-clamp amplifier. The analog signal is digitized by the analog to digital converter circuit of the DAQ so that a computer can store and processes it. Although the DAQ device provides analog filtering options, the signals may be acquired at higher bandwidths and digitally filtered at a later time. Analog output is used to deliver voltage signals from the DAQ device to the patch-clamp amplifier and piezoelectric stage as external command. Complex voltage protocols are required to automate the electrical stimulation of the membrane and movement of the PI stage. Application software is required to interface the user with the DAQ device. LabVIEW is commonly used for this purpose because it contains extensive support for interfacing to devices and instruments. DAQ device requires a driver engine that communicates between the device and application software by performing low-level register writes and reads on the DAQ device, while exposing the application program interface (API) to user applications software. We chose a NI-DAQmx device driver engine because it includes a DAQ assistant for configuration of channels, automation, and measurement tasks with simpler API for creating DAQ applications.

3. Laser Alignment. The alignment of the laser is verified by observing the diffraction pattern of the beam from the adjustable circular aperture. Adjust the angle of mirrors until the laser is aligned. Place the adjustable circular aperture at a right angle to the incident laser beam and observe the diffraction pattern of the beam by placing a piece of paper near the aperture. When the circular aperture is uniformly illuminated, the diffraction pattern has a bright region in the center, known as the Airy disk with a series of concentric bright rings around it

called the Airy pattern. Carefully narrow the width of the aperture until the airy patterns disappear. When the bead is aligned, the intensity of the airy disk will be uniform.

4. Primary cultures of neurons and hair cells. Membrane mechanics experiments on living cells require unrestricted access to their surface. This precludes *in vivo* or slice preparations. Isolated cells, ideally in a long-term culture system that is less complex than found *in vivo* are maintained *in vitro* under cell culture conditions. Hair cells should be used in <4 h after removal from the cochlea—make sure all dissection tools, solution, and instrumentation are ready before sacrificing the Guinea pig. The acute isolation of neurons from the ventral cochlear nucleus in adult guinea pigs was described first in [12]. Early developmental stage neurons are less susceptible to damage during the processing required for their culture. Glial cells are the major source of contamination in neuronal cultures and early developmental cultures contain fewer glial cells. Protocols for embryonic stage (E14–18) hippocampal neurons were described elsewhere [13]. These protocols in conjunction with the knowledge of rodent brainstem anatomy gained from the adult guinea pig experiments can be applied to embryonic rats and mice to harvest, culture, and isolate embryonic bushy cells from the VCN.
5. Viscous damping of the bead displacement is negligible at low frequencies, becoming greater as the frequency increases. Limitations on high-frequency electromechanical force measurements, resulting from viscous damping, are similarly determined by applying the above stimulus and observing bead displacement above the noise floor. Calibration of the trap allows for the correction of the frequency-dependent decreases in magnitude and increase in phase lag.
6. Membrane viscosity measurements. Tethers also retracted rapidly when the trap was turned off, suggesting that these tethers have the same viscous properties as tethers pulled from lipid vesicles without cytoskeleton [14]. For each pulling speed, the tether force increases exponentially and approaches a specific steady-state value (F_{ss}) where a faster pulling rate increases the steady-state value.

Acknowledgements

This work was supported by NIH/NIDCD grants R01 DC000354 and DC002775. Dr. Brenda Farrell and Vivek Rajasekharan have generously provided help in building, learning, and mastering the optical tweezers system.

References

1. Ilin V, Malyshev A, Wolf F, Volgushev M (2013) Fast computations in cortical ensembles require rapid initiation of action potentials. *J Neurosci* 33(6):2281–2292
2. Yang S, Saif MT (2007) Force response and actin remodeling (agglomeration) in fibroblasts due to lateral indentation. *Acta Biomater* 3(1):77–87
3. Mosbacher J, Langer M, Horber JK, Sachs F (1998) Voltage-dependent membrane displacements measured by atomic force microscopy. *J Gen Physiol* 111(1):65–74
4. Hochmuth RM (2000) Micropipette aspiration of living cells. *J Biomech* 33(1):15–22
5. Oghalai JS, Patel AA, Nakagawa T, Brownell WE (1998) Fluorescence-imaged microdeformation of the outer hair cell lateral wall. *J Neurosci* 18(1):48–58
6. Sit PS, Spector AA, Lue AJ, Popel AS, Brownell WE (1997) Micropipette aspiration on the outer hair cell lateral wall. *Biophys J* 72(6):2812–2819
7. Block SM (1992) Making light work with optical tweezers. *Nature* 360(6403):493–495
8. Li Z, Anvari B, Takashima M, Brecht P, Torres JH, Brownell WE (2002) Membrane tether formation from outer hair cells with optical tweezers. *Biophys J* 82(3):1386–1395
9. Dai J, Sheetz MP (1995) Axon membrane flows from the growth cone to the cell body. *Cell* 83(5):693–701
10. Brownell WE, Bader CR, Bertrand D, de Ribaupierre Y (1985) Evoked mechanical responses of isolated cochlear outer hair cells. *Science* 227(4683):194–196
11. Brownell WE, Qian F, Anvari B (2010) Cell membrane tethers generate mechanical force in response to electrical stimulation. *Biophysical J* 99(3):845–852
12. Manis PB, Marx SO (1991) Outward currents in isolated ventral cochlear nucleus neurons. *J Neurosci* 11(9):2865–2880
13. Kaech S, Bunker G (2006) Culturing hippocampal neurons. *Nat Protoc* 1(5):2406–2415
14. Waugh RE, Bauserman RG (1995) Physical measurements of bilayer-skeletal separation forces. *Ann Biomed Eng* 23(3):308–321
15. Raucher D, Sheetz MP (2000) Cell spreading and lamellipodial extension rate is regulated by membrane tension. *J Cell Biol* 148(1):127–136

Chapter 21

An Overview of Nanoparticle Based Delivery for Treatment of Inner Ear Disorders

**Ilmari Pykkö, Jing Zou, Annelies Schrott-Fischer,
Rudolf Glueckert, and Paavo Kinnunen**

Abstract

Nanoparticles offer new possibilities for inner ear treatment as they can carry a variety of drugs, protein, and nucleic acids to inner ear. Nanoparticles are equipped with several functions such as targetability, immuno-transparency, biochemical stability, and ability to be visualized in vivo and in vitro. A group of novel peptides can be attached to the surface of nanoparticles that will enhance the cell entry, endosomal escape, and nuclear targeting. Eight different types of nanoparticles with different payload carrying strategies are available now. The transtympanic delivery of nanoparticles indicates that, depending on the type of nanoparticle, different migration pathways into the inner ear can be employed, and that optimal carriers can be designed according to the intended cargo. The use of nanoparticles as drug/gene carriers is especially attractive in conjunction with cochlear implantation or even as an inclusion in the implant as a drug/gene reservoir.

Key words Targeted drug delivery, Growth factor delivery, Gene therapy, Repair of inner ear

1 Introduction

The World Health Organization (WHO) has estimated that 278 million people worldwide suffer from moderate to profound hearing loss in both ears, therefore making hearing loss one of the most prevalent chronic conditions worldwide [1]. The EU has ranked hearing impairment in the seventh place on the disability list with more than 60 million citizens affected by hearing loss at an annual cost of 107 billion euros [2]. In Europe, presbycusis is the most common form of hearing impairment in persons over the age of 60, affecting every third person 65 years of age or older with prevalence increasing with age [3]. The burden for hard of hearing is considerable, in terms of physical, social, and mental well-being, educational development, and employment [4].

The inner ear comprises the vestibular apparatus for balance control and the coiled cochlea (Fig. 1a). Hair cells convey sound

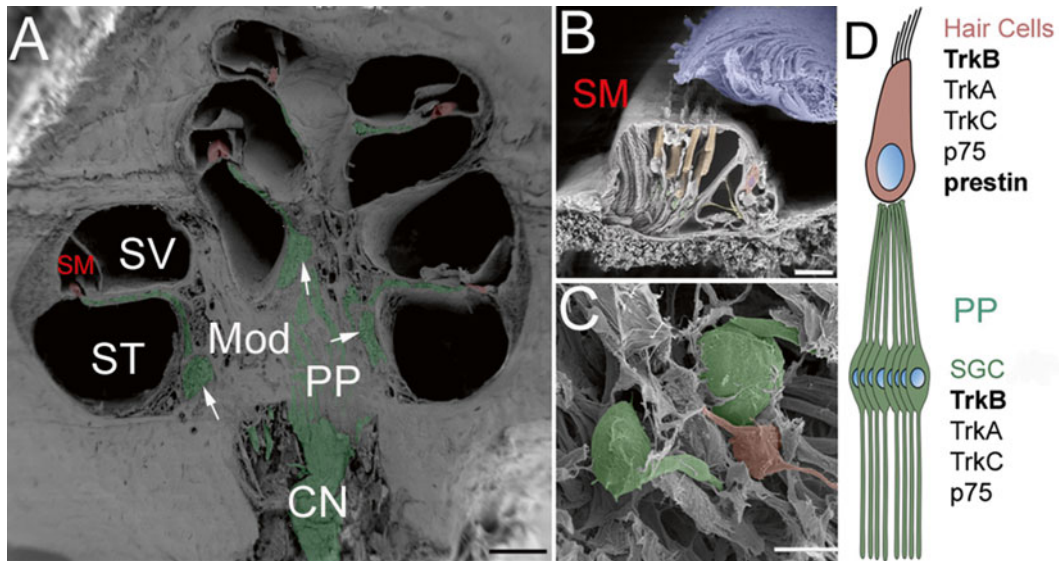


Fig. 1 Scanning electron micrographs showing anatomical structures of the human inner ear and targets for cell specific pharmaco-/gene therapy. **(a)** Three fluid-filled compartments characterize the mammalian hearing endorgan with nerve fibers and their cell bodies (green) and sensory epithelia (red). Sound enters the cochlea via the oval window and into the scala vestibuli (SV) that is confluent on the apical tip with the scala tympani (ST). Both contain perilymph, whereas the scala media (SM) contains endolymph. Primary processes (PP) of the cochlear nerve (CN). **(b)** The sensory epithelium consists of outer hair cells (orange), inner hair cells (red) with an overlying tectorial membrane (TM, blue) and an underlying basilar membrane (BM) that is bathed in the endolymph of the SM. **(c)** Electrical signals from hair cells travel via type 1 (green) and type 2 (red) primary neurons of the CN (shown in **a**) that traverses the spiral canal (arrows in **a**) of the modiolus (Mod) on its way to the central nervous system. **(d)** Target cells, including hair cells and spiral ganglion cells (SGC) and their selected molecular markers, for cell specific therapy in the inner ear. Scale bars = 1 mm (**a**), 50 µm (**b**), and 20 µm (**c**).

into electrical signals and wind up into 32–40 mm two and a half turns around the spindle shaped modiolus that contains spiral ganglion cells—the primary neurons. The sensory epithelium contains one row of inner hair cells and 3–4 rows of outer hair cells and rests on the basilar membrane (Fig. 1b) that vibrates when stimulated by sound in a tonotopic manner. High frequencies show maximum vibration in the basal part while low frequencies are mapped in apical regions. The motile outer hair cells actively tune the displacement of the basilar membrane and thereby amplify and sharpen the pitch discrimination. Loss of hair cells and retrograde degeneration of spiral ganglion cells (Fig. 1c) lead to irreversible hearing loss. Cochlear Implants can partly replace lost hair cells by direct electrical stimulation of the cochlear nerve. The cochlea is a relatively immuno-privileged enclave, fairly isolated from other organs and surrounded by a hard bony shell. The cochlear windows, the round window and oval window, are permeable to small

molecules and can be used as an access route to the inner ear [5]. The oval window was more efficient than round window in imaging of the membranous labyrinth in targeted delivery of contrast agents as gadolinium chelate [6, 7] and in visualization of inner ear diseases [8–10].

By using manganese-enhanced MRI even the central auditory pathway in living animals can be traced after either topical or systemic administration [11, 12]. The manganese-enhanced MRI has been used to follow neural activity in the brain, tinnitus-related brain regions, noise-induced activity increases in the brain, and central neuroplasticity (including hyperactivity) and neurodegenerative mechanisms associated with age-related hearing loss [13, 14]. In profound deafness, cochleostomy in connection with cochlear implant electrodes provides a route to the inner ear for prolonged delivery of therapeutic agents. The inner ear is, therefore, an attractive model organ for treatment as it contains circumscribed sensory elements that can be systematically analyzed such as neurons and vasculature. Currently, the most intensive activity in the quest for gene therapy is the search for vectors that can efficiently deliver growth factors and DNA to cellular targets [15–17]. Examples of these delivery systems are nanocarriers used for treating cancer [18], viral carriers for treating arterial occlusions [19], and viral vectors used in therapy for cardiovascular diseases [20]. However, as in the case of viral carriers, synthetic carriers also face the same problems for the inner ear treatment: limited access and poor uptake into the inner ear cells. The diffusion to the inner ear shows a gradient of expression, and the expression is often short-lived and toxic in repeated trials [21]. These and other results indicate that we have not been capable of introducing local (drug, peptide, or gene) therapies because of a shortage in technically advanced and safe carrier systems for humans.

It is a challenge and an opportunity for synthetic vectors such as targeted nanoparticles to be the future carriers for therapeutic agents. In the present review, we report on the current status of nanoparticle-based carrier systems designed for prevention, repair and regeneration of inner ear structures.

2 Use of Nanoparticles as a Treatment Vector

A nanoparticle is by definition a solid particle, often self-assembled systems with a particle size less than 100 nm (Fig. 2). For medical use, a nanoparticle matrix should be composed of materials approved by EMEA and FDA. For targeted delivery, specific ligands linked to the surface of nanoparticles will assist in cellular targeting. They should be designed to pass through cell membranes or tissue partitions by surface “functionalization” and to transport the cargo into the cells to either the cytoplasm or the

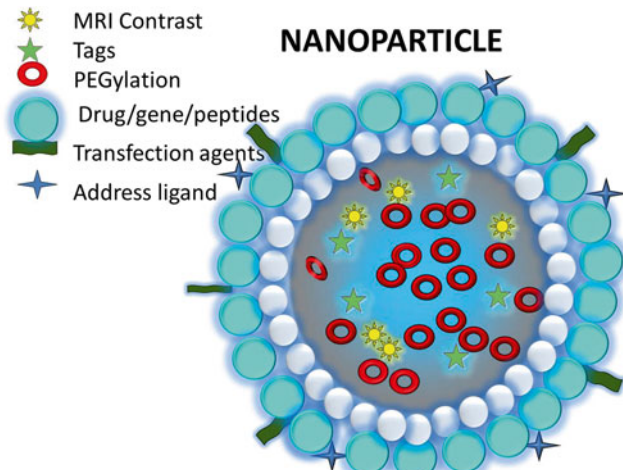


Fig. 2 Schematic construction of a nanoparticle based carrier system

nucleus. For experimental work in vitro and in vivo, signaling molecules are added on the nanoparticles. The use of paramagnetic ions, such as gadolinium chelate or superparamagnetic iron nanoparticles (SPION), assists the visualization of the flow of nanoparticles with magnetic resonance imaging in vivo. The manufacturing process is quite demanding, as it has to deliver sterile products. Organic solvents should be avoided, since nontoxic materials should be selected for use in humans. Nanoparticle sterilization should be avoided if possible because it is generally laborious and can induce problems by altering the surface structure or by denaturing the cargo. Before use, the NPs are sterilized by passing them through a $0.2\text{ }\mu\text{m}$ cellulose acetate syringe filter. The optimization of targeting and internalization of nanoparticles is important to minimize nonspecific distribution and uptake.

At present several different types of multifunctional nanoparticles for controlled drug/gene/peptide delivery have been produced, and they are available in the market; some of them are even in clinical trials (Fig. 3) [18, 22, 23]. The nanoparticles can incorporate a range of cargo molecules including drugs, proteins, genes, and small interfering RNA (siRNA). One of the key points is to ensure that the nanoparticles can be stored at room temperature for at least 21 days to facilitate logistics and testing. The particles should show minimal changes in their activity and no aggregation. The leakage of the drug out of the nanoparticles should be also minimal. Finally the characterization of nanoparticles is a demanding and often neglected task. Several measurements should be performed and to name a few, particle size analysis in the liquid phase by dynamic light scattering (DLS), flow field fractionation (FFF), and zeta potential measurements.

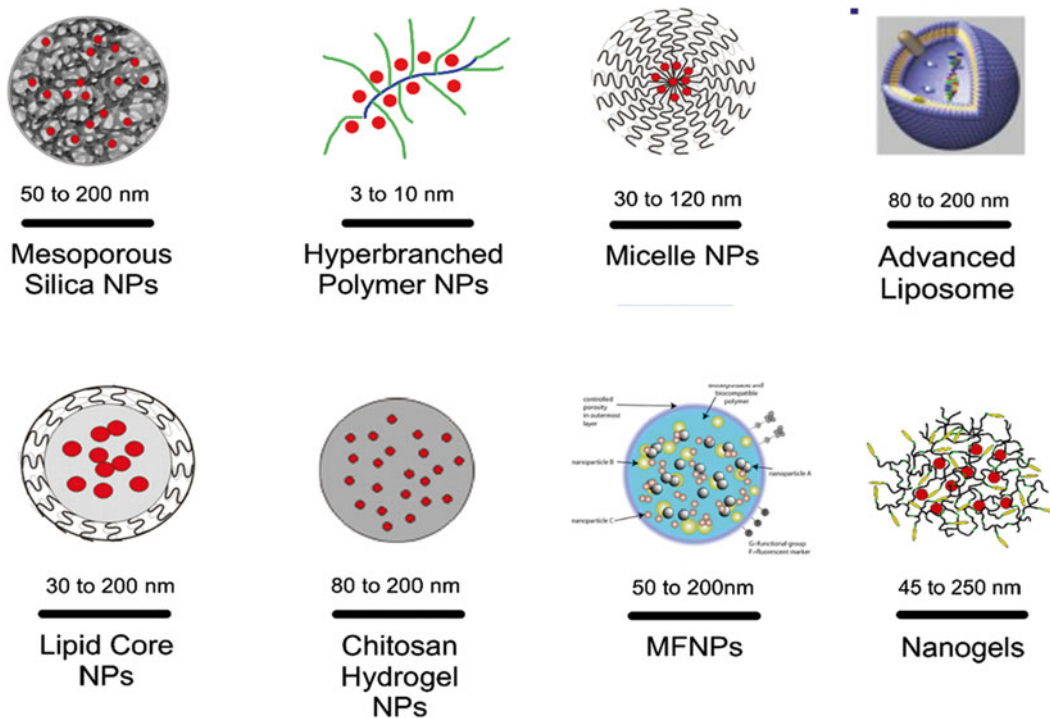


Fig. 3 Different types of nanoparticles and their size

Nanogels are a new group of nanoparticles. Polyethylenimide (PEI)-based nanogel nanoparticles can be placed on the round window membrane (RWM) to produce a delayed, targeted delivery of the cargo. High water content is a characteristic feature of nanogel, and nanoparticles are formed by specific chemical reactions that occur under physiological conditions. In situ gelling materials, based on pluronic copolymers containing different kinds of nanoparticles, are already in clinical trial [24]. The stability of the gels can be enhanced by partially cross-linking through star-shaped PEGs. SPION have been incorporated to form ferrogels that are responsive to magnetic fields [25].

3 Types of Nanoparticles

3.1 Advanced Liposomes/Lipoplexes

The liposomes/lipoplexes are the most commonly used nanoparticles and are made out of the same material as a cell membrane. They are used to deliver drugs and genes to combat cancer and other diseases. State-of-the-art lipoplexes are currently commercially available. First generation lipoplexes are readily available using commercial cationic lipids, such as Lipofectamine®. It is important that these lipoplexes are immediately used after mixing

of the plasmid and the commercial cationic lipid. The resulting lipoplexes are suitable for the transfection of cultivated cells; however, their composition often needs to be optimized for different cell types.

Recently, advanced liposomes/lipoplexes have been manufactured, which are stable, target specific, and have PEG coatings (Fig. 4). The general “work horse” can be tailored for individual needs, for instance they can be made to be hydrophilic, hydrophobic, anionic, or cationic. The physiochemical properties of the nanoparticle surface can be tailor-made to meet a variety of required conditions by coating it with PEG. Different ligands can be attached to their surface, making it possible to target different nerve cells at different sites in the body. Therapeutic agents, such as genes and signal molecules, can be incorporated or attached to them to create a controlled, trackable delivery and release system. Li et al. [26] reported the use of 60–70 nm size doxorubicin containing lipoplexes that were coated with DSP-PEG2000-COOH “the stealthy liposomes” and targeted to transferrin receptors. The targeted nanoparticles provided higher drug concentrations in the tumor tissue than nontargeted lipoplexes. Thus, for anticancer therapy where the tumor surface expresses an increased amount of transferrin receptors [27] and the arteries demonstrate vascular porosity, the targeted nanoparticle-based carrier system is sufficient

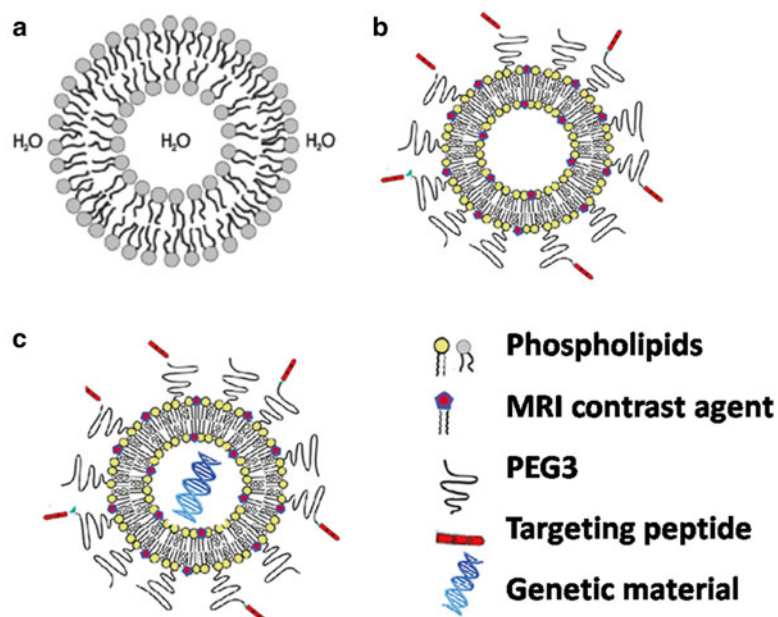


Fig. 4 Illustrations of advanced liposomes. (a) Cross section of a unilamellar liposome. (b) Schematic representation of targeted liposomes. (c) Schematic representation of targeted lipoplexes

for clinical treatment. However, the optimal coating of “the stealth liposomes” was not evaluated.

Liposome-mediated gene transfer is an attractive method because of its simplicity and low toxicity, and the method holds promise to be a major breakthrough for future therapies. The liposomes of today show only a modest transfection efficacy; however, several disease models have been successfully modulated by a liposome vector system. The main reason for modest transfection efficacy of liposomes was due to poor endosomal escape. To enhance the utility of these vectors it is necessary to improve target cell specific transfection to increase the level and duration of gene expression. A large international collaboration is necessary to protect genes against DNases, to target specific cells, to promote the cellular uptake, and to find a nuclear pore complex. A DNA-carrier system must have solid diameters less than 40 nm to allow transportation of the cargo through nuclear pore complexes into the nucleoplasm [28]. Sometimes the DNA or plasmid is too large to fit into the nanoparticle, and in these cases the DNA can be “packed” with hyperbranched polylysine nanoparticles. Lipoplexes form the stealth coat that brings the second particle into the cell cytoplasm from which the cargo is released to be taken up into the nucleus. In applications of gene delivery to the inner ear, lipoplexes have to pass the middle–inner ear barriers (round window and oval window) after intratympanic administration. We have observed obvious uptake of liposomes with the size of 240 nm in rat inner ear post-transtympanic injection [29].

3.2 Lipidic Nanocapsules

In recent years, a new generation of biomimetic delivery systems has been developed, lipidic nanocapsules (LNCs), whose structure resembles that of lipoproteins. Using biopolymer coating the liposome makes them more stable, and, after entering the cell, the biopolymer layer can be degraded and the released lipoplexes can target the cell nucleus. These LNCs are biocompatible and biodegradable and the ease and speed of their preparation give them an edge over other comparable drug delivery systems. Their formulation lies on a rapid and irreversible destabilization of a bicontinuous network obtained after successive phase inversions (thermal effect) of an appropriate emulsified system. This approach allows the elaboration of nanometric structures in the form of nanocapsules (a lipid core surrounded by a rigid surfactant shell). The mean LNC size can be adjusted very precisely in a range of 10–200 nm and the monodispersity of the size is remarkably narrow [30–32]. LNCs with a mean size of 50 nm passage through the middle–inner ear barriers *in vivo* [33].

To enhance the utility of an LNC as a vector, further improvements are possible, such as modifying their coating, increasing their packing capacity, enhancing transfection efficacy, and improving their target cell specificity. LNC-mediated gene transfer is an

attractive method, because of its simplicity, low toxicity, and potential to provide a major breakthrough for future therapy [34]. Their stability after dispersion in biological media is also an important criterion. Evidence shows that lecithin, located in the inner part of the shell, is an important parameter to formulating stable LNCs [35].

LNCs are suitable for the encapsulation and release of different kinds of hydrophilic drugs. In this case, it is necessary to formulate a lipophilic complex (lipoplexes or reverse micelle). This complex is introduced inside the LNC core. For reverse micelles, preliminary in vitro results with doxorubicin (a small hydrophilic anticancer drug) show an encapsulation rate of about 90 % and sustained release over several days. This technique can be adapted for the incorporation of small peptides as well as various compact proteins or oligonucleotides.

3.3 Chitosan Nanoparticles

Chitosan is a linear polymer consisting of randomly distributed D-glucosamine and N-acetyl-D-glucosamine. This natural polysaccharide is obtained by alkaline deacetylation of chitin, which is found in the shells of crustaceans like crabs and shrimp [36]. In the deacetylation process, acetamido groups of chitin are replaced by amino groups (Fig. 5), and the degree of deacetylation defines the quantity of amino groups in chitosan [37]. Compared to the other nonviral vectors, chitosan is considered as a safer alternative for gene delivery. Cationic lipids and cationic polymers, such as polyethylenimine (PEI) and poly(L-lysine) (PLL), have demonstrated toxicity, thereby limiting their applicability [36, 38, 39].

Chitosan–DNA nanoparticles are prepared using a complex coacervation technique. In acidic pH, amino groups of chitosan are protonated and interact efficiently with negatively charged phosphate groups of DNA. To enhance the phase separation, sodium sulfate can be used as a dissolving agent. Electrostatic interactions result in the formation of nanoparticles immediately after mixing these two oppositely charged polyelectrolytes at the applicable pH and temperature [40].

Parameters used in nanoparticle synthesis, such as concentrations of chitosan and plasmid DNA, molecular weight of chitosan,

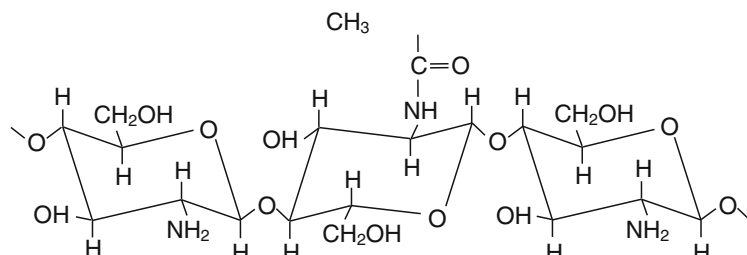


Fig. 5 Chemical structure of chitosan nanoparticles

degree of deacetylation, nitrogen to phosphate (N/P) ratio, and pH, affect the size, zeta potential, and stability of nanoparticles [40, 41]. Evidence shows that the zeta potential of nanoparticles has a strong influence on cellular uptake. The release of DNA from nanoparticles after cellular uptake is dependent on the properties of the chitosan. Transfection efficiency can be enhanced by optimizing parameters such as serum concentration [42]. Furthermore, modification of nanoparticle surface, by conjugating targeting ligands onto the surface after nanoparticle synthesis, enables targetability and more efficient transfection [40, 43, 44]. Transfection efficiency of the chitosan–DNA nanoparticles is cell-type dependent [39, 40]. Transfection is more efficient compared to naked DNA, but it has been shown that the transfection efficiency is lower compared to commercial Lipofectamine® [45]. Efficiency of low molecular weight chitosan has been reported to be equivalent to PEI, which is one of the most efficient nonviral vectors [46].

3.4 Amorphous Silica

Mesoporous silica nanoparticles (MSNs), with typical particle diameters of 50–200 nm, a narrow particle size distribution, and pore dimensions of 3–4 nm, have attracted a great deal of interest for use as imaging agents and delivery systems for biologically active components both in vitro and in vivo. MSNs exhibit several attractive features, including particle size control, relatively straightforward functionalization using well-established routes, biocompatibility, and degradability under physiological conditions. The high specific pore volume and surface area of MSN (typical values range from 0.6–1 cm³/g to 700–1000 m²/g, respectively) make it possible to reach drug loadings exceeding 30 wt% and allow tuning of the drug loading to that of the particle concentration to minimize particle induced toxicity. The particles can be produced to exhibit multifunctional properties, simultaneously carrying, for example, fluorescent dyes and/or MRI active functions for imaging [47–52], and/or ligands for targeting specific cells [53–59]. This makes functionalized MSNs very interesting for a wide range of biomedical applications, including cellular tracking both in vitro [41, 60] and in vivo [48, 52], and delivery of different drugs, genes, proteins, as demonstrated under in vitro conditions [61–68]. However, the efficacy is unknown of MSNs transportation across the middle–inner ear barriers.

3.5 Polymersomes

Amphiphilic block copolymers can self-assemble into polymersome nanoparticles in an aqueous environment. Polymersomes are vesicular, nano-sized spheres that encapsulate an aqueous solution. The synthetic amphiphilic block copolymers from which they are formed consist of hydrophilic and hydrophobic units joined together. Preparation is by slow addition of a block-copolymer solution in a water miscible organic solvent to water. Upon addition, the polymer chains self-assemble, the hydrophobic units of

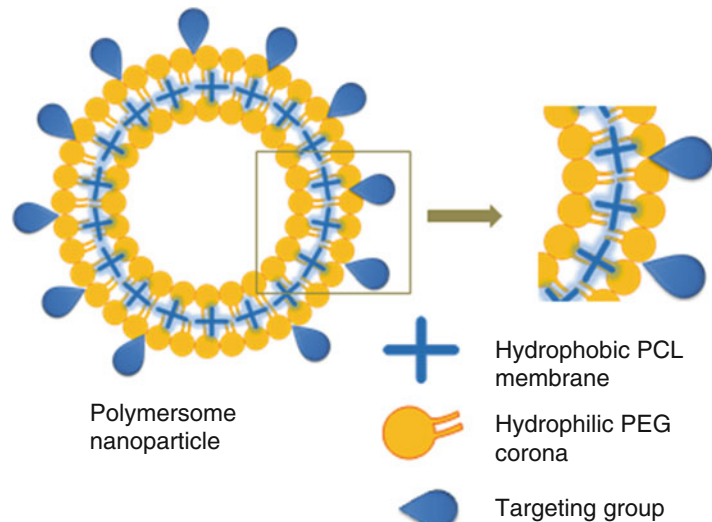


Fig. 6 PEG-*b*-PCL block copolymers self-assemble to form polymersome structures. The PCL units of the polymer form a hydrophobic core membrane, whereas the PEG units form a hydrophilic corona and line the interior cavity of the polymersome. The surface can be functionalized with targeting moieties

the polymer form a spherical membrane with an aqueous core. Then the hydrophilic chains form the surrounding corona as well as line the interior aqueous cavity of the polymersome (Fig. 6). The diameter of the core is several times smaller than the hydrodynamic radius [69].

Small molecular weight hydrophobic molecules can be incorporated into the membrane [70] and hydrophilic molecules encapsulated within the aqueous core [71]. The polymersome can be surface-functionalized to promote cellular uptake [72] or target specific cell types [73–75]. One of the block copolymers that can be used to form polymersomes is poly(ϵ -caprolactone)-*b*-poly(ethylene glycol) [69] (PEG-*b*-PCL). PCL, which forms the hydrophobic core, is an FDA-approved, biodegradable polyester polymer and is currently used in medical applications including suture material. PEG, which comprises the hydrophilic corona of the polymersome, is noted for its biocompatibility and resistance to both protein adsorption and cell adhesion [76], resulting in prolongation of circulation times of the polymersome within the body.

Polymersomes have the potential for a specific cell targeting to SGNs in cochlear organotypic explant cultures, when functionalized with short peptide sequences derived from NGF [77]. Moreover, when attached to polymersomes the peptide is capable of activating the tyrosine kinase B (TrkB) receptor [77]. Polymersomes

labeled with Tet1 [78], a short peptide sequence that binds to the GT1b ganglioside receptor, are capable of targeting the auditory nerve *in vivo* [74]. Surovtseva et al. [64] used a novel prestin binding peptide identified by phage display to target polymersomes to hair cells in cochlear explant cultures. By using polymersomes loaded with disulfiram, a drug that induces cell death, polymersomes are capable of delivering a drug payload to the inner ear *in vivo*, whereas unloaded polymersomes do not cause toxicity or hearing loss [79].

3.6 Hyperbranched Poly-L-Lysine

Hyperbranched poly-L-lysine is synthesized by the thermal polymerization of L-lysine*HCl. The reaction is performed at 150 °C in the presence of an alkaline metal base (MOH) to neutralize the amine hydrochloride and to create the corresponding free amino acid base [80]. In contrast to dendrimers, which are structurally perfect and monodisperse, hyperbranched polymers contain defects and are polydisperse. The characteristic parameters that describe the structure of hyperbranched polymers are the degree of branching [81] and the average number of branches (ANB) (Fig. 7). The ANB describes the average number of branches deviating from the linear direction per non-terminal unit [82]. Determination of degree and number of branching requires knowledge of the fraction of dendritic, terminal and linear units in the hyperbranched polymer. In addition to dendritic and terminal units, L-lysine can be incorporated in two isomeric linear forms, which are linked either via the α -amine group (α -linear, L α) or via the ϵ -amine group (ϵ -linear, L ϵ). The assignment of each of the α -CH signals allowed

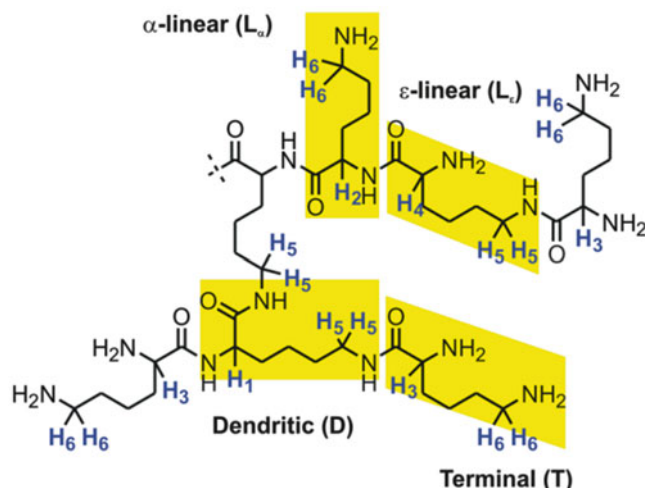


Fig. 7 Structural characterization of hyperbranched poly-L-lysine. The figure delineates also dendritic (D), terminal (T), and linear (L) units in the hyperbranched polymer that are used to characterize the hyperbranched poly-L-lysine

estimation of the relative fractions of the different structural units. Hyperbranched poly-L-lysine successfully passed the middle–inner ear barriers *in vivo* and expressed Math1 *in vitro* [83].

3.7 PLLA-mPEG and PLGA Polymeric Nanoparticles

Polymeric nanoparticles have been used in the last few years as delivery systems for a variety of therapeutic compounds, including small hydrophobic drugs, hydrophilic substances and biomolecules, such as peptides and proteins [84]. In our work, we mainly focus on two biocompatible polymer systems: poly-lactide-co-glycolide (PLGA) and a diblock copolymer consisting of poly-L-lactide and polyethylene glycol (PLLA-mPEG) (Fig. 8). In manufacturing the nanoparticles, high purity copolymer PLLA-mPEG is synthesized via ring-opening polymerization using PEG, L,L-lactide, and stannous 2-ethylhexanoate in anhydrous toluene [85]. After polymerization, the product is precipitated and washed a few times to remove unreacted chemicals. The strategy for the preparation of PLLA-mPEG and PLGA nanoparticles is based on an emulsion/evaporation technique that allows not only to form nanoparticles with a narrow size distribution, but also to accurately tailor their average hydrodynamic size. An oil-in-water (O/W) nano-emulsion is obtained after exposing the reaction mixture containing the polymer in the oil phase and a surfactant in the aqueous phase to ultrasound three times for 1 min each. Organic solvent removal is then obtained by evaporation, resulting in the formation of nanoparticles of PLLA-PEG block copolymer or PLGA.

To load drugs and therapeutic agents in the polymer nanoparticles, novel processing methods are used based on the use of nanoemulsion techniques. This approach is very versatile and can be easily modified to incorporate different types of drugs, mainly

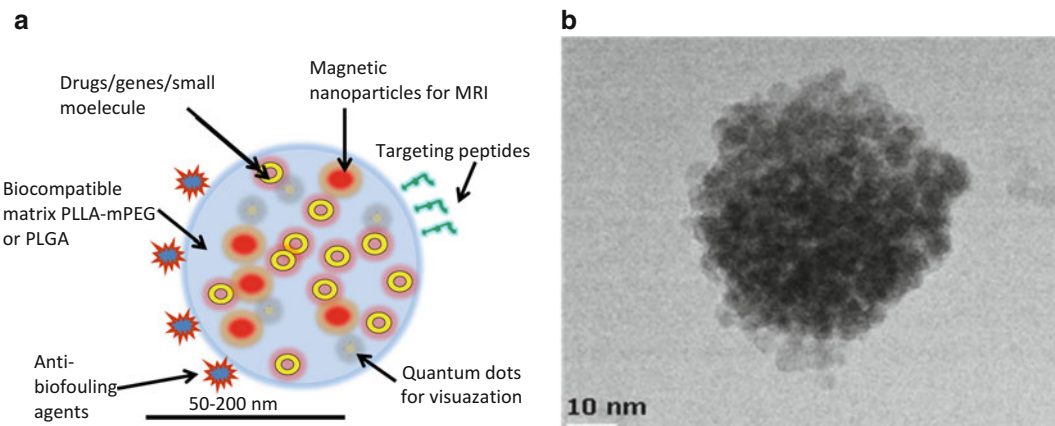


Fig. 8 Morphology of PLLA-mPEG and PLGA polymeric nanoparticles. **(a)** Schematic view of PLLA-mPEG or PLGA based multifunctional nanoparticles. **(b)** TEM image of multifunctional nanoparticles containing superparamagnetic iron oxide nanoparticles for MRI, quantum dots for fluorescent visualization, and a hydrophobic drug (not visible) embedded in a PLLA-mPEG matrix (not visible)

hydrophobic ones, at a sufficient loading capacity as well as visualization agents, such as SPION and/or fluorescent quantum dots. An additional layer, made of a suitable amphiphilic copolymer, can be added on the polymeric nanoparticles for loading hydrophilic compounds with different constituents. This layer acts as a diffusion barrier for the prevention of undesired drug release, but can cause increased complexity in the controlled release of drugs. Presently, the extent of penetration through middle-inner ear barriers is unknown for PLLA-PEG block copolymer or PLGA nanoparticles.

3.8 Nanogels

Hydrogel nanoparticles, so-called nanogels, are three dimensionally cross-linked hydrophilic polymer networks with finite dimensions in the sub-micrometer range (Fig. 9). They combine characteristics of hydrogels such as high water content, diffusion processes into and through the network, as well as tunable chemical and mechanical properties with the features of colloids such as high surface area. Traditionally, microgels and nanogels are prepared by free radical precipitation polymerization [86–88]. An alternative concept for the preparation of nanogels is based on cross-linking of well-defined macromolecular building blocks, either by direct interaction between

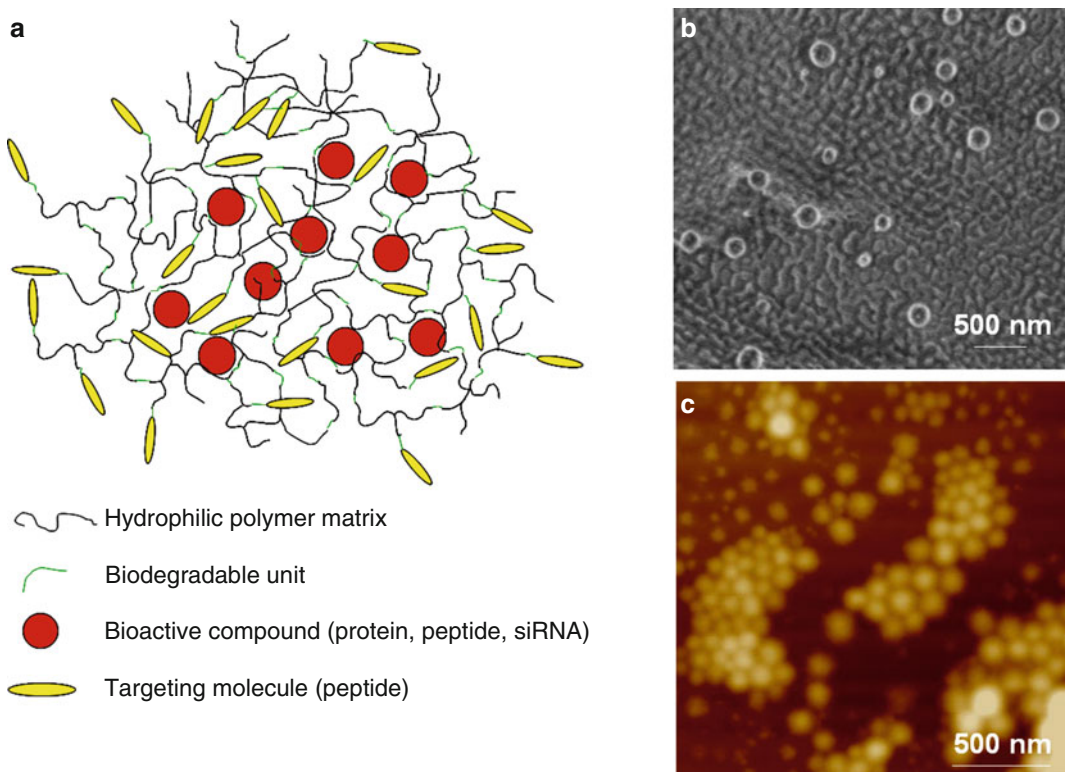


Fig. 9 The morphology of biodegradable nanogel. (a) Schematic representation of the biodegradable nanogel with the encapsulated drug. (b) Cryo-SEM and (c) AFM images of the disulfide cross-linked nanogels

the (pre-)polymers or by the use of low-molecular weight cross-linkers [89]. Such a pre-polymer condensation concept allows the use of building blocks with predefined tailored properties and the choice of cross-linking chemistries that tolerate functional groups that interfere with radical polymerization. Furthermore, cross-linking can be performed under application-relevant conditions such as physiological temperature, ion-strength and pH value. For these reasons, nanogels prepared by this method are particularly suitable for biomedical applications such as targeted delivery of low molecular weight drugs, siRNA, proteins, peptides, or plasmids into cells. Especially intriguing are the degradable nanogels prepared by oxidation of thiol functional prepolymers [90]. They allow the incorporation of peptides and proteins in particles that are stable in extracellular physiological conditions, but degrade after uptake by cells within the reductive environment of the cytosol, where, for example, glutathione cleaves disulfides to thiols.

4 Importance of Nanoparticle Surface Properties

The purpose of nanoparticle surface engineering is to obtain drug carriers with long circulation times in the bloodstream by minimizing the adsorption of opsonins, as well as ensuring cell-specific targeting through surface decoration with the appropriate ligands. A common strategy therefore is nanoparticle coating with poly (ethylene glycol) (PEG) chains, so-called pegylation [91, 92]. PEG is a highly hydrophilic polymer that is nontoxic, non-immunogenic, and FDA approved for biomedical applications. The “stealth” properties of PEG coated nanoparticles arise from steric hindrance and repulsion effects against blood components [93]. As a result, PEG acts as a shield protecting the drug-loaded nanoparticle from aggregation, enzyme degradation, rapid renal clearance, and interaction with cell membrane proteins. In addition, pegylation increases drug stability [94]. Generally, pegylation can be obtained either by nanoparticle formation in the presence of the PEG bearing copolymers, or by surface modification through physical or chemical polymer coupling onto the surface. The free terminus of the PEG chain can be used for the attachment of biological signals, thus enabling tissue specific targeting. Opsonization strongly depends on PEG molecular weights as well as PEG chain density at the surface of the particles [95]. In contrast to flat substrates, where the end groups of the PEG polymer brush are all located in close vicinity to the liquid interface, end group localization is significantly different for nanoparticles with diameters less than 100 nm. The PEG end groups and thus also the attached targeting ligands possess significantly more spatial freedom and are distributed throughout the polymer brush, which may affect accessibility of the ligands and thus targeting efficiency.

5 Targeting

Nanoparticle based targeted drug delivery may offer increased efficacy and reduced drug-associated side effects [73]. Usually nanoparticles are conjugated with ligands to bind with high selectivity to molecules that are uniquely expressed on the cell surface. However, in most cases the nanoparticle adsorption and internalization take place nonselectively, irrespective of the nanoparticle surface composition. To maximize internalization, specificity and transfection efficiency, it is beneficial that nanoparticles bind only to the target cells but not to the non-targeted cells. Cell uptake by endocytosis is, therefore, a critical factor in the targeted drug/gene delivery process. At present, in order to gain entry to the targeted cells, nanoparticles may use caveolae, clathrin, and integrin endocytotic pathways in addition to nonspecific, macropinocytosis to traverse the middle ear to the inner ear. The optimal nanoparticle size for cargo capacity and for cellular trafficking seems to be around 80 nm, but for nuclear entry nanoparticle size poses challenges for successful gene delivery.

Selectivity might be achieved by using targeting ligands. Several possible targets exist in the inner ear, which in many instances contain cell membrane with unique proteins. One is a transmembrane protein called prestin, a motor protein located in the cell membrane of outer hair cells. The construction of targeting ligand can be performed on the basis of a phage display technique that yields specific peptide constructs that bind to the epitopes on the cell surface. The binding properties of the targeting motifs are commonly evaluated in a fluorescent resonance energy transfer (FRET) technique on an organotypic culture of cochlear cells. One cell line expressing prestin is the HEI-OCI immortalized hair cell line [73].

Vestibular hair cells and spiral ganglion nerve cells express TrkB receptors, which can be used for targeting [96, 97]. Phage displays have yielded several possible ligands specific to TrkB receptors, but many of these are poorly selective. We have retrieved two novel targeting peptides consisting of 12 or 18 amino acids for the TrkB receptor, which bind to TrkB on the same site as BDNF. Targeting efficacy and selectivity can be measured in organotypic cultures (Fig. 10) and in an SH-SH5Y cell line, which is an established model for controlled TrkB expression. The A371 peptide (derived from HNgf_EE peptide, a TrkB ligand)-conjugated nanoparticles revealed enrichment in nerve fibers, spiral ganglion cells, and hair cells *in vivo* [98]. Non-functionalized nanoparticles and nanoparticles with scrambled ligand sequences showed non-specific uptake throughout the different cell populations of the inner ear.

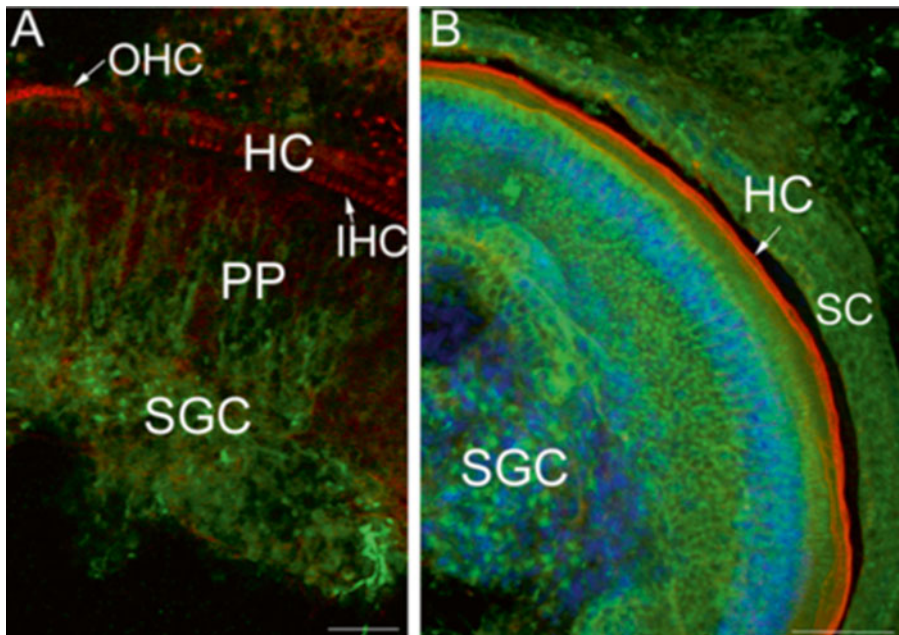


Fig. 10 Confocal microscopy of mice cochlear organotypic culture at 14 h post-incubation with polymersomes. (a) Enrichment of peptide A371 (TrkB ligand)-conjugated polymersomes (green) within the spiral ganglion cells (SGC) and their peripheral processes (PP) which contact the hair cell (red). (b) Scramble peptide-conjugated polymersomes (green) show nonspecific distribution in the cochlea. IHC inner hair cells, OHC outer hair cells, SC supporting cells

The inner ear contains both glucocorticoid and mineralocorticoid receptors, which provide substrates for the biological action of corticosteroids. Consequently, this steroid is used therapeutically in inner ear diseases, such as sudden onset sensorineural hearing loss and Meniere's disease. Bachmann et al. [99] demonstrated that, after transtympanic steroid application, the concentration in the scala tympani reached a peak of 1 mg/ml after 1 h, which is equal to 2 % of the steroid concentration of the solution applied to the round window. Thus, corticosteroids pass from the middle ear to the inner ear and produce a higher concentration in perilymph than through systemic administration [100, 101]. Recently, packing corticosteroids into nanoparticles has changed the delivery dynamics by allowing prolonged, high concentration delivery [102, 103]. Due to complexity of the targeting moieties, genes controlling the cell function, drugs used to prevent trauma, and possible gene therapy, there are several targets in the inner ear for vector design and targeting. Table 1, shows some efforts that are under progress or is considered important to be targeted to prevent or treat the hearing loss.

Table 1
Potentials and challenges for inner ear therapy

Cell type	Effect on cell physiology	Specific surface epitope	Regulator growth factor	Drug for trauma protection	Gene therapy	gene to be silenced
Outer hair cells	Survival	Prestin, TRPV4	GDNF, NT3	Dexa	GDNF,	Not decided yet
Inner hair cells	Survival, maintain stereocilia function	TRPV4	GDNF, NT3	Dexa	Myo7a, Otof	Not decided yet
Spiral ganglion neurons	Survival, induce sprouting	TrkB	BDNF, FGF, NT3	Dexa	BDNF	p75
Dormant precursor cells	Migrate, differentiate	SH3	BDNF, GDNF, FGF, NT3	Dexa	BDNF, GDNF	?
Supporting cells	Stimulate, migrate, differentiate	KHRI-1	GDNF	Dexa	Atoh1	Ids
Deiter cells	Keep functional	Kir4.1	?	Dexa	Atoh1	Ids
Marginal cells	Survival	TRPV4	?	Dexa		?
Spiral ligament cells	Induce gap junction expression	Not known	?	Dexa	Cx 26, Cx 30 heteromeric forms	?

Desired treatment effects on organs. *Dexa* dexamethasone, *TRPV4* transient receptor potential channel subfamily V member 4, *TrkB* tyrosine kinase growth factor receptor B, *BDNF* brain-derived nerve growth factor, *GDNF* glial-derived nerve growth factor, *FGF* fibroblast growth factor, *NT3* neurotrophin-3 growth factor, *Myo7a* myosin 7a protein coding gene, *Otof* otoferlin protein coding gene, *p75* low affinity nerve growth factor receptor p75, *SH3* src homology 3 domain regulatory protein, *Atoh1* Atonal homolog 1 (*Drosophila*) gene, *Cx26* connexin 26 coding gene, *Cx30* connexin 30 coding gene, *KHRI-1* murine monoclonal antibody against supporting cell, *ids* DNA binding protein inhibitor gene, *Kir-4.1* inwardly rectifying potassium channel

6 Transtympanic Delivery of Nanoparticles

Drugs can be applied transtympanically via the RWM or via a cochleostomy through microinjection; with injection from fluid-based delivery systems or from a reservoir in connection with cochlear implant electrodes. The cochleostomy pathway is suitable especially for patients with severe hearing impairment. The RWM delivery approach is a minimally traumatic method that can be applied to humans with minimal risks of permanent hearing loss.

Zou et al. [104, 105] studied the distribution of gadolinium chelate, following RWM application, and showed that loading of the perilymphatic space started within 10 min with a gradual filling

of the labyrinth that reached the apex of the cochlea. The cochlea completely cleared gadolinium chelate 7 h after the application of the agent [106]. Evaluation of RWM permeability in guinea pigs with constant infusion shows that permeability was dependent on the size of molecules, but with large individual variation [98]. Variation in RWM permeability to agents was defined by a factor of 34 for fluorescence and of 41 for dexamethasone-phosphate molecules [107]. Moreover, substances may also enter the perilymph through bony capsules from the middle ear, as shown when using tracers [108]. However, this study did not exclude the possibility that the tracers could penetrate the inner ear via the annular ligament of the oval window. PLGA nanoparticles, silica nanoparticles, and lipid core nanocapsules were distributed in the inner ear after intratympanic administration [33, 109, 110]. Here, the RWM was suspected as the main route for nanoparticle infiltration of the inner ear. Finally, to further demonstrate transport efficacy through the RWM, studies show that even large molecules such as insulin and proteins such as growth factors can pass the RWM. TGF- α passes through the RWM of guinea pig in an amount sufficient to stimulate hair cell regrowth with the potential to restore hearing [111].

So far, studies on RWM permeability have been limited to selective nanoparticles [33], such as SPION coated with PLGA (size 175 nm) or oleic acid coated SPION incorporated in PLGA (size 180 nm) [112]. SPIONs can be packed with drugs and magnetic forces applied, to transport the agents through the RWM into the inner ear. Magnetic forces supersede diffusion forces so that electric or magnetic forces can be applied to assist RWM permeation. Table 2 shows that most designed nanoparticles pass through the RWM and are detected within the cochlea.

One of the key elements in treating inner ear disorders with drug administration is to understand the mechanisms for nanoparticle trafficking through the RWM. The ultrafine structure of the RWM is still poorly understood, although there are some electron microscopy data for humans and animals [113]. In guinea pigs, the RWM is thinner but has the same basic components as in humans; epithelial layer, connective tissue layer and endothelial layer [114]. The epithelial layer, which has gap junctions between the cells, consists of two layers in animals whereas humans have more. The thickness of the RWM is about 70 μm in humans, 10–30 μm in guinea pigs, 15–20 μm in cats, 10–14 μm in chinchillas, and 12 μm in rats. The thickness of the RWM may also interfere with nanoparticle transportation through the barrier. The middle layer has collagen fibers that show 60 nm periodicity and the inner epithelial layer consists of 2–3 cell layers (Fig. 11). The ultrastructure of the RWM in humans, rats, and guinea pigs demonstrates many vesicles within the cells. Elements for clathrin and caveolae pathways are shown in the rat RWM, which indicates the potential involvement of these pathways in the transportation of nanoparticles through the RWM.

Table 2
Nanoparticles tested for round window membrane passage and distribution in cochlea

Nanoparticle	Animal (n = cochlear) and timing	Spiral ganglion	Organ of Corti	Lateral wall	Other structure
Liposomes LPX-12UH.IB Rhodamine	Mouse (n = 3) 1 and 3 days	+	+	+	
Polymersomes P1-NL-DL-77 USOU, Dil	Mouse (n = 3) 1 and 3 days	+	+/-	+	Glial cells labeled
Mesoporous silica nanoparticles ABO TRITC	Rat (n = 3) 1 h, 1 day, 3 days	+ Axons labeled	+	+	Good RW penetration
Hyperbranched poly-L-lysine EPFL Fluorescein	Mouse, rat (n = 6) 1 and 3 days	+ Nuclear entry	+	+/-	All membranes labeled Otic capsule labeled
PLGA KTH 9+10 mixture 109 + 498 nm	Mouse, rat (n = 5) 1 and 3 days	+	+	+ Labeled erythrocytes	Strongly labeled otic capsule
PLLA-mPEG KTH 11-13 165 + 150 + 200 nm	Mouse, rat (n = 4) 1 and 3 days	+ Axons labeled	+/-	-	Red (150 nm)— best penetration
Lipidic nanocapsules UA 5/50 Rhodamine	Mouse, rat (n = 4) 1 and 3 days	+	-	-	Basilar membrane labeled

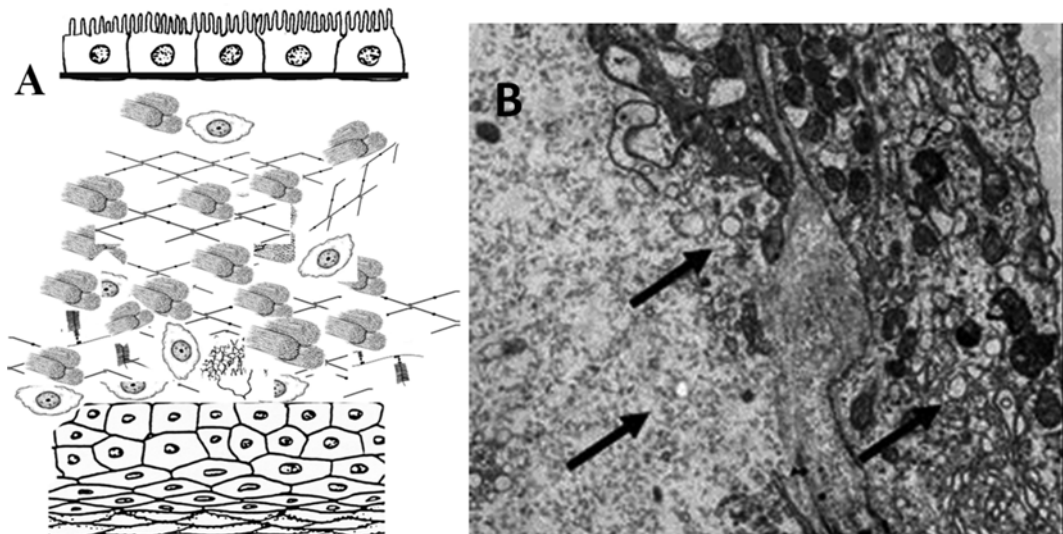


Fig. 11 Ultrastructure of guinea pig round window membrane (RWM). **(a)** Vesicular trafficking (arrows are visible in all layers of the RWM shown by transmission electron microscopy (TEM)). **(b)** Reconstruction of guinea pig TEM evaluation of RWM (Nykänen et al., unpublished results)

Agents that break down the tightness of the RWM tight junctions have been sought to assist nanoparticle passage through the RWM. One study showed that O-streptolysin formed large pores in the membrane with permeability increasing in a dose-dependent manner [115]. However, RWM permeability was highly variable and in some animal membranes there were no permeability changes. Recently, Zou et al. [5] demonstrated in rat that the application of agents on the RWM, using gelatinous sponge-based diffusion, was as effective as injection of the agent in the tympanic cavity. Thus, for small molecule drugs, even a short exposure time is satisfactory for RWM passage and trafficking into the perilymph.

In rats with intratympanic application of contrast agent, the scala vestibuli showed higher signal intensities than the scala tympani. The difference was maintained after 3 h of post-intratympanic administration [116]. In humans after 2 h, the application of contrast agent into the tympanic cavity passes the RWM and starts to load the perilymphatic space. After 12 h, the middle turn is filled and after 24 h the contrast agent reached the apex, indicating full loading in the cochlea. The distribution of gadolinium in the inner ear in MRI showed that the scala tympani and scala vestibuli were loaded at the same time. Furthermore, the vestibulum showed contrast before the cochlea. The authors indicated transligamental and transmodiolar spreading of the contrast agent within the cochlea [104, 106].

We have tested and evaluated the intracochlear localization of seven different types of nanoparticles applied on the RWM in mouse and rat (Table 2). All nanoparticle types were detected in the spiral ganglion cells, some nanoparticles such as silica-based nanoparticles were also found in axons. Much less nanoparticle distribution was found in the organ of Corti (mainly supporting cells) and the lateral wall [98]. Strong specific nanoparticle localization in the otic capsule (PLGA nanoparticles) or membranes (hyperbranched poly-L-lysine) was observed as well. All nanoparticle types were localized in the cytoplasm of the cells, while hyperbranched poly-L-lysines were detected in the nuclei of spiral ganglion neurons. No morphological alterations were detected after nanoparticle application. Also, no functional changes (no detectable threshold shift in the frequency range 1–40 kHz and no decrease in otoacoustic emission amplitudes) were observed within 15 days (mice) or on day 30 (rats) post-nanoparticle delivery.

7 Internalization of Nanoparticles

Even for small nanoparticles sizes of 7–15 nm, a simple nonendocytotic massive transport across cell membrane seems improbable [117]. A major drawback of current nanoparticle trafficking, when

compared with viruses, is their poor ability to enter the cytoplasm [118]. Internalization can be promoted by mechanisms that are known for viral infections. This approach is important if the purpose is to deliver the gene or shRNA constructs into to the target cells.

The idea behind attaching a peptide motif on the surface is that pegylated nanoparticles have neutral charge and their nonspecific internalization is limited on cell populations. Although most studies have reported the effect of surface functional ligands/motifs on nanoparticle cellular uptake, the impact of ligand arrangement is examined seldom on nanoparticle surfaces. It seems likely that the organization and density of surface motifs are important in internalization [92, 119].

The TAT (transactivator of transcription) peptide, which is present in HIV, enhances the cellular uptake of nanoparticles [120]. There is controversy concerning the pathway, and numerous possible internalization routes for TAT were proposed, such as lipid raft-mediated macropinocytosis, caveolae-mediated endocytosis, and clathrin-independent and -dependent endocytosis [117–120]. However, the uptake characteristics of the TAT peptide alone and of TAT-conjugated cargoes differ significantly [121–123]. Furthermore, the TAT-mediated internalization process may be dependent on the properties of the cargo molecule, TAT concentration, and cell line [121, 124, 125]. The incorporation of a biotinylated, pH-responsive polymer poly(propylacrylic acid) enhances the nuclear localization of TAT-conjugated vector [126]. Table 3 demonstrates the peptide sequences for TAT and TAT-hemagglutinin-2 peptides.

TAT-peptide was used in nanogel to enhance nuclear entry [127]. The NanoEar Research Consortium showed that TAT peptide on the surface of nanogels doubled the amount of uptake by the cells (Fig. 12), due to the presence of the positively charged amino acids, lysine and arginine [128]. In addition, the presence of TAT peptide on the nanoparticle appears to facilitate the release of the nanoparticle from the endosome, which might be improved by using a peptide that contains three TAT motifs and one HA-2 motif [128, 129].

Table 3
Peptide sequences for TAT and TAT-hemagglutinin 2 peptides and their random sequence used for comparison to improve cellular uptake and nuclear incorporation

Ran-C peptide	GARGEGINGC
TAT-C peptide	YGRKKRRQRRRC
HA2-C peptide	GLFEAIAGFIENGWEGMIDGC
TAT-HA2-C peptide	YGRKKRRQRRGLFEAIAGFIENGWEGMIDGC

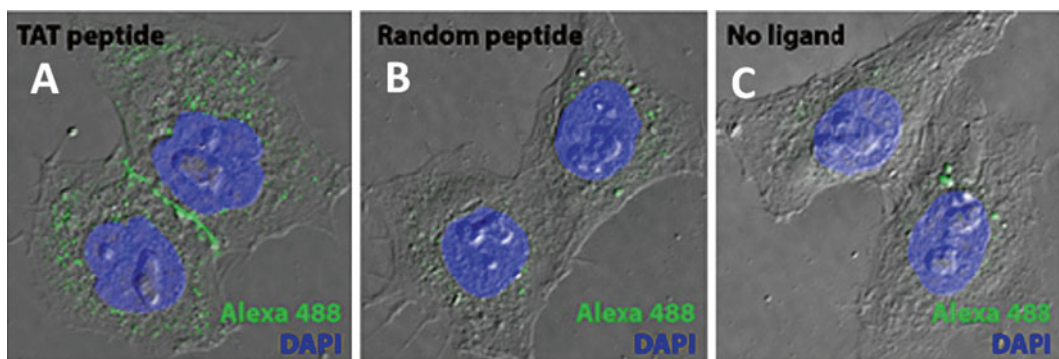


Fig. 12 Uptake of nanogel. **(a)** Uptake of nanogel in Alexa 488 labeled TAT-nanogel particles in cell culture, **(b)** ranC-nanogel particles, and **(c)** plain nanogel particles

The current understanding of cellular trafficking of nanoparticles is limited and more studies are needed on nanoparticle plasma membrane interactions and internalization of nanoparticles. These processes can be facilitated using viral proteins, such as the TAT-peptide, to enhance the internalization process. For testing nanoparticle trafficking in vitro, quantum dots can be used alone or incorporated into multifunctional nanoparticles. Colloidal semiconductor quantum dots are single crystals ranging in diameter sizes of 2–10 nm. Their size and shape can be precisely controlled during chemical synthesis, by choosing and tailoring the precursor's composition, reaction temperature, duration, and ligand molecules [130]. These nanocrystals can emit light at a specific wavelength, when excited by an external source, due to quantum confinement of the photoexcited electrons. The optical properties of the nanocrystal (i.e., color of the emitted light) can be tuned by changing the size of such nanostructures [131].

Intensive research has focused on the use of transferring mediated ligand internalization both in cancer cells and in passing the blood-brain barrier [53, 132, 133]. Transferrin-coated nanoparticles may enter the cell through a clathrin-mediated endocytosis pathway or a caveolae-mediated pathway [134]. Their entry and exocytosis seem to be dependent on nanoparticle sizes. An important finding was that the cell penetrating fusogenic biomolecules retain their properties upon conjugation with nanoparticles and may be effective importers of nanomaterial.

7.1 Endosomal Uptake and Lysosomal Escape of Nanoparticles

Several organelles in the cell have specific functions in sorting the substances entering the cell. The composition and identity of cell organelles are dictated by a flux of lipids and proteins they receive and lose through cytosolic exchange and membrane trafficking. The early endosomes are tubular and vesicular structures that receive direct input from the plasma membrane and are precursors of the mature endosomes [119]. These have a key role in sorting

material for recycling and degradation. The late endosomes receive cargo from early endosomes and deliver them to lysosomes where the cargo molecules are degraded. An alternative path from early endosomes is to recycling endosomes. The recycling endosomes are structures that are mainly composed of narrow-diameter tubules, which might be an intermediate station of a trans-Golgi network. Many proteins and hormones are trafficking as secretory granules in trans-Golgi networks [119]. The last cisternae in this network contain clathrin on their buds and are assumingly able to secrete the content to neighboring cells and facilitate a transcellular pathway as in the round window membrane [135].

The classic internalization process uses the endosome pathway predominantly, where a large fraction of therapeutic cargo is finally sequestered into lysosomes [136]. Lysosomal trafficking is routinely cited as a “critical barrier to non-viral gene therapy” [137]. Endo-lysosomal trafficking represents a classic consequence of clathrin-mediated endocytosis in that the nanoparticle is coated by the cell membrane envelope and guided to early endosomes, then to late endosomes, and finally sorted out in lysosomes [138]. The acidic milieu will lead to cargo degradation. Many receptor-mediated cellular trafficking vehicles use those pathways [139] as for example, transferrin [140] and growth factor receptor-mediated pathways [141].

The caveolae-mediated pathway may deliver cargo to the endoplasmatic reticulum and thus escape the lysosome system, although the caveolae-mediated pathway also often delivers the cargo to lysosomes [142]. A previous study used transferrin-coated PLGA nanoparticles of 63–90 nm, to study cellular trafficking using endothelial cells *in vitro* [133]. When blocking the caveolae pathway with indomethacin, internalization was reduced in half. These results indicate that a transferring receptor can mediate internalization through both clathrin and caveolae pathways. In a second study, polylysine nanoparticles were used, which condensed plasmid DNA into rods and ellipsoids with a minimum diameter less than 25 nm [143]. Particles were well internalized and localized in perinuclear regions. Moreover, larger particles of 43 nm were mainly found in lysosomes, when colocalizing using lysosome tracker with nanoparticles. The larger particles were internalized mainly through clathrin-coated pits. The smaller particles trafficked in the endoplasmatic reticulum but not in the Golgi complex, as demonstrated using a Golgi tracker. According to the authors, the smaller particles were probably internalized by a non-caveolae, nonclathrin, noncholesterol dependent pathway. However, these observations may not be universal for small particle sizes [92].

Improved internalization and endosomal escape can be achieved by modifying the surface of nanoparticles. Hatakeyama et al. [144] demonstrated that improved internalization occurred

by modifying the pegylating surface of lipoplexes with a peptide sensitive for cleavage by metallo-matrix protein. By adding 2 % acid sensitive fusogenic GALA peptide, siRNA delivery *in vivo* was improved sixfold. Lysosomal escape can be facilitated by using pegylated nanoparticles by diorthoester linkage, which is highly sensitive to acidic conditions and breaks lysosomal membranes [145]. Acid labile vinyl ester can also be applied for that purpose [146]. It is interesting to note that nanogels have a special characteristic of swelling up in an acidic environment and releasing the cargo from endosomes.

Another approach for nanoparticles to escape from endosomes and lysosomes is to use pH-labile bonds [147]. With this technique, an endosomolytic agent is linked to a nanoparticle shell allowing endosomal disruption and cytoplasmic release of the biologically active compound [148]. This concept was first realized by using a chemical modification of the cationic peptide mellitin [149]. Mayer et al. [150] used this formulation with covalently coupled PLL and noted luciferase gene expression increased 1800 X when compared with unmodified PLL. A similar approach used amphiphilic polycation (butyl methacrylate) with PEG via pH-sensitive acetal bonds [151]. Recently, conjugates between PEG and PEI have been developed [152]. One interesting approach is to incorporate a masked endosomolytic agent with siRNA delivery *in vivo* [148]. Here, siRNA is conjugated with osmolytic poly butyl and amino vinyl ether compounds via labile disulfide bonds, then the compounds are covered with new maleate derivatives that contain PEG. Injection of this 20 nm sized dynamic polyconjugate into a vein caused significant inhibition in the animal target organ [153]. Research in this field is rapidly increasing, but so far most of the success is derived by trial-and-error.

7.2 Nuclear Incorporation

Application of gene therapy to restore hearing loss focuses on three aims in the inner ear: (1) restoration or (2) preservation of hair cell populations, (3) transdifferentiation of supporting cells. Even though dysfunctional genes are identified in many cases of hearing loss, current clinical application of gene therapy is limited due to a lack of reliable tools for gene transfer. Two cellular processes have been identified as major barriers to DNA transfection using nanoparticles: insufficient migration of DNA through the cytoplasm and transportation across the nuclear pore complex (NPC). Once released from endosomes, DNA traverses through the cytoplasm to reach the nuclear envelope. However, diffusion of large (>500 kDa) molecules is highly restricted through the molecularly crowded and sterically obstructed environment of the cytoplasm [154]. The unique structural properties of DNA further attenuate its diffusion. The mobility of linear DNA in HeLa cell cytoplasm was impeded for fragments larger than 250 bp. The mobility of large fragments was greatly hindered, with little or no diffusion observed for fragments >2000 bp [155].

The NPC, perhaps the largest protein complex in the cell, is responsible for controlled exchange of components between the nucleus and cytoplasm and for preventing the transport of material not destined to cross the nuclear envelope. Even if a DNA vector reaches the nuclear envelope, it must be transported across the NPC to reach its destination. The NPC, which operates as a selective conduit for nucleocytoplasmic exchange in eukaryotes, supports two modes of transport. Particles smaller than 8–9 nm may enter by diffusion, while larger particles are ushered selectively by soluble receptors of the karyopherin/importin- β family, which recognize specific nuclear localization signal (NLS) peptides displayed by the cargo. This mode is used to transport objects smaller than 40 nm in diameter [28]. Given its large hydrodynamic radius and the lack of a NLS, DNA is transported very poorly through the NPC. Unless assisted, DNA transport through nuclear pores is limited to very short segments, on the order of approximately 100–500 bp [156]. Obstruction of these two important cellular processes therefore renders transfection efficiency by synthetic carrier unacceptably weak, particularly in the case of non-dividing cells and localized gene delivery.

The amount of nanoparticle bound plasmids and free plasmids in a cell line, when delivered with PEI, Poly-L-lysine (PLL), or lipoplexes, has been previously evaluated qualitatively, using RT-PCR methods [157]. The results indicated that the dynamics of cellular incorporation, plasmid release in the cytoplasm, and gene activation varied among carriers. The transgene expression (protein product) of the luciferase gene did not correlate with the free content of the plasmid DNA in the cytoplasm or the cellular incorporation efficiency of the nanocarriers. Transcription efficiency was 16 times greater and translation was 160 times more effective with virus delivery. They reported that PEI was approximately 10–100 times more efficient in gene transfection than PLL. The cellular uptake was dependent on the cell cycle phase and was about 70 times more effective in G1 compared to S phase. Tachibana et al. [158] compared cationic lipoplex and PEI in their relative transcription efficacy of plasmid DNA, and reported that no single event in delivery, such as intake into cells, amount of free cytoplasmic pDNA, or cell cycle uptake or expression could predict gene expression. Lipoplexes were about twice as effective in delivering plasmid to the nucleus as PEI vector, whereas the elimination rate of the plasmid in the nucleus was four times greater in PEI than in lipoplex. The transfection rate in lipoplex was estimated to be 7 times greater than for PEI. The pharmacokinetically determined average exposure of nucleus to plasmid was 17 times greater for lipoplex than for PEI. Overall lipoplex was 13 times more effective than PEI in gene delivery. Thus the transcriptional availability is determined by several factors that need further investigation. Another study compared intracellular trafficking and gene expression between adenovirus and a lipoplexes-based carrier system

[159]. Both delivery systems transferred DNA into the nucleus at comparable rates, but there was a substantial difference in transcription efficiency.

Extensive effort has been placed on enhancing nuclear import of DNA delivered by direct or indirect association with NLS moieties. This effort has been challenging because the size and chemical properties of DNA dramatically attenuate its transport in the cell cytoplasm and through the NPC. The resulting poor nuclear transfer and, consequently, biological activity is further exacerbated by the fact that, in most cases, the DNA remains epi-chromosomal, necessitating repeated administrations. At the basic science level, the trafficking of DNA inside cells and across the nuclear envelope is not completely understood, and the interaction between cellular components and biological material is poorly characterized, as are the effects produced by the latter on living systems. A further hindrance in the development of successful gene therapy is the detrimental response of the immune system. Understanding the sequence of inflammatory responses, which occur after delivery, may enable us to identify the points at which immune modulation may dramatically improve the efficacy of gene therapy. Nuclear plasmid delivery induced by nanoparticle carriers may be an option for improving transgene expression especially in non-dividing or growth-arrested cells [160–162]. Hyperbranched poly-lysine nanoparticles (HPNPs) are internalized into the nucleus of different cell types, including rat cochlear cells in vitro and in vivo [74, 83] (Fig. 13). This demonstrates the potential for HPNPs as carriers to deliver genes to the cochlear cell nucleus.

7.3 Use of DNA Transposons to Enhance Incorporation of Genetic Materials into Native Chromosomes

It would be useful if genes could be integrated with chromosomes that are naturally present in cells, allowing the inserted gene to continuously produce protein for therapeutic purposes. Incorporating the gene into the target cell genome is a technique made possible by retroviral and lentiviral gene therapies [163]. These systems appear less exclusive with the use of DNA transposons, which are capable of economically incorporating modified genes into the target cell genome, exclusive of size [164]. Many different types of transposon systems for mammalian gene transfer are available, including *hAT*-like *Tol2*, the only naturally active vertebrate transposon isolated from the Japanese medaka fish genome, a *Tcl*-like transposon known as *Sleeping Beauty* (*SB*), and the *PiggyBac* (*PB*) isolated from the cabbage looper moth *Trichoplusia ni* [165, 166]. Using the *SB* transposon, a gene trap procedure was used with the mouse germ line for the rapid generation and analysis of mutant mice [167]. *SB* was assembled by combining fragments of silent and defective *Tc1/mariner* elements from salmonid fish and this reconstructed *SB* showed high transposition efficiencies in vertebrate cells [168].

Fraser et al. discovered *PB* in the *Trichoplusia ni* cell line, TN-368, a repetitive element that was isolated by Cary et al. [169],

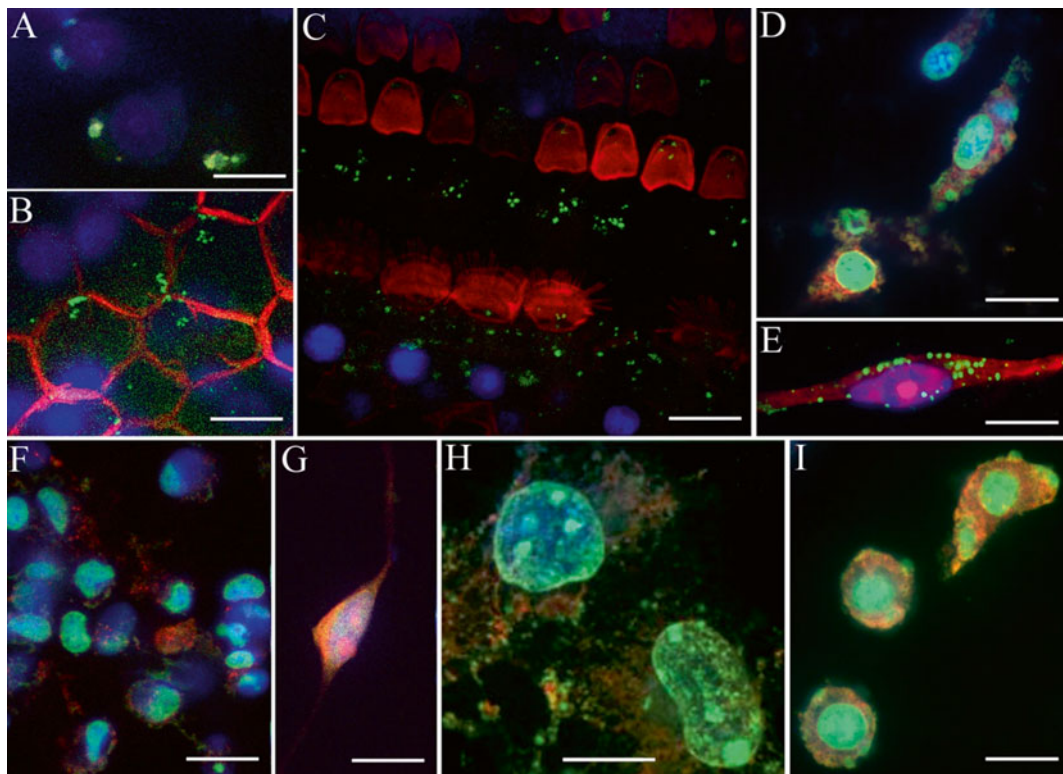


Fig. 13 Internalization of hyperbranched polylysine nanoparticles in different cell types. **(a–c)** Internalization of hyperbranched polylysine nanoparticles in adult rat cochlea, **(a)** Spiral ganglion cell, **(b)** Stria vascularis, **(c)** Organ of Corti. *Green* = nanoparticles, *red* = F-actin, *blue* = Nuclei; **(d–g)** Internalization of hyperbranched polylysine nanoparticles in cochlear primary cell culture, *green* = nanoparticles, *red* = Nucleolin, *blue* = Nuclei; **(h)** Internalization of hyperbranched polylysine nanoparticles in COS cells; **(i)** Internalization of hyperbranched polylysine nanoparticles in PC12 cells, *green* = nanoparticles, *red* = Nucleolin, *blue* = nuclei. Note: Nucleolin staining was used for the mechanism study of HPNPs nuclear import. Reports suggest that nucleolin is the cell surface target of DNA nanoparticles and that nucleolin is essential for the internalization and/or transport of the DNA nanoparticle from the cell surface into the nucleus. With permission of Int J Nanomedicine [74]

[170]. Later it was found to transpose efficiently in many different species [112, 172]. One advantage of the *PB* over *SB* transposon is that it does not leave a footprint, as it is precisely excised when a transposition takes place, whereas *SB* TA-dinucleotide gets duplicated upon transposition [173, 174]. *PB* is very efficient for germ line mutagenesis in mice and has significantly higher transposition activity in mammalian cell lines than *SB* and *Tol2* [175, 176]. *Tol2* is a naturally occurring hAT superfamily fish transposon that also shows activity in a wide range of vertebrate species, including human cells [177]. One of the advantages of this transposon system is that it can transfer genes of up to 11 kb with minimal loss of transposition activity compared to *SB*. *Tol2*, however, has lower

transposition activity compared to both *SB* and *PB*. *PB* carries larger cargo of up to 14 kb of foreign genes in the mouse germ line; however, recently, the *PB* system has been modified to deliver up to 18 kb inserts in hES cells [175, 178].

Until now site specific integration is not feasible but several attempts have been pursued. For instance, a recent study showed that a chimeric *PiggyBac* transposase, with GAL4DBD attached to its N-terminus, resulted in targeting a specific site upstream of the UAS (GAL4-binding) site in a plasmid assay system in *Aedes aegypti* embryos [179]. However, this kind of transposase modification seems feasible for *PB* rather than *SB* or *Tol2*, since the latter two seem to tolerate less N-terminal modifications [180]. The potential genotoxicity of *PB* will depend on the frequency of integration into genes and the expression level of the cargo. However, genotoxicity decreases by adapting insulator elements [181, 182].

One of the difficulties in using transposons is that they are mutagens that can cause mutations in several ways. If a transposon inserts itself into a functional gene, it will probably damage it. Insertion into exons, introns, and even into DNA flanking the genes (which may contain promoters and enhancers) can destroy or alter a gene's activity. Faulty repair of the gap left at the old site (in cut and paste transposition) can lead to mutations at that site. Although many modifications and further studies are needed in this field, the Recombinant DNA Advisory Committee, in 2008, approved the first human gene therapy clinical trial that used transposons [183]. If this trial succeeds, this approach could be the advent for clinical trials using transposons.

8 Gene Therapy and Therapeutic Agents

In order to pack and deliver genes noninvasively into the inner ear, several important criteria have to be met: RWM penetration of the vector and cargo [21], uniform diffusion and distribution of the vector in the treated area [184], and safety with respect to insertional mutagenesis and low toxicity. In these aspects, synthetic polycationic carriers offer the potential to confer the overall positive charge to the desired nucleic acid and thus enhance its trans-cellular transport [21]. Although the PEI complex is internalized in the respective cell type and expression of the reporter protein is achieved, two major drawbacks appear when comparing lipoplex to PEI-based cochlear delivery [185]. First, lower transfection efficiency is attained in the cochlea apical turns, and, second, hair cell loss occurs that is associated with scala media inoculation. These factors may limit the future potential use of PEI for clinical applications. As for viral gene vectors, despite their penetration through the round window membrane [186], the quantity is too low to be effective in gene therapy [187].

8.1 Math1

Cell fate decisions, coordinated cell division, pattern formation, and differentiation [188] are controlled hierarchically. Normally, after the last round of cell division, precursor cells of the inner ear sensory epithelium exit the cell cycle and differentiate. Cyclin kinase inhibitor p27kip1 in supporting cells and retinoblastoma protein pRb in hair cells are required to prevent cellular mosaics of sensory hair cells and non-sensory supporting cells. Supporting cell division is a highly regulated developmental event involving their reentry into the cell cycle [189, 190]. In mice that are mutant for p27, hair cell precursors continue to proliferate, even in the postnatal and adult organ of Corti to result in an extra row of hair cells [191, 192]. Age-dependent changes in supporting cell proliferative capacity are due in part to changes in the ability to down-regulate the cyclin-dependent kinase inhibitor p27^{Kip1} [193]. Inhibition of p27kip1, expression of Math1(Atoh1), and targeting to supporting cells, offers a chance to regenerate hair cells in the mammalian cochlea. Recently overexpression of Math1 (Atoh 1) in guinea pig cochlea forced supporting cells to differentiate into functioning hair cells [15].

The morphological formation of an organism is the result of an integrated network of differentiation programs and signaling pathways that control cell cycle exit. The timely ordered expression of tissue-specific genes is executed by transcription factors of the basic helix-loop-helix (bHLH) family. Following binding to Id proteins, bHLH cannot contact DNA, and the result is a loss of transcriptional activity and inhibition of differentiation [194]. Thus, Id proteins are natural inhibitors of Math1 protein-mediated transcription in cochlear hair cell regeneration. Our group has recently applied shRNA in vitro to silence Id1, Id2, and Id3 gene expression for regulating cochlear hair cell regeneration. Additional experiments in vivo should be carried out to confirm the results in vitro.

8.2 Nerve Growth Factors, BDNF

The deafferented peripheral processes of the auditory nerve will degenerate, following the loss of hair cells in the inner ear. In time, spiral ganglion cells (SGCs) and their central projections also die. Death appears due to apoptosis from loss of survival factors (largely neurotrophins) provided by the normal inner ear. Data from animal and human studies now unanimously support the view that different neurotrophin (BDNF, GDNF, NT-3) treatments extend the survival and excitability of the remaining auditory nerves following deafness, as occurs in the optic nerve and CNS [195, 196]. Brain-derived neurotrophic factor (BDNF) has been extensively investigated in both animals and humans. Early administration of neurotrophins in vivo can protect the SGCs from degeneration following deafness. We among others have demonstrated that BDNF is essential for the survival and regeneration of SGCs in humans and other animals. These findings support studies

conducted by others in the peripheral nervous system, which demonstrate that immediate administration of various neurotrophic factors *in vivo* reduce neuronal death after injury and deafferentation [197]. Even after prolonged SGC loss that represents years in a human life, BDNF reportedly restores cochlear nerve function, probably by inducing outgrowth of peripheral processes [198]. Another explanation is that BDNF is transforming precursor auditory nerve cells to functioning nerve cells [199].

We have recently demonstrated that BDNF activates precursor nerve cells and transforms them to SGCs in cultured human and animal cells [200, 201]. This observation provides an opportunity to highly impact deafened patients despite the lapse of several years since the onset of deafness. To design gene constructs coding full-length BDNF, a pair of specific nucleotide primers was synthesized (BLAST NM_012513.3): GTproBDNF forward, 5'-GTG ATG ACC ATC CTT TT-3' and GTproBDNF reverse 5'-CTA TCT TCC CCT TTT AAT G-3'. The PCR fragment was cloned to vector pcDNA6.2/C-EmGFP-DEST (Invitrogen) to produce full-length BDNF with a GFP tag.

Production of recombinant growth factors is a demanding task. A baculovirus system of protein expression has many advantages. The recombinant protein does not require folding and the protein is glycosylated, which is not possible if BDNF is produced using a bacterial system for protein expression. To produce and characterize recombinant rat BDNF from insect cells, we use a gene plasmid for baculovirus expression of BDNF. Isolation of recombinant protein is accomplished by chelating chromatography on Ni-agarose resin. In our hands, this system initially produces a proBDNF form, which is then transformed to mature BDNF in SF9 insect cells.

An understanding of the receptors that bind neurotrophins is essential to treatment. SGCs express the neurotrophin receptors, tropomyosin-related kinase (Trk) receptor tyrosine kinase and p75 neurotrophin receptor (NTR), a member of the tumor necrosis factor receptor superfamily [202]. Nanoparticles targeted to trkB receptors have been designed for drug delivery [203, 204]. The p75NTR binds all neurotrophins and also interacts with Trk receptors to modulate ligand binding specificity, affinity, and functionality within certain cell types [205]. Neurotrophin stimulation of differentiating neurons, over time, transforms the initially trophic character of p75 signaling into negative growth control and apoptosis. Thus, long-term BDNF treatment for SGC degeneration has negative effects, since p75NTF may induce apoptosis. Downregulation of p75NTF expression with peptide is essential in promoting neural axonal regeneration in CNS [206]. Short hairpin RNA (shRNA)-mediated transient silencing of p75NTR mRNA might also be helpful in promoting SGC regeneration with BDNF.

Finally, in the nervous system, Id2 interacts with core subunits in primary neurons through a destruction box motif (D box) [194]. Mutants of Id2 D-box enhance axonal growth in cerebellar granule neurons in vitro and in the context of the cerebellar cortex [207], and overcome myelin inhibitory signals for growth. Presently, we are attempting to deliver D-box mutated Id2 gene (mDB_Id2) using a nano-carrier.

8.3 RNA Interference

The development, cell fate, patterning, and innervation of both the sensory and nonsensory regions of the inner ear are governed by tight regulation involving, among others, transcription factors and microRNAs (miRNAs). In humans, mutations in specific miRNA genes are associated with hearing loss. MiRNAs and their pathways have been demonstrated recently [208]. One of the most exciting findings in recent years has been the discovery of RNA interference (RNAi). RNAi enables sequence-specific gene silencing through targeted degradation of mRNA by cognate double-stranded RNA (dsRNA). The dsRNA binds to the nuclease complex to form an RNA-induced Silencing Complex (RISC) and, with Agronuate 2 enzyme, “splices” in a sequence specific manner the complementary messenger RNA. Therefore, it offers a strategy to silence disease-causing genes *in vivo* [209–211]. However, if a dsRNA longer than 30 base pairs is used, an interferon pathway is activated and all the protein production of the cell is downregulated. Recent advances in synthetizing siRNAs of 21–22 nucleotides evades the interferon response and makes the therapy possible in humans [212]. RNAi can be elicited transiently in mammalian cells by transfection with siRNAs or plasmids expressing small hairpin RNAs (shRNAs). The shRNA-mediated transient silencing of p75NTR neurotrophin receptor mRNA can be used as mentioned before, to enhance the efficacy of BDNF and thereby promote SGC growth.

Delivery of siRNA has been problematic because siRNA is anionic and has difficulties in passing through the plasmalemma. However, using a TAT-based transfection agent and shielding the siRNA with a charge-neutralizing peptide carrier results in more effective gene silencing than using a Lipofectamine-based transporter system [129]. Lipofectamine had adverse effects in this study, such as undesired gene upregulation and possible immunogenicity with inflammation, while the peptide-based carrier showed no adverse effects either in gene upregulation or in the expression of immunogenic markers. However, experiments *in vivo* were limited to mucosal exposure only.

Mutations of the GJB2 gene result in a nonfunctional connexin 26 protein and hearing loss [213]. This autosomal dominant disorder is controlled by silencing the gene with siRNAs [214]. Recently, the protective effect of anti-apoptotic Bcl-2 proteins,

against gentamycin caused ototoxicity, has been shown following intratympanic delivery of viral vector containing a Bcl-2 nucleotide sequence [215]. We are also interested in delivering shRNA to improve the function of *Atoh 1* transcription and allow supporting cells to divide and differentiate into functioning outer hair cells.

In order to restore inner ear function, different nanoparticles with different characteristics can carry varying types of cargos. Lipid nanocapsules (LNC), mesoporous silica, and polymersomes are all suitable for carrying payloads of small molecular weight hydrophobic compounds. The hyperbranched polymers and chitosan nanoparticles are effective delivery vehicles for DNA/RNA. Lipoplexes are capable of carrying both DNA and hydrophobic/hydrophilic drugs. Some nanoparticles, such as mesoporous silica, can be formulated with 2–13 nm pores that can incorporate hydrophilic or hydrophobic drugs and can have a signaling agent (gadolinium chelate) covalently bound to their surface. Nanogels can be designed to degrade in the cytosol after endocytosis and can carry hydrophilic payloads such as peptides and DNA/RNA. They can be covalently endowed with tracers for visualization both in vitro (fluorescence dyes) and in vivo (gadolinium chelate). All of the nanoparticles are capable of having short peptide sequences attached to their surface for cellular targeting and internalization. Table 4 shows character and payload carrying properties of different nanoparticles.

Table 4
Summary of nanoparticle characteristics

Nanoparticle	Site of contrast agent	Hydrophilic drug	Hydrophobic drug	Peptides/BDNF	DNA/RNA	Optimal size
PLGA	Inside/outside	Yes		Yes	Yes	?
Silica	Outside and/or inside	If covalently attached	Yes	Small on surface	Small on surface	30–100 nm (non-porous), 100 nm porous
LNC	Inside	Yes	Yes	Yes	Yes	50 nm
Lipoplexes	Inside/outside	Yes	Yes	Yes	Yes	80 nm
Hyperbranched polymers	At the exterior	Yes	No	Yes	Yes (optimal cargo)	<50 nm
Chitosan	Inside/outside	Yes	Yes	Yes	Yes	70 nm
Polymersome	Inside	No	Yes	Yes	No	50 nm
Nanogel	Inside/outside		Yes	Yes	Yes	100 nm

9 Visualization of Nanoparticles with MRI

9.1 Gadolinium Chelate

Technically, it should be possible to detect the distribution of nanoparticles within the inner ear *in vivo* with MRI, if the nanoparticles contain paramagnetic agents such as gadolinium chelate (Fig. 14). Gadolinium chelate can be detected in the millimolar range, a concentration that is nontoxic for the inner ear [216]. The disadvantage of using gadolinium chelate is that the amount must be relatively high for visualization, and, therefore, a significant part of the nanoparticle carrier capacity is reserved for this agent. When compared to, for example, SPION the detectable amount of gadolinium chelate must be about 100–500 times greater than SPION. Imaging *in vivo* can demonstrate biocompatibility, membrane penetration, and targetability of multifunctional nanoparticles within the cochlea (Fig. 15). Therefore, imaging has benchmarking value in validating different types of nanoparticles.

Gadolinium chelate can be conjugated to the surface of different types of nanoparticles. In proper testing, targetability and visualization should be first tested *in vitro* on a phantom template in MRI, or by using, for example, S5-SH5Y cells, if TrkB receptor targeting is evaluated *in vitro*. Thereafter, MRI should be

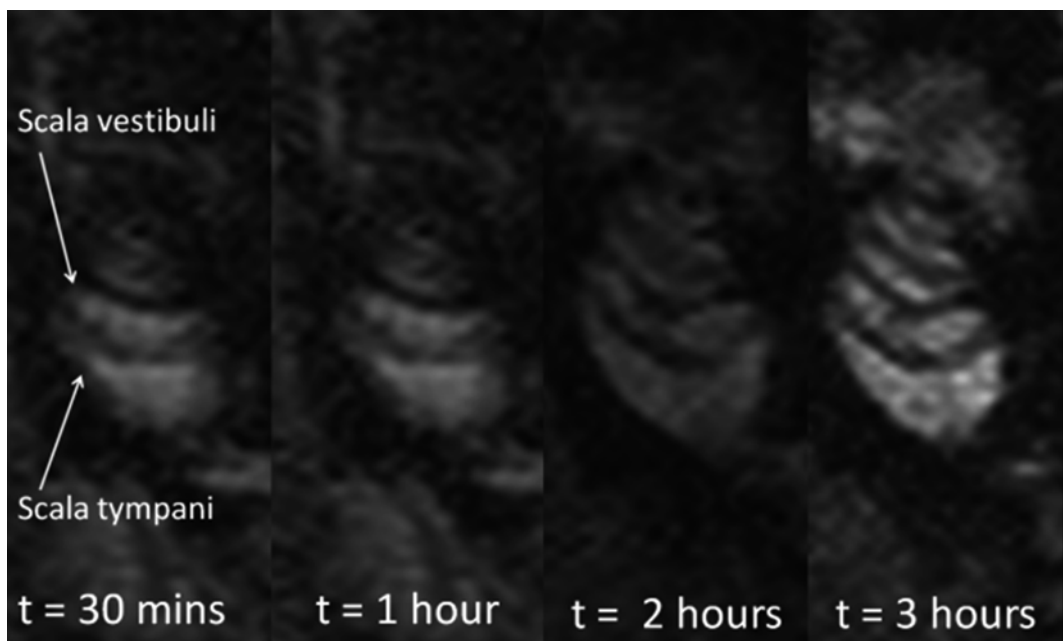


Fig. 14 2D RARE T1 MR images of left cochlea, showing dynamic uptake of Gd-DOTA post-intratympanic administration in rat. 40 μ L of Gd-DOTA was injected in the left middle ear cavity via tympanic membrane penetration and imaged after 30 min through 3 h. Enhancement of both scala tympani and scala vestibuli begin from the basal turn of the cochlea and progress over time to fill the entire cochlea to maximal brightness by 3 h

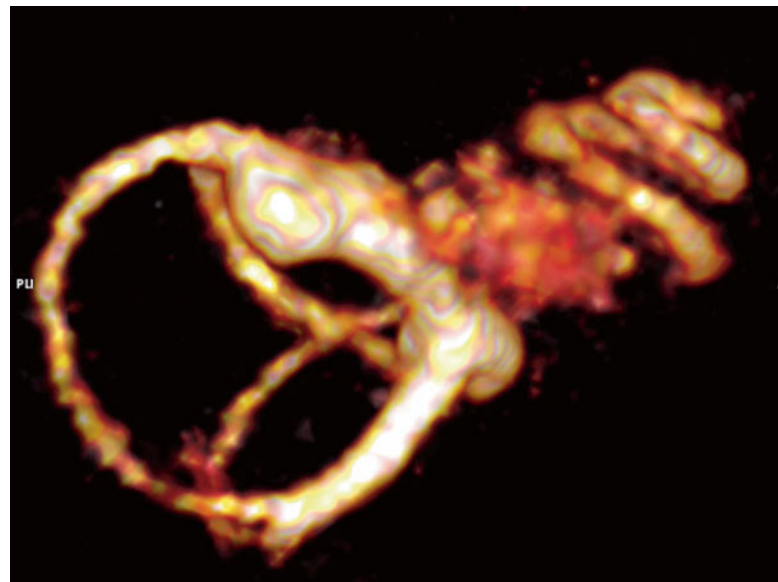


Fig. 15 2D RARE T2 MR image 180 min after left intracochlear catheter injection of 5 μL of POA@SPION. The right non-treated cochlea shows normal fluid bright T2-weighted signal. The left cochlea shows normal bright signal only in the scala media compartment containing endolymph. The perilymph is darkened by the T2 attenuating effect of the SPIONs within the perilymph space (scala tympani and scala vestibuli). Modified from Ref. [222]

performed *in vivo*, using T1-weighted sequences (Fig. 14). Targetability was evaluated previously by comparing the dynamics of nanoparticles in the perilymphatic compartments and spiral ganglion region [5, 105, 116].

SPION have been recently developed and used in biomedical applications, especially as a biocompatible contrast agent for MRI, due to their particular magnetic properties [217]. Usually, SPION composed of iron oxide cores and a polymeric shell are used as a T2-contrast agent [218]. The term “superparamagnetic” refers to the fact that, in very small nanoparticles, the magnetic moment is not locked along a specific crystallographic direction, but is free to move inside the material. Small nanoparticles below a critical size are magnetic only when applying an external magnetic field. For magnetite the critical size at room temperature is about 15–17 nm [219]. The magnetic “core” typically consists of nanocrystalline iron oxide; magnetite (Fe_3O_4) or maghemite ($\text{g-Fe}_2\text{O}_3$), [220]. Biocompatible polymers, peptides, antibodies, small organic ligands, and proteins are the main compounds used to coat and functionalize the SPION, to protect the magnetic nanocrystals, and to stabilize the nanoparticle suspension [221]. Recently, environmentally sensitive materials (mainly polymers) have been used

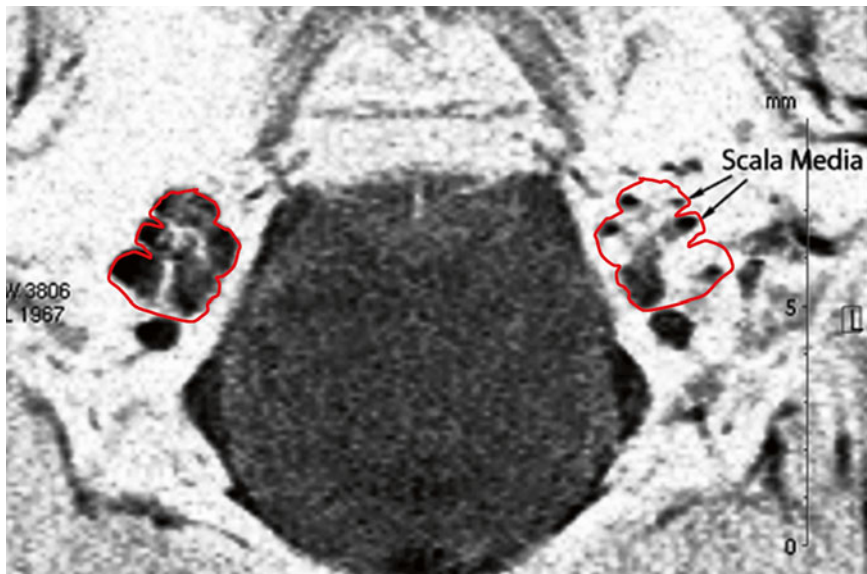


Fig. 16 3D volume reconstruction from a 3D T2 MR image 100 min after left intracochlear catheter injection of 5 μL of POA@SPION. The SPION signal will “kill” the water signal of perilymph and only endolymphatic space is visualized. The scala media of cochlea and endolymphatic space of vestibulum and semicircular canals are visualized. Modified from Ref. [260]

to coat and functionalize SPION and increase the sensitivity and specificity of such materials for MRI imaging [217, 222]. We have used Pluronic® coated SPION, which are functionalized by using an amphiphilic copolymer that interacts with the oleic acid molecules on the surface of the iron oxide. These SPION show excellent contrast properties for T2 weight imaging in MRI, due to their particular surface structure [218]. Applications *in vivo* of such nanoparticles demonstrate the feasibility of using this material for MRI visualization of inner ear structures (Fig. 16).

Recently, SPION have been developed as a gene delivery technology called Magnetofection [223, 224]. Magnetofection is based on magnetic nanoparticles coated with cationic molecules, such as polymers or lipids that can, upon applying an appropriate magnetic field gradient, transfer all types of nucleic acids and vectors into cells. This method exploits a magnetic gradient field to concentrate and confine the nucleic acids at the target cells or tissues within a few minutes [225, 226]. This technology also allows magnetic targeting *in vitro* and *in vivo*. The time course of magnetic nanoparticle intracellular distribution reveals that most are localized in the cytosol, demonstrating the need to develop a new technology with efficient nuclear uptake.

10 Toxicity

Nanoparticles, which are intended to deliver a pharmaceutical to the inner ear, must themselves be biologically inert or nontoxic to the surrounding cells and tissues. In order to test nanoparticle toxicity *in vitro*, established protocols are in place for cytotoxicity testing. However, final proof of toxicity is made only by testing *in vivo*, to determine immune responses, liver accumulation, and kidney excretion [227].

For standardized testing *in vitro*, we recommend using Balb/c 3T3 mouse fibroblast cells that are incubated for 48 h with the nanoparticle in question trying to use as high a concentration as possible. Thereafter, we test the cytotoxicity of the nanoparticle in serial dilutions. The comparison between *in vitro* tests and *in vivo* tests showed that in some nanoparticles the difference in toxicity can be even 100–1000 less *in vivo* than *in vitro* [228]. Toxicity was found in hyperbranched polylysine and silica (SiO_2) particles. The observed cytotoxicity of high amounts of nanoparticles is most likely due to nanoparticle overload, which was observed previously [231] and in our laboratory, with polycationic particles. Cytotoxicity was no longer observed with lowered nanoparticle concentration. All nanoparticles tested ended up inside cells and most were taken up by endocytosis. Particles were trapped in endosomes and had to escape in order to deliver their payload. Therefore, a tendency is to include in the nanoparticles surface endosomolytic peptides for enhancing gene delivery in nanoparticles [147]. However, it is also important to note that the dispersion medium can have a profound influence on the toxicity of the nanoparticles. For example, in our experience we did not observe any toxicity for silica nanoparticles dispersed in HEPES buffer even at high concentrations, while solvent-induced toxicity was observed for silica nanoparticles dispersed in DMSO.

For tests *in vivo*, the main objective is to assess kidney clearance of selective nanoparticles and to determine possible immune responses. Preliminary observations indicate that there is little excretion in the urine, following intravenous administration of positively charged hyperbranched polylysine nanoparticle. This result raises the possibility of retention at the renal glomerular microvasculature, where filtration is expected of nanoparticles, when coupled with the observation that the reticuloendothelial system is efficient in scavenging nanoparticles. The filtration barrier at this site is negatively charged due to the presence of glycosaminoglycans and sialic acid. Silver nanoparticles displayed strong activities in antibacterial, antiviral, and antifungal studies and was reportedly efficient in treating otitis media [232] and the distribution of silver nanoparticles in the middle and inner ear can be seen in micro CT [233]. The silver nanoparticles are toxic [228] and

may cause hearing loss and interferes with the kidney filtration by causing permeability changes in basement membrane and leading to its dysfunction. The silver nanoparticles were translocated in kidney tissue and deposited on the kidney's basilar membrane in glomerulus impairing urine filtration [227]. As a result albuminuria followed that was measured in vivo with SDS-Page [227]. The mechanism seems to be that the nanoparticles interfere with the upregulation of hyaluronic acid that is a key component in basement membrane [227]. Therefore, retention of positively charged nanoparticles is quite likely. Furthermore, neutralization of the naturally present negative charges, by the positively charged nanoparticles, may increase the permeability of the filtration barrier to proteins, resulting in proteinuria. This outcome may prove to be an adverse effect of nanoparticle-based drug or gene delivery strategies. Therefore, awareness of this effect is important in the context of nanoparticle-based delivery [234, 235].

Administration of nanomaterials via various routes, including biodistribution (the movement of materials through tissues), phagocytosis, opsonization, and endocytosis, is likely to cause cell/organ toxicity [236]. So far, our understanding of nanoparticle-induced toxicity is incomplete, and nanoparticle biodistribution to specific sites can occur, depending on their particular characteristics. Their small size facilitates uptake into cells and transcytosis across epithelium and endothelium into blood and lymph circulation, reaching potentially sensitive target sites such as bone marrow, lymph nodes, spleen, and heart. Access to the central nervous system and ganglia has also been observed via translocation along axons and dendrites of neurons. Endocytosis is largely dependent on nanoparticle surface chemistry (coating) and surface modifications. Their greater surface area per mass, compared with larger-sized particles of the same chemistry, renders them more biologically active.

As mentioned above, excretion of nanoparticles could occur via filtration by the kidneys. The endothelial layer, the basement membrane and the epithelial layer of glomerular capillaries constitute the filtration barrier. This barrier permits free passage of small diameter molecules such as water (0.2 nm), urea (0.32 nm), sodium (0.4 nm), chloride (0.35 nm), and glucose (0.7 nm), but does not permit free passage of larger particles such as erythrocytes (8000 nm) or large plasma proteins. Small plasma proteins such as albumin (3.6×15 nm) are not freely filtered but do get through this barrier in small amounts. Thus, the glomerular capillary filtration barrier behaves as if it were a filtering membrane containing aqueous "pores" with a diameter of 7.5–10 nm. These pores are not specialized membrane proteins; rather, they are aqueous channels between cells and within the basement membrane of the barrier.

In a recent toxicological study on hyperbranched poly-L-lysine nanoparticles *in vivo*, small and heavy positively charged nanoparticles were 100 % lethal in mice within 1 h, following an intravenous injection of 1200 µg. Thirty percent of animals that received 400 µg died within 4 h of injection. Smaller doses of 0.4 and 4.0 µg/animal were tolerated well (Lianos, personal observation).

The insignificant excretion of positively charged hyperbranched poly-L-lysine nanoparticles in the urine indicates that, following their intravenous injection, there is prompt distribution to and retention by tissues. The renal glomerular microvasculature in one site where positively charged NP could be retained owing to the fact that the wall of glomerular capillaries is positively charged. Neutralization of this charge could increase permeability of these capillaries to protein. Thus, depending on their diameter, circulating nanoparticles may or may not permeate into the layers and pass through the filtration barrier. Another determinant of their ability to permeate into the barrier is alteration of their surface characteristics performed in the manufacturing process in order to achieve functionalization of this surface. For example, nanoparticles with a positively charged surface are more likely to permeate into and be retained by the negatively charged filtration barrier.

Nanoparticles can also elicit an immune response. This response involves nanoparticle uptake by phagocytes (mainly macrophages) and dendritic cells. Both cell types are key players in a process known as antigen presentation, which generates a population of memory T-cells. We have recently shown that, macrophages took up nanoparticles and that these nanoparticles accumulated primarily in the cytoplasm with some localization in acidic lysosomes (Lianos et al. personal observation). Lysosomal localization of nanoparticles was previously described in two studies [236, 237]. In the first, internalized poly (γ -glutamic acid) nanoparticles were mostly detected in dendritic cell lysosomes [237]. In contrast, the second showed that gelatin nanoparticles did not accumulate in lysosomes, suggesting that these nanoparticles may have escaped into the cytoplasm as a result of endolysosomal membrane disruption [237]. Godbey et al. postulated that the presence of NH₂ termini may help the nanoparticle escape from lysosomes after causing their lysis [238]. According to this hypothesis, the buffering capacity of tertiary amino groups leads to osmotic swelling and endosomal rupture, resulting in the release of polymer into the cytoplasm. Although we did not evaluate hepatic toxicity of nanoparticles, Kupffer cells in the liver are specialized macrophages that behave similarly to the macrophages in our study. It is known that nanoparticle PEGylation prevents uptake in the reticuloendothelial system.

Exposure to MWCNTs through the major route of respiratory system causes sustained inflammation, macrophage

activation with or without granuloma formation, and fibrosis in the lung of rodents [239, 240]. Impairments in the lung, kidney, liver, and spleen were reported in immune-competent mice receiving high dosages of intravenously injected silica nanoparticles. The porosity and surface characteristics of the silica nanoparticles were suspected to affect nanoparticles–protein and nanoparticles–endothelial cell interactions, and eventually contributed to changes in hydrodynamic size of silica nanoparticles [241]. High dosages of intraperitoneally injected MSNPs caused a nuclear factor kappa B (NF- κ B) pathway-mediated inflammatory response and renal interstitial fibrosis [242]. Rodent studies *in vivo* show that AgNPs induce liver and neural toxicity after intravenous injection [243]. Intratympanic administration of high dosage AgNPs causes inner ear impairments [147, 227, 228]. AuNPs cause toxic effects on human lung epithelial cells through inducing ROS production [244].

During the defense procedure, alveolar macrophages produce pro-inflammatory and anti-inflammatory cytokines, which is a complex interplay in the immune response. Macrophages undergo highly reversible and transient polarization processes in response to comprehensive environmental signals, and are named M1 and M2 macrophages [245, 246]. M1 macrophages refer to classically activated macrophages that mediate defense of the host against a variety of bacteria, protozoa and viruses. M1 macrophages are involved in antitumor immunity mainly through secretion of cytokines including tumor necrosis factor- α (TNF- α), interleukin-1 β (IL-1 β), IL-6, etc. M2 macrophages, in turn, represent alternatively activated macrophages that have anti-inflammatory function and regulate wound healing mediated by the upregulated expression of cytokine IL-10 and growth factors including transforming growth factor- β 1 (TGF- β 1) and vascular endothelial growth factor (VEGF) [245, 247]. mRNA levels of TNF, IL-1 β , IL-6, IL-8, and IL-10 in macrophages have been selected as parameters in modeling response to silver nanoparticles [248].

Endotoxin contamination can also be a source for activation of the immune system. Contamination by endotoxic particles (usually fractions of bacterial wall) during nanoparticle synthesis is an important consideration with regard to their medical application [249]. Whether CD40 or CD86 induction indicates nanoparticle immunogenic potential needs further exploration, because the mere exposure of CD-type co-stimulatory molecules may cause upregulation. In this regard, previous studies showed that coating of carboxylated (negatively charged) polystyrene microparticles with poly-L-lysine increased the extent of uptake by dendritic cells and induced the CD83 maturation index [236].

11 Cochlear Implant Based Delivery

Currently there are more than 300,000 cochlear implant users worldwide, and this number increases by around 30,000 per year [250]. Cochlear implant candidates can be profoundly deaf, or during the last decade, can possess functional low frequency residual hearing at 1 kHz and below. In the latter case, the electrode array is inserted only into the first turn of the scala tympani and device design and surgical procedures are optimized for low frequency hearing preservation [251]. These implant users enjoy improved sound quality and hearing ability using a combination of electric and acoustic stimulation, a hybrid approach that opens a new field of opportunities, where the acoustic hearing of a cochlear implant user is preserved or enhanced using pharmacological approaches [252, 253]. For example, we might envisage an approach where, following the traumatic insertion of a short electrode array, medication is intermittently delivered to assist in hearing preservation. The auditory nerve itself is also a target for preservative or restorative therapies, to enhance its ability to transmit signals to the brain. Such therapies would either improve the status of degenerated fibers, target proliferation through activation of progenitors, or attempt process regrowth to electrode arrays, for improved spatial selectivity of stimulation [254, 255].

Cochlear implantation also offers a unique opportunity to deliver pharmacological agents deep into cochlear fluids and in close proximity to targeted structures, thereby avoiding the steep concentration gradients needed for round window delivery [184]. Nanoparticles released deep in the scala tympani can readily diffuse through the last few millimeters of perilymph before reaching all cochlear structures.

Currently, intensive research focuses on different techniques to deliver drugs, biologics and nanoparticles [256]. The simplest approach is to use a disposable, flexible cannula designed specifically for deep insertion into the cochlea with slow progressive injections of a substance prior to implantation (Fig. 17) [257]. This substance can consist of a concentrated suspension of particles for release from openings along the array or a less concentrated suspension for delivery from the cannula tip. In the latter case, the agent progressively displaces the perilymph, which is flushed out of the cannula entry point. Further drug diffusion into the apical region of the cochlea occurs post-implantation. Feasibility of the procedure has been investigated *in situ*. In eight temporal bones the catheter was inserted into the cochlea and an iodine solution injected. CT scans of the temporal bones showed that the injected liquid was located in the scala tympani. Histology has revealed no perforation of the basilar membrane after gentle injection of 10 µL of solution with a µL-syringe. Certain particles or drugs might also be held in a matrix that coats the electrode array for fast or slow release, depending on the properties of the

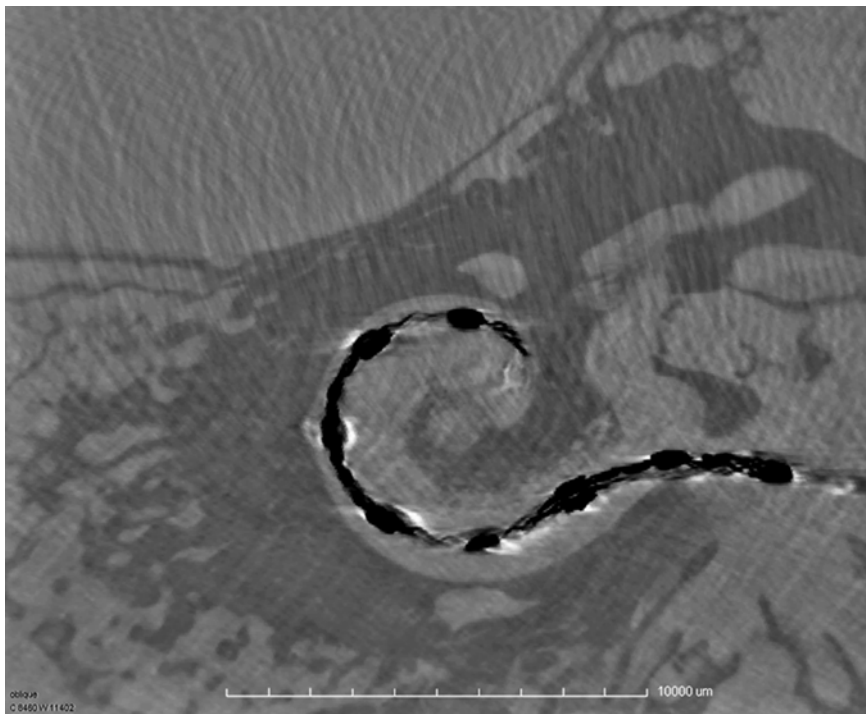


Fig. 17 Human cochlear preparation with flexible cannula inserted 20 mm deep into scala tympani. (Courtesy of NanoCl Research Consortium)

matrix (Fig. 18) [258]. This approach, however, limits the amount of drug applied and may alter the physical characteristics of the electrode array when loaded with the high drug concentrations critical for trauma reduction. Semichronic delivery of particles can also be achieved by incorporation of a reservoir within the body of the electrode array. The concept involves a single, wide channel, extending most of the length of the electrode array and (potentially) beyond the intracochlear portion by several centimeters. In this case particles are released by passive diffusion over a period of hours to months, depending on the geometry of the reservoir itself. Openings along the array would control both site and rate of particle release. The drug might alternatively be added to the reservoir in powder form for release by fluid ingress into the outlets. For more uniform delivery of fluid-based agents over time, an implanted micropump could be incorporated in principle [259]. Finally, prolonged delivery of agents might be achieved using a reservoir with a port and septum arrangement for injection into a holding reservoir through the skin. One embodiment under development contains a hydrogel plug at a single outlet to the cochlea, which swells upon contact with the drug suspension, thereby

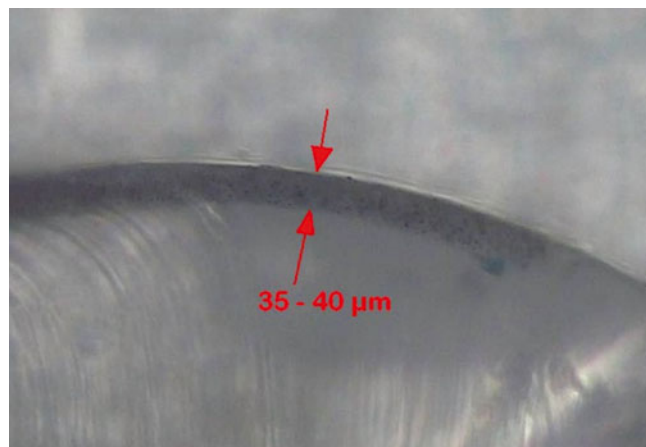


Fig. 18 Cross section of a cochlear implant electrode array. Incorporated into the surface of the electrode one can see a 35–40 μm thick coating. The matrix of the thin film (*black*) at the surface contains a drug (*Courtesy of C. Jolly Med-El Co*)

controlling the rate of drug transfer and fluid exchange. In summary, the future of hearing restoration likely involves a number of implanted combination devices, incorporating agents for pharmaceutical enhancement of the cochlea or the electrode/nerve interface.

12 Conclusions

The “non-druggable” targets that are not currently amenable to conventional therapeutics can be made “druggable” with nanoparticle-based therapy. In nanoparticle therapy the therapeutic agent, DNA or siRNA can be targeted into cells of a particular organ, where it directly affects the target cells, upregulates therapeutic gene expression, or releases a therapeutic protein from the cells. Novel synthetic gene transfer vehicles can be modified to facilitate DNA condensation, targeting the nucleus and transportation through nuclear pore complexes. The types of nanoparticles that will be manufactured and tested include hybrid nanoparticles, aqueous core lipid nanocapsules (ACLN) and different magnetic nanoparticles encapsulated with PLGA matrix. By virtue of their surface chemistry, these carriers are expected to induce DNA condensation, which facilitates cellular entry by endocytosis, helps endosomal escape, and protects against nucleases. Finally, the targeting of nuclear pore complexes and the transport of molecules through them will be promoted by conjugating nuclear localizing signal moieties.

Acknowledgments

HEI-OCI immortalized hair cell line (kindly provided by Prof. Federico Kalinec). Dr. Anna Minasyan kindly helped in structuring the manuscript. This project is supported by EU NanoEar Integrated Project NMP4-CT-2006-026556. We also acknowledge Kellomäki Minna (Tampere University of Technology), Linden Mika (Åbo Akademi University), Vihinen-Ranta Maija (University of Jyväskylä), Muhammed Mamoun (Royal Institute of Technology), Möller Martin and Kroll Juergen (RWTH, Aachen), Saulnier Patrick (Université d'Angers-INSERM U646), Stöver Timo (Medizinische Hochschule Hannover), Klok Harm-Anton (Ecole Polytechnique Fédérale de Lausanne), Popelar Jiri (Institute of Experimental Medicine, Prague), Rask-Andersen Helge (Uppsala University Hospital), Lianos Elias (University of Athens School of Medicine), Newman Tracey (University of Southampton), Jolly Claude (MED-EL Corporation, Austria), and Löbler Marian (University of Rostock) for their comments and contributions to this work.

References

- WHO (2006) Primary ear and hearing care. Training resource. Advanced level. World Health Organization
- WHO (2008) The World Health Report
- Gates GA, Cooper JC (1991) Incidence of hearing decline in the elderly. *Acta Otolaryngol* 111(2):240–248
- Ruben RJ (2000) Redefining the survival of the fittest: communication disorders in the 21st century. *Laryngoscope* 110(2 Pt 1):241–245
- Zou J, Zhang W, Poe D, Zhang Y, Ramadan UA, Pyykko I (2010) Differential passage of gadolinium through the mouse inner ear barriers evaluated with 4.7T MRI. *Hear Res* 259(1–2):36–43
- Zou J, Yoshida T, Ramadan UA, Pyykko I (2011) Dynamic enhancement of the rat inner ear after ultra-small-volume administration of Gd-DOTA to the medial wall of the middle ear cavity. *ORL J Otorhinolaryngol Relat Spec* 73(5):275–281
- Zou J, Poe D, Ramadan UA, Pyykko I (2012) Oval window transport of Gd-dOTA from rat middle ear to vestibulum and scala vestibuli visualized by in vivo magnetic resonance imaging. *Ann Otol Rhinol Laryngol* 121(2):119–128
- Nakashima T, Naganawa S, Sugiura M et al (2007) Visualization of endolymphatic hydrops in patients with Meniere's disease. *Laryngoscope* 117(3):415–420
- Naganawa S, Yamazaki M, Kawai H, Bokura K, Sone M, Nakashima T (2010) Visualization of endolymphatic hydrops in Meniere's disease with single-dose intravenous gadolinium-based contrast media using heavily T(2)-weighted 3D-FLAIR. *Magn Reson Med Sci* 9(4):237–242
- Zou J, Pyykko I (2015) Enhanced oval window and blocked round window passages for middle-inner ear transportation of gadolinium in guinea pigs with a perforated round window membrane. *Eur Arch Otorhinolaryngol* 272(2):303–309
- Watanabe T, Frahm J, Michaelis T (2008) Manganese-enhanced MRI of the mouse auditory pathway. *Magn Reson Med* 60(1):210–212
- Zou J, Pyykko I (2015) Calcium metabolism profile in rat inner ear indicated by MRI after tympanic medial wall administration of manganese chloride. *Ann Otol Rhinol Laryngol* 125(1):53–62
- Jin SU, Lee JJ, Hong KS et al (2013) Intratympanic manganese administration revealed sound intensity and frequency dependent functional activity in rat auditory pathway. *Magn Reson Imaging* 31(7):1143–1149
- Groschel M, Hubert N, Muller S, Ernst A, Basta D (2014) Age-dependent changes of calcium related activity in the central auditory pathway. *Exp Gerontol* 58:235–243

15. Izumikawa M, Minoda R, Kawamoto K et al (2005) Auditory hair cell replacement and hearing improvement by Atoh1 gene therapy in deaf mammals. *Nat Med* 11(3):271–276
16. Kawamoto K, Yagi M, Stover T, Kanzaki S, Raphael Y (2003) Hearing and hair cells are protected by adenoviral gene therapy with TGF-beta1 and GDNF. *Mol Ther* 4:484–492
17. Shou J, Zheng JL, Gao WQ (2003) Robust generation of new hair cells in the mature mammalian inner ear by adenoviral expression of *Hath1*. *Mol Cell Neurosci* 23(2):169–179
18. Dickerson EB, Blackburn WH, Smith MH, Kapa LB, Lyon LA, McDonald JF (2010) Chemosensitization of cancer cells by siRNA using targeted nanogel delivery. *BMC Cancer* 10:10
19. Miller VM, Hunter LW, Chu K, Kaul V, Squillace PD, Lieske JC, Jayachandran M (2009) Biologic nanoparticles and platelet reactivity. *Nanomedicine (Lond)* 4(7):725–733
20. Theoharis S, Krueger U, Tan PH, Haskard DO, Weber M, George AJ (2009) Targeting gene delivery to activated vascular endothelium using anti E/P-selectin antibody linked to PAMAM dendrimers. *J Immunol Methods* 343(2):79–90
21. Swan EE, Messcher MJ, Sewell WF, Tao SL, Borenstein JT (2008) Inner ear drug delivery for auditory applications. *Adv Drug Deliv Rev* 60(15):1583–1599
22. Wang Z, Chui WK, Ho PC (2010) Integrin targeted drug and gene delivery. *Expert Opin Drug Deliv* 7(2):159–171
23. Wojtowicz AM, Shekaran A, Oest ME, Dupont KM, Templeman KL, Hutmacher DW, Guldberg RE, Garcia AJ (2010) Coating of biomaterial scaffolds with the collagen-mimetic peptide GFOGER for bone defect repair. *Biomaterials* 31(9):2574–2582
24. Gong CY, Shi S, Dong PW et al (2009) In vitro drug release behavior from a novel thermosensitive composite hydrogel based on Pluronic f127 and poly(ethylene glycol)-poly(epsilon-caprolactone)-poly(ethylene glycol) copolymer. *BMC Biotechnol* 9:8
25. Albornoz C, Jacobo SE (2006) Preparation of a biocompatible magnetic film from an aqueous ferrofluid. *J Magn Magn Mater* 305(1):12–15
26. Li X, Ding L, Xu Y, Wang Y, Ping Q (2009) Targeted delivery of doxorubicin using stealth liposomes modified with transferrin. *Int J Pharm* 373(1–2):116–123
27. Anabousi S, Laue M, Lehr CM, Bakowsky U, Ehrhardt C (2005) Assessing transferrin modification of liposomes by atomic force microscopy and transmission electron microscopy. *Eur J Pharm Biopharm* 60(2):295–303
28. Pante N, Kann M (2002) Nuclear pore complex is able to transport macromolecules with diameters of about 39 nm. *Mol Biol Cell* 13(2):425–434
29. Zou J, Sood R, Zhang Y, Kinnunen PK, Pykkö I (2014) Pathway and morphological transformation of liposome nanocarriers after release from a novel sustained inner-ear delivery system. *Nanomedicine (Lond)* 9(14):2143–2155
30. Deda DK, Uchoa AF, Carita E, Baptista MS, Toma HE, Araki K (2009) A new micro/nanoencapsulated porphyrin formulation for PDT treatment. *Int J Pharm* 376(1–2):76–83
31. Heurtault B, Saulnier P, Pech B, Proust JE, Benoit JP (2002) A novel phase inversion-based process for the preparation of lipid nanocarriers. *Pharm Res* 19(6):875–880
32. Heurtault B, Saulnier P, Pech B, Venier-Julienne MC, Proust JE, Phan-Tan-Luu R, Benoit JP (2003) The influence of lipid nanocapsule composition on their size distribution. *Eur J Pharm Sci* 18(1):55–61
33. Zou J, Saulnier P, Perrier T, Zhang Y, Manninen T, Toppila E, Pykkö I (2008) Distribution of lipid nanocapsules in different cochlear cell populations after round window membrane permeation. *J Biomed Mater Res B Appl Biomater* 87(1):10–18
34. Schepel V, Wolf M, Scholl M et al (2009) Potential novel drug carriers for inner ear treatment: hyperbranched polylysine and lipid nanocapsules. *Nanomedicine (Lond)* 4(6):623–635
35. Vonarbourg A, Saulnier P, Passirani C, Benoit JP (2005) Electrokinetic properties of non-charged lipid nanocapsules: influence of the dipolar distribution at the interface. *Electrophoresis* 26(11):2066–2075
36. Lai WF, Lin MC (2009) Nucleic acid delivery with chitosan and its derivatives. *J Control Release* 134(3):158–168
37. Khan TA, Peh KK, Ch'ng HS (2002) Reporting degree of deacetylation values of chitosan: the influence of analytical methods. *J Pharm Pharm Sci* 5(3):205–212
38. Kiang T, Wen J, Lim HW, Leong KW (2004) The effect of the degree of chitosan deacetylation on the efficiency of gene transfection. *Biomaterials* 25(22):5293–5301
39. Corsi K, Chellat F, Yahia L, Fernandes JC (2003) Mesenchymal stem cells, MG63 and HEK293 transfection using chitosan-DNA nanoparticles. *Biomaterials* 24(7):1255–1264
40. Mao HQ, Roy K, Troung-Le VL et al (2001) Chitosan-DNA nanoparticles as gene carriers: synthesis, characterization and transfection efficiency. *J Control Release* 70(3):399–421

41. Huang DM, Hung Y, Ko BS et al (2005) Highly efficient cellular labeling of mesoporous nanoparticles in human mesenchymal stem cells: implication for stem cell tracking. *FASEB J* 19(14):2014–2016
42. Ishii T, Okahata Y, Sato T (2001) Mechanism of cell transfection with plasmid/chitosan complexes. *Biochim Biophys Acta* 1514(1): 51–64
43. Guang Liu W, De Yao K (2002) Chitosan and its derivatives—a promising non-viral vector for gene transfection. *J Control Release* 83(1):1–11
44. Huang M, Fong CW, Khor E, Lim LY (2005) Transfection efficiency of chitosan vectors: effect of polymer molecular weight and degree of deacetylation. *J Control Release* 106(3):391–406
45. Lee KY, Kwon IC, Kim YH, Jo WH, Jeong SY (1998) Preparation of chitosan self-aggregates as a gene delivery system. *J Control Release* 51(2–3):213–220
46. Koping-Hoggard M, Varum KM, Issa M, Danielsen S, Christensen BE, Stokke BT, Artursson P (2004) Improved chitosan-mediated gene delivery based on easily dissociated chitosan polyplexes of highly defined chitosan oligomers. *Gene Ther* 11(19):1441–1452
47. Hsiao JK, Tsai CP, Chung TH et al (2008) Mesoporous silica nanoparticles as a delivery system of gadolinium for effective human stem cell tracking. *Small* 4(9):1445–1452
48. Kim J, Kim HS, Lee N et al (2008) Multifunctional uniform nanoparticles composed of a magnetite nanocrystal core and a mesoporous silica shell for magnetic resonance and fluorescence imaging and for drug delivery. *Angew Chem Int Ed Engl* 4(44):8438–8441
49. Lin Y-S, Wu S-H, Hung Y et al (2006) Multifunctional composite nanoparticles: magnetic, luminescent and mesoporous. *ChemMater* 18:5170–5172
50. Liu HM, Wu SH, Lu CW et al (2008) Mesoporous silica nanoparticles improve magnetic labeling efficiency in human stem cells. *Small* 4(5):619–626
51. Taylor KM, Kim JS, Rieter WJ, An H, Lin W (2008) Mesoporous silica nanospheres as highly efficient MRI contrast agents. *J Am Chem Soc* 130(7):2154–2155
52. Wu SH, Lin YS, Hung Y, Chou YH, Hsu YH, Chang C, Mou CY (2008) Multifunctional mesoporous silica nanoparticles for intracellular labeling and animal magnetic resonance imaging studies. *Chembiochem* 9(1):53–57
53. Brevet D, Gary-Bobo M, Raehm L et al (2009) Mannose-targeted mesoporous silica nanoparticles for photodynamic therapy. *Chem Commun (Camb)* 12:1475–1477
54. Lebret VRL, Durand JO, Smahi M et al (2008) Surface functionalization of two-photon dye-doped mesoporous silica nanoparticles with folic acid: cytotoxicity studies with HeLa and MCF-7 cancer cells. *J Sol-Gel Sci Technol* 48:32–39
55. Liang M, Lu J, Kovochich M, Xia T, Ruehm SG, Nel AE, Tamanoi F, Zink JI (2008) Multifunctional inorganic nanoparticles for imaging, targeting, and drug delivery. *ACS Nano* 2(5):889–896
56. Park IY, Kim IY, Yoo MK, Choi YJ, Cho MH, Cho CS (2008) Mannosylated polyethylenimine coupled mesoporous silica nanoparticles for receptor-mediated gene delivery. *Int J Pharm* 359(1–2):280–287
57. Rosenholm JM, Meinander A, Peuhu E, Niemi R, Eriksson JE, Sahlgren C, Linden M (2009) Targeting of porous hybrid silica nanoparticles to cancer cells. *ACS Nano* 3(1):197–206
58. Rosenholm JM, Peuhu E, Eriksson JE, Sahlgren C, Linden M (2009) Targeted intracellular delivery of hydrophobic agents using mesoporous hybrid silica nanoparticles as carrier systems. *Nano Lett* 9(9):3308–3311
59. Tsai C-P, Chen CY, Hung Y, Chang F-H, Mou C-Y (2009) Monoclonal antibody-functionalized mesoporous silica nanoparticles (MSN) for selective targeting breast cancer cells. *J Mater Chem* 19:5737–5743
60. Lin Y-S, Tsai C-P, Hung H-Y et al (2005) Well-ordered mesoporous silica nanoparticles as cell markers. *Chem Mater* 17:4570–4573
61. Giri S, Trewyn BG, Lin VS (2007) Mesoporous silica nanomaterial-based biotechnological and biomedical delivery systems. *Nanomedicine (Lond)* 2(1):99–111
62. Mortera R, Vivero-Escoto J, Slowing II, Garrone E, Onida B, Lin VS (2009) Cell-induced intracellular controlled release of membrane impermeable cysteine from a mesoporous silica nanoparticle-based drug delivery system. *Chem Commun (Camb)* 22:3219–3221
63. Slowing II, Vivero-Escoto JL, Wu CW, Lin VS (2008) Mesoporous silica nanoparticles as controlled release drug delivery and gene transfection carriers. *Adv Drug Deliv Rev* 60(11):1278–1288
64. Slowing BG, Trewyn S, Giri V, Lin S-Y (2007) Mesoporous silica nanoparticles for drug delivery and biosensing applications. *Adv Funct Mater* 17(8):1225–1236
65. Liang M, Angelos S, Choi E, Patel K, Stoddart JF, Zink JI (2009) Mesostructured multifunctional nanoparticles for imaging and drug delivery. *J Mater Chem* 19:6251–6257
66. Liu J, Stace-Naughton A, Jiang X, Brinker CJ (2009) Porous nanoparticle supported lipid

- bilayers (protocells) as delivery vehicles. *J Am Chem Soc* 131(4):1354–1355
67. Lu J, Liang M, Zink JI, Tamanoi F (2007) Mesoporous silica nanoparticles as a delivery system for hydrophobic anticancer drugs. *Small* 3(8):1341–1346
 68. Wang S (2009) Ordered mesoporous materials for drug delivery. *Microporous Mesoporous Mater* 117(1–2):1–9
 69. Johnston AH, Dalton PD, Newman TA (2010) Polymersomes, smaller than you think: ferrocene as a TEM probe to determine core structure. *J Nanopart Res* 12(6):1997–2001
 70. Ghoroghchian PP, Lin JJ, Brannan AK, Frail PR, Bates FS, Therien MJ, Hammer DA (2006) Quantitative membrane loading of polymer vesicles. *Soft Matter* 2(11):973–980
 71. Lomas H, Canton I, MacNeil S et al (2007) Biomimetic pH sensitive polymersomes for efficient DNA encapsulation and delivery. *Adv Mater* 19(23):4238–4243
 72. Christian NA, Milone MC, Ranka SS et al (2007) Tat-functionalized near-infrared emissive polymersomes for dendritic cell labeling. *Bioconjug Chem* 18(1):31–40
 73. Roy S, Johnston AH, Newman TA et al (2010) Cell-specific targeting in the mouse inner ear using nanoparticles conjugated with a neurotrophin-derived peptide ligand: potential tool for drug delivery. *Int J Pharm* 390(2):214–224
 74. Zhang W, Zhang Y, Lobler M, Schmitz KP, Ahmad A, Pyykkö I, Zou J (2011) Nuclear entry of hyperbranched polylysine nanoparticles into cochlear cells. *Int J Nanomed* 6:535–546
 75. Surovtseva E, Johnston A, Zhang W et al (2011) Prestin binding peptides as ligands for targeted polymersome mediated drug delivery to outer hair cells in the inner ear. *Int J Pharm.* 2012 Mar 15;424(1–2):121–7. Epub 2011 Dec 30
 76. Halperin A (1999) Polymer brushes that resist adsorption of model proteins: design parameters. *Langmuir* 15(7):2525–2533
 77. Roy S, Glueckert R, Johnston AH, Perrier T, Bitsche M, Newman TA, Saulnier P, Schrott-Fischer A (2012) Strategies for drug delivery to the human inner ear by multifunctional nanoparticles. *Nanomedicine (Lond)*. 7(1):55–63. doi: 10.2217/nmm.11.84. Epub 2011 Nov 22
 78. Liu JK, Tenga QS, Garrity-Moses M, Federici T, Tanase D, Imperiale MJ, Boulis NM (2005) A novel peptide defined through phage display for therapeutic protein and vector neuronal targeting. *Neurobiol Dis* 19(3):407–418
 79. Buckiová D, Ranjan S, Newman TA et al (2011) Minimally invasive drug delivery to the cochlea through application of nanoparticles to the round window membrane. *Nanomedicine (Lond)*. 2012 Sep;7(9):1339–54. Epub 2012 Apr 4
 80. Scholl M, Nguyen TQ, Bruchmann B, Klok H-A (2007) The thermal polymerization of amino acids revisited; Synthesis and structural characterization of hyperbranched polymers from L-lysine. *J Polym Sci Part A Polym Chem* 45:5494–5508
 81. Hawker CJ, Lee R, Fréchet JMJ (1991) The one-step synthesis of hyperbranched dendritic polyesters. *J Am Chem Soc* 113:4303–4313
 82. Höltner D, Burgath A, Frey H (1997) Degree of branching in hyperbranched polymers. *Acta Polymer* 48:30–35
 83. Zhang Y, Zhang W, Johnston AH, Newman TA, Pyykkö I, Zou J (2011) Targeted delivery of Tet1 peptide functionalized polymersomes to the rat cochlear nerve. *Int J Nanomed*. 2012;7:1015–1022.
 84. Qin J, Jo YS, Ihm JE, Kim DK, Muhammed M (2005) Thermosensitive nanospheres with a gold layer revealed as low-cytotoxic drug vehicles. *Langmuir* 21:9346–9351
 85. Jo JS, Kim M-C, Kim DK, Kim C-J, Jeong Y-K, Kim K-J, Muhammed M (2004) Mathematical modeling and in-vitro experiment for the controlled-release of indomethacin-loaded PLA-PEO nanospheres. *Nanotechnology* 15:1186–1194
 86. Kabanov AV, Vinogradov SV (2009). In: *Angew Chem Int Ed* (ed) vol 48, p 14
 87. Oh JK, Drumright R, Siegwart DJ, Matyjaszewski K (2008) The development of microgels/nanogels for drug delivery applications. *Prog Polym Sci* 33:448–447
 88. Peppas NA, Hilt JZ, Khademhosseini A, Langer R (2006) Hydrogels in biology and medicine: from fundamentals to bionano-technology. *Adv Mater* 18:1345–1360
 89. Hennik WE, van Nostrum CF (2002) Novel crosslinking methods to design hydrogels. *Adv Drug Deliv Rev* 54(1):13–36
 90. Groll J, Singh S, Albrecht K, Möller M (2009) Biocompatible and degradable nanogels via oxidation reactions of synthetic thiomers in inverse miniemulsion. *J Polymer Sci Part A Polymer Chem* 47(20):5543–5549
 91. Wattendorf U, Merkle HP (2008) PEGylation as a tool for the biomedical engineering of surface modified microparticles. *J Pharm Sci* 97(11):4655–4669
 92. Verma A, Stellacci F (2010) Effect of surface properties on nanoparticle-cell interactions. *Small* 6(1):12–21
 93. He Q, Zhang J, Shi J, Zhu Z, Zhang L, Bu W, Guo L, Chen Y (2010) The effect of PEGylation of mesoporous silica nanoparticles

- on nonspecific binding of serum proteins and cellular responses. *Biomaterials* 31:1085–1092
94. Harris JM, Chess RB (2003) Effect of pegylation on pharmaceuticals. *Nat Rev Drug Discov* 2(3):214–221
 95. Gref R, Luck M, Quellec P et al (2000) “Stealth” corona-core nanoparticles surface modified by polyethylene glycol (PEG): influences of the corona (PEG chain length and surface density) and of the core composition on phagocytic uptake and plasma protein adsorption. *Colloids Surf B Biointerfaces* 18(3–4):301–313
 96. Schimmang T, Minichiello L, Vazquez E, San Jose I, Giraldez F, Klein R, Represa J (1995) Developing inner ear sensory neurons require TrkB and TrkC receptors for innervation of their peripheral targets. *Development* 121(10):3381–3391
 97. Ylikoski J, Pirvola U, Moshnyakov M, Palgi J, Arumae U, Saarma M (1993) Expression patterns of neurotrophin and their receptor mRNAs in the rat inner ear. *Hear Res* 65(1–2):69–78
 98. Zou JZY, Zhang W, Ranjan S, Sood R, Mikhailov A, Kinnunen P, Pyykko I (2009) Internalization of liposome nanoparticles functionalized with TrkB ligand in rat cochlear cell populations. *Eur J Nanomed* 3:8–14
 99. Bachmann G, Su J, Zumegen C, Wittekindt C, Michel O (2001) Permeability of the round window membrane for prednisolone-21-hydrogen succinate. Prednisolone content of the perilymph after local administration vs. systemic injection. *HNO* 49(7):538–542
 100. Parnes LS, Sun AH, Freeman DJ (1999) Corticosteroid pharmacokinetics in the inner ear fluids: an animal study followed by clinical application. *Laryngoscope* 109:1–17
 101. Chandrasekhar SS, Rubinstein RY, Kwartler JA, Gatz M, Connelly PE, Huang E, Baredes S (2000) Dexamethasone pharmacokinetics in the inner ear: comparison of route of administration and use of facilitating agents. *Otolaryngol Head Neck Surg* 122(4):521–528
 102. Borkholder DA (2008) State-of-the-art mechanisms of intracochlear drug delivery. *Curr Opin Otolaryngol Head Neck Surg* 16(5):472–477
 103. Chen G, Hou SX, Hu P, Hu QH, Guo DD, Xiao Y (2008) In vitro dexamethasone release from nanoparticles and its pharmacokinetics in the inner ear after administration of the drug-loaded nanoparticles via the round window. *Nan Fang Yi Ke Da Xue Xue Bao* 28(6):1022–1024
 104. Zou J, Pyykko I, Bretlau P, Klason T, Bjelke B (2003) In vivo visualization of endolymphatic hydrops in guinea pigs: magnetic resonance imaging evaluation at 4.7 tesla. *Ann Otol Rhinol Laryngol* 112(12):1059–1065
 105. Zou J, Ramadan UA, Pyykko I (2010) Gadolinium uptake in the rat inner ear perilymph evaluated with 4.7 T MRI: A comparison between transtympanic injection and gelatin sponge-based diffusion through the round window membrane. *Otol Neurotol* 31(4):637–641
 106. Nakashima T, Naganawa S, Katayama N, Teranishi M, Nakata S, Sugiura M, Sone M, Kasai S, Yoshioka M, Yamamoto M (2009) Clinical significance of endolymphatic imaging after intratympanic gadolinium injection. *Acta Otolaryngol Suppl* 560:9–14
 107. Hahn H, Kammerer B, DiMauro A, Salt AN, Plontke SK (2006) Cochlear microdialysis for quantification of dexamethasone and fluorescein entry into scala tympani during round window administration. *Hear Res* 21(1–2):236–244
 108. Mikulec AA, Plontke SK, Hartsock JJ, Salt AN (2009) Entry of substances into perilymph through the bone of the otic capsule after intratympanic applications in guinea pigs: implications for local drug delivery in humans. *Otol Neurotol* 30(2):131–138
 109. Tanuma A, Sato H, Takeda T et al (2007) Functional characterization of a novel missense CLCN5 mutation causing alterations in proximal tubular endocytic machinery in Dent’s disease. *Nephron Physiol* 107(4):87–97
 110. Praetorius M (2007) Active middle ear implants: more than “just” a hearing aid. *HNO* 55(9):681–683
 111. Witte MC, Kasperbauer JL (2000) Round window membrane permeability to transforming growth factor-alpha: an in vitro study. *Otolaryngol Head Neck Surg* 123(1 Pt 1):91–96
 112. Kopke RD, Wassel RA, Mondalek F, Grady B, Chen K, Liu J, Gibson D, Dormer KJ (2006) Magnetic nanoparticles: inner ear targeted molecule delivery and middle ear implant. *Audiol Neurotol* 11(2):123–133
 113. Nomura Y (1984) Otological significance of the round window, vol 33. *Advances in otorhinolaryngology*, Karger, Basel
 114. Yoshihara T, Kaname H, Ishii T, Igarashi M (1995) Subepithelial fiber components of the round window membrane of the guinea pig: an ultrastructural and immunohistochemical study. *ORL J Otorhinolaryngol Relat Spec* 57(3):115–121
 115. Engel F, Blatz R, Kellner J, Palmer M, Weller U, Bhadki S (1995) Breakdown of the round

- window membrane permeability barrier evoked by streptolysin O: possible etiologic role in development of sensorineural hearing loss in acute otitis media. *Infect Immun* 63(4):1305–1310
116. Zou J, Poe D, Bjelke B, Pyykko I (2009) Visualization of inner ear disorders with MRI in vivo: from animal models to human application. *Acta Otolaryngol Suppl* 560:22–31
 117. Banerji SK, Hayes MA (2007) Examination of nonendocytotic bulk transport of nanoparticles across phospholipid membranes. *Langmuir* 23(6):3305–3313
 118. Wattiaux R, Laurent N, Wattiaux-De Coninck S, Jadot M (2000) Endosomes, lysosomes: their implication in gene transfer. *Adv Drug Deliv Rev* 41(2):201–208
 119. De Matteis MA, Luini A (2008) Exiting the Golgi complex. *Nat Rev Mol Cell Biol* 9(4):273–284
 120. Rudolph C, Schillinger U, Ortiz A, Tabatt K, Plank C, Muller RH, Rosenecker J (2004) Application of novel solid lipid nanoparticle (SLN)-gene vector formulations based on a dimeric HIV-1 TAT-peptide in vitro and in vivo. *Pharm Res* 21(9):1662–1669
 121. Jarver P, Langel U (2004) The use of cell-penetrating peptides as a tool for gene regulation. *Drug Discov Today* 9(9):395–402
 122. Lindsay MA (2002) Peptide-mediated cell delivery: application in protein target validation. *Curr Opin Pharmacol* 2(5):587–594
 123. Richard JP, Melikov K, Brooks H, Prevot P, Lebleu B, Chernomordik LV (2005) Cellular uptake of unconjugated TAT peptide involves clathrin-dependent endocytosis and heparan sulfate receptors. *J Biol Chem* 280(15):15300–15306
 124. Koppelhus U, Awasthi SK, Zachar V, Holst HU, Ebbesen P, Nielsen PE (2002) Cell-dependent differential cellular uptake of PNA, peptides, and PNA-peptide conjugates. *Antisense Nucleic Acid Drug Dev* 12(2):51–63
 125. Nakase I, Niwa M, Takeuchi T et al (2004) Cellular uptake of arginine-rich peptides: roles for macropinocytosis and actin rearrangement. *Mol Ther* 10(6):1011–1022
 126. Rinne J, Albaran B, Jylhava J et al (2007) Internalization of novel non-viral vector TAT-streptavidin into human cells. *BMC Biotechnol* 7:1
 127. Ayame H, Morimoto N, Akiyoshi K (2008) Self-assembled cationic nanogels for intracellular protein delivery. *Bioconjug Chem* 19(4):882–890
 128. Löbler M, Rohm H, Perrier T et al (2012) Nanoparticle mediated drug delivery. End report from NanoEar Consortium. 120 p
 129. Eguchi A, Meade BR, Chang YC, Fredrickson CT, Willert K, Puri N, Dowdy SF (2009) Efficient siRNA delivery into primary cells by a peptide transduction domain-dsRNA binding domain fusion protein. *Nat Biotechnol* 2(6):567–571
 130. Sugunan A, Jafri HM, Qin J, Blom T, Toprak MS, Leifer K, Muhammed MJ (2010) Low-temperature synthesis of photoconducting CdTe nanotrapods. *J Mater Chem* 20:1208–1214
 131. Park J, Joo J, Kwon SG, Jang Y, Hyeon T (2007) Synthesis of monodisperse spherical nanocrystals. *Angew Chem Int Ed Engl* 46(25):4630–4660
 132. Anabousi S, Bakowsky U, Schneider M, Huwer H, Lehr CM, Ehrhardt C (2006) In vitro assessment of transferrin-conjugated liposomes as drug delivery systems for inhalation therapy of lung cancer. *Eur J Pharm Sci* 29(5):367–374
 133. Chang J, Jalloul Y, Kroubi M, Yuan XB, Feng W, Kang CS, Pu PY, Betbeder D (2009) Characterization of endocytosis of transferrin-coated PLGA nanoparticles by the blood-brain barrier. *Int J Pharm* 379(2):285–292
 134. Chithrani BD, Chan WC (2007) Elucidating the mechanism of cellular uptake and removal of protein-coated gold nanoparticles of different sizes and shapes. *Nano Lett* 7(6):1542–1550
 135. Lee MC, Miller EA, Goldberg J, Orci L, Schekman R (2004) Bi-directional protein transport between the ER and Golgi. *Annu Rev Cell Dev Biol* 20:87–123
 136. Sahay G, Alakhova DY, Kabanov AV (2010) Endocytosis of nanomedicines. *J Control Release* 145(3):182–195
 137. Lechardeur D, Verkman AS, Lukacs GL (2005) Intracellular routing of plasmid DNA during non-viral gene transfer. *Adv Drug Deliv Rev* 57(5):755–767
 138. Mayor S, Pagano RE (2007) Pathways of clathrin-independent endocytosis. *Nat Rev Mol Cell Biol* 8(8):603–612
 139. Mousavi SA, Malerod L, Berg T, Kjeken R (2004) Clathrin-dependent endocytosis. *Biochem J* 377(Pt 1):1–16
 140. Widera A, Norouziyan F, Shen WC (2003) Mechanisms of TfR-mediated transcytosis and sorting in epithelial cells and applications toward drug delivery. *Adv Drug Deliv Rev* 55(11):1439–1466
 141. Gaborik Z, Hunyady L (2004) Intracellular trafficking of hormone receptors. *Trends Endocrinol Metab* 15(6):286–293
 142. Laakkonen JP, Makela AR, Kakkonen E et al (2009) Clathrin-independent entry of baculovirus triggers uptake of *E. coli* in non-phagocytic human cells. *PLoS One* 4(4):e5093

143. Lai SK, Hida K, Man ST, Chen C, Machamer C, Schroer TA, Hanes J (2007) Privileged delivery of polymer nanoparticles to the perinuclear region of live cells via a non-clathrin, non-degradative pathway. *Biomaterials* 28(18):2876–2884
144. Hatakeyama H, Ito E, Akita H, Oishi M, Nagasaki Y, Futaki S, Harashima H (2009) A pH-sensitive fusogenic peptide facilitates endosomal escape and greatly enhances the gene silencing of siRNA-containing nanoparticles in vitro and in vivo. *J Control Release* 139(2):127–132
145. Li W, Nicol F, Szoka FC Jr (2004) GALA: a designed synthetic pH-responsive amphipathic peptide with applications in drug and gene delivery. *Adv Drug Deliv Rev* 56(7):967–985
146. Shin J, Shum P, Thompson DH (2003) Acid-triggered release via dePEGylation of DOPE liposomes containing acid-labile vinyl ether PEG-lipids. *J Control Release* 91(1–2):187–200
147. Ahmad A, Ranjan S, Zhang W, Zou J, Pyykko I, Kinnunen PK (2015) Novel endosomolytic peptides for enhancing gene delivery in nanoparticles. *Biochim Biophys Acta* 1848(2):544–553
148. Wolff JA, Rozema DB (2008) Breaking the bonds: non-viral vectors become chemically dynamic. *Mol Ther* 16:16–29
149. Rozema DB, Ekena K, Lewis DL, Loomis AG, Wolff JA (2003) Endosomolysis by masking of a membrane-active agent (EMMA) for cytoplasmic release of macromolecules. *Bioconjug Chem* 14(1):51–57
150. Meyer M, Zintchenko A, Ogris M, Wagner E (2007) A dimethylmaleic acid-melittin-polylysine conjugate with reduced toxicity, pH-triggered endosomolytic activity and enhanced gene transfer potential. *J Gene Med* 9(9):797–805
151. Murthy N, Campbell J, Fausto N, Hoffman AS, Stayton PS (2003) Bioinspired pH-responsive polymers for the intracellular delivery of biomolecular drugs. *Bioconjug Chem* 14(2):412–419
152. Knorr V, Allmendinger L, Walker GF, Painter FF, Wagner E (2007) An acetal-based PEGylation reagent for pH-sensitive shielding of DNA polyplexes. *Bioconjug Chem* 18(4):1218–1225
153. Rozema DB, Lewis DL, Wakefield DH et al (2007) Dynamic PolyConjugates for targeted in vivo delivery of siRNA to hepatocytes. *Proc Natl Acad Sci U S A* 104(32):12982–12987
154. Verkman AS (2002) Solute and macromolecule diffusion in cellular aqueous compartments. *Trends Biochem Sci* 27(1):27–33
155. Lukacs GL, Haggie P, Seksek O, Lechardeur D, Freedman N, Verkman AS (2000) Size-dependent DNA mobility in cytoplasm and nucleus. *J Biol Chem* 275(3):1625–1629
156. Lutdko JJ, Zhang G, Sebestyen MG, Wolff JA (1999) A nuclear localization signal can enhance both the nuclear transport and expression of 1 kb DNA. *J Cell Sci* 112(Pt 12):2033–2041
157. Mannisto M, Reinisalo M, Ruponen M, Honkakoski P, Tammi M, Urtti A (2007) Polyplex-mediated gene transfer and cell cycle: effect of carrier on cellular uptake and intracellular kinetics, and significance of glycosaminoglycans. *J Gene Med* 9(6):479–487
158. Tachibana R, Ide N, Shinohara Y, Harashima H, Hunt CA, Kiwada H (2004) An assessment of relative transcriptional availability from nonviral vectors. *Int J Pharm* 270(1–2):315–321
159. Hama S, Akita H, Iida S, Mizuguchi H, Harashima H (2007) Quantitative and mechanism-based investigation of post-nuclear delivery events between adenovirus and lipoplex. *Nucleic Acids Res* 35(5):1533–1543
160. Carlisle RC, Bettinger T, Ogris M, Hale S, Mautner V, Seymour LW (2001) Adenovirus hexon protein enhances nuclear delivery and increases transgene expression of polyethylenimine/plasmid DNA vectors. *Mol Ther* 4(5):473–483
161. Dean DA, Strong DD, Zimmer WE (2005) Nuclear entry of nonviral vectors. *Gene Ther* 12(11):881–890
162. Pollard H, Remy JS, Loussouarn G, Demolombe S, Behr JP, Escande D (1998) Polyethylenimine but not cationic lipids promotes transgene delivery to the nucleus in mammalian cells. *J Biol Chem* 273(13):7507–7511
163. Antoniou MN, Skipper KA, Anakok O (2013) Optimizing retroviral gene expression for effective therapies. *Hum Gene Ther* 24(4):363–374
164. Kim A, Pyykko I (2011) Size matters: versatile use of PiggyBac transposons as a genetic manipulation tool. *Mol Cell Biochem* 354(1–2):301–309
165. Pledger DW, Coates CJ (2005) Mutant Mos1 mariner transposons are hyperactive in *Aedes aegypti*. *Insect Biochem Mol Biol* 35(10):1199–1207
166. Kawakami K, Shima A, Kawakami N (2000) Identification of a functional transposase of the Tol2 element, an Ac-like element from the Japanese medaka fish, and its transposition in the zebrafish germ lineage. *Proc Natl Acad Sci U S A* 97(21):11403–1140

167. Horie K, Yusa K, Yae K et al (2003) Characterization of sleeping beauty transposition and its application to genetic screening in mice. *Mol Cell Biol* 23(24):9189–9207
168. Ivics Z, Hackett PB, Plasterk RH, Izsvák Z (1997) Molecular reconstruction of sleeping beauty, a *Tc1*-like transposon from fish, and its transposition in human cells. *Cell* 91(4):501–510
169. Fraser MJ, Smith GE, Summers MD (1983) Acquisition of host cell DNA sequences by baculoviruses: relationship between host DNA insertions and FP mutants of *Autographa californica* and *Galleria mellonella* nuclear polyhedrosis viruses. *J Virol* 47(2):287–300
170. Cary LC, Goebel M, Corsaro BG, Wang HG, Rosen E, Fraser MJ (1989) Transposon mutagenesis of baculoviruses: analysis of *Trichoplusia ni* transposon IFP2 insertions within the FP-locus of nuclear polyhedrosis viruses. *Virology* 172(1):156–169
171. Lobo N, Li X, Fraser MJ Jr (1999) Transposition of the piggyBac element in embryos of *Drosophila melanogaster*, *Aedes aegypti* and *Trichoplusia ni*. *Mol Gen Genet* 261(4–5):803–810
172. Thibault ST, Singer MA, Miyazaki WY et al (2004) A complementary transposon tool kit for *Drosophila melanogaster* using P and piggyBac. *Na Genet* 36(3):283–287
173. Elick TA, Bauser CA, Fraser MJ (1996) Excision of the piggyBac transposable element in vitro is a precise event that is enhanced by the expression of its encoded transposase. *Genetica* 98(1):33–41
174. Fraser MJ, Ciszczon T, Elick T, Bauser C (1996) Precise excision of TTAA-specific lepidopteran transposons piggyBac (IFP2) and tagalong (TFP3) from the baculovirus genome in cell lines from two species of Lepidoptera. *Insect Mol Biol* 5(2):141–151
175. Ding S, Wu X, Li G, Han M, Zhuang Y, Xu T (2005) Efficient transposition of the piggyBac (PB) transposon in mammalian cells and mice. *Cell* 122(3):473–483
176. Wu S, Ying G, Wu Q, Capecchi MR (2007) Toward simpler and faster genome-wide mutagenesis in mice. *Nat Genet* 39(7):922–930
177. Kawakami K (2007) Tol2: a versatile gene transfer vector in vertebrates. *Genome Biol* 8(Suppl 1):S7
178. Lacoste A, Berenshteyn F, Brivanlou AH (2009) An efficient and reversible transposable system for gene delivery and lineage-specific differentiation in human embryonic stem cells. *Cell Stem Cell* 5(3):332–342
179. Maragathavally KJ, Kaminski JM, Coates CJ (2006) Chimeric Mos1 and piggyBac transposases result in site-directed integration. *FASEB J* 20(11):1880–1882
180. Wu SC, Meir YJ, Coates CJ, Handler AM, Pelczar P, Moisyadi S, Kaminski JM (2006) piggyBac is a flexible and highly active transposon as compared to sleeping beauty, Tol2, and Mos1 in mammalian cells. *Proc Natl Acad Sci U S A* 103(41):15008–15013
181. Nienhuis AW, Dunbar CE, Sorrentino BP (2006) Genotoxicity of retroviral integration in hematopoietic cells. *Mol Ther* 13(6):1031–1049
182. Evans-Galea MV, Wielgosz MM, Hanawa H, Srivastava DK, Nienhuis AW (2007) Suppression of clonal dominance in cultured human lymphoid cells by addition of the cHS4 insulator to a lentiviral vector. *Mol Ther* 15(4):801–809
183. Skipper KA, Andersen PR, Sharma N, Mikkelsen JG (2013) DNA transposon-based gene vehicles—scenes from an evolutionary drive. *J Biomed Sci* 20:92
184. Plontke SK, Mynatt R, Gill RM, Borgmann S, Salt AN (2007) Concentration gradient along the scala tympani after local application of gentamicin to the round window membrane. *Laryngoscope* 117(7):1191–1198
185. Tan BT, Foong KH, Lee MM, Ruan R (2008) Polyethylenimine-mediated cochlear gene transfer in guinea pigs. *Arch Otolaryngol Head Neck Surg* 134(8):884–891
186. Jero J, Mhatre AN, Tseng CJ et al (2001) Cochlear gene delivery through an intact round window membrane in mouse. *Hum Gene Ther* 12(5):539–548
187. Crumling MA, Raphael Y (2006) Manipulating gene expression in the mature inner ear. *Brain Res* 109(1):265–269
188. Fekete DM, Muthukumar S, Karagogeos D (1998) Hair cells and supporting cells share a common progenitor in the avian inner ear. *J Neurosci* 18(19):7811–7821
189. Frolov MV, Dyson NJ (2004) Molecular mechanisms of E2F-dependent activation and pRB-mediated repression. *J Cell Sci* 117(Pt 11):2173–2181
190. Taylor R, Forge A (2005) Developmental biology. Life after deaf for hair cells? *Science* 307(5712):1056–1058
191. Lowenheim H, Furness DN, Kil J et al (1999) Gene disruption of p27(Kip1) allows cell proliferation in the postnatal and adult organ of corti. *Proc Natl Acad Sci U S A* 96(7):4084–4088
192. Chen P, Segil N (1999) p27(Kip1) links cell proliferation to morphogenesis in the developing organ of Corti. *Development* 126(8):1581–1590
193. White PM, Doetzlhofer A, Lee YS, Groves AK, Segil N (2006) Mammalian cochlear supporting

- cells can divide and trans-differentiate into hair cells. *Nature* 441(7096):984–987
194. Jones JM, Montcouquiol M, Dabdoub A, Woods C, Kelley MW (2006) Inhibitors of differentiation and DNA binding (Ids) regulate Math1 and hair cell formation during the development of the organ of Corti. *J Neurosci* 26(2):550–558
 195. Murphy JA, Clarke DB (2006) Target-derived neurotrophins may influence the survival of adult retinal ganglion cells when local neurotrophic support is disrupted: implications for glaucoma. *Med Hypotheses* 67(5):1208–1212
 196. Horton CD, Qi Y, Chikaraishi D, Wang JK (2001) Neurotrophin-3 mediates the autocrine survival of the catecholaminergic CAD CNS neuronal cell line. *J Neurochem* 76(1):201–209
 197. Ito J, Endo T, Nakagawa T, Kita T, Kim TS, Iguchi F (2005) A new method for drug application to the inner ear. *ORL J Otorhinolaryngol Relat Spec* 67(5):272–275
 198. Shibata SB, Cortez SR, Beyer LA, Wiler JA, Di Polo A, Pfingst BE, Raphael Y (2010) Transgenic BDNF induces nerve fiber regrowth into the auditory epithelium in deaf cochleae. *Exp Neurol* 223(2):464–472
 199. Rask-Andersen H, Bostrom M, Gerdin B, Kinnefors A, Nyberg G, Engstrand T, Miller JM, Lindholm D (2005) Regeneration of human auditory nerve. In vitro/in vivo demonstration of neural progenitor cells in adult human and guinea pig spiral ganglion. *Hear Res* 203(1–2):180–191
 200. Bostrom M, Khalifa S, Bostrom H, Liu W, Friberg U, Rask-Andersen H (2010) Effects of neurotrophic factors on growth and glial cell alignment of cultured adult spiral ganglion cells. *Audiol Neurotol* 15(3):175–186
 201. Oshima K, Senn P, Heller S (2009) Isolation of sphere-forming stem cells from the mouse inner ear. *Meth Mol Biol* 493:141–162
 202. Green SH, Bailey E, Wang Q, Davis RL (2012) The Trk A, B, C's of neurotrophins in the cochlea. *Anat Rec (Hoboken)* 295(11):1877–1895
 203. Zou J, Zhang Y, Sanjeev W, Sood R, Mikhailov A, Kinnunen P, Pyykkö I (2009) Internalization of liposome nanoparticles functionalized with TrkB ligand in rat cochlear cell population. *Eur J Nanomed* 2:9–14
 204. Ranjan R, Kholmovski EG, Blauer J et al (2012) Identification and acute targeting of gaps in atrial ablation lesion sets using a real-time magnetic resonance imaging system. *Circ Arrhythm Electrophysiol* 5(6):1130–1135
 205. Liu W, Glueckert R, Kinnefors A, Schrott-Fischer A, Bitsche M, Rask-Andersen H (2012) Distribution of P75 neurotrophin receptor in adult human cochlea—an immunohistochemical study. *Cell Tissue Res* 348(3):407–415
 206. Vega JA, San Jose I, Cabo R, Rodriguez S, Represa J (1999) Trks and p75 genes are differentially expressed in the inner ear of human embryos. What may Trks and p75 null mutant mice suggest on human development? *Neurosci Lett* 272(2):103–106
 207. Yu P, Zhang YP, Shields LB et al (2011) Inhibitor of DNA binding 2 promotes sensory axonal growth after SCI. *Exp Neurol* 231(1):38–44
 208. Rudnicki A, Isakov O, Ushakov K, Shavitzi S, Weiss I, Friedman LM, Shomron N, Avraham KB (2014) Next-generation sequencing of small RNAs from inner ear sensory epithelium identifies microRNAs and defines regulatory pathways. *BMC Genomics* 15:484
 209. Dash-Wagh S, Jacob S, Lindberg S, Fridberger A, Langel U, Ulfendahl M (2012) Intracellular delivery of short interfering RNA in rat organ of Corti using a cell-penetrating peptide PeppFect6. *Mol Ther Nucleic Acids* 1:e61
 210. Rybak LP, Mukherjea D, Jajoo S, Kaur T, Ramkumar V (2012) siRNA-mediated knockdown of NOX3: therapy for hearing loss? *Cell Mol Life Sci* 69(14):2429–2434
 211. Oishi N, Chen FQ, Zheng HW, Sha SH (2013) Intra-tympanic delivery of short interfering RNA into the adult mouse cochlea. *Hear Res* 296:36–41
 212. Oliveira S, Storm G, Schiffelers RM (2006) Targeted delivery of siRNA. *J Biomed Biotechnol* 2006(4):63675
 213. Marziano NK, Casalotti SO, Portelli AE, Becker DL, Forge A (2003) Mutations in the gene for connexin 26 (GJB2) that cause hearing loss have a dominant negative effect on connexin 30. *Hum Mol Genet* 12(8):805–812
 214. Maeda Y, Fukushima K, Nishizaki K, Smith RJ (2005) In vitro and in vivo suppression of GJB2 expression by RNA interference. *Hum Mol Genet* 14(12):1641–1650
 215. Pfannenstiel SC, Praetorius M, Plinkert PK, Brough DE, Staeker H (2009) Bcl-2 gene therapy prevents aminoglycoside-induced degeneration of auditory and vestibular hair cells. *Audiol Neurotol* 14(4):254–266
 216. Kakigi A, Nishimura M, Takeda T, Okada T, Murata Y, Ogawa Y (2008) Effects of gadolinium injected into the middle ear on the stria vascularis. *Acta Otolaryngol* 128(8):841–845
 217. Qin J, Asempah I, Laurent S, Fornara A, Muller RN, Muhammed M (2009) Injectable

- superparamagnetic ferrogels for controlled release of hydrophobic drugs. *Adv Mater* 21:1354–1357
218. Qin J, Laurent S, Suk JY, Roch A, Mikhaylova M, Bhujwalla ZM, Muller RN, Muhammed M (2007) A high-performance magnetic resonance imaging T2 contrast agent. *Adv Mater* 19:1874–1878
 219. Fornara A, Johansson P, Petersson K et al (2008) Tailored magnetic nanoparticles for direct and sensitive detection of biomolecules in biological samples. *Nano Lett* 8(10): 3423–3428
 220. Salazar-Alvarez G, Qin J, Sepelak V et al (2008) Cubic versus spherical magnetic nanoparticles: the role of surface anisotropy. *J Am Chem Soc* 130(40):13234–13239
 221. Laurent S, Forge D, Port M, Roch A, Robic C, Vander Elst L, Muller RN (2008) Magnetic iron oxide nanoparticles: synthesis, stabilization, vectorization, physicochemical characterizations, and biological applications. *Chem Rev* 108(6):2064–2110
 222. Poe P, Zou J, Zhang W, Qin J, Abo Ramadan U, Fornara A, Muhammed M, Pykkö I (2009) MRI of the cochlea with superparamagnetic iron oxide nanoparticles compared to gadolinium chelate contrast agents in a rat model. *Eur J Nanomed* 2:29–36
 223. Namgung R, Singha K, Yu MK, Jon S, Kim YS, Ahn Y, Park IK, Kim WJ (2010) Hybrid superparamagnetic iron oxide nanoparticle-branched polyethylenimine magnetoplexes for gene transfection of vascular endothelial cells. *Biomaterials* 31(14):4204–4213
 224. Mondalek FG, Zhang YY, Kropp B, Kopke RD, Ge X, Jackson RL, Dormer KJ (2006) The permeability of SPION over an artificial three-layer membrane is enhanced by external magnetic field. *J Nanobiotechnology* 4:4
 225. Plank C, Anton M, Rudolph C, Rosenecker J, Krotz F (2003) Enhancing and targeting nucleic acid delivery by magnetic force. *Expert Opin Biol Ther* 3(5):745–758
 226. Schillinger U, Brilla T, Rudolph C et al (2005) Advances in magnetofection—magnetically guided nucleic acid delivery. *J Mag Magnet Mat* 293(1):501–508, 228
 227. Feng H, Pykkö I, Zou J (2015) Hyaluronan up-regulation is linked to renal dysfunction and hearing loss induced by silver nanoparticles. *Eur Arch Otorhinolaryngol* 272(10): 2629–2642
 228. Zou J, Feng H, Mannerstrom M, Heinonen T, Pykkö I (2014) Toxicity of silver nanoparticle in rat ear and BALB/c 3T3 cell line. *J Nanobiotechnology* 12:52
 229. Kadlecova Z, Baldi L, Hacker D, Wurm FM, Klok HA (2012) Comparative study on the in vitro cytotoxicity of linear, dendritic, and hyperbranched polylysine analogues. *Biomacromolecules* 13(10):3127–3137
 230. Farcal L, Torres Andon F, Di Cristo L et al (2015) Comprehensive in vitro toxicity testing of a panel of representative oxide nanomaterials: first steps towards an intelligent testing strategy. *PLoS One* 10(5):e0127174
 231. Moss OR, Wong VA (2006) When nanoparticles get in the way: impact of projected area on in vivo and in vitro macrophage function. *Inhal Toxicol* 18(10):711–716
 232. Martinez-Gutierrez F, Boegli L, Agostinho A, Sanchez EM, Bach H, Ruiz F, James G (2013) Anti-biofilm activity of silver nanoparticles against different microorganisms. *Biofouling* 29(6):651–660
 233. Zou J, Hannula M, Misra S, Feng H, Labrador RH, Aula AS, Hyttinen J, Pykkö I (2015) Micro CT visualization of silver nanoparticles in the middle and inner ear of rat and transportation pathway after transtympanic injection. *J Nanobiotechnology* 13:5
 234. Schmidt-Wolf GD, Schmidt-Wolf IG (2003) Non-viral and hybrid vectors in human gene therapy: an update. *Trends Mol Med* 9(2):67–72
 235. Wang G, Uludag H (2008) Recent developments in nanoparticle-based drug delivery and targeting systems with emphasis on protein-based nanoparticles. *Expert Opin Drug Deliv* 5(5):499–515
 236. Thiele L, Rothen-Rutishauser B, Jilek S, Wunderli-Allenspach H, Merkle HP, Walter E (2001) Evaluation of particle uptake in human blood monocyte-derived cells in vitro. Does phagocytosis activity of dendritic cells measure up with macrophages? *J Control Release* 76(1-2):59–71
 237. Coester C, Nayyar P, Samuel J (2006) In vitro uptake of gelatin nanoparticles by murine dendritic cells and their intracellular localisation. *Eur J Pharm Biopharm* 62(3):306–314
 238. Godbey WT, Wu KK, Mikos AG (1999) Tracking the intracellular path of poly(ethylenimine)/DNA complexes for gene delivery. *Proc Natl Acad Sci U S A* 96(9):5177–5181
 239. Muller J, Huaux F, Moreau N et al (2005) Respiratory toxicity of multi-wall carbon nanotubes. *Toxicol Appl Pharmacol* 207(3):221–231
 240. Kobayashi N, Naya M, Ema M, Endoh S, Maru J, Mizuno K, Nakanishi J (2010) Biological response and morphological assessment of individually dispersed multi-wall carbon nanotubes in the lung after intratracheal instillation in rats. *Toxicology* 276(3): 143–153
 241. Yu T, Greish K, McGill LD, Ray A, Ghandehari H (2012) Influence of geometry,

- porosity, and surface characteristics of silica nanoparticles on acute toxicity: their vasculature effect and tolerance threshold. *ACS Nano* 6(3):2289–2301
242. Chen X, Zhouhua W, Jie Z, Xinlu F, Jinqiang L, Yuwen Q, Zhiying H (2015) Renal interstitial fibrosis induced by high-dose mesoporous silica nanoparticles via the NF-kappaB signaling pathway. *Int J Nanomed* 10:1–22
 243. Kim YS, Song MY, Park JD et al (2010) Subchronic oral toxicity of silver nanoparticles. Part Fibre Toxicol 7:20
 244. Schlinkert P, Casals E, Boyles M et al (2015) The oxidative potential of differently charged silver and gold nanoparticles on three human lung epithelial cell types. *J Nanobiotechnol* 13:1
 245. Mantovani A, Sica A, Sozzani S, Allavena P, Vecchi A, Locati M (2004) The chemokine system in diverse forms of macrophage activation and polarization. *Trends Immunol* 25(12):677–686
 246. Liao X, Sharma N, Kapadia F et al (2011) Kruppel-like factor 4 regulates macrophage polarization. *J Clin Invest* 12(7):2736–2749
 247. Mantovani A, Sozzani S, Locati M, Allavena P, Sica A (2002) Macrophage polarization: tumor-associated macrophages as a paradigm for polarized M2 mononuclear phagocytes. *Trends Immunol* 23(11):549–555
 248. Mukherjee D, Royce SG, Sarkar S et al (2014) Modeling in vitro cellular responses to silver nanoparticles. *J Toxicol* 2014:852890
 249. Vallhov H, Qin J, Johansson SM, Ahlborg N, Muhammed MA, Scheynius A, Gabrielsson S (2006) The importance of an endotoxin-free environment during the production of nanoparticles used in medical applications. *Nano Lett* 6(8):1682–1686
 250. Jeschke M, Moser T (2015) Considering optogenetic stimulation for cochlear implants. *Hear Res* 322:224–234
 251. von Ilberg C, Kiefer J, Tillein J, Pfenningdorff T, Hartmann R, Sturzebecher E, Klinke R (1999) Electric-acoustic stimulation of the auditory system. New technology for severe hearing loss. *ORL J Otorhinolaryngol Relat Spec* 61(6):334–340
 252. Haake SM, Dinh CT, Chen S, Eshraghi AA, Van De Water TR (2009) Dexamethasone protects auditory hair cells against TNFalpha-initiated apoptosis via activation of PI3K/Akt and NFkappaB signaling. *Hear Res* 255(1–2):22–32
 253. Strecker H, Jolly C, Garnham C (2010) Cochlear implantation: an opportunity for drug development. *Drug Discov Today* 15(7–8):314–21255
 254. Hansen S, Mlynářík R, Volkenstein S, Stark T, Schwaab M, Dazert S, Brors D (2009) Growth behavior of spiral ganglion explants on cochlear implant electrodes and their materials. *HNO* 57(4):358–363
 255. Shepherd RK, Coco A, Epp SB (2008) Neurotrophins and electrical stimulation for protection and repair of spiral ganglion neurons following sensorineural hearing loss. *Hear Res* 242(1–2):100–109
 256. Jolly C, Garnham C, Mirzadeh H, Truy E, Martini A, Kiefer J, Braun S (2010) Electrode features for hearing preservation and drug delivery strategies. *Adv Otorhinolaryngol* 67:28–42
 257. Ibrahim HN, Truy E, Bossard D, Hessler R, Jolly C (2010) Disposable drug delivery catheter for use in cochlear implantation: radiological study in cadaver temporal bones. *Cochlear Implants Int* 11(Suppl 1):431–433
 258. Richardson RT, Wise AK, Andrew JK, O'Leary SJ (2008) Novel drug delivery systems for inner ear protection and regeneration after hearing loss. *Expert Opin Drug Deliv* 5(10):1059–1076
 259. Fiering J, Mescher MJ, Leary Swan EE et al (2009) Local drug delivery with a self-contained, programmable, microfluidic system. *Biomed Microdevices* 11(3):571–578
 260. Zou J, Zhang W, Poe D et al (2010) MRI manifestation of novel superparamagnetic iron oxide nanoparticles in the rat inner ear. *Nanomedicine (Lond)* 5(5):739–754

Part VI

Screening of Cells and Bioactive Compounds

Chapter 22

Development of Cell-Based High-Throughput Chemical Screens for Protection Against Cisplatin-Induced Ototoxicity

Tal Teitz, Asli N. Goktug, Taosheng Chen, and Jian Zuo

Abstract

Various compounds have been tested in recent years for protection against cisplatin-induced hearing loss, but no compound has yet been FDA approved for clinical use in patients. Towards this goal, we developed an unbiased, high-throughput, mammalian cochlear cell-based chemical screen that allowed quantification of the protection ability of bioactive compounds and ranked them for future testing ex vivo in cochlear explant cultures and in vivo in animal models. In our primary screens, protection in the HEI-OC1 organ of Corti immortalized cell line was measured by the ability of each compound to inhibit caspase-3/7 activity triggered by cisplatin treatment (50 μ M cisplatin for 22 h). A total of 4385 unique bioactive compounds were tested in a single dose of 8 μ M and promising compounds were validated by dose response curves covering ten, 1:3 serial diluted concentrations. Primary hits were defined as having more than 60 % inhibition of the caspase-3/7 activity. Toxicity of the top compounds was measured by a CellTiter-Glo (CTG) assay that measured the viability of the cells in the presence of compound alone in similar dose responsive analysis. A combination of the caspase-3/7 inhibition activity assay (as measured by IC₅₀) and the CTG viability assay (as determined by LD₅₀) identified the top protective compounds in the HEI-OC1 cells. In the future, the top hits in our screens will be tested for their protective ability ex vivo in mouse cochlear explants and in vivo in animal models. Our mammalian cochlear cell-based, high-throughput chemical screening assays described here can be further modified and represent an initial successful step towards therapeutic intervention of hearing disorders, an unmet medical need of our society.

Key words Cisplatin, HEI-OC1 cells, Hair cells, Caspase 3/7-Glo assay, Cell Titer Glo viability assay, IC₅₀, LD₅₀

1 Introduction

High-throughput screening (HTS) of bioactive compound libraries has become a hallmark technique for picking potential drugs for diseased states [1–3]. Cell-based screens allow the feasibility of testing large amount of compounds in a single assay and are widely used in the pharmaceutical sector to identify novel chemical entities for drug discovery. In the hearing field specifically, screens have been used for testing compounds with potential for regeneration

or protection capacities against insults such as chemotherapy and aminoglycosides. Recently, Walters et al. screened for p27^{Kip1} transcriptional inhibitors to enhance regeneration of supporting cells in the ear by employing HeLa cells transfected with a luciferase reporter plasmid driven by the p27^{Kip1} promoter [4] and Edge et al. had used the embryonic kidney cell line (HEK) expressing a luciferase gene controlled by an Atoh1 enhancer and promoter sequences to screen for compounds activating Atoh1 gene expression in cells and thereby increasing regeneration [5]. More recently, murine cochlear micro-explants have been directly used for a medium-throughput screen for protective compounds against aminoglycoside ototoxicity [6]. Interestingly, screens for protective compounds against ototoxic insults have been successfully performed in zebrafish model systems for identifying compounds that can protect the lateral line neuromasts from aminoglycosides [7–9] or cisplatin [9–11].

Screens in the present study were designed for identifying compounds that can protect mammalian inner ear cells from the ototoxic effect of cisplatin. We aimed to conduct an unbiased, large-scale screen and for that reason chose an inner ear cochlear cell line HEI-OC1 [12] to perform the screen. The screen was designed for 384-well microplate format by utilizing a state-of-the-art HTS platform with the aid of a robot. Two separate assays were performed sequentially on the same day for each compound tested: the Caspase-Glo 3/7 activity assay and the CellTiter-Glo (CTG) viability assay. The caspase-3/7 activity assay measured the ability of the test compounds to inhibit the Caspase-3/7 activity induced by cisplatin treatment after 22 h co-incubation while the CTG assay recorded the viability of the cells after 22 h incubation with the test compounds alone. Consistency and reproducibility of each assay measured by the Z'-factor parameter was of utmost importance to assure confidence in the results [13]. Interestingly, while most HTS screens, such as the screens described above, involved addition of one test compound to cells (per well) to test its effects, the screens described here involved addition of two separate drugs (i.e., cisplatin and a test compound), and thus required double attention to ensure consistency in time and reproducibility of drug delivery to the cells.

1.1 Cisplatin Otoprotection

Cisplatin (cis-diamminedichloroplatinum II) is one of the most widely used drugs in oncologic therapy in both pediatric and adult age groups. It is used clinically for head and neck, lung, bladder, cervical, ovarian, testicular, and gastrointestinal cancers as well as childhood cancers such as neuroblastoma and medulloblastoma [14]. One of its major side effects is irreversible sensorineural hearing loss that occurs with an average incidence of 62 % of patients treated with cisplatin [15]. Several molecular pathways have been implicated in cisplatin-induced ototoxicity in the ear with

generation of reactive oxygen species (ROS), MAPK signaling pathways and activation of caspases as critical events in the process [16–19]. There is substantial overlap among the biological pathways involved in cisplatin-, aminoglycoside-, and noise-induced hearing loss [20, 21] and many compounds tested for one of these insults have shown some protective effects for the other insults. Thus, we hypothesized that screening drugs that protect against cisplatin ototoxicity will also protect against aminoglycoside- and noise-induced hearing loss. Moreover, we hypothesized that mammalian-specific screens will effectively yield more protective compounds than screens in zebrafish, a lower vertebrate species. Finally, there are currently no other cochlear derived cells that are more suitable than HEI-OC1 cells for such a large-scale high-throughput screen and we believe that subsequent characterization of a limited number of initial hit compounds in murine cochlear explants can circumvent many undesired compromising properties of HEI-OC1 cells.

1.2 Inhibition of Caspase-3 Activation: Screening Against Cell Death in the Inner Ear

Caspase-3 activation is an important downstream molecular event known to occur in the majority of cellular pathways leading to cell death (apoptosis) including in the inner ear cells [22, 23]. Previous work has shown that inhibition of caspases, for example by zVAD-FMK, an irreversible general caspase inhibitor, confers robust protection against cisplatin-induced cell death [22]. For this screen, we chose caspase-3/7 activity as the endpoint readout indicating cisplatin-induced cell death, as it would allow us to detect inhibition of cell death at any molecular cellular target upstream of caspase-3/7 cleavage in the HEI-OC1 cell line.

1.3 HEI-OC1 Cells

These cells can be used to measure death induced by cisplatin in cochlear hair cells, and we utilized the HEI-OC1 immortalized inner ear cell line isolated originally from P7 organs of Corti of the Immortomouse [12]. Despite some undesired properties, this cell line has been shown to serve as a good model of inner ear cells [24], and we have independently confirmed by qRT-PCR that the cells we used in this screen express the reported hair cell markers Myo6 and Myo7a. Currently no other cell lines from the mammalian inner ear have been characterized suitable for HTS.

1.4 Positive Reference and Quality Control Compounds for Screening

For the Caspase-3/7-Glo assay, we utilized compound Pifithrin- α [25, 26] as a positive reference compound, as it provided good protection against cisplatin ototoxicity by inhibiting caspase-3 cleavage at an IC₅₀ of 17 μ M. Another positive reference compound that was also identified as a hit in our screen is zVAD-FMK, a known general irreversible inhibitor of caspases. The dose responses for the compounds Pifithrin- α and zVAD-FMK in the two assays are shown in Fig. 1. The quality control compounds in the screens (positive and negative control compound for each screen) are indicated in Fig. 2.

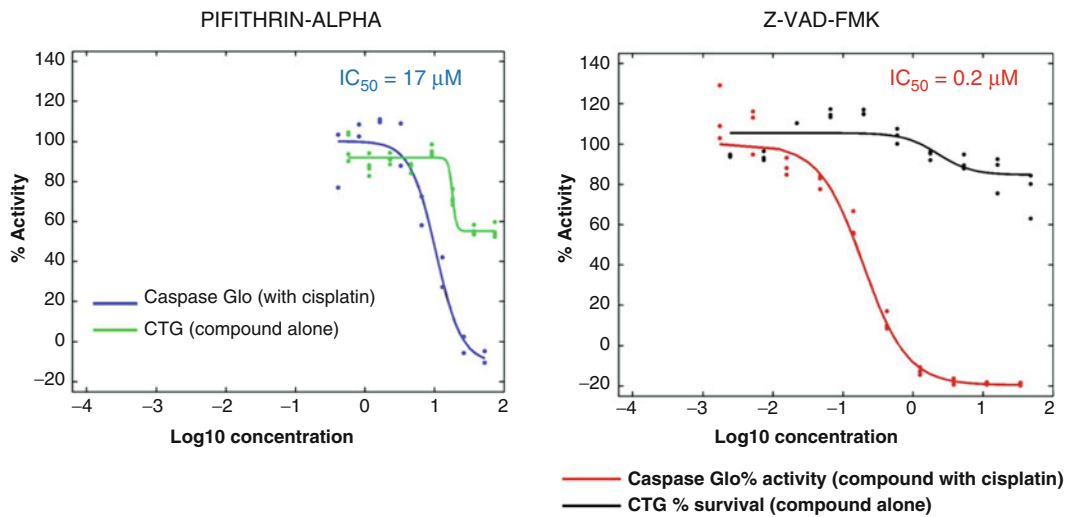


Fig. 1 Positive reference control compound in the screen was Pifithrin- α that was included in each screening plate and positive compound that came up as a hit in the screen was zVAD-FMK, a known general inhibitor of caspases

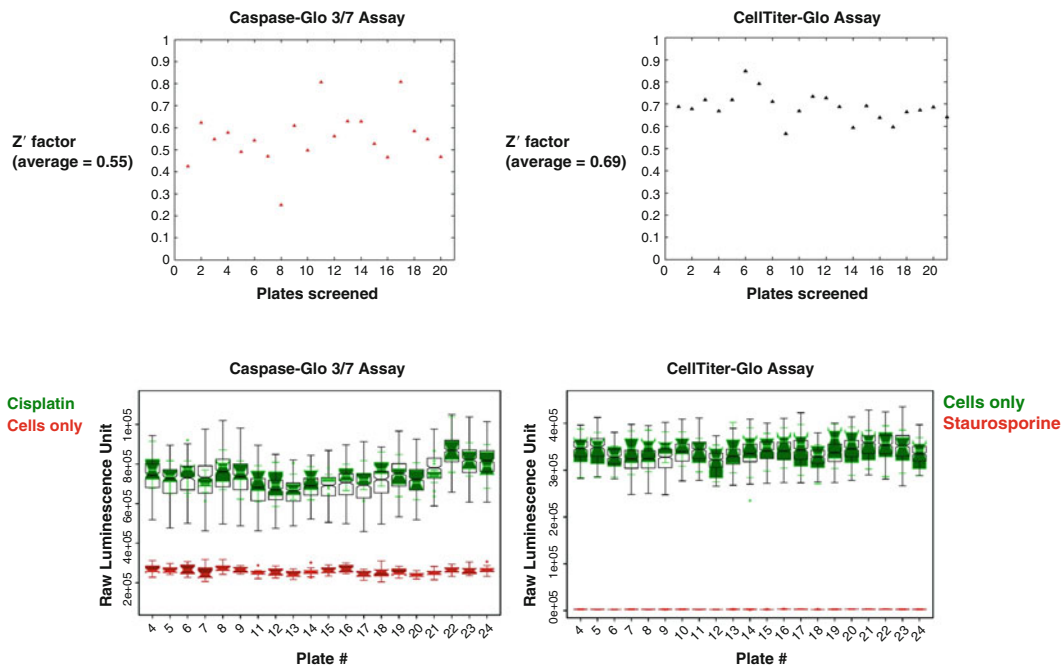


Fig. 2 Screen quality controls from a representative dose-response screen: Caspase-Glo 3/7 and CellTiter-Glo assays were performed sequentially on the same day and Z'-factors were determined for each plate screened. Compounds were tested in triplicates

1.5 Screen Optimization and Validation

Before starting the automated HTS, we optimized assay conditions in small-scale experiments performed off-deck including the assessment of best cell seeding density (1600 cells/well in 25 μL

media), best cisplatin concentration (50 µM, which gave the peak caspase 3/7 activity in the dose-response curve), optimum assay incubation time after cisplatin addition (22 h at 33 °C, 10 % CO₂, gave the highest caspase-3/7 activity in the assay), the highest Dimethyl sulfoxide (DMSO) concentration that would not affect cisplatin's caspase-3/7 activity (0.5 %) and concentration of the positive control compound Pifithrin-α. We validated the linearity of Caspase-Glo 3/7 and CTG assays to be within the detection range of our plate reader and verified that 0.5 % DMSO had no effect on cell death kinetics. After optimization of the screening conditions, validation of the assay performance using automated laboratory instruments and robotics was performed according to the HTS Assay Validation guidelines provided in the Assay Guidance Manual by Eli Lilly & Company and the National Center for Advancing Translational Sciences [27, 28].

2 Materials

2.1 HEI-OC1 Cell Growth Reagents

1. Phosphate-buffered saline (PBS), pH 7.4.
2. Dulbecco modified Eagle's medium (DMEM, Gibco, Gaithersburg, MD, cat. no. 11995-065).
3. Fetal bovine serum (FBS)
4. Interferon-gamma from mouse (Sigma-Aldrich, St Louis, MO).
5. Ampicillin.
6. Trypsin-EDTA (0.25 %).

2.2 Control and Test Compounds

1. Dimethyl sulfoxide (DMSO); cell culture tested.
2. 2500 µM cisplatin stock solution in PBS:cis-diammineplatinum(II) dichloride (powder, Sigma cat no. 479306). Weigh and dissolve cisplatin powder on day of screening to final concentration of 2500 µM in PBS by incubating 30 min at 37 °C. Use this cisplatin stock solution within 24 h of preparation to ensure stability (*see Note 1*).
3. Cisplatin dilutions for Caspase-Glo 3/7 screening: Dilute 2500 µM cisplatin stock solution using DMEM to final concentration of 50 µM in the cells' wells (Add 10 µL volume cisplatin solution with the help of a WellMate dispenser to 25 µL volume of cells).
4. Pifithrin-α (Enzo Life Sciences, Farmingdale, NY). Dissolve in DMSO for making stock solutions in the range of 60–17 mM and dilute with Pintool to the final concentrations needed for the cells' wells.
5. Staurosporine (Selleck Chemicals, Houston, TX): Prepare 25 mM stock solution in DMSO.

6. Test compound Library: In the primary screens, use 5–10 mM compound stock solutions dissolved in 100 % DMSO and aliquot to compound plates (10–15 µL/well) to get final concentration of ~8 µM. In secondary screens, generate dose response curves by using ten 1:3 dilutions of the primary compound stock solutions to get final concentrations in the plate wells in the range of ~40 µM to ~2 nM.

2.3 Equipment and Reagents

1. Fully automated HighRes HTS platform that involves a 6-axis Staubli robot arm.
2. Pintool compound transfer device.
3. Three Matrix WellMate reagent dispensers (Thermo Scientific, Waltham, MA).
4. BigBear orbital shaker.
5. Agilent VSpin microplate centrifuge.
6. Perkin Elmer EnVision plate reader to perform screens. Validate automation instrument performance prior to screens and monitor throughout the runs for an error-free operation [29].
7. Assay microplates for plating HEI-OC1 cells: 384-well, flat, solid-bottom, white, tissue-culture treated, polystyrene (Corning, Corning, NY). Give microplates unique barcode numbers to allow easy tracking.
8. Compound plates: Clear, v-bottom, polypropylene 384-well plates (Corning).
9. Caspase-Glo 3/7 luminescent assay (Promega, Madison, WI).
10. CellTiter-Glo luminescent cell viability assay (Promega).

3 Methods

1. Grow HEI-OC1 cells prior to screening in DMEM with 10 % FBS, 45 µg/mL ampicillin, and 25 U/mL Mouse interferon-gamma at 33 °C in a 10 % CO₂ incubator as described by Kalenic et al. [12].
2. For screening seed HEI-OC1 cells in 384-wells plates, 1600 cells/well in volume of 25 µL, in media without interferon-gamma and incubate for 24 h at 33 °C in a 10 % CO₂ incubator (*see Note 2*).
3. Include in the screens negative and positive quality control compounds for each assay (*see Note 3* and Fig. 2).
4. Additionally, in the caspase-Glo 3/7 assay, include a dose response of the positive reference compound Pifithrin-alpha in each cell plate (*see Note 4*) and a control cell plate for the cis-platin dose response (*see Note 5*).

5. Conduct screen campaign in two steps: primary screen and secondary dose-response screen. Carry out primary screen at a single test compound concentration (~8 μ M), which is then followed by a confirmatory dose-response screen of the “hit” compounds. Perform the primary screen only with the Caspase-Glo 3/7 assay (*see Note 6*) in single copy, due to the large number of compounds to be tested. Perform the dose-response screen sequentially on the same day with both caspase 3/7 and CTG assays (*see Note 7*) in triplicate and with 10 compound concentrations (1:3 serially diluted). The main steps of the caspase-Glo 3/7 and the CTG viability screens are summarized in Figs. 3 and 4 and detailed in Subheading 3, steps 6–12.
6. A day after plating the HEI-OC1 cells, transfer test compounds to the assay plates with a 384-well pintoool device at ~30 nL/well to give a final concentration of ~8 μ M in the primary screen or final concentrations of ~40 μ M to ~2 nM in the dose response screen.
7. In the Caspase-Glo 3/7 assay, follow this step immediately by the addition of 10 μ L of cisplatin solution to each well using an 8-channel reagent dispenser to give a final concentration of 50 μ M cisplatin with the final assay volume of 35 μ L. In the CTG viability assay no cisplatin is added, leaving the assay volume at 25 μ L/well, in order to test the toxicity of the test compounds alone.

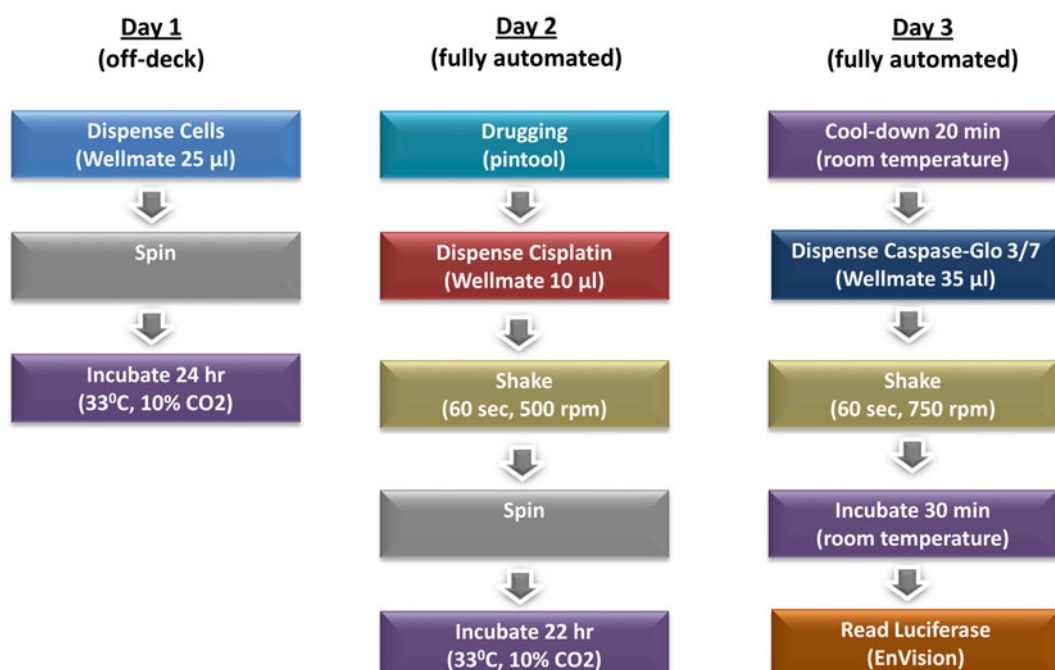


Fig. 3 Screening workflow for the Caspase-Glo 3/7 assay. Final assay volume per well: 35 μ L

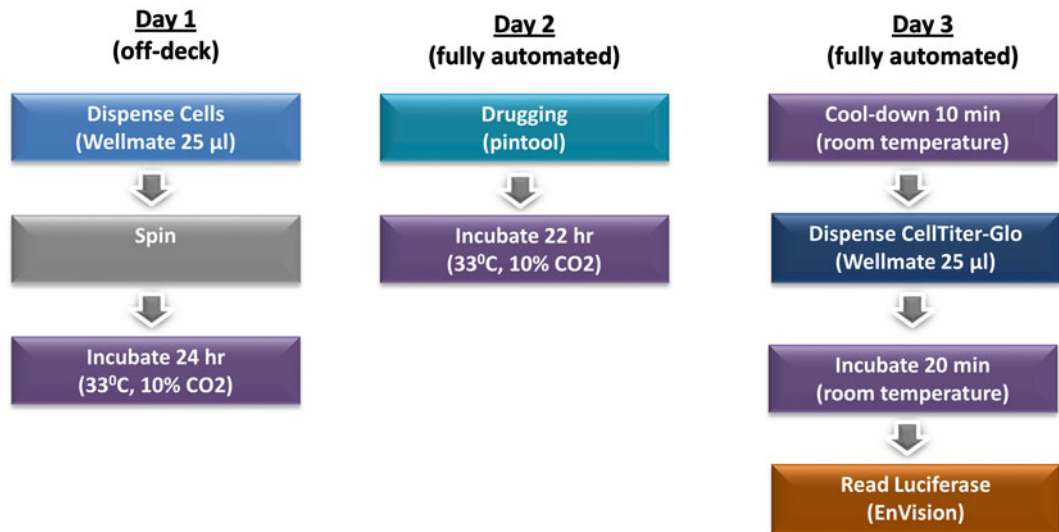


Fig. 4 Screening workflow for the CellTiter-Glo assay. Final assay volume per well: 25 μ L

8. In the Caspase-Glo 3/7 assay, after adding cisplatin shake the 384-well cells plates for 60 s at 500 RPM in a Bigbear orbital shaker and spin to enhance assay reproducibility (*see Note 8*).
9. Incubate cell plates from both assays, Caspase-3/7 and CTG, with the test compounds for 22 h at 33 °C in a 10 % CO₂ incubator.
10. Bring Caspase-Glo 3/7 assay solution to room temperature. Add 35 μ L of solution to an equal volume of cells using a WellMate dispenser. Shake the cell plates for 1 min at 750 RPM in an orbital shaker. Read luciferase assay in an EnVision plate reader 30 min after addition of the Caspase-Glo 3/7 reagent to the cells.
11. Bring CTG Assay reagent to room temperature. Add 25 μ L of this reagent to an equal volume of cells using a WellMate dispenser. Read Luciferase assay in the EnVision plate reader 20 min after addition of the CTG reagent to the cells.
12. Calculate Z'-factor for each screen and perform percent activity normalization [30] to select “hit” compounds using the positive and negative control conditions with 60 % “hit cut-off” in the primary screen (*see Note 9*). Calculate IC₅₀ and LD₅₀ for each compound in the dose response screens to identify promising “hit” compounds (*see Note 10*).

4 Notes

1. Cisplatin is inactive in the presence of high DMSO concentrations, so for that reason special attention is given to dissolve cisplatin in PBS and not DMSO and to add it to the cells independently of the tested compounds, which are dissolved in DMSO. In all screen wells, DMSO concentration are never above 0.5 %, a concentration that we found to not have impact on cisplatin's ability to induce caspase-3/7 activity in this assay.
2. Plating to the 384-well plates in the screen is done in media containing no interferon-gamma to slow cells' growth and mimic more closely the non-proliferative and post mitotic state of hair cells *in vivo*. Also, we filter the HEI-OC1 cells' suspension through a 70 µm sterile filter, after applying Trypsin-EDTA solution and before plating to the 384-well screening plates. The aim, here, is to obtain a single cell suspension and thus plating a consistent number of cells in each well.
3. For the Caspase-Glo 3/7 primary screen, cisplatin (50 µM) and DMSO (0.08 %) are used as positive and negative controls for caspase 3/7 activations, respectively. In the dose-response screen, the negative control can be modified to 0.35 % DMSO to accommodate for larger volumes of test compounds. For the CTG assay, staurosporine at a final concentration of 20 µM is used as a positive control, since it causes 100 % cell death at the 22 h time point, and 0.49 % DMSO is used as a negative control with 100 % cell viability.
4. Pifithrin- α , a small molecule that inhibits p53, was shown to suppress the expression of p53, and caspases-3 and -1 in mouse cochlear explants [25, 26]. Pifithrin- α was shown in previous studies to confer reasonable protection from cisplatin-induced death in cell lines and, importantly, in mouse cochlear explants at concentrations of 20–100 µM [25, 26], although at these doses it was reported to damage the hair cells' stereocilia.
5. For quality control in the Caspase-Glo 3/7 assay, include in every run a cisplatin dose response plate of the HEI-OC1 cells: ten, 1:2 dilutions of cisplatin stock solutions from concentrations of 1.75–900 µM are manually added to a HEI-OC1 cell plate (10–25 µL volume in well plate) to create a dose response for the specific day of the screen.
6. Caspase-Glo 3/7 assay—Assay that measures the luminescence light emitted as a result of cleavage of a substrate, containing the caspase-3/7 DEVD site and suitable for HTS for caspase-3/7 activity. IC₅₀ of a compound is identified as the concentration that inhibits 50 % of caspase-3/7 activity induced by 50 µM of cisplatin after 22 h of incubation.

7. Cell Titer Glo assay—Assay that measures the amount of ATP released from live cells as a result of a luminescence reaction and is suitable for HTS. LD₅₀ is identified as the dose of a compound that causes death of 50 % of the cells induced by 50 µM of cisplatin after 22 h incubation.
8. The spinning and shaking steps of the plates described in this protocol are important in increasing reproducibility and consistency of the screen (achieving high Z'-factor values).
9. In-house analysis software is used to perform percent activity normalizations and to calculate the IC₅₀ and LD₅₀ of the compounds from the dose response curves. In addition, we recommend visualizing by the naked eyes the Hill plots of each compound to ensure an appropriate sigmoidal curve is generated in the tested concentration range before deciding the correct IC₅₀ and LD₅₀ Hill coefficient in the two assays. We screened more than 8000 compounds (most compounds have more than one copy in the library, total 4385 unique bioactive compounds) in the primary screen, while >150 unique compounds were followed up for dose-response experiments.
10. This screen was utilized four separate times in the last two years, screening >8000 compounds and each time obtaining reproducible and consistent results, with Z'-factor averages of 0.55 and 0.69 for caspase-3/7 and CTG viability assays, respectively. Thus, we hope this test will prove useful for investigators in the auditory field in screening potential compounds against cisplatin and other forms of ototoxicity.

Acknowledgments

This work was supported in part by grants from the NIH (DC006471, CA21765, DC013879), the Office of Naval Research (N00014-12-1-0191, N00014-12-1-0775, N00014-09-1-1014) and the American Lebanese Syrian-Associated Charities of St. Jude Children's Research Hospital. We thank Drs. Federico Kalinec and Gilda Kalinec at the House Research Institute for providing the HEI-OC1 cells.

References

1. Macarron R, Banks MN, Bojanic D et al (2011) Impact of high-throughput screening in biomedical research. *Nat Rev Drug Discov* 10:88–195
2. Sharma LK, Leonardi R, Lin W (2015) A high-throughput screen reveals new small-molecule activators and inhibitors of Pantothenate kinases. *J Med Chem* 58:1563–1568
3. Wang P, Alvarez-Perez J, Felsenfeld DP et al (2015) A high-throughput screen reveals that harmine-mediated inhibition of DYRK1A increases human pancreatic beta cell replication. *Nat Med* 21:383–390

4. Walters JB, Lin W, Diao S et al (2014) High-throughput screening reveals alsterpaullone, 2-cyanoethyl as a potent p27Kip1 transcriptional inhibitor. PLOS One 9:e91173
5. Edge A et al (2013) Patent: small molecule compounds to treat hearing loss. International publication number WO 2013/126805 A2
6. Ryals M, Pak K, Ryan A (2015) Kinase inhibitor library screen to identify targets involved in aminoglycoside-induced ototoxic damage to murine organ of Corti. ARO 38th annual meeting PS-293, 38:176–177
7. Ou HC, Cunningham LL, Francis SP, Brandon CS, Simon JA, Raible DW, Rubel EW (2009) Identification of FDA-approved drugs and bioactives that protect hair cells in the zebrafish (*Danio rerio*) lateral line and mouse (*Mus musculus*) utricle. J Assoc Res Otolaryngol 10:191–203
8. Ou HC, Santos F, Raible DW, Simon JA, Rubel EW (2010) Drug screening for hearing loss: using the zebrafish lateral line to screen for drugs that prevent and cause hearing loss. Drug Discovery Today 15:265–271
9. Vlasits AL, Simon JA, Raible DW, Rubel EW, Owens KN (2012) Screen of FDA-approved drug library reveals compounds that protect hair cells from aminoglycosides and cisplatin. Hear Res 294:153–165
10. Ou H, Simon JA, Rubel EW, Raible DW (2012) Screening for chemicals that affect hair cell death and survival in the zebrafish lateral line. Hear Res 288:58–66
11. Niihori M, Platto T, Igarashi S et al (2015) Zebrafish swimming behavior as a biomarker for ototoxicity-induced hair cell damage: a high-throughput drug development platform targeting hearing loss. Transl Res. 166(5): 440–450
12. Kalenic GM, Webster P, Lim DJ, Kalenic F (2003) A cochlear cell line as an in vitro system for drug ototoxicity screening. Audiol Neurootol 8:177–189
13. Zhang JH, Chung TD, Oldenburg KR (1999) A simple statistical parameter for use in evaluation and validation of high throughput screening assays. J Biomol Screen 4(2):67–73
14. Chirites F, Albu S (2014) Prevention and restoration of hearing loss associated with the use of cisplatin. BioMed Res Int. doi:[10.1155/2014/925485](https://doi.org/10.1155/2014/925485)
15. Marshak T, Steiner M, Kaminer M, Levy L, Shupak A (2014) Prevention of cisplatin-induced hearing loss by intratympanic dexamethasone: a randomized controlled study. Otolaryngol Head Neck Surg 150:983–990
16. Mukherjea D, Rybak LP, Sheehan KE, Kaur T, Ramkumar V, Jajoo S, Sheth S (2011) The design and screening of drugs to prevent acquired sensorineural hearing loss. Expert Opin Drug Discov 6:491–505
17. Schacht J, Talaska AE, Rybak LP (2012) Cisplatin and aminoglycosides antibiotics: hearing loss and its prevention. Anat Rec 295:1837–1850
18. Wong ACY, Ryan AF (2015) Mechanisms of sensorineural cell damage, death and survival in the cochlea. Front Aging Neurosci 7:58
19. Casares C, Ramirez-Camacho R, Trinidad A, Roldan A, Jorge E, Garcia-Berrocal JR (2012) Reactive oxygen species in apoptosis induced by cisplatin: review of physiopathological mechanisms in animal models. Eur Arch Otorhinolaryngol 269:2455–2459
20. Rybak LP, Ramkumar V (2007) Ototoxicity. Kidney Int 72:931–935
21. Forge A, Van De Water TR (2008) Protection and repair of inner ear sensory cells. In: Salvi RJ, Popper AN, Fay RR (eds) Hair cell regeneration, repair, and protection. Springer Science, New York, pp 199–256
22. Liu W, Staeker H, Stupak H, Malgrange B, Lefebvre P, Van De Water TR (1998) Caspase inhibitors prevent cisplatin-induced apoptosis of auditory sensory cells. Neuroreport 9:2609–2614
23. Yakovlev AG, Faden AI (2001) Caspase-dependent apoptotic pathways in CNS injury. Mol Neurobiol 24:131–144
24. Kim H, Lee J, Kim S et al (2010) Roles of NADPH oxidases in cisplatin-induced reactive oxygen species generation and ototoxicity. J Neurosci 30:3933–3946
25. Zhang M, Liu W, Ding D, Salvi R (2003) Pifithrin- α suppresses p53 and protects cochlear and vestibular hair cells from cisplatin-induced apoptosis. Neuroscience 120: 191–205
26. Ding D, Allman BL, Salvi R (2012) Review: ototoxic characteristics of platinum antitumor drugs. Anat Rec 295:1851–1867
27. Iversen PW, Beck B, Chen Y-F et al (2004) HTS assay validation. In: Sittampalam GS, Gal-Edd N, Arkin M et al (eds) Assay guidance manual [Internet]. Eli Lilly & Co. and the National Center for Advancing Translational Sciences, Bethesda, MD. <http://www.ncbi.nlm.nih.gov/books/NBK83783/>. Accessed 29 Sept 2014
28. Chai SC, Goktug AN, Chen T (2015) Assay validation in high throughput screening—

- from concept to application. In: Vallisuta O (ed) Drug discovery and development—from molecules to medicine. InTech, Rijeka, Croatia
29. Chai SC, Goktug AN, Cui J, Low J, Chen T (2013) Practical considerations of liquid handling devices in drug discovery. In: El-Shemy H (ed) Drug discovery. InTech, Rijeka, Croatia
30. Goktug AN, Chai SC, Chen T (2013) Data analysis approaches in high throughput screening. In: El-Shemy H (ed) Drug discovery. InTech, Rijeka, Croatia

Chapter 23

Profiling Specific Inner Ear Cell Types Using Cell Sorting Techniques

**Taha A. Jan, Lina Jansson, Patrick J. Atkinson,
Tian Wang, and Alan G. Cheng**

Abstract

Studies of specific tissue cell types are becoming increasingly important in advancing our understanding of cell biology and gene and protein expression. Prospective isolation of specific cell types is a powerful technique as it facilitates such investigations, allowing for analysis and characterization of individual cell populations. Such an approach to studying inner ear tissues presents a unique challenge because of the paucity of cells of interest and limited cell markers. In this chapter, we describe methods for selectively labeling and isolating different inner ear cell types from the neonatal mouse cochlea using fluorescence-activated cell sorting.

Key words Inner ear, Single cell analysis, Fluorescence-activated cell sorting, Profiling

1 Introduction

The inner ear auditory and vestibular organs comprise heterogeneous cell types with diverse functional and morphological features. The regional differences of the cochlea (apex versus base) and the utricle (striola versus extrastriola) at various ages create additional layers of complexity, and opportunities to dissect differences of individual cell populations. Most studies have relied on histological and electrophysiological techniques to delineate such regional difference. In addition, studies using microdissection to manually separate the cochlear domains have revealed distinct profiles of gene expression and cell behavior [1–3]. Thus, the next frontier in probing the biology of the inner ear involves resolving the differences of specific cell types at a more refined level.

There exists a variety of techniques for isolating distinct cell types, including those based on size and density using gradient centrifugation [4], immunopanning [5], magnetic beads [6], and flow cytometry. In order to investigate different cell types, others

and we have demonstrated the use of fluorescence-activated cell sorting (FACS) to study cell behavior using a variety of culturing conditions [7, 8], gene expression profiling [9, 10], or proteomic analyses [11]. While the use of FACS for these applications is not novel in other organ systems, the poor viability and paucity of cochlear cells present unique challenges.

Here, we describe the use of FACS to isolate subpopulations of cochlear cell types based on cell surface markers and fluorescence-conjugated probes to selectively label rare cell populations from transgenic or wild-type mice. We detail steps for microdissection of the neonatal cochlea, tissue dissociation, labeling of cell types using fluorescent-conjugated primary antibodies or fluorogenic substrates, and cell sorting.

2 Materials

2.1 Solutions and Antibodies

1. Accutase (Stock solution—eBioscience “Accutase—Enzyme Cell Detachment Medium,” San Diego, CA).
2. Ethanol: 70 % in distilled water.
3. Phosphate buffered solution (PBS) (mM): 1.06 KH₂PO₄, 2.97 Na₂HPO₄·7H₂O, 155.2 mM NaCl, pH 7.4.
4. Hanks’ balanced salt solution (HBSS) (mM): 1.26 CaCl₂, 0.49 MgCl₂·6H₂O, 0.41 MgSO₄·7H₂O, 5.33 KCl, 0.44 KH₂PO₄, 4.17 NaHCO₃, 137.93 NaCl, 0.34 NaHPO₄, 5.55 Dextrose.
5. 0.5 mg/mL thermolysin.
6. 10 mM HEPES (4-(2-hydroxyethyl)-1-piperazineethanesulfonic acid) buffer: dilute from 1 M stock solution in deionized water.
7. Fetal bovine serum (FBS).
8. FACS buffer: 1× Dulbecco’s phosphate buffered saline in 4 % FBS.
9. FACS tubes with integrated cell strainer cap.
10. Standard 12×75, 5 mL round-bottomed, polystyrene FACS tubes.
11. Fluorescent-conjugated monoclonal mouse anti-CD146, diluted 1:1000 (Phycoerythrin, PE, BioLegend, San Diego, CA).
12. Fluorescent-conjugated monoclonal mouse anti-CD326, diluted 1:1000 (PE/Cy7, BioLegend).
13. Rabbit polyclonal anti-CD271 primary, diluted 1:2000 (Millipore, Billerica, MA).
14. Goat anti-rabbit fluorescence-conjugated (Cy5 or Alexa) secondary antibody, diluted 1:250 (Jackson ImmunoResearch, West Grove, PA).

15. 1 µg/mL propidium iodide (PI).
16. 0.3 mM stock solution of DRAQ7 far-red viability dye: Dilute to a final concentration of 3 µM (1:100) dilution in FACS.
17. 0.25 % Trypsin-EDTA stock solution.
18. Trypsin inhibitor/DNaseI cocktail: 100 mg trypsin inhibitor and 100 µg of DNaseI in 20 mL of PBS, sterilize using a 0.2 µm sterile syringe filter and store at -20 °C.
19. DMEM/F12 stock solution: Mix DMEM with Ham's F12 v/v.
20. Ampicillin sodium salt: 1000× stock solution in Milli-Q water (50 mg/mL), filter-sterilize with 0.2 µm sterile syringe filter and store in 500-µL aliquots at -20 °C. Dilute to final working concentration of 50 µg/mL on day of use.
21. Full Media: To 500 mL of DMEM/F12, add 365.1 mg/L of L-Glutamine, 10 mL of B-27 Serum-Free Supplement (Invitrogen, Carlsbad, CA), 5 mL N-2 Supplement (Invitrogen), 25 mg ampicillin solution (as prepared in Subheading 2, step 21), and the following (ng/mL): 10 human fibroblast growth factor-basic (bFGF), 50 mouse insulin-like growth factor-1 (IGF-1), 20 human epidermal growth factor (EGF), 50 heparan sulfate proteoglycan (HS).
22. 3-carboxyumbelliferyl β-D-galactopyranoside (CUG) working Solution: Dilute CUG from FACS labeling kit (Marker Gene Technologies, Eugene, OR), add stock “Substrate Reagent” from kit (50 mM) and dilute into full media 1:50 for final concentration of 1 mM. Use a dark hood with minimum light exposure and make fresh solution at the time of use.
23. CUG stopping solution: 400 µL FBS in 10 mL of sterile 10 mM HEPES (see Subheading 2, step 7), to be made fresh at the time of use.

2.2 Animals and Equipment

1. Wild type CD1 (Charles River Laboratories, Wilmington, MA), *Axin2lacZ/+* mice in CD1 background [12] (#009120, Jackson Laboratory, Bar Harbor, ME), and Lgr5-EGFP [13] (#008875, Jackson Laboratory).
2. Special equipment: FACSAria (Becton Dickinson, San Jose, CA) or other equivalent sorter equipped with 405-nm, 488 and 640-nm lasers and appropriate filters for your chosen fluorophores/reporter mice.
3. 23 gauge blunt aluminum needle (MONOJECT™ Blunt Cannulas, Covidien, 23 × 1" Orange) (VWR International, Radnor, PA).
4. 1 mL syringe (VWR International).
5. Bürker chamber (or other hemocytometer).

6. Ice block, 22.9 × 10.8 × 3.8 cm (Koolit Refrigerants, Cold Chain Technologies, Holliston, MA).
7. Dissecting equipment: Two #5 and two #55 Dumont forceps, and extra-fine Bonn scissors (Fine Science Tools, Foster City, CA), Olympus SZ61 dissection microscope (Shinjuku, Tokyo).
8. Tubes and plates: 35 × 10 mm polystyrene sterile petri dish, 60 × 15 mm polystyrene sterile petri dish, sterile seal-rite 1.5 mL microcentrifuge tube, p300 pipette tips (Eppendorf Dualfilter TIPS 20–300 µL, 55 mm, PCR clean and sterile or equivalent), standard p20–p1000 µL pipette tips, 6-well non-tissue culture dish (Greiner Bio-One, Non-Treated Plates, 6 wells or equivalent), sterile blue 40 µm filter (BD Falcon Cell Strainers; BD Biosciences), 15 mL polystyrene sterile conical centrifuge tube.
9. FACS tubes: Falcon round-bottom tubes, polystyrene, 12 × 75, 5 mL (VWR International).

3 Methods

3.1 Microdissection of the Cochlea

1. Prepare dissection microscope under hood by wiping surfaces with 70 % ethanol and setting out ice blocks (*see Note 1*).
2. Prepare 10–15 35 mm petri dishes under sterile conditions and fill with ~2 mL of sterile ice-cold HBSS.
3. Prepare two 35 mm petri dishes under sterile conditions and fill with ~2 mL of sterile 1× PBS.
4. Sterilize microforceps with 70 % ethanol. Instruments should be periodically sterilized using a standard autoclave (*see Note 1*).
5. In a separate room from the sterile hood, use iris scissors to sacrifice 12–15 postnatal (P) 0–3-day-old mice and place heads onto a 60 mm petri dish on ice block (*see Note 1*). Transgenic reporter mice may be used here to allow for examination of specific cell populations of interest. All animal studies should be approved by the institutional IACUC according to NIH guidelines.
6. Using #5 Dumont forceps and fine microscissors, excise the mandible and tongue and cut through the skull base at the level of the palate.
7. Remove the overlying skin of the calvaria and transect the skull base by inserting the scissors at the inferior part of the foramen magnum to the middle of the palate.
8. Make another incision with fine microscissors from the cut edge of the palate to the superior aspect of the calvaria on both sides, being careful not to damage the otic capsule.

9. Complete the isolation of the temporal bone by making two 45° angled incisions starting from the superior aspect of the foramen magnum, extending to the coronal cut at the hard palate.
10. Place isolated temporal bones in 35 mm petri dishes containing ice-cold HBSS.
11. Collect temporal bones from about 12–15 animals that have been sacrificed, for a total of 24–30 temporal bones (*see Note 2*).
12. Transfer petri dish with isolated temporal bones to previously prepared sterile dissection hood.
13. Transfer four temporal bones to each preprepared 35 mm petri dish containing HBSS and place on ice block.
14. Begin microdissection using two #5 forceps to gently remove the brain in the temporal bone overlying the otic capsule.
15. Chip away from parts of the cochlear capsule, beginning at the entrance of the vestibulocochlear nerve.
16. Following exposure of the base of the cochlea, gently pull out the cochlea and surrounding tissues. Remove any remaining spiral ganglion and the stria vascularis, beginning at the base by peeling away like a ribbon. You may choose to keep the spiral ganglia and/or stria vascularis if this is a region of interest.
17. Transfer cochlea to 35 mm petri dish containing PBS on ice block.
18. For optimal tissue viability, the total time of dissection should be less than 60 min.
19. If reporter mice are used, then repeat above steps for 3–5 wild-type (WT) P0–P3 mice as controls.

3.2 Cochlea Removal and Cell Dissociation

3.2.1 Cell Surface Marker Labeling for Wild-Type Cochlea

1. Transfer a maximum of 20 dissected cochleae per tube into 1.5 mL Eppendorf tubes using forceps or a p1000 pipettor.
2. Add 100 µL of 0.5 mg/mL thermolysin in 10 mM HEPES medium without serum for 20 min in a 37 °C water bath.
3. Add 200 µL of room temperature stock Accutase and re-incubate in the 37 °C water bath for 6 min. Gently agitate the tube by flicking it once or twice at the 3-min mark.
4. Using a 23 gauge blunt aluminum needle and a 1 mL syringe, triturate 10× at room temperature.
5. Add an additional 300 µL of DPBS with 10 % FBS to each Eppendorf tube.
6. Pass cells through a 40 µm strainer. Cells can be collected in a non-tissue culture 6-well dish.
7. Transfer filtered samples into new sterile 1.5 mL Eppendorf tubes.

8. Spin cells at $300 \times g$ for 5 min.
9. Aspirate supernatant. Leave approximately 50 μL at the bottom of the tube to prevent disruption of the cells as in most cases the pellet will not be visible.
10. Resuspend cells in 200–1000 μL volume of FACS buffer with antibody combination of choice (*see Note 3*). For example, anti-CD146 antibody, to label cells in the greater epithelial ridge, anti-CD326 antibody, to label all epithelial cells in the cochlear duct, and anti-CD271 antibody, to label supporting cells in the organ of Corti and cells in the lesser epithelial ridge.
11. In addition to the sample tube also prepare tubes with: unstained control, single stained controls for each antibody-fluorophore combination used and FMO (fluorescence minus one) controls for each gate to be set in the sorter (*see Note 4*).
12. Gently triturate 3–4× using a 1000 μL pipette tip.
13. Keep cells on ice (or at 4 °C), while protecting all tubes from light using aluminum foil wrapping or a covered icebox, and allow to sit for 25 min for antibody labeling.
14. Wash cells with 3× volume FACS buffer and spin at $300 \times g$ for 5 min.
15. Aspirate supernatant, again leaving about 50 μL of volume at the bottom of the tube, to prevent disruption of the non-visible pellet.
16. Resuspend cells in FACS buffer with fluorescence-conjugated (Cy5 or Alexa) secondary goat anti-rabbit antibody, to label the anti-CD271 antibody.
17. Incubate cells over ice (or at 4 °C) for 25 min while keeping all tubes light protected using aluminum foil wrapping or a covered icebox.
18. Repeat steps 14 and 15.
19. Cells may now be combined and transferred to standard FACS tubes and resuspended in a volume of 200–1000 μL FACS buffer.

3.2.2 Fluorescent Reporter Mice [14]

1. Place 200 μL of sterile PBS into a 1.5 mL Eppendorf tube.
2. Transfer up to 20 cochleae into each tube.
3. Pre-warm 50 μL aliquots of 0.125 % trypsin for ~2 min in a 37 °C water bath (*see Note 5*).
4. Add 200 μL of pre-warmed 0.125 % trypsin to PBS containing the cochleae.
5. Place Eppendorf tube at 37 °C for 15 min.
6. To terminate trypsinization, add 100 μL of soybean trypsin inhibitor to each tube.

7. Using a 300 μL blunt pipette tip with a p200 pipettor set at 150 μL , gently triturate cells 80–100 \times , being careful not to create bubbles.
8. Following trituration pass cells through a 35 μm Falcon cell strainer into a standard 5 mL FACS tube. To avoid losing sample, a tube is recommended with an integrated cell strainer cap.
9. Split cells from wild-type cochleae into two tubes. Cells in one tube will be used as an unstained control and those in the other will be stained at a later step with a viability dye (*see Note 4*).
10. Place 400 μL of dissociated cells from cochleae from GFP reporter mice [12] in each FACS tube.
11. At this juncture, there should be four categories of tubes with the following contents. Do not add viability dye at this step:
 - Wild-type—no viability dye (unstained control for FACS setup).
 - Wild-type—with viability dye (single stained control and FMO control for FACS setup).
 - GFP reporter—alone (single stained control and FMO control for FACS setup).
 - GFP reporter—with viability dye (for actual cell sorting).
12. Place cells on ice and protect from light.

3.2.3 Cell Dissociation of Cochleae from LacZ Reporter Mice

for Substrate Fluorogenic Labeling [15]

1. Place 50 μL of sterile PBS in the center of a well in a 6-well non-coated culture dish.
2. Transfer up to 20 cochleae into each 50 μL droplet of PBS. A new 50 μL droplet of PBS should be used for more than 20 cochleae.
3. Pre-warm 50 μL aliquots of 0.125 % trypsin for ~2 min in a 37 °C water bath.
4. Add 50 μL of pre-warmed 0.125 % trypsin to PBS containing the cochleae.
5. Place a 6-well dish at 37 °C for 8 min, taking care not to shake the dish.
6. To terminate trypsinization, add 50 μL of soybean trypsin inhibitor to each 100 μL droplet.
7. Add an additional 50 μL of Full Media.
8. Using a 300 μL blunt pipette tip with a p200 pipettor set at 125 μL , gently triturate cells 80–100 \times , being careful not to create bubbles.
9. Following trituration of each droplet, add an additional 200 μL of media to each well.

10. Pass cells through into FACS tube with integrated 35 μm cell strainer cap (~300 μL remains following trituration and filtration).
11. Split cells from wild-type cochleae into three tubes, diluting 100 μL with 300 μL media in each tube. The cells in one tube are used as an unstained control, while those in the second are stained with a viability dye (not to be added at this step). The cells in the last tube are stained with CUG to detect background fluorescence (*see Notes 4 and 6*).
12. Place 400 μL of dissociated cells from cochleae from LacZ reporter mice in each FACS tube. As a CUG single stain control, dilute 10 μL of cells in 390 μL media. Bring volume of any remaining tubes to 400 μL .
13. Pre-warm working CUG at 37 °C for 3–5 min.
14. Incubate cells in a 37 °C humidified incubator for 10 min.
15. Add 200 μL of working CUG solution, prepared as described in Subheading 2, **step 23**, to each appropriate FACS tube requiring staining. For tubes not designated to have CUG, add full media only.
16. At this juncture, there should be five categories of tubes with the following contents (do not add viability dye at this step):
 - Wild-type—without CUG or PI (unstained control for compensation).
 - Wild-type—with viability dye only (single stained control for compensation).
 - Wild-type—with CUG and viability dye (FMO/substrate control for gating).
 - LacZ reporter—with CUG only (single stained control for compensation).
 - LacZ reporter—with CUG and viability dye (for actual cell sorting).
17. Protect all tubes from light and incubate them in a 37 °C humidified incubator for 25 min.
18. Add 1.8 mL of ice-cold HEPES solution (CUG stopping solution), prepared as described in Subheading 2, **step 24**, to each FACS tube under a sterile hood with lights off to minimize light exposure.
19. Centrifuge cells at 300 $\times g$ for 5 min.
20. Remove supernatant and resuspend cells in 300 μL Full Media. Pool all aliquots for the sorting sample, including cochleae from LacZ reporter mice stained with CUG and PI (*see Note 7*).
21. Place cells on ice and protect from light.

3.3 Cell Sorting

1. A trained flow cytometer operator is highly recommended for all sorting and is usually required in most core facilities (*see Note 8*). Although this protocol outlines a general sorting procedure, it is important to follow protocols in place for the facility and the machine you are using.
2. We use a BD FACSaria II equipped with 405-, 488-, and 640-nm lasers. Detection of CUG for LacZ cells is done using the 405-nm laser; GFP and PI are both excited with the 488-nm laser and DRAQ7 is detected using the 640-nm laser. Always check that the machine you plan to use has the appropriate lasers and filters for your combination of fluorophores before you start your experiment.
3. Begin by turning on the cell sorter and warming up the lasers. We have found that the use of a 100 μm nozzle is optimal for viability of cochlear cells. After achieving a stable stream, perform quality control and optimize laser settings and drop delay using manufacturer/core facility's instructions.
4. Run the samples on a flow rate as low as possible, while still keeping events per second optimal for each machine. Using our facility cytometers to sort our samples, we aim for around 2000–3000 events. If the sample is too dilute to achieve this, it is recommended to spin down the cells and resuspend them in a smaller volume of FACS buffer. In addition, because we sort cells under sterile conditions, it is critical to follow your machine's decontamination protocol (e.g., bleach or ethanol).
5. Add viability dye to cells (a final concentration of 1 $\mu\text{g}/\text{mL}$ for propidium iodide or 3 μM for DRAQ7), no more than 30 min before the start of the sort.
6. Begin compensation setup by running unstained control cells and adjusting photo multiplier tube (PMT) voltages for Forward Scatter (FSC) and Side Scatter (SSC) so that the cell population of interest is clearly shown on the dot plot (Fig. 1a). Then run single-stained controls and either manually adjust compensation or collect data for the machine to calculate the compensation matrix (BD sorters running DIVA software routinely perform automatic compensation).
7. After compensation is calculated and applied to the experiment file, set up your worksheet with the relevant plots. Set gates to exclude doublets, using Height versus Width or Area versus Width parameters (Fig. 1b). Sequentially arrange your plots to exclude nonviable cells using your viability dye of choice and to select out the cell population(s) of interest (Figs. 2 and 3, *see Note 9*). Set each gate using your FMO controls.
8. If the sorter is equipped with a cooling chamber for the sample tube and/or collection tubes, set the temperature to 4 °C to help preserve cell viability (*see Note 10*).

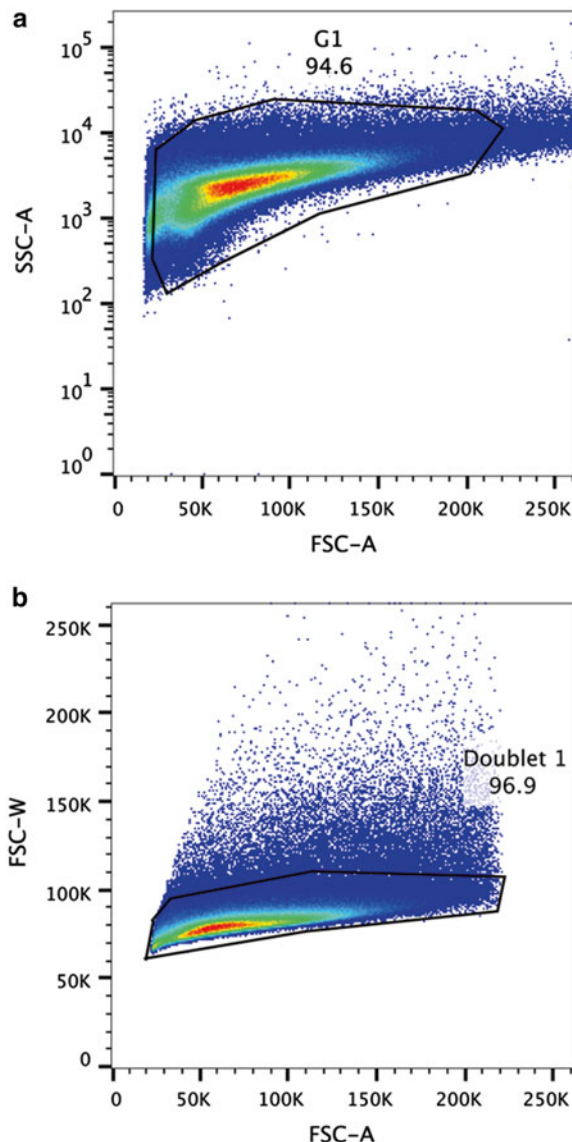


Fig. 1 Cell sorting to remove cell debris and doublets. **(a)** Dot plot of dissociated cochlear cells undergoing sorting using Forward Scatter Area (FSC-A) and Side Scatter Area (SSC-A) on axes for distinguishing debris from cell populations. A single gate is set (G1) with 94.6 % of cells selected here. Note that the lower threshold for individual events here is set at 25,000 on the x-axis to exclude debris. FSC is represented here on a linear scale while SSC is a logarithmic one. **(b)** FSC-A versus the Forward Scatter Width (FSC-W) is used to exclude doublets. Similarly, area versus height may also be used to generate a diagonal distribution of events, assuming that area scaling is set using sample cells and not beads. Events deviating from the expected linear nature of the plot are excluded. In this plot, 96.9 % of cells are deemed singlets and the remaining events excluded. This technique is standard for excluding doublets on the assumption that two or more cells that adhere together will not have the same width versus area dimensions as single cells and that all cells are spherical

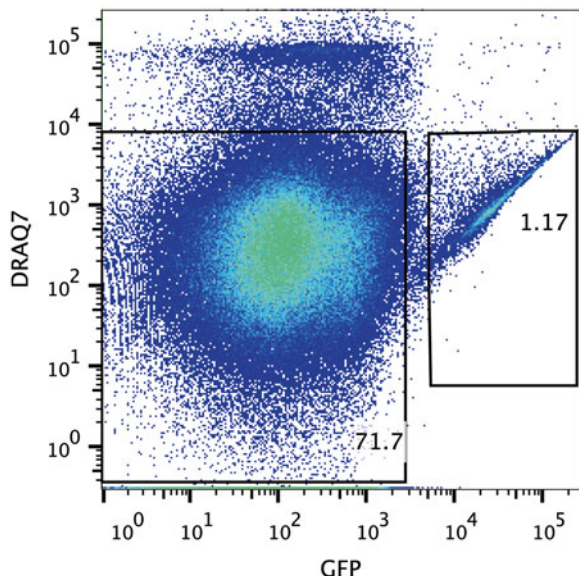


Fig. 2 Cell sorting to rid nonviable cells and select cell population of interests. Dissociated cochlear cells from neonatal Lgr5-GFP mice are distributed on the x-axis as detected by the 488 nm-laser while the DRAQ7 viability red dye is used to exclude nonviable cells seen as a distinct group of events high on the y-axis (~5.2 %). Of the cells selected, viable Lgr5-GFP-positive cells constitute approximately 1.2 % and viable Lgr5-GFP-negative cells about 71.7 % of the parent cell population

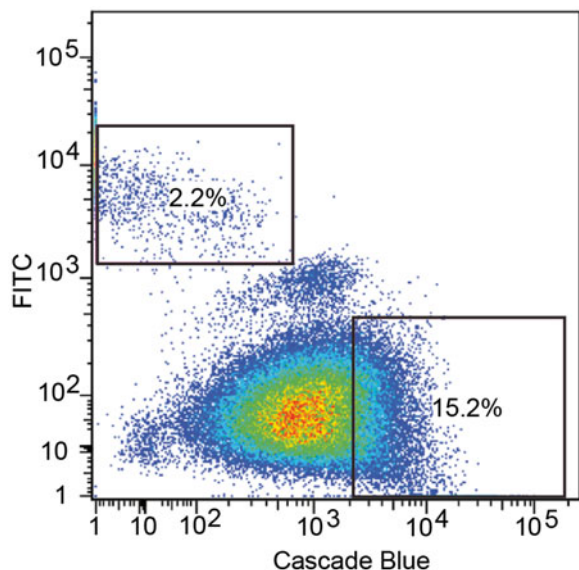


Fig. 3 Cell sorting to select multiple cell population of interests. FACS plot demonstrating the final gating strategy for isolation of Axin2-lacZ-high cells (15.2 % stained by CUG) and Lgr5-GFP-positive cells. All events on this plot have already been gated to exclude debris, doublets, and nonviable cells. Cochlear cells from Axin2-lacZ, Lgr5-GFP double reporter mice were used to generate this plot

9. Based on the gating strategy, sort the cell populations into FACS tubes containing 500 µL Full Media for cells meant to be cultured or into Eppendorf tubes with appropriate buffer (RNAlater, Trizol or other lysis buffer) for RNA expression analysis. For clonal assays, sort desired numbers of cells into culture plates with Full Media. When possible, also include a reanalysis of a few of your sorted cells to verify proper sort settings and viability of sorted cells.
10. Record your sorts, including the number of cells sorted by the FACS machine for each population.

4 Notes

1. We have a dedicated room for primary tissue culture under a laminar flow hood [16, 17]. Sacrifice of animals and dissection to the level of temporal bones occurs in a separate room to minimize contamination for subsequent steps. All surfaces are wiped down frequently with 70 % ethanol. A surgical facemask should be worn during dissection and gloves at all times with frequent glove changes. A separate set of finer microforceps is reserved strictly for steps subsequent to the temporal bone isolation.
2. We find that at least 20 cochleae should be dissected as a minimum for each sort, given the paucity of cells that are lost through the process. The yield of cells also depends on the subpopulation being isolated, as rare populations will need more starting materials (i.e., more cochleae).
3. Sinkkonen et al. [9] identified an array of markers for microdissection of the cochlear cells using a combination of a GFP-reporter for hair cells along with anti-CD146, anti-CD326, and anti-CD271 antibody. The latter three cell surface markers were found to label different parts of the cochlea, including the greater epithelial ridge, the cochlear ductal epithelial cells, and the lesser epithelial ridge supporting cells, respectively. Using this combination, along with the GFP-reporter for hair cells and the remaining negative populations at the different steps, allows for separation of the cells into five subpopulations. Of course, other transgenic mice that label different subpopulations of supporting cells may be substituted here.
4. Several controls are needed, depending on the type of experiment planned. In general, an unstained control (cells with no reporter or antibody staining) and single stain controls are necessary. When using an antibody panel, a single stained control is required for each individual antibody-fluorophore combination used in the sort. Similarly, if fluorescent cells from transgenic reporter mice are used, a sample of these cells with no other fluorophore/dye is necessary. In addition, a control sample is required with cells stained with a viability dye of choice

with no other fluorophore. In combination, these controls are used for compensation of spectral overlap between different fluorophores. As long as the appropriate compensation controls are performed, most sorters will perform the compensation matrix. The data collected from the controls reflect the amount of light emitted by different fluorophores into the different detection channels on the machine. This allows for the mathematical subtraction of any spillover into neighboring channels close to the chosen detection channel for a given fluorophore. Unstained and single stain controls are processed alongside the sample you wish to sort, but require fewer cells. It is reasonable to use two cochleae per stain required or about 50,000 stained cells. In addition to compensation controls, most sorts will also require FMO (Fluorescence Minus One) controls to guide the gates for sorting. FMO controls contain all the fluorophores in your panel minus the one you are setting for the gate. This is because a combination of fluorophores generally gives you a higher overall background fluorescence than unstained cells in any given channel. Positive and negative population gating that is based on unstained cells runs the risk of shifting your gate significantly, so that your positive population is interpreted as larger than it actually is. Ideally you would need one FMO control for each antibody/fluorophore/reporter in your staining panel, but they are most important when the signal of interest spans a range instead of representing distinctly separated populations. Lastly, some sorts may also require an isotype control or a substrate control, to estimate background binding of antibodies or staining of substrates. These controls are needed when dealing with intracellular stains, such as the one described above for LacZ/CUG. Before attempting this kind of sort, it is recommended to consult with an experienced FACS operator to discuss appropriate controls.

5. Different digestion techniques are used when surface markers are labeled versus the use of transgenic reporter mice. We utilize trypsinization for the dissociation of cells from LacZ or GFP reporter mice. Accutase and thermolysin are utilized for cell dissociation of cell surface markers, as trypsinization affects cell surface antigens, thereby affecting labeling.
6. The use of fluorescence-conjugated substrates to label LacZ-positive cochlear cells prior to cell sorting presents several technical challenges that would not be encountered when sorting fluorescent reporter (e.g., GFP-positive) cells from transgenic mice. We use a known fluorescent substrate of β -galactosidase called 3-carboxyumbelliferyl β -D-galactopyranoside (CUG) [18]. To maximize substrate specificity, we determine the level of nonspecific labeling by processing wild-type cochleae with the same CUG staining procedure in each experiment. This specific FMO/substrate control is necessary (*see Note 4*) to

create a threshold for setting the gates used to identify LacZ-high cells, which we define as the most fluorogenic cells from the LacZ-reporter cochleae, especially since this protocol typically generates a “range” of LacZ-positive cells.

7. Another challenging aspect of this technique is the paucity of cells in the cochlea, making isolation of rare subpopulations difficult. In order to overcome this, we simply increase the number of mice utilized for each experiment (20–50 mice). The mouse strain CD-1 is known to routinely have large litters between 10 and 15 mice per litter. Homozygous transgenic mice can be crossed with this CD1 strain to increase litter size.
8. During the sorting process, an experienced FACS user is needed to maintain the settings constant across experiments. Most importantly, it is ideal to become familiar with cochlear cells using one FACS machine to avoid large reconfigurations during each experiment and thus potential variability. This allows for faster processing of cells and, thereby, increases cell viability. However, even with an ideally maintained machine there is still inherent variability in sample staining intensities and viability from experiment to experiment. Therefore the stated controls should be included each time a sort is run.
9. Gating of viable cells during sorting must remain consistent among different experiments as the operator selects the final gating parameters. Make sure that sufficient events are used, so that nonviable cells are distinguished clearly from viable ones. Verify the gate using your FMO control.
10. It is critical to maintain cell viability prior to cell sorting. The following steps were found to be important in optimizing cell viability: (a) Minimize dissection time: we coordinated a team of dissectors (2–3 persons) to shorten the duration of harvesting cells. We routinely completed dissections of 80 cochleae in less than two hours with a team of 3; (b) Gentle trituration: it is important to perform this step using a blunt tip pipette in a gentle manner; (c) Keep dissociated cells on ice: we found that keeping tissues/cells on ice as much as possible improved subsequent cell viability; (d) To further increase viability, we found the use of a 100 µm nozzle superior to the 70 µm nozzle.

Acknowledgements

The authors would like to thank R. Chai for figure illustration. This work was supported by grants from the Swedish Research Council C0657401 (L.J.), NIH/NIDCD K08DC011043, RO1DC013910, Department of Defense W81XWH-14-1-0517, the Akiko Yamazaki and Jerry Yang Faculty Scholar Fund, and the California Initiative in Regenerative Medicine RN3-06529 (A.G.C.).

References

1. Oshima K et al (2007) Differential distribution of stem cells in the auditory and vestibular organs of the inner ear. *J Assoc Res Otolaryngol* 8:18–31
2. Zhang Y et al (2007) Isolation, growth and differentiation of hair cell progenitors from the newborn rat cochlear greater epithelial ridge. *J Neurosci Meth* 164:271–279
3. Yoshimura H et al (2014) Deafness gene expression patterns in the mouse cochlea found by microarray analysis. *PloS One* 9:e92547
4. Shiono H, Ito Y (2003) Novel method for continuous cell separation by density gradient centrifugation: evaluation of a miniature separation column. *Prep Biochem Biotechnol* 33:87–100
5. Foo LC et al (2011) Development of a method for the purification and culture of rodent astrocytes. *Neuron* 71:799–811
6. Neurauter AA et al (2007) Cell isolation and expansion using Dynabeads. *Adv Biochem Engin Biotechnol* 106:41–73
7. Chai R et al (2012) Wnt signaling induces proliferation of sensory precursors in the postnatal mouse cochlea. *Proc Natl Acad Sci U S A* 109:8167–8172
8. White PM, Doetzlhofer A, Lee YS, Groves AK, Segil N (2006) Mammalian cochlear supporting cells can divide and trans-differentiate into hair cells. *Nature* 441:984–987
9. Sinkkonen ST et al (2011) Intrinsic regenerative potential of murine cochlear supporting cells. *Sci Rep* 1:26
10. Scheffer DI, Shen J, Corey DP, Chen ZY (2015) Gene expression by mouse inner ear hair cells during development. *J Neurosci* 35:6366–6380
11. Herget M et al (2013) A simple method for purification of vestibular hair cells and non-sensory cells, and application for proteomic analysis. *PloS One* 8(6):e66026
12. Lustig B et al (2002) Negative feedback loop of Wnt signaling through upregulation of conductin/axin2 in colorectal and liver tumors. *Mol Cell Biol* 22:1184–1193
13. Barker N et al (2007) Identification of stem cells in small intestine and colon by marker gene Lgr5. *Nature* 449:1003–1007
14. Chai R et al (2011) Dynamic expression of Lgr5, a Wnt target gene, in the developing and mature mouse cochlea. *J Assoc Res Otolaryngol* 12:455–469
15. Jan TA et al (2013) Tympanic border cells are Wnt-responsive and can act as progenitors for postnatal mouse cochlear cells. *Development* 140:1196–1206
16. Jan TA, Chai R, Sayyid ZN, Cheng AG (2011) Isolating LacZ-expressing cells from mouse inner ear tissues using flow cytometry. *J Vis Exp* 58:e3432
17. Oshima K, Senn P, Heller S (2009) Isolation of sphere-forming stem cells from the mouse inner ear. *Meth Mol Biol* 493:141–162
18. Zeng YA, Nusse R (2010) Wnt proteins are self-renewal factors for mammary stem cells and promote their long-term expansion in culture. *Cell Stem Cell* 6:568–577

Part VII

Physiological Protocols

Chapter 24

Optical Coherence Tomography to Measure Sound-Induced Motions Within the Mouse Organ of Corti In Vivo

Zina Jawadi, Brian E. Applegate, and John S. Oghalai

Abstract

The measurement of mechanical vibrations within the living cochlea is critical to understanding the first nonlinear steps in auditory processing, hair cell stimulation, and cochlear amplification. However, it has proven to be a challenging endeavor. This chapter describes how optical coherence tomography (OCT) can be used to measure vibrations within the tissues of the organ of Corti. These experimental measurements can be performed within the unopened cochlea of living mice routinely and reliably.

Key words Cochlear mechanics, Basilar membrane, Tectorial membrane, Vibrometry, Sound encoding, Biomechanics, In vivo imaging

1 Introduction

Different techniques have been used historically to measure basilar membrane motion.

The measurement of basilar membrane motion was pioneered by von Békésy in the 1950s using stroboscopic illumination [1]. In the post-mortem cochlea of multiple species, he identified the presence of traveling waves. The first vibratory measurements in living animals came in 1967 from Johnstone and Boyle, who studied the guinea pig using the Mössbauer technique [2]. In 1971, Rhode also used this approach, in which a radioactive source was placed on the undersurface of the basilar membrane. He identified that sound-induced vibrations of the squirrel monkey basilar membrane were nonlinear [3]. This nonlinear gain increases the dynamic range of mammalian hearing and is termed cochlear amplification [4].

Laser Doppler vibrometry is primarily for surface measurements. From the 1980s to the late 2000s, laser Doppler vibrometry was the predominant technique for measuring sound-induced vibrations of the basilar membrane. Most commonly, the cochlear base was studied near or at the round window, and the most

common animals used were those with large cochleae that protrude prominently into the middle ear space, including the guinea pig, gerbil, and chinchilla. With this technique, the otic capsule bone was opened, a small reflective glass bead was dropped onto the undersurface of the basilar membrane, and the laser was focused on the bead. Motion-induced Doppler shifts in the reflected light could then be measured.

This approach provided the highest available sensitivity and was used to define most of what is currently known about cochlear amplification (for review, *see* [5]). While it has been possible to collect data using laser Doppler vibrometry without placing a reflective bead [6, 7], this approach is challenging because of the low reflectance of the basilar membrane. In addition, some data has been collected from the cochlear apex [8–10]. However, this method, too, has proven difficult because opening the Reissner's membrane to drop a reflective bead onto the surface of the tectorial membrane can disrupt the endocochlear potential and thus alter cochlear function.

Besides the technical difficulties associated with opening the cochlea, laser Doppler vibrometry has a limitation in that its depth resolution is defined by the numerical aperture (NA) of the objective used to focus the light. However, a long working distance objective, which usually has a relatively low NA, makes it easier to target the laser and thus perform the *in vivo* experiments. This means that without the use of a bead to define the spot being measured, reflections from multiple surfaces along the path of the laser may occur, producing artifacts. With the use of the bead, however, the measurement technique is limited to surface measurements. For this reason and the technical issues explained above, laser Doppler vibrometry has primarily been used to measure basilar membrane motion. The remaining structures within the organ of Corti have essentially been unstudied because of their inaccessibility.

Optical coherence tomography (OCT) is an optical imaging modality that permits depth-resolved measurements and is widely used for imaging the eye and coronary arteries. Recent investigations using animal models of the middle and inner ear illustrate the growing demand for the high fidelity tomographic and vibratory information accessible with OCT for interrogating the function of the ear [11–15]. In 2006, OCT was first used to measure vibrations within the living guinea pig cochlea [16]. Further studies performed within the guinea pig cochlear base after opening the otic capsule bone have been used to identify differences between the vibration of the reticular lamina and of the basilar membrane [17].

OCT fundamentally measures the magnitude and phase of light field reflected from a sample as a function of depth. The magnitude is used to render tomographic images where small changes

in refractive index provide contrast. The imaging depth of OCT is both tissue and wavelength dependent, but typically falls in the range of 1–2 mm. The axial and lateral resolutions are typically in the range of 1–15 μm and 10–30 μm , respectively. The phase of the light field may be used to measure small relative changes in refractive index or position of the reflectors in the sample. For applications in the ear, the refractive index is typically assumed to be constant with respect to time; hence, any modulation of the phase is attributed to motion. By monitoring the phase as a function of time, relative motion as small as a few picometers can be measured enabling spatially resolved vibrometry [18]. Note that while the relative motion is resolved in 3D space, the position of the moving tissues is only known to the spatial resolution noted above for the tomographic images and only motion parallel to the illumination beam is measured. In other words, while the relative motion can be known to a few picometers, the tissue structures that are moving are only typically known to a few microns and only the projection of the motion on the optical axis (parallel to the light illumination) is resolved.

There are several methods for realizing an OCT system based on either time-domain or spectral-domain interferometry. Time-domain methods use a moving reference arm reflector in an interferometer to encode the depth of the tissue reflectors in time. Small relative motion is typically measured by monitoring the Doppler shift of the light returning from the sample. This is analogous to laser Doppler vibrometry except that the position of the moving tissue is spatially resolved. In spectral-domain methods, the depth of the tissue reflectors is encoded in the spatial frequency (wave-number, k) of the reflected light. A Fourier transform converts from spatial frequency to space. The magnitude of the result is the tomographic image. The phase of the Fourier transform can be monitored as a function of time for vibrometry. The earliest systems developed for OCT typically used time-domain methods, however it has been shown that the spectral-domain methods have an inherent sensitivity advantage of 20–30 dB [19–21].

Spectral interferometry for OCT may be accomplished in one of two ways: a broad wavelength band light source and spectrometer to resolve the light as a function of spatial frequency or a narrow wavelength band light source where the center frequency is swept as a function of time and detected with a photodiode. The former is typically called Fourier-domain OCT (FD-OCT) and the latter is called swept-source OCT (SSOCT).

OCT permits the noninvasive measurement of sound-induced motion within the intact mouse cochlea. A key goal in understanding cochlear mechanics is to measure the motions of the various microstructures that compose the organ of Corti, not just the basilar membrane. These structures are highly organized and presumably work together to develop cochlear amplification. Ideally, these

measurements would be made in an intact (i.e., unopened) cochlea to minimize trauma to the cochlea and to permit increased experimental reliability. In addition, the ability to study the mouse cochlea would offer some benefits because transgenic strains with altered biomechanics are available. To achieve these goals, we developed a FD-OCT system that permitted vibrometry within the apical turn of the mouse cochlea [11, 13, 22] and discovered complex micro-mechanical vibratory characteristics within the supporting cells of the organ of Corti [12]. However, this OCT system was not as sensitive as laser Doppler vibrometry, and therefore averaging of repeated measurements was required in order to achieve a reasonable noise floor. This meant that experimental time was longer than ideal, which is an issue when performing *in vivo* experiments.

We then developed a new technique based upon SSOCT, termed volumetric optical coherence tomography vibrometry (VOCTV), which overcomes these limitations. The technique offers depth-resolved displacement measurements with sensitivity and speed comparable to laser Doppler vibrometry. Using VOCTV in the mouse cochlea, we measured the traveling wave within both the basilar membrane and the tectorial membrane, and we found key differences that explain unusual features found in auditory nerve single unit recordings [18]. With this approach, we open the middle ear bulla but do not open the cochlea. The success rate for an experiment using VOCTV in our lab is roughly 90 %, and we routinely perform experiments on 2–3 mice per day. Unsuccessful experiments occur if the mouse dies unexpectedly or if the experimenter inadvertently damages the tympanic membrane or ossicular chain during the surgical exposure.

This chapter describes the dissection process, the imaging process, and the vibratory measurement calculations that we use to make these measurements in living mice. Our current optical setup design has been published [18], and frankly, given the rapid advances in optics, it is already out of date. However, any OCT setup can be used with the animal preparation we describe to make similar recordings.

2 Materials

2.1 Supplies for Mouse Anesthesia

1. We use a combination of ketamine and xylazine to anesthetize the mice. The anesthetic dose for mice is ketamine 100 mg/kg and xylazine 10 mg/kg. We dilute and then mix these two drugs together in the correct proportions so that only one injection needs to be given.
2. 0.9 % NaCl, 100 mg/mL ketamine, 20 mg/mL xylazine.
3. Ketamine working solution: Mix 0.6 mL ketamine with 2.4 mL NaCl to make 3 mL of diluted ketamine (20 mg/mL).

4. Xylazine working solution: Mix 0.05 mL xylazine with 2.94 mL NaCl to make 3 mL of diluted xylazine (2 mg/mL).
5. Final anesthetic solution: Mix diluted ketamine with diluted xylazine to make 6 mL of anesthetic solution at a concentration of 10 mg/mL ketamine and 1 mg/mL xylazine. Store at room temperature.

2.2 Surgical Equipment

2.2.1 Surgical Apparatus

1. Stage with manual 2D movement controls fixed to a vibration isolation table, which is used to adjust the mouse position relative to the dissecting microscope.
 2. Thermoregulated heating pad placed on top of stage.
 3. Head holder attached to stage (*see Note 1*).
 4. 70 % Ethanol to sterilize head holder.
 5. Dissecting microscope with attached OCT system positioned over the stage (Fig. 1).
 6. Speaker to generate the sound stimuli positioned near the stage.
1. Small gauze pads.
 2. Cotton balls.

2.2.2 Surgical Instruments (Fig. 2)

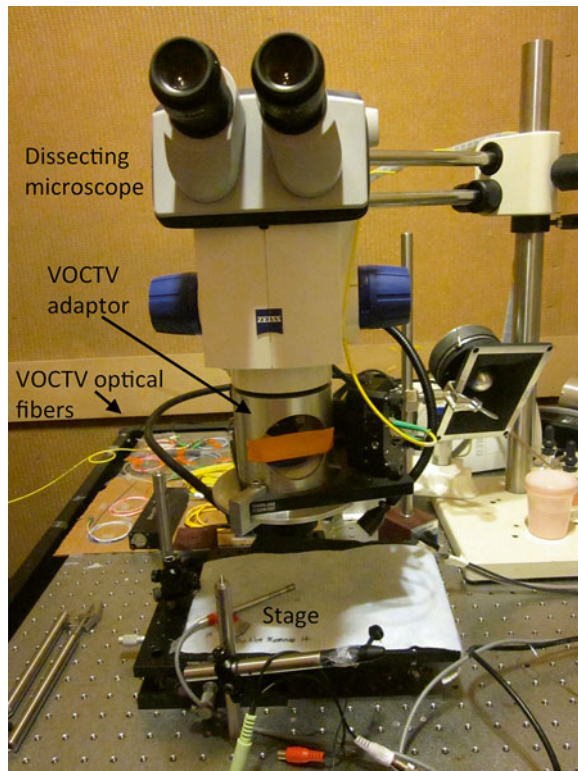


Fig. 1 Our experimental setup containing the VOCTV system

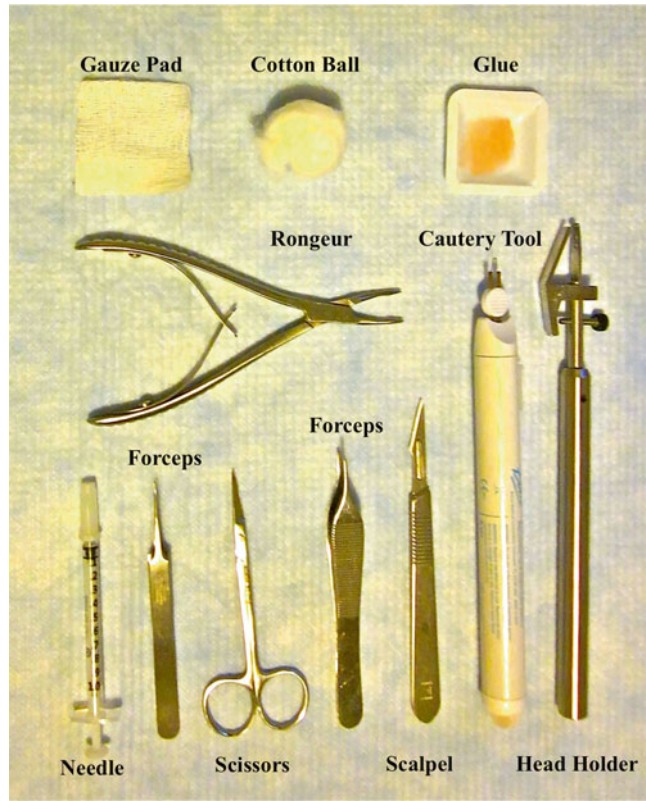


Fig. 2 Surgical instruments: battery-operated cautery tool, forceps, glue, head holder, needle, one cotton ball, one small gauze pad, rongeur, scalpel, and scissors

3. Battery-operated cautery tool.
4. Dissection instruments: forceps, scissors, straight pick or needle, scalpel, rongeurs.
5. Methyl methacrylate glue, both the powder and liquid components (Co-Oral-Ite Dental Mfg., Diamond Springs, CA).
6. Small cup or weighing boat and Q-tips to mix glue solution.
7. Anesthetic Monitoring Worksheet.

2.2.3 Optical Equipment

1. Broad band laser, either swept source or wide-bandwidth (e.g., MEMS-VCSEL, Thorlabs, Newton, NJ).
2. Photodetector (e.g., WL-BPD600MA, Wieserlabs).
3. Digitizer (e.g., NI-5772, National Instruments, Austin, TX).
4. Field programmable gate array (FPGA) (e.g., NI-7966R, National Instruments).
5. 2D galvo mirror (e.g., OIM101, Optics In Motion, Long Beach, CA).

3 Methods

3.1 Anesthetization

The institutional animal care and use committee should approve all animal procedures according to the appropriate guidelines.

1. Use adult mice, aged P28 to P42 to perform an intraperitoneal (IP) injection of the proper dose.
2. Weigh mouse and inject proper volume of anesthetic solution based on using 0.1 mL/10 g at the beginning of the experiment.
3. Perform a paw pinch test, to determine whether the mouse needs additional anesthesia by using forceps to gently squeeze the foot. If the leg withdraws, additional anesthesia is required. Do not start surgical procedures until there is no withdrawal.
4. Supplement anesthetic every 30 min, although the time-length may vary depending on each individual animal. Typically we give 0.05 mL of the anesthetic solution.
5. Use an Anesthetic Monitoring Worksheet (Fig. 3) throughout each experiment to document monitoring procedures and all anesthesia injections. Keep these records in a binder for semi-annual IACUC inspections.

3.2 Mouse Placement in Head Holder

1. Once fully anesthetized, use scissors to gently remove the scalp between both ears. The left ear will be used as an example. Leave the pinna in place or transect the ear canal and remove the pinna depending on experimental needs.
2. Dry the scalp with a gauze pad, and insert the head into the head holder (Fig. 4a) (*see Note 2*).
3. Glue skull to head holder using methyl methacrylate glue (Fig. 4b) and allow it to harden for 5–10 min.
4. Gently rotate the mouse and head holder to expose the left ear.

3.3 Surgical Exposure of Cochlea [23]

1. Remove skin covering the ventral side of the left ear and the left masseter muscle with scissors (Fig. 4c).
2. Remove the submandibular gland and perform a deeper dissection with the scissors and scalpel to divide the edge of the trapezius muscle and the posterior belly of the digastric muscle. Use the cautery where needed to control bleeding. The tympanic bulla then becomes visible (Fig. 4d) (*see Note 2*).
3. Remove part of the jaw, in order to view the cochlear apex, by first removing the masseter muscle, which lies on the lateral surface of the mandible, with the cautery. Use the rongeurs to remove the ramus of the mandible (*see Note 3*).
4. Open the bulla medial to the tympanic annulus with care (Fig. 4e) by first scraping the bulla with the tip of a small scalpel

Mouse Anesthetic Monitoring Form

Date:

Researcher:

PI:

APLAC #:

Induction Anesthesia:

Ketamine: 100 mg/kg

Xylazine: 10 mg/kg

Time	Anesthesia Given (Induction)	Level of Anesthesia (Assessed by signs of movement or withdrawal reflex)	Respiratory Rate & Pulse (Assessed visually)	Body Temperature (Assessed with heating blanket temperature probe)	Color (View skin around eyes and paws)
0:00	_____ ml (____ g)	<input type="radio"/> OK <input type="radio"/> Sacrifice <input type="radio"/> Not OK <input type="radio"/> Recover	<input type="radio"/> OK <input type="radio"/> Not OK	<input type="radio"/> OK <input type="radio"/> Not OK	<input type="radio"/> OK <input type="radio"/> Not OK
0:15	_____ ml	<input type="radio"/> OK <input type="radio"/> Sacrifice <input type="radio"/> Not OK <input type="radio"/> Recover	<input type="radio"/> OK <input type="radio"/> Not OK	<input type="radio"/> OK <input type="radio"/> Not OK	<input type="radio"/> OK <input type="radio"/> Not OK
0:30	_____ ml	<input type="radio"/> OK <input type="radio"/> Sacrifice <input type="radio"/> Not OK <input type="radio"/> Recover	<input type="radio"/> OK <input type="radio"/> Not OK	<input type="radio"/> OK <input type="radio"/> Not OK	<input type="radio"/> OK <input type="radio"/> Not OK
0:45	_____ ml	<input type="radio"/> OK <input type="radio"/> Sacrifice <input type="radio"/> Not OK <input type="radio"/> Recover	<input type="radio"/> OK <input type="radio"/> Not OK	<input type="radio"/> OK <input type="radio"/> Not OK	<input type="radio"/> OK <input type="radio"/> Not OK
1:00	_____ ml	<input type="radio"/> OK <input type="radio"/> Sacrifice <input type="radio"/> Not OK <input type="radio"/> Recover	<input type="radio"/> OK <input type="radio"/> Not OK	<input type="radio"/> OK <input type="radio"/> Not OK	<input type="radio"/> OK <input type="radio"/> Not OK
1:15	_____ ml	<input type="radio"/> OK <input type="radio"/> Sacrifice <input type="radio"/> Not OK <input type="radio"/> Recover	<input type="radio"/> OK <input type="radio"/> Not OK	<input type="radio"/> OK <input type="radio"/> Not OK	<input type="radio"/> OK <input type="radio"/> Not OK
1:30	_____ ml	<input type="radio"/> OK <input type="radio"/> Sacrifice <input type="radio"/> Not OK <input type="radio"/> Recover	<input type="radio"/> OK <input type="radio"/> Not OK	<input type="radio"/> OK <input type="radio"/> Not OK	<input type="radio"/> OK <input type="radio"/> Not OK
1:45	_____ ml	<input type="radio"/> OK <input type="radio"/> Sacrifice <input type="radio"/> Not OK <input type="radio"/> Recover	<input type="radio"/> OK <input type="radio"/> Not OK	<input type="radio"/> OK <input type="radio"/> Not OK	<input type="radio"/> OK <input type="radio"/> Not OK
2:00	_____ ml	<input type="radio"/> OK <input type="radio"/> Sacrifice <input type="radio"/> Not OK <input type="radio"/> Recover	<input type="radio"/> OK <input type="radio"/> Not OK	<input type="radio"/> OK <input type="radio"/> Not OK	<input type="radio"/> OK <input type="radio"/> Not OK
2:15	_____ ml	<input type="radio"/> OK <input type="radio"/> Sacrifice <input type="radio"/> Not OK <input type="radio"/> Recover	<input type="radio"/> OK <input type="radio"/> Not OK	<input type="radio"/> OK <input type="radio"/> Not OK	<input type="radio"/> OK <input type="radio"/> Not OK
2:30	_____ ml	<input type="radio"/> OK <input type="radio"/> Sacrifice <input type="radio"/> Not OK <input type="radio"/> Recover	<input type="radio"/> OK <input type="radio"/> Not OK	<input type="radio"/> OK <input type="radio"/> Not OK	<input type="radio"/> OK <input type="radio"/> Not OK
2:45	_____ ml	<input type="radio"/> OK <input type="radio"/> Sacrifice <input type="radio"/> Not OK <input type="radio"/> Recover	<input type="radio"/> OK <input type="radio"/> Not OK	<input type="radio"/> OK <input type="radio"/> Not OK	<input type="radio"/> OK <input type="radio"/> Not OK
3:00	_____ ml	<input type="radio"/> OK <input type="radio"/> Sacrifice <input type="radio"/> Not OK <input type="radio"/> Recover	<input type="radio"/> OK <input type="radio"/> Not OK	<input type="radio"/> OK <input type="radio"/> Not OK	<input type="radio"/> OK <input type="radio"/> Not OK
3:15	_____ ml	<input type="radio"/> OK <input type="radio"/> Sacrifice <input type="radio"/> Not OK <input type="radio"/> Recover	<input type="radio"/> OK <input type="radio"/> Not OK	<input type="radio"/> OK <input type="radio"/> Not OK	<input type="radio"/> OK <input type="radio"/> Not OK
3:30	_____ ml	<input type="radio"/> OK <input type="radio"/> Sacrifice <input type="radio"/> Not OK <input type="radio"/> Recover	<input type="radio"/> OK <input type="radio"/> Not OK	<input type="radio"/> OK <input type="radio"/> Not OK	<input type="radio"/> OK <input type="radio"/> Not OK

Fig. 3 Mouse anesthetic monitoring form

to soften it. Then, use a straight pick or needle to remove the bone fragments. Do not open the bulla until all bleeding is stopped, since any blood seeping into the middle ear space reduces the quality of the OCT image.

5. Note the cochlea on the floor of the middle ear cavity. Adjust the head holder to tilt the head at roughly a 45° angle, which brings the cochlear apex in line with the optical axis of the microscope and permits imaging of most of the apical turn. The dissection is now complete.

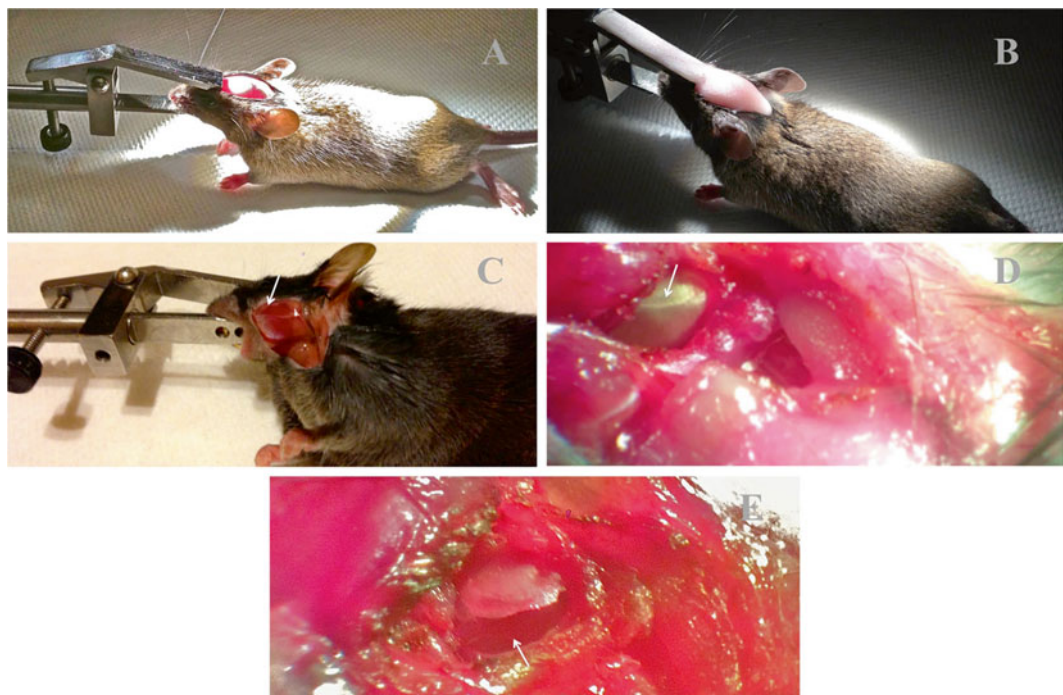


Fig. 4 Surgical exposure of the mouse cochlear apex. (a) The anesthetized mouse is placed in the head holder. (b) The head is glued to the head holder to provide rigid fixation. (c) The ventral approach to the tympanic bulla. The masseter muscle is noted (arrow). (d) The tympanic bulla has been exposed. The tympanic annulus (arrow) defines the attachment of the tympanic membrane. (e) After opening the bulla, the cochlea (arrow) is barely visible on the floor of the middle ear cavity

3.4 Imaging: Investigating the Mouse Cochlea

3.4.1 OCT Imaging Terminology

1. A-line: Park the x and y scan mirrors at one position, and collect a line image along the optical path of the laser (*see Note 4*).
2. B-scan. Move the scan mirrors so that the laser is moved along a linear path, and collect multiple sequential A-lines. Plot these to give a planar image along the $x-z$ axes.
3. C-scan or Volume scan. The scan mirrors are moved to cover the entire $x-y$ range, while collecting A-lines. This scan creates a 3D $x-y-z$ image.
4. M-scan. Park the scan mirrors at one location and collect multiple A-lines over time. The magnitude of the signal from any given voxel does not change, but its phase varies if the structure is vibrating. The vibration of one or more pixels along the z -direction is measured with this technique.
5. BM-scan. Scan mirrors move the laser step-by-step along a linear path, stopping at evenly spaced intervals to collect an M-scan, allowing the measurement of vibrations over a 2D region of space.
6. CM-scan. This scan is similar to a BM-scan, but measures vibration throughout a volume of tissue.

3.4.2 Identifying Regions of Interest

1. Image the cochlea, in order to identify a region of interest for measuring vibrations, by rapidly collecting B-scans with the VOCTV system.
2. Collect B-scans continuously and align the mouse under the system until identifying a mid-modiolar cross-section of the cochlea (*see Note 5*).
3. Ensure that the quality of the image is sharp (Fig. 5). We use dispersion compensation to account for differences in the amount of glass in the sample and reference arms of the VOCTV system. We have many different algorithms stored, and the user can switch between them to see which one gives the best image. In addition, adjusting the polarization paddles contained within the optical path of the sample arm may help.
4. Once a region of interest is found, save the image. This image is used later, to show where the measurement was made when analyzing the vibratory data.

3.4.3 Measuring Vibratory Responses from a Single Point

1. Select a measurement location for study on the B-scan image. Commonly, this location is the mid-portion of the basilar membrane; however, one can use any pixel within the image.
2. Present sound stimuli of varying frequencies and intensity to the ear, while collecting M-scans to measure vibratory responses at this point (*see Note 6*).
3. Begin collecting data (Fig. 6a), which is completed in ~2–3 min.
4. Analyze the vibratory responses at the selected point. If desired, vibrations can be processed and analyzed at all points along the A-line as the information is collected simultaneously.

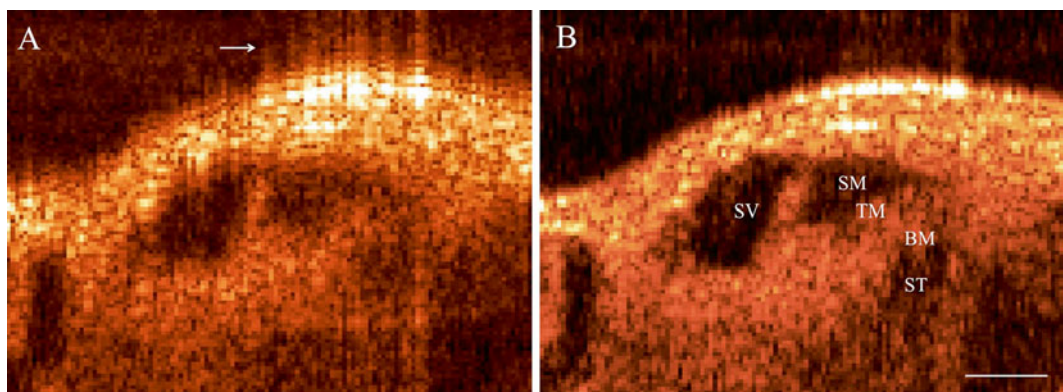


Fig. 5 B-scans of the cochlear apex. **(a)** This image demonstrates poor dispersion compensation. Reflections at the boundary between the air and the otic capsule bone are particularly noticeable (arrow). **(b)** A B-scan after application of appropriate dispersion compensation. Scala Vestibuli (SV), Scala Media (SM), Scala Tympani (ST), Tectorial Membrane (TM), Basilar Membrane (BM). Scale bar 100 μ m

3.4.4 BM-Scans

This process is similar to single-point measurements; however, vibratory data are collected from multiple points.

1. Collect a B-scan image first, by selecting an area for study using the computer mouse. We usually select the organ of Corti, from the osseous spiral lamina to the spiral ligament.
2. Set the step size, which defines the number of points at which the scan mirrors will stop along the scan path, thereby setting the sampling resolution along the horizontal axis. Note that the resolution along the vertical axis (the z direction) is determined by the bandwidth of the laser used for the VOCTV system.
3. Set the sound stimulus parameters, which are sequentially repeated for each step in the scanning process. This can dramatically increase the data collection time and it is recommended that the user carefully consider the number of stimulus frequencies and intensities to be studied.
4. Collect the data (Fig. 6b).

3.4.5 CM-Scan

The CM-scan is performed similarly to the BM-scan; however, selecting the region of interest is more complex, because it must be done in 3D. Therefore, this scan is similar to collecting an image Z-stack on a confocal microscope. However, the starting and stopping points of the scan are defined in the y -axis rather than the z -axis.

1. Collect a volume scan of the cochlea, and then scroll through the B-scans to define the starting and stopping points in the y -dimension. The region of interest in the x and z dimensions is selected with the computer mouse as described above for the BM-scan.

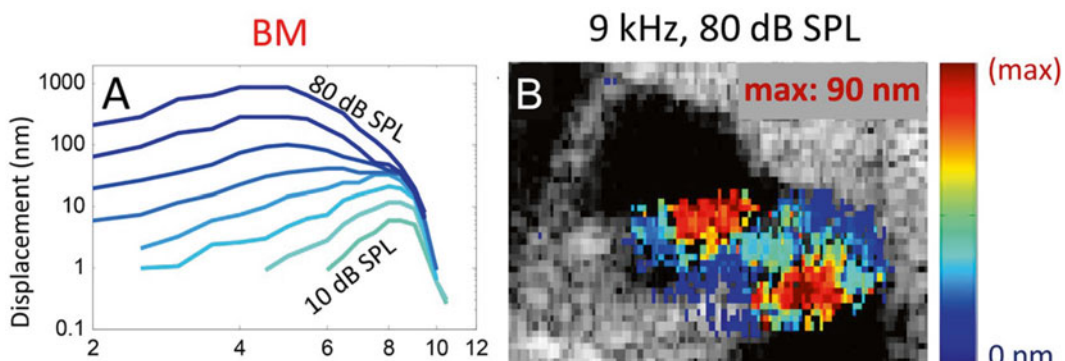


Fig. 6 Vibratory responses. (a) A single point tuning curve from the mouse basilar membrane. (b) A BM scan from the mouse organ of Corti. Only magnitude data are shown in these representative examples. Reproduced from Ref. [18] with permission

2. Set step sizes for both the x and y dimensions. We usually use 20 μm .
3. Set sound stimuli parameters.
4. Collect the data.

3.5 Completion of the Experiment

When analyzing the data, it is important to calculate the ratio of the vibratory responses to the intensity of the sound that entered the cochlea. While the frequency response of the speakers are calibrated prior to each experiment, the ear canal, tympanic membrane, and ossicular chain all filter the sound stimuli.

1. Measure the vibratory response of the ossicular chain after all cochlear measurements have been completed. In the mouse, we typically target the laser onto the orbicular apophysis of the malleus.
2. Present all sound frequencies at 80 dB SPL and collect vibratory data. Because the vibration of the ossicular chain is linear, these data can be scaled as needed.
3. Euthanize the mouse at the end of the experiment with an overdose of anesthesia solution and confirm according to guidelines.

3.6 Analysis

3.6.1 Phase Measurements to Displacement Magnitude and Phase

The data collected when performing vibrometry with VOCTV is phase versus time. For a single point measurement, this is simply one array. For a BM-scan or CM-scan, there will be an array for each voxel contained within the selected region of interest (*see Note 7*).

1. Perform a Fourier transform to identify the vibratory magnitude and phase at the stimulus frequency (*see Note 8*).
2. Commonly measured characteristics that can be calculated during data analysis include:
 - The Characteristic Frequency (CF) is the frequency of maximal vibration to stimuli of very low intensity (typical 10–20 dB SPL), which defines the measurement location along the cochlear tonotopic map.
 - The Best Frequency (BF) is the maximal frequency of vibration response to the stimulus intensity. At low stimulus intensities, the BF equals the CF; however, the BF shifts to a lower frequency with higher intensity stimuli.
 - The $Q_{10\text{dB}}$ is a quantification of sharpness of tuning. Originally, it was defined for use with auditory nerve tuning curves. However, it can be adapted for use with vibratory measurements by dividing the CF by the bandwidth measured 10 dB below the vibratory magnitude at the CF.

- The *gain* is calculated by dividing the peak vibratory magnitude at the CF measured in the live animal by peak vibratory magnitude in the dead animal.

4 Notes

1. The head holder is necessary to rigidly fix the head in order to reduce movements from other sources that might affect the vibratory measurements.
2. Take care to prevent damage to structures. The heat of the cautery can potentially damage the bulla and cochlea. In addition, it is critically important to note the white line through the bone of the tympanic bulla, the tympanic annulus, which marks the edge of the tympanic membrane. Care must be taken so that this structure is not damaged when opening the bulla.
3. Bleeding can occur from the pterygoid muscles just deep to the mandible. Staying close to the bone of the mandible is the best way to prevent bleeding. Cautery is often ineffective if bleeding starts in this area. Instead, cotton wisps can be used to pack off this region. The venous bleeding will stop with time.
4. The *A-line* measures the image intensity versus depth at one x , y position.
5. To achieve this cross-section, the head holder is physically adjusted and/or the direction of the scan is changed. On our system, a scan rotation angle of -30° works well.
6. These stimulus parameters need to be set in software. Our standard parameters for measuring vibrations within the apex of the mouse cochlea are to sweep the frequency from 2 to 14 kHz in steps of 0.5 kHz and to sweep the intensity from 10 to 80 dB SPL in steps of 10 dB.
7. To convert this to displacement, use the following equation:

$$D = \varphi \times \frac{\lambda}{4\pi n} \quad (1)$$

where D is the displacement at each point in time, φ is the phase at each point in time, λ is the center wavelength of the light used, and n is the refractive index of the sample. At 1300 nm, the refractive index of water is ~ 1.32 .

8. Because of the fixed time delay for sound to propagate from the speaker into the ear, and the filtering response of the middle ear, the phase of intra-cochlear structures are referenced to the phase of the ossicular chain. This is accomplished by subtracting the phase of the ossicular chain from the phase of the cochlear structure used in measuring.

Acknowledgements

The authors appreciate the assistance of Jinkyung Kim, Hee Yoon Lee, Xiao Fang Liu, Patrick Raphael, and Anping Xia. This project was funded by NIH grants DC014450, DC013774, DC010363, and the Stanford CNC Seed Grant Program.

References

- Von Bekesy G (1960) Experiments in hearing. McGraw-Hill, New York
- Johnstone BM, Boyle AJ (1967) Basilar membrane vibration examined with the Mossbauer technique. *Science* 158:389–390
- Rhode WS (1971) Observations of the vibration of the basilar membrane in squirrel monkeys using the Mossbauer technique. *J Acoust Soc Am* 49(Suppl 2):1218+
- Davis H (1983) An active process in cochlear mechanics. *Hear Res* 9:79–90
- Robles L, Ruggero MA (2001) Mechanics of the mammalian cochlea. *Physiol Rev* 81:1305–1352
- Ren T (2002) Longitudinal pattern of basilar membrane vibration in the sensitive cochlea. *Proc Natl Acad Sci U S A* 99:17101–17106
- Legan PK, Lukashkina VA, Goodyear RJ, Kossi M, Russell IJ et al (2000) A targeted deletion in alpha-tectorin reveals that the tectorial membrane is required for the gain and timing of cochlear feedback. *Neuron* 28:273–285
- Cooper NP, Rhode WS (1995) Nonlinear mechanics at the apex of the guinea-pig cochlea. *Hear Res* 82:225–243
- Cooper NP, Rhode WS (1997) Mechanical responses to two-tone distortion products in the apical and basal turns of the mammalian cochlea. *J Neurophysiol* 78:261–270
- Khanna SM (2002) Non-linear response to amplitude-modulated waves in the apical turn of the guinea pig cochlea. *Hear Res* 174:107–123
- Gao SS, Raphael PD, Wang R, Park J, Xia A et al (2013) In vivo vibrometry inside the apex of the mouse cochlea using spectral domain optical coherence tomography. *Biomed Opt Express* 4:230–240
- Gao SS, Wang R, Raphael PD, Moayedi Y, Groves AK et al (2014) Vibration of the organ of Corti within the cochlear apex in mice. *J Neurophysiol* 112:1192–1204
- Gao SS, Xia A, Yuan T, Raphael PD, Shelton RL et al (2011) Quantitative imaging of cochlear soft tissues in wild-type and hearing-impaired transgenic mice by spectral domain optical coherence tomography. *Opt Express* 19:15415–15428
- Nguyen CT, Jung W, Kim J, Chaney EJ, Novak M et al (2012) Noninvasive in vivo optical detection of biofilm in the human middle ear. *Proc Natl Acad Sci U S A* 109:9529–9534
- Subhash HM, Davila V, Sun H, Nguyen-Huynh AT, Nuttall AL et al (2010) Volumetric in vivo imaging of intracochlear microstructures in mice by high-speed spectral domain optical coherence tomography. *J Biomed Opt* 15:36024
- Choudhury N, Song G, Chen F, Matthews S, Tschinkel T et al (2006) Low coherence interferometry of the cochlear partition. *Hear Res* 220:1–9
- Chen F, Zha D, Fridberger A, Zheng J, Choudhury N et al (2011) A differentially amplified motion in the ear for near-threshold sound detection. *Nat Neurosci* 14:770–774
- Lee HY, Raphael PD, Park J, Ellerbee AK, Applegate BE et al (2015) Noninvasive in vivo imaging reveals differences between tectorial membrane and basilar membrane traveling waves in the mouse cochlea. *Proc Natl Acad Sci U S A* 112:3128–3133
- De Boer JF, Cense B, Park BH, Pierce MC, Tearney GJ et al (2003) Improved signal-to-noise ratio in spectral-domain compared with time-domain optical coherence tomography. *Opt Lett* 28:2067–2069
- Choma M, Sarunic M, Yang C, Izatt J (2003) Sensitivity advantage of swept source and Fourier domain optical coherence tomography. *Opt Express* 11:2183
- Leitgeb R, Hitzenberger CK, Fercher AF (2003) Performance of fourier domain vs. time domain optical coherence tomography. *Opt Express* 11:889–894
- Applegate BE, Shelton RL, Gao SS, Oghalai JS (2011) Imaging high-frequency periodic motion in the mouse ear with coherently interleaved optical coherence tomography. *Opt Lett* 36:4716–4718
- Wenzel GI, Xia A, Funk E et al (2007) Helper-dependent adenovirus-mediated gene transfer into the adult mouse cochlea. *Otol Neurotol* 28:1100–1108

Chapter 25

Method for Dissecting the Auditory Epithelium (Basilar Papilla) in Developing Chick Embryos

Snezana Levic and Ebenezer N. Yamoah

Abstract

Chickens are an invaluable model for exploring auditory physiology. Similar to humans, the chicken inner ear is morphologically and functionally close to maturity at the time of hatching. In contrast, chicks can regenerate hearing, an ability lost in all mammals, including humans. The extensive morphological, physiological, behavioral, and pharmacological data available, regarding normal development in the chicken auditory system, has driven the progress of the field. The basilar papilla is an attractive model system to study the developmental mechanisms of hearing. Here, we describe the dissection technique for isolating the basilar papilla in developing chick inner ear. We also provide detailed examples of physiological (patch clamping) experiments using this preparation.

Key words Basilar papilla, Patch clamping, Hair cells, Development

1 Introduction

1.1 Chick as a Model System to Study Auditory Development

Audition is of critical importance to a wide range of behaviors in birds. It is used for prey capture, individual and species recognition, as well as vocal learning and mate selection. Avian auditory systems have principally been studied in the context of brainstem development (*see Ref. [1]* for a review of chick), as models of sound localization (*see Ref. [2]* for a review of barn owls), and for studies of song production and learning (*see Ref. [3]* for a review of passerines). Chick's auditory system represents an ideal starting point for comparative studies of the evolution and development of avian hearing. Comparative data suggest that the organization of the auditory system of chickens represents the primitive (plesiomorphic) condition [4]. The developmental and embryological aspects of the auditory system in this species have been the focus of work in a number of independent laboratories. The use of the chicken has been widespread, in part due to the wide availability of chicken eggs and to the accessibility of the embryo to perform experimental manipulations. In addition, the existence of a detailed description

of the normal stages of embryonic development [5] has been an invaluable tool for these kinds of studies. The extensive morphological, physiological, behavioral, and pharmacological data available regarding normal development in the chick auditory system has driven the progress of the field (for a review *see* Ref. [1]). In addition, the auditory systems of both humans and chicks are at comparable stages at birth [6]. Also, both species start to hear during gestation [7, 8], making the chick cochlea, known as the basilar papilla, an attractive model system to study developmental mechanisms of hair cells.

1.2 Basic Anatomy of the Vertebrate Peripheral Auditory System

The basic function of the ear is to transduce sound waves to the brain's auditory processing centers. The vertebrate ear contains three main parts. The outer ear contributes to collecting the sound and funneling it through the external canal to the tympanic membrane. The middle ear contains a system of bony ossicles to convey the vibrations to the inner ear and match the impedance of the air to that of the cochlear fluid (for recent review *see* Ref. [9]). The inner ear consists of a fluid filled space containing the auditory sensory epithelium, which develops as an out-pouching of the vestibular system. The auditory epithelium consists of a basilar membrane (BM) on which lie the auditory receptor cells known as hair cells. Sound reaches the hair cells via vibrations of the BM. Hair cells are designed to transduce mechanical stimuli into electrical responses via a transduction apparatus consisting of a hair bundle. This bundle, which sits on the apex of the receptor cell, is composed of 30–100 stereocilia, whose tips project into a gelatinous structure known as the tectorial membrane. The hair bundle contains mechanoreceptive transduction channels and has the ability to couple the energy of bundle deflection to the gating of these channels. The stereocilia, which are arranged in rows of increasing height are connected at their tips with small extracellular filaments of ~5–10 nm in diameter, called tip links. Mechanical stimulation towards the tallest stereocilia increases tension in these tip links [10], thereby increasing the probability of opening the mechano-electrical transduction channels located at the insertion site of the link into the stereocilia [11, 12]. Once open, the transduction channels allow the influx of K⁺ and Ca²⁺ ions from the endolymph, which has an unusually high concentration of K⁺, into hair cells resulting in membrane depolarization. The depolarization spreads to the basolateral membrane of the hair cells to activate voltage-gated Ca²⁺ channels that mediate the release of neurotransmitter onto afferent fibers projecting to the auditory brain stem.

1.3 Anatomy of the Chicken Inner Ear

In the adult chicken, the cochlea is a tubular structure, approximately 5 mm long, containing the basilar papilla, the tegmentum vasculosum (a vascularized secretory tissue), three scalae fluid filled compartments, and the cochlear ganglion [13, 14]. The avian

homologue of the organ of Corti, the basilar papilla, is an auditory epithelium that contains about 10,000 hair cells and twice as many supporting cells [15]. Covering the hair cells is the tectorial membrane, which is mechanically tuned [16, 17] and forms the base of the scala media. The hair cells are arranged in a tonotopic gradient along the cochlea, responding to the 50–5000 Hz range sound [18, 19]. Low frequencies are detected at the apical end and high frequencies at its base. There are two principal morphologically distinct hair cell types found in the chicken basilar papilla. Tall hair cells typically are thought to receive primarily afferent innervation, thus being more similar to inner hair cells of mammals. The short hair cells receive primarily efferent innervation [13, 14], and are thought to be analogous to the outer hair cells of the mammalian cochlea [19]. Although both types of hair cells can be found throughout the tonotopically organized papilla, their general trend of innervation varies.

Unlike the mammalian cochlea, where there is an orderly arrangement of a single row of inner hair cells and three rows of outer hair cells along the tonotopic axis, there are many hair cells distributed across the chick basilar membrane at any given tonotopic location. The number of rows of hair cells varies according to the width of the basilar membrane: approximately a dozen hair cells at high-frequency encoding basal locations, where the basilar membrane is narrow, to over 40 hair cells at low-frequency encoding apical locations, where the basilar membrane is wide.

1.4 Functional Development of Hearing

The chicken inner ear is morphologically and functionally close to maturity at the time of hatching. Low frequency sound-evoked responses are reported from E10 in chicken cochlear nuclei. This threshold decreases with development, and is markedly improved between E18 and hatching (E21), coinciding with the filling of the middle ear with air rather than liquid [20]. The cochlear ganglion contains primary afferent neurons of the vertebrate auditory and vestibular systems and constitutes the first synaptic relay after the transduction of sound. Cochlear (acoustic) neurons are bipolar, with a central process that makes synapses in the brainstem, and a peripheral process that terminates on the sensory epithelium of the inner ear. Cochlear and vestibular ganglia develop in the early embryo as one single unit, the cochleovestibular (CV) ganglion, where the majority of neurons arise by migration from the otic vesicle. As development proceeds, the CV ganglion splits into two distinct ganglia, the cochlear and vestibular ganglia. The neurons develop peripheral processes and innervate the sensory epithelium. Innervation begins around day 6 of development in the chick (14–15 gestation days in mouse), by which time most ganglionic cells have undergone terminal mitosis. The developmental process proceeds in parallel with hair cell maturation, where first synaptic contacts form by days 8–9 [21] and mature synapses by day 15–17 (gestation day 18, and postnatal mouse respectively [22]).

2 Materials

2.1 Tools/Labware

1. Marsh automatic incubator (e.g., Lyon Electric, Chula Vista, CA).
2. Dissecting microscope.
3. Microscissors.
4. Pair of fine Dumont #5 or #55 forceps.
5. Petri dishes (35 mm × 10 mm).

2.2 Dissection, Recording, and Drug Solutions

Prepare all solutions in Milli-Q water.

1. Chick saline solution for dissection (mM): 155 NaCl, 6 KCl, 4 CaCl₂, 2 MgCl₂, 5 HEPES, and 3 glucose at pH 7.4.
2. Extracellular solution: 145 NaCl, 6 KCl, 2 CaCl₂, 10 D-glucose, 10 HEPES, pH 7.3.
3. Intracellular solution for perforated patch experiments (mM): 145 KCl, 2 MgCl₂, 10 HEPES, 1 EGTA, 10 D-glucose, 250 µg/mL amphotericin pH 7.3.

3 Methods

3.1 Isolating the Chick Basilar Papilla

from Embryonic Day 6 to Post-Hatching

3.1.1 Growing and Staging Chick Embryos

1. Obtain fertilized chicken eggs from approved local supplier.
2. Incubate fertilized eggs at 37 °C in a chick egg automatic incubator (e.g., Marsh, Lyon Electric, Chula Vista, CA).
3. Prior to experiments, stage embryos according to the number of somites present [5]. The numbers of somites often closely follow the days of incubation.

3.1.2 Dissecting the Basilar Papilla

1. Decapitate the embryo using scissors using a pair of scissors.
2. Sagittally section the head using scissors or a scalpel blade (*see Note 1*).
3. Remove brain to expose the bony labyrinth. The cranial bone is soft until about embryonic day 16 and is easily cut and removed by microscissors and a pair of fine forceps.
4. Cut around the bony labyrinth using small scissors or a small scalpel to isolate the tissue.

5. Transfer the bony labyrinth to a smaller petri dish (35 mm × 10 mm) and continue dissecting tissue around the cochlear duct.
6. Carefully begin to expose the cochlear duct using tweezers (*see Note 2*).
7. Cut the VIIth nerve using small scissors and remove basilar papilla using tweezers. Make sure that the basilar papilla moves as one whole piece and is attached only to the nerve (*see Note 3*).

3.2 Example of Using the Basilar Papilla in Physiological Experiments

3.2.1 Spontaneous Electrical Activity in Developing Chick Hair Cells

Isolated chick basilar papilla preparation can be used for a variety of physiological and cellular experiments. The hair cells are accessed after careful removal of the tectorial membrane using fine tweezers or eye lash glued to the wooden stick. This exposes the apical surface of hair cells. To access more basal end, the tissue needs to be pierced with the cleaning pipette (which is the same kind as recording pipette, but once the pipette is used for cleaning, it is changed with the new one for recording).

Using the isolated chick basilar papilla (Fig. 1), one can determine if spontaneous electrical activity in the developing hair cell exists (Fig. 2 [23]). This early activity may influence the overall connectivity and development of the auditory system, which in part may be dependent on the spike shape and frequency. Thus, this electrical activity may serve some developmental functions, which we investigated in subsequent studies using the methods described above.

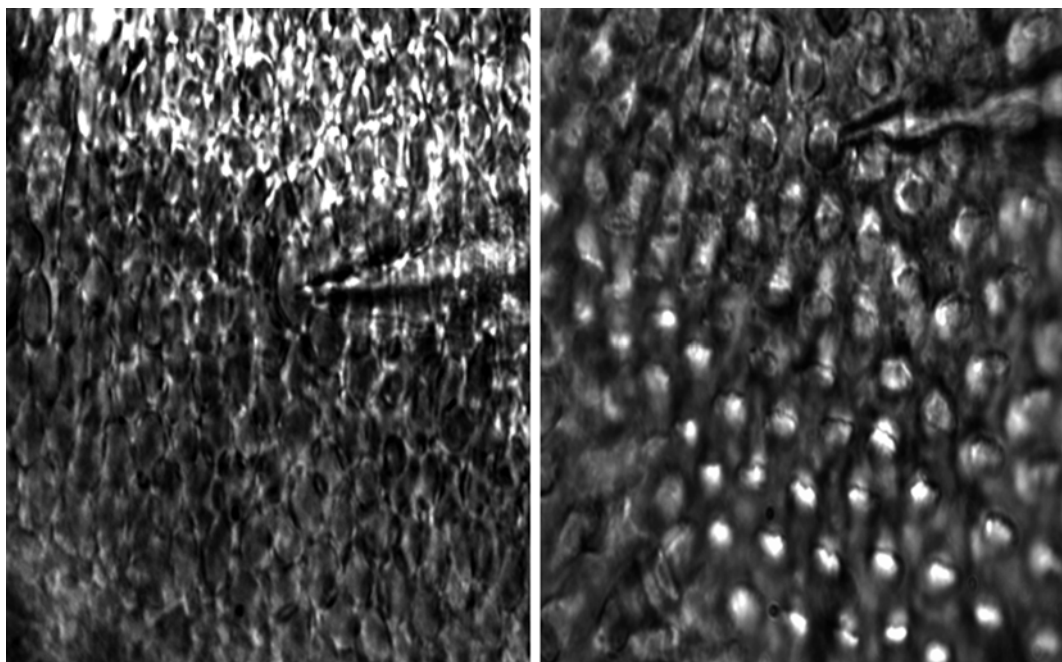


Fig. 1 Differential contrast interference images of the intact basilar papilla at E12 (*left*) and P2 (*right*), showing individual hair cells from their apical surface and patch pipette

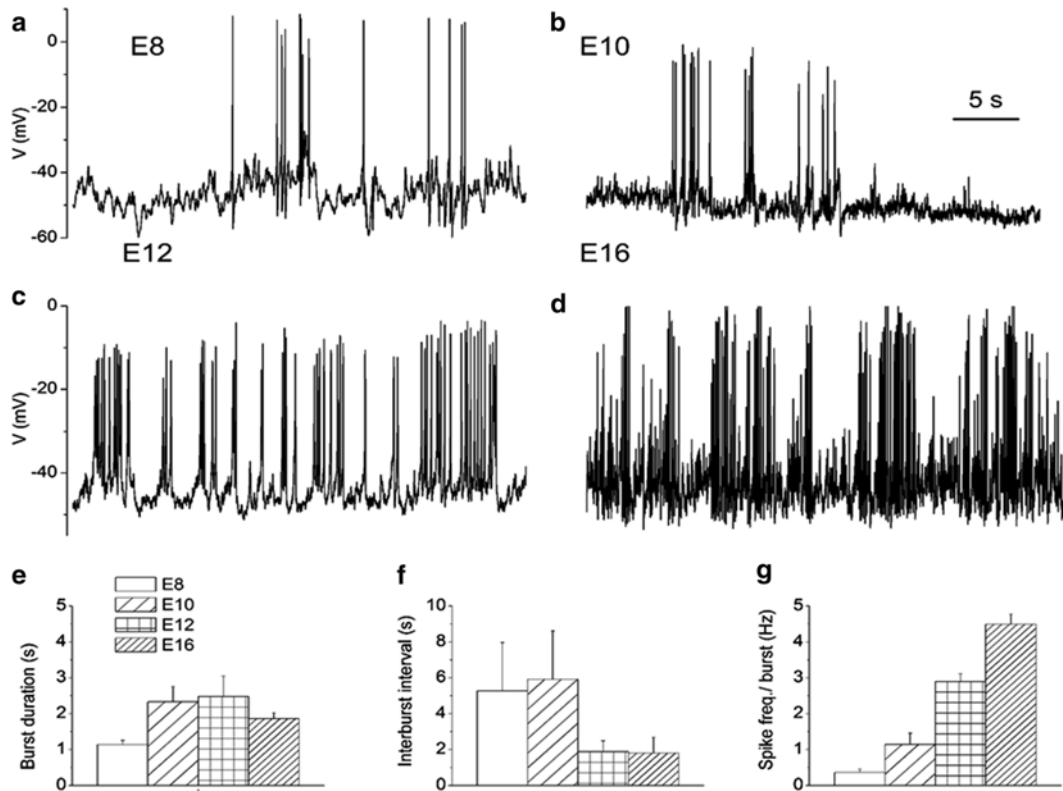


Fig. 2 Discharge pattern of action potentials in hair cells was altered during development. **(a–d)** Examples of changes in bursting activity in developing hair cells from E8 to E16 are shown E8 (a), E10 (b), E12 (c), E16 (d). **(e–g)** Summary data of the duration of burst (e), inter-burst intervals (f), and the spike frequency within a burst (g) at different stages in development (E8–E16) are illustrated in the histograms (24)

4 Notes

1. The head must be immediately FULLY submerged in oxygenated chicken saline using a petri dish of ~15 cm in diameter or some other dish that allows for full submersion of the entire head (naturally head size increases with age). It is very important for the tissue to never come in contact with air. A petri dish is coated with Sylgard Elastomere Kit—by covering 1 mm thickness and baking it at 65 °C for ~1 h). Prepare all solutions in Milli-Q water (18 MΩ cm) with a total organic content of less than 5 parts/billion. Oxygenate the chick saline solution for a minimum of 20 min on ice, with 95 % O₂/5 % CO₂. To oxygenate the saline solution, fill a 500 mL beaker with 250 mL of saline. Attach an oxygen tank using plastic tubing with a glass stem bubbler at the end (or use fine tubing with a diameter of ~1–2 mm) and a stopper to control gas flow.

2. The bony labyrinth can be seen through the skull ventrally. Remove the cartilaginous capsule surrounding the duct of the basilar papilla very carefully, piece by piece, making sure not to damage the basilar papilla.
3. The tegmentum vasculosum and the tectorial membrane are removed mechanically using fine forceps (Dumont #55) and an eyelash glued to the tip of the wooden stick. Chick basilar papillae can be stored in a 37 °C incubator in Minimum Essential Medium (Invitrogen, Carlsbad, CA) or ice-cold dissecting solution before subsequent manipulations.

Acknowledgements

We thank members of our laboratory for comments on the manuscript. This work was supported by grants to ENY from NIH (R01 DC0100386; DC007592; DC003826).

References

1. Rubel EW, Parks TN (1988) Organization and development of the avian brain-stem auditory system. In: Edelman GM, Einar Gall W, Maxwell Cowan W (eds) *Brain function*. Wiley, New York, pp 3–92
2. Konishi M (1999) Deciphering the brain's codes. In: Abbott L, Sejnowski TJ (eds) *Neural codes and distributed representations: foundations of neural computation*. MIT Press, Cambridge, pp 1–18
3. Konishi M (1985) Birdsong: from behavior to neuron. *Annu Rev Neurosci* 8:125–170
4. Carr C, Code R (2000) The central auditory system in reptiles and birds. In: Dooling R, Fay R, Popper A (eds) *Comparative hearing: birds and reptiles*. Springer, Berlin
5. Van Hamburger HL (1951) A series of normal stages in the development of the chick embryo. *J Morphol* 88:49–82
6. Rubel EW, Fritzsch B (2002) Auditory system development: primary auditory neurons and their targets. *Ann Rev Neurosci* 25:51–101
7. Jackson H, Rubel EW (1978) Ontogeny of behavioral responsiveness to sound in the chick embryo as indicated by electrical recordings of motility. *J Comp Physiol Psychol* 92:682–696
8. Birnholz JC, Benacerraf BR (1983) The development of human fetal hearing. *Science* 222(4623):516–518
9. Stenfelt S, Goode R (2005) Bone-conducted sound: physiological and clinical aspects. *Otol Neurotol* 26:1245–1261
10. Pickles JO, Comis SD, Osborne MP (1984) Cross-links between stereocilia in the guinea pig organ of Corti, and their possible relation to sensory transduction. *Hear Res* 15:103–112
11. Assad JA, Shepherd GMG, Corey DP (1991) Tip-link integrity and mechanical transduction in vertebrate hair cells. *Neuron* 7:985–994
12. Hudspeth AJ (1992) Hair-bundle mechanics and a model for mechanochemical transduction by hair cells. *Soc Gen Physiol Ser* 47:357–370
13. Hirokawa N (1978) The ultrastructure of the basilar papilla of the chick. *J Comp Neurol* 181:361–374
14. Tanaka K, Smith CA (1978) Structure of the chicken's inner ear. *Am J Anat* 153:251–271
15. Tilney LG, Tilney MS (1986) Functional organization of the cytoskeleton. *Hear Res* 22:55–77
16. von Békésy G (1960) *Experiments in hearing*. McGraw-Hill, New York
17. Gummer AW, Smolders JWT, Klinke R (1987) Basilar membrane motion in the pigeon measured with the Mossbauer technique. *Hear Res* 29:63–92
18. Gray L, Rubel EW (1981) Development of responsiveness to suprathreshold acoustic stimulation in chickens. *J Comp Physiol Psychol* 95(1):188–198
19. Manley GA, Meyer B, Fischer FP, Schwabedissen G, Gleich O (1996) Surface morphology of

- basilar papilla of the tufted duck *Aythya fuligula*, and domestic chicken *Gallus gallus domesticus*. J Morph 227:197–212
- 20. Saunders JC, Coles RB, Richard Gates G (1973) The development of auditory evoked responses in the cochlea and cochlear nuclei of the chick. Brain Res 63:59–74
 - 21. Rebillard M, Pujol R (1983) Innervation of the chicken basilar papilla during its development. Acta Otolaryngol 96:379–388
 - 22. Anniko M, Nordemar H, Sabin A (1983) Principles in embryonic development and differentiation of vestibular hair cells. Otolaryngol Head Neck Surg 91(5): 540–549
 - 23. Levic S, Nie L, Tuteja D, Harvey M, Sokolowski BH, Yamoah EN (2007) Development and regeneration of hair cells share common functional features. Proc Natl Acad Sci U S A 104(48):19108–19113

Chapter 26

Whole-Cell Patch-Clamp Recording of Mouse and Rat Inner Hair Cells in the Intact Organ of Corti

Juan D. Goutman and Sonja J. Pyott

Abstract

Whole-cell patch clamping is a widely applied method to record currents across the entire membrane of a cell. This protocol describes application of this method to record currents from the sensory inner hair cells in the intact auditory sensory epithelium, the organ of Corti, isolated from rats or mice. This protocol particularly outlines the basic equipment required, provides instructions for the preparation of solutions and small equipment items, and methodology for recording voltage-activated and evoked synaptic currents from the inner hair cells.

Key words Inner hair cell, Cochlea, Organ of Corti, Whole-cell patch-clamp, Voltage clamp, Voltage-activated current, Evoked synaptic current

1 Introduction

Whole-cell patch-clamp electrophysiology has been used to measure the electrical potential and currents from a variety of cell types including the sensory hair cells from various animals, including (but not limited to) frog [1], turtle [2], chick [3], guinea pig [4], rat [5], and mouse [6]. These recordings have been invaluable to examining the biophysical mechanisms underlying function of these sensory cells, including mechanoelectrical transduction [7], electrical tuning in nonmammalian hair cells [8], membrane properties of mammalian inner and outer hair cells [9], the mechanisms of afferent neurotransmitter release [10], and synaptic transmission at olivocochlear efferent synapses [11]. While whole-cell patch-clamp recordings were originally performed on isolated hair cells, the ability to perform recordings in the intact organ of Corti has greatly expanded the capacity to examine the physiology of the sensory hair cells genetically, tonotopically, and in association with their synaptic contacts and neighboring cells. Recordings from the intact organ of Corti have proven essential to our increasing understanding of the developmental changes underlying the maturation

of the sensory hair cells, afferent and efferent synaptic transmission, and glutamate uptake by neighboring support cells. This chapter describes the materials and protocols necessary for recording whole-cell currents from inner hair cells in the acutely isolated organ of Corti. Although emphasis is placed on the recording and isolation of voltage-gated currents and evoked synaptic currents, very similar techniques can be used to record currents from the outer hair cells [12], the afferent boutons [13], as well as supporting cells within the organ of Corti [14]. Finally, although this chapter discusses only the whole-cell configuration, the methods outlined can be adapted to investigate other patch-clamp configurations.

2 Materials

2.1 Isolating the Organ of Corti

1. Dissecting stereomicroscope (e.g., Olympus SZ51 or Leica MZ75).
2. Dissection scissors and forceps (Fine Science Tools).
3. 35-mm petri dishes.

2.2 Coverslip Fabrication to Hold the Isolated Organ of Corti

1. Glass coverslips (e.g., 0.8–12 cm diameter round glass coverslips).
2. Stainless steel insect (minutien) pins (e.g., length of 1 cm and diameter of 0.1 mm, Fine Science Tools).
3. Heating platform.
4. Sylgard.

2.3 Electrode Fabrication and Filling

1. Programmable pipet puller (e.g., Narashige PC-10 or Sutter Instrument Company P-97).
2. Thin-walled borosilicate glass tubing (e.g., 1 mm capillaries with filament, World Precision Instruments).
3. Recording electrode filling pipet (e.g., MicroFil needle, World Precision Instruments).

2.4 Whole-Cell Patch-Clamp Recordings

1. Patch-clamp microscope with DIC (e.g., Zeiss AxioExaminer, Olympus BX51).
2. Precision micromanipulators and electrode holder for patch clamping (e.g., Sutter Instrument Company MP-285).
3. Patch-clamp amplifier and digitizer (e.g., Molecular Devices Multiclamp 700A and Digidata 1322A).
4. Acquisition and analysis software (e.g., pClamp and/or WinWCP [Windows Whole Cell Program] developed by John Dempster at the University of Strathclyde Glasgow).

5. Vibration isolation table, perimeter, and Faraday cage (e.g., TMC).
6. Gravity-fed, local perfusion system (*see Note 1*).
7. Drug delivery pipet (e.g., MicroFil needle, World Precision Instruments).
8. Coarse micromanipulator (e.g., Sutter Instrument Company MP-85).
9. Isolated constant current stimulator (e.g., Digitimer Ltd. DS3).
10. Stimulating electrode holder (e.g., electrode holder for theta glass, Warner Instruments).
11. Theta-glass tubing (e.g., Warner Instruments).
12. Insulated silver wire (e.g., 0.25 mm, teflon coated silver wire, Warner Instruments).

2.5 Solutions

Prepare all solutions using ultrapure water and analytical grade reagents.

1. Household bleach (e.g., Clorox).
2. External solution (mM): 155 NaCl, 5.8 KCl, 0.9 MgCl₂, 1.3 CaCl₂, 0.7 NaH₂PO₄, 5.6 D-glucose, and 10 HEPES, pH 7.4, 300 mOsm.
3. Internal solution (mM): 150 KCl, 3.5 MgCl₂, 0.1 CaCl₂, 5 EGTA, 5 HEPES, and 2.5 Na₂ATP, pH 7.2, 290 mOsm (*see Note 2*).

3 Methods

3.1 Experiment Preparation

Solutions, coverslips, and both cleaning and stimulating electrodes can be made well in advance of experiments. Recording electrodes should be made the day of experiments.

3.1.1 Solutions

1. Prepare external solution, usually in 1 L volumes, filter, and store at 4 °C for at most 2 weeks.
2. Prepare internal solution usually in 50 mL or 100 mL volumes on ice, aliquot in 5 mL volumes, and store at -20 °C for at most 2 months. Keep on ice and use immediately once thawed for experiments. Discard any extra solution.

3.1.2 Coverslip Fabrication to Hold the Isolated Organ of Corti

1. Place the coverslip on a very warm hot plate.
2. Place a minutien pin across the diameter of the coverslip.
3. Use a standard pipet tip to place a drop of prepared Sylgard on one end of the pin to secure it to the coverslip. The heat cures the Sylgard immediately. Be careful the Sylgard drop is not too

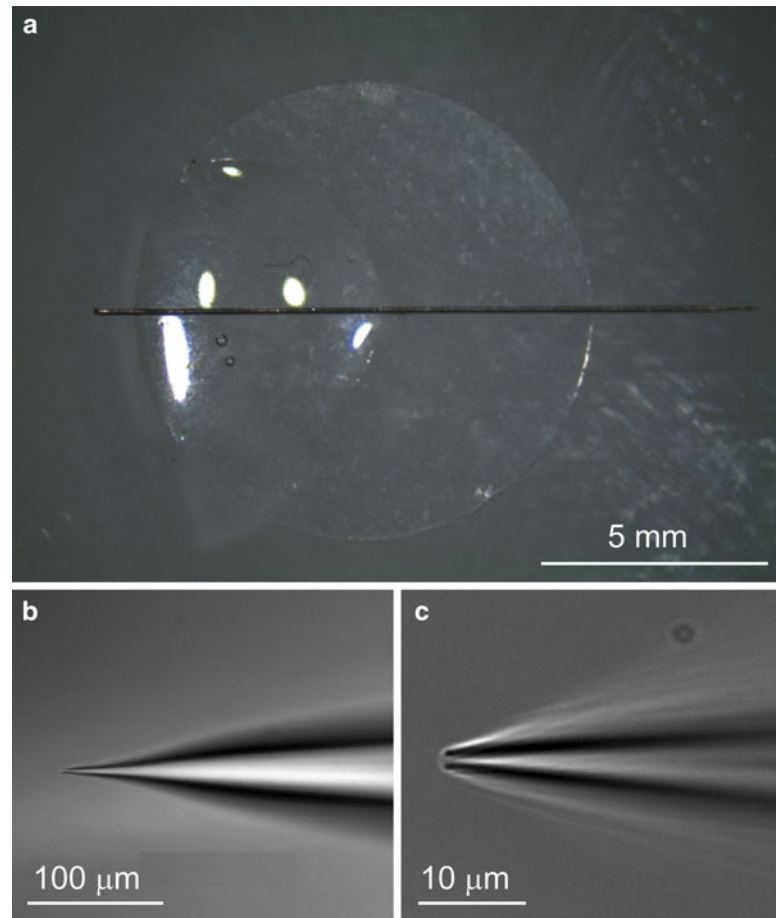


Fig. 1 Preparation of coverslips and recording electrodes. (a) A properly prepared coverslip is fabricated from round coverslip glass (with a diameter of approximately 1 cm) and an insect pin (with a length of approximately 1 cm and diameter of 0.1 mm) affixed with a drop of Sylard. (b, c) An appropriately shaped recording electrode, at lower magnification (b) and also higher magnification (c), tapers rapidly and has an opening diameter generally between 1 and 2 μm

high or it can obstruct access to the organ of Corti during patch-clamp recordings. A finished coverslip is shown in Fig. 1a.

4. Coverslips can be rinsed with distilled water after experiments and reused.
1. Pull recording electrodes from borosilicate glass using a multi-stage puller. A starting protocol is: Heat 1: 65.1, Heat 2: 58.0 (Narishige PC-10). However, adjustments will need to be made. In most cases, the temperature of the final pull needs to be increased/decreased to pull electrodes with smaller/larger tip diameters, respectively.

3.1.3 Recording Electrode Fabrication

2. Examine the tip for shape and diameter under a compound microscope. The tip should taper rather steeply, and the final diameter varies depending on the recordings being performed (Fig. 1b, c). Tip diameters of approximately 2 μm have resistances of 1–3 $\text{M}\Omega$ with the above solutions, whereas smaller tip diameters (1 μm) have resistances of 5–6 $\text{M}\Omega$. See Note 3 for more discussion on electrode resistances.

3.1.4 Cleaning Pipet Fabrication

1. Under a stereomicroscope break the tip of a recording electrode with dissecting forceps so that the tip diameter is approximately 10–30 μm .

3.1.5 Stimulating Electrode Fabrication

Electrodes for stimulating olivocochlear efferent terminals can be fabricated from the same glass pipets used for recordings (creating a unipolar electrode) or, alternatively, from theta-glass capillaries (creating a bipolar electrode). Fabrication of a bipolar electrode is described below. Fabrication of a unipolar electrode would be similar except that the second pole is connected to the bath ground.

1. Cut two pieces of insulated silver wire to a length of approximately 5 cm.
2. Remove insulation from one end of each of the silver wires to expose about 0.5–1 cm of uninsulated wire.
3. Immerse the exposed part of the wires in full strength household bleach for 15–30 min until the wire obtains a purple-gray color. Rinse with distilled water and use.
4. Remove insulation from the other end of each of the silver wires to expose about 3–4 mm or just enough to allow for electrical continuity with stimulator.
5. Pull the theta-glass capillary using the following protocol: single step with a heating value of 65.1 (Narishige PC-10).
6. Under a stereomicroscope, break the tip of the stimulating electrode with dissecting forceps, so that the tip diameter is approximately 20–40 μm . See Subheading 3.1.5, step 9 for instructions on measuring the resistance values.
7. Fill each compartment of the stimulating electrode approximately half way with external solution.
8. Insert a silver wire into each compartment of the stimulating electrode and mount the electrode to a holder.
9. With the aid of a fine micromanipulator, place the tip of the stimulating electrode inside the recording bath (filled with extracellular solution). Use a voltmeter to measure the electrode resistance across the cable connectors of the electrode holder. Resistance for bipolar electrodes should not be greater than 1–2 $\text{M}\Omega$.
10. Connect the mounted electrode to the stimulator.

3.2 Isolating the Organ of Corti for Patch-Clamp Recordings

Isolating the organ of Corti (for patch-clamp recordings and other techniques) requires practice and is best learned with the help of someone experienced in the dissection. An excellent video tutorial is available [15]. Isolation of the organ of Corti generally becomes more difficult as the animals mature and the structures of the inner ear calcify. Apical (low frequency turns) are generally easier to isolate than basal (high frequency) turns. Organs of Corti are best isolated from rats and mice younger than 1 month of age (although older ages are possible). The age of animals used to obtain tissue, also depends on the intent of the experiments: many voltage-gated currents show developmental changes in expression [16].

1. Remove the temporal bone containing the inner ear from the skull using dissecting scissors and place immediately in a 35 mm petri dish filled with ice-cold external solution.
2. Under a dissecting microscope isolate the inner ear from the temporal bone using forceps and place into a new 35 mm petri dish filled with ice-cold external solution containing the submerged coverslip.
3. Remove the organ of Corti from the inner ear using forceps.
4. Remove the overlying tectorial membrane using forceps.
5. Position the organ of Corti under the insect pin of the cover-slip so that the inner hair cells are accessible from one side of the pin (in the *y*-axis). A properly positioned organ of Corti is shown in Fig. 2 (see Note 4).

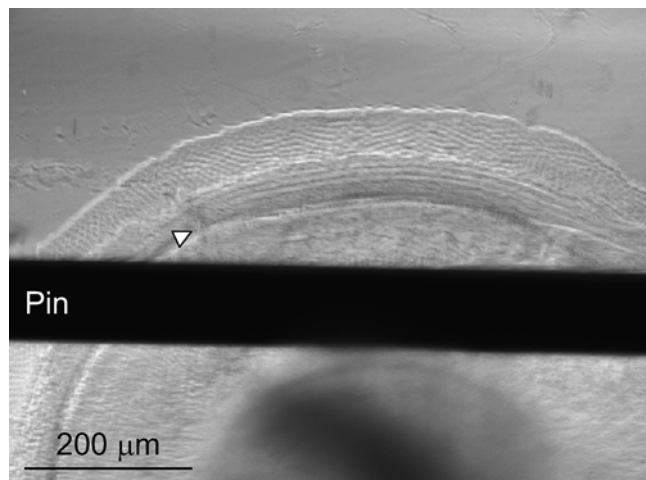


Fig. 2 Low magnification micrograph of an isolated organ of Corti positioned on a coverslip. A properly positioned organ of Corti is firmly and flatly anchored under the insect pin and also allows for ample room to access the row of inner hair cells (open arrowhead) by the recording electrode

3.3 Preparing the Isolated Organ of Corti for Patch-Clamp Recordings

Depending on the recordings to be performed, a necessary step described here is the removal of supporting cells that overlie the basal ends of the inner hair cells and/or the terminals of the efferent projections.

1. Place the coverslip with the organ of Corti into the recording chamber. The organ of Corti must be kept under constant perfusion at a rate of approximately 1–3 mL/min.
2. Bring the organ of Corti into view first under low power (10×) and then under higher power (40× or 60×). Gently raise the objective but (ideally) keep the objective in contact with the bath (external) solution. Raising the objective allows room to position the cleaning pipet.
3. Place the cleaning pipet onto the electrode holder. Use the micromanipulators to position the cleaning electrode into the bath and under the microscope objective.
4. Incrementally lower the cleaning pipet and objective until the cleaning pipet is in the same field of view as the organ of Corti.
5. Gently position the cleaning pipet onto the organ of Corti just below the row of inner hair cells (toward the spiral ganglion cells in the *y*-axis). Apply gentle suction while moving the cleaning pipet below the row of inner hair cells. (Suction can also be applied with the aid of a 50 mL syringe connected to the electrode holder.) The goal is to carefully remove the supporting cells and connective tissue that cover the base of the inner hair cells (*see Note 5*).
6. Repeat this step until the basal ends of at least a few inner hair cells have been sufficiently exposed. An organ of Corti before and after cleaning is shown in Fig. 3.
7. Raise the objective (while still keeping it in contact with the bath solution) and retract and dispose of the cleaning pipet.

3.4 Achieving the Whole-Cell Patch-Clamp Recording Configuration

The procedure for whole-cell patch clamping inner hair cells is very similar to the procedures used to patch-clamp other cells. In all cases, ideal procedures are somewhat personal and can vary from cell to cell. Excellent reviews outlining the general theory and application of patch clamping are available elsewhere [17].

1. Fill the recording electrode approximately halfway with filtered internal solution (*see Note 2*). Be sure there are no air bubbles in the tip. Place the recording electrode onto the electrode holder and apply positive pressure. The electrode should be at approximately a 30° angle with the coverslip and organ of Corti.
2. Use the micromanipulators to position the recording electrode into the bath and under the microscope objective.

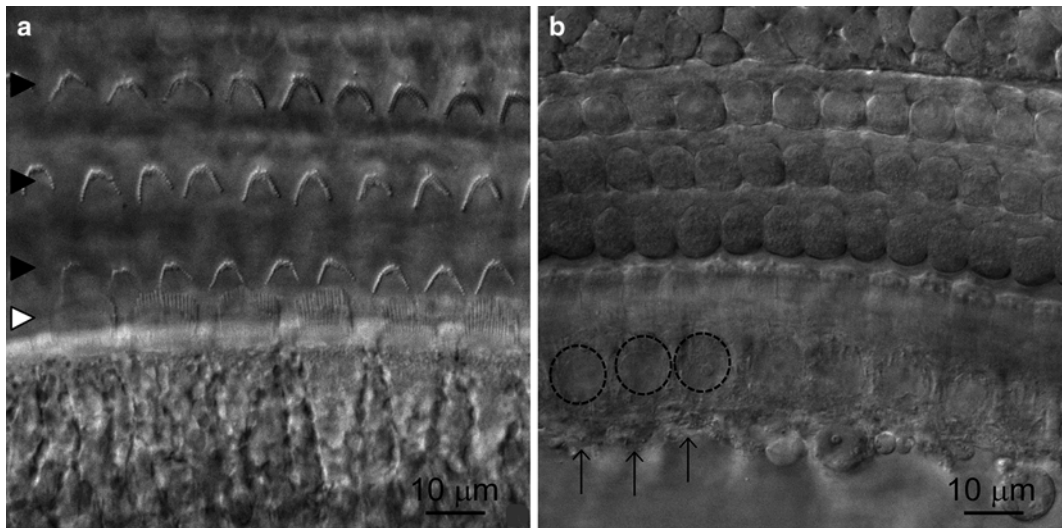


Fig. 3 High magnification of an isolated organ of Corti before and after cleaning. **(a)** Hair cell stereocilia are visible in a preparation before cleaning. The three rows of outer hair cells (*closed arrowheads*) and a single row of inner hair cells (*open arrowhead*) are indicated. **(b)** In the cleaned organ of Corti, the relative positions of the hair cells are similar but the basal ends are now exposed for the first three inner hair cells (*arrows*). Nuclei are also clearly visible (*circled*)

3. Verify the appropriate resistance (size) of the electrode with a test pulse (*see Note 3*).
4. Verify the appropriate (negative) holding potential.
5. Incrementally lower the recording electrode and objective until the recording electrode is in the same field of view as the organ of Corti.
6. Verify the appropriate positive pressure on the electrode. There should be a visible stream from the tip of the electrode and yet pressure should not be so high as to cause cells to detach from the organ of Corti.
7. Choose a healthy hair cell for patching. Indicators of poor condition (indicating a hair cell should not be patched) include disrupted or missing stereocilia, cell swelling, particle movement in the nucleus or cytoplasm.
8. Bring the recording electrode alongside the base of the inner hair cell to be patched. The electrode tip and the cell membrane of the hair cell should be in the same plane. Focus up and down to verify that the tip of the electrode is indeed in the same plane as the hair cell and neither above nor below.
9. Gently slide the recording electrode along the lateral wall of the hair cell to verify that the electrode is positioned on the hair cell membrane (and not the membrane of a supporting cell).

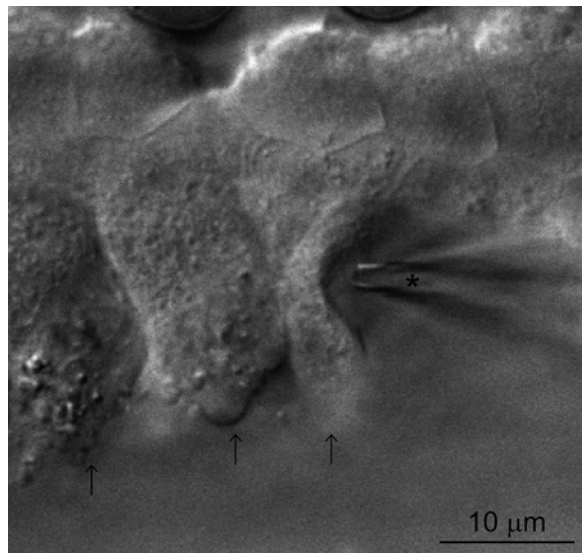


Fig. 4 High magnification of an isolated organ of Corti showing the proper approach to an inner hair cell with a recording electrode. Supporting cells surrounding the inner hair cells have been removed to allow access by the recording electrode (*) to the basal ends of the first three inner hair cells (arrows). The membrane of one of the inner hair cells and the tip of the recording electrode are in focus (in the same plane) and the positive pressure of the recording electrode forms a visible indentation on the inner hair cell membrane

10. If necessary readjust positive pressure and/or the position of the recording electrode so that there is a visible indentation of the hair cell membrane by the recording electrode (Fig. 4).
11. Release positive pressure and simultaneously apply slight negative pressure to the recording electrode.
12. Monitor the membrane resistance. (Both software packages referred to above are able to continuously measure and check this parameter). It should increase and achieve a gigaohm seal. For some hair cells, changes in resistance happen quickly, whereas for other hair cells changes happen more gradually. If the membrane resistance stabilizes without reaching a gigaohm seal, increase negative pressure gradually until a gigaohm seal is achieved.
13. Once a gigaohm seal has been achieved, apply gentle, rapid negative suction to achieve the whole-cell configuration.
14. If a gigaohm seal cannot be achieved, raise the objective (while still keeping it in contact with the bath solution), retract and dispose of the recording electrode, and begin with a new recording electrode and hair cell.
15. The approximate membrane properties of a healthy cell in the whole-cell configuration are (in voltage clamp mode) a mem-

brane capacitance of 10 pF, a membrane resistance of 200–400 M Ω , a series resistance of up to 20 M Ω , and (in current clamp mode) a resting membrane potential of –60 mV. These values depend on a variety of factors, especially the size of the cell, the size of the recording electrode, the quality of the whole-cell configuration, and the solutions.

16. In voltage-clamp mode, large outward (potassium) currents are evoked in response to depolarizing voltage steps and are another indication that the whole-cell configuration is established correctly.
17. The isolated organ of Corti, under constant perfusion and at room temperature, can last for up to 1 h. Indications that the preparation should be replaced include loss of integrity of the cell membranes, swollen cells, and particle movement in the nuclei or cytoplasm.

3.5 Recording and Analyzing Whole-Cell Voltage Clamp Currents

The biophysical properties of the currents to be recorded determine the voltage clamp protocols. The most conspicuous voltage-gated currents in inner hair cells from hearing animals are relatively quickly activating BK currents and relatively slowly activating K⁺ currents. Recording and isolating these currents is described here to illustrate the general principles required to analyze whole-cell currents.

1. As part of preparing for experiments (*see Subheading 3.1*), make 5–10 mL of 100 nM IBTX in external solution and load into a gravity-fed, local perfusion system (*see Note 1*).
2. After preparing the isolated organ of Corti for patch-clamp recordings (*see Subheading 3.3*), use a coarse micromanipulator to position the drug delivery pipet approximately 300 μ m from the recording electrode and just above the sensory epithelium.
3. After achieving the whole-cell configuration (*see Subheading 3.4*), apply on-line series resistance correction. With low resistance recording electrodes, series resistances are typically 5 M Ω and can often be compensated by 70 % on-line. Series resistance correction may need to be adjusted during the recordings.
4. From a hyperpolarized membrane potential (–60 mV) depolarize the membrane to approximately 40 mV in 10 mV steps. Depolarization durations should be approximately 20–100 ms to achieve steady-state outward currents. Allow sufficient time between depolarization steps (2–10 s) (*see Note 6*). Finally, leak subtraction can be incorporated into these protocols. Previous experiments [18, 19] have utilized a standard P/4 protocol [20]. Finally, because of their fast activation, low pass filter BK currents at 10 kHz and sample (digitize) at 50 kHz.

3.5.1 Pharmacological Isolation

Although less than ideal, BK currents can be separated from the more slowly activating K⁺ currents by the time of measurement. Because BK currents activate with a tau of <1 ms, which is much faster than the other slowly activating K⁺ currents (tau ≈ 6 ms), currents measured 1 ms after application of the depolarizing step are mostly BK currents [18]. Pharmacological isolation of currents is often the preferred method of isolation (*see Note 6*). BK currents can be isolated from the remaining K⁺ currents by off line subtraction after pharmacological blockade. IBTX is a toxin highly specific for BK channels [21].

1. Record whole-cell currents in IBTX using the same voltage protocol used in control (no toxin) conditions (*see Note 8*).
2. Offline subtract records obtained in IBTX from those obtained in control conditions (which represent the total K⁺ currents) to obtain the isolated BK currents. (Most acquisition and analysis software provides features to subtract records.) Further analyses of these records can be performed as required. For example, activation kinetics can be fit to the original records and/or the isolated BK currents. In addition, current-voltage (*I-V*) or conductance-voltage (*G-V*) relationships can be calculated from the original records and/or the isolated BK currents. Excellent explanations on preparing and analyzing *I-V* and *G-V* curves are available elsewhere [17].

3.6 Recording Evoked Synaptic Currents

Before the onset of hearing, efferent terminals originating from the medial superior olive in the brainstem contact IHCs [22]. This direct efferent innervation of the IHCs peaks functionally during the second postnatal week [23]. Spontaneous efferent synaptic activity can be recorded postsynaptically from the IHC using methodology similar to that described above. Efferent synaptic activity can also be evoked and recorded postsynaptically from the IHC using the protocol described below.

1. After preparing the isolated organ of Corti for patch-clamp recordings (*see Subheading 3.3*), use a precision micromanipulator to position the extracellular stimulating electrode under the row of IHCs and in contact with the preparation.
2. After achieving the whole-cell configuration (*see Subheading 3.4*), deliver stimulating pulses at a rate of 1 Hz while holding the IHC at -90 mV. Begin with pulse amplitudes between 100 and 200 μA and durations of current (or voltage) between 100 and 500 μs (*see Note 9*).
3. If no synaptic currents are elicited, reposition the stimulating electrode towards or away from the row of IHCs (in the *y*-axis) and/or into or out of the organ of Corti (in the *z*-axis). Stimulation of the efferent terminals projecting to the IHCs is achieved most efficiently by placing the stimulating electrode

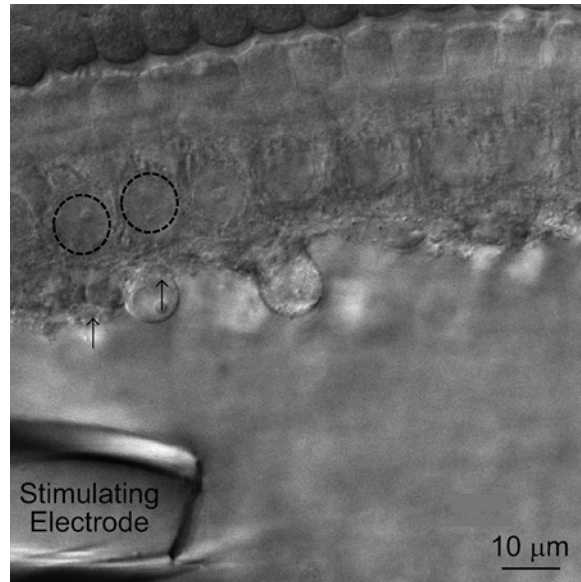


Fig. 5 High magnification of an isolated organ of Corti showing the proper positioning of recording and stimulating electrodes. The basal ends of two inner hair cells (arrows) and their nuclei (circled) are visible relative to the stimulating electrode

near the row of IHCs, but not necessarily directly below the recorded IHC. When repositioning the stimulating electrode, do so slowly and carefully so as not to compromise the whole-cell patch-clamp configuration. A properly positioned stimulating electrode is shown in Fig. 5.

4. The amplitude and duration of the pulse is another factor that can be modified for successful stimulation. Importantly, the stronger the stimulation, the more fibers are recruited and the larger the synaptic response (also, the lower the failure rate). Changing the polarity of the pulse may also affect the response.
5. From these records, quantal analyses can be performed to determine important parameters of neurotransmitter release at the efferent-IHC synapse and are described excellently elsewhere [24].

4 Notes

1. The gravity-fed, local perfusion system can be very simple and consist of a syringe connected to the delivery pipet by nothing more than tubing and a stopcock. On the other hand, a variety of commercially available and also computer-driven systems (e.g., Warner Instruments VC-8) are available for use.

Application of solutions using a picospritzer (Parker) may be preferable, to precisely control small ejection volumes (pL) and ejection times (ms) [12].

2. Typically the osmolarity of the internal solution is 10–15 mOsm less than that of the external solution to promote formation of a gigaohm and obtain long and stable recordings. K⁺-based internal solutions are also suitable for recording synaptic currents. An alternative to K⁺-based internal solutions, especially when recording Ca²⁺ currents, is the following solution (mM): 120 CsMeSO₃, 13 TEA, 5 HEPES, 0.35 CaCl₂, 3.5 MgCl₂, 1 EGTA, 2.5 Na₂ATP, pH 7.2, 290 mOsm). CsMeSO₃ can be replaced by CsCl, or CsGluconate.
3. In general, more rapidly tapering electrodes are preferable to more slowly tapering electrodes, since the former reduces electrode resistance. The size of the electrode depends on the size of the currents to be recorded. While smaller (higher resistance) electrodes more easily form gigaohm seals, larger lower resistance electrodes reduce series resistance errors associated with large recorded currents. Series resistance errors are deviations of the membrane potential from the clamped potential caused by currents passing across the electrode and cell resistances in series. Series resistance errors make voltage-dependent outward currents appear to activate more slowly and have lower magnitudes at steady state. These effects become more dramatic as the current and associated voltage deviation, $V=IR$, increases.
4. Proper positioning of the organ of Corti under the insect pin is important. Enough of the organ of Corti must be exposed above the insect pin to allow access to the inner hair cells by the recording electrode. At the same time, enough of the epithelium must be securely positioned under and below the pin to firmly anchor the organ of Corti to the coverslip. Finally, the organ of Corti must be flatly positioned under the pin. If the organ of Corti is too loose, cleaning of supporting cells may dislodge the organ of Corti from the coverslip. Approaching cells with the recording electrode becomes more difficult if the epithelium is not positioned flatly under the pin.
5. The basal ends of inner hair cells are more inaccessible in organs of Corti obtained from younger animals (<P12) but become more exposed in older organs of Corti (>P14). Depending on the recording age, cleaning overlying cells may or may not be necessary. If the cleaning of overlying cells is not necessary, a recording electrode, filled with external solution and under positive pressure, can be pushed through the tissue below the row of IHCs, to open space for later access with another recording electrode filled with internal solutions.

6. In general, when recording large, outward K⁺ currents, it is best to keep the depolarization duration as short as possible. Short durations avoid the accumulation of extracellular K⁺, which shifts the Nernst potential of K⁺, thereby reducing the driving force of K⁺ efflux and decreasing current magnitudes in a time-dependent manner. Longer durations between depolarizing steps and continuous perfusion with external solution also prevent accumulation of extracellular K⁺. Importantly, previous work shows that K⁺ accumulation is minimal under these conditions [17].
7. Blocking substances are used in one of two main ways to separate currents. First, it may be possible to block all currents except the current of interest. Depending on the range of channels present, this may involve one or more blockers, sometimes in combination with ionic substitution. Secondly, a blocker that is specific for the channel of interest may be used. Current is recorded in the presence of the blocker and that result is subtracted from current obtained in the absence of the blocker to visualize the current of interest.
8. IBTX is difficult to washout. Ideally, to verify recording stability, whole-cell currents should be measured after washout of the pharmacological agent, using the same voltage protocol used in control and treatment conditions. Control and washout currents should be comparable to verify stability.
9. Repositioning the stimulating electrode is preferable to applying very large or prolonged electrical stimuli. Larger stimuli reduce recording stability. Prolonged stimuli can result in stimulation artifacts that overlap with evoked synaptic currents.

References

1. Lewis RS, Hudspeth AJ (1983) Voltage- and ion-dependent conductances in solitary vertebrate hair cells. *Nature* 304(5926):538–541
2. Art JJ, Fettiplace R (1987) Variation of membrane properties in hair cells isolated from the turtle cochlea. *J Physiol* 385:207–242
3. Fuchs PA, Nagai T, Evans MG (1988) Electrical tuning in hair cells isolated from the chick cochlea. *J Neurosci* 8(7):2460–2467
4. Santos-Sacchi J, Dilger JP (1988) Whole cell currents and mechanical responses of isolated outer hair cells. *Hear Res* 35(2–3):143–150
5. Glowatzki E, Fuchs P (2000) Cholinergic synaptic inhibition of inner hair cells in the neonatal mammalian cochlea. *Science* 288(5475):2366–2368
6. Kros CJ, Ruppersberg JP, Rusch A (1998) Expression of a potassium current in inner hair cells during development of hearing in mice. *Nature* 394(6690):281–284
7. Fettiplace R, Kim KX (2014) The physiology of mechanoelectrical transduction channels in hearing. *Physiol Rev* 94(3):951–986
8. Fettiplace R, Fuchs PA (1999) Mechanisms of hair cell tuning. *Annu Rev Physiol* 61:809–834
9. Housley GD, Marcotti W, Navaratnam D, Yamoah EN (2006) Hair cells—beyond the transducer. *J Membr Biol* 209(2–3):89–118
10. Glowatzki E, Grant L, Fuchs P (2008) Hair cell afferent synapses. *Curr Opin Neurobiol* 18(4):389–395
11. Katz E, Elgoyhen AB (2014) Short-term plasticity and modulation of synaptic transmission at mammalian inhibitory cholinergic olivocochlear synapses. *Front Syst Neurosci* 8:224

12. Wersinger E, McLean WJ, Fuchs PA, Pyott SJ (2010) BK channels mediate cholinergic inhibition of high frequency cochlear hair cells. *PLoS One* 5(11):e13836
13. Glowatzki E, Fuchs PA (2002) Transmitter release at the hair cell ribbon synapse. *Nat Neurosci* 5(2):147–154
14. Glowatzki E, Cheng N, Hiel H, Yi E, Tanaka K, Ellis-Davies G, Rothstein J, Bergles D (2006) The glutamate-aspartate transporter GLAST mediates glutamate uptake at inner hair cell afferent synapses in the mammalian cochlea. *J Neurosci* 26(29):7659–7664
15. Grant L, Yi E, Goutman JD, Glowatzki E (2011) Postsynaptic recordings at afferent dendrites contacting cochlear inner hair cells: monitoring multivesicular release at a ribbon synapse. *J Vis Exp* (48)
16. Kros CJ (2007) How to build an inner hair cell: challenges for regeneration. *Hear Res* 227(1–2):3–10
17. Sontheimer H, Ransom CR (2002) Whole-cell patch-clamp recordings. In: Walz W, Boulton AA, Baker GB (eds) *Patch clamp analysis: advanced techniques*, vol 35, *Neuromethods*. Springer, New York, pp 35–67
18. Pyott SJ, Glowatzki E, Trimmer JS, Aldrich RW (2004) Extrasynaptic localization of inactivating calcium-activated potassium channels in mouse inner hair cells. *J Neurosci* 24(43):9469–9474
19. Pyott S, Meredith A, Fodor A, Vázquez A, Yamoah E, Aldrich R (2007) Cochlear function in mice lacking the BK channel alpha, beta1, or beta4 subunits. *J Biol Chem* 282(5):3312–3324
20. Bezanilla F, Armstrong CM (1977) Inactivation of the sodium channel. I. Sodium current experiments. *J Gen Physiol* 70(5): 549–566
21. Galvez A, Gimenez-Gallego G, Reuben JP, Roy-Contancin L, Feigenbaum P, Kaczorowski G, Garcia ML (1990) Purification and characterization of a unique, potent, peptidyl probe for the high conductance calcium-activated potassium channel from venom of the scorpion *Buthus tamulus*. *J Biol Chem* 265(19): 11083–11090
22. Simmons DD (2002) Development of the inner ear efferent system across vertebrate species. *J Neurobiol* 53(2):228–250
23. Katz E, Elgooyhen AB, Gomez-Casati ME, Knipper M, Vetter DE, Fuchs PA, Glowatzki E (2004) Developmental regulation of nicotinic synapses on cochlear inner hair cells. *J Neurosci* 24(36):7814–7820
24. Goutman J, Fuchs P, Glowatzki E (2005) Facilitating efferent inhibition of inner hair cells in the cochlea of the neonatal rat. *J Physiol* 566(Pt 1):49–59

Chapter 27

Glass Probe Stimulation of Hair Cell Stereocilia

Anthony W. Peng and Anthony J. Ricci

Abstract

Hair cells are designed to sense mechanical stimuli of sound using their apical stereocilia hair bundles. Mechanical deflection of this hair bundle is converted into an electrical signal through gating of mechano-electric transduction channels. Stiff probe stimulation of hair bundles is an invaluable tool for studying the transduction channel and its associated processes because of the speed and ability to precisely control hair bundle position. Proper construction of these devices is critical to their ultimate performance as is appropriate placement of the probe onto the hair bundle. Here we describe the construction and use of a glass probe coupled to a piezo-electric actuator for stimulating hair bundles, including the basic technique for positioning of the stimulating probe onto the hair bundle. These piezo-electric stimulators can be adapted to other mechanically sensitive systems.

Key words Piezo-electric stimulation, Hair cell stereocilia, Mechanotransduction, Mechanical stimulator, Auditory system, Hair cells, Hair bundle

1 Introduction

In the auditory and vestibular system, tiny hair bundles protrude from the apical surface of sensory hair cells. These hair bundles consist of a staircased array of actin filled stereocilia and convert mechanical vibrations induced by sound into electrical signals. Much of our knowledge about the mechanisms of how hair cells convert mechanical vibrations into electrical signals was discovered through the use of controlled hair bundle stimulation, while simultaneously recording membrane currents of the hair cell. This technique allows the characterization of the mechanically sensitive ion channel responsible for the mechano-electrical transduction (MET) process. To accurately biophysically assess the properties of ion channels, stimulation must occur at a rate faster than the gating properties of the channel. Thus, voltage-clamp speed is critical for investigating voltage-gated channels, rapid drug application for investigating ligand-gated ion channels, and rapid mechanical stimulations for characterizing mechanosensitive ion channels.

A common method for stimulating the stereocilia hair bundle is to use a stiff glass probe attached to a piezo-electric device. The piezo-electric device moves a given distance for a driving voltage applied to the device with excellent repeatability and accuracy down to the nanometer scale. The first experiments using piezo electric devices were done using piezo-electric bimorphs [1–6]. More recently there has been a shift toward using piezo-electric stacks because of their higher resonant frequency, allowing faster stimulation speeds [7–11].

Other stimulation techniques exist, including another popular method, a fluid jet. The fluid jet stimulation involves using a stream of fluid that is directed at the stereocilia hair bundle. Fluid jets are achieved either using pressure generated from a compressor or from fluid displacement by piezo-electric disk benders. The stimulus is inherently different from the stiff glass probe stimulation since the fluid acts as a force stimulus on the hair bundle, whereas the stiff glass probe acts as a displacement stimulus.

Each stimulation technique has its benefits and drawbacks. The stiff probe is an order of magnitude faster (10 s of μ s rise time) than the fluid jet (100 s of μ s rise time). The fluid jet is able to stimulate the hair bundle without introducing any displacement bias, since it does not require touching the hair bundle (assuming there is no standing pressure from the tip). The stiff probe bypasses any hair bundle mechanics by delivering a displacement rather than a force stimulus like that delivered by the fluid jet. Stiff probes may not stimulate mammalian cochlear hair bundles uniformly, depending on how contact is made [12], whereas the fluid jet has this potential, since the fluid can hit all stereocilia simultaneously. However, this strongly depends on how cohesive the bundle behaves. In this chapter, we will only be discussing the stiff probe stimulation of hair bundles.

We have further developed the piezo electric stack driven glass probe stimulators to increase their stability, reliability, and speed. We will discuss the construction of these stimulators as well as the basic experiment of stimulating mammalian auditory hair bundles. These techniques and stimulators can also be adapted for stimulation of other hair bundle types like those found in the vestibular system or other mechanical systems like touch.

2 Materials

2.1 Recording Solutions

1. Prepare all solutions using ultrapure water (e.g., 18.2 M Ω MilliQ water).
2. Extracellular solution: 140 mM NaCl, 2 mM KCl, 2 mM CaCl₂, 2 mM MgCl₂, 10 mM HEPES, 2 mM creatine monohydrate, 2 mM Na-pyruvate, 2 mM ascorbic acid, 6 mM dextrose, pH to 7.4 using NaOH, 300–305 mOsm using NaCl (*see Note 1*).

3. Intracellular solution: 125 mM CsCl, 3.5 mM MgCl₂, 5 mM ATP, 5 mM creatine phosphate, 10 mM HEPES, 1 mM cesium BAPTA, 3 mM ascorbic acid, pH to 7.2 using CsOH, and 280–290 mOsm using CsCl (*see Note 1*).
4. 4 mm diameter syringe filter, 0.20 µm pore (Corning, Acton, MA) for filtering solutions before loading into pipettes.
5. Eppendorf Microloader (Eppendorf, Hamburg, Germany) for loading solutions into patch pipettes.

2.2 Microscope and Patch Clamp Setup

1. Microscope for viewing stimulator positioning on the hair bundle with transmitted light. We use an upright fixed stage microscope (Olympus BX51 WI) for high magnification (60–100×) images of the hair bundles. Other fixed stage electrophysiology microscopes are also acceptable.
2. Patch clamp amplifier for recording electrical responses from hair cells. We use the Axon 200B for low noise and high bandwidth. Other amplifiers are likely acceptable.
3. Vibration isolation table is absolutely required to minimize vibrations in the setup, which would translate into mechanical responses detected by the hair cell.
4. Full size stable micromanipulator for holding the piezo stimulator like the Sutter MP-285 mechanical or Scientifica PatchStar. Lightweight and small manipulators are not sufficient to carry the load of the piezo stimulator.
5. Mechanically stable stage is another important requirement. Cantilevered stages (only supported on one side of the stage) are less desirable as they add low mechanical resonances to the system. We use a custom stage cut out from 95 mm optical rail supported on both sides. *See Note 2*.
6. Recording dish that allows adjustment of the tissue position. We use a custom recording dish that uses strands of dental floss to anchor the tissue (Fig. 1), which sits on top of two small pieces of cover slip.
7. An apical perfusion pipette with a tip diameter of ~100 µm to protect hair bundles from calcium chelators in the internal solution (*see Note 3*). This requires a perfusion system using a peristaltic pump or gravity flow system. Gravity flow systems are less likely to have pulsating flow. An example of the organization of the pipettes under the microscope is shown in Fig. 1.
8. Custom dual photodiode circuit for optical readout of the motion of the piezo stimulator. We use a 10× eyepiece to project the microscope image onto the photodiode from a quad port adapter on the camera output of the microscope trinocular (*see Note 4*). The photodiode can be on X–Y translation and rotation stages for positioning of the photodiode in the field of view of the microscope (Fig. 2).

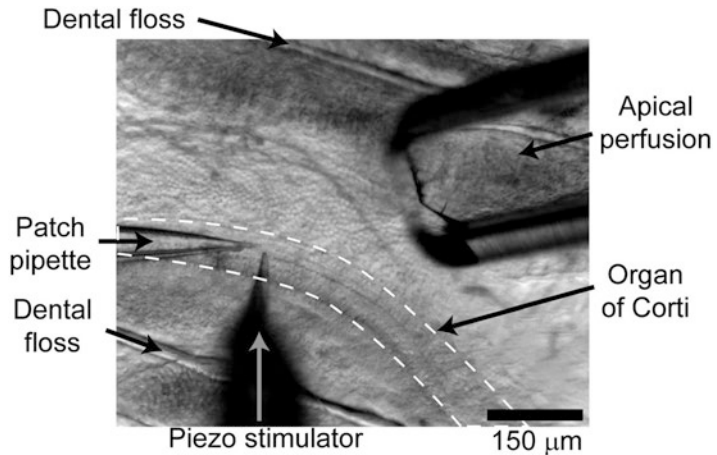


Fig. 1 Example setup of pipettes under the microscope. Dental floss holds the preparation down. An apical perfusion pipette controls the solution that bathes the hair bundles. Patch pipette records electrically from the hair cell. Piezo stimulator moves the hair bundles

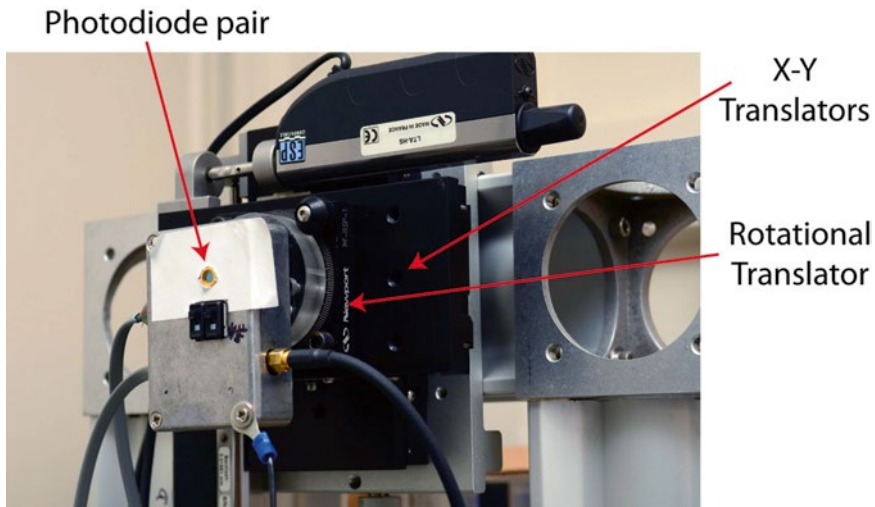


Fig. 2 Example setup of photodiode

9. At least a two channel oscilloscope to monitor the photodiode and patch amplifier outputs. Set the oscilloscope to trigger on the stimulus waveform of the piezo actuator to look at the patch amplifier response a few milliseconds after the onset of the stimulus.

2.3 Piezo Stimulator

1. High voltage piezo driver amplifier. We use a custom high voltage amplifier using an MP38 power operational amplifier with ten times gain. *See Note 5.*

2. Proper connectors to connect the piezo stack to the high voltage amplifier. We use BNC connectors that breakout into banana plugs and connect to the piezo stack using two wire-shielded cable with a flexible jacket like silicone rubber (Cooner Wire, Roseville, CA).
3. Variable attenuator PA5 (Tucker Davis Technologies, Alachua, FL) for easy control of the size of the stimulus. This is not absolutely necessary, but is an added convenience.
4. Variable 8 Pole low-pass Bessel filter (Frequency Devices Inc., Ottawa, IL), removing high frequencies that would excite mechanical resonances in the system.
5. Loctite Epoxy Marine (Loctite, Westlake, OH) (*see Note 6*) used to bond together the piezo stack with the probe holder on one end and the rod on the other for mounting to the manipulator.
6. Tungsten rod. We use 0.5" diameter (*see Note 7*).
7. Bare piezoelectric stack actuator (piezo stack). We use a $6.5 \times 6.5 \times 10$ mm with max displacement of 9.1 μm (Thorlabs, Newton, NJ) (*see Note 8*). Other bare stacks are also available depending on the application.
8. Custom aluminum probe holder to hold a 1 or 1.5 mm diameter glass pipette (Fig. 3; *see Note 9*).
9. Glass capillaries for making micro-probes. We use 1 mm or 1.5 mm capillaries.
10. Micropipette puller (e.g., Sutter P-1000; Sutter Instruments, Novato, CA).
11. Aluminum foil.

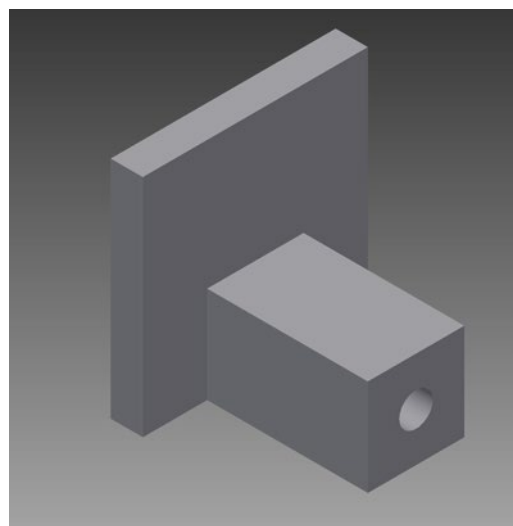


Fig. 3 Example of the custom holder for the glass pipette

12. Hard Signet wax.
13. Microforge (e.g., Narishige MF-900; East Meadow, NY) to make probe tips.
14. Soldering iron.
15. Chromerge Glass Cleaner.
16. Clamp or weight to apply compression force during epoxy curing.

3 Methods

3.1 Making a Piezo Stimulator

1. Epoxy the stack actuator to one end of the tungsten rod with the wires pointing toward the rod. Keep the actuator off-center to one side of the surface of the rod without any part hanging off of it (Fig. 4a; see Note 10).

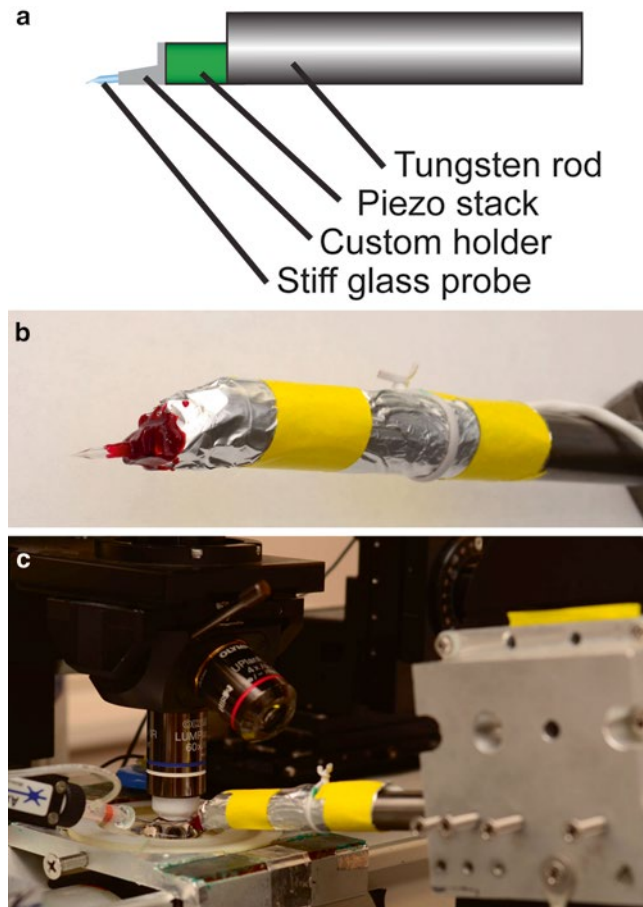


Fig. 4 Piezo Stimulator. (a) Schematic of the piezo stimulator. (b) Image of a completed piezo stimulator. (c) Image of the piezo stimulator on a Scientifica Patchmaster with a custom holder

2. Apply a compression force using a clamp or weight while the epoxy dries overnight.
3. Epoxy the custom glass probe holder to the free end of the piezo stack, also applying compression force while letting it dry overnight.
4. Solder the piezo stack lead wires to the 2-wire shielded cable. Pay attention to have the correct polarity of stimulation delivered to the piezo stack from the amplifier.
5. Tape down the shield of the 2-wire cable to the tungsten rod to ground the shield.
6. Shield the entire piezo stack and lead wires with aluminum foil. Ensure the aluminum foil is in good electrical contact with the tungsten rod and the custom front holder (*see Note 11*).
7. Connect the stimulator, move everything close to final experimental positions, and test for capacitive artifacts in the patch amplifier output during a fast step stimulation of the piezo stack. If artifacts are present, check the grounding in Subheading 3.1, steps 5 and 6.
8. Use the micropipette puller to make a pipette from glass capillaries. Short and stubby pipettes are preferred for higher resonance frequencies.
9. Using a microforge, polish the tip of a pipette to shape it into the rounded V shape of an outer hair cell bundle or a flat shape like the inner hair cell bundle (*see Note 12*).
10. Cut the shaped pipette shank to the length required to fit under the objective. This may be 11–15 mm depending on the objective. A short shank is better since it decreases the cantilever of the probe and thus minimizes unwanted vibrations.
11. Insert the shaped pipette into the custom glass probe holder and immobilize it using the hard Signet wax, by using a soldering iron to melt the wax.
12. Coat the Signet wax around the metal holder to insulate it from any liquid that may contact the custom glass probe holder when under the objective. A complete stimulator is shown in Fig. 4b.
13. Put the stimulator in the micromanipulator (*see Fig. 4c*) and make sure it is visible under the objective in the microscope. Problems here may require slight modification of the design so that none of the microscope components touch the stimulator.
14. Position the image of the shaped probe on the photodiode. The photodiode pair should be oriented perpendicular to the direction of motion of the piezo stack. Moving the image of the probe across the diode should produce a signal waveform like that shown in Fig. 5. Place the probe in the region indicated for maximum sensitivity.

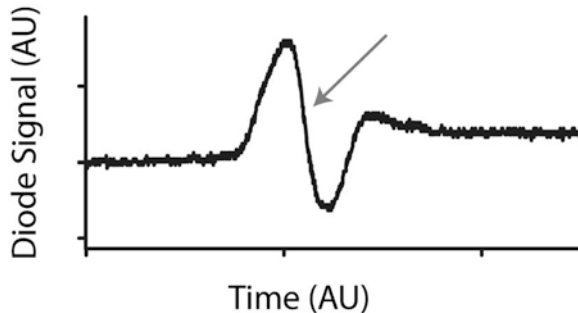


Fig. 5 Photodiode signal trace. An example of the photodiode output signal when an OHC probe is moved perpendicularly across the photodiode pair. The gray arrow indicates the region of greatest sensitivity where the photodiode should be aligned for measurements of probe movement

15. Start with a filter setting of about 30 kHz on the 8-pole Bessel filter. If significant resonance is present, lower the filter cutoff frequency until the level of resonance in the step response is minimal. If this level is below 10 kHz, then improvements to the stimulator are advised (*see Note 13*).
16. Visualize the probe motion on a camera and mark the position of the probe before and after a large actuation of about 1 μm to ensure that the probe is moving straight (*see Note 14*).

3.2 Calibration of the System

1. Calibrate the photodiode magnification by placing a micrometer scale under the objective and measure the magnification at the photodiode.
2. Calibrate the displacement size of the stimulating probe using the photodiode by placing a set voltage to the stack and record the diode signal.
3. Repeat **step 2**, Subheading 3.2 at different voltages to ensure linearity of the photodiode signal.
4. With the probe in the same position, move the photodiode a known displacement (a distance that is equivalent to about 0.5 μm under the objective) and record the photodiode signal.
5. Calculate the displacement sensitivity of photodiode and apply that calibration to the measured photodiode signals in **steps 1** and **2**, Subheading 3.2, to get a value of displacement per volt of the piezo stack. This calibration is used as the displacement of the hair bundle during probe stimulation (*see Note 15*).

3.3 Recording Mechano-electric Transduction Currents

1. Immerse the stiff probe in Chromerge for a few minutes and wash with water. Do this prior to the start of recordings from a new preparation. Do not allow the Chromerge to touch the wax, if possible, as it will slowly deteriorate the wax.
2. Dissect an organ of Corti and place it in the recording dish under the microscope. Keep the stria vascularis attached.

Position the tissue such that the hair bundles are standing upright, parallel to the microscope light path. This can be achieved by adjusting the position of the dental floss anchors seen in Fig. 1.

3. Lower the apical perfusion pipette into the recording chamber and position it to ensure good perfusion of the tissue's apical surface.
4. Bring the stimulator into view in the microscope before patching the hair cell and place it close to the epithelial surface, so that it is easy to position the stimulator onto the hair bundle after patching the hair cell.
5. Ensure no liquid is in direct contact with the grounded/conducting parts of the stimulator, as this will affect the grounding of the patch amplifier. This will be evident as an unstable patch amplifier signal offset when the patch pipette is lowered into the grounded solution.
6. Prior to patching a hair cell, use a pipette to clean the surface of the epithelium with gentle suction around the hair bundles, as debris can sometimes build up around the hair bundles.
7. Patch a hair cell with a hair bundle that closely matches the shape of the stimulating probe.
8. After patching, wait 5 min for the internal solution to equilibrate in the cell before collecting data. During this time, bring the stimulating probe close to the hair bundle of the patched hair cell (*see Note 16*).
9. Put a repeating square waveform of about 100 nm on the probe to test the mechanotransduction current of the hair bundle. We achieve this using our patch application software (jClamp, SciSoft Inc, New Haven, CT), but this can also be achieved using a function generator.
10. Move the probe into the hair bundle, stimulating in the direction of sensitivity of the hair bundle, while watching the response of the cell using the oscilloscope (*see Note 17*). For lateral position, we position the probe such that the peak current is maximized for the given step size while simultaneously maximizing adaptation (*see Note 18*).
11. Run a step protocol (family of curves, example stimulus waveforms shown in Fig. 6a), going from negative displacements to positive displacements. A positive bias on the stack is required to allow for negative displacements. This is accomplished by placing a bias in the piezo amplifier.
12. Look at the saturation of the MET current at large positive stimulations (Fig. 6b). If the current is not saturated, decrease the attenuation of the drive signal and run the protocol again, until the peak MET current is saturating.

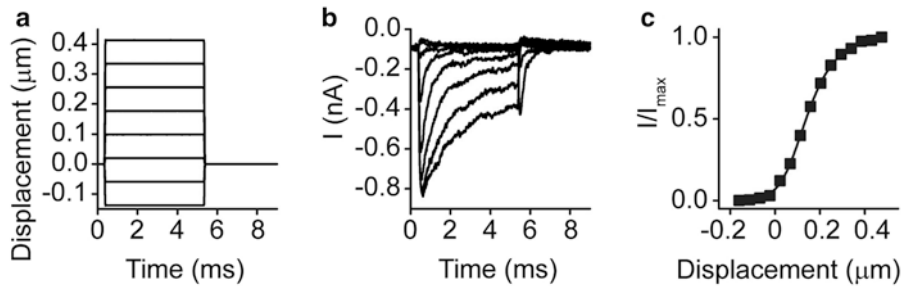


Fig. 6 Waveform and resulting currents. (a) Simulator waveform. (b) Example of MET currents resulting from stimulus waveform in (a). (c) IX curve generated from the peak MET current from each step size from (b). (b) Displays only a subset of the traces, whereas (c) has the data from all traces

13. Look at the amount of adaptation. If adaptation is not fast and robust, try removing the probe from the hair bundle and clean the probe as in Subheading 3.3, step 8 (see Note 19).
14. For each stimulus size, find the peak current immediately following the probe step onset and plot that against the displacement size to generate an activation curve (current-displacement plot) for the MET channel (Fig. 6c).

4 Notes

1. Extracellular solution can be made by the following procedure:
 - A 10× stock of salts is prepared with (mM): 1400 NaCl, 20 KCl, 20 CaCl₂, 20 MgCl₂, 100 HEPES.
 - A 1 M stock solution of Na-pyruvate and ascorbic acid is made ahead of time and stored at -20 °C in 4 mL aliquots.
 - On the day of experiments, make 500 mL of extracellular solution by adding ~350 mL of H₂O to a beaker with a stir-bar and then adding 50 mL of the 10× extracellular stock solution, 1 mL of 1 M Na-pyruvate and ascorbic acid, 2 mM creatine monohydrate, and 6 mM dextrose. Adjust the pH to 7.4 using NaOH.
 - Using a volumetric flask, bring the volume to 500 mL with H₂O and adjust the osmolality of the solution to 300–305 mOsm using NaCl.
 - Intracellular solution can be made by the following procedure:
 - 25 mL of the intracellular solution is made using: 125 mM CsCl, 3.5 mM MgCl₂, 5 mM ATP, 5 mM creatine phosphate, 10 mM HEPES, 1 mM cesium BAPTA, 3 mM ascorbic acid. Adjust pH to 7.2 using CsOH.

- Using a volumetric flask, bring volume to 25 mL with H₂O and osmolality to 280–290 mOsm using CsCl. Aliquot and store at -20 °C. Thaw on day of experiment.
2. Commercial stages are available from ThorLabs, Sutter, and Scientifica. When assessing these stages, look for mechanical stability and strength of springs in the stages. Higher tension springs are better for optimal vibration performance.
 3. Positive pressure in the back of the patch pipette is often used when patch clamping to keep the pipette clean. This will cause a small amount of the internal solution to flow out of the pipette. This solution often contains Ca²⁺ chelators to maintain a low Ca²⁺ concentration. These Ca²⁺ chelators will break the tip-links in the hair bundles and decrease the MET current [13, 14].
 4. The photodiode is designed using a pair of photodiodes with a differential trans-impedance amplifier. The desired magnification of the photodiode system is dependent on the application and desired displacement sizes. More magnification is desired for smaller step size applications and less is desired for larger step applications in order to keep the object in the linear range of the photodiode during the stimulation. Increasing the distance between the photodiode and the projection lens will increase the magnification [4]. There is a tradeoff between magnification and required light intensity as more light is required for a good diode signal as magnification is increased.
 5. The main criteria for choosing a piezo amplifier are a high current output and a voltage range that matches your piezo stack. The actual bandwidth of stimulation depends on the size of the piezo actuator with larger actuators having smaller bandwidths. The output of the amplifier can also be biased to different baseline voltages to allow for negative displacements of the piezo actuator.
 6. This epoxy is chosen because of the stiffness of the cured epoxy. The stiffer the epoxy, the better force translation and resonant performance. Softer, rubbery epoxies do not perform as well. The long cure time is a tradeoff for better performance. Other epoxies are also available that are heat cured for shorter periods of time, which also provide comparable stiffness.
 7. Steel rods can also be used. We choose denser materials because we want a large mass to help dampen any resonance. This could conceivably also be achieved with a large block that the stimulator is connected to, but we have not tested this.
 8. The specific piezo stack may vary depending on application. As a rule of thumb, for bare stacks used in open-loop high-speed stimulation, only use about 10 % of the total displacement the stack can achieve. The longer the stack, the more it can move, but the lower the resonant frequency, translating to a lower

operating frequency for nonresonant motion. Prepackaged and preloaded stacks are also a popular solution, but preload-ing decreases the resonant frequency of the stack. Stacks that are too thin (piezo-chips) have a very high resonant frequency, but have a large off-axis motion. Correcting this off-axis motion increases the load and lowers the resonant frequency of the system.

9. Aluminum is used here because we want the material to be lightweight and conductive. The piezo stack sees this piece as a load. The lower the load mass the better because as load mass increases, resonant frequency decreases according to the equation [15]:

$$f_{\text{Loaded}} = f_{\text{Stack}} \sqrt{\frac{m_{\text{effective}}}{m_{\text{effective+load}}}} \quad (1)$$

Lowering the load mass will increase the resonant frequency. A conductive material is required to shield the capacitive artifacts of the piezo actuator from the patch amplifier signal.

10. This maximizes the clearance to get the device as close as possible to the objective and at as flat an angle as possible. Use only a small dab of epoxy in the center of the piezo stack surface, so that the epoxy does not excessively spill out when compressed together with the rod.
11. Good electrical contact is essential for shielding the capacitive artifact during step displacements of the piezo stimulator. Good contact can be measured using a multimeter with desired resistances between materials being $<1 \Omega$. Make sure all pieces are grounded only once as multiple grounding points will introduce electrical noise through ground loops.
12. To achieve a flat shape, polish the pipette to make it a solid core by touching the tip to the hot polishing filament. Break the glass fiber back until the desired size and lightly polish the end to remove any sharp edges. For the outer hair cell bundle, follow similar procedures for the inner hair cell, but the size of the probe is smaller and should be polished more to achieve the rounded shape. Ideally, to better match the V shape of the outer hair cell bundle, a freshly pulled pipette of the right dimensions can be used and polished until the end of the pipette is sealed, which will round the end of the pipette. An advanced variation is to put a slight bend in the pipette as seen in the schematic of Fig. 4a. This allows the pipette to clear the modiolar side of the tissue and prevent the shank from rubbing against the epithelial surface.
13. Factors that affect the performance of the probe include: fixation of the probe to the holder, length of the glass probe and

strength of epoxy bonds. If you experience a resonance during stimulation with 10 kHz filtering. Make the probe as short as possible and ensure the probe is well attached to the aluminum holder.

14. If motion is not straight, it could mean that piezo actuator motion is constrained or damaged. One common reason for constrained motion is that too much epoxy was used and the epoxy has come into contact with the actuating layers of the stack.
15. An alternative calibration technique is to use the camera. Calibrate the camera image using a micrometer scale under the objective to determine the number of microns/pixel or microns per mm on the screen. Put the probe on the camera, and deliver a large step of 1–2 μm . Record the driving voltage, and measure the actual displacement of the probe using the camera image. This method assumes linearity of the piezo electric stack up to the large displacements used in the calibration.
16. If the probe has gotten dirty with cell debris, bring the stimulating probe away from the preparation and change the filtering frequency with no attenuation. This should “buzz” the stimulating probe and often shake off any debris. Repeat this as necessary to clean the probe. If the probe cannot be cleaned this way, take it out of the recording chamber and clean with Chromerge. Make sure to thoroughly rinse the probe with water before submerging into the dish.
17. We generally position the probe as low as possible without touching the surface of the epithelium. We achieve this by lowering the probe until we know we are touching the surface and then move up slightly.
18. When first performing these MET experiments, explore the parameter space of probe placement. Purposely place the probe in incorrect positions to see how it affects the response of the MET current. Be sure to include positions too far left, right, forward, back, up, and down from the hair bundle. This provides valuable insight as to how probe position affects the resulting MET currents. From this, you can determine which probe placement you believe is correct. Our MET currents assume the placement of the probe to maximize peak current and adaptation. Beware of baseline shifts, since the baseline shift will adapt away over longer timescales. Be sure to pull the probe back sufficiently to negate any baseline shift and let the cell re-equilibrate and reapproach the hair bundle.
19. Sometimes there is transparent material that can prevent the probe from contacting the hair bundle directly and slows the adaptation response. This can also manifest as the probe visually not touching the hair bundle, but a significant MET current is present.

Acknowledgments

We thank Thomas Effertz for critically reading the manuscript. Work was supported by K99 DC013299 to AWP, and by R01 DC003896 from NIDCD to AJR.

References

1. Hudspeth AJ, Corey DP (1977) Sensitivity, polarity, and conductance change in the response of vertebrate hair cells to controlled mechanical stimuli. *Proc Natl Acad Sci U S A* 74:2407–2411
2. Eatock RA, Corey DP, Hudspeth AJ (1987) Adaptation of mechanoelectrical transduction in hair cells of the bullfrog's sacculus. *J Neurosci* 7:2821–2836
3. Corey DP, Hudspeth AJ (1983) Kinetics of the receptor current in bullfrog saccular hair cells. *J Neurosci* 3:962–976
4. Crawford AC, Fettiplace R (1985) The mechanical properties of ciliary bundles of turtle cochlear hair cells. *J Physiol (Lond)* 364:359–379
5. Corey DP, Hudspeth AJ (1980) Mechanical stimulation and micromanipulation with piezoelectric bimorph elements. *J Neurosci Methods* 3:183–202
6. Russell IJ, Richardson GP, Cody AR (1986) Mechanosensitivity of mammalian auditory hair cells in vitro [published erratum appears in *Nature* 321:888]. *Nature* 321:517–519
7. Ricci AJ, Crawford AC, Fettiplace R (2003) Tonotopic variation in the conductance of the hair cell mechanotransducer channel. *Neuron* 40:983–990
8. Ricci AJ, Kennedy HJ, Crawford AC, Fettiplace R (2005) The transduction channel filter in auditory hair cells. *J Neurosci* 25:7831–7839
9. Stepanyan R, Belyantseva IA, Griffith AJ, Friedman TB, Frolenkov GI (2006) Auditory mechanotransduction in the absence of functional myosin-XVa. *J Physiol* 576:801–808
10. Stauffer EA, Holt JR (2007) Sensory transduction and adaptation in inner and outer hair cells of the mouse auditory system. *J Neurophysiol* 98:3360–3369
11. Peng AW, Effertz T, Ricci AJ (2013) Adaptation of mammalian auditory hair cell mechanotransduction is independent of calcium entry. *Neuron* 80:960–972
12. Nam JH, Peng AW, Ricci AJ (2015) Underestimated sensitivity of mammalian cochlear hair cells due to splay between stereociliary columns. *Biophys J* 108:2633–2647
13. Indzhykulian AA, Stepanyan R, Nelina A, Spinelli KJ, Ahmed ZM, Belyantseva IA, Friedman TB, Barr-Gillespie PG, Frolenkov GI (2013) Molecular remodeling of tip links underlies mechanosensory regeneration in auditory hair cells. *PLoS Biol* 11:e1001583
14. Assad JA, Shepherd GM, Corey DP (1991) Tip-link integrity and mechanical transduction in vertebrate hair cells. *Neuron* 7: 985–994
15. Dynamic Operation (2015). Piezoelectrics in Positioning: Tutorial on Piezotechnology in Nanopositioning Applications. www.pi.ws [cited 2015 06/18/2015]

Chapter 28

A Walkthrough of Nonlinear Capacitance Measurement of Outer Hair Cells

Lei Song and Joseph Santos-Sacchi

Abstract

Nonlinear capacitance (NLC) measures are often used as surrogate measures of outer hair cell (OHC) electromotility (eM), since the two are commonly thought to share many biophysical features. The measurement of NLC is simpler than direct measurements of eM and, therefore, many investigators have adopted it. A standard patch-clamp hardware configuration is sufficient for recording NLC, given the proper software interface. Thus, the approach is cost effective. We use the software jClamp since it is tailored to capacitance measurement. Here we detail steps that we use to measure NLC. The walk through includes isolation of guinea pig OHCs, building voltage commands, recording, and analysis.

Key words Nonlinear capacitance, Outer hair cells, Electromotility, Prestin, Cochlea, Inner ear

1 Introduction

The OHC lateral membrane protein prestin [1] powers electromotility [2–5], key to mammalian cochlear amplification [6]. Direct measurement of OHC motility requires a number of additional techniques (such as microchamber [7–9] or equipment (such as fast camera [10] or photodiode [7, 8, 11] which are not standard additions to the usual patch clamp [12] setup. For the investigation of prestin function in nonnative cells [13–15], although electromotility measurement is possible, a micro chamber is required to deform the cell [1] and the magnitude of motility is an order of magnitude smaller than that of the native OHC [1, 13–15]. NLC, a surrogate measure of motility, is the electrical signature of prestin activity. NLC can substitute for measures of motility, and can be carried out on a typical patch-clamp setup without additional equipment. The advantage of NLC is more evident in the assessment of prestin function in transfected cell lines which often express much less prestin, but requires relatively fast measures to acquire large number of cells for statistics [13, 14, 16].

Conventional methods for measuring cell capacitance use step-induced transient analysis (charge integration) or the use of a lock-in amplifier to interrogate phase responses to sine wave stimuli [17–19]. Using a phase detector, the phase tracking method follows the current changes attributed to capacitance changes. Limitations include having low and stable membrane conductance, and these measures are subject to influence of fast (stray) capacitance between pipette and bath solution [18, 20]. We use two-sine method where the additional set of recorded parameters from the second sine is used to solve capacitance which is more resistive to fast conductance change. Data analysis can alternatively be performed on one of the recorded sine wave currents if desired so it offers flexibility in data analysis.

Here we introduce the measurement of NLC of OHCs, a procedure that circumvents the mechanical measurement of OHCs. An example of using two types of stimuli (dual-sine and transient step perturbations atop a voltage ramp) on the same OHC is shown (Fig. 1) where a stair-step stimulus we previously used to detect OHC capacitance [9] and a two-sine stimulus are each applied to

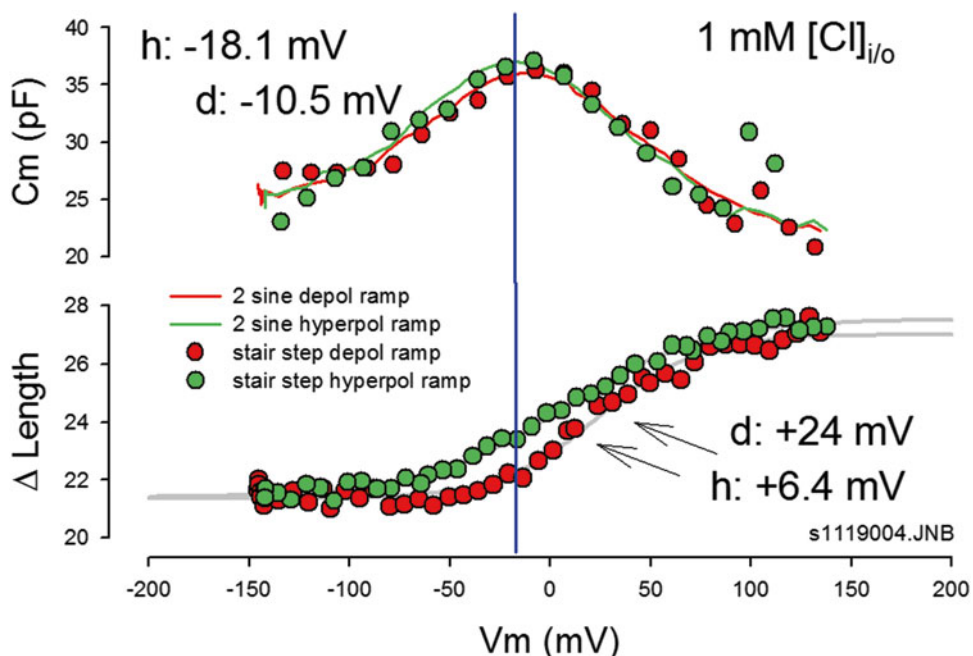


Fig. 1 Example traces of NLC collected from same OHC by using a stair step stimulus (upper panel, circle) and 2-sine (upper panel, solid lines). Stimulus of either depolarization or hyperpolarization ramp are color coded. In general the two stimulus methods generate NLC curves that are overlapping, except the curves that were generated by using 2-sine are less “noisier” than those acquired by step stimulus. *Bottom panel* shows simultaneous measurement of motility. Blue line is the voltage at peak capacitance for a hyperpolarized ramp. A depolarized shift of V_h in motility measurement is marked for each depolarized and hyperpolarized stimulus

the same whole-cell patched OHC. Two-sine analysis is less noisy than that acquired by stair-step stimuli (upper panel, Fig. 1), although mechanical measurement obtained by each ramp stimulus almost overlap (lower panel, Fig. 1). We focus on measuring NLC in OHCs by using the two-sine method. We routinely use the software jClamp (jClamp, www.scisoft.com) in our daily data collection so our introduction is unavoidably based on the operation of that software. However, the basic steps can be replicated by a skilled physiologist/programmer by referring to original publications [21, 22].

We introduce the basic steps for acquiring NLC so a trained electrophysiologist who is familiar with patch clamping can start the measurement with minimal modifications such as the addition of software. Major procedures include isolating OHCs, preparation of the experiment solutions, building stimulus command, and recordings. Some notes are provided to offer tips to acquire high quality data.

2 Materials

2.1 Patch-Clamp

Hardware and Software

1. PC running on windows (XP, Vista, Win 7, and Win 8).
2. Pipette puller (Sutter P-2000 or similar) and soft glass thin wall pipette (WPI, Sarasota, FL).
3. Amplifier (Axon 200 series or 700 series) and headstage.
4. D/A converter: Axon 13xx, 14xx series (Molecular Devices, Sunnyvale, CA), National Instrument Austin, TX) or IO Tech (Measurement Computing Corp, Norton, MA).
5. A Windows compatible camera is optional for measuring NLC and electromotility simultaneously, but is also helpful in monitoring OHC conditions.
6. Software: jClamp (*see Note 1*).

2.2 Solutions

All solutions are made in deionized water.

1. Ionic blocking extracellular solutions (mM): Mix 92 NaCl, 20 TEACl, 20 CsCl, 1 CaCl₂, 2 CoCl₂, 1 MgCl₂, 10 HEPES, in 950 mL of H₂O. Use 1–2 M NaOH to adjust pH 7.2–7.4, then top off to 1 L. Use d-Glucose to increase osmolality of solution to ~300 mOsm (*see Note 2*). Store at 4 °C.
2. Intracellular pipette solution (mM): 136 CsCl, 2 MgCl₂, 10 HEPES, 10 EGTA, start from a smaller volume such as 180 mL. Use 1–2 M CsOH to adjust pH 7.2–7.4 as in Subheading 2.2, step 1. Then top off to 200 mL (you can make smaller volume based on your consumption of pipette solution). Use d-glucose to adjust osmolality to ~300 mOsm.

Be sure to keep intracellular and extracellular solution to within 2 mOsm. When making “physiological” intracellular chloride concentration, gluconate is used as an anion substitute for chloride (*see Note 3*). Store at 4 °C.

3. Filter all solutions with a 0.22 µm filter after the solution is made.
4. (Dispase I, 10 U/mL, Roche).

2.3 Equipment

1. pH meter (e.g., Corning pH meter 430 or similar).
2. Dissecting tools: Scissor (assorted sizes), hemostat, Malleus Bone Nipper, No. 3, No. 5 and fine forceps.

3 Methods

3.1 Isolating Guinea Pig Outer Hair Cells

All animal protocols should be approved by the institutional animal care and use committee according to NIH guidelines.

1. Euthanize animals with isoflurane overdose.
2. Dissect and isolate temporal bones and place in a petri dish filled with 1x PBS.
3. Refrigerate unused second cochlea at 0–4 °C for later use (up to 4 h).
4. Open bulla with a Malleus Bone Nipper, to expose cochlea and remove ossicles with No. 3 forceps.
5. Press and crack the apical part of the cochlea using blunted or No. 3 forceps. Lift the cracked bone to create an opening.
6. Carefully tuck between the bone and spiral ligament and press toward the bone (outward) using the blunted forceps tip or No. 3 forceps. Cracked bone chips will then be lifted away. Start from the opening and work down toward the base to expose the whole Organ of Corti.
7. Carefully strip off Organ of Corti (*see Note 4*).
8. Place stripped Organ of Corti in either extracellular solution or PBS with Dispase (5 U/mL).
9. Incubate for 10–12 min at room temperature, then transfer the organ of Corti strip to the recording chamber with a few drops of extracellular solution.
10. Gently triturate the Organ of Corti strip using a flame thinned pipette tip (200-µL pipette tip) mounted on a 1 cc syringe (*see Note 5*).
11. Leave the suspension solution in the recording chamber for about 15–20 min for cells to sink and stick to the glass bottom.
12. Fill the dish with extracellular solution and start recording (*see Note 6*).

3.2 Preparing for Whole-Cell Patch Clamping of Outer Hair Cells

1. Prepare a recording pipette with a resistance of 4–6 MΩ. We typically use thin-walled electrodes (TW150-4 from WPI, Sarasota, FL) (*see Note 7*).
2. Use standard whole-cell patch-clamp technique to form a GΩ seal and then rupture membrane to form a whole-cell configuration. OHC membrane tension (evidenced by changes in cell turgor) should be monitored during pipette washout. This is a crucial step to avoid artifacts since NLC is sensitive to turgor pressure-induced membrane tension [23–27] (*see Note 8*).

3.3 Recording Nonlinear Capacitance

1. Prior to building a command file, make sure the system calibration file is correct (*see Note 9*). Always use an electrical cell model to verify that the measurement system is working properly.
2. Build command file in jClamp within the command building utility. We routinely apply two-sine stimulus [21, 22] superimposed onto a voltage ramp. For construction of command, see help file in jClamp (*see Note 10*).
3. Save command file in the quick access RPD (Rapid Parameter Directory) window to allow quick activation of commands during online recording. Once activated, a command window will pop up and stimulus parameters can be modified online.
4. Use “init” button in the command utility window (or the RPD buttons) to start recording (*see Note 11*). Changes of the command are not saved automatically unless the save button is clicked. Nevertheless, each data file possesses the command protocol for reconstruction.
5. Select Cm vs. Vm in Results window. The data will be displayed as NLC curves online following each data collection. Each stimulus condition can be repeated until stabilization of NLC is reached, usually when intracellular pipette solution exchange is accomplished.

3.4 Data Analysis

1. Open Analysis window then select data file by using open folder icon to load raw data.
2. Select part(ition) 3 by clicking “Sel” for the two-sine ramp collection we typically use (Fig. 2). Only part 3 of the command (ramp) is selected and displayed.
3. Select Yaxis: Cm in the drop down window and Xaxis: Voltage to plot NLC curve.
4. Check “Rs” for series resistance correction.
5. Check “DtR” for detrending of data prior to FFTing (optional, *see Note 12*).
6. Fit NLC curve by select fitting icon and move cursor by left clicking and holding.

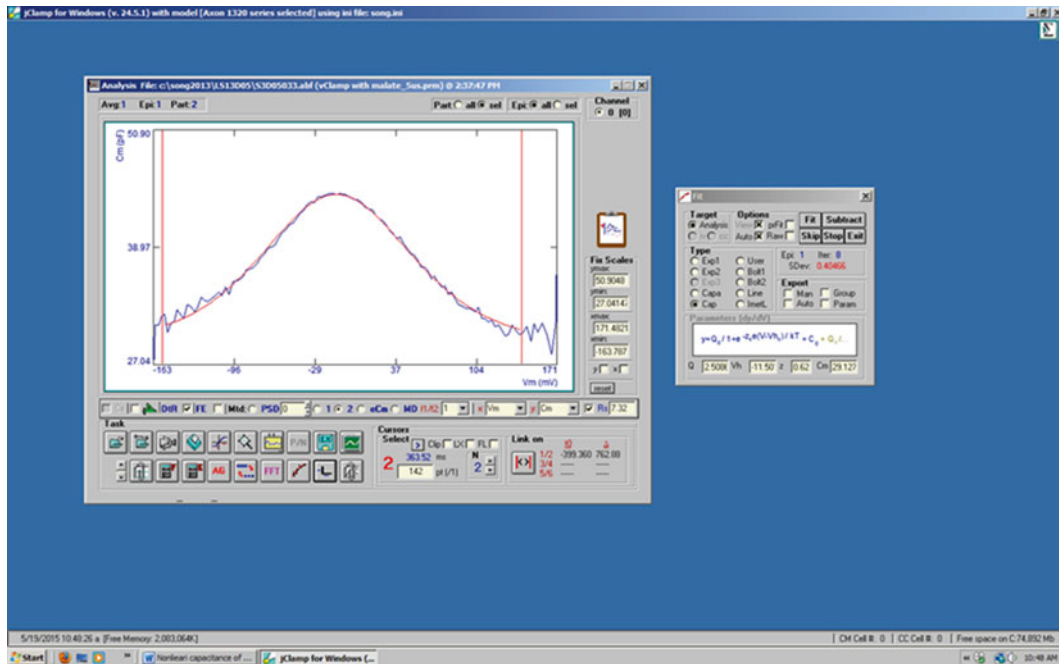


Fig. 2 Screenshot of data analysis window. Red lines/cursors highlight the voltage range fitted. Activate the cursor by clicking the fitting icon on the bottom row of buttons, 7th from the left. Then click each cursor and drag to the proper place. Before fitting, remember to check R_s so the series resistance is corrected. Right window pops up when selecting curve fitting icon. Select Cap and click “fit” button. Fitting parameters are shown in the bottom windows. You can export those fitting parameters by selecting “Param” in “Export” panel (see jClamp help files for more detailed explanations)

7. Select the range for fitting and in the pop up window, select “CAP” fit. Parameters shown in the windows are Q_{\max} (total charge moved), V_h (voltage at peak capacitance), z (valence), and C_{lin} (linear capacitance) (Fig. 2).
8. Export fitted parameters. Select “Param” and then click “Fit” button. Select “Auto” will include fitted curve in the export file so traces can be used in other plotting software, such as SigmaPlot.
9. Plot NLC curve in supported extremal software. Left click on the software icon and drag to the data analysis window and release. Refer to Help file in jClamp for detailed instructions (see Note 13).

4 Notes

1. Although other common software used for patch clamping can also measure NLC, the analyses were very often carried out in a separate program post hoc [28–31]. Our in house developed

software jClamp (distributed through Scisoft, Ridgefield, CT) is by far the easiest software to measure and analyze linear/nonlinear capacitance. The online display of NLC and a number of data analysis features offer handy functions when tracking voltage shifts of NLC. Once an investigator becomes familiar with the program, the data acquisition and analysis are routine.

2. When possible, ionic blocking solutions are used to eliminate current that may interfere with NLC measurements. When “physiological” solutions are needed for your investigation, check the current (by selecting in the analysis window “Vm vs. Im”). If a nonlinear current is present at the voltage where NLC is present, you need to take precaution when interpreting your data, because nonlinear currents can interfere with NLC assessment.
3. Intracellular chloride is the key anion that modulates prestin’s function [32]. When an experiment requires reduction of intracellular chloride, substitute anions often shift NLC curve toward different directions along the voltage axis [32–35]. Errors in fitting for parameters occur if the NLC is moved out of the stimulus voltage range [33, 34]. In general, gluconate substitution maintains NLC curves within the voltage range of the amplifier so that both ends of the curve reach a steady state. Fitting is more reliable under those conditions. When another anion substitution is required, adjust voltage range of stimulation accordingly within the limit of amplifier so that the NLC curve is clearly within the voltage range. Remember, you cannot fit a NLC curve where the peak is not clearly resident, with substantial capacitance measures on either side.
4. Use a forceps to press from under the coiled organ of Corti to break the bone from the modiolus. Start from apex then work down toward base. An alternative is to separate the organ of Corti from the apex and use fine forceps to hold the broken end, while carefully pulling along the spiral of the modiolus.
5. The 200- μ L pipette tips are flame heated in the middle of the taper then pulled to thin the wall. Then trim the base of pipette tip to fit a 1 cc syringe and cut the thinned tube so the opening is just large enough to suck in the strip of the organ of Corti. Metal needles or glass pipettes are not appropriate, as cells tend to adhere to the surface of glass and metal.
6. Fill extracellular (bath) solution gently so OHCs, which adhere to the bottom of the dish, will not float away. An alternative is to use a large opening patch pipette to move an individual OHC settled at the bottom of the dish to the recording chamber.

7. Typical pipette resistances in 140 mM Cl solution are around 4 M Ω . When the gluconate substitute is used, the resistance is raised to 5–6 M Ω in 5 mM Cl pipette solution.
8. Membrane tension: Outer hair cell membrane tension is a strong modulator of NLC [10, 24, 25, 27]. Increased membrane tension (e.g., caused by turgor pressure) can shift NLC curve over 50 mV [10, 25, 26]. Such a shift in V_h may create errors in data interpretation; we strongly recommend investigators to control turgor pressure in OHC recordings during NLC and motility measurements. Tension changes can occur due to a variety of reasons including imbalanced osmolality between intracellular and extracellular solution, higher intracellular chloride levels [36] or influx of chloride [35] or other ions, plugged pipette, and positive pressure clamped to the pipette [10, 24, 26]. Therefore, either controlling or close monitoring of membrane tension is important to obtain unbiased data. We routinely adopt two approaches to reduce artifacts derived from membrane tension changes: (1) to monitor cell turgor/length change with a video camera [36], and (2) to collapse the cell by suctioning the pipette. If turgor tension is not the focus of study, collapsing cells is the best approach to eliminate the problem. When membrane tension is part of the study or a “natural” condition is desired especially in motility measurement, collapse the cell at the end to acquire recordings as a control condition. Capturing images and making measurements of cell length change also gives helpful indications of turgor changes and is highly recommended when a video camera is available.
9. Calibration should be done prior to the experiment and needs to be repeated after some time period, or whenever the system changes—new sampling clock, different filter setting on the amplifier, change in amplifier gain, etc. If the calibration is wrong then the data are WRONG! On the headstage, remove the pipette holder. Insert a 10 M Ω resister and connect to the ground. Run the calibration according to the menu instruction. This is a step easily ignored by investigators. Do not use wrong calibration files! File names should be saved to contain time and amplifier filter frequency and clock information so that earlier calibration files are all identifiable. Calibrations are saved with data files.
10. Building command file: A command file is built in the Command Utility interface prior to the experiment and a shortcut can be used. Move cursor to the left of screen and point to the command utility icon (6th from the top) and open the panel (shown on the right). Load command protocols by clicking folder icon in Command Utility window and select from the command file folder. If a command is used frequently,

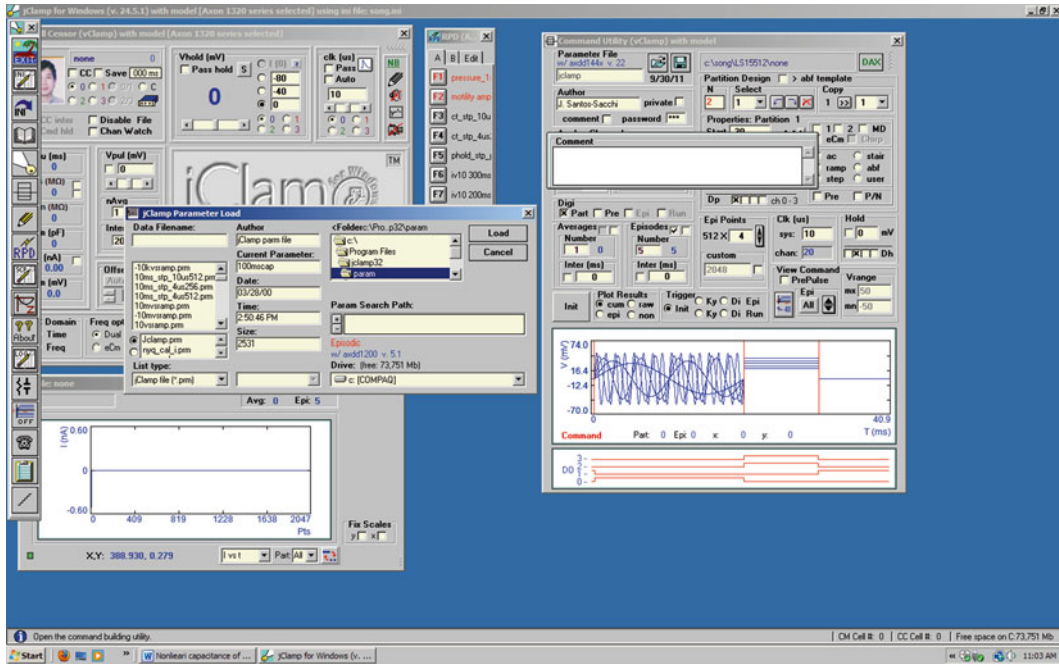


Fig. 3 Screenshot of command building window. Left column is activated by moving cursor to the left. Then select 6th icon from the list to activate command utility window. Click open folder icon to select command file to work on. Command files are saved in “Param” subfolder in jClamp folder

you may save it in the “RPD” window (Shown in small panel with quick access keys, (Fig. 3) to enable quick access. A typical dual-sine ramp command is shown below in command utility window. We use four sections to define the command. The sections 1 and 4 have matching holding potentials. Partition 2 defines the beginning of ramp voltage. Partition 3 is the ramp where the start voltage is at the end of the ramp (-200 mV in the screenshot). Command Cm window needs to be selected and typical resolution is 2.56 ms if two-sine [22, 33] is to be superimposed onto the ramp (Fig. 4).

11. Quick access key (RPD) is the fast approach to activate a saved command file frequently used. We use it only at the beginning of the recording series. Upon activation of a command, the command utility window and Result Window data display will both pop up. Change the data display to Vm vs. Cm in drop down window so the NLC is displayed online. If the command needs repeated, use “init” key to activate the command during the continuous recording of the cell. The advantage of doing so is the ability to keep all the prior NLC curves on the data display window so you can track the changes of NLC online. This is particularly useful in determining the completion of cell dialysis [35] and tracking whether the cell has reached steady

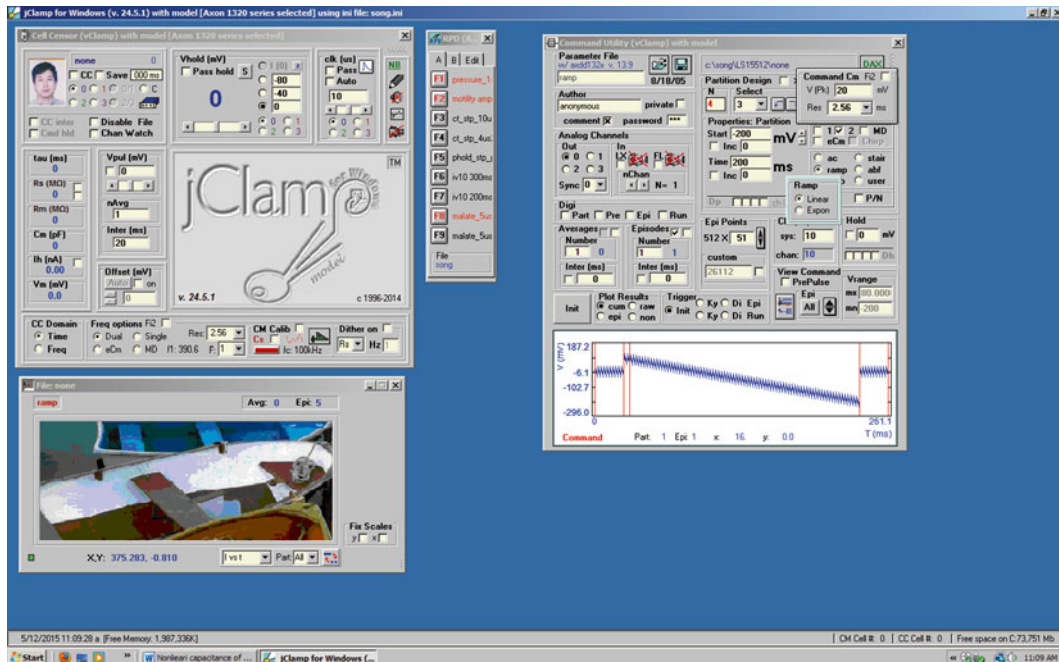


Fig. 4 Screenshot of window when building a ramp command with superimposed two-sine. First check “ramp.” Then move cursor to 2 (two-sine). “Command Cm” box will pop up when box of “2” is checked. Typical two-sine resolution is 2.56 ms and two-sine voltage is 10–20 mV (shown in the figure). Each section has to have 2-sine enabled. Start voltage of the ramp is +80 mV in partition 2 and –200 mV in partition 3. Typical ramp duration is 200–300 ms

state upon various manipulations (perfusion of extracellular solution containing drugs, change holding potential, change membrane tension, etc.). We routinely record NLC online until a few overlapping NLC traces appear before advancing to the next manipulation in the experiment. This is essential in acquiring high quality data.

12. Detrending is a method to properly prepare the data prior to FFT analysis and extraction of NLC. Detrending removes slow changes in the current response but leaves behind clear dual-sine currents, which possess the capacitance information. For example, without detrending, a fast ramp or sine wave superimposed with a two-sine stimulus will erroneously result in NLC peaks larger than slower ramp or sine stimuli. Detrending uses a small scale “piece-wise linear” approach to remove the trend generated by the underlying ramp or sinusoid stimulus. Users may choose to enable “detrending” if the underlying stimulus rate is fast and a small noise increase is not crucial.
13. jClamp can be linked to other data analysis or plotting software such as Excel, SigmaPlot, Matlab, and Origin. You need to

select in the ini file to link the software (*see* jClamp help files for detailed steps). The linked software will appear on the upper right corner in jClamp analysis window (the SigmaPlot icon in the screenshot, (Fig. 2)). To export the plot, simply left click and drag the software icon to the NLC curve analysis window and release. A generic plot will automatically be generated in the selected software.

References

1. Zheng J, Shen W, He DZ, Long KB, Madison LD, Dallos P (2000) Prestin is the motor protein of cochlear outer hair cells. *Nature* 405:49–155
2. Brownell WE, Bader CR, Bertrand D, de Ribaupierre Y (1985) Evoked mechanical responses of isolated cochlear outer hair cells. *Science* 227:194–196
3. Ashmore JF (1987) A fast motile response in guinea-pig outer hair cells: the cellular basis of the cochlear amplifier. *J Physiol* 388:323–347
4. Santos-Sacchi J, Dilger JP (1988) Whole cell currents and mechanical responses of isolated outer hair cells. *Hear Res* 35:143–150
5. Iwasa KH, Kachar B (1989) Fast in vitro movement of outer hair cells in an external electric field: effect of digitonin, a membrane permeabilizing agent. *Hear Res* 40:247–254
6. Ashmore J, Avan P, Brownell WE et al (2010) The remarkable cochlear amplifier. *Hear Res* 266:1–17
7. Dallos P, Evans BN, Hallworth R (1991) Nature of the motor element in electrokinetic shape changes of cochlear outer hair cells. *Nature* 350:155–157
8. He DZ, Evans BN, Dallos P (1994) First appearance and development of electromotility in neonatal gerbil outer hair cells. *Hear Res* 78:77–90
9. Huang G, Santos-Sacchi J (1993) Mapping the distribution of the outer hair cell motility voltage sensor by electrical amputation. *Biophys J* 65:2228–2236
10. Song L, Santos-Sacchi J (2013) Disparities in voltage-sensor charge and electromotility imply slow chloride-driven state transitions in the solute carrier SLC26a5. *Proc Natl Acad Sci U S A* 110:3883–3888
11. Santos-Sacchi J, Song L (2014) Chloride-driven electromechanical phase lags at acoustic frequencies are generated by SLC26a5, the outer hair cell motor protein. *Biophys J* 107:126–133
12. Hamill OP, Marty A, Neher E, Sakmann B, Sigworth FJ (1981) Improved patch-clamp techniques for time-resolved capacitance measurements in single cells. *Pflugers Archiv* 411: 137–146
13. Bai JP, Navaratnam D, Samaranayake H, Santos-Sacchi J (2006) En block C-terminal charge cluster reversals in prestin (SLC26A5): effects on voltage-dependent electromechanical activity. *Neurosci Letts* 404:270–275
14. Bai JP, Surguchev A, Bian S et al (2010) Combinatorial cysteine mutagenesis reveals a critical intramonomer role for cysteines in prestin voltage sensing. *Biophys J* 99:85–94
15. Bian S, Koo BW, Kelleher S, Santos-Sacchi J, Navaratnam DS (2010) A highly expressing Tet-inducible cell line recapitulates in situ developmental changes in prestin's Boltzmann characteristics and reveals early maturational events. *Am J Physiol Cell Physiol* 299:C828–C835
16. Bai JP, Surguchev A, Ogando Y, Song L, Bian S, Santos-Sacchi J, Navaratnam D (2010) Prestin surface expression and activity are augmented by interaction with MAP1S, a microtubule-associated protein. *J Biol Chem* 285:20834–20843
17. Joshi C, Fernandez JM (1988) Capacitance measurements. An analysis of the phase detector technique used to study exocytosis and endocytosis. *Biophys J* 53:885–892
18. Lindau M, Neher E (1988) Patch-clamp techniques for time-resolved capacitance measurements in single cells. *Pflugers Archiv* 411: 137–146
19. Neher E, Marty A (1982) Discrete changes of cell membrane capacitance observed under conditions of enhanced secretion in bovine adrenal chromaffin cells. *Proc Natl Acad Sci U S A* 79:6712–6716
20. Debus K, Hartmann J, Kilic G, Lindau M (1995) Influence of conductance changes on patch clamp capacitance measurements using a lock-in amplifier and limitations of the phase tracking technique. *Biophys J* 69:2808–2822
21. Santos-Sacchi J (2004) Determination of cell capacitance using the exact empirical solution

- of partial differential Y/partial differential C_m and its phase angle. *Biophys J* 87:714–727
22. Santos-Sacchi J, Kakehata S, Takahashi S (1998) Effects of membrane potential on the voltage dependence of motility-related charge in outer hair cells of the guinea-pig. *J Physiol* 510:225–235
 23. Santos-Sacchi J, Shen W, Zheng J, Dallos P (2001) Effects of membrane potential and tension on prestin, the outer hair cell lateral membrane motor protein. *J Physiol* 531:661–666
 24. Santos-Sacchi J, Rybalchenko V, Bai JP, Song L, Navaratnam D (2006) On the temperature and tension dependence of the outer hair cell lateral membrane conductance G_{metL} and its relation to prestin. *Pflugers Archiv* 452:283–289
 25. Santos-Sacchi J, Navarrete E, Song L (2009) Fast electromechanical amplification in the lateral membrane of the outer hair cell. *Biophys J* 96:739–747
 26. Song L, Santos-Sacchi J (2010) Conformational state-dependent anion binding in prestin: evidence for allosteric modulation. *Biophys J* 98:371–376
 27. Kakehata S, Santos-Sacchi J (1995) Membrane tension directly shifts voltage dependence of outer hair cell motility and associated gating charge. *Biophys J* 68:2190–2197
 28. Oliver D, Fakler B (1999) Expression density and functional characteristics of the outer hair cell motor protein are regulated during postnatal development in rat. *J Physiol* 519:791–800
 29. Dong XX, Iwasa KH (2004) Tension sensitivity of prestin: comparison with the membrane motor in outer hair cells. *Biophys J* 86: 1201–1208
 30. Iwasa KH (1993) Effect of stress on the membrane capacitance of the auditory outer hair cell. *Biophys J* 65:492–498
 31. Muallem D, Ashmore J (2006) An anion antiporter model of prestin, the outer hair cell motor protein. *Biophys J* 90:4035–4045
 32. Oliver D, He DZ, Klöcker N et al (2001) Intracellular anions as the voltage sensor of prestin, the outer hair cell motor protein. *Science* 292:2340–2343
 33. Rybalchenko V, Santos-Sacchi J (2003) Cl⁻ flux through a non-selective, stretch-sensitive conductance influences the outer hair cell motor of the guinea-pig. *J Physiol* 547:873–891
 34. Rybalchenko V, Santos-Sacchi J (2008) Anion control of voltage sensing by the motor protein prestin in outer hair cells. *Biophys J* 95:4439–4447
 35. Song L, Seeger A, Santos-Sacchi J (2005) On membrane motor activity and chloride flux in the outer hair cell: lessons learned from the environmental toxin tributyltin. *Biophys J* 88:2350–2362
 36. Santos-Sacchi J, Song L, Zheng J, Nuttall AL (2006) Control of mammalian cochlear amplification by chloride anions. *J Neurosci* 26:3992–3998

Chapter 29

In Vitro Functional Assessment of Adult Spiral Ganglion Neurons (SGNs)

**Jeong Han Lee, Choongryoul Sihn, Wanging Wang,
Cristina Maria Perez Flores, and Ebenezer N. Yamoah**

Abstract

Spiral ganglion neurons (SGNs) faithfully encode acoustic waves from hair cells to the cochlear nucleus (CN) using voltage-dependent ion channels. A sizable portion of our knowledge on SGN functions have been derived from pre-hearing neurons. In post-hearing SGNs, the mechanisms of how they encode the massive sound information without delay and precisely are largely unknown. Mature SGNs are housed in the central bony labyrinth of the cochlea, protected by a well-insulated myelin sheath, making it a technical feat to isolate viable neurons for rigorous functional electrophysiology. Recently, we have overcome the previous intractable hindrance in SGN functional analyses. We provide a step-by-step user-friendly protocol with practical applications, including patch-clamp recordings and imaging by using cultured SGNs.

Key words Spiral ganglion neurons (SGNs), Hair cells (HCs), Auditory system, Modiolus, Myelin sheath, Unmyelinated, Matured SGNs

1 Introduction

In the inner ear the cochlea converts sound energy into neural signals that are transmitted to the brainstem. The organ of Corti along the cochlea axis contains inner hair cells (IHC), which are responsible for the sensory transduction and synaptic activation of the primary afferent auditory neurons, spiral ganglion neurons, (SGNs). The outer hair cells (OHC) serve as the cochlear amplifier; they receive afferent innervation through numerous thin and unmyelinated fibers of type II SGNs, which correspond ~5 % of the cochlear afferents [1]. The IHCs function in the detection of auditory stimuli, and they transmit precise and reliable information about the amplitude, duration, and frequency of acoustic waves. The IHCs are innervated by the unbranched and myelinated type I SGNs, which comprise ~95 % of the cochlear afferents (10–20 of these neurons extend single neurites to exclusively innervate a single IHC) [1–3]. The two SGNs cell-types could be distinguishable

by morphological features and/or double staining of TuJ and peripherin (both markers are positive for Type II SGNs) [4, 5].

In mice after the birth, it takes ~2 weeks for the onset of hearing [6]. Whereas pre-hearing SGNs rely faithfully on outputs from spontaneously active developing hair cells, the electrical phenotypes of post-hearing neurons are shaped by distinct rapid and graded receptor potentials from hair cells [7, 8]. To date, technical difficulties in isolation of fragile post-hearing neurons from the rigid bony labyrinth of the inner ear have hindered analyses of the electrical phenotype of SGNs. Therefore, we have recently developed new strategies to isolate post-hearing mouse SGNs for functional analyses. One of the most powerful advantages of using mouse model is that mouse has well established genetic models. Genetically modified mice are commonly used for the human disease model as well as in the inner ear research. Here, we describe the primary culture technique of adult SGNs from mice and other applications.

2 Materials

2.1 SGN Culture Components

- All reagents are mixed in Milli-Q distilled water ($18.2\text{ M}\Omega$).
1. 1 mg/mL laminin ready to use (Sigma-Aldrich, St Louis, MO).
 2. 100 U/ μL penicillin G.
 3. 15 mm round glass coverslips.
 4. 2.5 % trypsin ready to use.
 5. 40 μm cell strainer.
 6. 6–8 Week-old mice, $N=3$.
 7. B27 (ready to use, Life Technologies, 50 \times).
 8. BDNF: Mix 10 ng/ μL in 0.1 % BSA solution (Sigma-Aldrich, St Louis, MO).
 9. Bovine serum albumin: Mix 0.1 % in distilled water (Sigma-Aldrich, St Louis, MO).
 10. Collagenase I: Mix 10 mg/mL in MEM Hanks' buffer (Hanks' solution (mM) 137 NaCl, 5.4 KCl, 0.25 Na_2HPO_4 , 5 glucose, 0.44 KH_2PO_4 , 1.3 CaCl_2 , 1.0 MgSO_4 , 4.2 NaHCO_3).
 11. D-glucose: Mix 450 mg/mL in distilled water.
 12. Dishes: 4-well NUNC culture dish and 60 mm dish.
 13. Dissecting instruments: Dumont #4 and #5 fine forceps and surgical scissors.
 14. DNase I: Mix 1000 U/mL in MEM Hanks' (Sigma-Aldrich, St Louis, MO).

15. Dulbecco's phosphate-buffered saline (DPBS) without Ca²⁺ and Mg²⁺ (Life Technologies, Carlsbad, CA).
16. Fetal bovine serum (FBS).
17. Hanks' buffered saline solution (HBSS, Life Technologies, Carlsbad, CA).
18. Kynurenic acid.
19. L-glutamine.
20. MgCl₂: Make 1 M in distilled water.
21. Minimum essential medium (MEM) Hanks'.
22. NaOH: Make 1 M in distilled water.
23. Neurobasal A (Life Technologies 10888-022).
24. NT-3: Mix 10 ng/μL in 0.1 % BSA solution (Sigma-Aldrich, St Louis, MO).
25. Plastic tubes: 15 and 50 mL tubes.
26. Poly-D-lysine hydrobromide: Mix 0.5 mg/mL in distilled water (Sigma-Aldrich, St Louis, MO).
27. Sucrose.
28. Syringes: 10 and 50 mL.
29. Water-bath shaker.

2.2 Patch-Clamp Recording Components

1. Inverted microscope with fluorescence, e.g., Nikon TE2000 w/fluorescence (Nikon, Tokyo, Japan).
2. Narishige MF-830 microforge (Narishige International USA, East Meadow, NY).
3. Origin software (OriginLab Corporation, Northampton, MA).
4. Patch-clamp amplifier: Axopatch 200B (Molecular Devices, Sunnyvale, CA).
5. Precision micromanipulator and microscope mounting adaptors (EXFO, Newton, NJ).
6. Software and data acquisition interface, e.g., pCLAMP Digidata 1200 (Molecular Devices, Sunnyvale, CA).
7. Sutter P-97 programmable pipette puller (Sutter Instrument Company, Novato, CA).
8. Borosilicate glass with filament (ITEM #: BF150-86-10) (Sutter Instrument Company, Novato, CA).
9. Vibration isolation table and perimeter Faraday cage (TMC, Peabody, MA).
10. Internal pipette solution for calcium current isolation: Prepare (mM) 70 CsCl, 70 N-methyl-D-glucamine chloride, 1 MgCl₂, 10 HEPES, 2–5 EGTA, 1 CaCl₂, 4 Cs₂ATP, pH to 7.2 with CsOH.

11. Extracellular bath solution for calcium current isolation: Prepare (mM) 120 choline Cl, 20 tetraethylammonium chloride (TEACl), 5 4-aminopyridine (4-AP), 0.02 linopirdine, 2 CsCl, 1.8–5 CaCl₂, 0.5–5 MgCl₂, 10 HEPES, 5 d-glucose, pH 7.40, with NaOH (*see Note 1*).
12. Ca²⁺ channel blockers: Nimodipine (L type), ω -conotoxin MVIIA (CTX; N type), ω -agatoxin IVA (ATX; P/Q type), ω -theraphotoxin-Hg1a, ω -TRTXHg1a (rSNX-482; R type) (Alomone Labs), and mibepradil (T type) channels (*see Note 2*).
13. Internal pipette solution for measuring action potentials: Prepare (mM) 112 KCl, 2 MgCl₂, 0.1 CaCl₂, 5 K₂ATP, 0.5 GTP-Na, 1 EGTA, 10 HEPES, pH to 7.35 with KOH.
14. Extracellular bath solution for measuring action potentials: Prepare (mM) 130 NaCl, 5 KCl, 1 MgCl₂, 1 CaCl₂, 10 d-glucose, and 10 HEPES, pH 7.4 with NaOH.

3 Method

3.1 SGN Culture

3.1.1 Preparations

on the Day

Before Dissection

1. Clean coverslip with 70 % ethanol (EtOH) and autoclave. Keep coverslips in 70 % EtOH before use.
2. Autoclave tools including scissors and forceps (*see Note 3*).
3. Put two cleaned and sterilized round coverslip into 4-well culture plate.
4. Add 200 μ L (0.5 mg/mL) of poly-d-lysine to each coverslip and place them in the incubator for 6 h.
5. Wash them with PBS 3×.
6. Thaw 5 μ L laminin slowly on the ice bucket and dilute it with 250 μ L PBS. Apply the solution onto the coverslips, place them in the incubator for overnight (*see Note 4*).
7. Preparation of pre-dissecting solution (PDS): Weigh 10 mg kynurenic acid and add it to 50 mL MEM Hanks' and keep them in cold room (4 °C) on the shaker for overnight.
8. Preparation of pre-culture medium (PCM): Weigh 1 mg kynurenic acid and add it to the 5 mL "Neurobasal A" medium and keep them in cold room for overnight.
9. Solution 2: Prepare 2.5 mL of HBSS and 15.4 g of sucrose and add Milli-Q distilled water up to 50 mL (adjust to pH 7.5). Sterilize 50 mL Solution 2 using a 0.2- μ m filter and 50 mL syringe. Keep the solution 2 in cold room.

3.1.2 Preparations

Before Dissection

1. Prepare to use the following reagents: 40 mL MEM Hanks', pre-dissecting solution (PDS), pre-culture medium (PCM), 450 mg/mL glucose, B27, penicillin, 1 M MgCl₂, FBS,

L-glutamine, Milli-Q distilled water, DPBS, MEM Hanks', 10 and 50 mL syringes, 0.2 µm filter (*see Note 5*).

2. Aspirate laminin solution and rinse the well with PBS 3×, then fill with a mixture of Neurobasal/FBS (1:1). Keep in incubator at least 2 h before seeding with cells.
3. Prepare culture medium (CM). Sterilize 5 mL of pre-culture medium by filtering with a 0.2-µm filter attached to a 10 mL sterile syringe. Make fresh every time you culture cells. Add the following: 100 µL of B27 (final 2 %), 5 µL of penicillin (final 100 U/mL), and 12.5 µL of L-glutamine (final 0.5 mM).
4. Preparation of Dissecting Solution (DS). Sterilize 50 mL of pre-dissecting solution using a 0.2-µm filter and 50 mL syringe. Add 400 µL of MgCl₂ to obtain a final concentration of 10 mM, 110 µL of D-glucose, and 50 µL of penicillin.
5. Preparation of Digestive Solution (DGS): Add 2 mL of DS to a 15 mL tube and then add 40 µL of B27 (final 2 %) (*see Note 6*).
6. Add 2 mL FBS to the DS.
7. Aliquot 4 mL of centrifugation solution (CFS) into new 15 mL tube. This is pre-CFG.

3.1.3 Dissection

All animal protocols should be approved by the Institutional Animal Care and Use Committee according to the guidelines of the NIH.

1. Sacrifice the mice using CO₂ and decapitate using surgical scissors (*see Note 7*).
2. Clean the mouse head using 70 % EtOH. Cut the head and peel off the skin. Then bisect it.
3. Remove the temporal bone and place in cold MEM Hanks' buffer.
4. Under a dissecting microscope, isolate the cochlea from the temporal bone in DS.
5. Dissect the sample by shearing off the bony shell and removing the stria vascularis, including the organ of Corti (Fig. 1)
6. Keep spiral ganglion neurons in cold DGS.

3.1.4 Digestion

1. Take out collagenase type I and DNase I from freezer and thaw at RT.
2. Transfer the SGNs into a 15 mL tube and add 400 µL of DGS.
3. Add 50 µL collagenase type I and 50 µL DNase I and place in 37 °C water bath for 15 min at a vibration rate of 70 oscillations/min.
4. Add 50 µL of 2.5 % trypsin to the digesting solution. Keep ganglia in water bath for an additional 10 min at the same vibration rate (*see Note 8*).

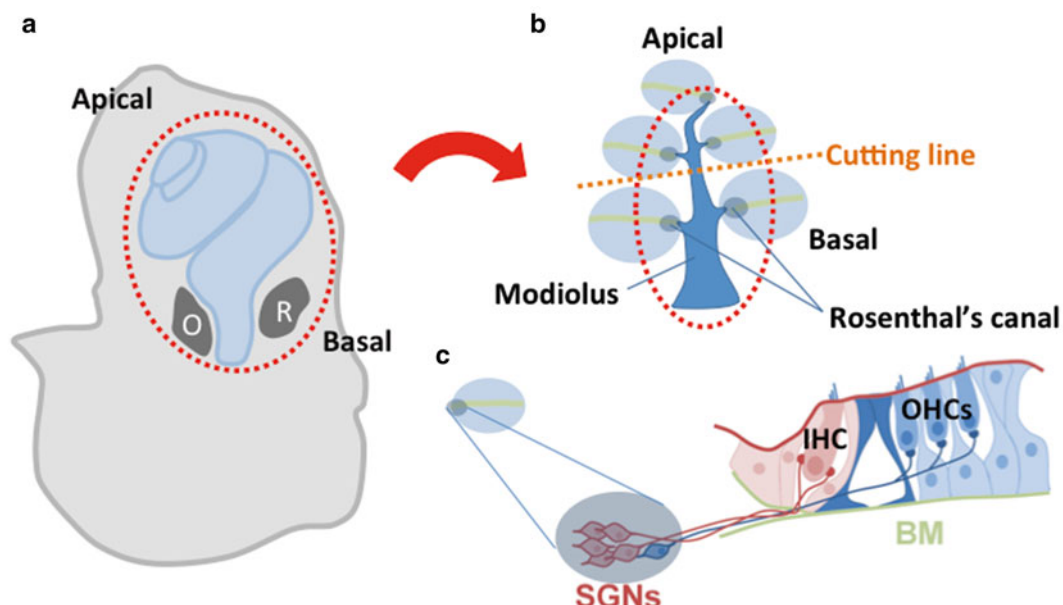


Fig. 1 (a) Schematic drawing of a mouse cochlea following isolation from the temporal bone. Red-dotted circle indicates the area to dissect out. (O: oval window, R: round window). (b) It shows an isolated modiolus surrounded by cochlear duct. Following removal of the cochlear duct from the modiolus cut through the orange dotted line to divide the apical from the basal turn. (c) Drawing showing SGNs cell bodies in Rosenthal's canal (BM basilar membrane)

5. Prepare 8 mL of CFG. Add 4 mL of solution 2 into pre-CFS.
6. Add 400 µL FBS to stop the enzyme activity.
7. Gently and slowly triturate samples 20× using a 1 mL pipette tip; then smash the remaining cochlear framework with tip. Gently triturate the samples again another 5×.
8. Transfer the samples to 4 mL of CFS and centrifuge at 80×*g* for 5 min (*see Note 9*).
9. Prepare the final CM by mixing 360 µL of CM, 60 µL of FBS, 1 µL of NT3, and 1 µL of BDNF)/well.
10. Discard supernatant carefully following centrifugation, then add final CM to the pellet in the tube.
11. Discard old medium in the 4-well culture plate.
12. Seed the cell suspension on coverslips and keep the cells in a 5 % CO₂ humidified incubator.

3.1.5 Day

*After Dissection:
Replacement of Medium*

1. Take the final CM.
2. Prepare new culture medium, containing 5 mL of Neurobasal-A, 100 µL of B27, 5 µL of penicillin, and 12.5 µL L-glutamine.
3. Mix 200 µL final CM with 200 µL new culture medium per well (final volume is 400 µL per well).
4. Add 1 µL NT3 and 1 µL BDNF per well (*see Note 10*).

3.2 Immunostaining of Cultured SGN

3.2.1 Prepare the Solution for Staining

3.2.2 Immunostaining

Blocking buffer: 10 % normal serum/0.1 % Triton X-100 in PBS (*see Note 11*).

Antibody dilution buffer: 1 % BSA/0.1 % Triton X-100 (*see Note 12*).

1. Aspirate medium, then cover cells with 4 % paraformaldehyde diluted in PBS.
2. Allow cells to fix for 15 min at room temperature.
3. Aspirate fixative; then rinse 3× in PBS for 10 min each.
4. Block the cells in blocking buffer for 60 min.
5. Prepare primary antibody by dilution in antibody dilution buffer.
6. Aspirate blocking buffer and apply diluted primary antibody and incubate overnight at 4 °C.
7. Wash 3× in PBS for 10 min each (*see Note 13*).
8. Incubate the cells in fluorescent-conjugated secondary antibody diluted in antibody dilution buffer for 1–2 h at room temperature in the dark.
9. Wash 3× in PBS for 10 min each (*see Note 14*).
10. Apply DAPI (1 µg/mL in PBS) for 15 min.
11. Rinse 2× in PBS for 10 min each.
12. Coverslip the slide with anti-fade reagent (*see Note 15*).
13. Image the specimens (Fig. 2).

3.3 Whole-Cell Patch-Clamp Recordings

3.3.1 Whole-Cell Voltage-Clamp Recording in SGNs

1. Place a coverslip on the recording chamber filled with external recording solution; select a cell and then filled the recording pipette with internal solution.
2. Position the cell at the center of the microscope's field of view. Cells are selected based on morphology (healthy SGN neurons have round cell body with smooth membranes and lack of membrane blebs). An advantage in recording from adult

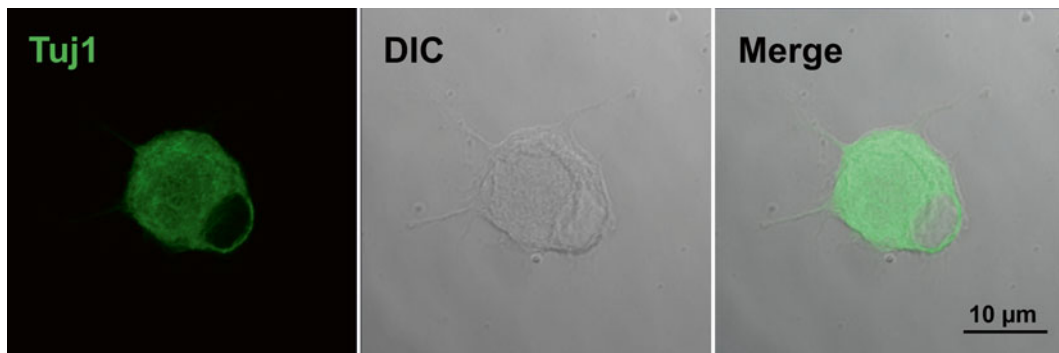


Fig. 2 Immunostaining data of spiral ganglion neuron (SGN). SGNs were stained with anti-Tuj1

neurons is that neurite outgrowth was less pronounced compared with prehearing neurons. Nonetheless, to minimize space clamp artifacts, we targeted spherical neurons with reduced neurite outgrowth for voltage-clamp experiments.

3. Apply a 5 mV repetitive test pulse (from a holding potential of 0 mV ~every second; often configured in the patch-clamp software with a “seal test” protocol), adjust the pipette potential (offset) to 0 before seal formation using the controls on the patch-clamp amplifier (“pipette offset”). Use fire-polished glass pipettes and apply slight positive pressure to the pipette (to keep debris off the tip) until contact is made with the neuronal cell membrane to facilitate the formation of the $G\Omega$ seal between the pipette and the cell membrane.
4. Bring the pipette recording down onto the cell membrane. Cancel fast capacitance transients; after formation of the $G\Omega$ seal (ideally $>1 G\Omega$).
5. Establish the whole-cell recording configuration by applying gentle suction pulses to rupture the patch of membrane in the pipette. To monitor the configuration, use repetitive biphasic (± 5 mV) pulses (5 ms duration).
6. Cancel slow-capacitance transients, due to cell membrane capacitance using the amplifier controls. Series resistance can then be compensated by ~80 %.
7. Acquire traces using standard patch-clamping software such as Clampex. In our experiments, we filter recordings at 2 kHz and sample at a rate of 5 kHz using a Digidata 1200 series interface (Axon Instruments). Input resistance can be calculated by recording voltage changes by injection of $\Delta 10$ -pA hyperpolarizing currents. Once whole-cell access is obtained, allow equilibration time of around 3–5 min so that the pipette solution dialyze the cell. The input resistance is monitored during this time (and throughout the recording) to ensure that it is stable. If the input resistance changes appreciably during recording, then the cell should be discarded.

3.3.2 Ca^{2+} Current Recording

1. Generate the inward Ca^{2+} current traces with depolarizing voltage steps from a holding potential of $-90/-70$ mV and stepped to varying positive potentials ($\Delta V=2.5-10$ mV).
2. Measure the whole-cell Ca^{2+} current amplitudes at varying test potentials at the peak and steady-state levels using a peak and steady-state detection routine; divide the current magnitude by the cell capacitance (pF) to generate the current density–voltage relationship.

3.3.3 Whole-Cell Current-Clamp Recording from SGNs

Whole-cell current-clamp technique records membrane potential changes (e.g., action potentials (APs) firing from SGNs *in vitro*).

1. After attaining the whole-cell configuration, the resting membrane potential (RMP) can be recorded at $I=0$ mode. Action Potentials (AP) are usually recorded at I-CLAMP FAST mode by injecting current.
2. Positive or negative current can be injected
3. To identify the contribution of specific current to the firing pattern of SGNs, known pharmacology blocks can be added to the external or internal recording solutions (Fig. 3 and *see Note 16*).

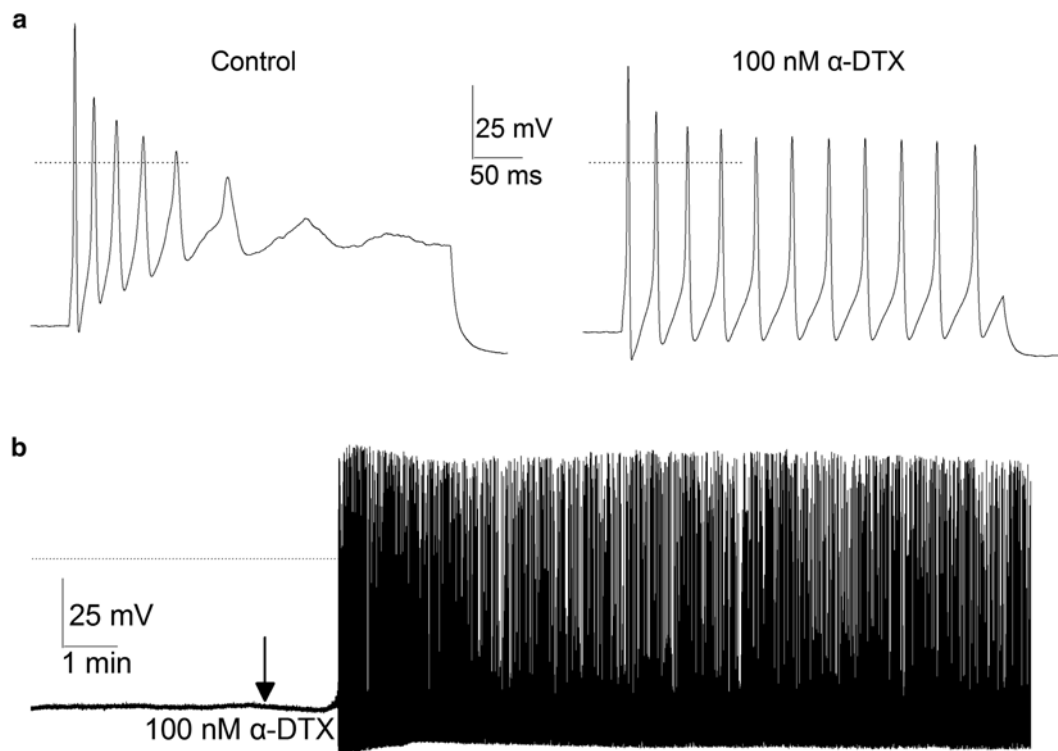


Fig. 3 α -DTX (dendrotoxin) increases the excitability of P12 (postnatal) SGNs in wild type mice. (a) Representative action potential was recorded by injecting 0.2-nA-current for 200-ms duration in SGN (*left panel*). Bath application of external solution containing 100 nM α -DTX resulted in increased spike activity. (b) Effect of α -DTX on quiescent neuron at baseline. The arrow indicates the time at which the external solution containing 100 nM α -DTX was perfused. α -DTX transformed quiescent neuron into spontaneously active SGN

4 Notes

1. In all cases when the Ca^{2+} concentration was altered, Mg^{2+} substitution was used to minimize membrane surface charge effects.
2. The stock solutions of all channel blockers and agonists should be made either in double-distilled water or DMSO and stored at $\sim 20^\circ\text{C}$. The final concentration of DMSO in the recording bath solution was $\sim 0.0001\%$. This concentration of DMSO has no effects on action potentials, nor did it alter Ca^{2+} current recordings (data not shown).
3. Sterilizers that use UV light can be useful before dissection.
4. The process of laminin dilution should be very gentle and avoid strong agitation otherwise the high molecular weight protein will be damaged, losing its effects.
5. Keep all solutions on the ice bucket.
6. Everything is the same concentration as DS. FBS is replaced with B27.
7. Follow the animal welfare guidelines appropriate for your institution.
8. Adjust the pH value of enzyme solution with 0.2 M NaOH to near pH 8.0 (optimum pH is 7.8–8.7).
9. Before the centrifugation, the single-cell suspension was collected using the cell strainer (40 μm).
10. Change half volume of the medium every 2 days with new culture medium above.
11. Use the normal serum from the same species as the secondary antibody.
12. Dilute the Triton X-100 as 10 % in PBS. To prepare 1 mL, add 0.1 mL Triton X-100 in 0.9 mL PBS. Mix well and keep at 4 $^\circ\text{C}$.
13. If using a fluorescent-conjugated primary antibody, then do not add secondary antibody reaction.
14. If using an antifade reagent with DAPI, then skip next step.
15. For the best results, allow the mounting media to harden overnight at room temperature in the dark. For long-term storage, keep slides at either 4 $^\circ\text{C}$ or -20°C protected from light.
16. The external solution is applied using either rapid perfusion systems or application by gravity.

References

1. Nayagam BA, Muniak MA, Ryugo DK (2011) The spiral ganglion: connecting the peripheral and central auditory systems. *Hear Res* 278:2–20
2. Morrison D, Schindler RA, Wersäll J (1975) A quantitative analysis of the afferent innervation of the organ of Corti in guinea pig. *Acta Otolaryngol* 79:11–23
3. Spoendlin H (1981) Differentiation of cochlear afferent neurons. *Acta Otolaryngol* 91:451–456
4. Huang LC, Thorne PR, Houley GD, Montgomery JM (2007) Spatiotemporal definition of neurite outgrowth, refinement and retraction in the developing mouse cochlea. *Development* 134:2925–2933
5. Barclay M, Ryan AF, Housley GD (2011) Type I vs type II spiral ganglion neurons exhibit differential survival and neuritogenesis during cochlear development. *Nerual Dev* 6:33
6. Kraus HJ, Aulbach-Kraus K (1981) Morphological changes in the cochlea of the mouse after the onset of hearing. *Hear Res* 4:89–102
7. Johnson SL, Echrich T, Kuhn S et al (2011) Position-dependent patterning of spontaneous action potentials in immature cochlear inner hair cells. *Nat Neurosci* 14:711–717
8. Marcotti W (2012) Functional assembly of mammalian cochlear hair cells. *Exp Physiol* 97:438–451

Chapter 30

Mapping Auditory Synaptic Circuits with Photostimulation of Caged Glutamate

Joshua J. Sturm, Tuan Nguyen, and Karl Kandler

Abstract

Photostimulation of neurons with caged glutamate is a viable tool for mapping the strength and spatial distribution of synaptic networks in living brain slices. In photostimulation experiments, synaptic connectivity is assessed by eliciting action potentials in putative presynaptic neurons via focal photolysis of caged glutamate, while measuring postsynaptic responses via intracellular recordings. Two approaches are commonly used for delivering light to small, defined areas in the slice preparation; an optical fiber-based method and a laser-scanning-based method. In this chapter, we outline the technical bases for using photostimulation of caged glutamate to map synaptic circuits, and discuss the advantages and disadvantages of using fiber-based vs. laser-based systems.

Key words Photostimulation, Fiber-based uncaging, Laser scanning, Glutamate uncaging, Synaptic input mapping, Auditory circuit connectivity

1 Introduction

Photostimulation with caged glutamate or “glutamate uncaging” has emerged as a robust and reliable tool for mapping functional synaptic connectivity in a variety of systems [1–6]. In the auditory system, glutamate uncaging has been used to reveal the organization of functional connectivity in the superior olivary complex [2, 7, 8], the ventral cochlear nucleus [9], the inferior colliculus [10], and the auditory cortex [11–15]. In glutamate uncaging studies, the origin and strength of synaptic inputs received by an individual neuron are determined by obtaining a whole-cell patch clamp recording from a neuron, exciting potential presynaptic neurons with glutamate uncaging, and assessing the resulting postsynaptic responses. Glutamate uncaging is achieved by brief (1–100 ms) pulses of light delivered to small, defined areas in the slice, either by an optical fiber [2, 6] or by a scanning laser [1, 4]. By systematically exciting many (100–1000s) discrete locations in the slice, the topographic distribution of stimulation sites that elicit postsynaptic

responses in the recorded neuron is used to generate synaptic input maps of excitatory and/or inhibitory connections.

In this chapter, we outline the basic conceptual and technical principles of using fiber- and laser-based glutamate uncaging to map local synaptic circuits in the auditory system. To assist the reader in determining which type of system will be most appropriate for his/her research questions and laboratory environment, we compare the advantageous and disadvantageous associated with fiber-based and laser-based uncaging. Although we focus on synaptic input mapping in the auditory brainstem and midbrain, the methods described here will be applicable to other brain regions as well.

2 Materials

Fiber-based and laser-based uncaging systems can each be incorporated into standard electrophysiological setups for visualized whole-cell recording in living brain slices (Fig. 1). A variety of caged compounds are commercially available from several vendors (Calbiochem, Temecula, CA; HelloBio, Bristol, UK; Life Technologies, Grand Island, NY; Molecular Technologies, Inc., Tocris, Bristol, UK).

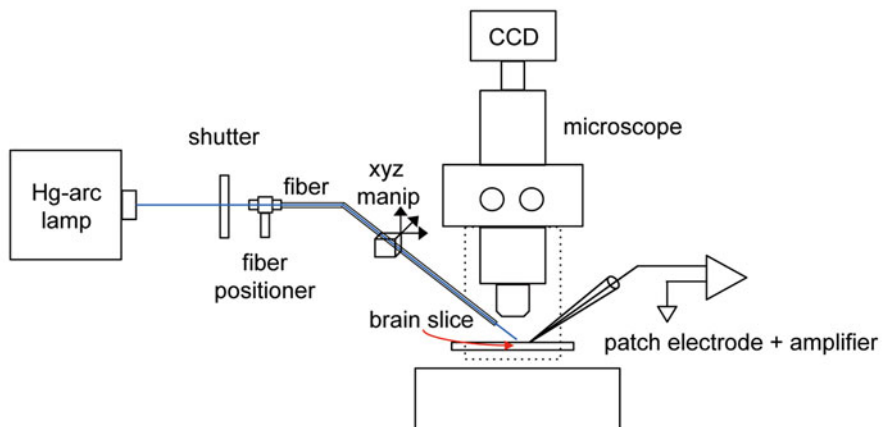
2.1 Fiber-Based Uncaging

1. Electronic shutter: Uniblitz Model LSG with AlMgF₂ coating (Vincent Associates, Rochester, NY).
2. Mercury arc Lamp: 100-W lamp with Series Q lamp housing and UV grade fused silica condenser (Oriel, Irvine, CA or Newport Corporation, Irvine, CA).
3. Optical fibers: 5–50 μm fibers (CeramOptec Industries Inc, Bonn, Germany or Polymicro Technologies, Phoenix, AZ).
4. Power supply (Opti Quip Inc., Highland Mills, NY).
5. Pulse generator (e.g., Master 8; A.M.P.I., Jerusalem, Israel).

2.2 Laser-Based Uncaging System

1. UV laser, 355 nm, 2 W (e.g., Model 3510-30; DPSS Lasers, Santa Clara, CA).
2. Polarizing beamsplitter for power attenuation (e.g., GT5-A, Thorlabs, Newton, NJ).
3. Mechanical shutter (e.g., Model LST200, nmLaser Products, San Jose, CA).
4. Galvo-driven mirrors (e.g., Model 6210H, Cambridge Technology, Bedford, MA).
5. Optical lenses: $f=10$ cm and $f=15$ cm (e.g., LA4380-UV and LA4874-UV, respectively, Thorlabs).
6. Dichroic beamsplitter (e.g., FF484-FDi01-25x36, Semrock, Rochester, NY).

a Optical fiber photostimulation



b Laser scanning photostimulation

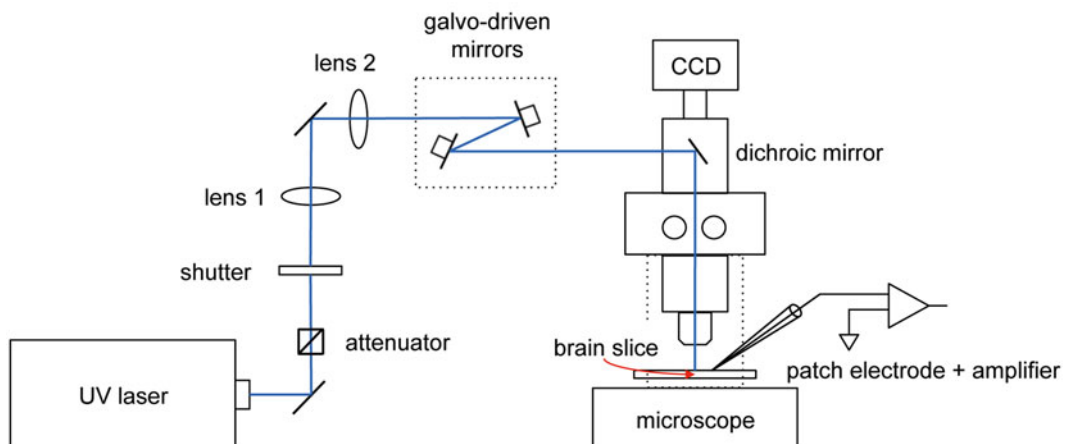


Fig. 1 Schematic illustration of fiber-based and laser-based UV photostimulation systems. **(a)** Optical fiber system. **(b)** Laser-scanning photostimulation system. The focal lengths and positions of the two lenses are chosen to ensure that the laser spot is parfocal with the image across the entire field-of-view. Light paths shown in blue. *CCD* camera

3 Methods

3.1 Photostimulation with Caged Glutamate

3.1.1 Caged Neurotransmitters

Synaptic input mapping with glutamate uncaging involves exciting small groups of presynaptic neurons by locally increasing the glutamate concentration with brief pulses of high intensity light and measuring postsynaptic responses in individual neurons via whole-cell patch-clamp recordings. Presynaptic stimulation is achieved via rapid photolysis of photo-labile caged glutamate, which is biologically inert under ambient lighting conditions, but which releases free

glutamate in response to light (Fig. 2a). A variety of caged glutamate compounds have been synthesized (e.g. [16–18]) and many are commercially available (*see* Subheading 2). Caged glutamate consists of a glutamate molecule covalently linked to a “caging” compound, which renders the glutamate biologically inactive. These covalent linkages undergo photolysis in response to light, at which point glutamate is “uncaged” and is able to activate glutamate receptors, thus eliciting action potentials in nearby neurons (Fig. 2a).

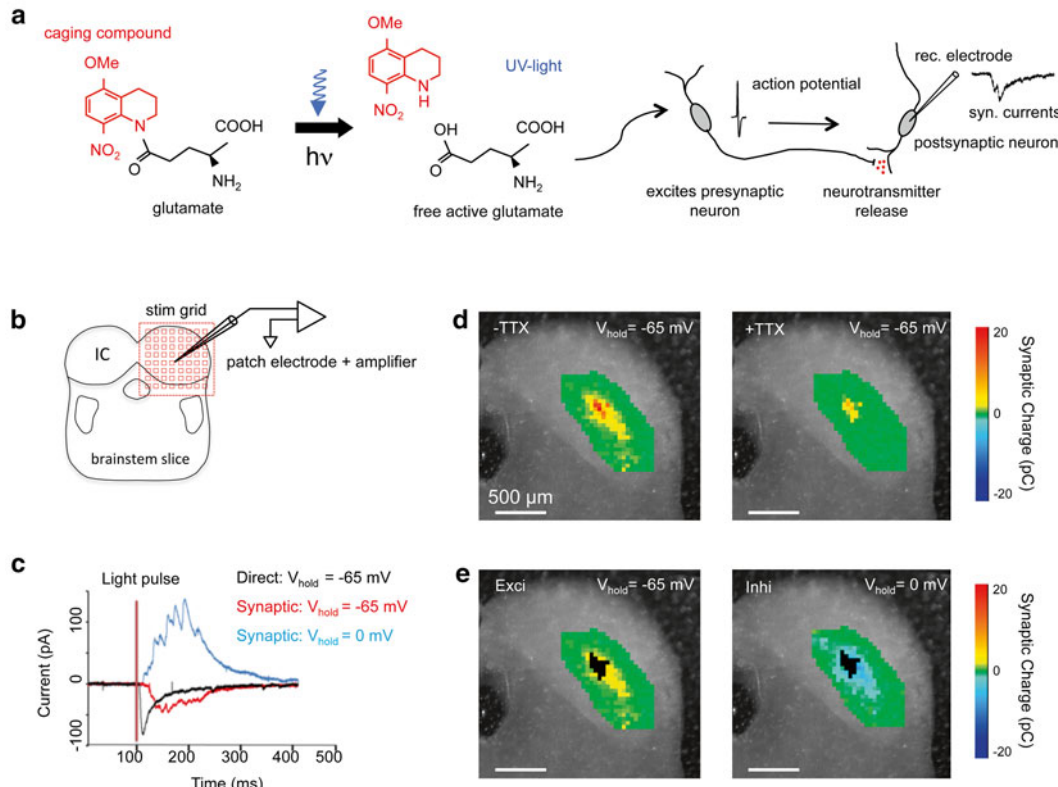


Fig. 2 Using laser scanning photo stimulation with caged glutamate to map synaptic connections in the inferior colliculus. (a) UV light hydrolyses the covalent linkage between glutamate (*black*) and the caging compound (*red*, caging group is 4-methoxy-7-nitroindolinyl (MNI) group from MNI-caged-L-glutamate, Tocris) (*left*), thereby releasing free glutamate (*middle*) that drives nearby neurons to spiking (*right*). Spiking in presynaptic neurons leads to neurotransmitter release and synaptic currents in the recorded postsynaptic neuron. (b) Schematic illustration of input mapping in the inferior colliculus (IC) with whole-cell path clamp recording electrode. Light pulses are delivered to a series of stimulation targets (stim grid) (c) Excitatory (*red* trace) and inhibitory (*blue* trace) synaptic inputs can be distinguished by holding the membrane potential of the recorded cell near the reversal potential for chloride (-65 mV) and glutamatergic neurotransmission (0 mV), respectively. Compared to direct stimulations (*black* trace), synaptic responses have longer onset latencies. (d) *Left*, Example of an excitatory synaptic input map obtained with laser-scanning photostimulation from an IC neuron in a P7 mouse. *Right*, Synaptic inputs are abolished by mapping in the presence of TTX, which blocks action potential generation leaving only direct responses intact. (e) Example of average excitatory (*left*, same map as 2D, *left*) and inhibitory (*right*) synaptic input maps. Direct response sites are shown in black. (Panel (c) modified from ref. [10])

Different caging compounds exhibit distinct biophysical (e.g., photolytic efficiency and kinetics, stability against spontaneous hydrolysis in the absence of light) and biological properties (agonist or antagonist action and potential toxicity). Most caged glutamate compounds are photolysed by light within the ultraviolet spectrum (300–400 nm), but a number of caging compounds have also been developed with sensitivity to wavelengths within the visible range (400–700 nm) (for example, RuBi-Glutamate, Tocris; [19]). Visible light allows greater tissue penetration and reduced photo-toxicity compared to UV light [20, 21], but caged compounds that are sensitive to visible light are also sensitive to ambient light, which requires careful light shielding during their usage. While the properties of most commercial caged compounds usually have been well characterized, the experimenter is advised to verify in their specific preparation that the chosen caged compound does not interact with their biological system, while in its supposedly inactive state. For example, the addition of caged glutamate to the external solution should have no effect on membrane potentials or synaptic transmission. Finally, the experimenter should also confirm that the UV light exposure necessary to elicit reliable action potential generation via uncaging does not itself interfere with the physiological properties of the neurons to be stimulated [22, 23].

3.1.2 Mapping Locations of Presynaptic Neurons

In a typical synaptic input mapping study, a whole cell recording is first obtained from an individual neuron in a living brain slice (Fig. 2b) immersed in a bath of recirculating artificial cerebrospinal fluid (ACSF). Caged glutamate is then added to the ACSF and allowed to reach a stable concentration (5–10 min) within the slice. Most studies use a working concentration of caged glutamate between 80 μ M and 3 mM [2, 3, 5, 7, 10–15], but the optimal concentration needs to be adjusted based upon the caged compound, the neurons to be stimulated, the uncaging system used, and the particular experimental conditions. An appropriate glutamate concentration will be high enough that uncaging reliably elicits action potentials, but low enough to both minimize buildup of free glutamate due to spontaneous hydrolysis and restrict the area of excitation (*see Subheading 3.1.4*). For uncaging, brief, focal UV light pulses (1–100 ms) are delivered to locations containing potential presynaptic neurons. Different stimulation sites are targeted either by moving an optical fiber above the slice (*see Subheading 3.2*) or by steering a laser light spot using computer-controlled galvanometers (*see Subheading 3.3*). If a photo-stimulation site contains neurons presynaptic to the recorded cell, a postsynaptic response will be recorded (*see Note 1*). At stimulation sites close to the recorded neuron, uncaged glutamate can also directly excite the recorded cell itself, giving rise to short latency (1–5 ms post-stimulus) membrane currents (“direct responses”). These direct responses can be distinguished from synaptic responses

by their shorter onset latencies and by their insensitivity to blocking axonal spike propagation with tetrodotoxin (TTX), which abolishes synaptic but not direct responses (Fig. 2*d, right*). By systematically testing hundreds to thousands of stimulation sites, the positions of neurons are revealed that make functional synaptic connections with the recorded neuron in the slice.

Excitatory and inhibitory presynaptic inputs can be distinguished by recording synaptic currents at different membrane voltages of the recorded neuron in voltage-clamp mode (Fig. 2*c, from [10]*). To isolate glutamatergic excitatory inputs, the membrane potential of the recorded cell is held at the reversal potential for chloride, which eliminates membrane currents through glycine and GABA_A receptors (Fig. 2*c, e, left*). Conversely, to isolate inhibitory synaptic inputs, the membrane potential of the recorded cell is held near the reversal potential for glutamatergic neurotransmission (Fig. 2*c, e, right*) (*see Note 2*). The contribution of GABAergic and glycinergic connections to inhibitory input maps may also be isolated pharmacologically using specific antagonists for GABA and glycine receptors [10] (*see Note 3*).

3.1.3 Synaptic Input Map Analysis

If synaptic response amplitudes are small and difficult to detect, or if there is a high level of spontaneous synaptic activity in the slice, which can make it difficult to categorize a synaptic event as an elicited response, mapping should be repeated several times to create averaged input maps (Fig. 3). These input maps can then be analyzed with respect to the amplitudes and the latencies of responses as well as the distribution of excitatory and inhibitory synaptic connections. For instance, investigators may wish to calculate quantities such as synaptic input area, total input charge (charge per map), or input charge density (charge per stimulation site). Such analyses have been used to characterize the processes of synaptic elimination and strengthening that occur during early development in the primary sound localization circuit formed by the medial nucleus of the trapezoid body (MNTB) and the lateral superior olive (LSO) (Fig. 4) [2, 7, 8], in the inferior colliculus (IC) [10] and in the auditory cortex [3, 5, 13, 14]. Spatial analyses can relate the shape of synaptic input maps to the anatomical or functional organization of the circuit, such as tonotopy. Comparing the excitatory and inhibitory input maps can quantify the degree of spatial overlap between synaptic excitation and inhibition, in order to estimate local synaptic excitation: inhibition balance. In the IC, for example, excitatory and inhibitory input maps were found to exhibit a high degree of spatial overlap, and this overlap was subject to significant developmental regulation [10].

3.1.4 Interpretation of Input Maps

The accurate interpretation of synaptic input maps to reveal underlying synaptic circuitry rests upon a number of important considerations. First, in addition to depending upon the kinetics and concentration of the caged compound being utilized and the

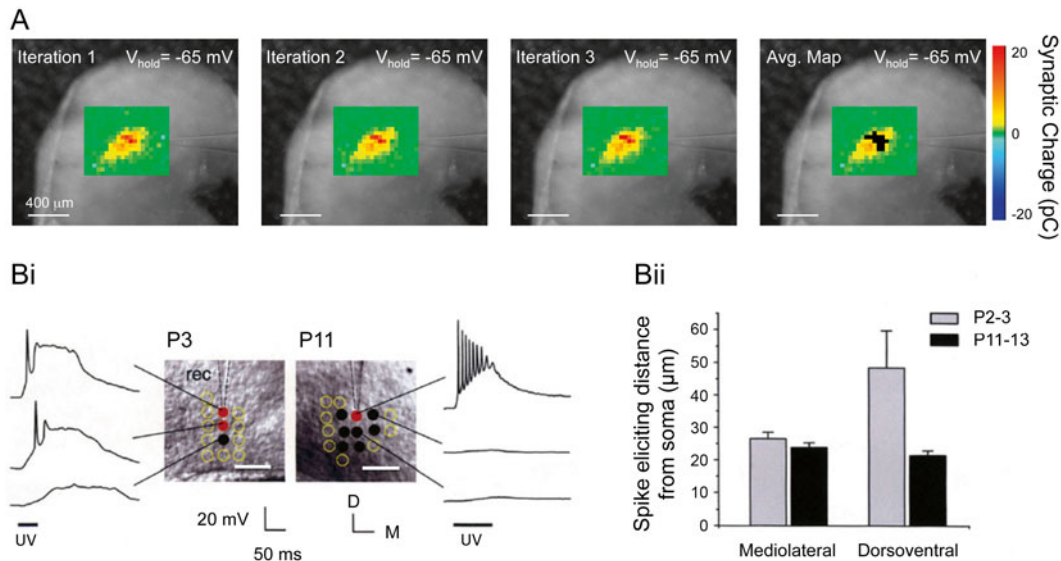


Fig. 3 Reliability and spatial resolution of synaptic input mapping. **(a)** Repeated mapping of excitatory inputs (Iterations 1–3) reveals very similar maps. Responses are averaged to generate an “average map” for further analysis. Stimulation sites eliciting direct responses in average map are shown in black. Example is from the IC of a postnatal day (P)8 mouse. V_{hold} —membrane holding potential. **(b)** Spatial resolution of glutamate uncaging with a 20 μ m diameter optical fiber in the medial nucleus of the trapezoid body (MNTB) of developing rats. **(Bi)** Uncaging elicited glutamate responses of individual MNTB neurons at P3 and P11. Stimulation sites that elicit action potentials (filled red circles) are found immediately around the cell body at the tip of the recording electrode (rec). Stimulation sites at greater distances elicit either subthreshold responses (black filled circles) or no responses (open yellow circles). D dorsal, M medial. Scale bar, 100 μ m. **(Bii)** Age-dependent changes in the average spike-eliciting distance along the mediolateral and dorsoventral dimensions of the MNTB. (Panel **b**) modified from ref. [2], Fig. 4)

power of the UV photo-stimulus, the effective resolution of input mapping is also influenced by morphological and physiological properties of the pre-synaptic neurons being stimulated [2, 4]. The dendritic geometry and the dendro-somatic distribution of glutamate receptors influence what uncaging positions will generate action potential in the neuron, thus influencing the spatial resolution of presynaptic input maps. For example, if presynaptic neurons have large dendritic fields with a high density of glutamate receptors, uncaging anywhere over the dendritic tree may be able to elicit spikes, making it difficult to infer the location of the pre-synaptic cell body from those uncaging sites. This uncertainty may increase if there exists heterogeneity (in terms of dendritic arbor size and sensitivity to glutamate) in the population of presynaptic neurons being stimulated.

Differences in animal age and associated degrees in axon myelination, tissue density, and neuron physiology affect light penetration into the slice and the sensitivity of presynaptic neurons to glutamate uncaging [2, 4, 7]. Therefore, it is necessary to calibrate the uncaging efficiency for differences in the experimental preparation [2, 7, 10].

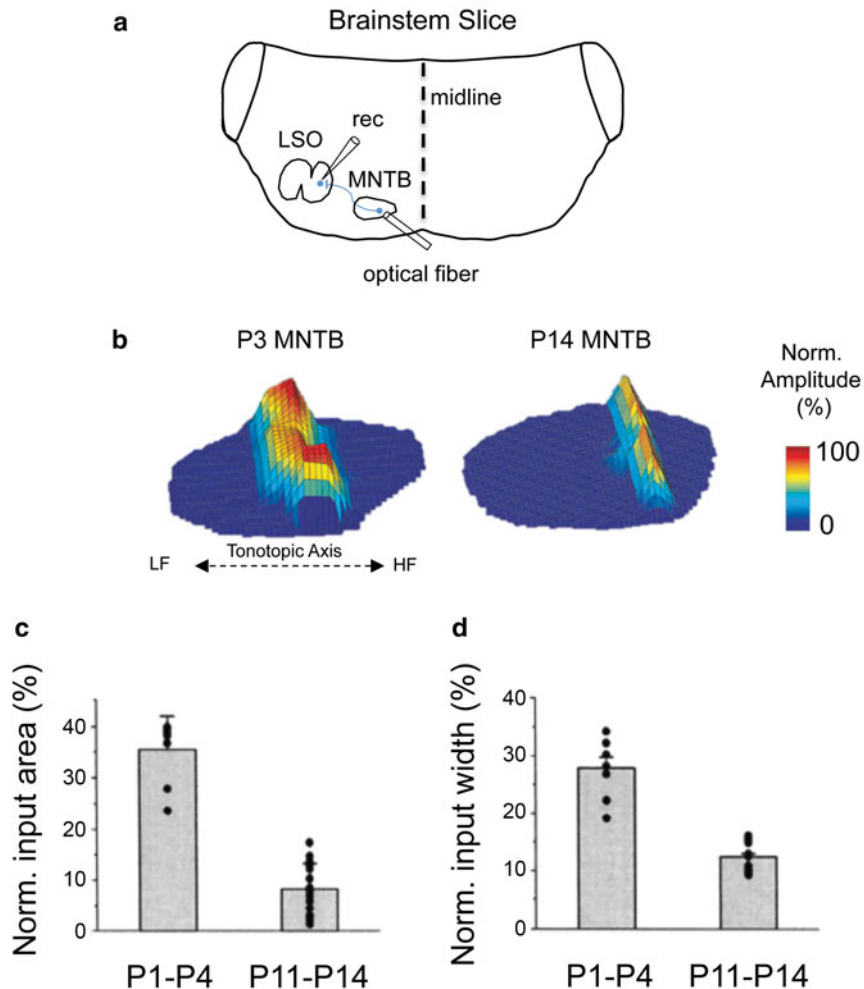


Fig. 4 Functional refinement of the developing MNTB-LSO pathway revealed by fiber-based glutamate uncaging. (a) Schematic illustration of the pathway from the medial nucleus of the trapezoid body (MNTB) to the lateral superior olive (LSO) and the experimental configuration; functional synaptic connections from the MNTB to the LSO are revealed by stimulating presynaptic MNTB neurons with uncaged glutamate, and measuring postsynaptic responses in the recorded LSO neuron. Light stimulation for glutamate uncaging is delivered by an optical fiber. (b) Examples of MNTB input maps obtained at P3 and P14. (c) Developmental changes in normalized input map area and input map width (d) along the tonotopic axis. Map area is normalized to MNTB cross-sectional area and input map width is normalized to mediolateral MNTB length. (Panels (b)–(d) modified from ref. [2])

This is best done by generating “excitability profiles,” which involves recording from putative presynaptic neurons while uncaging glutamate in their vicinity to determine the area over which glutamate uncaging leads to the generation of action potentials (Fig. 3b) [2, 4, 10]. If excitability profiles are similar for neurons across experimental conditions, then variations in the excitatory and inhibitory input maps between experimental conditions can be attributed to differences in connectivity rather than to differences in the ability of uncaged glutamate to drive presynaptic neurons.

A second issue in interpreting synaptic input maps is discerning whether responses are due to activation of monosynaptic or polysynaptic connections. One method for distinguishing monosynaptic responses from polysynaptic responses is to decrease neuronal excitability by raising the concentration of divalent cations in the ACSF and/or pharmacologically blocking NMDA receptor activation [4]. Decreasing circuit excitability reduces the likelihood that uncaging-driven spiking in presynaptic neurons will elicit action potentials in postsynaptic neurons, restricting the activation of polysynaptic pathways. If NMDA receptor currents are critical for presynaptic spike generation, activation of polysynaptic inputs can be decreased without NMDA receptor blockade by reducing the concentration of caged glutamate and/or the uncaging light intensity, in order to elicit only one or very few action potentials in presynaptic neurons. Finally, another method to evaluate whether input maps reflect monosynaptic connections is to disinhibit the brain slice with antagonists of inhibitory neurotransmission in order to favor the recruitment of polysynaptic responses. If excitatory input maps remain unchanged in the disinhibited slice, then this can be taken as further indication that they consist of monosynaptic connections [10].

3.2 Optical Fiber-Based Input Mapping

3.2.1 System Composition

A relatively simple and affordable method for creating movable localized UV light illumination in slices is the use of an optical fiber. A basic fiber-based photostimulation system is composed of a mercury arc lamp as a UV source, a condenser to focus the light into the optical fiber, an electronic shutter to control light pulse duration and an optical fiber for light delivery (Fig. 1a). The electronic shutter needs to allow short and precise opening/closing times (<10 ms) and withstand the high light and heat output from a mercury arc lamp. Additionally, to achieve a desired illumination spot size it is important to select an optical fiber with UV transmittance and an appropriate diameter (we have used fibers with diameters ranging from 5 to 200 μm). Constructing a fiber-based uncaging system is relatively simple and can be constructed in a few days; a detailed description of the necessary components and their assembly is given elsewhere (*see* [6]).

3.2.2 Advantages of Uncaging with Optical Fibers

The major advantages of using a fiber-based uncaging system over a laser-based uncaging system include its lower cost, reduced time for assembly, and the ability to use multiple fibers for simultaneous stimulation of several sites [24]. The cost of a fiber-based system, including the light source, electronic shutter, optical fiber and accessory equipment, is approximately \$5000, which is an order of magnitude lower than the cost of a laser-based system. A fiber-based system can be quickly added to an existing electrophysiology setup, and the location of the optical fiber above the brain slice, and hence the stimulation area, can be monitored and recorded via

the existing video camera of a visualized whole-cell patch clamping setup. If multiple optical fibers are needed, they can be added using the additional ports on the mercury lamp housing. Additional fibers may also allow the sharing of one lamp housing between several electrophysiological setups. Using multiple optical fibers enables the simultaneous stimulation of distinct sources of presynaptic input, in order to examine how different input sources are integrated.

3.2.3 Limitations of Uncaging with Optical Fibers

The major limitations of using a fiber-based uncaging system, compared to laser-based systems, include generally poorer spatial resolution and longer time for manually changing uncaging positions. The spatial resolution of a fiber-based system, as defined as the spike-eliciting area, will depend upon a number of factors including UV light power, UV flash duration, optical fiber diameter. In general, this area should be experimentally determined for the specific preparation. In our experience, the spatial resolution of an optical fiber with a 20 µm diameter light-conducting core (Polymicro Technologies, Phoenix, Arizona) is approximately 50 µm in the MNTB [2]. In general, fiber-based systems are less suitable for experiments that require very small, subcellular stimulation areas. Because the optical fiber is moved manually between uncaging positions, input mapping is slow, requiring that stable recordings for 1–3 h depending on the number of stimulation sites. In our hands, it takes about 2 h to stimulate 100–150 sites in the MNTB [2, 25]. Thus, fiber-based systems are less well-suited for uncaging experiments that requiring large numbers (>200) of stimulation positions or if long stable recordings cannot be obtained. In summary, fiber-based uncaging systems are inexpensive, flexible, and relatively easy to assemble, but their drawback is limited spatial resolution and slow scanning speed due to manual positioning (Table 1).

Table 1
Advantages and limitations of fiber-based and laser-based uncaging

Uncaging system	Advantages	Limitations
Optical fiber	Inexpensive	Spatial resolution
	Easy to set up and use	Temporal resolution
	Flexibility (multiple fibers and illumination size)	Manual control
UV laser	Spatial resolution	Cost
	Temporal resolution	Technical expertise required
	Automated control	

3.3 Laser Scanning-Based Input Mapping

3.3.1 System Composition

A typical laser-scanning photostimulation (LSPS) system consists of a UV laser for light generation, an attenuator to regulate light intensity, a mechanical shutter to control UV light pulse width, voltage-controlled galvo-driven mirrors to steer the location of the laser spot, lenses to focus the UV light, and a dichroic beam splitter to reflect laser light down through the microscope to the sample, while letting visible light from the sample pass through to the camera for visualization of the brain slice (Fig. 1b). Software programs control the mirror galvanometers (and thus the location of the laser spot in the field of view) to generate a series of laser targets that can be scanned through in random or defined sequences ScanImage & Ephus, are freely available software packages offered through openwiki.janelia.org. Stimulation/acquisition software, we have been using in ref. [10], is available up request from *nguyen@tcnj.edu*).

3.3.2 Advantages of Uncaging with LSPS

The major advantages of a laser-based uncaging system over a fiber-based uncaging system are its superior spatial and temporal resolution. Because light for uncaging is focused through the microscope objective, the uncaging spot can be very small when using high-magnification objectives. If required, spatial resolution (including in the Z-axis) can be improved further with two-photon uncaging, to the extent that individual dendritic spines may be stimulated [26, 27]. Because of the use of software-controlled mirror galvanometers, LSPS systems can rapidly scan through a very large number of stimulation sites, with the minimum inter-stimulus interval between sites effectively being determined by the duration of synaptic responses, rather than by the time required to move between targets. This allows for the mapping and examination of large input areas. For example, in our mapping studies in the IC, we usually scan about 500 discrete sites at 2 Hz, completing one map iteration in about 5–10 min. The speed of automated laser scanning also makes it feasible to repeat mapping protocols multiple times over relatively short periods, thereby, increasing input map reliability and investigating changes in input map organization after pharmacological or other experimental manipulations. Compared to fiber-based experiments, which require that neurons be held stable from 1 to 3 h, even extensive LSPS experiments can generally be completed in 30 min or less.

3.3.3 Limitations of Uncaging with LSPS

The major limitations of using an LSPS uncaging system compared to fiber-based systems include its higher cost, and the greater level of technical skill required to assemble the system. The most expensive item is the UV laser. We use a 355 nm solid-state UV laser with 2 W of power (DPPS lasers, Inc) costing approximately \$30,000. Additionally, while detailed instructions are available (*see* [4]), compared to a fiber-based system, assembly and trouble shooting of an LSPS system requires more time (at least several months) and

a higher level of technical skill. In summary, compared to fiber-based systems, LSPS-based uncaging systems afford superior spatial and temporal resolution, but they are more expensive and require greater technical expertise to operate (Table 1).

3.4 Choosing the Right Approach

Deciding which uncaging system is most appropriate for your laboratory will depend upon your specific research question and the available financial resources. In cases where synaptic input maps are relatively small and where the general locations of these inputs can be predicted from previous anatomical studies, a fiber-based system will likely prove effective. Additionally, investigators with little prior knowledge of optics, who aim to begin collecting data as soon as possible, may wish to opt for a fiber-based system. However, in cases where either the location or the number of synaptic inputs are unknown, or where the synaptic input maps are large, the higher mapping speed of a computer controlled, semi-automated LSPS-based system will be preferable.

4 Notes

1. If you are having trouble detecting postsynaptic responses, first check to make sure that sufficient uncaging light is indeed being delivered to the slice (if necessary, verify with photoactivatable fluorescent dyes). Next, ensure that the light is being delivered to the desired location, if not, system calibration will be necessary. If postsynaptic responses are still undetectable, increase the concentration of caged glutamate and/or increase the duration and power of the uncaging light pulse. To confirm that photostimulation is leading to robust action potential generation in presynaptic neurons, perform excitability mapping (*see Subheading 3.2*).
2. If you are having trouble visualizing inhibitory synaptic inputs, it may be worth increasing the driving force for chloride by changing to an internal solution with a higher chloride concentration to boost inhibitory synaptic inputs.
3. Caution should be taken when blocking glutamate receptors, because this interferes with the ability of uncaged glutamate to activate presynaptic neurons.

References

1. Callaway EM, Katz LC (1993) Photostimulation using caged glutamate reveals functional circuitry in living brain slices. *Proc Natl Acad Sci U S A* 90(16):7661–7665
2. Kim G, Kandler K (2003) Elimination and strengthening of glycinergic/GABAergic connections during tonotopic map formation. *Nat Neurosci* 6(3):282–290
3. Zhao C, Kao JP, Kanold PO (2009) Functional excitatory microcircuits in neonatal cortex connect thalamus and layer 4. *J Neurosci* 29(49):15479–15488

4. Shepherd GM (2012) Circuit mapping by UV uncaging of glutamate. *Cold Spring Harb Protoc* 9:998–1004
5. Viswanathan S, Bandyopadhyay S, Kao JP, Kanold PO (2012) Changing microcircuits in the subplate of the developing cortex. *J Neurosci* 32(5):1589–1601
6. Kandler K, Nguyen T, Noh J, Givens RS (2013) An optical fiber-based uncaging system. *Cold Spring Harb Protoc* 2:118–121
7. Hirtz JJ, Braun N, Griesemer D, Hannes C, Janz K, Lörke S, Müller B, Friauf E (2012) Synaptic refinement of an inhibitory topographic map in the auditory brainstem requires functional $\text{Ca}_v1.3$ calcium channels. *J Neurosci* 32(42):14602–14616
8. Clause A, Kim G, Sonntag M, Weisz CJ, Vetter DE, Rübsamen R, Kandler K (2014) The precise temporal pattern of prehearing spontaneous activity is necessary for tonotopic map refinement. *Neuron* 82(4):822–835
9. Campagnola L, Manis PB (2014) A map of functional synaptic connectivity in the mouse anteroventral cochlear nucleus. *J Neurosci* 34(6):2214–2230
10. Sturm J, Nguyen T, Kandler K (2014) Development of intrinsic connectivity in the central nucleus of the mouse inferior colliculus. *J Neurosci* 34(45):15032–15046
11. Barbour DL, Callaway EM (2008) Excitatory local connections of superficial neurons in rat auditory cortex. *J Neurosci* 28(44):11174–11185
12. Lee CC, Imaizumi K (2013) Functional convergence of thalamic and intrinsic projections to cortical layers 4 and 6. *Neurophysiology* 45(5–6):396–406
13. Meng X, Kao JPY, Kanold PO (2014) Differential signaling to subplate neurons by spatially specific silent synapses in developing auditory cortex. *J Neurosci* 34(26):8855–8864
14. Watkins PV, Kao JPY, Kanold PO (2014) Spatial pattern of intra-laminar connectivity in supragranular mouse auditory cortex. *Front Neural Circ* 8:15
15. Kratz MB, Manis PB (2015) Spatial organization of excitatory synaptic inputs to layer 4 neurons in mouse primary auditory cortex. *Front Neural Circ* 9:17
16. Stensrud K, Noh J, Kandler K, Wirz J, Heger D, Givens RS (2009) Competing pathways in the photo-Favorskii rearrangement and release of esters: studies on fluorinated p-hydroxyphenacyl-caged GABA and glutamate phototriggers. *J Org Chem* 74(15):5219–5227
17. Conrad PG 2nd, Givens RS, Weber JF, Kandler K (2000) New phototriggers: extending the p-hydroxyphenacyl pi-pi absorption range. *Org Lett* 2(11):1545–1547
18. Givens RS, Rubina M, Wirz J (2012) Applications of p-hydroxyphenacyl (pHP) and coumarin-4-ylmethyl photoremovable protecting groups. *Photochem Photobiol Sci* 11(3):472–488
19. Shembekar VR, Chen Y, Carpenter BK, Hess GP (2005) A protecting group for carboxylic acids that can be photolyzed by visible light. *Biochemistry* 44(19):7107–7114
20. Rial Verde EM, Zayat L, Etchenique R, Yuste R (2008) Photorelease of GABA with visible light using an inorganic caging group. *Front Neural Circ* 2:2
21. Fino E, Araya R, Peterka DS, Salierno M, Etchenique R, Yuste R (2009) RuBi-glutamate: two-photon and visible-light photoactivation of neurons and dendritic spines. *Front Neural Circ* 3:2
22. Leszkiewicz DN, Kandler K, Aizenman E (2000) Enhancement of NMDA receptor-mediated currents by light in rat neurones in vitro. *J Physiol* 524(Pt 2):365–374
23. Leszkiewicz DN, Aizenman E (2003) Reversible modulation of GABA(A) receptor-mediated currents by light is dependent on the redox state of the receptor. *Eur J Neurosci* 17(10):2077–2083
24. Kandler K, Katz LC, Kauer JA (1998) Focal photolysis of caged glutamate reveals an entirely postsynaptic form of long-term depression of hippocampal glutamate receptors. *Nat Neurosci* 1:119–123
25. Noh J, Seal RP, Garver JA, Edwards RH, Kandler K (2010) Glutamate co-release at GABA/glycinergic synapses is crucial for refinement of an inhibitory map. *Nat Neurosci* 13(2):232–238
26. Matsuzaki M, Ellis-Davis GC, Nemoto T, Miyashita Y, Lino M, Kasai H (2001) Dendritic spine geometry is critical for AMPA receptor expression in hippocampal CA1 pyramidal neurons. *Nat Neurosci* 4(11):1086–1092
27. Smith MA, Ellis-Davis GC, Magee JC (2003) Mechanism of the distance-dependent scaling of Schaffer collateral synapses in rat CA1 pyramidal neurons. *J Physiol* 548(Pt. 1):245–258

INDEX

A

- Acetonitrile 118, 119, 123, 124, 131, 140, 142, 146
Actin
 actin meshwork 6
 β-actin 6
 F-actin core 5
 γ-actin 6
Action potentials 223, 235, 237, 264, 468, 516, 521, 522, 528, 529, 531–533
ADE2 96
Agilent 2100 bioanalyzer 75, 77, 80, 85, 86, 90, 91
AH109 96, 98–102, 104–106
Airy disk 194, 197, 360, 361
Alignment ratio 306, 307, 314
A-line 457, 458, 461
Allografts. *See* Schwannomas
3-amino-1,2,4-triazole (3-AT) 98, 100, 105
Ammonium formate 140
Analgesic 65, 67
 buprenorphine 65, 67
Anaplastic 60
Anesthesia 44, 62, 65, 66, 247, 248, 452–453, 455, 460
 isoflurane/forane 62, 63
Anistropy
Antibiotics 5, 68, 74, 321
Antibody
 anti-whirlin HL5136 antibody 10–11
 GAD67 265–267, 272
 parvalbumin 263, 264, 266, 267
 primary antibody 9, 14, 150, 154, 155, 161, 163, 164, 196, 269, 272, 313, 340, 343, 519, 522
 secondary antibody 9, 14, 150, 155, 161, 164, 196, 269, 271, 272, 321, 331, 340, 344, 432, 519, 522
 colloidal gold 150
 vGAT 266, 272
Apical plasma membrane 6
Apoptosis 391, 392, 421
Artificial intron
 plasmid 27–28, 30
 sequence 28, 30, 32, 33, 38

- Astrocytomas 59
Atoh1 323, 379, 391, 420
Atypical 60
Auditory neurons
 current clamp 479, 480, 521–522
 physiology 531
 post-hearing 514
 pre-hearing 514
 synapse
 afferent synapse 471, 472
 efferent synapse 471
 voltage clamp 350–352, 357, 480, 487, 519–520, 530
Auditory pathway 264, 266, 267, 365
Auditory system 95–107, 121, 263–274, 350, 463, 464, 467, 525, 526
Autosomal-dominant 59

B

- Barrel 7, 14, 18, 22
Basilar papilla
 birds 463
 development 463–469
 hair cells 464, 465, 467–468
 hearing 463, 465–469
 patch-clamp 351, 352, 360, 520, 527
 physiology 471
 regeneration 365
β-galactosidase 444
Benign 60, 61, 63, 67, 68, 70
Ben-Me-1. *See* Cell culture
Best frequency (BF) 460
Bilateral. *See* Vestibular
Binomial distribution 195–196
Bioactive compound libraries 419
Biostatic transfection 15–16
Bioluminescence imaging (BLI) 61, 63, 67, 70.
 See also Imaging
 luciferin 63, 67, 69, 70
BioRad hand-held Helios® Gene Gun 5
 bullets 5, 6, 8, 12–14
BK currents 480, 481
BM-scan 457, 459, 460
Brainstem compression 59, 60
B-scan 457–459

Buffer

- blocking buffer.....154, 161, 163, 271, 308, 313, 519
- contrast staining buffer154
- Hanks balanced salt solution (HBSS)61, 432
- phosphate-buffered saline (PBS)61, 168, 268, 423
- solubilization buffer139, 141
- TE buffer98
- Tris-buffered saline (TBS), 61

Buprenorphine. *See* Analgesic

C

Calcium signaling

- ATP-dependent Ca^{2+} transients223
- Ca^{2+} -dependent action potentials223
- Carving283–285, 287, 289
- Caspase-Glo 3/7 assay422–427
- caspase 3/7 activation427

Cell

- cell-cell junctions5
- cell membrane350–352, 359, 365, 367, 376, 377, 382, 385, 520
- cell types4, 6, 136, 244, 258, 293, 356
- Deiter's cell5
- hair cell (*see* Hair cell)
- Myo15ash2* and *Whrnwi* hair cells10–11, 15–17
- sensory cell5, 18
- supporting cell4, 5, 265, 301, 378, 379, 382, 386, 391, 394, 420, 452, 465, 472, 477, 479
- terminally-differentiated cells4, 5
- vestibular hair cell10–11, 19, 20, 377

Cell culture

- NF2*-deficient benign human meningioma cell line
- Ben-Men-161, 63
- Nf2po* schwannoma cells61, 63
- primary schwann cell culture314
- schwann cells59, 63, 306, 313, 316
- spiral ganglion cells251, 364, 377, 378, 382, 391

Cell culture media

- DME/F12 medium61
- Dulbecco's modified eagles (DME) medium61, 191

Cell identification278, 281–284, 287

Cell seeker279, 281–284, 286, 289

Cell sorting432, 437–444

CellTiter-Glo (CTG) cell viability assay420

Characteristic frequency (CF)460, 461

Chicken otocyst27–40

Chick Ringer's Solution31, 35–37, 40

Cisplatin

- cisplatin-induced ototoxicity419–428
- protection against cisplatin-induced ototoxicity419–428
- Clic56, 18–20
- CM-scan457, 459–460
- Cochlea

- afferent fibers244, 264, 464
- chicken463–466, 468
- efferent fibers244, 250, 252–253, 264
- guinea pig356, 380, 381, 391, 449, 450, 471, 504

- inner hair cells19, 235, 237, 251, 264, 265, 364, 378, 465, 472, 476–479, 482, 483, 513
- mouse293–303, 382, 388, 390, 398, 427, 451, 452, 457–460, 518
- outer hair cells45, 46, 244, 245, 264, 350, 356, 364, 377, 378, 394, 465, 471, 472, 513
- ribbon synapse265

Cochlear implant305, 364, 365, 379, 402

Collagen-matrigel substrate295, 296

Confirming interactions104

Confocal microscope9, 15, 23, 224, 225, 250, 259, 459

Connectomics277

Connexin hemichannels235

- ATP release from connexin hemichannels235

Conventional transfection4

Cranial nerve palsy60

Cranial nerves60, 156, 162, 269

Cristae ampullares4

Current clamp480, 521

Cuticular plate4–6, 21

Cyclic alkylaminoluciferin (CycLuc1)69

Cytomegalovirus (CMV)62, 64, 68, 322

D

Deafness6, 59, 77, 79, 365, 391, 392

Decalcification150, 152, 157, 162, 270, 273

Degeneration10–11, 16, 17, 241, 244, 364, 391, 392

Desalting peptides140, 142

- C18 spin columns130, 140, 142

DFNB3115

Diffusion screen7, 8, 14, 21, 22

Dimer190

Dimethyl sulfoxide (DMSO)61, 100, 101, 139, 229, 230, 295, 321, 329, 398, 423, 424, 427, 522

Directed neurite growth317

Dispase294, 299, 302, 504

Dispersion184, 232, 370, 398, 458

Dissection

- basilar papilla38, 243, 463–469

- cochlea 273, 299
- spiral ganglion 250, 251, 299, 305–318, 364, 377, 378, 382, 389, 391, 396, 513–522
- d-luciferin potassium (*see* Luciferase)
- DMSO. *See* Dimethyl sulfoxide (DMSO)
- DNA
 - cDNA constructs 17
 - DNA-coated gold particles 5, 6
 - exogenous DNA 4, 5
- Drycap dehydrators 8, 13
- DsRed epitope tag 15
- E**
 - Ear afferents 253, 264, 513
 - Ear efferents 244
 - Egg windowing 35, 40
 - Electrode fabrication 30, 34, 472, 474–475
 - Electron microscopy 9, 20, 149–164, 204, 206, 256, 259, 277–289, 308, 310, 380
 - Electrophysiology 5, 471, 489, 533
 - Electroporation 3, 4, 16, 27–40, 101, 104, 107, 293
 - Embryo 4, 27, 31–32, 34–40, 44, 45, 52, 245, 249, 255, 257, 297, 298, 300, 302, 390, 463–469
 - Endotoxin free 20, 52, 53
 - Enzymatic digestion 298, 299
 - Ependymomas 59
 - Espin 6
 - Excitatory neurons
 - Arg3.1/arc 264, 266, 267, 272
 - vGlut2 267
 - Explant cultures
 - cochlea 46, 98, 121, 135–147, 149–164, 223, 233, 237, 238, 246, 252–253, 257, 258, 268–270, 298, 301, 311, 315, 361, 364, 380, 382, 390, 391, 395–397, 402, 404, 431, 432, 434, 435, 449, 450, 452, 455–457, 460, 504, 513, 517
 - sensory epithelium 4, 7, 11, 15, 19, 156, 244, 320, 364, 464, 480
 - spiral ganglion 250, 299, 305, 306, 313, 315, 364, 377, 378, 382, 389, 391, 435, 477, 513, 517
 - Expression constructs
 - Clic5-GFP 18–20
 - DsRed-Whirlin 10–11, 15
 - GFP- β -actin 10–11, 17
 - GFP-myosin 15a 15–17
 - F**
 - Facial nerve paralysis 59
 - FACS. *See* Fluorescence-activated cell sorting (FACS)
 - Fetal bovine serum (FBS) 11, 14, 20, 22, 45, 46, 55, 61, 63, 68, 191, 192, 208, 212, 229, 233, 302, 308, 312, 317, 321, 423, 424, 432, 433, 435, 515–518, 522
 - Fetal gene transfer 44
 - Filter-Aided Sample Preparation (FASP) 139, 145
 - Flow cytometry 330, 431
 - Fluorescence-activated cell sorting (FACS) 432–434, 436–439, 441–444
 - Fluorescence excitation
 - diode laser 239
 - light emitting diode (LED) 227, 228, 239–241
 - Fluorescence immunohistochemistry 263–274
 - Fluorescence immunostaining 6
 - Fluorescence microscopy
 - calcium imaging 240
 - confocal imaging
 - laser-scanning confocal microscopy 224
 - Ronchi ruling pattern 224
 - spinning disk confocal microscopy 239
 - two-color imaging 224, 235
 - image duplicator 225, 229, 230, 232, 233, 235, 239, 240
 - Fluorescent probes
 - calcium dyes 230
 - Fluo-4 AM 230, 235, 237, 238
 - Fura-Red AM 230, 234
 - voltage dyes
 - voltageFluor (Vf) 229
 - Focusing nozzle 18
 - Formic acid 139, 140, 142, 143, 145, 146
 - Forskolin 61
 - G**
 - Gain 112, 193, 232, 238, 246, 359, 377, 449, 490, 508
 - GAL4 95, 96, 99, 106, 390
 - Gene delivery
 - gene gun 4
 - lentivirus 62, 64
 - nanoparticle-based gene delivery 399
 - rAAV-mediated 46
 - Gene gun
 - acell (Aurogen) 18
 - bioRad hand-held Helios® gene gun 5, 18
 - Genetically engineered mouse (GEM) 60
 - GFP-myosin-XVa 10–11
 - GFP-Whrn 10–11
 - Glycobiology 115
 - Glycome 115
 - Gold
 - gold particle bombardment 6, 18
 - gold particles 5, 6, 12, 13, 15, 18, 21, 22, 150, 164
 - Green fluorescent protein (GFP) 30, 74
 - Ground truth 277

- Growth factor delivery 294, 319, 433
 Growth factors 320, 365, 380, 391, 392, 401
 Guinea pig 356, 361, 380, 381, 391, 449, 450, 471
- H**
- Hair cell
 differentiation 299, 320, 356
 imaging 209
 inner hair cell 19, 203, 204, 206, 210, 214, 215, 217, 223, 235, 237, 251, 265, 364, 378, 465, 471–484, 493, 498, 513
 outer hair cell 45, 46, 203, 204, 206, 244, 245, 264, 350, 356, 364, 377, 394, 465, 471, 472, 478, 493, 498, 501–511, 513
 patch clamp 206, 208, 209, 218, 241, 351, 352, 360, 489–490, 497, 501, 503, 505, 506, 515–516, 520, 527, 534
 transfected hair cell 5, 16–18
- Hamilton Neuros™ syringes 62, 65
- Hank's balanced salt solution (HBSS). *See* Buffer
- Head holder 453–457, 461
- Hearing loss 59, 305, 363–365, 373, 378, 379, 386, 393, 399, 420, 421
- Hearing restoration 404
- HEI-OC1 cells 421–424, 427
- Helium
 gas 6, 8, 14, 16, 17
 pressure 6, 8, 11, 14
- Heterologous gene expression 78
- High-throughput screens
 hill plots 428
 mammalian cochlear cell-based
 chemical screens 488, 501
 screen optimization and validation 422–423
 Z'-factor 420, 422, 426, 428
- His3 96, 99–100, 105
- Hopping probe ion conductance microscopy (HPICM)
 calibration 210–211
 glass nanopipettes 207–209
 image processing 213–216
 imaging live hair cells 209, 210, 213, 214
 imaging setup 206, 210, 214
 software 207, 213, 218, 219
- Human deafness 6
- Hydrocephalus 59
- I**
- Iberiotoxin (IBTX) 480, 481, 484
- IC₅₀ 421, 426–428
- Ilastik
 anisotropy 280, 287
 carving 283–285, 289
 feature selection 280, 288
- HDF5, 287–289
 pixel classification 278, 281, 288
- Imaging**
 bioluminescence imaging (BLI) 61, 63, 67, 69, 70
 confocal imaging 247, 259
 electron microscopy 256, 259, 310
 live cell 5
 magnetic resonance imaging (MRI) 60, 61, 67, 70, 365, 366, 371, 374, 382, 395–397
 multi-isotope imaging mass spectrometry 5
 single molecule imaging 192, 193
- Immortomouse 421
- Immunohistochemistry 39, 149, 164, 250, 255, 264, 265, 267, 269, 273, 323, 339
- transmission electron microscopy 204
- Immunostaining 9, 14, 23, 149, 265–267, 272, 300, 339, 340, 519
- Injectoporation 3, 4, 16
- Inner ear**
 hair cell (*see* Hair cell)
 spiral ganglion (*see* Spiral ganglion)
- Interferometry 310, 311, 451
- Intracranial 61, 62, 66
- Intra-nerve injection 65. *See* Orthotopic
- Intrauterine electroporation 3
- In vivo animal models 427
- Ion channel gating 350, 353
- Isoflurane/forane. *See* Anesthesia
- IVIS spectrum preclinical in vivo
 imaging system 63, 67
- K**
- Ketamine 452, 453
- Knockout mice 293
N?²⁹ 61, 63, 64
- L**
- Labeling cell/tissue lysates
 C18 spin column 130, 140, 142–143
 disulfide bonds 115, 119, 129, 386
 interfering substances in iTRAQ
 labeling 118–119
 isobaric tagging for relative and absolute quantification (iTRAQ) 114
 isotope coded affinity tag (ICAT) 111–114
- Laminar flow hood 14, 20, 156, 192, 315, 442
- Laminin 61, 63, 308, 310, 311, 318, 514, 516, 517, 522
- Laser Doppler vibrometry 449–452
- Laser scanning-based input mapping
 advantages of uncaging with LSPS 535
 limitations of uncaging with LSPS 535
 system composition 535

- Laser scanning images.....224, 527, 528, 535–536
- LD_{50}426, 428
- Lenti-CMV-Luc.....62, 64, 68
- Lentiviral transduction. *See* Gene delivery
- Li Acetate.....98
- Light emitting diode (TLED).....354
- Lipofection.....4, 16
- Liquid Chromatography-Tandem Mass Spectrometry (LC-MS/MS).....124, 131, 138, 140, 143, 146
nano.....140, 143
- LTQ-Orbitrap.....140, 143
- Luciferase
D-luciferin potassium.....63
luciferase-expressing meningioma cells,
Ben-Men-1-Luc.....64, 66, 67
luciferase-expressing schwannoma cells.....61, 64
reporter assay system62
- Lysate generation
phosphoprotein enrichment.....121, 128
reactive cysteines.....120
stable isotope labeling of amino acids in cell culture
(SILAC).....117–118
tandem mass tags (TMTs).....114–115
- ## M
- Magnetic resonance imaging (MRI). *See* Imaging
- Magnitude.....280, 356, 361, 450, 451, 457, 460, 461, 484, 488, 501, 520, 533
- Malignant transformation.....60
- Mask.....127, 194, 210, 285, 287–289, 307, 309, 315, 386, 442
- Mass spectrometry
label free quantitation137, 138, 147
tandem mass tags.....114, 115
- MAT α96
- MatTek glass bottom Petri dishes7
- Mechanical damage.....17
- Mechanosensory.....320, 335
- Mechanotransduction experiment
current recording520, 522
equipment selection.....208, 227, 246, 324, 354, 433–434, 453–454, 501, 504, 533
recording solution.....519, 521
- Membrane electromechanics.....349–361
- Membrane mechanics.....350–352, 357, 361
- Membrane/protein interactions.....350, 376
- Meninges.....60
- Meningomas.....59–70
xenografts in SCID mice.....60
- Mesenchymal stem cells (MSCs).....320–322
- Mesh.....285, 287
- Metabolic labeling.....136
- Microarray analysis.....77, 80, 85–86, 88, 90
- Microcarriers
gold microcarrier8, 12–13, 17
tungsten microcarrier.....8
- Microfabrication.....305, 309–310
- Microinjection.....4, 5, 31, 44, 45, 379
- Micromanipulator31, 36, 37, 226, 228, 233, 472, 473, 475, 477, 480, 481, 489, 493, 515
- Microscope
confocal250, 259, 459
electron9, 20, 149–164, 204, 206, 256, 259, 277–289, 308, 310, 364, 380, 381
hopping probe ion conductance.....203–219
- Mitogen-activated protein kinase
(MAPK)70, 421
- Molecular cloning.....73–91
- Morbidities.....60
- Mortality60
- Mouse
model.....514
mutant258
- Mouse experimental embryology
endolymphatic duct40
fast green30, 35, 36
otic vesicle45, 465
otocyst44–46
transuterine microinjection44, 45
- M-scan457
- Multiple reaction monitoring (MRM)
calibration peptides.....117
transition definitions.....116
transition states.....116
- Multiplicity of Infection (MOI).....64, 68
- Mutation15, 17, 60, 69, 110, 165, 390, 393
- Myosin
myosin Ic6
myosin VI6, 338
myosin VIIa6, 323, 338, 340
myosin XVa3, 6, 15–17
- ## N
- Nanodelivery365–367
- Nanoparticle-based gene delivery.....320, 370, 387, 398
- Nanoparticle(s)21, 361–371, 374–386, 388, 389, 394–402
- Natural killer (NK) cells69
- Neuregulin- β 1/herculein- β 1 epidermal growth factor domain (rhuHRG- β 1)61
- Neuroanatomical tracing
dextran amines245–248, 250, 255–257, 259
Golgi staining244–246, 257
lipophilic dyes245–247, 249–253, 255, 256, 258, 259

- Neurofibromatosis type 2 (NF2)
 NF2-associated 59–70
 tumor suppressor gene, NF2-deficient 60
- Neuron 5, 27, 243, 245, 248–251, 254–258, 263, 264, 266, 267, 277, 288, 306, 312, 316, 354, 356, 358, 361, 521, 525–533, 535, 536
- Neutral density filters 191, 196
- Nitrogen 8, 329
- Nonlinear capacitance
 detrending 510
 FFT 510
 linear capacitance 507
 maximum charge moved 506
 two-sine analysis 503
 voltage at peak capacitance 502, 506
- Non-obese diabetic (NOD) 69
- Non-viral gene delivery 320
- Nucleofection 320, 333

O

- Olivocochlear efferents
 lateral olivocochlear neurons (LOC) 530, 532
- OPMI Pro Magis surgical microscope 62, 66
- Optical coherence tomography (OCT) 449–461
- Optical fiber-based input mapping
 advantages of uncaging with optical fibers 533–534
 limitations of uncaging with optical fibers 534–535
 system composition 533
- Optical sectioning 233, 234
- Optical tweezers 350–352, 354, 355
- Organ of Corti 207–209, 211–213, 219, 224, 244, 250, 264, 301, 311, 449–461, 494, 504, 507, 513, 517
- Organotypic culture 6, 10, 11, 14, 22, 207, 233–234, 293–303, 377, 378
 cochlea 294, 298–302, 305, 311, 312, 315, 316, 319–344, 356, 361
- Orthotopic
 intra-nerve injection 65
 stereotactic injection 66–67
- Otic capsule 298, 299, 311, 315, 316, 434, 435, 450, 458
- Otoconia 11
- Outer hair cell
 electromotility 350, 501, 503
 isolating outer hair cells 431, 503, 504
 membrane tension 350, 351, 505, 508, 510
 prestin 190, 191, 195, 196, 198, 350, 501, 507
- Over-expression 293

P

- Particle
 bombardment 6, 11, 18
 delivery 20
- Patch clamp electrophysiology
 conductance-voltage (G-V) relationship 481
 current isolation 515, 516
 current-voltage (I-V) relationship 481
 electrode resistance 475, 483
 external (extracellular) bath solution 507, 516
 gigaohm seal 479, 483
 internal (intracellular) pipette solution 503, 505, 515, 516
- K⁺ accumulation 484
- leak subtraction 480
- low pass filtering 480
- membrane capacitance 520
- membrane resistance 479, 480
- recording electrodes 472–480, 483, 528, 531
- sampling (digitizing) frequency 480
- series resistance 506, 520
 compensation 438
 errors 483
- voltage clamp configuration 479–481
- whole cell configuration 505, 521
- Patterning 244
- PDZ
 domain 15, 16
 ligand 16
- Penicillin/streptomycin
 penicillin G sodium 61
 streptomycin sulfate 61
- pGADT7 102–106
- pGBK 102
- Phase 181, 184, 245, 350, 361, 450, 451, 457, 460–461, 502
- Phenobarbital anesthesia 44
 compounding anesthetic 52
- Phosphate buffered solution (PBS). *See* Buffer
- Phospholipids 349
- Photobleaching 190, 193, 237, 240, 241
- Photodiode detector 451
- Photopolymerization 306, 307
- Photostimulation of caged glutamate
 caged neurotransmitters 528
 interpretation of input maps 532
 mapping locations of presynaptic neurons 529
 synaptic input map analysis 530
- Piezo-electric stimulator
 amplifier 206
 calibration 355, 359, 499
 cleaning 211

- construction 205
 grounding 209
 hair bundle placement 209
 probe placement 207
 resonance 217
 stack selection 277–289
- Pifithrin- α 421–423, 427
 PI3K/AKT/mTOR 70
 Pixel classification 280
 Phosphatase inhibitors 139
 Photodiode detector 451
 Plasmid 5, 8, 12, 14, 17, 20–22, 27–40,
 46–49, 53, 89, 96, 98, 100–104, 106, 170, 322,
 332, 368–370, 376, 385, 387–390, 392, 393, 420
P0Cre;Nf2^{flox/flox} (Nf2^{PO}) 63
 Polybrene (hexadimethrine bromide) 62
 Poly-d-lysine 61, 354, 356, 515, 516
 Polyethylene glycol 98, 374
 Poly-L-lysine 61, 370, 373–374, 382,
 387, 400, 401
 Polymerase chain reaction (PCR) 30, 47, 48,
 50–51, 55, 63, 68, 77, 79, 81, 83, 86–88, 90,
 99–101, 149, 169, 170, 181, 182, 323, 387, 392,
 421, 434
 Post-embedding immunogold transmission
 electron microscopy 149–164
 Postnatal
 day 207, 264, 531
 mouse 206, 207, 211
 Povidone-Iodine 62, 65, 66
 pre-miRNA 28, 29, 32, 33
 Prestin 190, 191, 195,
 198, 350, 501
 Primer construction 88, 99, 169
 Progenitor cell and sphere assay 301
 Protein concentration 62, 64, 121, 130,
 136, 172, 181
 Protein digestion 139–142, 146
 Protein fractionation 140, 143
 ion exchange chromatography 119, 131,
 140, 143
 Protein identification 114, 132, 138,
 143, 144, 146
 database search engines 138
 MASCOT 138, 140, 143, 146
 SEQUEST 138
 XTANDEM 138
 Protein interactions 95–107, 111, 125, 352
 Protein labeling
 chemical mass tagging
 isobaric tag for relative and absolute
 quantification (iTRAQ) 136
 isotope coded affinity tag (ICAT) 136
 enzymatic labeling 136
 18O labeling 137
- immunogold labeling 160–161
 label-free
 peak intensities or area under the curve 137
 spectral counting 137, 138
 metabolic labeling 136
 stable Isotope Labeling (SILAC) 136
- Protein localization
 colloidal gold 150
 ultrastructural
 collection of thin tissue sections 340
 decalcification of bone 162
 fixation of tissues 51, 56
 immunohistochemistry 39, 149, 164,
 250, 255, 263–274, 323, 339
 staining for contrast 322–323
 tissue embedding 152
- Protein pilot 131
- Protein–protein interaction 95–107, 166
- Protein quantitation
 analysis of differentially expressed
 proteins 144–145
 software for label-free quantitation
 Elucidator 138
 ProteoIQ 138
 Scaffold 138, 140, 143, 144, 147
 spectral counts 135, 137, 138, 144–147
 normalizing (*see* Tandem mass tags)
- Proteomics 110, 111, 114, 116,
 135, 136, 138, 145
 shotgun proteomics 145
- Puromycin dihydrochloride 62
- Q**
- Q_{10dB} 460
- Qiagen RNeasy® kit 75, 76, 82, 90, 344
- R**
- Rat 10–11
- Real-time reverse transcription PCR
 (RT-PCR) 77, 79, 86, 87, 90,
 149, 387, 421
- RACE 77, 79, 86, 87
- Recombinant AAV (rAAV)-mediated gene transfer
 benzonase nuclease 47, 49
 centrifugal filter 47, 49, 50, 56, 168
 cytopathic effect (CPE) 55
 inverted terminal repeat 47, 53, 54
 packaging capacity 54
 polyethylenimine (PEI) 44, 47, 370
 risk group I reagent 52
 serotype 44, 46, 48, 52, 53, 56
 tropism 44, 53
 viral genomes 50, 51, 55
- Reporter lysis buffers. *See* Buffers

- Resin embedding 152
- Recording solutions 488–489
- Ribbon synapses 265
- RNA
 - RNA integrity number (RIN) 336
 - isolation 334
 - quality 77, 80, 82, 85, 91
 - RNAlater® 75, 80, 82–84
 - RNASeq 73–91
- RNase
 - contamination 323
 - RNaseZap® 75, 80, 82, 83, 90
- RNeasy® Mini Kit 75, 76, 80, 82, 84
- S**
 - Saccular macula (SM) 4, 301, 364
 - Sch10545/Sch10545-Luc 64, 65, 67, 68.
 - See* Schwannomas
 - Schwann cells. *See* Cell culture
 - Schwannomas
 - allografts 67–70
 - imaging in small animals (*see* Bioluminescence imaging and magnetic resonance imaging)
 - Nf2P0* schwannoma cells 61, 63
 - Sch10545-Luc schwannoma cells 65
 - Sch10545 schwannoma cells 64
 - spinal schwannomas 59
 - vestibular schwannomas (VS), 59
 - xenografts in SCID mice 60
 - Scintillation vials 8, 13
 - Seg3D 285, 289
 - Seizures 60
 - Sensory epithelium 3–23, 40, 156, 244, 320, 335, 364, 391, 464, 480
 - Sequencing
 - Illumina-Solexa sequencing 79, 86
 - RNASeq 73–91
 - Severe combined immunodeficiency (SCID) 60, 62, 65–67, 69
 - mice 60, 65–67
 - Shaker-2 15
 - Single cell analysis and profiling 440
 - Small interfering RNA (siRNA) 5
 - Sodium dodecyl sulfate (SDS) 167, 168
 - Spinal schwannomas. *See* Schwannomas
 - Spiral ganglion
 - afferent bouton 472
 - neuron culture
 - dissociated 356
 - explant 306
 - primary 361
 - type I 356
 - type II 321
 - Spiral ligament 11, 156, 162, 459, 504
 - Sporadic 60
 - unilateral 60
 - Staurosporine 423, 427
 - Step count 195, 198
 - Stereocilia
 - base of stereocilia 20
 - IHC stereocilia 20
 - stereociliary bundle 6, 11, 15, 17, 18, 21
 - stereociliary tips 5, 11, 16
 - Stereotactic
 - injection (*see* Orthotopic)
 - radiation 60
 - Stoichiometry 189–198
 - Stria vascularis 11, 157, 162, 211, 233, 435, 494, 517
 - Supervoxels 285
 - Supporting cells
 - 4, 5, 265, 301, 379, 382, 386, 391, 394, 420, 436, 442, 452, 472, 477, 479, 483
 - inner supporting cells 265, 378
 - Surface plasmon resonance
 - analyte 171–172
 - langmuir binding model 178
 - ligand 166, 171–172
 - ligand immobilization 168, 184
 - mass transfer limitation 185
 - pH scouting 173, 174, 176
 - residual plot 179
 - sensor chip 166, 169, 174, 175, 178, 183, 184
 - Synaptic transmission
 - evoked synaptic currents 472, 481–482, 484
 - quantal analysis 482
 - Synthetic dropout (SD) medium 97
 - T**
 - Tagged protein 15–17, 46, 167
 - Tandem mass tags
 - aminoxy TMT kit 115
 - Iodoacetyl TMT kit 115
 - Targeted nanoparticles 365, 368
 - Targeted visualization 365
 - TE buffer 98, 344
 - Tectorial membrane 11, 211, 213, 219, 364, 450, 452, 458, 464, 465, 467, 469, 476
 - Tether force 351, 352, 357, 358, 361
 - Tether formation force 358
 - Tetramer 190, 195
 - 3D reconstruction 250, 255
 - Tissue engineering 319–344
 - Tissue preparation
 - brain 83, 268, 269
 - cochlea 268, 270
 - sensory epithelium 11

- spiral ganglion 313
 - Tol2-plasmid
 - construction 30, 32–33
 - diagram 29
 - miRNA expression 29, 39
 - Tonotopic organization 465
 - Transbasilar-membrane approach 18
 - Transcriptional profiling 74, 75, 77–79, 81, 86–88
 - Transfection. *See* Gene delivery
 - Transgenic mouse reporters 294
 - Transmission electron microscopy (TEM) 149–164, 204, 381
 - post-embedding 149–164
 - Transient transfection 74, 89, 191
 - Trifluoroacetic acid 118, 123, 145
 - TRIO and F-actin binding protein (TRIOBP) 6
 - Tris-buffered saline (TBS). *See* Buffer
 - Trypsin
 - immobilized 119, 127, 128, 130
 - TPCK-treated 130
 - Tubing
 - syringe adaptor tubing 8
 - tefzel tubing 7, 8, 12, 21
 - tubing cutter 8, 12, 13
 - tubing prep station 7, 8, 12, 13
 - Tumors. *See* Schwannomas. *See also* Meningiomas
- U**
- Ultramicrotomy
 - histochemical staining solution 153
 - knives 152, 153, 158
 - semi-thin sectioning 152–153, 157–159
 - ultrathin-sectioning 153, 159–160
 - Ultrasonic cleaner 8
 - Ultrastructural
 - colocalization 149–164
 - interacting proteins 149–164
 - identification 149–164
 - Utricular macula 4, 40
 - UV photolysis 227–228, 232, 233, 239
 - of caged IP₃, 235, 238
- V**
- Vestibular
 - bilateral VS 59
 - vestibular branch of the 8th cranial nerve 59
 - vestibular periphery 4
 - vestibular sensory epithelium 11, 18
 - vestibular schwannomas (VS) (*see* Schwannoma)
 - Vectors
 - non-viral vectors 370, 371
 - pAcGFP1-actin vector 20
 - viral vectors 4, 5, 28, 44, 54, 68, 365, 394
 - Vetbond™ tissue adhesive 63, 65
 - Virus
 - comparison for transduction efficiency 53, 68
 - Voltage-activated currents 480, 481
 - Voltage-clamp 350–352, 357, 519, 520, 530
 - Volume scan 457, 459
 - Volumetric optical coherence tomography vibrometry (VOCTV) 452, 453, 458–460
- W**
- Watershed 109, 110
 - Wharton's jelly cells 319–344
- X**
- X-α-Gal 96
 - Xenografts in SCID mice. *See* Meningiomas. *See also* Schwannomas
 - Xenopus* 73–91, 248
 - A6 kidney cell line 81, 89
 - Xylazine 452, 453
- Y**
- Y187 96, 99, 102
 - Yeast DNA isolation 103–104
 - Yeast dropout media
 - Ade 98
 - His 98
 - Leu 98
 - Trp 98
 - Yeast media 97
 - Yeast Peptone Dextrose media (YPD) 97, 99–102
 - Yeast two-hybrid (Y2H) 95–107, 149
- Z**
- Zebrafish chemical screens 421
 - Zebrafish embryo 4
 - zVAD-FMK 421, 422